Tool Steels: 5th Edition
George Roberts, George Krauss, Richard Kennedy, p 1-6
DOI:10.1361/toos1998p001

Copyright © 1998 ASM International®
All rights reserved.
www.asminternational.org

CHAPTER 1
Introduction

Tool steels are the alloys used to manufacture the tools, dies, and molds that shape, form, and cut other materials, including steels, nonferrous metals, and plastics. This definition of tool steels has been expanded into the following description in the "Tools Steels" section of the Steel Products Manual of the Iron and Steel Society (Ref 1):

> Tool steels are either carbon, alloy or high-speed steels, capable of being hardened and tempered. They are usually melted in electric furnaces and produced under tool steel practice to meet special requirements. They may be used in certain hand tools or in mechanical fixtures for cutting, shaping, forming and blanking of materials at either ordinary or elevated temperatures. Tool steels are also used on a wide variety of other applications where resistance to wear, strength, toughness and other properties are selected for optimum performance.

This description implies that tool steel technology overlaps the technology of carbon and low-alloy carbon steels, produced in large tonnages, which may be hardened by quench and tempering heat treatments. Although this association between tool steels and other hardenable steels is true, most texts on tool steels exclude treatment of the high-tonnage bar steels that might also be used for tool applications such as hand tools (Ref 1–3). Also, while tool steels may be manufactured with properties for use in nontool applications, such as springs, magnets, bearings, or even structural applications, these uses also are not generally treated in texts that describe the characterization and selection of tool steels.

This edition of *Tool Steels*, as have previous editions, will also concentrate on those steels that are uniquely manufactured for tool applications, recognizing that some more recently developed ultrahigh-strength steels—such as maraging steels, AF1410, and Aeromet 100, developed for structural applications that require high toughness—are sometimes also used for tool applications. This chapter explores further the philosophies which make tool steels a very special class of steels, the long historical evolution of iron and steel manufacture, including steels for tools, and the more recent development of tool steels as they emerged from the development of iron and steel products in general. The classification of the many types of tool steels is described in Chapter 2, and subsequent chapters describe production, alloy design, heat treatment, and specific tool steels in detail.

Tool Steels as Special Alloys

Tool steels have long been considered to be a very special group of alloys with characteristics similar to but different from those of other steels. Marcus Grossmann and Edgar Bain, in their book on tool steels (Ref 4), written in 1930 when the physical metallurgy of steel was just beginning to be firmly established, eloquently commented on the relationships been tool and other carbon steels:

> In some cases, notably in high-speed steel, the resulting alloy steel possesses such remarkable properties that, in a sense, its relation to carbon steel is almost unrecognizable. Yet it is the authors' opinion that the fundamental similarity exists, and that it may profitably be recognized. In acquiring an understanding of alloy steels, great value attaches in particular to some sort of general theory or principle if it is faithfully in accord with the facts and explains them in terms of simple fundamental effects. It is believed that certain fundamentals of iron metallurgy are manifest in all steels, modified in a definite manner by the alloying elements.

In addition to alloying, tools steels are considered special because they are very difficult to manufac-

ture, demanding the highest quality in every processing step. Peter Payson, in his book *The Metallurgy of Tool Steels,* published in 1962 (Ref 3), reflects this consideration in support of separating tool steels from more mass-produced steels:

> Even tool steel is not perfect, but it is far superior to so-called "tonnage" steel in freedom from internal porosity, sizable undesirable nonmetallic inclusions, serious chemical segregation, and surface defects. Various physical methods are used for macroinspection, and metallographic procedures for microinspection, to assure that tool steels meet the minimum requirements set up by the consumer.

While Payson's statement reflects the manufacturing scenario in the mid-20th century, it is far from accurate today. Carbon and low-alloy bar steels currently are manufactured in high volume to the highest quality by electric furnace melting, ladle metallurgy for impurity and inclusion control, and continuous casting. Nevertheless, tool steels are special and require careful manufacturing. The very high alloy content and microstructure that make them desirable for severe applications also make them difficult to manufacture. The contradictory demands of ease in manufacture and high performance of tool steel products were early noted by Harry Brearley in the 1916 preface to his book on the heat treatment of tool steels (Ref 5):

> The ultimate value of a tool may depend as much on the manner in which it is worked into its finished shape, as on the material from which it is made. The skill and knowledge of the toolsmith and hardener must therefore always be taken into account. If for any reason whatever these cannot be relied upon, the softer steels which are not so readily overheated in forging, or cracked in hardening, are invariably introduced at the cost, and finally to the dissatisfaction, of the tool user.

Historical Evolution of Iron and Steel

The earliest uses of steel were for tools and weapons, and then as now, high hardness and durability were the valued properties for these applications. High hardness was coupled to three factors: the ability to produce iron, the introduction of carbon into the iron to make steel, and the heating and quenching of the steel to produce martensite. The early attainment of each of these factors, and their simultaneous incorporation into finished tools and weapons, must have required considerable experimentation, chance, intuition, and perceptive observation. Indeed, the production of hardened tool steels must be considered truly impressive. It was accomplished without analytical instruments or scientific understanding of chemistry, crystallography, or microstructure.

Iron can be traced to the Egyptians of 5000 to 6000 years ago, and numerous biblical references confirm this time period for the beginning use of iron (Ref 6, 7). Widespread replacement of bronze by iron occurred at about 1200 B.C., perhaps because of natural and economic disasters that interrupted the flow of tin, which was alloyed with copper to make bronze (Ref 7). As a result, the advantages of iron became known, despite its being an unfamiliar technology, as well as being softer and more subject to corrosion than bronze.

Maddin (Ref 7) explored the early hardening of steel and described a miner's pick—the earliest known example of a martensitic steel tool. The pick (Fig. 1-1) was found in Galilee and dates from the late 13th or early 12th century B.C. Figure 1-2 shows the hardened martensitic microstructure, which confirms that the pick was hardened by heating and quenching. Earlier steel objects have been

Fig.1-1 Miner's pick from Mt. Adir in northern Galilee (13th to 12th century B.C.). Arrow indicates flake, the microstructure of which is shown in Fig. 1-2. Source: Ref 7

Fig.1-2 Martensitic microstructure of hardened pick shown in Fig. 1-1. Light micrograph, estimated magnification 500 to 1000X. Source: Ref 7

documented, but their microstructures are pearlitic, indicating that quenching was not yet mastered. The following quotation from Homer's *Odyssey* (Ref 8), relating to the blinding of the giant Cyclops by Odysseus and his men, shows that quenching and metalworking must have been well established by 900 B.C., the approximate date of its writing (Ref 6, 7):

> And as when armorers temper in the ford
> The keen-edged pole-axe, or shining sword,
> The red-hot metal hisses in the lake;
> Thus in his eyeball hissed the plunging stake.

Steel, a workable combination of iron and carbon, has been historically difficult to produce efficiently and consistently. Two quite different approaches to steel production evolved over the millennia. One was based on smelted iron, which contained too little carbon and required subsequent carburization, while the other was based on the production of pig or cast iron, which contained too much carbon and required its subsequent removal. The earliest example of the first approach is the production of "wootz" steel in India, which dates back to about 350 B.C. (Ref 6, 7, 9). Iron ore was smelted with charcoal in forges; air was forced into the charge through tuyeres with bellows, enabling high temperatures to be attained. Nevertheless, temperatures were limited, and semisolid sponge iron containing considerable entrapped slag was produced. The slag was removed and fragmented into smaller particles by intense hammering or forging. This wrought iron was then carburized in crucibles with charcoal or rice husks to produce the wootz or crucible steel. An example of the type of forge used to produce wootz steels is shown in Fig. 1-3.

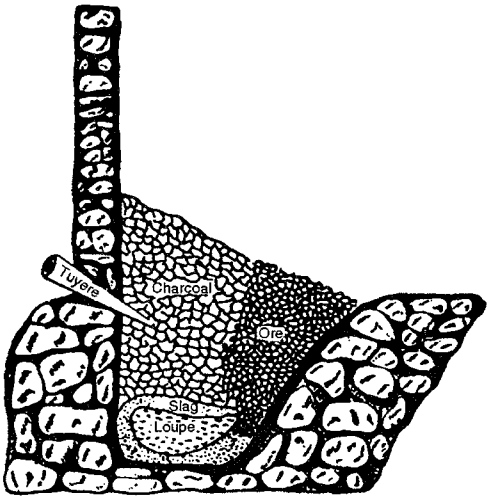

Fig.1-3 Sectional view of a Catalan forge. Source: Ref 10

Similar processing developed in Europe following the Dark Ages when wrought iron was carburized by heating in contact with charcoal to form what was known as blister steel, from the appearance of surface blisters or scale. The depth of carburization tended to be shallow and nonuniform. Later, short lengths of blister steel were stacked, forged, and welded to produce the product referred to as shear steel. The uniformity of the shear steel structure was improved, but variations in carbon could not be completely eliminated.

Wrought iron production in forges or bloomaries directly from ore, similar to those practices described for the production of wootz steel, continued to be the major production method for iron and steel well into the 19th century. However, blast furnaces, which converted iron ore by reduction with air, charcoal, and limestone flux into cast or pig iron, eventually developed to produce iron in larger quantities (Ref 6). Pig and cast irons were high in carbon, silicon, and phosphorus and quite brittle. The high carbon content lowered the melting point of iron, making it fluid and castable, but the associated iron carbides or graphite in the microstructure, together with other impurities, prevented working—as is characteristic of wrought steels with lower carbon content. Various low-volume production techniques to convert cast iron to steel were developed—for example, the puddling process described by Thackray in his informative account of the history of iron and steel (Ref 6)

Modern high-volume liquid steelmaking developed when the high-carbon content and other impurities in pig iron were oxidized in Bessemer converters and Siemens-Martins open hearth furnaces to create steel (Ref 6). In the Bessemer process, patented by Bessemer in 1856, hot air was blown through molten pig iron to reduce carbon and silicon; in the open hearth furnace, first successfully operated by Siemens in a plant in 1868, solid or liquid pig iron and scrap were melted in the furnace, and the oxygen for the conversion of the pig iron to steel was provided by iron ore. Liquid steelmaking has continued to evolve to this day, with the replacement of Bessemer converters and open hearth furnaces with other types of oxygen converters and electric arc furnaces. The latter developments have been largely applied to large-tonnage, low-alloy, carbon steels, while tool steel production has followed an independent path.

Tool Steel History

Early tool steel history is intimately related to the evolution of steels in general, since the inability to make steel in large quantities tended to concentrate steel applications to tools and weapons instead of the structural applications that dominate steel usage

today. Perhaps the best early examples of the skill and knowledge required for high-performance steel manufacture are the swords produced in China, Damascus, and Japan (Ref 9, 11). These swords were produced by layer welding of high- and low-carbon steel by multiple forging steps. Not only was a functional sword with the high hardness of high-carbon steel and the toughness of low-carbon steel produced, but the fine layered structure also yielded unique patterns of great beauty. Although pattern-welded steel technologies evolved over many centuries, recorded dates for Damascus blades originate from A.D. 540 (Ref 9), and Japanese swordmaking was clearly documented during A.D. 900 to 1000, when Japanese swordmakers began to inscribe their names on the blades (Ref 11).

Table 1-1 presents a chronological listing of developments in steels, emphasizing important dates or periods for tool and high-speed steel technology. The beginning of tool steel history is generally regarded as 1740, when Benjamin Huntsman, a clockmaker from Sheffield, England, melted pieces of blister steel in a crucible. The melting produced a much more homogeneous steel than the blister or shear steels produced by solid-state processing and provided the foundation for producing the high-quality steel required for not only Huntsman's clock springs but also the tool steels that were to come. The crucible melting process, typically handling amounts of tool steels about 100 lb in size, continued to dominate the making of tool steels well into the 20th century (Ref 4), until electric furnace melting, with heats of several tons in size, other melting processes, and powder metallurgy (P/M) production of tool steel were developed and applied as described in Chapter 3.

Table 1-1 Important dates in the development of high-speed tool steels

Date	Development
1200 B.C.	First documented hardened steel tool
350 B.C.	Wootz steels of India
A.D. 540	Damascus layered steel blades
A.D. 900	Japanese layered steel blades
Dark Ages	Steel production by carburizing of iron
1740	Crucible melting of steel: Huntsman
1868	Air-hardening tungsten alloy steel: Mushet
1898	High-speed steel high-heat hardening: Taylor/White
1903	0.70C-14W-4C prototype of modern high-speed steel
1904	Alloying with 0.3% V
1906	Electric furnace melting introduced
1910	18W-4Cr-1V (18-4-1) steel (T1) introduced
1912	3 to 5% C additions for added red hardness
1923	12% C for higher-speed machining
1939	High C high V superhigh-speed steels (M4 and T15)
1940	Start of substitution of molybdenum for tungsten
1953	Sulfurized free-machining high-speed steel
1961	Rockwell C 70 high-speed steel (M40 series)
1970	Introduction of powdered metal high-speed steels
1973	Higher silicon and nickel contents of M7 to increase hardness
1980	Development to cobalt-free superhigh-speed steels
1980	Titanium nitride ceramic coating of tool steels
1982	Aluminum-modified high-speed tool steels

Source: Modified from previous editions of *Tool Steels*, with additions from Ref 12

Modern tool steels depend strongly on alloying and heat treatment for their high hardness, and understanding of the interrelationships among carbon content, alloy composition, and processing came only gradually in the 19th century. The slow pace was caused in part by the necessary concurrent development of methods of precise chemical analysis and metallography, which could resolve the microstructure of steels. Often, fracture surfaces of steels were the only measure of steel structure and quality. Nevertheless, the use of alloying was beginning, and Huntsman and others were beginning to use manganese to deoxidize liquid steel (Ref 6).

Alloying, which initiated the era of modern tool steels, is attributed to Robert Mushet, who in 1868 added tungsten to a high-carbon steel. Until that time, and for 25 years thereafter, other steels for tools were made of unalloyed carbon steel. The composition of Mushet's steel, marketed as "R. Mushet's Special Tool Steel" through 1900, consisted of nominally 2% C, 2.5% Mn, 7% W, and often 0.50% Cr and 1.10% Si (Ref 13). This steel had the remarkable capacity to harden during air cooling after forging or heating and is regarded as the first high-speed steel.

Chromium, as reviewed by R.A. Hadfield (Ref 14), was investigated as an alloying element in steel, soon after its discovery in 1797. Practical benefits of hardening and toughening of steel by alloying with chromium were first claimed in an American patent filed by Julius Baur in 1865. Henri Brustlein, of Unieux, France, also investigated the production of ferrochrome and its addition to steel (Ref 14, 15), starting in 1876. The benefits of chromium, however, were not always consistently developed because the role that carbon played in hardening and the solid-state phase transformations that caused hardening were not clear at the time Hadfield wrote his review in 1892 (Ref 14).

At the same time, John W. Langley summarized the alloying of steel in a paper delivered to the Society of Civil Engineers (Ref 16). He emphasized that, in addition to iron, at least 0.30% C was necessary to make hardening possible in steel, and that manganese was essential to "neutralize the evil effects of sulphur and oxygen." The detrimental effect of phosphorus was also noted, as was the opinion that only tungsten, chromium, manganese, and nickel could be used to make useful alloy steels. Hardening was associated with rapid cooling "from a temperature a little above redness." Otto Thallner, in his book on tool steels, translated from German in 1902 (Ref 17), also summarizes the effects of manganese, tungsten, chromium, and nickel, the elements most commonly used for alloying tool steel at the turn of the century.

A dramatic period in the development of high-speed steel was precipitated by Fred W. Taylor and his colleague Maunsel White at the Bethlehem Steel Corporation in the years around 1900. The intrigue, technical status, discoveries, players, legal aspects, and importance of this period have been recorded and analyzed in detail in a very readable paper by Arthur Townsend (Ref 13). Briefly, Taylor and White, in the period from 1894 to 1898, discovered that very-high-temperature heating, much higher than typically applied at that time, and subsequent air cooling of chromium-tungsten steels, developed in that period by others in competition to the Mushet tungsten steels, could produce and maintain exceptional hardness during machining at high speeds, even at red heat. The high-temperature heating, its remarkable effects, and the benefits of high-temperature tempering, were truly innovative contributions by Taylor and White. Prior to 1898, air-hardening tool steels were commonly hardened only by cooling from relatively low temperatures after forging and were not reheated for hardening. Patents filed by Taylor and White were subjected to considerable legal argument because it was not clear whether they were claiming a new steel or a new heat-treating process.

The intense activity in heat treatment and alloy development of high-speed steels at the turn of the century continued and was rapidly joined by great advances in metallography, x-ray analysis, and scientific understanding of phase transformations and microstructure (Ref 18, 19), to make advances in the entire field of alloy tool steels. O.M. Becker summarizes the state of the art in 1910 and describes all the crystalline phases then identified in steels, including ferrite, cementite, austenite, and martensite (Ref 10). His descriptions of the transformations between the various phases show that this aspect of heat treatment was not yet fully understood at that time. Many new compositions were introduced for both tool and die applications.

By 1920, the number of principal tool steel grades had been extended to about 12; many of these types are still currently produced. Included in the alloy tool steels developed during this period were the tungsten-base and chromium-base hot-work die steels, manganese oil-hardening die steel, tungsten finishing steel, tungsten chisel steel, and chromium-vanadium and carbon-vanadium general-purpose steels. In the high-speed steel field, the improved red hardness from cobalt additions had been discovered, and three principal grades were available: 18W-4Cr-1V (18-4-1), 14W-4Cr-2V, and 18-4-1 with cobalt.

Also by 1920, nearly all of the American tool steel companies had organized metallurgical research departments, and the resulting scientific and technical effort brought additional tremendous progress in tool steel development. Included in the outstanding developments were (1) the importation of the high-carbon, high-chromium die steel compositions from England to the United States shortly after World War I, (2) the addition of molybdenum to the 1C-5Cr die steels to make them air hardening, (3) the development of the special die-casting die steels that have found so many other hot-working applications, (4) the combining of tungsten and chromium in die steels requiring maximum heat resistance, and (5) the development of various free-machining tool steels. In the last category are included the graphitic die steels introduced in 1937, the leaded steels first patented in 1939 and applied to diemaking in 1946, and the sulfurized tool steels.

New developments in high-speed steels since 1920 have also been impressive. In 1980, there were 41 different high-speed steel compositions, of which about 12 accounted for the bulk of high-speed steels used. The large variety is primarily the result of the cobalt additions and the substitution of molybdenum for tungsten due to the availability of vast resources of molybdenum made possible by the opening of the Climax Mine in Colorado and the shortage of tungsten because of World War II. These developments gave molybdenum a cost advantage, and molybdenum high-speed steels now occupy a major part of the market (a situation that has changed dramatically from 1902, when Thallner stated that its high price relative to tungsten prohibited its use).

The tendency of molybdenum grades to decarburize or lose carbon from surface layers during heating was a major early deterrent to the use of molybdenum steels. This problem was solved in 1930, when the Watertown Arsenal discovered that borax coatings greatly reduced decarburization during heating for forging or rolling. Also, salt bath and controlled-atmosphere furnaces were developed to prevent decarburization and maintain the precise temperature control required for the heat treatment of high-speed steels.

Another major high-speed steel development during this active period was the discovery that carefully balanced additions of high vanadium and increased carbon would form large amounts of very hard vanadium carbides, which greatly increase abrasion resistance. This discovery led to the so-called superhigh-speed steels that have given excellent service in die applications as well as outstanding tools for cutting purposes. High-speed steels containing cobalt have been developed with hardness close to 70 HRC after heat treatment.

More recently, new methods of manufacture of tool steels, including electroslag melting, vacuum arc remelting, and powder processing have been applied to produce uniformity in composition and structure and high quality. Surface-modification heat treatments such as gas carburizing and nitriding have long been applied to tool steels, and the most recent developments include carburizing and nitriding in vacuums and plasmas and the applica-

tion of thin ceramic layers such as titanium nitride by chemical and physical vapor deposition techniques (Ref 20).

Summary

This chapter has introduced the special set of alloys known as tool steels. The historical account shows that the development of tool steels could not be separated from the evolution of iron and steels in general until the concepts of alloying and its role in hardening were established in the second half of the 19th century. The making of steel, because its success depended so much on trial and error, was invariably shrouded in secrecy. However, with scientific enlightenment and rapidly expanding demand for manufactured goods came the need and willingness to share information.

Some of the pioneering manuscripts devoted to the manufacture and application of tool and high-speed steels published at the beginning of the 20th century have been noted here, including books by Thallner (1902), Becker (1910), and Brearley (1918). From 1920 on, with the scientific principles in place, continual development of instrumentation for analysis and control and rapidly expanding technology and manufacturing capacity, tool steel development increased dramatically. The results of these efforts are described in detail in the balance of this book.

REFERENCES

1. Tool Steels, *Steel Products Manual*, Iron and Steel Society, April 1988
2. G.A. Roberts and R.A. Cary, *Tool Steels*, 4th ed., American Society for Metals, 1980
3. P. Payson, *The Metallurgy of Tool Steels*, John Wiley & Sons, 1962
4. M.A. Grossmann and E.C. Bain, *High-Speed Steel*, John Wiley & Sons, 1931
5. H. Brearley, *The Heat Treatment of Tool Steel*, Longmans, Green and Co., London, 1918
6. G.E. Thackray, Notes on the History of Iron and Steel, *Trans. Am. Soc. Steel Treat.*, Vol 6, July–Dec 1924, p 443–490
7. R. Maddin, A History of Martensite: Some Thoughts on the Early Hardening of Iron, *Martensite*, G.B. Olson and W.S. Owen, Ed., ASM International, 1992, p 11–19
8. Homer, *The Odyssey*, Book IX:389–394, ca. 900 B.C.
9. L.S. Figiel, *On Damascus Steel*, Atlantis Arts Press, 1991
10. O.M. Becker, *High-Speed Steel*, McGraw-Hill, 1910
11. H. Tanimura, Development of the Japanese Sword, *J. Met.*, Feb 1980, p 63–72
12. A.M. Bayer and L.R. Walton, Wrought Tool Steels, *ASM Handbook*, Vol 1, (formerly *Metals Handbook*, Vol 1, 10th ed.), ASM International, 1990, p 764
13. A.S. Townsend, Alloy Tool Steels and the Development of High-Speed Steel, *Trans. Am. Soc. Steel Treat.*, Vol 21, Jan-Dec 1933, p 769–795
14. R.A. Hadfield, Alloys of Iron and Chromium, *J. Iron Steel Inst.*, Vol 42 (No. 2), 1892, p 49–110
15. M. Brustlein, On Chrome Pig Iron and Steel, *J. Iron Steel Inst.*, Vol 30 (No. 2), 1886, p 770–778
16. J.W. Langley, Discussion on Structural Steel, *Trans. Am. Soc. Civil Eng.*, Vol 27, July-Dec 1892, p 385–405
17. O. Thallner, *Tool-Steel: A Concise Handbook on Tool-Steel in General*, W.T. Brannt, trans., Henry Carey Baird & Co., 1902
18. C.S. Smith, *A History of Metallography*, University of Chicago Press, 1960
19. A. Sauveur, *The Metallography and Heat Treatment of Iron and Steel*, McGraw-Hill, 1912; 2nd ed., 1915; 3rd ed., 1926, 4th ed., 1935
20. A. Matthews, Titanium Nitride PVD Coating Technology, *Surf. Eng.*, Vol 1, (No. 2), 1985, p 93–104

Tool Steels: 5th Edition
George Roberts, George Krauss, Richard Kennedy, p 7-28
DOI:10.1361/toos1998p007

Copyright © 1998 ASM International®
All rights reserved.
www.asminternational.org

CHAPTER 2
Classification and Selection of Tool Steels

There are a great many specific grades or compositions of tool steels. These steels have been organized into groups or types that have evolved to perform specific functions, such as forging, cold work, die casting, and high-speed machining, in a variety of operating conditions. Within each group or type may be many grades that are similar but differ slightly from one another to accommodate somewhat different processing requirements, operating conditions, or work materials.

Classification of Tool Steels

The very large number of tool steels is effectively classified by the widely used system developed by the American Iron and Steel Institute (AISI) (Ref 1-3). This system is the starting point for the selection of the proper steel for a given function from the large number of steels available.

The AISI classification system arranges tool steels into groups that are based on prominent characteristics such as *alloying* (for example, tungsten or molybdenum high-speed steels), *application* (for example, cold-work or hot-work tool steels), or *heat treatment* (for example, water-hardening or oil-hardening tool steels). Table 2-1 lists nine main groups of tool steels and their identifying letter symbols, and Table 2-2 presents the AISI classification and the nominal compositions of the most widely used tool steels. In addition to the AISI classification, the steels are identified by designations in the Unified Numbering System (UNS) for Metals and Alloys, established in 1975 by the Society of Automotive Engineers (SAE) and the American Society for Testing and Materials (ASTM). Table 2-2 shows only nominal compositions of the major alloying elements in various tool steels. Composition ranges of the alloying elements for each steel are given in separate chapters on tool steel groups.

Although the AISI classification system is widely used, many countries have independent classification systems for tool steels. Table 2-3 lists AISI grades and cross-references to designations of comparable tool steels from German, Japanese, British, French, and Swedish systems (Ref 3, 4).

Previous editions of this book (Ref 5, 6) used a three-digit code to identify the different types of tool steels. Although this system has been replaced by the AISI system, it is described here because it represents an earlier stage in the development of the tool steel industry. The first digit of an alloy designation identified the group of steels, the first and second digits taken together identified the class, and all three digits together identified the steel within the class. This system subdivided tool steels into many more classes than the AISI system, as shown in Table 2-4. Compositions of the steels in each class are given in the first and fourth editions of this book, and many, but not all, of the steels identified by three-digit numbers were also assigned AISI classifications. Many of the tool steels assigned three-digit codes were used for very specialized applications and were manufactured in very small amounts. As a result, some tool steels, listed by their AISI designations in Table 2-5, are no longer in common use.

Table 2-1 Main groups of tool steels and AISI letter symbols

Group	Identifying symbol
Water-hardening tool steels	W
Shock-resisting tool steels	S
Oil-hardening cold-work tool steels	O
Air-hardening, medium-alloy cold-work tool steels	A
High-carbon, high-chromium cold-work tool steels	D
Mold steels	P
Hot-work tool steels, chromium, tungsten, and molybdenum	H
Tungsten high-speed tool steels	T
Molybdenum high-speed tool steels	M

Source: Ref 2

Table 2-2 AISI classification and nominal compositions of major tool steels

AISI	UNS No.	Identifying elements, % C	Mn	Si	Cr	V	W	Mo	Co	Ni
Water-hardening tool steels										
W1	T72301	0.60–1.40(a)	...	...	...	...	...	...	...	...
W2	T72302	0.60–1.40(a)	...	...	...	0.25	...	...	...	...
W5	T72305	1.10	...	...	0.50	...	...	...	...	...
Shock-resisting tool steels										
S1	T41901	0.50	...	...	1.50	...	2.50	...	...	...
S2	T41902	0.50	...	1.00	...	...	...	0.50	...	...
S5	T41905	0.55	0.80	2.00	...	...	...	0.40	...	...
S6	T41906	0.45	1.40	2.25	1.50	...	...	0.40	...	...
S7	T41907	0.50	...	...	3.25	...	...	1.40	...	...
Oil-hardening cold-work tool steels										
O1	T31501	0.90	1.00	...	0.50	...	0.50	...	...	...
O2	T31502	0.90	1.60	...	...	...	...	...	...	...
O6(b)	T31506	1.45	0.80	1.00	...	...	...	0.25	...	...
O7	T31507	1.20	...	...	0.75	...	1.75	...	...	...
Air-hardening, *medium*-alloy cold-work tool steels										
A2	T30102	1.00	...	...	5.00	...	...	1.00	...	...
A3	T30103	1.25	...	...	5.00	1.00	...	1.00	...	...
A4	T30104	1.00	2.00	...	1.00	...	...	1.00	...	...
A6	T30106	0.70	2.00	...	1.00	...	...	1.25	...	...
A7	T30107	2.25	...	...	5.25	4.75	1.00(c)	1.00	...	...
A8	T30108	0.55	...	...	5.00	...	1.25	1.25	...	...
A9	T30109	0.50	...	...	5.00	1.00	...	1.40	...	1.50
A10(b)	T30110	1.35	1.80	1.25	...	...	...	1.50	...	1.80
High-carbon, high-chromium cold-work steels										
D2	T30402	1.50	...	...	12.00	1.00	...	1.00	...	...
D3	T30403	2.25	...	...	12.00	...	...	...	...	...
D4	T30404	2.25	...	...	12.00	...	...	1.00	...	...
D5	T30405	1.50	...	...	12.00	...	...	1.00	3.00	...
D7	T30407	2.35	...	...	12.00	4.00	...	1.00	...	...
Low-alloy special-purpose tool steels										
L2	T61202	0.50–1.10(a)	...	...	1.00	0.20	...	...	...	...
L6	T61206	0.70	...	...	0.75	...	...	0.25(c)	...	1.50
Mold steels										
P2	T51602	0.07	...	...	2.00	...	...	0.20	...	0.50
P3	T51603	0.10	...	...	0.60	...	...	...	...	1.25
P4	T51604	0.07	...	...	5.00	...	...	0.75	...	...
P5	T51605	0.10	...	...	2.25	...	...	...	...	...
P6	T51606	0.10	...	...	1.50	...	...	...	...	3.50
P20	T51620	0.35	...	...	1.70	...	...	0.40	...	...
P21	T51621	0.20	1.20 (A1)	...	...	...	...	...	...	4.00
Chromium hot-work tool steels										
H10	T20810	0.40	...	...	3.25	0.40	...	2.50	...	...
H11	T20811	0.35	...	...	5.00	0.40	...	1.50	...	...
H12	T20812	0.35	...	...	5.00	0.40	1.50	1.50	...	...
H13	T20813	0.35	...	...	5.00	1.00	...	1.50	...	...
H14	T20814	0.40	...	...	5.00	...	5.00	...	...	...
H19	T20819	0.40	...	...	4.25	2.00	4.25	...	4.25	...
Tungsten hot-work tool steels										
H21	T20821	0.35	...	...	3.50	...	9.00	...	...	...
H22	T20822	0.35	...	...	2.00	...	11.00	...	...	...
H23	T20823	0.30	...	...	12.00	...	12.00	...	...	...
H24	T20824	0.45	...	...	3.00	...	15.00	...	...	...

(continued)

(a) Available with different carbon contents. (b) Contains graphite. (c) Optional. Source: Ref 2

Table 2-2 AISI classification and nominal compositions of major tool steels

AISI	UNS No.	Identifying elements, % C	Mn	Si	Cr	V	W	Mo	Co	Ni
Tungsten hot-work tool steels (continued)										
H25	T20825	0.25	...	...	4.00	...	15.00	...	...	...
H26	T20826	0.50	...	...	4.00	1.00	18.00	...	...	...
Molybdenum hot-work tool steels										
H42	T20842	0.60	...	...	4.00	2.00	6.00	5.00	...	...
Tungsten high-speed tool steels										
T1	T12001	0.75(a)	...	...	4.00	1.00	18.00	...	...	...
T2	T12002	0.80	...	...	4.00	2.00	18.00	...	...	...
T4	T12004	0.75	...	...	4.00	1.00	18.00	...	5.00	...
T5	T12005	0.80	...	...	4.00	2.00	18.00	...	8.00	...
T6	T12006	0.80	...	...	4.50	1.50	20.00	...	12.00	...
T8	T12008	0.75	...	...	4.00	2.00	14.00	...	5.00	...
T15	T12015	1.50	...	...	4.00	5.00	12.00	...	5.00	...
Molybdenum high-speed tool steels										
M1	T11301	0.80(a)	...	...	4.00	1.00	1.50	8.00	...	...
M2	T11302	0.85–1.00(a)	...	...	4.00	2.00	6.00	5.00	...	...
M3, class 1	T11313	1.05	...	...	4.00	2.40	6.00	5.00	...	...
M3, class 2	T11323	1.20	...	...	4.00	3.00	6.00	5.00	...	...
M4	T11304	1.30	...	...	4.00	4.00	5.50	4.50	...	...
M6	T11306	0.80	...	...	4.00	2.00	4.00	5.00	12.00	...
M7	T11307	1.00	...	...	4.00	2.00	1.75	8.75	...	...
M10	T11310	0.85–1.00(a)	...	...	4.00	2.00	...	8.00	...	...
M30	T11330	0.80	...	...	4.00	1.25	2.00	8.00	5.00	...
M33	T11333	0.90	...	...	4.00	1.15	1.50	9.50	8.00	...
M34	T11334	0.90	...	...	4.00	2.00	2.00	8.00	8.00	...
M36	T11336	0.80	...	...	4.00	2.00	6.00	5.00	8.00	...
Ultrahard high-speed tool steels										
M41	T11341	1.10	...	...	4.25	2.00	6.75	3.75	5.00	...
M42	T11342	1.10	...	...	3.75	1.15	1.50	9.50	8.00	...
M43	T11343	1.20	...	...	3.75	1.60	2.75	8.00	8.25	...
M44	T11344	1.15	...	...	4.25	2.00	5.25	6.25	12.00	...
M46	T11346	1.25	...	...	4.00	3.20	2.00	8.25	8.25	...
M47	T11347	1.10	...	...	3.75	1.25	1.50	9.50	5.00	...

(a) Available with different carbon contents. (b) Contains graphite. (c) Optional. Source: Ref 2

To provide an introductory overview of tool steels and some background for tool steel selection and application, each group of tool steels, as listed in Table 2-2, is described briefly in this chapter. Separate later chapters then describe each group in more detail. The chemical compositions of the tool steels listed in Table 2-2 include a wide range of carbon and alloy contents. As developed in detail in the chapters on alloy design and heat treatment, the combinations of the properties of the various groups of tool steels are strong functions of heat treatment processing as determined by the alloying. The final heat treatment of tool steels invariably consists of a three-stage process: heating for austenite formation, cooling to transform the austenite to martensite, and heating or tempering to eliminate retained austenite and form carbides within the martensite.

Several very general alloying and heat treatment principles are introduced at this point to provide a base for comparing the various groups of tool steels:

- The hardened microstructure of a typical tool steel consists of a matrix of tempered martensite containing various dispersions of iron and alloy carbides.
- High carbon and high alloy content promote hardenability or the ability to form martensite on cooling.
- The higher the carbon and alloy content in supersaturation in the martensite, as inherited from the parent austenite, the higher the density of carbides that can be formed on tempering.
- The higher the content of strong carbide-forming elements, the higher the density of carbides that are stable in austenite during hot work and austenitiz-

Table 2-3 Cross-references of AISI tool steels designations to designations in other national systems

United States (AISI)	West Germany (DIN)(a)	Japan (JIS)(b)	Great Britain (B.S.)(c)	France (AFNOR)(d)	Sweden (SS14)
Molybdenum high-speed steels (ASTM A 600)					
M1	1.3346	...	4659 BM1	A35-590 4441 Z85DCWV08-04-02-01	2715
M2, reg C	1.3341, 1.3343, 1.3345, 1.3553, 1.3554	G4403 SKH51 (SKH9)	4659 BM2	A35-590 4301 Z85WDCV06-05-04-02	2722
M2, high C	1.3340, 1.3342	...	...	A35-590 4302 Z90WDCV06-05-04-02	...
M3, class 1	...	G4403 SKH52	...	...	...
M3, class 2	1.3344	G4403 SKH53	...	A35-590 4360 Z120 WDCV06-05-04-03	(USA M3 class 2)
M4	...	G4403 SKH54	4659 BM4	A35-590 4361 Z130 WDCV06-05-04-04	...
M7	1.3348	G4403 SKH58	...	A35-590 4442 Z100DCWV09-04-02-02	2782
M10, reg C	...	...	...	...	...
M10, high C	...	...	...	...	...
M30	1.3249	...	4659 BM34	...	...
M33	1.3249	...	4659 BM34	...	...
M34	1.3249	...	4659 BM34	...	...
M35	1.3243	G4403 SKH55	...	A35-590 4371 Z85WDKCV06-05-05-04-02 A35-590 4372 Z90WDKCV06-05-05-04-02	...
M36	1.3243	G4403 SKH55, G4403 SKH56	...	A35-590 4371 Z85WDKCV06-05-05-04	2723
M41	1.3245, 1.3246	G4403 SKH55	...	A35-590 4374 Z110WKCDV07-05-04-04	2736
M42	1.3247	G4403 SKH59	4659 BM42	A35-590 4475 Z110DKCWV09-08-04-02	...
M43	...	...	...	A35-590 4475 Z110DKCWV09-08-04-02-01	...
M44	1.3207	G4403 SKH57	4659 (USA M44)	A35-590 4376 Z130KWDCV12-07-06-04-03	...
M46	1.3247	...	...	...	...
M47	1.3247	...	...	...	...
Intermediate high-speed steels					
M50	1.2369, 1.3551	...	...	A35-590 3551 Y80DCV42.16	(USA M50)
M52	...	...	...	...	...
Tungsten high-speed steels (ASTM A 600)					
T1	1.3355, 1.3558	G4403 SKH2	4659 BT1	A35-590 4201 Z80WCV18-04-01	...
T2	...	...	4659 BT2, 4659 BT20	4203 18-0-2	...
T4	1.3255	G4403 SKH3	4659 BT4	A35-590 4271 Z80WKCV18-05-04-01	...
T5	1.3265	G4403 SKH4	4659 BT5	A35-590 4275 Z80WKCV18-10-04-02	(USA T5)
T6	1.3257	G4403 SKH4B	4659 BT6	...	...
T8	...	...	...	...	...
T15	1.3202	G4403 SKH10	4659 BT15	A35-590 4171 Z160WKVC12-05-05-04	(USA T15)
Chromium hot-work steels (ASTM A 681)					
H10	1.2365, 1.2367	G4404 SKD7	4659 BH10	A35-590 3451 32DCV28	...
H11	1.2343, 1.7783, 1.7784	G4404 SKD6	4659 BH11	A35-590 3431 FZ38CDV5	...

(continued)

(a) Deutsche Industrie Normen (German Industrial Standards). (b) Japanese Industrial Standard. (c) British Standard. (d) l'Association Française de Normalisation (French Standards Association). Source: Ref 3, 4

Table 2-3 (continued)

United States (AISI)	West Germany (DIN)(a)	Japan (JIS)(b)	Great Britain (B.S.)(c)	France (AFNOR)(d)	Sweden (SS14)
Chromium hot-work steels (ASTM A 681) (continued)					
H12	1.2606	G4404 SKD62	4659 BH12	A35-590 3432 Z35CWDV5	...
H13	1.2344	G4404 SKD61	4659 BH13, 4659 H13	A35-590 3433 Z40CDV5	2242
H14	1.2567	G4404 SKD4	...	3541 Z40WCV5	...
H19	1.2678	G4404 SKD8	4659 BH19	...	...
Tungsten hot-work steels (ASTM A 681)					
H21	1.2581	G4404 SKD5	4659 BH21, 4659 H21A	A35-590 3543 Z30WCV9	2730
H22	1.2581	G4404 SKD5	...	...	...
H23	1.2625	...	...	...	...
H24	...	...	...	...	...
H25	...	...	...	...	...
H26	...	...	4659 BH26	...	...
Molybdenum hot-work steels (ASTM A 681)					
H42	...	...	...	3548 Z65WDCV6.05	...
Air-hardening, medium-alloy cold-work steels (ASTM A 681)					
A2	1.2363	G4404 SKD12	4659 BA2	A35-590 2231 Z100CDV5	2260
A3	...	...	...	...	...
A4	...	...	...	...	...
A5	...	...	...	...	...
A6	...	...	4659 BA6	...	...
A7	...	...	...	...	...
A8	1.2606	G4404 SKD62	...	3432 Z38CDWV5	...
A9	...	...	...	...	...
A10	...	...	...	...	...
High-carbon, high-chromium cold-work steels (ASTM A 681)					
D2	1.2201, 1.2379, 1.2601	G4404 SKD11	4659 (USA D2), 4659 BD2 4659 BD2A	A35-590 2235 Z160CDV12	2310
D3	1.2080, 1.2436, 1.2884	G4404 SKD1, G4404 SKD2	4659 BD3	A35-590 2233 Z200C12	...
D4	1.2436, 1.2884	G4404 SKD2	4659 (USA D4)	A35-590 2234 Z200CD12	2312
D5	1.2880	...	...	A35-590 2236 Z160CKDV12.03	...
D7	1.2378	...	...	2237 Z230CVA12.04	...
Oil-hardening cold-work steels (ASTM A 681)					
O1	1.2510	G4404 SKS21, G4404 SKS3, G4404 SKS93 G4404 SKS94, G4404 SKS95	4659 BO1	A35-590 2212 90 MWCV5	2140

(continued)

(a) Deutsche Industrie Normen (German Industrial Standards). (b) Japanese Industrial Standard. (c) British Standard. (d) l'Association Française de Normalisation (French Standards Association). Source: Ref 3, 4

Table 2-3 (continued)

United States (AISI)	West Germany (DIN)(a)	Japan (JIS)(b)	Great Britain (B.S.)(c)	France (AFNOR)(d)	Sweden (SS14)
Oil-hardening cold-work steels (ASTM A 681) (continued)					
O2	1.2842	...	4659 (USA 02) 4659 BO2	A35-590 2211 90MV8	...
O6	1.2206	...	...	A35-590 2132 130C3	...
O7	1.2414, 1.2419, 1.2442, 1.2516, 1.2519	G4404 SKS2	...	A35-590 2141 105WC13	...
Shock-resisting steels (ASTM A 681)					
S1	1.2542, 1.2550	G4404 SKS41	4659 BS1	A35-590 2341 55WC20	2710
S2	1.2103	...	4659 BS2	A35-590 2324 Y45SCD6	...
S5	1.2823	...	4659 BS5	...	...
S6	...	...	...	...	...
S7	...	...	...	...	...
Low-alloy special-purpose steels (ASTM A 681)					
L2	1.2235, 1.2241, 1.2242, 1.2243,	G4404 SKT3, G4410 SKC11	...	A35-590 3335 55CNDV4	...
L6	1.2713, 1.2714	G4404 SKS51, G4404 SKT4	...	A35-590 3381 55NCDV7	...
Low-carbon mold steels (ASTM A 681)					
P2	...	...	...	...	...
P3	1.5713	...	...	2881 Y10NC6	...
P4	1.2341	...	...	...	(USA P4)
P5	...	...	...	...	...
P6	1.2735, 1.2745	G4410 SKC31	...	2882 10NC12	...
P20	1.2311, 1.2328, 1.2330	...	4659 (USA P20)	A35-590 2333 35CMD7	(USA P20)
P21	...	...	...	...	...
Water-hardening steels (ASTM A 686)					
W1	1.1525, 1.1545, 1.1625, 1.1654, 1.1663, 1.1673, 1.1744, 1.1750, 1.1820, 1.1830	G4401 SK1, G4401 SK2, G4401 SK3 G4401 SK4, G4401 SK5, G4401 SK6 G4401 SK7, G4401 SK7, G4410 SKC3	4659 (USA WI), 4659 BW1A 4659 BW1B 4659 B,W1C	A35-590 1102 Y(1) 105, A35-590 1103 Y(1) 90 A35-590 1104 Y(1) 80, A35-590 1105 Y(1) 70 A35-590 1200 Y(2) 140, A35-590 1201 Y(2) 120 A35-596 Y75, A35-596 Y90	...
W2	1.1645, 1.2206, 1.283	G4404 SKS43 G4404 SKS44	4659 BW2	A35-590 1161 Y120V, A35-590 1162 Y105V A35-590 1163 Y90V, A35-590 1164 Y75V A35-590 1230 Y(2) 140C, A35-590 2130 Y100C2	(USA W2A) (USA W2B) (USA W2C)
W5	1.2002, 1.2004, 1.2056	...	...	A35-590 1232 Y105C	...

(a) Deutsche Industrie Normen (German Industrial Standards). (b) Japanese Industrial Standard. (c) British Standard. (d) l'Association Française de Normalisation (French Standards Association). Source: Ref 3, 4

ing. These carbides are retained as components of the microstructure in addition to those formed in martensite during tempering.

- The higher the carbon content of the martensite and the higher the density of carbides, the higher the hardness and wear resistance but the lower the toughness of a tool steel microstructure.

Water-hardening tool steels have the lowest alloy content of all the tool steels and are essentially carbon steels. Therefore, their hardenability is low, and water quenching is required to form martensite. Even with water quenching, only the surface of a tool may harden. However, the high carbon content of the water-hardening tool steels ensures that the martensite will be of high hardness where it forms. Consistent with the low-alloy content, only iron carbides are produced by heat treatment of the water-hardening tool steels.

Shock-resisting tool steels have been developed to provide high toughness and fracture resistance in combination with high strength and wear resistance under conditions of impact loading. The high toughness is achieved by maintaining carbon content at moderate levels, thereby keeping the carbon content of the martensite low and carbide dispersions fine. The alloy content of the shock-resisting tool steels is higher than that of the water-hardening tool steels; accordingly, the hardenability also is higher. The alloying elements also promote beneficial dispersions of carbides.

Oil-hardening, cold-work tool steels have been developed to provide very high wear resistance under cold-working conditions. High hardness is provided by high-carbon martensite tempered at low temperatures to provide very fine dispersions of carbides. Hardenability, because of high carbon and moderate alloy content, is sufficient to provide good depth of hardening by oil quenching. The alloying and very high carbon content of type O7 steel promote graphite formation, which enhances machinability and die life.

Air-hardening, medium-alloy cold-work tool steels also have high wear resistance under cold-working conditions. The various grades, due to ranges of carbon and alloy content, have various combinations of hardness and toughness. Similar to the oil-hardening steels, the wear resistance is provided by high-carbon martensite and fine carbide dispersions. However, because of the high alloy content, hardenability is high enough to permit martensite formation on air cooling. The very slow cooling minimizes distortion and promotes good dimensional stability during heat treatment. This group of tool steels also has a grade, A10, which contains graphite in its microstructure.

High-carbon, high-chromium cold-work tool steels have extremely high wear and abrasion resistance. Not only is tempered high-carbon martensite an important component of the microstructure, but large volume fractions of alloy carbides also play an important role in achieving high wear resistance. Some of the alloy carbides are produced by solidification and coexist with austenite during hot working and austenitizing, and some are produced by tempering. Again, the high alloy content provides excellent hardenability and makes possible martensite formation on air cooling with attendant benefits for dimensional control. Although the high abrasion resistance of the D-type tool steels is desirable for cold-work applications, the machining and grinding

Table 2-4 Classes of tool steels in three-digit classification system

Class	Description
Group 100: Carbon tool steels	
110	Carbon, with or without significant additions of V, Cr, Si, and Mn
120	Carbon-vanadium
130	Carbon-chromium
140	Carbon-chromium-vanadium
Group 200: Low-alloy tool steels	
210	Based on chromium up to 3% and >0.65% C
220	Based on chromium up to 3% and <0.65% C
230	Based on nickel and >0.65% C
240	Based on nickel and <0.65% C
Group 300: Special-purpose tool steels	
310	Silicon tool steels
320	Tungsten chisel steels
330	Nontempering chisel steels
340	Tungsten finishing steels
350	High-carbon, low-alloy tool steels
360	Semihigh-speed steels
370	Mold steels for hubbed and/or carburized cavities
380	Mold steels for machined cavities
390	Graphitic tool steels
Group 400: Die steels for cold work	
410	Oil-hardening cold-work die steels
420	Air-hardening cold-work die steels
430	High-carbon, high-chromium cold-work die steels
440	Special wear-resistant cold-work die steels
Group 500: Die steels for hot work	
510	3–4% Cr hot-work die steels
520	Chromium-molybdenum hot-work die steels
530	Chromium-tungsten hot-work die steels
540	Tungsten hot-work die steels
550	Molybdenum hot-work die steels
Group 600: High-speed steels	
610	Tungsten types
620	Tungsten-cobalt types
630	Molybdenum types
640	Molybdenum-cobalt types
650	Tungsten-molybdenum types
660	Tungsten-molybdenum-cobalt types
Group 700: Tool steels of historical interest	
710	Wortle die and self-hardening steels

Source: Ref 5, 6

operations during manufacture of finished dies and molds are difficult.

Low-alloy, special-purpose tool steels can be used in a variety of applications with characteristics overlapping those of water- and oil-hardening grades. The alloying provides moderate hardenability, in some cases suitable for oil hardening, but the availability of medium-carbon grades makes possible higher toughness compared to the high-carbon oil-hardening tool steels.

Mold steels have low-carbon contents relative to other tool steels in order to permit the shaping, by hubbing or machining, of cavities for plastic molding or metal die casting while the steels are in a soft annealed condition. The molds or dies are then carburized and hardened to obtain high surface hardness and wear resistance. A key requirement for molds and dies is good polishability and excellent surface finish. Sometimes martensitic stainless steels are used for plastic molding dies if corrosion resistance is a factor in performance of the lower-alloy P steels.

Chromium hot-work tool steels must have excellent resistance to high-temperature impact loading, to softening during high-temperature exposure, and to thermal fatigue. This demanding set of requirements—typical of forging, many other types of hot working, and die casting—is accomplished by

Table 2-5 Tool steels no longer in common use

	Composition, %					
Type	C	W	Mo	Cr	V	Others
High-speed steels						
M6	0.80	4.25	5.00	4.00	1.50	12.00 Co
M8	0.80	5.00	5.00	4.00	1.50	1.25 Nb
M15	1.50	6.50	3.50	4.00	5.00	5.00 Co
M45	1.25	8.00	5.00	4.25	1.60	5.50 Co
T3	1.05	18.00	...	4.00	3.00	...
T7	0.75	14.00	...	4.00	2.00	...
T9	1.20	18.00	...	4.00	4.00	...
Hot-work steels						
H15	0.40	...	5.00	5.00	...	...
H16	0.55	7.00	...	7.00	...	...
H20	0.35	9.00	...	2.00	...	...
H41	0.65	1.50	8.00	4.00	1.00	...
H43	0.55	...	8.00	4.00	2.00	...
Cold-work steels						
D1	1.00	...	1.00	12.00	...	...
D6(a)	...	...	...	...	...	...
A5	1.00	...	1.00	1.00	...	3.00 Mn
Shock-resisting steels						
S3	0.50	1.00	...	0.74	...	...
S4	0.55	...	...	...	...	2.00 Si, 0.80 Mn
Mold steel						
P1	0.10	...	...	...	...	...
Special-purpose steels						
L1	1.00	...	...	1.25	...	...
L3	1.00	...	...	1.50	0.20	...
L4	1.00	...	...	1.50	0.25	0.60 Mn
L5	1.00	...	0.25	1.00	...	1.00 Mn
L7	1.00	...	0.40	1.40	...	0.35 Mn
F1	1.00	1.25	...	...	...	...
F2	1.25	3.50	...	...	...	...
F3	1.25	3.50	...	0.75	...	...
Water-hardening tool steels						
W3	1.00	...	...	...	0.50	...
W4	0.60/1.40(b)	...	...	0.25	...	...
W6	1.00	...	...	0.25	0.25	...
W7	1.00	...	...	0.50	0.20	...

(a) Now included with D3 in Table 2-2. (b) Various carbon contents were available.

the use of medium-carbon contents and relatively high concentrations of chromium and other strong carbide-forming elements. The medium-carbon content promotes toughness by limiting the carbon concentration of the martensite and by limiting the size of alloy carbide particles. Good high-temperature strength is achieved by tempering at high temperatures where fine, stable dispersions of chromium and vanadium alloy carbides precipitate. These carbides coarsen only slowly in service. The high-alloy content of the H steels also provides excellent hardenability and permits the hardening of heavy sections by air cooling.

Tungsten hot-work tool steels have much greater resistance than the chromium hot-work steels to softening during high-temperature exposure. The improved resistance to softening is accomplished by the addition of substantial amounts of tungsten, which in addition to the chromium, produce large volume fractions of stable alloy carbides in the microstructure. The latter distributions of carbides, however, also reduce toughness.

Molybdenum hot-work tool steels. The H42 steel listed in this category in Table 2-2 has softening resistance comparable to the tungsten hot-work steels and thus, offers an alternate choice, depending on availability and cost. Molybdenum, another strong alloy carbide-forming element, is added with chromium, vanadium, and tungsten to provide a large volume fraction of alloy carbides, which results in stable microstructures when exposed to high-temperature forming operations.

Tungsten high-speed tool steels are used for high-speed cutting tool applications. The alloy content of strong carbide-forming elements, especially tungsten in amounts of 18% or more, is so high that these steels do not soften even when exposed to temperatures where the tool appears red. The T steels, by virtue of their relatively high carbon and very high alloy contents, have high hardenability and are processed to develop microstructures with large volume fractions of high-temperature stable carbides, which create excellent wear resistance and red hardness.

Molybdenum high-speed tool steels similar to the T group of high-speed steels, are used for high-speed cutting tool applications. Molybdenum replaces some of the tungsten of the T steels, but the performance characteristics of the T and M steels, except for the slightly higher toughness of the M steels, are essentially the same. Alloying considerations (namely, the formation of stable alloy carbides and the addition of cobalt to increase red hardness) and heat-treating processing are similar for both types of high-speed steels. However, the M steels more readily decarburize and require more care in hardening.

Ultrahard high-speed tool steels are capable of being hardened to 70 HRC, compared to the maximum hardness of 65/66 HRC attainable in the other high-speed steels. The very high hardness represents an optimization of the heat-treating and alloying design characteristic of high-speed steels i.e., very high densities of primary alloy carbides and fine alloy carbides produced by secondary hardening at high tempering temperatures and is achieved by higher carbon contents together with high contents of cobalt and the strong carbide-forming elements. Toughness at very high hardness levels is a major consideration in the application of the ultrahard high-speed steel, and often these steels are used with hardness below the maximum attainable.

Summary. The preceding sections have presented the AISI classification system for tool steels and briefly described the characteristics of the major groups. A discussion of the selection of tool steels follows. The remaining chapters will then describe the principles and details of the production, alloy design, heat treatment, microstructures, and selection of the various types of tool steels.

Selection of Tool Steels

As shown in previous sections, there are many types and grades of tool steels, all with different compositions and properties. Selection of a single tool steel for a specific operation must be based on two major considerations: (1) predicting the performance of a steel for an application and (2) analyzing the limitations associated with the manufacture of a tool, die, or mold with the selected steel. Within this framework, the ultimate basis of the proper selection of a tool steel is the final cost per unit part produced by the tool.

Table 2-6 presents an overview and comparison of the most important manufacturing and service characteristics of the various steel grades in the various classes of tool steels according to the AISI classification system. Qualitative ranking, in terms of low, medium, and high ratings, are provided to aid in the assessment of the various steels. Many of the manufacturing characteristics are related to heat treatment response, and service characteristics are rated relative to toughness, resistance to softening, and wear resistance. The following sections present information and a methodology that can be used to help select tool steels for specific applications based on performance requirements and manufacturing considerations.

Predicting the Performance of Tool Steels

Tool steels are used for many purposes, but all applications can be grouped into five basic types of operations: forming, shearing, cutting, molding, and miscellaneous (Table 2-7). After the major functions of a tool are identified, a first step in selecting an appropriate tool steel can be made based on performance requirements, such as

Table 2-6 Manufacturing and service characteristics of tool steels

AISI designation	Hardening and tempering: Resistance to decarburization	Hardening response	Amount of distortion(a)	Resistance to cracking	Approximate hardness(b), HRC	Fabrication and service: Machinability	Toughness	Resistance to softening	Resistance to wear
Molybdenum high-speed steels									
M1	Low	Deep	A or S, low; O, medium	Medium	60–65	Medium	Low	Very high	Very high
M2	Medium	Deep	A or S, low; O, medium	Medium	60–65	Medium	Low	Very high	Very high
M3 (class 1 and class 2)	Medium	Deep	A or S, low; O, medium	Medium	61–66	Medium	Low	Very high	Very high
M4	Medium	Deep	A or S, low; O, medium	Medium	61–66	Low to medium	Low	Very high	Highest
M6	Low	Deep	A or S, low; O, medium	Medium	61–66	Medium	Low	Highest	Very high
M7	Low	Deep	A or S, low; O, medium	Medium	61–66	Medium	Low	Very high	Very high
M10	Low	Deep	A or S, low; O, medium	Medium	60–65	Medium	Low	Very high	Very high
M30	Low	Deep	A or S, low; O, medium	Medium	60–65	Medium	Low	Highest	Very high
M33	Low	Deep	A or S, low; O, medium	Medium	60–65	Medium	Low	Highest	Very high
M34	Low	Deep	A or S, low; O, medium	Medium	60–65	Medium	Low	Highest	Very high
M36	Low	Deep	A or S, low; O, medium	Medium	60–65	Medium	Low	Highest	Very high
M41	Low	Deep	A or S, low; O, medium	Medium	65–70	Medium	Low	Highest	Very high
M42	Low	Deep	A or S, low; O, medium	Medium	65–70	Medium	Low	Highest	Very high
M43	Low	Deep	A or S, low; O, medium	Medium	65–70	Medium	Low	Highest	Very high
M44	Low	Deep	A or S, low; O, medium	Medium	62–70	Medium	Low	Highest	Very high
M46	Low	Deep	A or S, low; O, medium	Medium	67–69	Medium	Low	Highest	Very high
M47	Low	Deep	A or S, low; O, medium	Medium	65–70	Medium	Low	Highest	Very high
Tungsten high-speed steels									
T1	High	Deep	A or S, low; O, medium	High	60–65	Medium	Low	Very high	Very high
T2	High	Deep	A or S, low; O, medium	High	61–66	Medium	Low	Very high	Very high
T4	Medium	Deep	A or S, low; O, medium	Medium	62–66	Medium	Low	Highest	Very high
T5	Low	Deep	A or S, low; O, medium	Medium	60–65	Medium	Low	Highest	Very high
T6	Low	Deep	A or S, low; O, medium	Medium	60–65	Low to medium	Low	Highest	Very high
T8	Medium	Deep	A or S, low; O, medium	Medium	60–65	Medium	Low	Highest	Very high
T15	Medium	Deep	A or S, low; O, medium	Medium	63–68	Low to medium	Low	Highest	Highest
Chromium hot-work steels									
H10	Medium	Deep	Very low	Highest	39–56	Medium to high	High	High	Medium
H11	Medium	Deep	Very low	Highest	38–54	Medium to high	Very high	High	Medium
H12	Medium	Deep	Very low	Highest	38–55	Medium to high	Very high	High	Medium
H13	Medium	Deep	Very low	Highest	38–53	Medium to high	Very high	High	Medium

(continued)

(a) A, air cool; B, brine quench; O, oil quench; S, salt bath quench; W, water quench. (b) After tempering in temperature range normally recommended for this steel. (c) Carburized case hardness. (d) After aging at 510 to 550 °C (950 to 1025 °F). (e) Toughness decreases with increasing carbon content and depth of hardening.

Table 2-6 (continued)

AISI designation	Hardening and tempering: Resistance to decarburization	Hardening response	Amount of distortion(a)	Resistance to cracking	Approximate hardness(b), HRC	Fabrication and service: Machinability	Toughness	Resistance to softening	Resistance to wear
Chromium hot-work steels (continued)									
H14	Medium	Deep	Low	Highest	40–47	Medium	High	High	Medium
H19	Medium	Deep	A, low; O, medium	High	40–57	Medium	High	High	Medium to high
Tungsten hot-work steels									
H21	Medium	Deep	A, low; O, medium	High	36–54	Medium	High	High	Medium to high
H22	Medium	Deep	A, low; O, medium	High	39–52	Medium	High	High	Medium to high
H23	Medium	Deep	Medium	High	34–47	Medium	Medium	Very high	Medium to high
H24	Medium	Deep	A, low; O, medium	High	45–55	Medium	Medium	Very high	High
H25	Medium	Deep	A, low; O, medium	High	35–44	Medium	High	Very high	Medium
H26	Medium	Deep	A or S low; O, medium	High	43–58	Medium	Medium	Very high	High
Molybdenum hot-work steels									
H42	Medium	Deep	A or S, low; O, medium	Medium	50–60	Medium	Medium	Very high	High
Air-hardening medium-alloy cold-work steels									
A2	Medium	Deep	Lowest	Highest	57–62	Medium	Medium	High	High
A3	Medium	Deep	Lowest	Highest	57–65	Medium	Medium	High	Very high
A4	Medium to high	Deep	Lowest	Highest	54–62	Low to medium	Medium	Medium	Medium to high
A6	Medium to high	Deep	Lowest	Highest	54–60	Low to medium	Medium	Medium	Medium to high
A7	Medium	Deep	Lowest	Highest	57–67	Low	Low	High	Highest
A8	Medium	Deep	Lowest	Highest	50–60	Medium	High	High	Medium to high
A9	Medium	Deep	Lowest	Highest	35–56	Medium	High	High	Medium to high
A10	Medium to high	Deep	Lowest	Highest	55–62	Medium to high	Medium	Medium	High
High-carbon, high-chromium cold-work steels									
D2	Medium	Deep	Lowest	Highest	54–61	Low	Low	High	High to very high
D3	Medium	Deep	Very low	High	54–61	Low	Low	High	Very high
D4	Medium	Deep	Lowest	Highest	54–61	Low	Low	High	Very high
D5	Medium	Deep	Lowest	Highest	54–61	Low	Low	High	High to very high
D7	Medium	Deep	Lowest	Highest	58–65	Low	Low	High	Highest
Oil-hardening cold-work steels									
O1	High	Medium	Very low	Very high	57–62	High	Medium	Low	Medium
O2	High	Medium	Very low	Very high	57–62	High	Medium	Low	Medium
O6	High	Medium	Very low	Very high	58–63	Highest	Medium	Low	Medium
O7	High	Medium	W, high; O, very low	W, high; O, very low	58–64	High	Medium	Low	Medium
Shock-resisting steels									
S1	Medium	Medium	Medium	High	40–58	Medium	Very high	Medium	Low to medium
S2	Low	Medium	High	Low	50–60	Medium to high	Highest	Low	Low to medium
S5	Low	Medium	Medium	High	50–60	Medium to high	Highest	Low	Low to medium
S6	Low	Medium	Medium	High	54–56	Medium	Very high	Low	Low to medium

(continued)

(a) A, air cool; B, brine quench; O, oil quench; S, salt bath quench; W, water quench. (b) After tempering in temperature range normally recommended for this steel. (c) Carburized case hardness. (d) After aging at 510 to 550 °C (950 to 1025 °F). (e) Toughness decreases with increasing carbon content and depth of hardening.

Table 2-6 (continued)

AISI designation	Hardening and tempering: Resistance to decarburization	Hardening response	Amount of distortion(a)	Resistance to cracking	Approximate hardness(b), HRC	Fabrication and service: Machinability	Toughness	Resistance to softening	Resistance to wear
Shock-resisting steels (continued)									
S7	Medium	Deep	A, lowest; O, low	A, highest; O, high	45–57	Medium	Very high	High	Low to medium
Low-alloy special-purpose steels									
L2	High	Medium	W, low; O, medium	W, high; O, medium	45–63	High	Very high(c)	Low	Low to medium
L6	High	Medium	Low	High	45–62	Medium	Very high	Low	Medium
Low-carbon mold steels									
P2	High	Medium	Low	High	58–64(c)	Medium to high	High	Low	Medium
P3	High	Medium	Low	High	58–64(c)	Medium	High	Low	Medium
P4	High	High	Very low	High	58–64(c)	Low to medium	High	Medium	High
P5	High	...	W, high; O, low	High	58–64(c)	Medium	High	Low	Medium
P6	High	...	A, very low; O, low	High	58–61(c)	Medium	High	Low	Medium
P20	High	Medium	Low	High	28–37	Medium to high	High	Low	Low to medium
P21	High	Deep	Lowest	Highest	30–40(d)	Medium	Medium	Medium	Medium
Water-hardening steels									
W1	Highest	Shallow	High	Medium	50–64	Highest	High(e)	Low	Low to medium
W2	Highest	Shallow	High	Medium	50–64	Highest	High(e)	Low	Low to medium
W5	Highest	Shallow	High	Medium	50–64	Highest	High(e)	Low	Low to medium

(a) A, air cool; B, brine quench; O, oil quench; S, salt bath quench; W, water quench. (b) After tempering in temperature range normally recommended for this steel. (c) Carburized case hardness. (d) After aging at 510 to 550 °C (950 to 1025 °F). (e) Toughness decreases with increasing carbon content and depth of hardening.

wear resistance, toughness, and hot hardness, and manufacturing requirements related to heat treatment and finishing (Table 2-8).

Table 2-7 General groupings of tool steel applications

1. Forming
   - (a) Cold forming
   - (b) Hot forming
2. Shearing
   - (a) Blanking
   - (b) Punching
   - (c) Cutting (shear blades and slitters)
   - (d) Trimming
3. Cutting (material removal)
   - (a) Metal cutting
   - (b) Nonmetal cutting
   - (c) Chipping
4. Molding
   - (a) Die casting
   - (b) Plastic molding
   - (c) Ceramic molding
   - (d) Powder molding
5. Miscellaneous
   - (a) Wear parts
   - (b) Percussion tools
   - (c) Gages

Forming tools for either hot or cold work include such operations as die blocks and inserts, hot-forging machine tools, press-forming tools, deep-drawing tools, cold-heading dies and punches, thread-rolling dies, and extrusion tools. Such tools are in sliding contact with solid metal parts for a portion of their working time and may be subject to high stresses for short periods of time during operation. Thus, as seen in Table 2-8, their principal requirement is wear resistance; secondary requirements include toughness and machinability. Forming tools used for hot work have the additional requirement of hot hardness.

Shearing tools include shear blades, cutoff tools on forging or heading machines, trimming dies, blanking dies, slitters, punches, and piercers. They are subject to high stresses, particularly as the stock thickness increases, and require high toughness along with wear resistance to maintain the original edge contour and dimension. Safety in hardening and a minimum distortion on hardening are secondary requirements but are of prime importance in long blades and intricate blanking dies.

Cutting tools used for machining require hot hardness and wear resistance. Toughness and

grindability are listed as secondary needs. Cutting tools may also include chipping operations, so chisels requiring high toughness may be classified here.

Molding tools are classified to include not only plastic molding dies, but also die-casting and permanent molds for forming molten metals such as zinc, aluminum, and copper alloys, and tooling for P/M brick and ceramic briquetting, where solid material is received and formed.

Miscellaneous tools and parts include wear parts requiring high wear resistance, such as sand-slinger plates and milling and grinder plates, percussion parts requiring high toughness, and gages requiring high hardness, good finish, and size stability.

Performance Selection Factors

Wear resistance, toughness, and hot hardness are considered here and throughout this book to be the major performance factors for the selection of tool steels. Combinations of these properties determine the suitability of a steel for a given application and whether the steel is suited for short, medium, or long production runs. Minor selection factors, which may be of importance for certain functions, include working hardness, as related to yield strength or elastic limit, depth of hardening, and grain size.

In this book, a numerical system is used to rank steels for the major selection factors of wear resistance, toughness, and hot hardness. Each chapter on the various types of tool steels starts with a table that gives heat-treating data and ranks various properties by numbers. In the system used, 1 represents a low rating and 9 represents a high rating. The numbers are primarily for comparative ranking and are not intended to indicate quantitative differences, which may be considerably greater than 9 to 1. For example, Table 2-9 compares the wear resistance of several tool steels and shows that steels given the same rating may differ significantly in abrasion re-

Table 2-8 First step in selection of tool steels

If the tool:	These major characteristics are required in the tool steel:	And these minor charactertistics may be required:	Under these conditions:	These major properties(a) should be sought: Wear resistance	Tough-ness	Hot hardness
Cuts	Wear resistance and resistance to softening effect of heat	Grindability and toughness	Light cuts, slow speeds	4–8	1–3	1–6
			Heavy cuts, fast speeds	7–9	1–3	8–9
Shears	Wear resistance and toughness	Safety in hardening and slight distortion in hardening	Thin stock, short runs	4–6	1–7	(b)
			Thin stock, long runs	6–9	1–7	(b)
			Heavy stock, short runs	2–4	7–9	(b)
			Heavy stock, long runs	3–5	7–9	(b)
Forms	Wear resistance	Machinability and toughness	Cold, short runs	4–6	1–7	(b)
			Cold, long runs	7–9	1–4	(b)
			Hot, short runs	3–6	6–9	5–7
			Hot, long runs	4–6	6–9	7–9
Draws	Wear resistance	Slight distortion in hardening	Short runs	4–6	1–7	(b) (b)
			Long runs	7–9	1–4	
Extrudes	Resistance to softening effect of heat, toughness, and wear resistance	...	Cold	4–9	1–7	(b) 5–7
			Hot	3–6	6–9	
Rolls	Wear resistance	...	Short runs	4–6	1–7	(b)
			Long runs	7–9	1–4	(b)
Batters	Toughness	Wear resistance	Short runs	2–4	7–9	(b)

(a) See test for description of these properties and their numerical ratings. (b) Important only in hot working, as in examples under forming, extruding, or cutting.

Table 2-9 Relative wear resistance of selected tool steels(a)

AISI	Hardness, HRC	Abrasion weight loss, g × 10	Relative weight loss	Wear resistance rating
T15	67.4	1.5	1:1	9
A7	65.0	1.6	1.1:1	9
M4	67.4	2.3	1.5:1	9
D4	63.0	4.3	3:1	8
D2	62.3	9.1	6:1	8
A2	62.9	33.0	22:1	6
O7	64.5	41.0	30:1	5

(a) Flat specimen abraded by wet 28/35-mesh quartzite on rubber wheel at 250 rev/min under 40 lb load; total travel, 4000 surface feet. Data from Teledyne VASCO.

sistance. Minor factors in the system are given as follows: hardness on the Rockwell C scale (HRC), grain size by Shepherd fracture ratings at full hardness, and depth of hardening by the letters S (shallow), M (medium), and D (deep). The column on core hardness for 25 mm (1 in.) round bars is related to the depth of hardening.

Toughness, variously defined as the energy absorbed during fracture or the ability of a steel to resist fracture, is related in some way to almost all of the manufacturing and performance factors of tool steels. Steel carbon content, heat treatment, surface condition, hardness, and strength all affect toughness. Subsequent chapters discuss these factors relative to the toughness of specific groups of tool steels, and Chapter 17 discusses the relationship of microstructure to toughness and fracture as related to cracking that may occur in tool steels. Here, toughness is presented primarily to assist in tool steel selection and ranking.

Figures 2-1 and 2-2 show, respectively, combinations of toughness and wear resistance and toughness and hot hardness for various tool steels. Figure 2-1 shows that, in general, the toughness of tool steels decreases as wear resistance increases. According to the brief review of alloying principles and the classes of tool steels presented earlier in this chapter, higher wear resistance, but reduced toughness, is accomplished by increasing carbon and alloy content.

Figure 2-2 shows that the relationship of toughness to hot hardness is not as easy to generalize as is the relationship of toughness to wear resistance. This observation is very much related to the operating conditions under which the various tool steels must operate at high temperatures. For example, the hot-work H-type forging alloys are designed to resist heavy impact loads as well as softening at high temperatures, while the high-speed steel cutting tools are not subjected to the same heavy loading and thus can tolerate lower toughness, as they maintain high surface wear resistance at elevated temperatures. The latter considerations also dictate the choice of surface modifications that might benefit

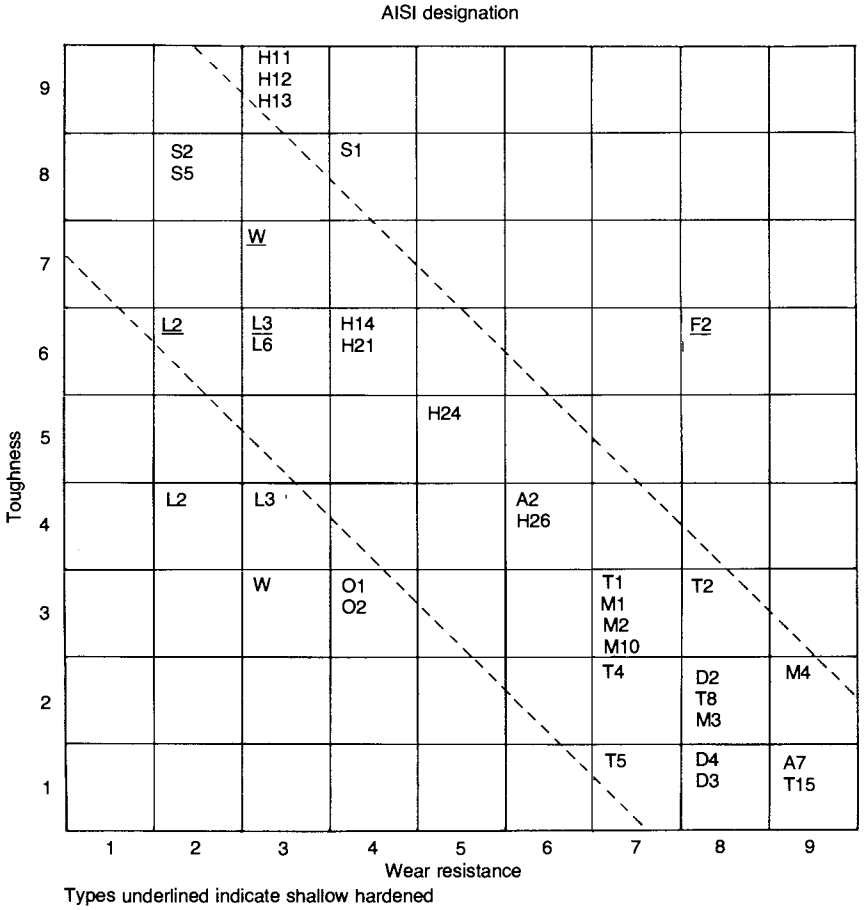

Fig. 2-1 Toughness versus wear resistance for commonly used tool steels

performance, as discussed in Chapter 16. The H-type steels are sometimes nitrided, a process capable of producing high surface hardness to reasonable case depths, while the high-speed steels are frequently coated with very thin layers of very hard ceramic materials such as titanium nitrides or carbides.

Manufacturing Limitations

After the major performance requirements for a tool steel application are identified, manufacturing limitations that affect cost and producibility of the tool or die from a given steel must be considered. The ranking of manufacturing factors used in this book includes availability, rated on a scale of 1 to 4; cost of the steel, rated on a scale of 1 to 5; machinability, rated on a scale of 1 to 9; quenching medium (W, water; O, oil; A, air; S, salt); hardening temperature required; dimensional change on hardening, rated H (high), M (medium), or L (low); and susceptibility to decarburization, also rated H, M, or L.

The column on cost is intended to reflect only the relative basic cost of a steel based on its alloy content, and is not intended to reflect the expected final cost of the tool or die. Alloying element costs are based on costs prior to publication of the fourth edition of *Tool Steels*, and may fluctuate, depending on the marketplace. Price variations related to various qualities of tool steels achievable by different manufacturing approaches also are not considered in the cost column. Steels of low initial cost may have higher final die cost, depending on equipment available to the manufacturer, hardening temperature, cost of hardening, straightening, machining, and grinding.

Examples of Tool Steel Selection

The selection of a tool steel begins with the identification of the group or groups of tool steels that best satisfy the requirements of a given tool or die application. Selection within a group then proceeds with a more detailed

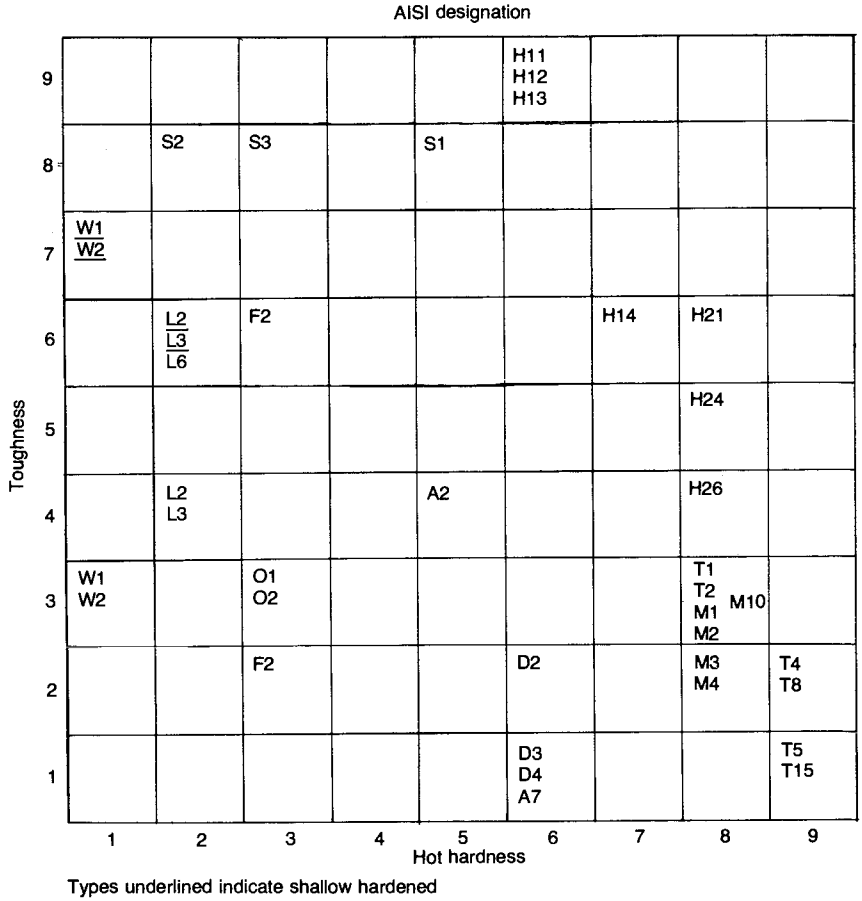

Types underlined indicate shallow hardened

Fig. 2-2 Toughness versus hot hardness for commonly used tool steels

evaluation of manufacturing and performance requirements of the grades of steel within that group. The chapters on the various types of tool steels describe in detail the basic metallurgy and properties of those groups of steels and give examples of the types of applications for which the steels have been used. The following sections present some examples of the selection process and the tool steels selected for specific applications, based on earlier case studies (Ref 5, 6). Operating experience, which supplements tabulations of properties and relative rankings, is invaluable in terms of the selection of tool steels, and comments regarding specific applications are included either in the text or in associated tables.

Selection of Steels for Cold-Heading Dies

Cold-heading dies frequently fail by wear, galling, and splitting; they also fail from fatigue on inner or working surfaces. Occasionally, failure by sinking or enlarging of the die form is encountered. Because of this and the high stresses encountered in cold heading, steels with high hardness on the working surfaces (generally about 62 HRC) are preferred. The materials most commonly used for punches and dies are water-hardening steels W1 and W2. These are shallow-hardening materials in which the control of hardenability is of greatest importance. For dies, hardenability is generally adjusted in accordance with the size of the die. Splitting along the longitudinal axis of the die can be avoided by selecting materials with a greater hardenability or by raising the hardening temperature. Although vanadium generally provides shallower-hardening materials than the plain carbon tool steels, other elements in the composition may be adjusted to compensate for this, while providing the high toughness of a finer-grained vanadium modification.

The wear resistance of the water-hardening steels is distinctly limited even at maximum normal working hardness of 62 to 64 HRC. Thus, when longer production runs are desired, the use of more highly alloyed steels such as D2, M2, or A2 is desirable. The lower toughness ratings of these steels, however, make it almost impossible to use them as solid dies. Accordingly, they are often used as an insert in a casing made from tough (9) H11 steel at a hardness of 48 to 50 HRC.

Punches used with cold-heading dies are also frequently made from steels W1 or W2. Where wear resistance can be sacrificed and toughness is of utmost importance, or where breakage is encountered, punches made from shock-resisting steel S1 may also be employed. Where greater wear resistance is required for cold-heading punches, steels D2 or M2 are used.

Selection of Steels for Coining Dies

The considerations here are not dissimilar from those for cold-heading dies, but coining dies may be considerably larger or more intricate, so that distortion in hardening, machinability, and cost may be of greater importance. Coining dies may fail by wear, sinking, or cracking. With low pressures and soft workpiece material, die failure by wear is sometimes caused by metal pickup.

Much industrial coining is done in the silverware industry on drop hammers. Here, water-hardening steels such as W1 treated to a surface hardness of 59 to 61 HRC are almost always used—whether silver, copper alloys, or stainless steels are coined. The shallow-hardening characteristics of the water-hardening steel and control of its hardenability are important. When coining deep designs, failure of the water-hardening steels often occurs by cracking. To solve this problem, deeper-hardening carbon tool steels may be employed, or lower-carbon steels such as S1 or L6 with toughness ratings of 6 to 8 at hardnesses of 57 to 59 HRC may be selected. Where maximum toughness (9) is required, steels H11 or H12 are used at 45 to 52 HRC. At this low hardness, scoring can be prevented by hard chromium plating of 0.127 to 0.254 mm (0.005 to 0.010 in.) for small dies, and for greater wear resistance oil-hardening steel O1 or air-hardening steels A2 and D2 are employed at 56 to 58 HRC.

Preferably, cold-coining dies are made by hubbing with master hobs, which is considerably less expensive than machining. Steels O1 and A2 can be satisfactorily cold hubbed, but sometimes intermediate anneals are necessary between several hubbings. Steel W1 can be more readily hubbed, the impression generally being about twice as deep for a given hub pressure in this grade as compared to steel A2.

Selection of Steels for Cold-Work Dies and Punches

This widely encountered application for tool and die steels includes the operating characteristics from Table 2-7 in categories 1(a), 2(a), 2(b), and 2(c). The requirements for tool steels may vary from those of high productivity or high wear resistance to those where toughness is the principal consideration. Consequently, many steels are actually employed; the principal ones are listed in Table 2-10 along with wear resistance and toughness ratings.

Since cold work is involved, hot hardness is not considered. Wear resistance rates from 3 to 9 and toughness ratings from 1 to 7 are used for cold-working operations. High-speed steels and high-carbon, high-chromium steels provide the greatest wear resistance but the lowest toughness, whereas higher toughnesses, when required, are obtained with steels of lower alloy content.

When dies are extremely small and size change from hardening is not a serious consideration, water-hardening steels are quite satisfactory. As part size increases, use of water- and oil-hardening steels is reduced in favor of air-hardening materials such as A2 and D4. This is particularly true in blanking parts that are 76.2 mm (3 in.) in width or

greater. The same trend would be noted as parts become more intricate in design.

As the thickness of the stock being punched or formed increases, greater toughness is often required. Occasionally, when parts must be punched from metals of 6.35 mm (0.25 in.) in thickness, shock-resisting steels S1 or S5, with a toughness rating of 8 and a wear resistance rating of 2 to 4, are recommended. Low wear resistance of silicon and tungsten chisel steels is sometimes overcome by carburizing to obtain a surface carbon content of about 0.75% to a depth of from 0.254 to 0.508 mm (0.010 to 0.020 in.). Further changes in wear resistance of steels O1, A2, and D2 to improve the life of blanking die punches may be obtained by nitriding, employing a gas-nitriding cycle of about 12 h at 540 °C (1000 °F). This treatment is most popular on steel D2 because of its resistance to softening at the nitriding temperature, which prevents a soft core underneath the relatively hard, brittle nitrided case. For maximum production runs, high-speed steels such as M2 or M4 may be used.

In the manufacture of blanking dies and punches, the cost of the steel is low compared to the cost of the die. This is particularly true for small dies, where the cost of steel D2 has been only about 10% of the total die cost. For larger dies, approximately 305 mm (12 in.) in size, the cost of steel has been as much as 50% of the total die cost.

Punches used in connection with cold-work, blanking, or trimming dies have a limited slenderness ratio of punch diameter to sheet thickness, which for aluminum, brass, and steel is about 2.5 to 1 for unguided punches and 1 to 1 for guided punches. The limiting slenderness ratio of punch diameter to sheet thickness for piercing spring steel and stainless steel is between 1.5:1 and 3:1 for unguided punches and between ½:1 and 1:1 for accurately guided punches. The change in recommended hardness of steels W1, D2, and M2 as a function of punch diameter is shown in Fig. 2-3. Punches used in short-run blanking dies when made from water-hardening steels W1 or W2 may be left in a relatively soft condition so that they can be peened to compensate for wear.

Table 2-10 Wear resistance and toughness of tool steels for cold-work dies and punches for blanking

	Rating for:	
Steel	Wear resistance	Toughness
W1	4	7
W2	4	7
L6	3	6
O1	4	3
O2	4	3
A2	6	5
D2	8	2
D4	8	1
A7	9	1
T1	7	3
M2	7	3
M4	9	2

Selection of Tool Steels for Cold Forming Hexagon Nuts

As an example of a specific task in selecting steels for punches and dies, the application of manufacture of hexagon nuts by cold forming is shown in Fig. 2-4. The first operation (Fig. 2-4a) involves cold upsetting of a precut steel rod, forming a partial chamfer on one end. The two pins illustrated are accurately guided and have a relatively low requirement for wear resistance because there is little lateral movement of the steel slug against the end surface of the pin. Wear resistance is not a prime requirement, and because the pins are accurately guided, the choice was to manufacture them from carbon tool steel drill rod—even though they would harden through their small cross section and thus have a low toughness rating of 3. Pins were hardened to 58 to 60 HRC by water quenching from 790 °C (1450 °F) and tempering 3 h at 230 °C (450 °F). The sizing die shown in Fig. 2-4(a) is in fact a die holder forming a guide for the upper pin and serving to contain the sizing die insert. As such, there is no requirement for high wear resistance; however, the

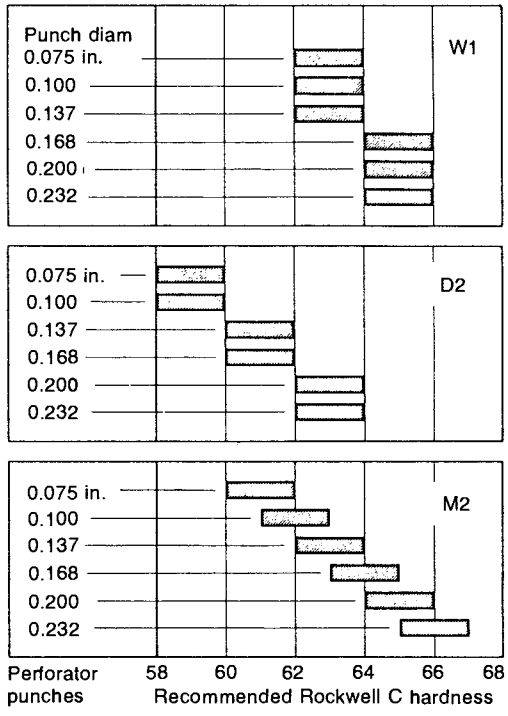

Fig. 2-3 Suggested hardness for tool steel perforator punches. Punches should be tempered to 56 to 60 HRC when subjected to heavy shock or used to pierce thick material.

steel should be of high strength but low notch sensitivity, and thus high toughness (9), and readily manufactured.

Such holding or compression rings are quite frequently manufactured from air-hardening steel H11, which can be tempered for accurate size stability because of its secondary-hardening nature. In this instance, the sizing die was treated to 48 to 50 HRC by air cooling from 995 °C (1825 °F) and double tempering for 2.5 plus 2.5 h at 565 °C (1050 °F). The sizing die insert is subject to considerable wear and must have reasonably high strength and hardness. In this particular application, high-speed steels were selected; steels T1 and M4 both were tried to determine if the added wear resistance of the latter would significantly improve performance. Because wear conditions were moderate, either steel performed satisfactorily at a hardness of 60 to 62 HRC.

In the second operation (Fig. 2-4b), the part is further upset and heavy chamfers coined on both ends. A water-hardening steel was selected for the two pins and was treated to the same hardness. The small diameter of these pins suggests the choice of an oil- or air-hardening steel for added safety in hardening and lack of distortion. Steels O1, A2, or high-speed steels T1 and M2 also could have been used. The doming die and doming punch are large masses subjected to splitting forces similar to a cold-heading die and require high toughness (7). Therefore, water-hardening steel W1 with 1.00% C and shallow-hardening characteristics was selected. The dies were heated to 800 °C (1475 °F) and quenched (by flushing water through the center hole only) to create a hard case on the inside diameter of the die and punch. They were tempered for 3 h at 190 °C (375 °F) for a hardness of 62 to 64 HRC.

The third operation (Fig. 2-4c) involves the use of two forming pins that create a prepiercing operation on the slug and at the same time form the outside surface of the slug into its desired hexagon shape. The punches must have considerably higher wear resistance (7 to 9) than would be afforded by a water-hardening steel. Therefore, steel T1 was selected, hardened to 58 to 60 HRC by oil quenching from 1260 °C (2300 °F) and tempered for 2.5 plus 2.5 h at 595 °C (1100 °F). The hexing die holder is not in contact with the work and, similar to the example of Fig. 2-4(b), was made from the tough steel H11, hardened to 48 to 50 HRC. The die insert with its hexagonal inside surface is subject to considerable wear, and high-speed steels were chosen.

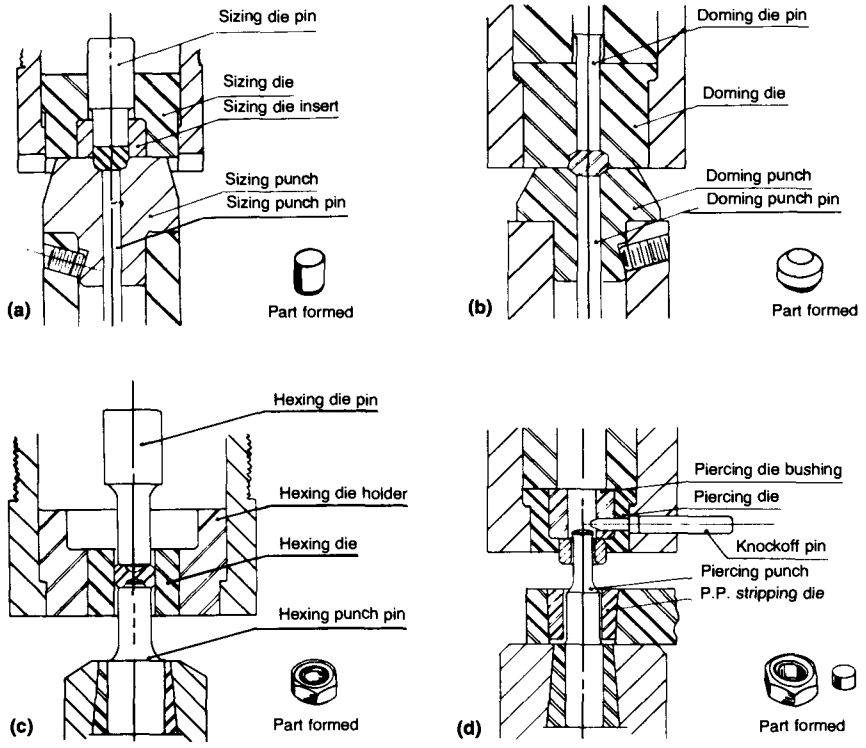

Fig. 2-4 Tooling for cold forming a hexagon nut. (a) First operation: upsetting. (b) Second operation: upsetting and chamfering. (c) Third operation: forming and prepiercing. (d) Final operation: piercing

Using steel T1 with a wear resistance of 7, oil quenched from 1270 °C (2320 °F) and tempered 2.5 plus 2.5 h at 595 °C (1100 °F), gave a production of 350,000 parts. Changing to M4 steel, one of the superhigh-speed steels containing 4% V and having a wear resistance rating of 9, gave a production of more than 1 million parts. This latter steel was still further improved by carburizing in a charcoal pack at 1065 °C (1950 °F), then air cooling and tempering for 2.5 plus 2.5 h at 555 °C (1030 °F) for a final surface hardness of 63 to 65 HRC. A production of 2.4 million pieces was obtained.

The final series of operations involves piercing the center hole of the nut (Fig. 2-4d). The piercing-die bushing and stripping die required a higher compressive strength (higher hardness) than would be possible to obtain on steel H11 used in the holding rings of the earlier operations. The wear resistance requirement was not vital; consequently, steel A2 was selected and hardened by air cooling from 995 °C (1750 °F) and tempering for 2.5 h at 218 °C (425 °F) to a hardness of 59 to 61 HRC. The piercing punch required a considerably higher toughness than could be obtained on steels of maximum wear resistance such as D2, D4, or A7. Consequently, the high-speed steel T1 was selected as a compromise between the needed wear resistance and required toughness on this unsupported and unguided punch. The piece was hardened by quenching in oil from 1260 °C (2300 °F) and tempering for 2.5 plus 2.5 h at 595 °C (1100 °F) to a hardness of 59 to 61 HRC. Finally, the knockoff pin was made from an oil-hardening steel O1 drill rod heat treated to 58 to 60 HRC by quenching in oil from 790 °C (1450 °F) and tempering 2.5 h at 205 °C (400 °F). It also could have been manufactured from steel W1 or steel A2 at low cost and reasonable economy.

Selection of Steels for Cold Extrusion

This operation involves the displacement of metal by plastic flow and a steady, nearly uniform pressure and may involve either forward or backward extrusion. Cold-impact extrusion is a special form of this process. High compressive strength (hardness) of the die is the most important factor required. Because of high pressures, toughness is sacrificed to obtain high strength, and a steel of low toughness (1 to 5) frequently is selected; dies are usually prestressed in compression by pressure of the shrink rings made from tough (9) steel H11 employed to hold them in place. Table 2-11 lists popular steels and their working hardnesses. Steels A2, D2, and M2 may be used; the last generally gives near-maximum die life. For extremely difficult jobs where failure by cracking is encountered, especially in the extrusion of steel, medium-carbon steels such as H11 give the best results, with toughness ratings of 6 to 9 and wear resistance ratings of 3 to 6. Conversely, for improvements in wear resistance (to 9) over steel M2, steels M4 or T15 may be used.

Selection of Steels for Shears

Shearing can be performed either hot or cold and on materials with thicknesses from less than 0.0254 mm (0.001 in.) up to 152 mm (6 in.). Consequently, as in most other tool steel applications, requirements for wear resistance and toughness will vary over the entire available range of those properties. Table 2-12 gives examples of steels that have been selected for shears on different applications.

Table 2-11 Tool steels for cold extrusion

Steel	Rating for: Wear resistance	Toughness	Working hardness, HRC
Punches			
T15	9	1	64–66(a)
M4	9	2	64–66(a)
D4	8	1	62–64(a)
D2	8	2	60–62
Punch shank or mandrel			
A2	6	5	56–58
O1	4	3	56–58
S1	4	8	56–58
S5	2	8	56–58
Die insert			
T15	9	1	65–67
M4	9	2	64–66
D4	8	1	62–64
M2	7	3	64–65
D2	8	2	60–62
Die base			
A2	6	5	54–56
S1	4	8	54–56
L6	3	6	54–56
O1	4	3	54–56
Die holder			
H11	3	9	48–50
Knockout pin			
H11	3	9	53–55
S5	2	8	54–56
L6	3	6	54–56
O1	4	3	54–56
S1	4	8	54–56
Die anvil			
M4	9	2	60–62
D2	8	2	58–60
A2	6	5	58–60
O1	4	3	58–60

(a) Or 60–63 HRC under conditions requiring slightly higher toughness

Selection of Steels for Die-Forging and Press-Forging Tools

Tool steels found in most press-forging and drop-hammer forging operations (Table 2-13) are employed at a hardness generally not exceeding 510 HB. For the press forging of high-temperature alloys, particularly those with a nickel or cobalt base, certain high-alloy hot-work steels, including H26, are used at hardnesses up to 577 HB. Whether the forging dies are to be used on a drop hammer or a press is a greater influence on the

Table 2-12 Tool steels for shears

	Rating for:			
Steel	Wear resistance	Toughness	Hot hardness	Applications
S2	2	8	2	Cold shearing heavy stock; scrap shears; hot shears for moderate life
S5	2	8	3	
S1	4	8	5	
H11	3	9	6	For shock conditions; hot or cold shearing; hot shearing heavy sections
A8	4	8	6	
O1	4	3	3	Cold-work shears for high production on thin or medium-thickness stock
A2	6	5	5	
D2	8	2	6	
M3	8	2	8	Long-lift cold shears for thin or medium-thickness stock; highest wear resistance
M4	9	2	8	

Table 2-13 Tools steels for hot-forging

	Rating for:			
Steel	Wear resistance	Toughness	Hot hardness	Applications
S1	4	8	5	Short runs; die temperature in 480 °C (900 ° F); dies can be cooled. If die design is critical, use H12 to minimize warpage.
H12	3	9	6	Long runs; die temperature in service not over 480 °C; dies can be water cooled. A8 provides better resistance to wear. Resistance to softening to 480 °C is good. Steels have high toughness for abuse in service. Most widely used steel for application is H12.
H11	3	9	6	
H13	3	9	6	
A8	4	8	6	
H21	4	6	8	Long or short runs; die temperatures above 480 °C. Steels H24 and H26 have best wear resistance. Most widely used in H21. H26 used for press forging of nickel– and cobalt–base high–temperature alloys.
H20	4	6	8	
H24	5	5	8	
H25	4	6	8	
H26	6	4	8	

Table 2-14 Tool steels for rolling–mill rolls

	Rating for:			
Steel	Wear resistance	Toughness	Hot hardness	Applications
L3	3	6	2	Cold rolls up to 75–125 mm (3–5 in.) round. Shallow hardening; 65 HRC minimum surface hardness; brine quenched
O1	4	3	3	Cold rolls 6.4–100 mm (¼–4 in.) round. Through-hardening in oil; 60–62 HRC
A2	6	5	5	Cold rolls 6.4–250 mm (¼–10 in.) round. Through-hardening in air; 58–62 HRC; work rolls and backup rolls
D2	8	2	6	Cold rolls 6.4–300 mm (¼–12 in.) round; through-hardening in air; 58–62 HRC; Sendzimir mill work rolls
M4	9	2	8	Cold rolls 6.4–150 mm (¼–6 in.) round; high-speed steel; 62–65 HRC: Sendzimir mill work rolls
H11	3	9	6	Hot rolls; short runs; backup rolls; low temperatures; 40–48 HRC
H21	4	6	8	Hot rolls; medium runs; medium temperatures; 40–50 HRC
H26	6	4	8	Hot rolls; long runs; special materials; high temperatures; 45–58 HRC

selection of the hardness range than is the die composition, although both should be considered.

Dies can be operated at a higher hardness in a press since they are subject to less impact. However, dies in a press usually run hotter, necessitating use of steels of slightly higher alloy content. For example, when a hammer is used, low-alloy die steels at 341 to 375 HB are suggested to make forgings of a simple part from carbon or alloy steel. When the same part is forged on a press, higher-alloy die block materials such as steel H12 may be used, hardened to 369 to 388 HB. Although steels H11, H12, and H13 can be used interchangeably as inserts or as complete blocks, steel H12 is generally preferred because of its tungsten content, which is considered to provide longer life in forging operations.

Trimming tools used in conjunction with forging operations are frequently made from cold-work die steels A2 or D2. The latter has a longer life because of its greater wear resistance. Where toughness is important, trimming may be done with steel H11, especially if the trimming operation is performed hot.

The cost of the steels for small dies represents only a minor portion of total die cost for these tools as for most others. However, for very large die blocks used to forge material up to 610 mm (24 in.) thick, the steel cost may amount to 50 to 75% of the cost of the die.

Selection of Steel for Additional Uses

Further examples of steel selection for specific applications are given in tabular form only. Selection of tool steels for rolls, both hot and cold (Table 2-14), for die-casting dies (Table 2-15), for hot-ex-

Table 2-15 Tool steels for die-casting dies

Steel	Rating for: Wear resistance	Toughness	Hot hardness	Applications
P20	1	8	2	Prehardened to 300 HB; used for white metal dies; short to medium runs. Holder blocks for aluminum die-casting die inserts
H11	3	9	6	General purpose for aluminum die casting; long runs for white metal die casting.
H13	3	9	6	47 HRC preferred hardness; air hardening. General secondary tooling for die-casting machines
H12	3	9	6	
H14	4	6	7	Long runs on aluminum die-casting dies. Only rarely employed. 47–49 HRC
H21	4	6	8	Short runs on brass die casting; 38–42 HRC
H19	5	6	7	Medium runs on brass die casting; 38–43 HRC
H23	5	5	8	Medium runs on brass die casting; 32–39 HRC. Highest tempering resistance

Table 2-16 Tool steels for hot extrusion

Steel	Rating for: Wear resistance	Toughness	Hot hardness	Applications
S1	4	8	5	General secondary tooling for white metal extrusion; dies for steel extrusion
A2	6	5	5	Dies for white metal extrusion
D2	8	2	6	Dies for white metal extrusion
H11	3	9	6	Dies, dummy blocks, rams, liners for magnesium and aluminum. Rams and
H13	3	9	6	liners for copper alloy extrusion. Die holders for extrusion. Dummy blocks for
H12	3	9	6	copper, brass; 42–47 HRC. Mandrels for copper alloys; 50–52 HRC
H10	3	9	6	Dies for aluminum extrusion
H21	4	6	8	Dies and dummy blocks for copper alloy extrusion. Dies for brass and copper; 42–45 HRC. Dummies for cupronickel; 41–44 HRC
H26	6	4	8	Dies for copper alloy extrusion. Dies for brass and copper; 40–44 HRC
T15	9	1	9	Dies for refractory metal extrusion and high-temperature alloy extrusion

Table 2-17 Tool steels for thread-rolling dies

Steel	Rating for: Wear resistance	Toughness	Hot hardness	Applications
A2	6	5	5	Circular and flat dies; 10–50% less life than D2 or M2. More popular on dies ground after hardening
D2	8	2	6	Long-run circular and flat dies
M1	7	3	8	Long-run circular and flat dies
M2	7	3	8	Long-run circular and flat dies

Table 2-18 Tool steels for structural use

Steel	Rating for: Wear resistance	Toughness	Hot hardness	Applications
L2	1	7	2	Machine elements, cams, shafts, spindles, gears, sprockets
S1	4	8	5	
P20	1	8	2	
P21	1	8	4	
H11	3	9	6	Ultrahigh-strength steel used for aircraft and missile structures, bolts at
H10	3	9	6	1515–2070 MPa (220–300 ksi) ultimate tensile strength
A8	4	8	6	For strengths of 1790–2205 MPa (260–320 ksi). Less ductility than H11
A9	4	8	6	
M50	6	3	6	High-temperature bearings; strengths up to 2585 MPa (375 ksi), low ductility
M10	7	3	8	
M2	7	3	8	

trusion tooling (Table 2-16), for thread-rolling dies (Table 2-17), and for structural use (Table 2-18) is covered.

REFERENCES

1. Steel Products Manual: Tool Steels, Iron and Steel Society, 1988
2. Tool Steels, *Heat Treater's Guide: Practices and Procedures for Irons and Steels,* H. Chandler, Ed., ASM International, 1995, p 517–669
3. J.G. Gensure and D.L. Potts, *International Metallic Materials Cross-Reference,* 3rd ed., Genium Publishing, 1988
4. C.W. Wegst, *Key to Steel,* Verlag Stahlschlüssel Wegst, 1989
5. G.A. Roberts, J.C. Hamaker, Jr., and A.R. Johnson, *Tool Steels,* 3rd ed., American Society for Metals, 1962
6. G.A. Roberts and R.A. Carey, *Tool Steels,* 4th ed., American Society for Metals, 1980

Tool Steels: 5th Edition
George Roberts, George Krauss, Richard Kennedy, p 29-43
DOI:10.1361/toos1998p029

Copyright © 1998 ASM International®
All rights reserved.
www.asminternational.org

CHAPTER 3
Manufacture of Tool Steels

Tool steels are produced by numerous manufacturers located around the world. These materials also cover a broad range of compositions, from plain carbon to very highly alloyed high-speed steels (see Chapter 2). Therefore, a wide variety of manufacturing equipment is employed and no universal practice is followed. This chapter describes some of the more typical manufacturing practices, along with their benefits and limitations. A few of the more recently introduced processes that hold considerable promise for producing tool steels or finished tools at lower cost or with improved quality also are reviewed.

Primary Melting

Electric arc furnace (EAF) melting continues to be the principal process for the production of tool steels. However, significant changes have occurred in the melt area since the fourth edition of this book was published—specifically, the incorporation of secondary refining operations such as argon oxygen decarburization (AOD), vacuum oxygen decarburization (VOD), and ladle furnaces (Ref 1). The steelmaking process has been split into two stages. The first stage consists essentially of only melting with little or no refining, and the equipment and operation can be optimized for this purpose (e.g., with ultrahigh-powered electric arc furnaces). In the second stage, hot metal from the electric arc furnace is transferred to a ladle or converter vessel where the majority of refining takes place. The principal benefits associated with secondary refining are reduced furnace time and increased overall capacity. Yields, quality, consistency, and reproducibility are also improved.

Raw materials account for a significant portion of the cost of a final tool steel bar or coil product. Thus, competitive pressures dictate using the lowest-cost materials consistent with obtaining the desired chemistry. Tool steel scrap makes up a large percentage of each charge, typically 75%. This can be internal mill scrap (commonly referred to as *revert*) consisting of end crops, bar and billet macroslices, and turnings, as well as purchased scrap of all forms. Special care must be taken to avoid scrap contamination, especially from undesirable elements such as nickel, cobalt, and copper, which cannot be oxidized out of the melt. Alloy additions of chromium, tungsten, molybdenum, vanadium, silicon, and manganese are usually made in the AOD in the form of ferroalloys. Molybdenum, cobalt, and vanadium can also be added as oxides, which can be reduced in the AOD.

The raw material charge is usually melted as rapidly as possible, then transferred to a secondary refining vessel such as the AOD (Fig. 3-1), where refining is accomplished by the injection of controlled ratios of O_2 and argon or N_2 by means of a submerged tuyere. Excellent control of chemistry, including carbon, sulfur, phosphorus, O_2, and H_2, is possible. Nitrogen can also be removed to some degree, depending on the alloy, or purposefully added by nitrogen blowing. Since there is no supplementary heat source for the AOD, temperature control is achieved by controlling the rate of blowing. Additional heat can be obtained by adding aluminum or silicon as fuel for the exothermic oxidation reaction.

When the desired chemistry has been achieved and the proper temperature reached, the heat is poured into a ladle and transferred to the casting (teeming) station. Ingots can be either top or bottom poured. Teeming rates are higher in bottom pouring since several molds are filled simultaneously from a common down sprue. Bottom pouring also permits the use of mold flux, which can improve ingot surface quality. Internal quality, including the amount of pipe and carbide segregation, may also be improved by bottom pouring. Following casting, ingots are usually annealed to prevent cracking (depending on the alloy) or hot stripped and heated directly for forging.

Electroslag Remelting

Electroslag remelting or refining (ESR) is a progressive melting process in which the end of an electrode, produced in a previous process such as EAF-AOD, is submerged in a reactive, molten slag contained in a water-cooled copper mold. Heat is generated by the passage of high current (usually alternating current) through the molten slag. As the end of the electrode melts, droplets of molten metal fall through the slag, are refined, and collect in a pool in the mold, building an ingot as the electrode is consumed. There are two basic variants of the process: one employing a long, static mold and the other a short, collar mold. In the latter case, relative movement occurs between the mold and the solidifying ingot. This is achieved by either withdrawing the ingot from the bottom of a stationary mold or raising the mold relative to the stationary ingot. Because of the good heat removal of the system and the fact that only a relatively small portion of metal is molten at any one time, solidification rates are significantly higher than in a comparably sized static cast ingot, and as-cast structures thus are substantially improved. The process is shown schematically in Fig. 3-2. A typical ESR tool steel ingot is shown in Fig. 3-3.

Since ESR is a batch process that operates at relatively low rates (typically a few pounds per minute), it is expensive for some materials. Therefore, the process has found application for tool steels only where improvements in yield, cleanliness, sulfur reduction, or structure are required.

The benefits of ESR stem directly from the way the process operates. A smooth ingot surface, which is ideal for subsequent hot working, is achieved as a result of the constant melt rate and the thin slag layer that solidifies on the mold wall. Progressive solidification conditions also produce an ingot that is completely sound, with no pipe or porosity. Uniform, relatively rapid solidification leads to an improvement in the uniformity of macrostructure and a reduction in the tendency for center segregation (Fig. 3-4). Microstructural features such as the eutectic cell size (Fig. 3-5) and the eutectic carbide

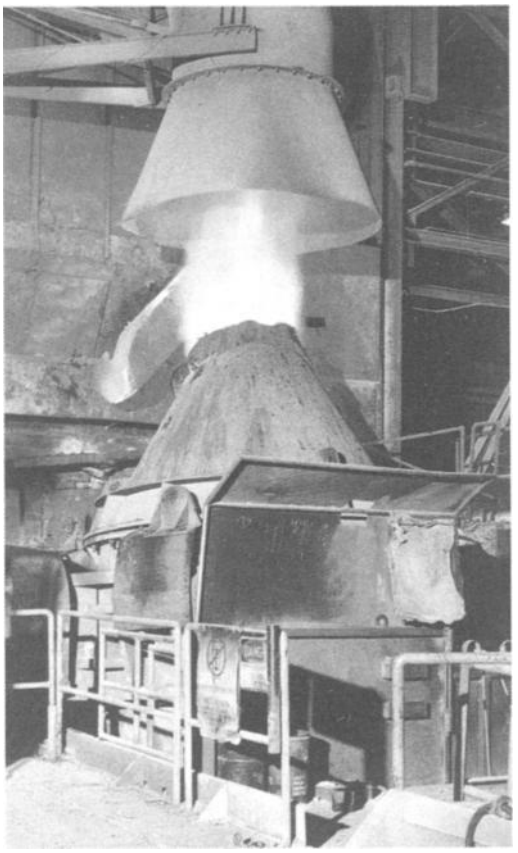

Fig. 3-1 AOD furnace in operation. Courtesy of Allvac

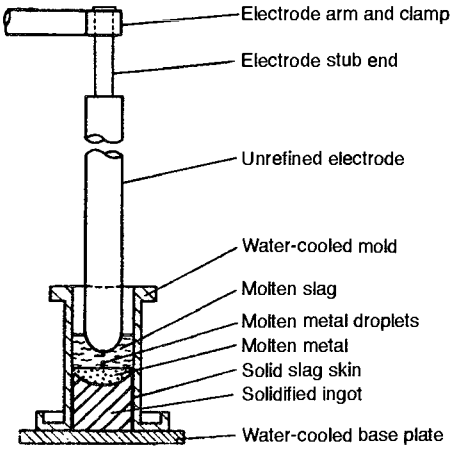

Fig. 3-2 Schematic of ESR process. Source: Ref 2

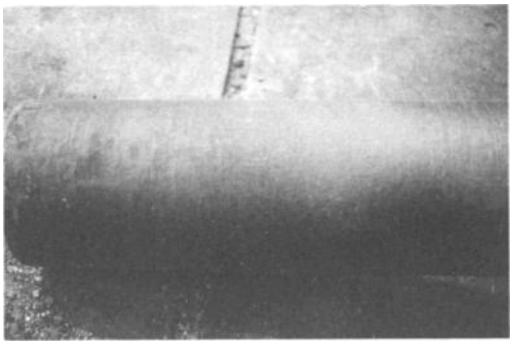

Fig. 3-3 Typical ESR tool steel ingot, 300 mm (12 in.) diam M42. Courtesy of Allvac

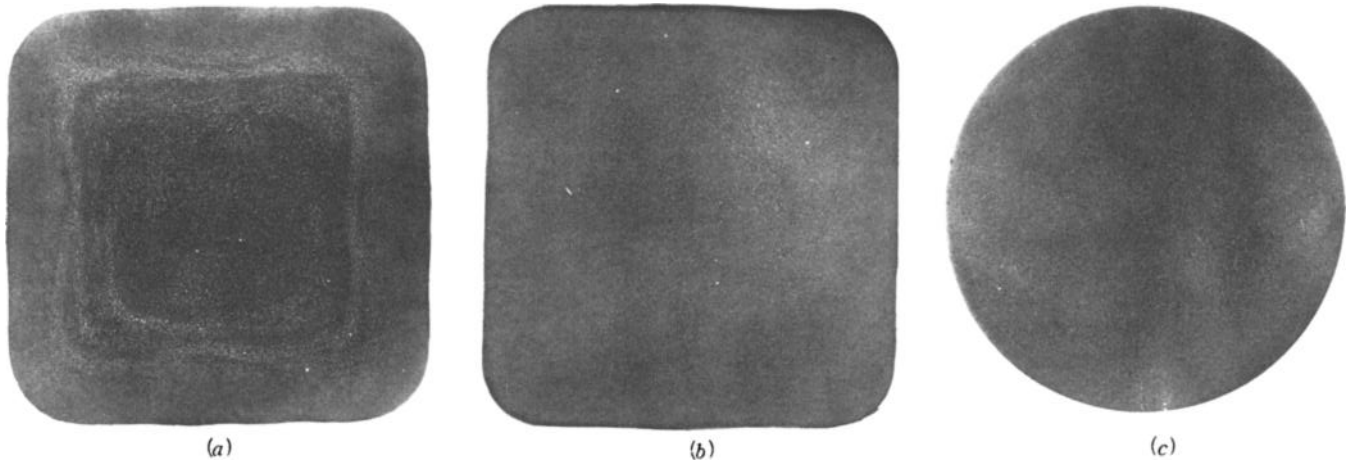

Fig. 3–4 Macroetch quality of high-carbon sulfurized M2-type high-speed steel produced conventionally and by electroflux remelting. (a) From static cast 350 mm (14 in.) square ingot. Disks hardened and tempered. (b) and (c) From electroflux remelted 400 mm (16 in.) diam ingot. Polished and etched with nital. Source: Ref 3

particle size (Fig. 3-6) are also reduced. These results have been documented previously (Ref 4). Cleanliness of ESR-melted product is significantly improved over that of air-melted EAF product (Ref 5). The highly reactive ESR slag removes exogenous oxide inclusions at the tip of the melting electrode, as molten droplets fall through the slag bath and from the molten metal pool (Ref 2). Chemical uniformity of ESR ingots is improved over static ingots (Ref 4), and sulfur is substantially reduced (to at least 70%) (Ref 6). These features, in turn, result in a number of significant benefits, including improved hot workability and thus processing yields, reductions in degree of carbide banding, carbide size, grain size (Ref 2, 3) (Fig. 3-7), and better transverse tensile ductility and fatigue properties (Ref 4, 6) (Fig. 3-8).

Despite this long list of significant improvements resulting from ESR melting, its use in the manufacture of tool steels is quite limited due to economics. Even though yield significantly improves, the resulting cost savings may not repay the cost of extra processing associated with the ESR step. Thus, it is probably most often applied to certain specialized tool steel applications where the end user is willing to pay the extra cost for premium ESR quality.

Vacuum arc remelting (VAR) is a companion process to ESR, which has limited application to tool steels. Like ESR, VAR is a progressive solidification process that results in a refined macrostructure and microstructure, excellent chemical uniformity, and a sound ingot with minimal hot-top pipe. In the VAR process, an arc in a high-vacuum environment replaces the resistance-heated molten slag as the heat source. There is very little change in chemistry and no sulfur reduction in VAR, compared to ESR, but O_2, N_2, and volatile elements (e.g., manganese, lead, and bismuth) can be removed to some degree. Use of VAR for tool steels is limited to certain critical bearing and a few other specialized customer applications.

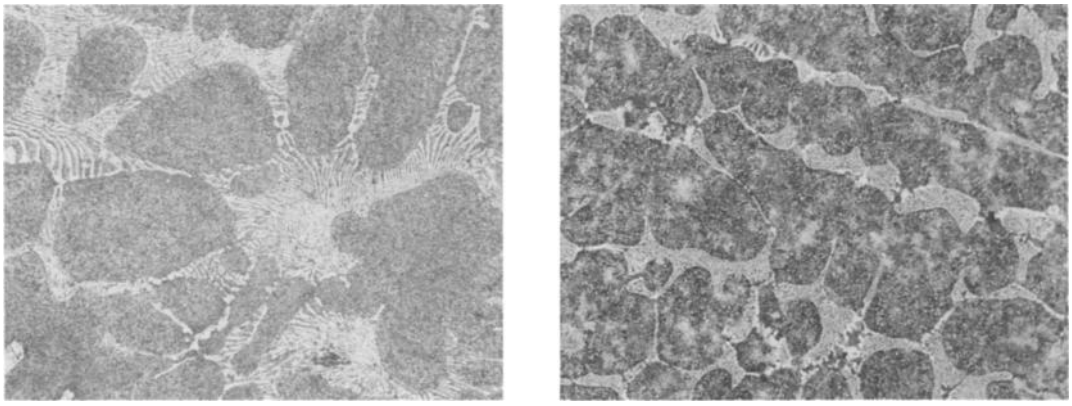

(a) (b)

Fig. 3-5 Eutectic cell size for 1360 kg (3000 lb) M42 high-speed steel ingots produced by conventional static casting (a) and ESR (b). 30×, center position. Courtesy of Allvac

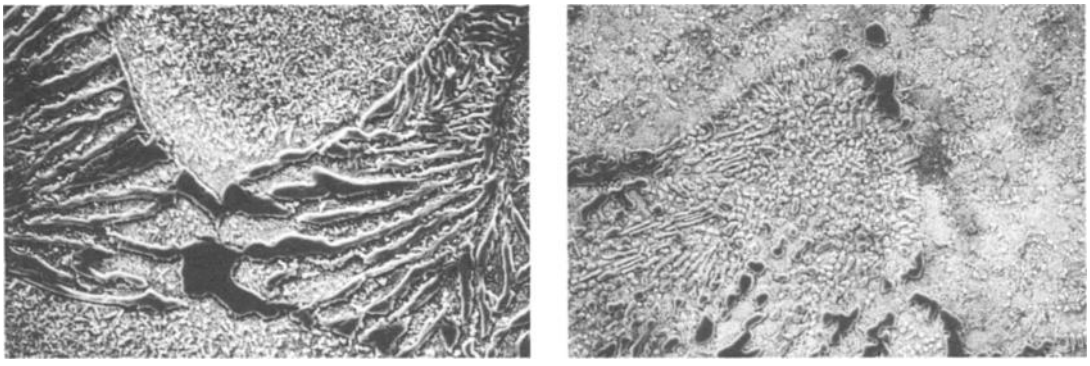

(a) (b)

Fig. 3-6 Eutectic carbide particle size for 1360 kg (3000 lb) M42 high-speed steel ingots produced by conventional static casting (a) and ESR (b). 610×, center position. Courtesy of Allvac

Primary Breakdown

It is difficult to generalize about the practices employed in the working of tool steels, as they are undoubtedly as varied as the number of manufacturers and all the different sizes and types of equipment used. Because the size of the tool steel market is relatively small, tool steel manufacturers generally also produce a variety of other alloys, varying from steels to nickel-base alloys and titanium, and thus their equipment is not necessarily tailored strictly to tool steels. In almost all cases, however, it is safe to say that the competitive nature of the tool steel business has ended the era of manually manipulated hammers and hand mills and replaced it with automated or continuous operations with substantially greater throughput and efficiency.

The initial breakdown practice for tool steel ingots, to some degree, depends on the final product. For long products (billet, bar, or rod coil), the process would usually start on an open-die hydraulic press or a modern rotary forging machine. In some cases, breakdown may also be done by rolling on large blooming mills as, for example, plate and sheet products or round-cornered square (RCS) reroll billet. Products from these operations may be sold as large-diameter bar from which various tools could be made directly or as billet to be reforged to produce a final component shape. Round-cornered squares or round reroll billet would be intended for further processing by rolling to bar.

The newest and most modern piece of equipment used for hot working of tool steels is the precision rotary forge. Several of these large, high-powered machines have been installed by producers of tool steels in the 1980s and 1990s. Ideally suited to the forging of tool steels, they are extremely versatile and highly productive. A precision rotary forge consists of a forging box with four radially opposed hammers and a handling device, or chuckhead, on each side that passes the workpiece back and forth through the forging hammers as it is reduced in cross section (Fig. 3-9).

These machines are very productive and require only a single operator. The high hammer stroke rate (180 to 310 strokes per minute) and heavy reductions (up to 40% reduction of area per pass) cause adiabatic heating and permit reductions of up to 16:1 without reheating. They are also flexible. Size capability ranges from 320 to 650 mm (12.5 to 26 in.) diam maximum input to 80 mm (3 in.) diam output. Finished lengths of 6 to 13 m (20 to 43 ft) are possible. Squares, rectangles, hollows, and stepped cross sections can also be forged, and finished product quality is excellent. Finished bar is very straight with a diameter tolerance of about 1.5% and excellent surface finish with few cracks, laps, or seams.

Rolling

Finish rolling operations have also been transferred from old hand mills to modern, efficient, continuous rolling mills (Ref 7, 8) (Fig. 3-10). These operations consist of as many as 26 rolling mill stands in a continuous line. A starting billet as large as 135 mm (5.3 in.) in diameter or RCS by 10 m (33 ft) in length and weighing up to 1360 kg (3000 lb) can be rolled in a single operation to a bar size of 12.5 to 75 mm (0.5 to 3 in.) in diameter or to a continuous rod-coil down to 6 mm (0.22 in.) in diameter. Heating for rolling can be done in typical gas-fired pusher or walking-beam furnaces or in high-powered induction furnaces capable of heating a 135 mm (5.3 in.) diam billet from room tempera-

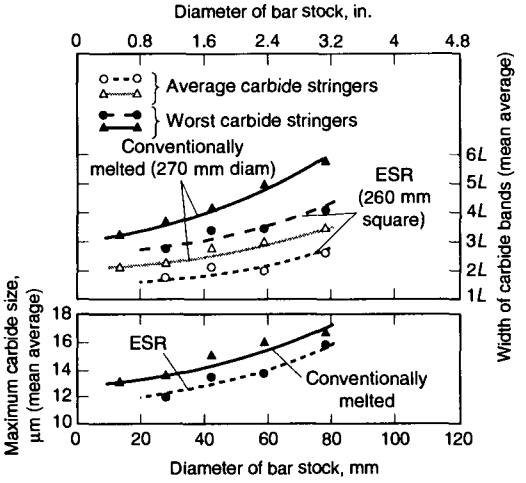

Fig. 3-7 Carbide banding and carbide size of as-rolled M2 high-speed steel. Source: Ref 2

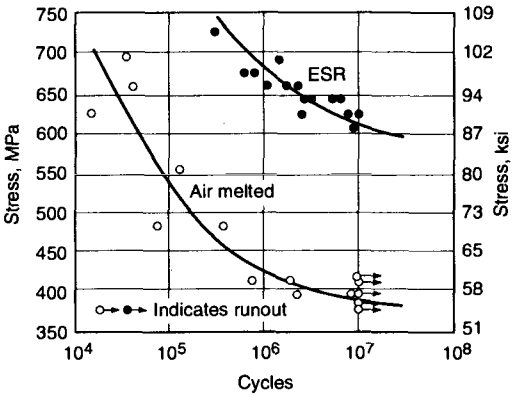

Fig. 3-8 *S-N* curves for tension-compression fatigue testing of transverse air-melted and ESR A2 specimens. Source: Ref 4

ture to a rolling temperature of approximately 1150 °C (2100 °F) in 10 min. Such rapid heating is very effective in preventing decarburization in tool steels. Thus, the entire heating and rolling process, from room temperature to a finished coil, can be accomplished in less than 12 min. A variety of high-tech devices are used in these operations to control, improve, and monitor the quality of rolled products. Computers automate the systems that run the mills and gather the statistical process control data required by current standards. Multiple optical pyrometers spaced throughout the mill measure compliance to required metallurgical controls. Automated measuring devices and hot-eddy-current testers give continuous readings of the diameter tolerance and surface quality of the entire length of each coil.

Hot workability of tool steels varies widely due to the range of chemistries involved. The highly alloyed high-speed steels are the most difficult to hot work. In general, the workability of tool steels is intermediate, falling somewhere in between easily worked aluminum and carbon or alloy steels and the more difficult-to-work nickel and iron-base superalloys. As-cast ingot workability, as measured by Gleeble high-strain-rate testing, is significantly lower than that of an intermediate product (e.g., a reroll billet) that has undergone some prior working (Fig. 3-11). This is presumably due to coarse, as-cast grains and carbide segregation inherent in solidification of the ingot and suggests that initial working operations should be less aggressive than those applied to intermediate product. Typical hot-working operations start at temperatures of 1090 to 1190 °C (2000 to 2175 °F). Minimum finishing temperatures vary over a wide range, from 955 to 1010 °C (1750 to 1850 °F), depending on the particular operation and grade. High-speed steels can be forged with reductions of up to at least 13:1 in a single heating if finishing temperatures are maintained.

Fig. 3-9 Precision rotary forging machine. Courtesy of Allvac

In addition to achieving the required final shape and dimensions, the purpose of hot working is to improve the properties of the alloy and thus the performance of the final tool. This is accomplished by refining the grain size and carbide distribution. The change in carbide distribution with progressive amounts of hot work for an M7 high-speed steel is shown in Fig. 3-12. After hot working, forged or rolled bars usually must be annealed to avoid the danger of cracking in machining, grinding, or reheating for further work.

Hot and Cold Drawing

Drawing operations are often employed on tool steels to produce better tolerances, smaller sizes than can be achieved in hot rolling, or squares, rectangles, hexagons, or other special shapes. The inherent properties of these materials—high strength and limited ductility—restrict cold drawing in extreme cases to a single, relatively light pass (e.g., 20% reduction of area) in order to prevent breakage. The bar or coil must then be cleaned, annealed, and recoated before another draw pass. Warm drawing at temperatures up to about 540 °C (1000 °F) will reduce the degree of work hardening and permit multiple draw passes without intermediate annealing.

There is a growing tendency to supply high-speed steel rod product in the as-drawn condition rather than with the historic centerless ground finish. This can be accomplished with great efficiency today with automatic machines that start with an annealed, hot-rolled coil, cold draw to a tight tolerance, straighten, eddy-current inspect, and cut to length in a single, continuous operation. This equipment is shown in Fig. 3-13. The as-drawn product requires careful control in hot working and annealing to eliminate decarburization since no surface removal is taken.

Continuous Casting

Many attempts have been made to continuous cast tool steels for the usual economic reasons. As might be expected, because of their relatively high

alloy content and wide solidification range (particularly in high-speed steels), segregation and cracking are frequently cited as problems.

Waters, et al. (Ref 9) reported on trials that began in 1954 with a 100 mm (4 in.) square vertical caster. Severe center carbide segregation occurred in a T1-type steel unless casting speeds were slowed to one-third of normal. At such slow speeds, metal-handling problems occurred and economics were judged unfavorable. Trials with horizontal casting of 25 mm (1 in.) diam bar of high-speed steel at low speed (<450 kg/h, or 1000 lb/h) resulted in rather severe witness marks and internal cracking due to thermal stresses (Ref 10).

As recently as November 1992, no indication of continuous casting of tool steels was noted in a summary of equipment and operators in the United States and Canada (Ref 11), but progress has been reported in Europe. Casting of tonnage quantities of a variety of steels, including high-carbon bearing, tool, and high-speed steels, has been accomplished on a horizontal machine at speeds "remarkably lower" than for stainless or low-alloy steels (Ref 12). Electromagnetic stirring is also considered essential to obtain satisfactory carbide structure, but

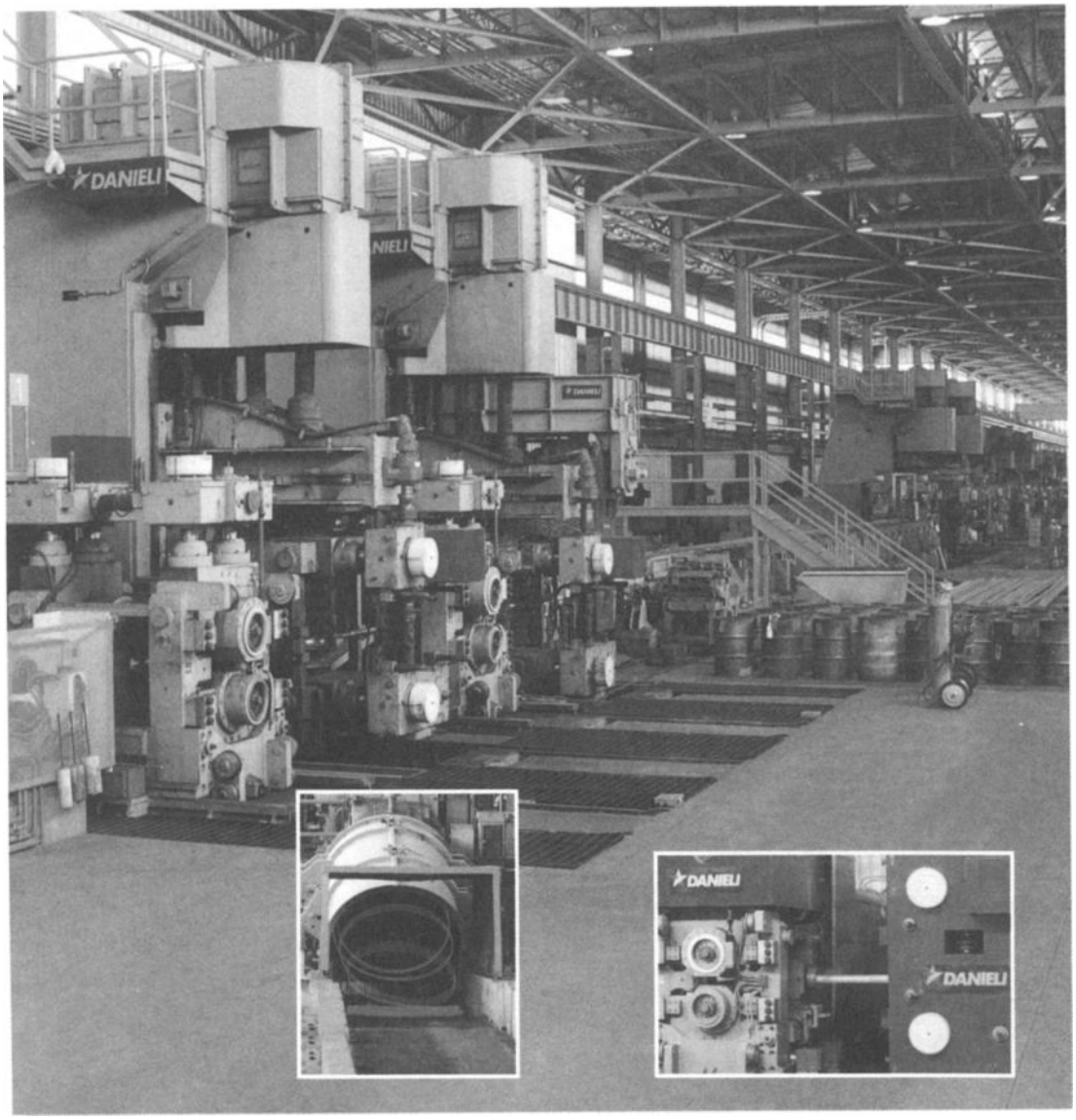

Fig. 3-10 Continuous rod and bar mill. Courtesy of Allvac

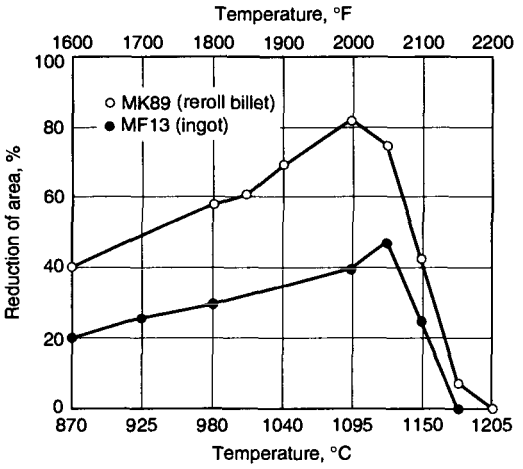

Fig. 3-11 Gleeble hot ductility curve for M7 high-speed

good final product results were reported for various tool steel grades made from 200 mm (8 in.) diam continuous-cast billet.

Success has also been reported for continuous casting of tool steels on a vertical caster (Ref 13). Various sizes, from 100 mm (4 in.) RCS to 140 by 185 mm (5.5 by 7.3 in.) are possible. Proper cooling conditions (both in the mold and during secondary cooling) and electromagnetic stirring are critical to obtaining a good cast structure. As-cast carbide networks for an M2 high-speed steel and a ledeburitic steel were reported to be finer than those in standard 250 mm (10 in.) ingot cast steels. Following casting, billets are annealed and sometimes ground. Grinding weight loss is from 4 to 6%. Billets are then hammer forged or rotary forged and rolled. Central porosity is closed and the cast carbide network broken up in the initial forging. Minimum reduction ratios of 2:1 in forging followed by 2.5:1 in rolling are required to obtain fully dense cores.

The most recent attempt at continuous casting of tool steels is the electroslag rapid remelting (ESRR) process (Ref 14). This approach is unique in that it combines some of the best features of ESR—a sound, homogeneous ingot with good surface quality—in a process that can cast small-diameter ingots (e.g., 160 mm, or 6.3 in., diam) from larger starting electrodes (250 mm, or 10 in., diam). The process operates with a T-shape mold (Fig. 3-14) and runs at melt rates considerably higher than standard ESR rates (Fig. 3-15). Billets completely free of centerline porosity and segregation have been produced,

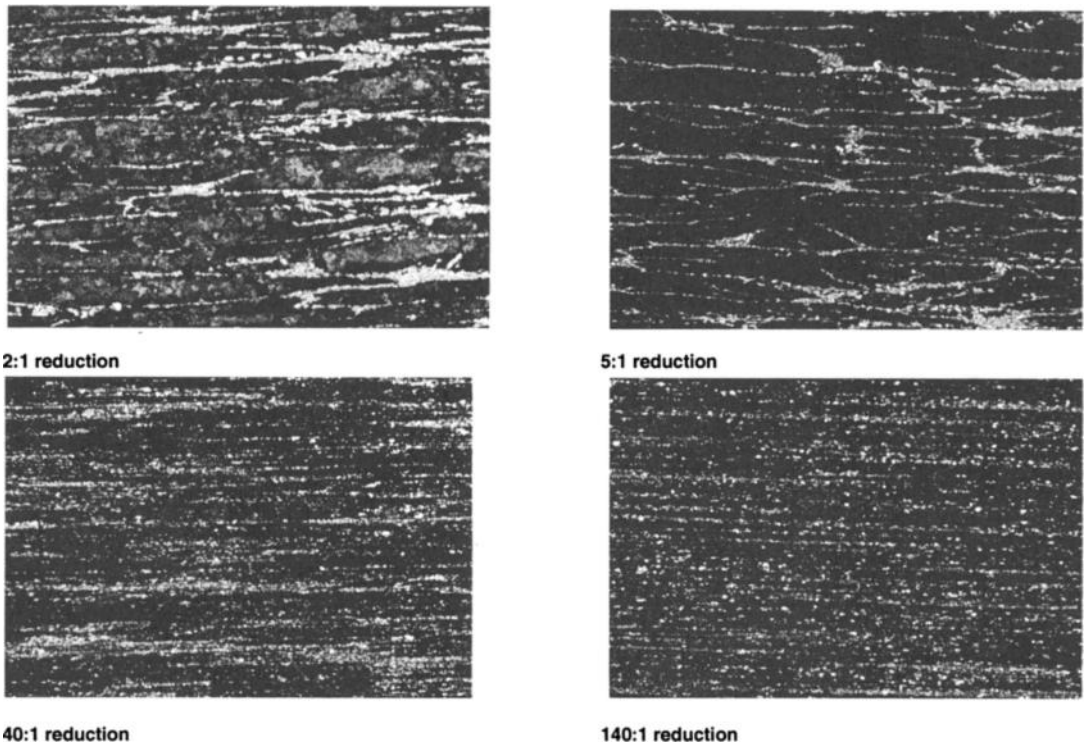

Fig. 3-12 Refinement of carbide structure of M7 with increasing amounts of hot working. Courtesy of Allvac

and direct hot working of the as-cast billets has been demonstrated.

Powder Metallurgy

Perhaps the most significant change in the manufacturing methods for tool steels since the fourth edition of *Tool Steels* was published has been the rapid advance of powder metallurgy (P/M) for production of the most highly alloyed steels, such as high-carbon, high-chromium (D series) and high-speed (T and M series) (see Chapter 2). The P/M business is estimated to be growing at a rate of 10% (Ref 15) to 15% (Ref 16) annually, far in excess of the overall market for tool steels. Despite more than 100 years of manufacturing history, the high-carbon, high-alloy tool steels remain particularly difficult to process by the conventional ingot metallurgy route. The relatively slow cooling of the conventional static cast ingot allows the formation of coarse eutectic carbide structures (Fig. 3-5), which are difficult to break down during hot working. Reduction ratios of greater than 100:1 may be required to develop a fine, uniform carbide structure (Fig. 3-12). A variety of problems may occur as a

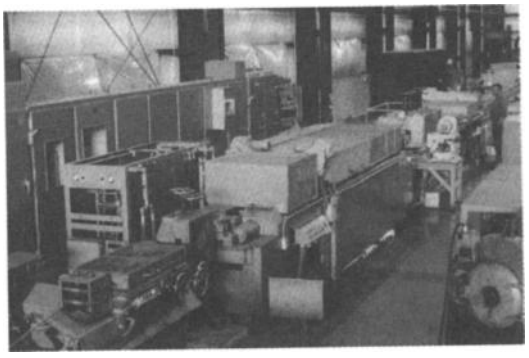

Fig 3-13 Combination drawing line for automatic drawing, straightening, eddy-current inspection, and cutting to length. Courtesy of Allvac

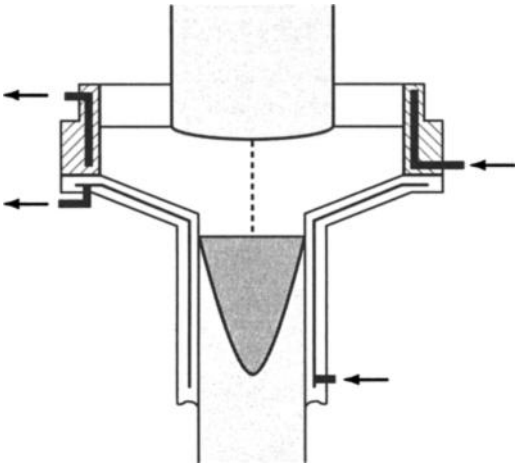

Fig 3-14 Principle of the ESRR process. Source: Ref 14

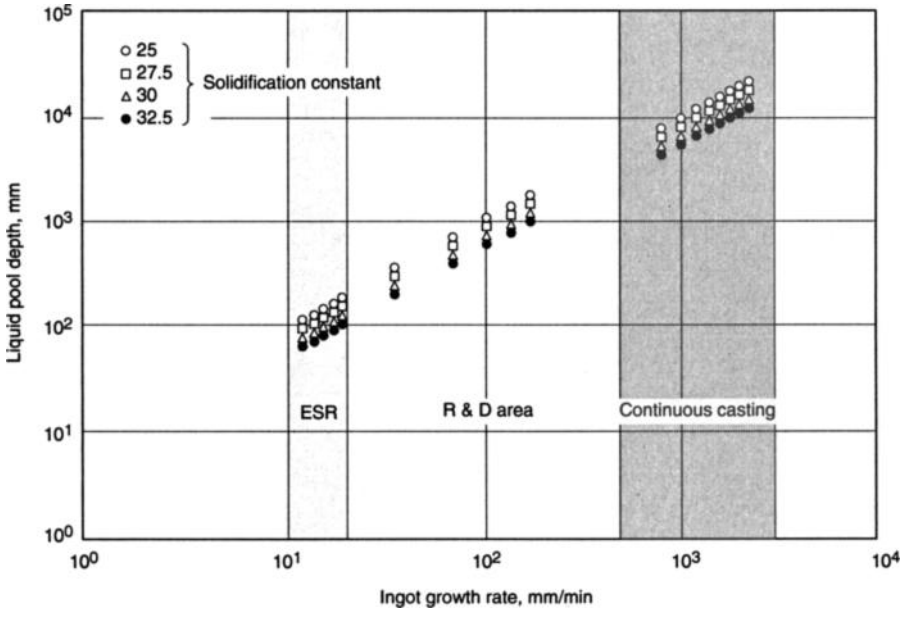

Fig. 3-15 Pool depth versus casting/remelting rate for 160 mm (6.3 in.) diam ingot. Source: Ref 14

result of the less than desirable carbide structure, including nonuniform and excessive grain growth, nonuniform heat-treat response (hardness), poor transverse properties, and low toughness. The ability of P/M to overcome these problems stems from the fundamental ability of the process to produce a fine, uniform distribution of carbides as a result of rapid solidification during atomization. The first full-scale commercialization of P/M tool steels in the United States was announced in December 1970 (Ref 17) and was followed shortly thereafter in Sweden (Ref 18). Today, numerous companies throughout the world are involved at all levels of activity, ranging from research to full-scale production.

Although production figures are not readily available, the gas atomization process would appear to be the most widely used for P/M tool steels based on the number of companies employing this method. Figure 3-16 shows a schematic of the gas atomization process. Molten metal is poured through a small-diameter nozzle into jets of high-pressure gas that break the stream into small droplets. Each droplet can be considered a mini-ingot that solidifies during free-fall to the bottom of the chamber.

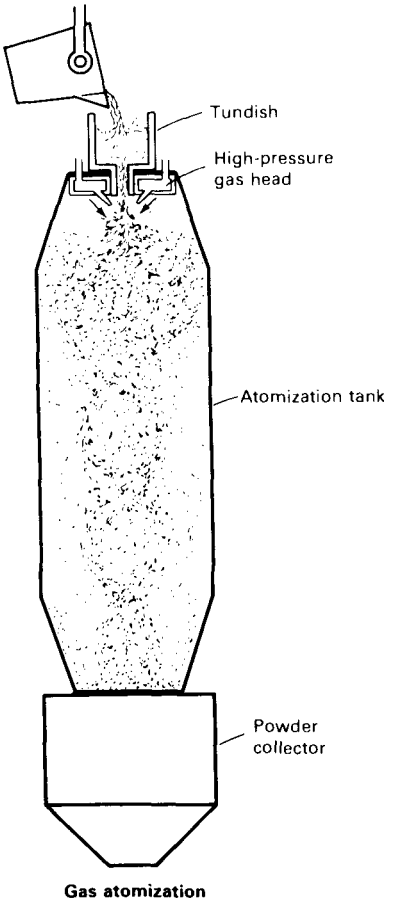

Fig. 3-16 Schematic of the gas atomization process. Source: Ref 19

It is important to minimize oxygen content in the powder; therefore, nitrogen is the most commonly used atomizing gas. Nitrogen is substantially less costly than argon and is not considered harmful in tool steels. In addition, argon entrapment in powder can lead to porosity on high-temperature heat treatment (thermally induced porosity).

The highly spherical nature of powders produced by the gas atomizing process means that final parts cannot be produced by the conventional press-and-sinter technique due to a lack of adequate green strength. Thus, hot isostatic pressing (HIP) has become the most common consolidation technique for P/M tool steels. In this method, a mild steel container is filled with loose powder that is vibrated to achieve a maximum packing density. The container or can is then evacuated and hermetically sealed. The container may then be directly hot isostatically pressed or, in some cases, an intermediate cold isostatic pressing (CIP) operation may be added to improve the density and raise thermal conductivity. Billets produced by HIP are usually hot worked by a combination of press or rotary forging and rolling, depending on final product size. It is also possible to substitute a sintering operation and direct rotary forging for the HIP-and-forge process. Since full density can be achieved by hot isostatic pressing, working following HIP is not necessary. As-compacted tool steels can be made in very large sizes, up to at least 1 m (3.3 ft) in diameter (Ref 20), have isotropic properties, and show no out-of-roundness on heat treating. Figure 3-17 illustrates a very large tool made from P/M high-speed steel.

Water-atomized tool steel powders are highly irregular in shape and thus, after annealing, are suitable for conventional die pressing operations. Sintering to full density in finished parts is difficult to

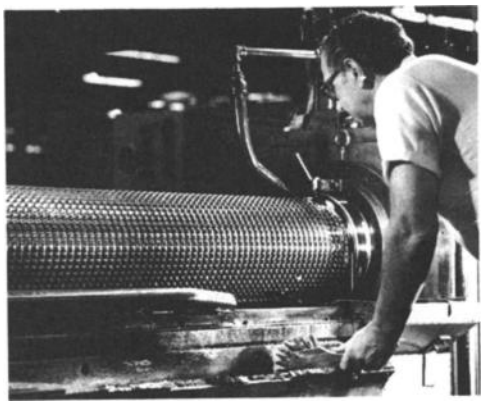

Fig. 3-17 Large broaching tool made from P/M high-speed tool steel. Source: Ref 21

achieve, however. Rapid densification to near theoretical can be aided by liquid phase sintering, but carbide and grain growth can be very rapid under these conditions, leaving a narrow processing window for producing acceptable product (Ref 22, 23).

Solidification rates for gas or water atomization are several orders of magnitude higher than those of the conventional static ingot practice. These high solidification rates can suppress the eutectic carbide reaction and result in an extremely fine, uniform carbide distribution. The dramatic difference in carbide particle distribution for P/M tool steels is shown in Fig. 3-18 and is illustrated quantitatively in Fig. 3-19. Both the maximum and the average carbide particle sizes are significantly smaller in the P/M product. In fact, the maximum carbide particle in P/M is smaller than the average carbide particle in the ingot metallurgy product.

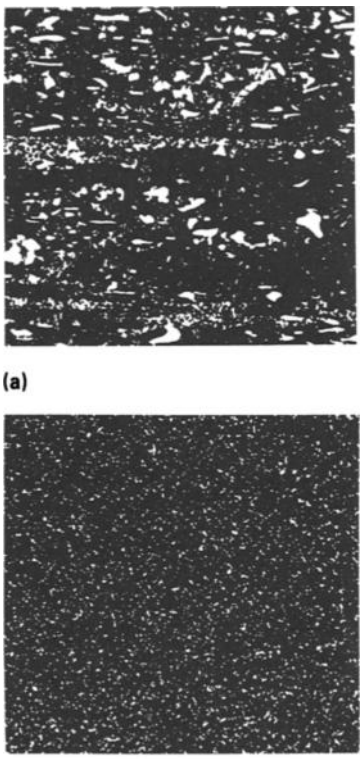

(a)

(b)

Fig. 3-18 Microstructure of T15 tool steel. (a) Wrought (b) P/M processed. Source: Ref 24

The advantages of P/M tool steels are a direct result of their fine, uniform carbide distribution. These include improved machinability in the annealed condition (Ref 26) and faster response to hardening heat treatment (Fig. 3-20). Improved grindability in the fully hardened condition and toughness are illustrated in Table 3-1 (Ref 25). The only apparent negative in performance for P/M high-speed steels is a reduction in wear resistance (see Table 3-3 in the next section).

The P/M process has also extended the alloy range for high-speed steels, much as for P/M nickel-base alloys. Alloy T15 has generally been considered to be the practical upper limit for conventional ingot metallurgy alloys (Ref 25). While higher alloy content and vanadium carbide content would be expected to improve performance, the severe alloy segregation and coarse, banded carbide structure from conventional static ingots result in decreased ingot hot workability, reduced tool grindability, and lower tool toughness. The P/M process allows the successful production of high-speed steel tools with much higher alloy and VC content, and an entire series of improved-performance alloys has been developed on this basis (Table 3-2).

Metal injection molding (MIM) is a variant of the P/M process that is growing at an estimated rate of 20 to 25% annually (Ref 16) and which holds significant potential for tool steels. In MIM, extremely fine (10 to 20 μm) powders are blended with a polymer, and the mixture is injection molded in a manner similar to plastic injection molding. Molded or green parts are usually heated at a low temperature to remove most of the organic binder, followed

Table 3-1 Mechanical properties of high-speed steels: P/M versus conventional

		Toughness				
		Charpy C-notch impact value		Bend fracture strength		
Grade (a)	Hardness, HRC	J	ft · lbf	MPa	ksi	Grinding ratio
CPM T15	67	19	14	4675	678	2.2
T15 conventional	66	5	4	2151	312	0.6
CPM M4	64	43	32	5350	776	...
CPM M4	65	32	24	5378	780	2.7
M4 conventional	64	14	10	3585	520	1.1
M2 conventional	65	18	13	3820	554	3.9

(a) CPM is a trademark of Crucible Industries. Source: Ref 25

by a high-temperature treatment in a protective atmosphere for final binder removal and sintering. The process is capable of making extremely intricate parts and complex geometries, with high density and good mechanical properties. Parts produced by MIM are typically 95 to 97% dense, with properties approaching wrought materials. Limitations of the process are the high cost of very fine powder, long debinding times, high tooling costs, and part size limitations of usually less than 25 mm (1 in.) (Ref 27).

Although P/M tool steels are an outstanding metallurgical accomplishment, they constitute only about 10% of the domestic high-speed steel market, which in turn represents only a portion of the total tool steel market. The bulk of this market is still supplied by product made by the highly cost-competitive conventional ingot metallurgy approach. Users are frequently unwilling to pay the premium for P/M steels over conventional grades, estimated at from 5 to 50% (Ref 25, 28), when the conventional product meets their requirements.

Osprey Process

Osprey processing of tool steels is currently a very small activity limited to work in Japan and the U.K., but the process warrants discussion here because of its technical and commercial potential and because it is the most advanced and well known of the spray-forming processes. A schematic view of the process in a horizontal billet-making mode is shown in Fig. 3-21. The process is similar to gas atomization in that molten alloy is poured from an induction furnace through a nozzle that directs the stream into high-pressure gas atomization jets, frag-

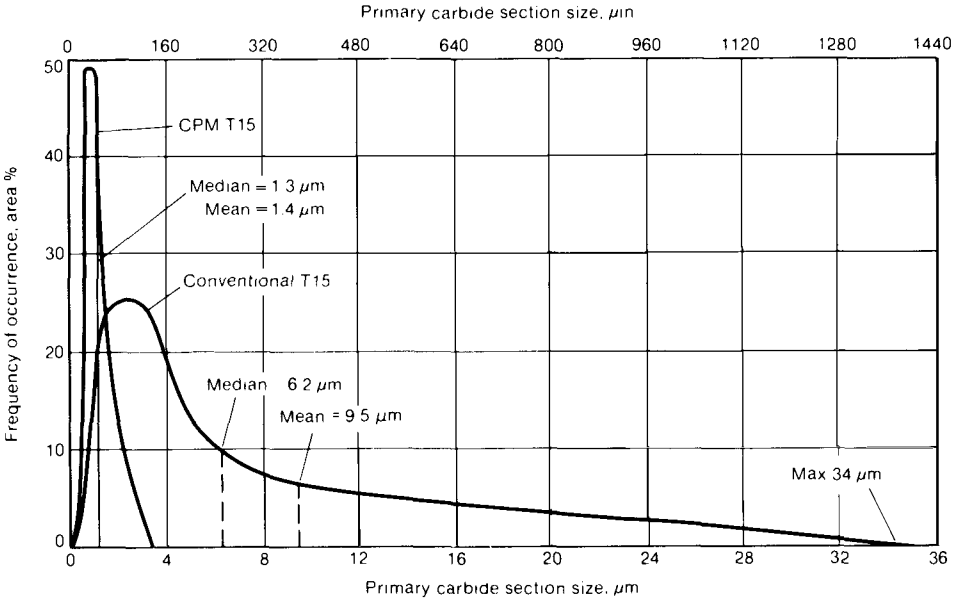

Fig. 3-19 Primary carbide distributions in T15 high-speed steel produced conventionally and by crucible particle metallurgy (CPM). Source: Ref 25

Table 3-2 P/M high-speed steels

Grade (a)	Composition, %					
	C	Cr	W	Mo	V	Co
T15 Conventional	1.55	4.75	12.5	...	5.0	5.0
CPM 6V	2.20	4.0	10.0	5.3	6.5	8.5
CPM Rex 76	1.5	3.75	10.0	5.25	3.0	9.0
CPM 9V	1.75	5.25	...	1.35	8.75	...
CPM 10V	2.5	5.0	...	1.3	10.0	...
ASP 60	2.3	4.25	6.5	7.0	6.5	10.5

(a) CPM is a trademark of Crucible Industries. ASP is a trademark of Soderfors Powder, AB.

menting it into a large number of small droplets. Rather than allowing the droplets to free-fall and solidify in the chamber, however, a collector is inserted into the spray of particles at a specific distance from the atomizing nozzle and is rotated and withdrawn at a rate matching the buildup of the depositing spray. Depending on the particular arrangement, a wide variety of spray-formed products can be made, including billet, hollows, and sheet. Large volumes of an inert atomizing gas are employed, usually nitrogen or argon, which remove most of the heat in the process.

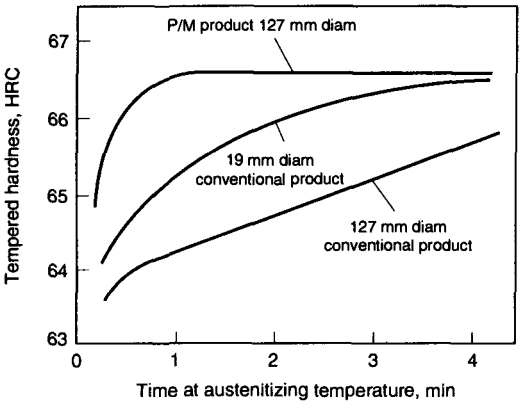

Fig. 3-20 Comparison of hardening response of P/M product and conventional product. Source: Ref 20

Commercialization of the Osprey process for tool steels effectively began in 1986 with a pilot plant of 400 kg (preform) capacity in Japan. A commercial plant with 800 kg capacity was subsequently built in 1991. Rolls up to 800 mm in diameter by 500 mm long (30 by 20 in.) can be produced (Ref 30). High-carbon high-speed steel and high-chromium cast irons are the alloys being sprayed as roll sleeves for use on the intermediate and finishing stands of round bar, flat bar, wire rod, and section mills (Ref 29) (Fig. 3-22).

The benefits of Osprey tool steels are similar to those of P/M product and likewise stem from the

Table 3-3 T15 properties: relative values

Property	Osprey metallurgy	Powder metallurgy	Ingot metallurgy
Carbide size, μm	5–6	2–3	15–20
Bend strength	90	100	60
Wear resistance	100	90	100
Grindability	80	100	25
Toughness	90	100	60

Courtesy of Osprey Metals Ltd.

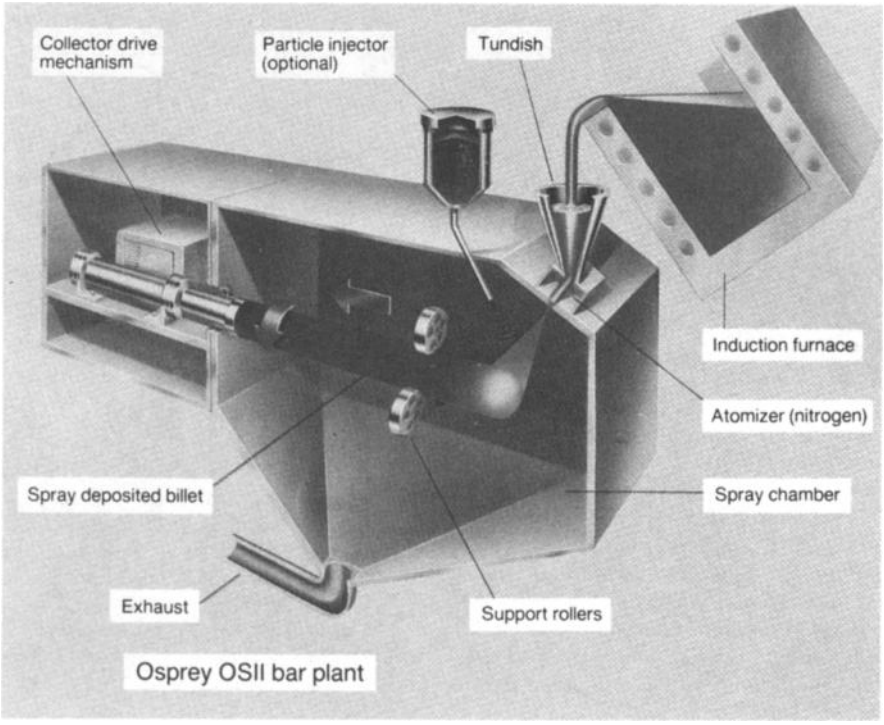

Fig. 3-21 Horizontal concept of spray forming round billets. Source: Ref 29

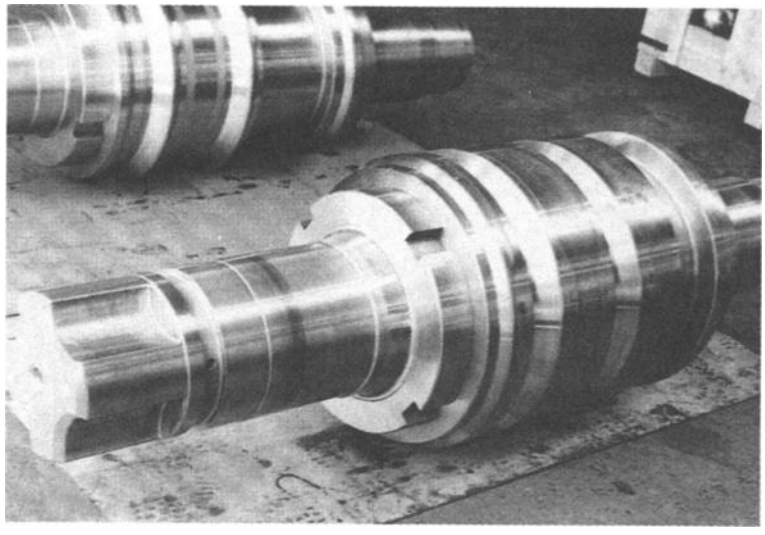

Fig. 3-22 *Spray-formed rolls. Source: Ref 29*

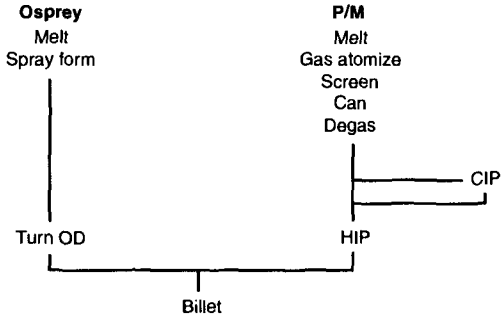

Fig. 3-23 Comparison of Osprey and P/M processing routes for producing tool steel billet suitable for forging or rolling

refinement of structure obtained by the process. Large volumes of gas used in Osprey processing, sometimes a 1:1 basis per pound of metal, extract the superheat and much of the latent heat from the sprayed droplets and from the top of the preform, providing rapid solidification conditions (10^3 to 10^5 °C/s, or 1.8×10^3 to 1.8 to 10^5 °F/s) (Ref 31).

As-sprayed rolls have very high density (>98%) and a fine, uniform carbide distribution free of any of the eutectic carbides observed in the comparable ingot metallurgy product. Roll lives, as a consequence, are 1.6 to 3 times as long as the equivalent cast rolls of the same alloy. Lives of 10 times the conventional rolls are reported for new alloys developed especially for the spray-forming process (Ref 30).

High-speed steel tools made from Osprey material have a uniform distribution of fine carbides of a size very close to P/M products. As a result, performance benefits compared to ingot metallurgy product are very similar to those of P/M high-speed steels (Table 3-3). The most attractive aspects of Osprey processing are the considerably fewer steps necessary in the manufacturing cycle and the very high-spray deposition rates. Process flow routes for Osprey and P/M are shown in Fig. 3-23, illustrating this difference. Flow rates for spraying are reported from 5 to 60 kg/min (10 to 130 lb/min) (Ref 32).

Limiting aspects of the process include spraying yields generally reported to be in the mid-70% range and a sprayed billet diameter limited to about 300 mm (12 in.). Substantial progress has been made on both issues. A four-year development project is currently under way and has successfully produced 400 mm (16 in.) diam D2 tool steel preforms at a 90% yield (Ref 33). Progress on these issues could make the Osprey process economically competitive for tool steels, at least for P/M tool steels.

REFERENCES

1. K.W. Lange, Thermodynamic and Kinetic Aspects of Secondary Steelmaking Processes, *Int. Mater. Rev.*, Vol 3 (No. 2), 1988, p 53–89
2. G. Hoyle, *Electroslag Processes, Principles and Practices,* Applied Science, Essex, U.K., 1983
3. R. Schlatler, Electroflex Remelting of Tool Steels, *Met. Eng. Q.*, Feb 1972, p 48–60
4. T.V. Philip, ESR: A Means of Improving Transverse Mechanical Properties in Tool and Die Steels, *Met. Technol.*, Dec 1975, p 554–564
5. W.E. Duckworth and G. Hoyle, *Electroslag Refining,* Chapman & Hall, London, 1969

6. W. Holzgruber, K. Petersen, and P.E. Schneider, "Comparison of Product and Economics from Large AC-ESR, VAR and DC-ESR Ingots," paper presented at Vacuum Metallurgy Conference, (Beverly Hills, CA), American Vacuum Society, 10–13 June 1968
7. W. Huskonen, World Class Bar/Rod Mill, *33 Met. Prod.*, July 1989, p 17–20
8. R. Brooks, State of the Art Becomes a Science, *33 Met. Prod.*, Jan 1992, p 10–13
9. B.H.C. Waters, W.H. Pritchard, A. Graybrook, and G.T. Harris, Continuous Casting of High Speed Steel, *J. Iron Steel Inst.*, Nov 1958, p 233–248
10. D.C. Briggs and R. Thompson, The Properties of High Speed Steel Produced by Horizontal Casting, in *Cutting Tool Materials*, F.W. Gorsten, Ed., American Society for Metals, 1981
11. Continuous Caster Roundup—USA, Canada, *Iron Steelmaker*, Nov 1992, p 20–30
12. E. Bachmer, W. Meyer, and E. Reisl, Development of Horizontal Continuous Casting of Special Steels, *Metall. Ital.*, Vol 84 (No. 7), Aug 1992, p 615–619
13. G.R. Rosegger, H. Buhl, H. Scherl, and W. Kahr, Casting and Processing of Continuous Cast, High-Alloyed Tool and High Speed Steels at Breitenfeld, *Radex Rundsch.*, Dec 1989, p 154–166
14. W. Holzgruber and H. Holzgruber, Production of High Quality Billets with the New Electroslag Rapid Remelting Process, *Proceedings of the 1997 International Symposium on Liquid Metals Processing & Casting*, American Vacuum Society, 1997
15. North American Powder Metals Market, Confidential Multi Client Market Study Leading Edge Reports, 1990
16. D.G. White, P/M in North America, *Int. J. Powder Metall.*, Vol 32 (No. 3), 1996, p 221–228
17. J.J. Obrzut, PM Tool Steels Come Out Swinging, *Iron Age*, 1 Jan 1971
18. J. Tengzelius and O. Grinder, P/M in Sweden, *Int. J. Powder Metall.*, Vol 32 (No. 3), 1996, p 203–210
19. U.K. Patent 1,389,750, 1972
20. P. Ray and P.K. Pal, 31 High Speed Steel Semis—Alternate Production Routes, *World Conference on Powder Metallurgy*, Vol 2, Institute of Metals, London, 1990, p 159–168
21. J.R. Davis, Ed., *ASM Specialty Handbook: Tool Materials*; ASM International, 1995
22. F.V. Lenel, *Powder Metallurgy Principles and Applications*, Metal Powder Industries Federation, 1980
23. G. Hoyle, *High Speed Steels*, Butterworths, London, 1988
24. Atomization, *Powder Metallurgy*, Vol 7, *Metals Handbook*, 9th ed., American Society for Metals, 1984
25. A. Kasak and E.J. Dulis, Powder Metallurgy Tool Steels, *Powder Metall.*, Vol 2, 1978, p 114–121
26. H.A. Garner and G.J. Del Corso, Powder Metallurgy Tool Steels, *Adv. Mater. Process.*, April 1996, p 25–26
27. K.H. Miska, Ed., Merits of Metal Injection Molding, *Manuf. Eng.*, July 1990, p 87–90
28. D.R.G. Davies and A.R.E. Singer, Spray Forming by Centrifugal Spray Forming, *Adv. P/M Part. Mater.*, Vol 1, 1992, p 301–317
29. A. Leatham, Commercial Spray Forming: Exploiting the Metallurgical Benefits, *Mater. World*, June 1996, p 317–320
30. T. Itami and Y. Kawashima, The Production of Rolling Mill Rolls and High Speed Cutting Tools at Sumitomo Heavy Industries, *Spray Forming: Science, Technology, and Application*, Metal Powder Industries Federation, 1992, p 77–91
31. Osprey Breaks New Ground in Spray Deposition Technology, *Met. Power Rep.*, Oct 1987, p 712–716
32. A.G. Leatham and L.G. Elias, The Osprey Process, *Spray Forming: Science Technology, and Application*, Metal Powder Industries Federation, 1992, p 59–65
33. L.H. Shaw and C. Spiegelhauer, Spray Forming and Evaluation of Large Diameter Billets in Special Steels, *3rd Conf. Spray Forming*, Osprey Metals, 1996, p 101–113

Tool Steels: 5th Edition
George Roberts, George Krauss, Richard Kennedy, p 45-65
DOI:10.1361/toos1998p045

Copyright © 1998 ASM International®
All rights reserved.
www.asminternational.org

CHAPTER 4
Tool Steel Alloy Design

Steels are alloys of iron and other elements. Carbon is the major alloying element for many types of steels, and tool steel technology, similar to that of low-alloy carbon steels, is in large part based on the control of the effects of carbon on microstructure and properties. The carbon contents of tool steels, however, are generally higher than those of most carbon structural steels. In addition, tool steels, with few exceptions (e.g., water-hardening tool steels), are much more highly alloyed than plain or low-alloy carbon steels.

The high carbon and alloy contents of tool steels are used to produce very high strength and hardness by the formation of crystalline phases such as martensite and various carbides. The phases are arranged into microstructures by solidification or powder processing, hot rolling, and heat treatment. In hardened tool steels, the typical microstructure consists of a dispersion of hard carbides in a matrix of tempered martensite. Many variations of this microstructure exist, depending on alloying and processing conditions. Tool steels are, in effect, complex microstructural systems, where every microstructural component of the system is affected by alloying and processing, and eventually plays a role in the performance of a steel under specific service conditions.

This chapter describes the various phases that form in tool steels, starting from the base of the Fe-C system, and then the effects of the major alloying elements. The emphasis is on the phases themselves: their chemical compositions, crystal structures, and properties. Details about how the various phases are arranged into finished microstructures by phase transformations and other mechanisms of microstructural change during heat treatment are discussed in Chapter 5.

Phases and Phase Diagrams: General Considerations

Phases are the independent microstructural units, with unique structures and chemical compositions, that make up an alloy system. The various chemical components of a system distribute themselves among the phases according to thermodynamic principles, and the number of phases that may exist depends on alloy composition, temperature, and pressure (Ref 1). Almost all processing and use of tool steels occur at atmospheric pressure; therefore, pressure is generally assumed constant in the representation of alloy phase equilibria. Thus, the phases present are a function of chemical composition and temperature, assuming constant pressure of 1 atm, and phase equilibria are conveniently represented in plots of temperature and composition. These plots are referred to as phase diagrams.

Phase diagrams assume equilibrium—in other words, that the phases and the phase combinations present at a given temperature in a given alloy have the lowest free energy possible and have had sufficient time to attain that state. In the processing of tool steels, however, often there is insufficient time for the alloying elements to completely partition themselves between the various phases by solid-state diffusion; therefore, equilibrium phase diagrams may represent only the state which is approached rather than the state which is actually attained.

When an alloy is cooled from one temperature to another where different phases are stable, phase transformations must occur. Equilibrium phase diagrams identify only the phases present at the beginning and end of phase transformations, and they provide no information about mechanisms, transformation kinetics, or the distribution of phases produced by various types of phase transformations. The latter type of information is available from other sources, as discussed later in this chapter and in other chapters. Nevertheless, despite limitations associated with nonequilibrium conditions, phase diagrams represent a powerful guide to tool steel alloy development and processing.

Determination of Equilibrium Phase Diagrams

Traditionally, phase diagrams have been determined by applying a variety of experimental techniques. The requirement that equilibrium must be attained, along with the large number of temperatures and alloy compositions that must be evaluated to determine even a small portion of an alloy system, makes experimental determination of equilibrium phase diagrams a difficult process, especially when three or more chemical components are present. This section briefly describes some of the experimental and calculation techniques used to determine phase diagrams of importance to tool steels; refer to the cited literature for details.

Light microscopy and selective etching of specimens quenched from a given temperature are used to identify the number and distribution of phases present at that temperature (Ref 2). It is assumed that sufficiently rapid quenching "freezes-in" high-temperature equilibria after sufficient time at temperature and that no further chemical changes occur as a result of rapid cooling to room temperature. In the case of steels where austenite is stable at high temperatures, quenching will cause transformation of the austenite to martensite, but the martensite, because diffusion is suppressed, will have the same composition as the austenite. Although light microscopy and high-resolution electron microscopy are important techniques that characterize sizes, morphologies, and microstructural arrangements of phases, such microscopic techniques cannot, except by experience, fully identify and characterize the phases revealed.

In order to characterize and unambiguously identify phases, x-ray diffraction is used to determine crystal structure, and x-ray fluorescent analysis (where the intensity of characteristic x-rays from the chemical components of the phases is measured) is used to determine the chemical composition of individual phases (Ref 3, 4). However, because the diameter of the x-ray beams used to excite the characteristic x-rays in x-ray spectrometers is generally much larger than the crystal particles within a microstructure, the particles—in particular, the alloy carbides that are present in tool steels—must be extracted by chemical or electrochemical dissolution of the iron-rich matrix in which the carbides are embedded (Ref 5, 6). The resulting residue of extracted carbides can then be chemically analyzed, either by x-ray fluorescent spectroscopy or other chemical procedures.

More recently, electron microprobe analyzers with highly focused electron beams have made possible the generation of characteristic x-rays from small particles within a metallographic specimen without the need for particle extraction (Ref 7). Electron microprobes use single-crystal spectrometers set to diffract only the radiation from a given element, a process referred to as wavelength dispersive spectroscopy (WDS) and which is capable of high-precision chemical analysis. Characteristic x-ray intensity from the chemical components of fine particles can also be measured in scanning and scanning transmission electron microscopes by energy-dispersive spectroscopy (EDS), where x-ray intensities from the various chemical components are collected with solid-state detectors; the precision, however, is somewhat less than that obtained by WDS (Ref 7).

In addition to the identification of phases and their compositions, the temperatures that mark the boundaries between various phase fields are important features of equilibrium phase diagrams. These boundaries are determined by measurements of volumetric, thermal, electrical, or magnetic changes as a function of temperature. For example, heat given off while new phases form on cooling, as measured by thermocouples attached to specimens, causes a change in cooling rate. This change marks the temperature of the beginning of a phase transformation as the high-temperature phase or phases are replaced. Similarly, changes in specimen length or volume when a new phase with a different density replaces another can be measured by dilatometric analysis. Dilatometry is widely used to determine phase field boundaries and to generally characterize the progress of phase transformations (Ref 8). The temperatures at which diffusion-controlled phase transformations begin are a function of cooling rate: The higher the cooling rate, the lower the transformation start temperature. Equilibrium phase diagram boundaries, therefore, must be determined by measurements at very slow cooling or heating rates or extrapolations to negligible rates of heating or by cooling.

Another method of determining phase equilibria and equilibrium phase diagrams is by calculation based on thermodynamic parameters of various phases. This powerful approach, now broadly applicable to many of the alloy systems of importance to tool steels, was initiated and developed by Hillert and colleagues at the Royal Institute of Technology in Stockholm (Ref 9). As noted relative to the experimental determination of phase diagrams, the stable phases as a function of temperature and chemical composition are those with minimum free energy. Equation 4-1 presents the framework for the calculations that establish the Gibbs free energy of a mole of a given phase, G_m^{α} (Ref 10):

$$G_m^{\alpha} = \sum_J x_J^{\alpha o} G_J^{\alpha} + RT \sum_J x_J^{\alpha} \ln x_J^{\alpha} + {}^{E}G_m^{\alpha} \quad \text{(Eq 4-1)}$$

where J is the number of components in the system and x_J is the mole fraction of the components. The first term is the summation of the Gibbs free energy of the pure components in the same structure; the second term is the summation of the entropy contributions to the free en-

ergy, assuming ideal or random mixing of the various component atoms; and the third term is the excess free energy if the mixing is not ideal. The application of Equation 4-1 to determine the stable phase or phases in a system at a given temperature is then based on further assumptions and analytical expressions and the availability of databases for the thermodynamic properties of various phases in alloy systems of interest (Ref 10, 11).

The determination of phase equilibria by thermodynamic calculations requires the storage and manipulation of large amounts of data and thus has been closely coupled to the development of high-speed computing and associated software development (Ref 11). Many of the developments have been published in *CALPHAD*, a journal dedicated to the computer calculation of phase diagrams from thermochemical information. For alloy systems of interest to tool steel technology, a thermochemical computerized databank, Thermo-Calc, has been developed (Ref 12). A great advantage of this computer program is that complex phase equilibria in multicomponent systems can be evaluated, a process that could be accomplished only with great difficulty and expense by experimental techniques. Databanks for these calculations are based on previously attained experimental measurements from binary, ternary, and higher-order systems. With careful assessment, the data can be extrapolated to more complicated multicomponent alloys for which no experimental information is available. Ongoing effort is devoted to extending and assessing the data for the databanks used in the thermodynamic calculations (Ref 11, 12).

The Iron-Carbon Phase Diagram: Ferrite, Austenite, and Cementite

Figure 4-1 shows the portion of the Fe-C phase diagram of most interest for commercial alloys (Ref 13). Steels may contain up to 2.0 wt% C, and cast irons are based on Fe-C alloys containing more than 2.0 wt% C. As Table 2-2 shows, some tool steels have medium levels of carbon content, but many have carbon contents exceeding 0.8 wt%.

Three phases exist in Fe-C alloys: austenite, ferrite, and cementite. Each phase may be referred to by a variety of terms. For example, austenite may also be referred to as gamma-iron, γ-Fe, or simply γ. Figure 4-1 shows that ferrite forms in two temperature ranges. Low-temperature ferrite is also referred to as alpha-ferrite, α-Fe, or α, while high-temperature ferrite is referred to as delta-ferrite, δ-Fe, or δ. Cementite is also referred to as iron carbide, theta-carbide, θ-carbide, or Fe_3C. Cementite is actually metastable; under some conditions, and in the presence of high carbon content and alloying elements such as silicon, the most stable form of carbon may be graphite rather than cementite. Tool steels O6 and A10, as noted in Chapter 2, and gray and ductile cast irons, with very high carbon contents compared to steels (between 3.0 and 4.0 mass% C) (Ref 14), are designed to have graphite as an important microstructural constituent. Graphite nucleates only with difficulty in medium-carbon steels, but it has been shown that boron nitrides effectively accelerate nucleation and growth of graphite in a 0.53 wt% steel (Ref 15). The dashed lines in Fig. 4-1 show the boundaries of phase fields when graphite coexists with the other phases.

The face-centered cubic (fcc) crystal structure of austenite is shown in Fig. 4-2 (Ref 16). The atoms are not drawn to scale; in fact, they are in contact along face diagonals or ⟨110⟩ directions of the unit cell and are packed as closely as possible on {111} planes. Figure 4-3 presents a more realistic representation of the fcc crystal structure of austenite (Ref 17). Although the hard sphere representation of the iron atoms is an oversimplification of actual atomic structures consisting of electrons surrounding a positively charged nucleus, the schematic representation in Fig. 4-3 effectively shows where atoms are in contact. Austenite in Fe-C alloys has a high solubility for carbon, up to 2.11 wt% at 1148 °C (2098 °F), as shown in Fig. 4-1. The carbon atoms are much smaller than iron atoms and occupy octahedral interstitial sites (i.e., sites at the midpoint of the edges and in the center of the unit cell) between the iron atoms (Ref 18, 19). Figure 4-3 shows schematically the relative sizes of the carbon and iron atoms and the locations of carbon atoms in the interstitial sites.

Figures 4-4 and 4-5 show the body-centered cubic (bcc) crystal structure of ferrite. Atoms are in contact along body diagonals or ⟨111⟩ directions of the unit cell, but the atomic structure is more open than that of austenite. As a result, there is a volume expansion in specimens when austenite transforms to ferrite. Carbon atoms in ferrite occupy octahedral interstitial sites between iron atoms, and in the bcc structure these sites are located at the midpoints of the faces and the edges of the unit cell (Ref 18, 19). In contrast to austenite, the solubility of carbon in ferrite is very low because of the closer spacing of iron atoms along unit cell edges or ⟨100⟩ directions in the bcc crystal structure. In fact, the solubility of carbon in ferrite is so low that the single-phase alpha-ferrite field is not shown in Fig. 4-1. Figure 4-6 is an enlarged portion of the iron-rich side of the Fe-C phase diagram, which shows that the maximum amount of carbon that can dissolve in ferrite is 0.0218 wt% at 727 °C (1341 °F) and that the solubility of carbon in ferrite decreases to negligible values with decreasing temperature.

Cementite has an orthorhombic crystal structure; that is, the axes of the unit cell are perpendicular, but the lattice parameters that define the size of the unit cell are all different. Figure 4-7 shows the unit cell of cementite. Its crystal structure is complex, with 12 iron atoms and 4 carbon atoms per unit cell.

Figure 4-8 more realistically depicts cementite by representing the atoms as hard spheres, emphasizing the regularity of the iron and carbon arrangements in the structure. Ferrite and austenite are interstitial solid solutions of iron and carbon and can dissolve a range of carbon contents up to maximum levels of 0.02 and 2.11 wt%, respectively (Fig. 4-1 and 4-6). Cementite, however, is an intermetallic compound with a specific ratio of three iron atoms to one carbon atom and does not exist over a range of compositions. The composition of cementite, therefore, is 25 at.% C and 75 at.% Fe, or on a mass basis, 6.67 wt% C and 93.33 wt% Fe.

Figure 4-1 shows the temperature and composition ranges over which the various phases of the Fe-C binary system are stable. The solid lines are the boundaries between regions of different combinations of ferrite, austenite, and cementite, while the dashed lines are the boundaries between ferrite, austenite, and graphite. Carbon is an austenite-stabilizing element, and as carbon content increases, the size of the single-phase austenite field increases. Eventually, the solubility of carbon in austenite is exceeded, and the excess carbon is accommodated by cementite formation, resulting in the two-phase field where austenite and cementite coexist. At low tempera-

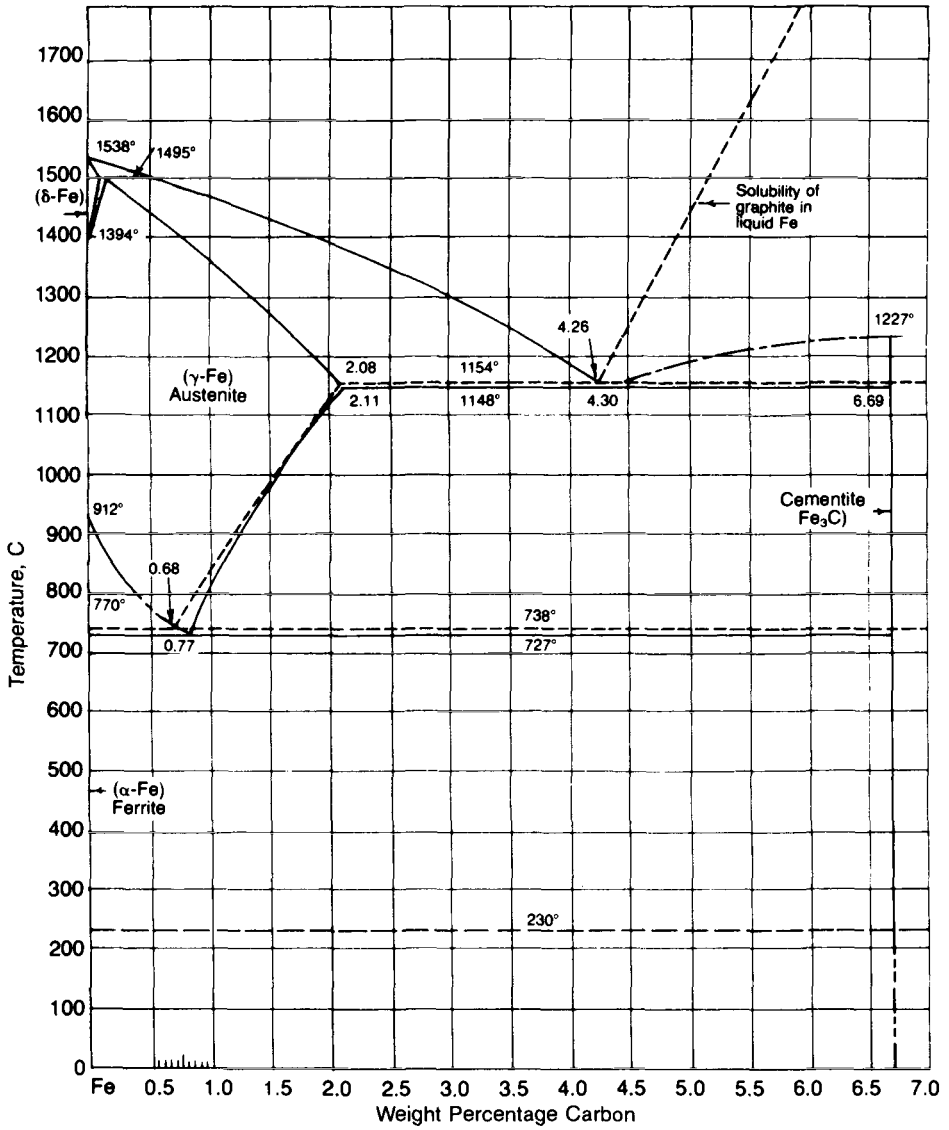

Fig. 4-1 Fe-C phase diagram up to 6.67 wt% C. Solid lines indicate boundaries of phase fields when Fe_3C is the metastable form of carbon, and the dashed lines indicate the boundaries when graphite is the stable form of carbon. Source: Ref 13

tures, because the low solubility of carbon in ferrite is readily exceeded, the lower part of the Fe-C diagram is dominated by the two-phase ferrite and cementite equilibrium. The horizontal line at 727 °C (1341 °F) marks the range of alloy compositions where austenite, ferrite, and cementite can coexist and designates the lowest temperature of austenite stability under equilibrium conditions.

The austenite phase field is extremely important for the hot deformation and heat treatment of tool steels and other low-alloy carbon steels. Figure 4-9 emphasizes the austenite phase field and its boundaries or associated critical temperatures (Ref 20). As noted earlier, the boundaries are shifted from equilibrium when cooling and heating rates are more rapid than those required for equilibrium. As a result, there are sets of temperatures for heating, cooling, and equilibrium that mark the boundaries for each phase field. The temperatures are designated as A, for arrest points, and given the subscripts c for heating (from the French *chauffant*) and r for cooling (from the French *refroidissant*). The equilibrium austenite/ferrite-austenite temperatures, austenite/cementite-austenite temperatures, and the lower critical temperature for austenite stability are designated A_3, A_{cm}, and A_1, respectively.

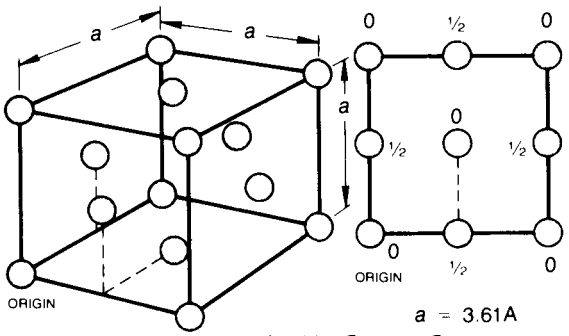

Fig. 4-2 Face-centered cubic crystal structure. *A1* is the structure (Strukturbericht) symbol, and copper is the prototype metal with the fcc structure. Austenite on steel is fcc. Source: Ref 16

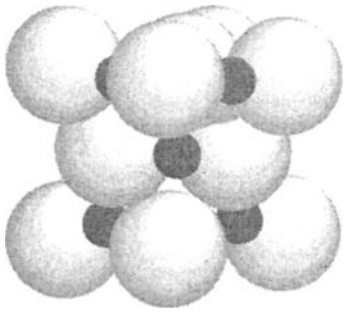

Fig. 4-3 Representation of fcc structure of austenite. White spheres represent iron atoms, and black spheres represent carbon atoms in octahedral sites between iron atoms. Source: Ref 17

Alloying Elements: Effects on Ferrite and Austenite Stability

The alloying elements commonly used in tool steels may significantly shift the phase field boundaries shown on the Fe-C phase diagram. Each element, depending on its atomic size and electronic structure, as related to its atomic number or position in the periodic table, may stabilize either the ferrite crystal structure or the austenite crystal structure. Thus, the alloying elements are categorized either as ferrite-stabilizing elements or austenite-stabilizing elements. Table 4-1 lists the various ferrite- and austenite-stabilizing elements found in tool steels.

The eutectoid reaction in steel is the solid-state reaction where austenite transforms to ferrite and cementite and thus corresponds to a state where three phases are in equilibrium. Further, under equilibrium conditions, the temperature of the eutectoid reaction is fixed at the A_1 temperature (i.e., the lowest temperature at which austenite may exist), and the compositions of the three coexisting phases are fixed. The effect of various alloying elements on the eutectoid temperature is shown in Fig. 4-10. Ferrite-stabilizing elements raise the eutectoid temperature (i.e., extend the temperature range over which ferrite is stable), and austenite-stabilizing elements lower the eutectoid temperature (i.e., increase the temperature range over which austenite is stable to lower temperatures). Figure 4-11 shows that the eutectoid carbon content is decreased by all alloying elements. The eutectoid carbon content is the carbon content of the austenite that transforms to ferrite and cementite at the A_1 temperature. In the Fe-C binary system, the carbon content of the fully austeni-

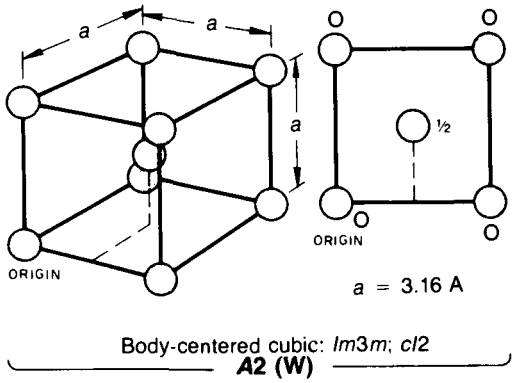

Fig. 4-4 Body-centered cubic crystal structure. *A2* is the structure (Strukturbericht) symbol, and tungsten is the prototype metal with the bcc structure. Ferrite in steel is bcc. Source: Ref 16

tic structure that will transform to ferrite and cementite corresponds to 0.77 wt% C, as shown in Fig. 4-1.

Figures 4-12 to 4-14 show, respectively, the effects of increasing amounts of manganese, chromium, and molybdenum on the size of the single-phase austenite field (Ref 20). In each figure, the dashed lines show the extent of the austenite field in plain carbon steels. Figures 4-12 to 4-14 were determined experimentally. However, now the effects of alloying can also be determined by thermodynamic calculations (Ref 21). For example, Fig. 4-15 shows the calculated effect of chromium on the austenite phase field.

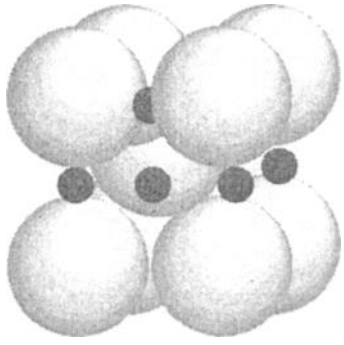

Fig. 4-5 Representation of bcc structure of ferrite. White spheres represent iron atoms, and black spheres represent carbon atoms in octahedral sites between iron atoms. Source: Ref 17

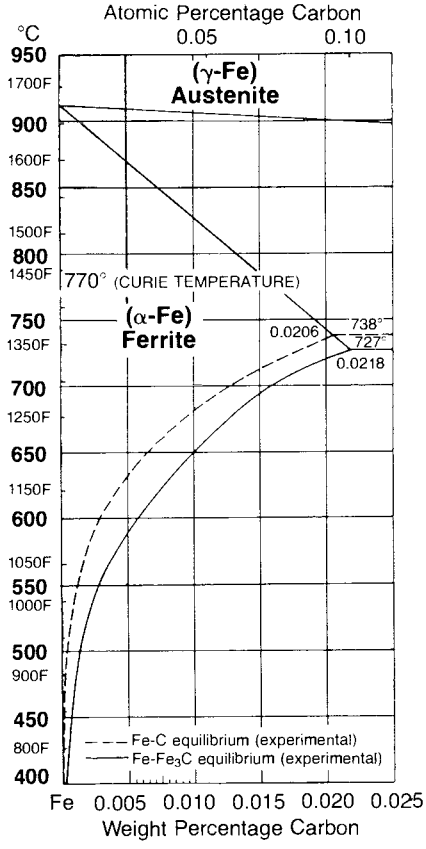

Fig. 4-6 Iron-rich side of the Fe-C diagram, showing extent of ferrite phase field and decrease of carbon solubility with decreasing temperature. Source: Ref 13

Figure 4-12 shows that manganese, an austenite-stabilizing element and a moderately strong carbide-forming element, depresses the A_3 temperature but raises the A_{cm}. Figures 4-13 and 4-14 show that chromium and molybdenum, respectively, both very strong carbide-forming elements as well as ferrite-stabilizing elements, significantly shrink the size of the austenite phase field when added in substantial quantities. These changes in phase equilibria have major effects on the processing of tool steels. As a result of reduced size of the single-phase austenite field, especially at high-carbon contents, many tool steels are hot worked and austenitized at temperatures where austenite and carbides are stable. Therefore, hot working of tool steels may be more difficult than hot working of low-alloy steels, where it can be performed on single-phase austenite. Also, austenitizing in austenite-carbide multiphase fields can be used to adjust carbide and austenite compositions and amounts during hardening of steels. These consequences of alloying on processing are discussed in more detail in other chapters.

Martensite

The formation of martensite is a major objective of alloy design and processing of tool steels and hardenable low-alloy steels. Martensite is a unique phase, but it is a nonequilibrium phase and thus does not appear on the Fe-C equilibrium diagram shown in Fig. 4-1. Martensitic phases, named after the German metallurgist Adolf Martens, are found

Table 4-1 Effect of alloying elements in tool steels

Ferrite-stabilizing elements
Chromium
Molybdenum
Niobium
Silicon
Tantalum
Titanium
Tungsten
Vanadium
Zirconium
Austenite-stabilizing elements
Carbon
Cobalt
Copper
Manganese
Nickel
Nitrogen

in many alloy systems, including those that constitute the bases for ferrous alloys, nonferrous alloys, and ceramic systems (Ref 22). The key to identifying a martensitic phase is the nature of the solid-state phase transformation by which the martensite forms. Martensitic phase transformations are accomplished by shearing and cooperative movement of the atoms of the parent phase into the product martensite, rather than by atom-by-atom diffusion from the parent phase to the product phase. The mechanisms that produce martensitic phases produce displacements, or characteristic surface tilting, when the martensite crystals intersect free surfaces; consequently, martensitic transformations are also referred to as displacive transformations (Ref 23).

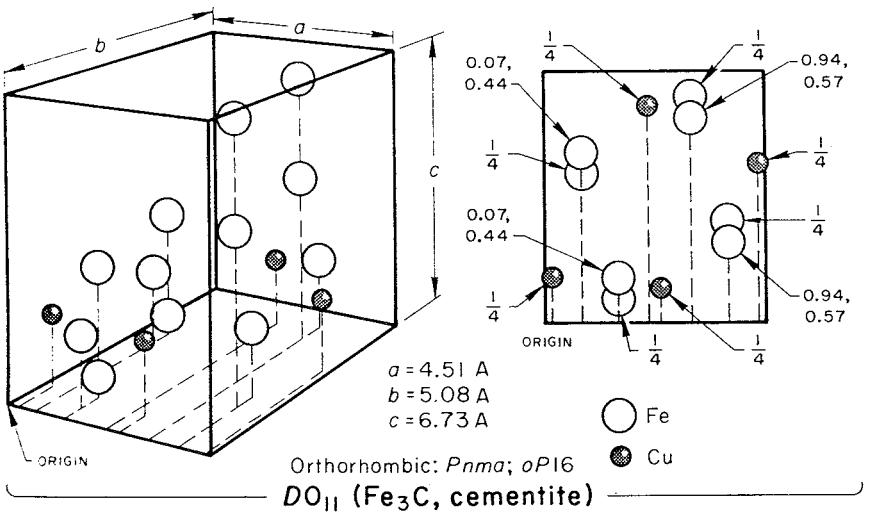

Fig. 4-7 Orthorhombic crystal structure. DO_{11} is the structure (Strukturbericht) symbol, and cementite is the prototype compound with the orthorhombic structure. Source: Ref 16

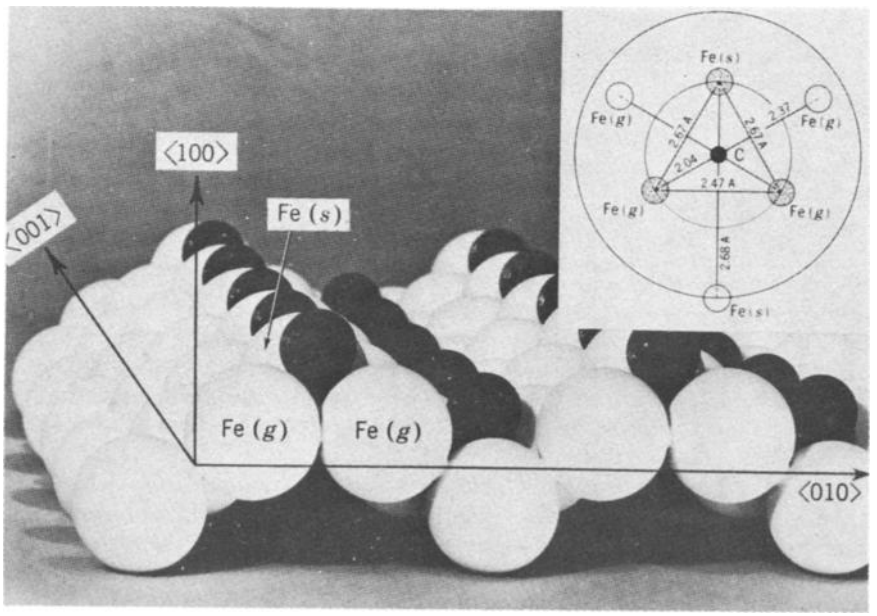

Fig. 4-8 Representation of orthorhombic crystal structure of cementite. White spheres represent iron atoms, and black spheres represent carbon atoms. Source: Ref 18

Figure 4-16 shows schematically the shearing and surface tilting associated with the formation of a martensite crystal from austenite in Fe-C alloys and steels (Ref 24). The surface tilting is produced by plane strain parallel to certain crystallographic planes, termed habit planes, in the parent austenite crystals. Although the plane strain deformation appears homogeneous on a microscopic scale, it is actually accomplished by two deformations. One deformation is referred to as the lattice deformation and constitutes the strains required to change the crystal structure from that of austenite to martensite.

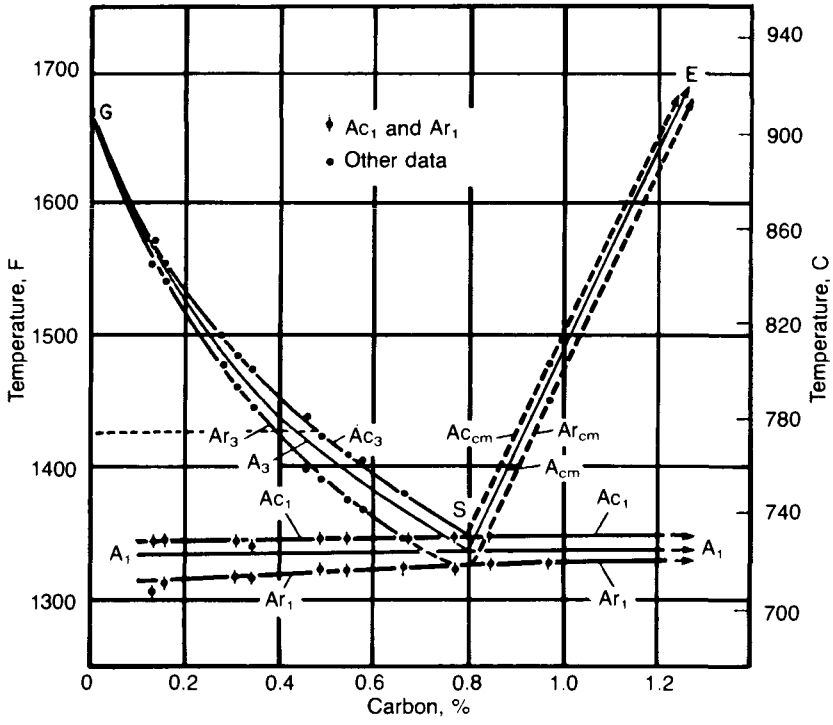

Fig. 4-9 Cooling (Ar_1, Ar_3, Ar_{cm}), heating (Ac_1, Ac_3, Ac_{cm}), and equilibrium (A_1, A_3, A_{cm}) critical temperatures for Fe-C alloys. Heating and cooling at 0.125 °C/min (0.225 °F/min). Source: Ref 20

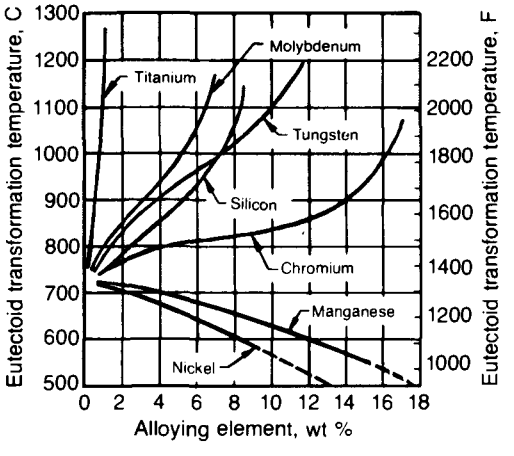

Fig. 4-10 Effect of alloying elements on eutectoid temperature in steel. Source: Ref 20

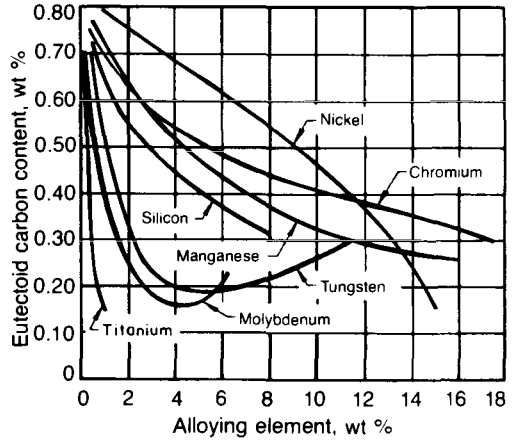

Fig. 4-11 Effect of alloying elements on the carbon content of the austenite that transforms eutectoidally to ferrite and cementite. Source: Ref 20

In ferrous systems this lattice deformation is termed the Bain strain. The lattice deformation, however, does not produce plane strain. Therefore, another deformation, termed the lattice invariant deformation, is required. This accommodation deformation is accomplished by characteristic plastic deforma-

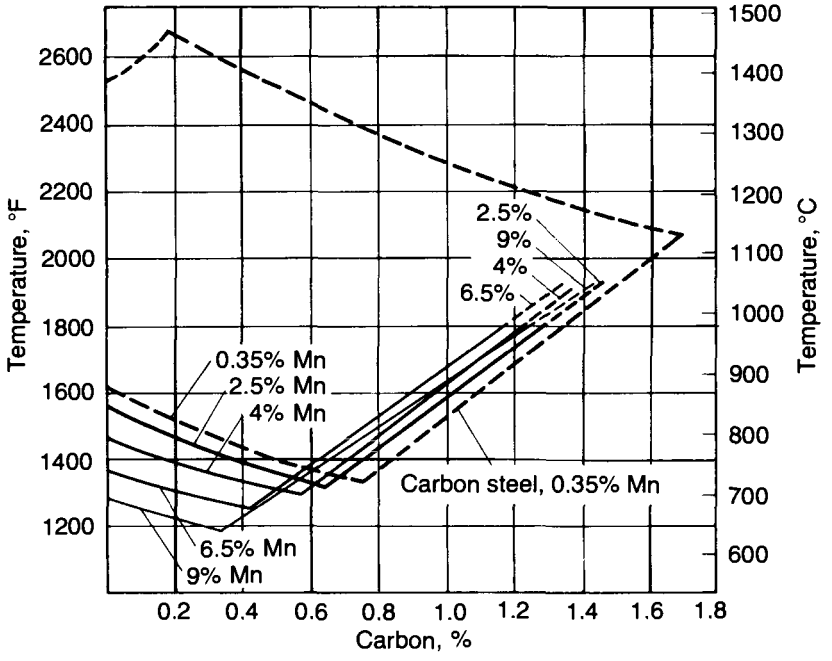

Fig. 4-12 Effect of manganese content on the A_1 and A_{cm} temperatures that define the austenite phase field of Fe-Mn-C alloys. Source: Ref 20

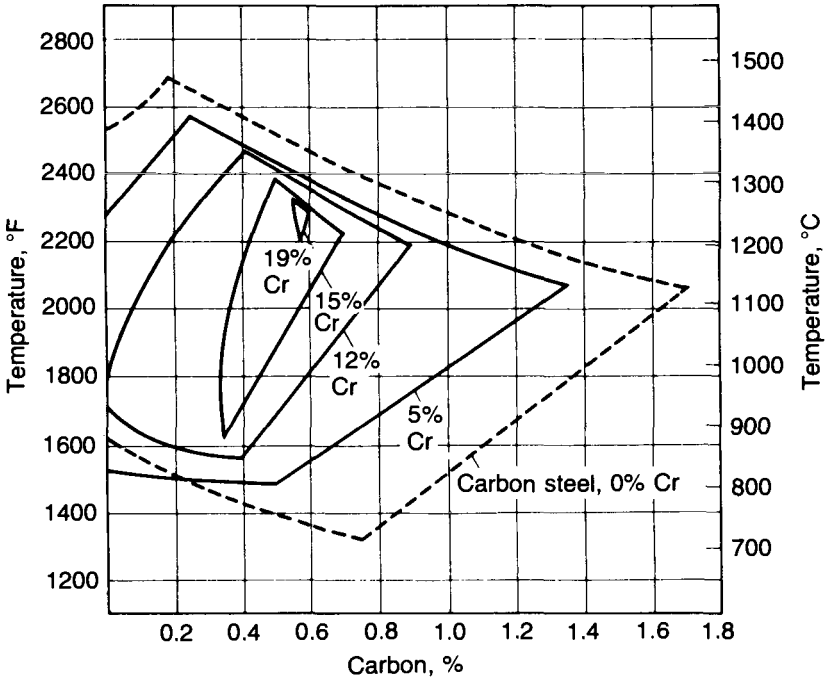

Fig. 4-13 Effect of chromium content on the austenite phase field in Fe-Cr-C alloys. Source: Ref 20

tion mechanisms such as fine-scale twinning or dislocation motion at the habit plane interface of the growing martensite crystal and the parent austenite. The analysis and characterization of martensitic shear transformations is the basis of the crystallographic or phenomenological theory of martensitic transformations (Ref 22-24).

As a result of the diffusionless martensitic transformation, there is no change in chemical composition when martensite forms from austenite; the carbon and alloying element atoms that are dissolved in the fcc structure of austenite during austenitizing are directly inherited and incorporated into the martensite. Figure 4-17 shows the body-centered tetragonal (bct) crystal structure of martensite in Fe-C alloys and steels (Ref 25). Similar to the structure of ferrite, the structure of martensite is body-centered, with an iron atom located in the center of the unit cell. However, the unit cell of martensite is tetragonal; that is, one cell edge, as characterized by the *c* parameter, is longer that the other two, as characterized by the *a* parameters. The tetragonality is a result of the carbon atoms trapped in one set of the octahedral interstitial sites in the body-centered structure of the martensite. The number of sites occupied by carbon atoms, and thus the tetragonality of the martensite, is a direct function of the carbon content of the parent austenite (Fig. 4-18).

The temperature range over which martensite forms and can coexist with austenite is important for the processing and heat treatment of tool steels. Figure 4-19 shows M_s temperature (i.e., the temperature at which martensite starts to form on cooling) as a function of carbon content in Fe-C alloys (Ref 26). Below the M_s temperature, martensite coexists with austenite and increases in amount with decreasing temperature. Alloying elements lower M_s temperatures. The effects of alloying and martensite kinetics are described in more detail in Chapter 5 with regard to control of retained austenite in the microstructure of tool steels.

Figure 4-19 shows that the temperature and composition domain of martensite formation is divided into two parts, with an intervening mixed region. In the low-carbon region, the martensite that forms is termed lath martensite, whereas in the high-carbon region, the martensite is termed plate martensite. The terms lath and plate refer to the morphology and microstructural distribution of the martensitic crystals in a transformed microstructure. Lath martensite crystals, as revealed by light microscopy and transmission electron microscopy (TEM), form parallel to one another in groups referred to as packets. The parallel arrangement of the crystals gives the impression of stacks of lath- or board-shaped crystals. The habit planes of lath martensite are {557}, and the internal structure of each crystal contains a high density of dislocations (Ref 26, 27). Figure 4-20 shows an example of lath martensite that formed in H13 tool steel (Ref 28).

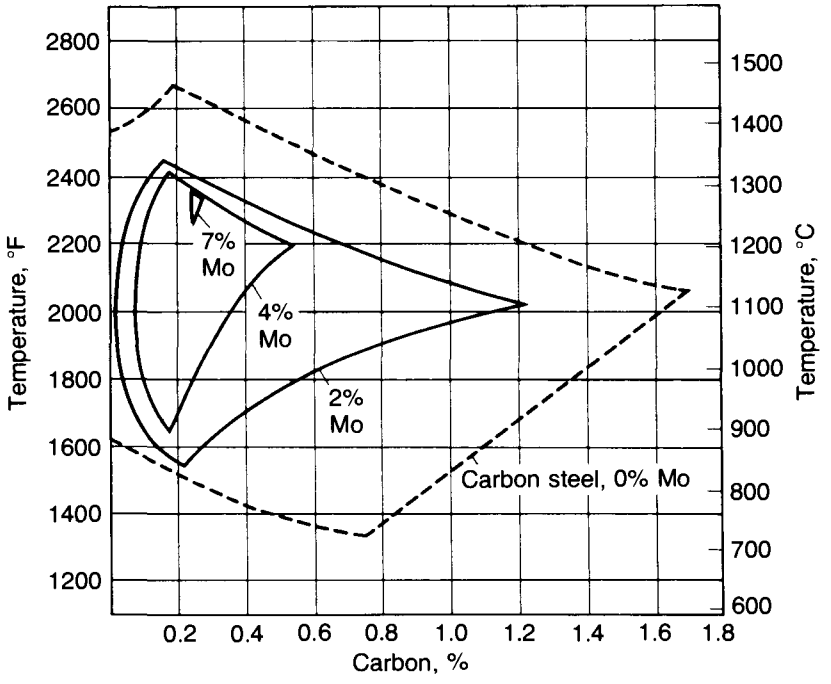

Fig. 4-14 Effect of molybdenum content on the austenite phase field in Fe-Mo-C alloys. Source: Ref 20

crystal contains a high density of dislocations (Ref 26, 27). Figure 4-20 shows an example of lath martensite that formed in H13 tool steel (Ref 28).

Plate martensite crystals in three dimensions have plate-shaped morphologies, and the cross sections through the plates on two-dimensional metallographic surfaces appear needlelike or acicular. The plates form in nonparallel arrays. This feature, as well as the many variants of the {225} and {259} habit planes on which the crystals form in austenite, gives plate martensitic microstructures a zigzag appearance. Because the M_s temperatures are low, large amounts of retained austenite generally are associated with plate martensite, and the retained austenite often appears as triangular patches between the martensite crystals. The lower temperature range of plate martensite formation also increases the amount of fine twinning by which the lattice invariant deformation is accomplished. Figure 4-21 shows a plate martensitic microstructure in a specimen of A2 tool steel. Plates of martensite and retained austenite are shown; because of the high alloy content of the A2 steel, spherical alloy carbides are also retained in the microstructure (Ref 28).

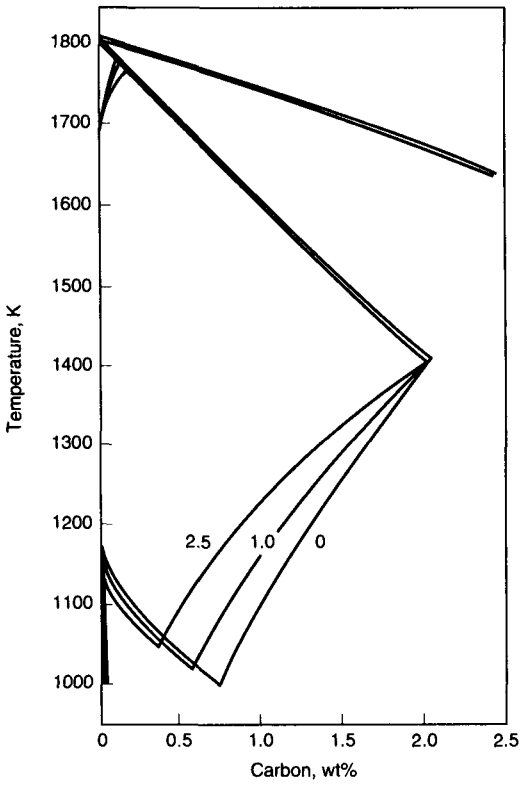

Fig. 4-15 Calculated effect of chromium on the austenite phase field in Fe-Cr-C alloys. Source: Ref 21

The carbon atoms trapped in the martensitic structure constitute a nonequilibrium, supersaturated structure. The equilibrium structure in the temperature range over which martensite forms, as shown in Fig. 4-1, is a combination of ferrite and cementite, or in the case of highly alloyed tool steels, a combination of ferrite and alloy carbides. Therefore, when martensite is heated, in the heat treatment step referred to as tempering, the carbon supersaturation is relieved by the precipitation of carbides. At low tempering temperatures, cementite and other iron carbides are formed; at high tempering temperatures, where substitutional alloying element atoms are able to diffuse, alloy carbides are precipitated. Although tempering causes the martensitic structure to decompose, martensite plays an important role in the evolution of tool steel microstructure by presenting a supersaturated matrix structure for carbide precipitation and secondary hardening. The structure and property changes produced by tempering are discussed in more detail in subsequent chapters.

Alloy Carbides and Tool Steel Alloy Design

Alloying to produce large volume fractions of alloy carbides is a major difference in the design of tool steels compared to the design of low-alloy steels. Large volume fractions of carbides provide the high hardness and wear resistance required to shape other materials, but also make hot deformation, heat treatment, and machinability of the tool steels themselves more difficult. The alloy carbides may be produced during solidification, during hot work or austenitizing for hardening, and during tempering of martensitic microstructures. Equilibrium phase diagrams and considerations of phase equilibria indicate which carbides will be present in a given steel, and knowledge of the effects of processing operations, as discussed in other chapters, predict the microstructural distribution of the carbides.

Table 4-2 lists the various types and some of the characteristics of alloy carbides that may form in tool steels (Ref 29). The letter M in the carbide designation represents the metal content of the carbide and reflects the fact that more than one metal component may occupy the metal lattice sites in the crystal structure for a carbide. For example, the atoms of several metals may substitute for iron atoms in the structure of cementite described in Fig. 4-7 and 4-8. Jack and Jack (Ref 30) describe in detail the various carbide and nitride crystal structures that form in steel.

The stability of the various carbides is a function of the balancing of atomic sizes and electronic structure of the various alloying elements to produce crystallographic structures of minimum free energy. The transition elements, in which the

(Ref 31). The group VIII elements are weak carbide-forming elements or form no carbides. The transition metal carbides have strong interatomic bonding, high melting points, and unique electrical properties and, in addition to their use in tool steels, are often used in pure form (Ref 31). A measure of carbide stability is the free energy of formation, as listed for various carbides in Table 4-4 (Ref 32). A high negative free energy of formation is a measure of high carbide stability and strong carbide-forming tendency of the component atoms.

Alloy carbides have very high hardness. Therefore, large volume fractions of high-hardness alloy carbides are incorporated by design into the microstructures of tool steels. However, not all applications require the highest hardness, especially in applications where fracture resistance is critical. As a result, the various tool steel classes have evolved to achieve the best balance of carbides and properties for a given type of tooling. Figures 4-22 and 4-23 and Table 4-5 show comparisons of hardness characteristic of the various types of alloy carbides and tool steel microstructures (Ref 29, 33-35).

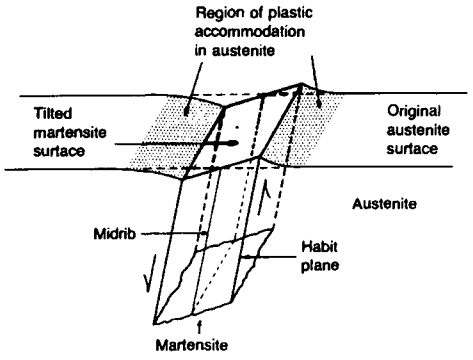

Fig. 4-16 Schematic diagram of sphere and surface tilt associated with formation of a martensite plate in austenite. Source: Ref 24, revised courtesy of M.D. Geib

Martensite and cementite, the base microstructural components of hardened plain carbon and low-alloy steels, have significantly lower hardness than the alloy carbides. Therefore, incorporation of alloy carbide dispersions into tempered martensitic matrix microstructures contributes to the enhanced performance of tool steels for severe forming applications. In general, the higher the carbide-forming alloy element content and the higher the carbon content, the higher the alloy carbide content and hardness of a tool steel. For example, high-speed steels are highly alloyed to provide very high hardness for metal machining operations and, as shown in Fig. 4-24, have very large fractions of alloy carbides incorporated into their microstructures (Ref 36).

As described previously, strong carbide-forming elements introduce new phases and may dramatically change phase equilibria in tool steels. Therefore, the equilibrium phase diagrams for multicomponent tool steel alloying systems differ significantly from the Fe-C phase diagram shown in Fig. 4-1. The multiple alloying element additions in tool steels greatly increase the composition ranges over which more complex phase equilibria must be represented, and with more than three components,

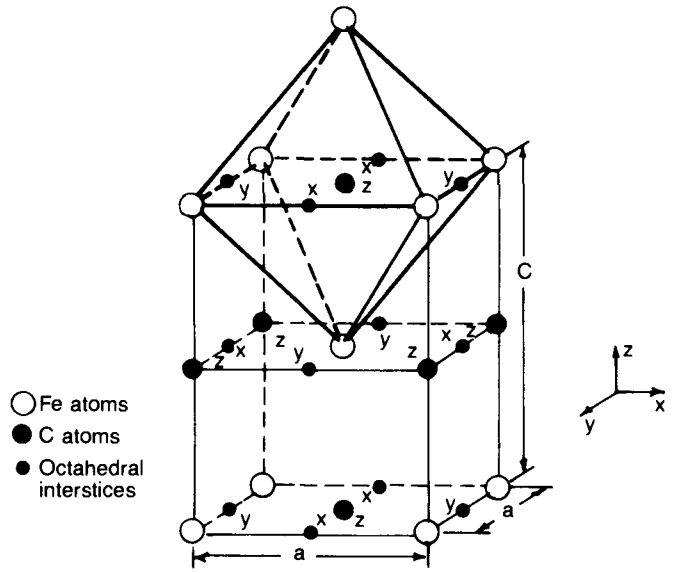

Fig. 4-17 Body-centered tetragonal crystal structure of martensite in Fe-C alloys. Source: Ref 25

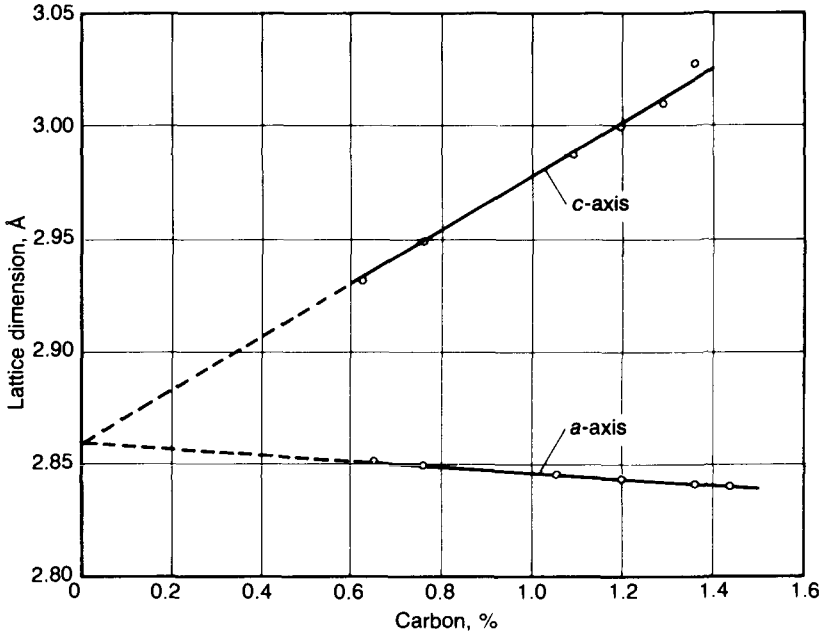

Fig. 4-18 Effect of carbon content on the *a* and *c* lattice parameters of martensite unit cells. Source: Ref 20

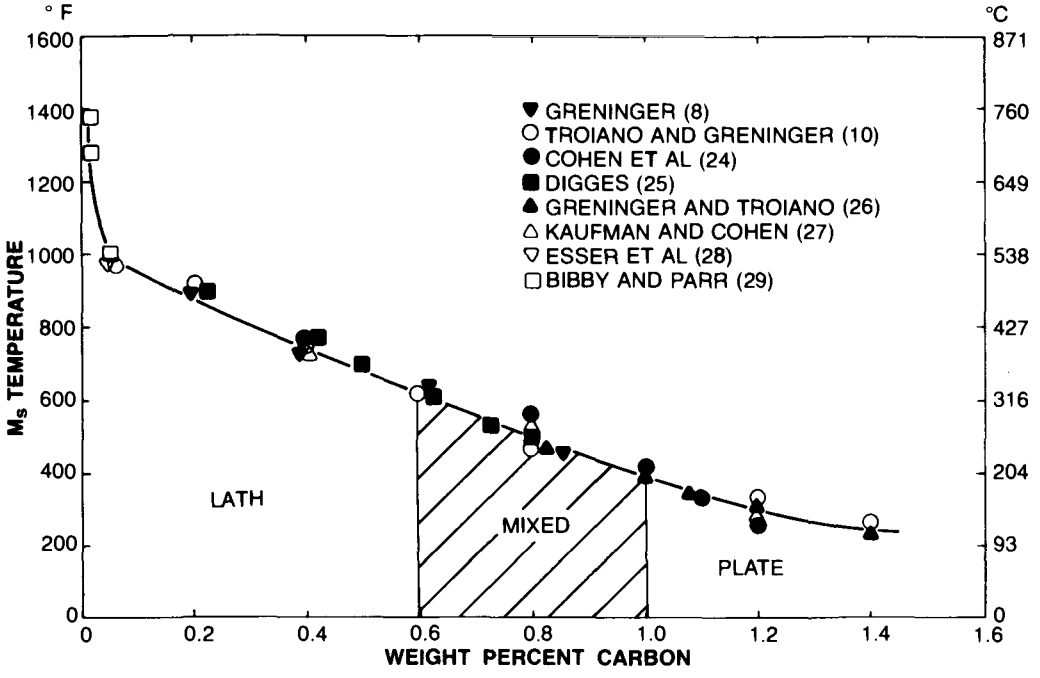

Fig. 4-19 M_s temperature as a function of carbon content in Fe-C alloys and steels. Composition ranges of lath and plate martensite are also shown. Source: Ref 26; investigations noted are identified by their numbers in Ref 26.

there are insufficient dimensions to graphically represent complete system phase equilibria. Computer calculations coupled with experimental work, as described earlier, are powerful techniques currently used to establish phase equilibria in selected composition ranges of multicomponent tool steel systems (Ref 10-12, 38, 39).

However, before the advent of thermodynamic calculations, experimental studies, which restricted alloy compositions or temperatures, were exclusively used to establish portions of tool steel phase diagrams. For example, Fig. 4-25 and 4-26 show examples of vertical sections through the Fe-Cr-C alloy system, where chromium content has been held constant at 5 and 13 wt%, respectively (Ref 40). The vertical sections shown are similar to the Fe-C diagram but show many more phase fields than the Fe-C diagram because of the alloy carbide phases formed by chromium. Vertical sections are very useful for establishing temperature ranges of phase stability and in setting temperatures for hot work and heat treatment for specific alloys but do not give the chemical compositions of the coexisting phases in the multiphase fields (Ref 1).

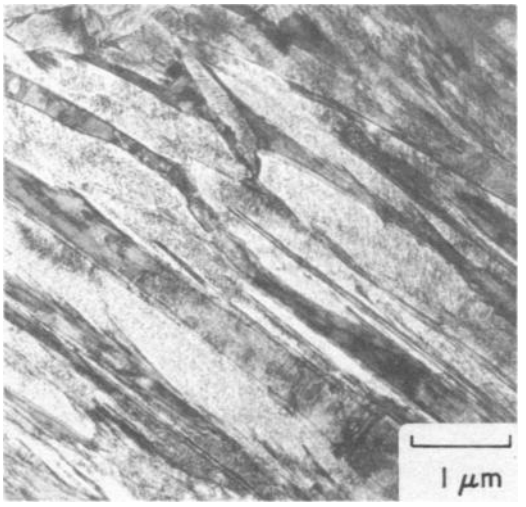

Fig. 4-20 Lath martensite in H13 tool steel. Source: Ref 28

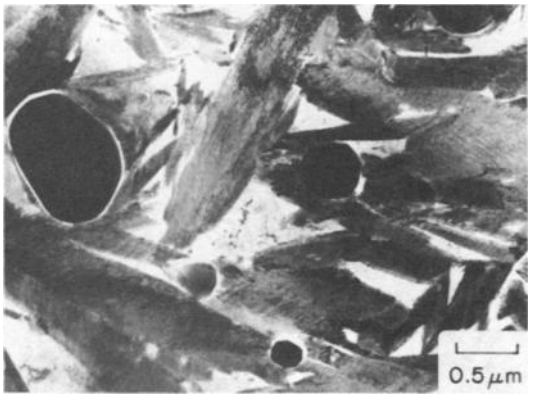

Fig. 4-21 Plate martensite in A2 tool steel. Retained austenite is present between the nonparallel plates of martensite. Source: Ref 28

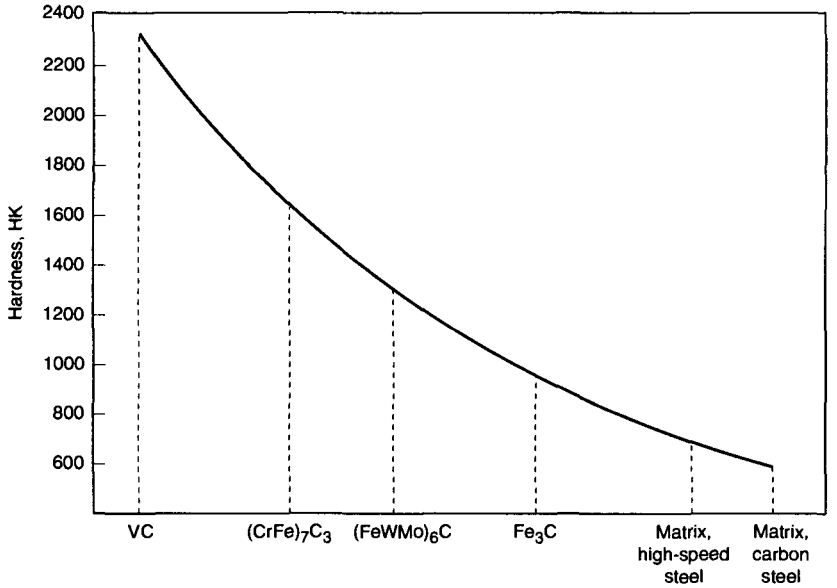

Fig. 4-22 Hardness comparisons of alloy carbides and hardened matrix in tool steels. Source: Ref 29

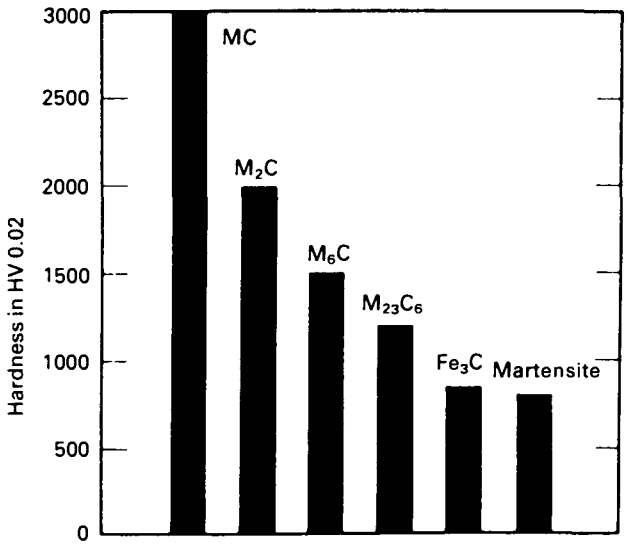

Fig. 4-23 Relative hardness of alloy carbides, cementite, and martensite in high-speed steels. Source: Ref 33

Table 4-2 Characteristics of alloy carbides in tool steels

Type of carbide	Lattice type	Remarks
M_3C	Orthorhombic	A carbide of the cementite (Fe_3C) type. M may be Fe, Mn, Cr, with a little W, Mo, V.
M_7C3	Hexagonal	Mostly found in Cr alloy steels. Resistant to dissolution at higher temperatures. Hard and abrasion resistant. Found as a product of tempering high-speed steels.
$M_{23}C_6$	Face-centered cubic	Present in high-Cr steels and all high-speed steels. The Cr can be replaced with Fe to yield carbides with W and Mo.
M_6C	Face-centered cubic	A W- or Mo-rich carbide. May contain moderate amounts of Cr, V, Co. Present in all high-speed steels. Extremely abrasion resistant.
M_2C	Hexagonal	W- or Mo-rich carbide of the W_2C type. Appears after temper. Can dissolve a considerable amount of Cr.
MC	Face-centered cubic	V-rich carbide. Resists dissolution. Small amount that does dissolve reprecipitates on secondary hardening.

Source: Ref 29

Table 4-3 Transition metal carbides

Carbide formation is fairly common among the transition elements, except for the second and third rows of group VIII (a).

III	IV	V	VI	VII	VIII		
$Sc_{2-3}C$ ScC_2 Sc_2C_3	TiC	V_2C VC	$Cr_{23}C_6$ Cr_7C_3 Cr_3C_2	$Mn_{23}C_6$ Mn_3C Mn_5C_2 Mn_7C_3	Fe_3C	Co_3C Co_2C	Ni_3C
Y_2C Y_2C_3 YC_2	ZrC	Nb_2C NbC	Mo_2C Mo_3C_2 MoC_{1-x}	TcC	Ru	Rh	Pd
LaC_2	HfC	Ta_2C TaC	W_2C W_3C_2 WC	ReC	OsC	Ir	Pt

(a) ☒ indicates no carbide formation for this element. Source: Ref 31

In addition to vertical sections through ternary and higher-order systems that show phase equilibria as a function of temperature and composition, two other types of representations of phase equilibria are commonly used. One type consists of the projection of high-temperature phase equilibria on composition axes of ternary systems, and the other consists of the representation of phase equilibria as a function of composition at some fixed temperature. The latter representations are referred to as isothermal sections. The former type of representation is commonly used to characterize liquidus surfaces and solidification reactions, while the second type is used to characterize phase relationships at some temperature of interest for thermomechanical or heat treatment processing of alloys in a given system. These two types of diagrams are illustrated in Fig. 4-27 and 4-28, respectively, for the Fe-Cr-C system, which is of great importance to tool steel and stainless steel development, production, and application. The importance of the Fe-Cr-C alloy system is demonstrated by the review of 45 literature references concerning various studies of Fe-Cr-C phase diagrams in the phase diagram volume edited by Raynor and Rivlin (Ref 41). The phase equilibria and diagrams for other ternary systems of importance to tool steels have been similarly reviewed and summarized (Ref 41), and a 10-volume set of ternary alloy phase diagrams has been published (Ref 42).

Table 4-4 Free energies of formation of carbides

Carbide	Free energy, kJ/kg·K
TaC	−268
TiC	−180
ZrC	−155
SiC	−51
VC	−50
WC	−35
Cr_7C_3	−30
$Cr_{23}C_6$	−18
Mn_3C	−4
Fe_3C	+6
Co_2C	+7
Ni_3C	+11

Source: Ref 32

Figure 4-27 shows the liquidus surface projection for the iron-rich portion of the Fe-Cr-C system (Ref 41). Constant-temperature contours show the temperatures where solidification of the various phases begins as function of chromium and carbon content. Between the dark, arrowed lines, solidification occurs by the nucleation and growth of a single phase. Along the dark lines, referred to as lines of twofold saturation, solidification occurs by the formation of two phases, and the arrows point in the direction of decreasing temperature. Where three lines of twofold saturation come together, at compositions or points of threefold saturation, solidification proceeds by various reactions that involve four phases: the liquid phase and three solid phases (Ref 1). Table 4-6 identifies the various liquidus reactions in the Fe-Cr-C system and in its three constituent binary systems (Ref 41).

Figure 4-28 shows a schematic isothermal section at 870 °C (1600 °F), based on an experimental study of the Fe-Cr-C system at this temperature (Ref 6). The one- and two-phase fields are labeled, and the three-phase fields are represented as triangles. The corners of the triangles give the compositions of the three coexisting phases. For example, the points J, B, and C give the compositions of γ, M_3C, and M_7C_3, respectively, which coexist in alloys whose compositions are located within the J-B-C triangle. The boundaries of the two-phase fields give the ranges of compositions of the two phases that coexist. For example, the line AB shows that cementite or the carbide M_3C can dissolve chromium up to the level B. When the amount of chromium in an alloy exceeds that amount, the solubility of chromium in the M_3C structure is exceeded, and the excess chromium is accommodated by the formation of the M_7C_3 carbide. Similarly, when the chromium content in an alloy exceeds the amount soluble in the M_7C_3 structure, the excess chromium is accommodated by the formation of the $M_{23}C_6$ carbide crystal structure. Figure 4-28 represents only the phase equilibria at a single temperature. As temperature changes, the boundaries shift or new phases appear as the phase equilibria change. With respect to the hardening of tool steels, the austenite present at austenitizing temperatures, such as 870 °C (1600 °F) transforms to martensite on cooling to room temperature, and whatever carbides are stable at the

Table 4-5 Comparative hardness of some carbides and microstructures found in tool steels

Material	Average hardness(a), HK	Material	Average hardness(b), HRC
Oil-hardening tool steel (60.5 HRC)	790	Matrix of hardened high-speed steel	66.0
Cementite in plain carbon tool steel	1150	$(Fe, W, Mo)_6C$ in high-speed steel	75.2
Cr_7C_3 in high-carbon, high chromium steel	1820	WC in carbide tool bit	82.5
Al_2O_3 in grinding weel	2240	VC in high-carbon, high-vanadium high-speed steel	84.2
VC in high-carbon, high-vanadium steel	2520		

(a) From Ref 34. Indentations made with 25 g load. (b) From Ref 35. Rockwell C hardness converted from 25 g Vickers readings

Table 4-6 Invariant liquidus reactions in the C-Cr-Fe system

System	Symbol	Temperature °C	Temperature °F	Reaction
C-Fe	p_1	1493	2719	$L + \delta Fe \leftrightarrow \gamma Fe$
	e_1	1153	2107	$L \leftrightarrow \gamma Fe + C$
C–Cr	e_2	1490	2714	$L \leftrightarrow (Cr) + Cr_{23}C_6$
	p_2	1520	2768	$L + Cr_7C_3 \leftrightarrow Cr_{23}C_6$
	p_3	1780	3236	$L + Cr_3C_2 \leftrightarrow Cr_7C_3$
	p_4	1895	3443	$L + C \leftrightarrow Cr_3C_2$
Cr-Fe		None		
C-Cr-Fe	U_1	1275	2327	$L + \delta Fe \leftrightarrow M_{23}C_6 + \gamma Fe$
	U_2	1255	2291	$L + M_{23}C_6 \leftrightarrow M_7C_3 + \gamma Fe$
	U_3	1160	2120	$L + M_7C_3 \leftrightarrow M_3C + \gamma Fe$
	U_4	1156	2113	$L + M_3C \leftrightarrow \gamma Fe + C$
	P_1	1230	2246	$L + M_7C_3 + C \leftrightarrow M_3C$
	U_5	1585	2885	$L + M_3C_2 \leftrightarrow M_7C_3 + C$

Source: Ref 41

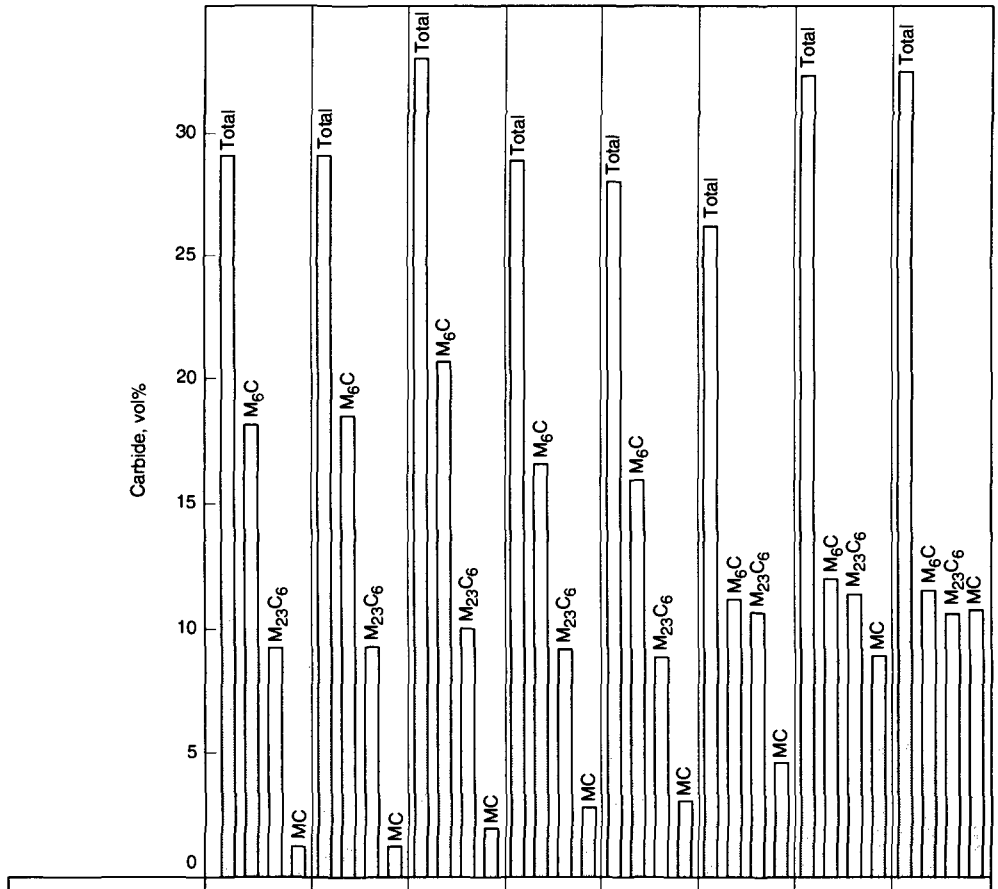

Composition, wt%	18-4-1	18-4-1-5	18-4-2	1.5-9-4-1	6-5-4-2	0-9-4-2	6-5-4-4	12-5-5-5
Austenitizing temperature, °C	1290	1290	1290	1200	1220	1220	1220	1250
AISI steel type	T1	T4	T2	M1	M2	M10	M4	T15

Fig. 4-24 Volume percentages of carbides in high-speed steels as-annealed (white bars) and after austenitizing for hardening (black bars). Compositions of tungsten high-speed steels is given in weight percent as W-Cr-V-Co and of molybdenum high-speed steels as W-Mo-Cr-V. Source: Ref 36, as reproduced in Ref 37

austenitizing temperature are incorporated into the martensitic microstructure.

Figure 4-29 shows a portion of the 870 °C (1600 °F) isothermal section of the Fe-Cr-C system (Ref 6). The nominal compositions of four alloys in which chromium is a major alloying element have been plotted on the isothermal section (Ref 43). The 420 alloy is a martensitic stainless steel sometimes used for tooling applications, and the H13, A2, and D2 steels are tool steels whose complete compositions are given in Table 2-1. All the alloys contain other elements that would shift the boundaries of the phase fields somewhat, but the plotting of the chromium and carbon contents on the isothermal sections demonstrates some of the alloying principles that lead to different classes of tool steels.

The chromium hot-work steel H13 (0.35% C, 5% Cr) must have good toughness; therefore, carbon content is maintained at a level where only a small amount of carbides will form, as indicated by the location of the H13 composition on the boundary of the austenite-M_7C_3 two-phase field in Fig 4-29. The cold-work tool steel A2 (1.0% C, 5% Cr) requires greater wear resistance, as is achieved by increasing the carbon content and thereby increasing the content of M_7C_3 carbides in the microstructure. Even higher wear resistance is achieved by increasing both carbon and chromium in the cold-work tool steel D2 (1.5% C and 12.0% Cr) in order to produce higher volume fractions of M_7C_3 carbides in hardened microstructures. These comments apply only to the microstructural alloy carbide contents that are established by austenitizing. Significant hardening is also produced by chromium and other alloy carbide precipitation in martensite during tempering, but these reactions are established by low-temperature equilibria where ferrite rather than austenite is the stable phase coexisting with the carbides.

References

1. F.N. Rhines, *Phase Diagrams in Physical Metallurgy*, McGraw-Hill, 1956
2. G.F. Vander Voort, *Metallography: Principles and Practice*, McGraw-Hill, 1984
3. B.D. Cullity, *Elements of X-Ray Diffraction*, Addison-Wesley, 1978
4. Powder Diffraction File (PDF), International Centre for Diffraction Data (ICDD), Newton Square, PA
5. M. Waldenstrom, An Experimental Study of Carbide-Austenite Equilibria in Iron-Base Alloys with Mo, Cr, Ni and Mn in the Temperature Range

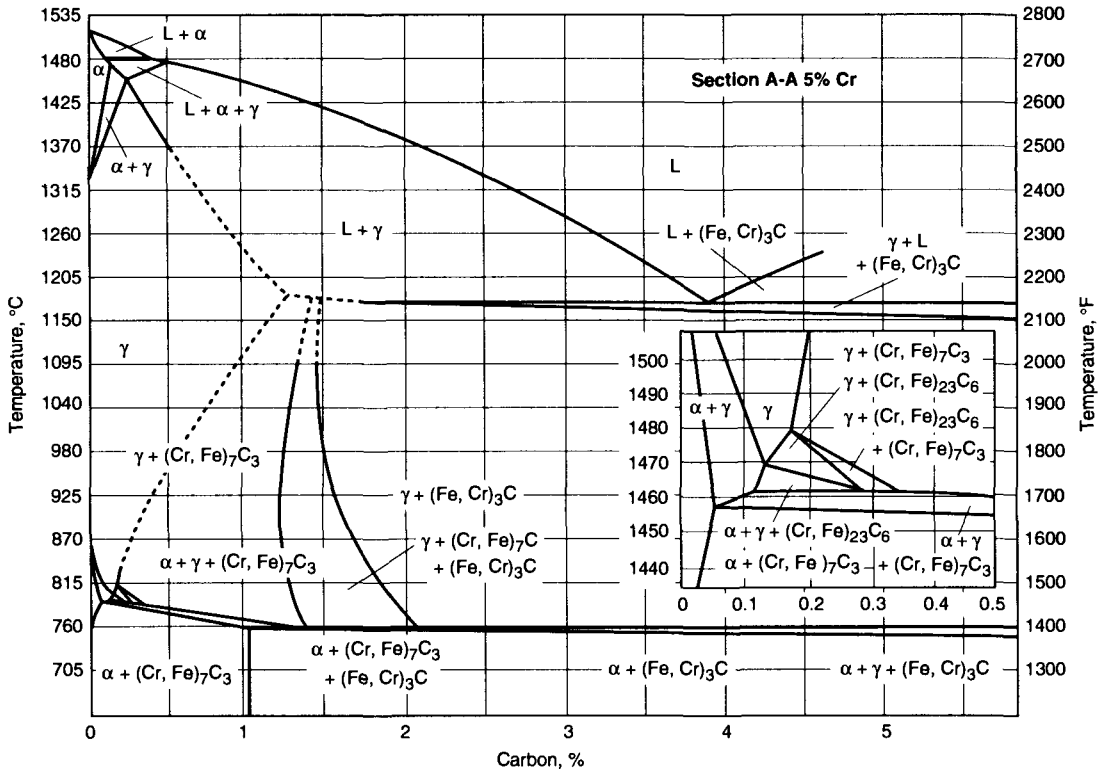

Fig. 4-25 Vertical section of the Fe-C-Cr system at 5% Cr. Source: Ref 40

1173 to 1373 K, *Metall. Trans. A*, Vol 8A, 1977, p 1963–1977
6. L.R. Woodyatt and G. Krauss, Iron-Chromium-Carbon System at 870 C, *Metall. Trans. A*, Vol 7A, 1976, p 983–989
7. J. I. Goldstein, D.E. Newbury, P. Echlin, D.C. Joy, C. Fiori, and E. Lifshin, *Scanning Electron Microscopy and X-ray Microanalysis*, Plenum Press, 1981
8. G.T. Eldis, A Critical Review of Data Sources for Isothermal and Continuous Cooling Transformation Diagrams, *Hardenability Concepts with Applications to Steel*, D.V. Doane and J.S. Kirkaldy, Ed., TMS-AIME, 1978, p 126–148
9. Formation of Microstructures: The Mats Hillert Symposium in Materials Science, *Scand. J. Metall.*, Vol 20, 1991, p 1–124
10. M. Hillert, Prediction of Iron-Base Phase Diagrams, *Hardenability Concepts with Applications to Steel*, D.V. Doane and J.S. Kirkaldy, Ed., TMS-AIME, 1978, p 5–26
11. B. Sundman, Thermodynamic Databanks, Visions and Facts, *Scand. J. Metall.*, Vol 20, 1991, p 79–85
12. B. Sundman, B. Jansson, and J.-O. Andersson, The Thermo-Calc Databank System, *CALPHAD*, Vol 9 (No. 2), 1985, p 153–190
13. *Metallography, Structures and Phase Diagrams*, Vol 8, *Metals Handbook*, 8th ed., American Society for Metals, 1973, p 275, 276
14. Gray and Ductile Iron Castings Handbook, C.F. Walton, Ed., Gray and Ductile Iron Founders' Society, 1971
15. T. Iwamoto, T. Hoshino, K. Amano, and Y. Nakano, An Advanced High Strength Steel for Machining and Cold Forging Uses, *Fundamentals and Applications of Microalloying Forging Steels*, C.J. Van Tyne, G. Krauss, and D.K. Matlock, Ed., TMS, 1996, p 277–286
16. C.S. Barrett, Crystal Structure of Metals, *Metallography, Structures and Phase Diagrams*, Vol 8, *Metals Handbook*, 8th ed., American Society for Metals, p 233–250
17. C. Hammond, *Introduction to Crystallography*, Ox-

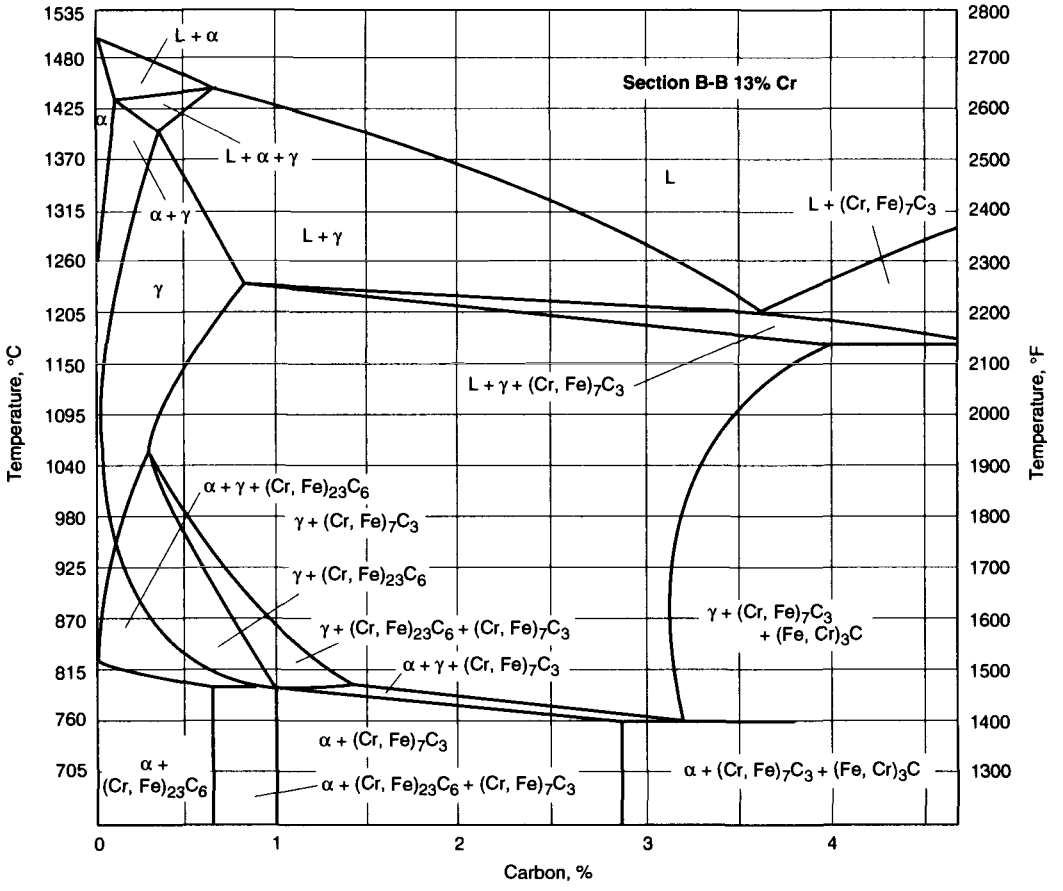

Fig. 4-26 Vertical section of the Fe-C-Cr system at 13% Cr. Source: Ref 40

ford University Press, Oxford, U.K.,1990
18. C.S. Barrett and T.B. Massalski, *Structure of Metals*, 3rd ed., McGraw-Hill, 1966
19. G. Krauss, *Steels: Heat Treatment and Processing Principles*, ASM International, 1990
20. E.C. Bain and H.W. Paxton, *Alloying Elements in Steel*, 2nd ed., American Society for Metals, 1961
21. J.S. Kirkaldy, B. A. Thomson, and E. Baganis, Prediction of Multicomponent Equilibrium and Transformation Diagrams for Low Alloy Steels, *Hardenability Concepts with Applications to Steel*, D.V. Doane and J.S. Kirkaldy, Ed., TMS-AIME, 1978, p 82–119
22. C.M. Wayman, *Introduction to the Crystallography of Martensite Transformations*, Macmillan, 1964
23. G.B. Olson and W.S. Owen, Ed., *Martensite*, ASM International, 1992
24. B.A. Bilby and J.W. Christian, The Crystallography of Martensite Transformations, *J. Iron Steel Inst.*, Vol 197, 1961, p 122–131
25. M. Cohen, The Strengthening of Steel, *Trans. TMS-AIME*, Vol 224, 1962, p 638–656
26. A.R. Marder and G. Krauss, The Morphology of Martensite in Iron-Carbon Alloys, *Trans. ASM*, Vol 60, 1967, p 651–660
27. A.R. Marder and G. Krauss, The Formation of Low-Carbon Martensite in Fe-C Alloys, *Trans. ASM*, Vol 62, 1969, p 957–964
28. J.R.T. Branco, "Development of Nb-Modified AISI H13/H11 Type Tool Steels", Ph.D. thesis, Colorado School of Mines, 1989
29. R. Wilson, *Metallurgy and Heat Treatment of Tool Steels*, McGraw-Hill, London, 1975
30. D.H. Jack and K.H. Jack, Carbides and Nitrides in Steel, *Mater. Sci. Eng.* Vol 11, 1973, p 1–27
31. L.E. Toth, *Transition Metal Carbides and Nitrides*, Academic Press, 1971
32. F.D. Richardson, The Thermodynamics of Metallurgical Carbides and of Carbon in Iron, *J. Iron Steel Inst.*, Vol 175, 1953, p 33
33. H. Brandis, E. Haberling, and H.H. Weigard, Metallurgical Aspects of Carbides in High Speed Steels, *Processing and Properties of High Speed Tool Steels*, M.G.H. Wells and L.W. Lherbier, Ed., TMS-AIME, 1980, p 1–18
34. L.P. Tarasov, The Microhardness of Carbides in Tool Steels, *Met. Prog.*, Vol 54 (No. 6), 1948, p 846
35. P. Leckie-Ewing, A Study of the Microhardness of the Major Carbides in Some High-Speed Steels, *Trans. ASM*, Vol 44, 1952, p 348
36. F. Kayser and M. Cohen, Carbides in High Speed Steel— Their Nature and Quantity, *Met. Prog.*, Vol 61 (No. 6), 1952, p 79
37. H.W. Rayson, Tool Steels, *Constitution and Properties of Steels*, F.B. Pickering, Ed., VCH Publishing, 1992, p 581–640

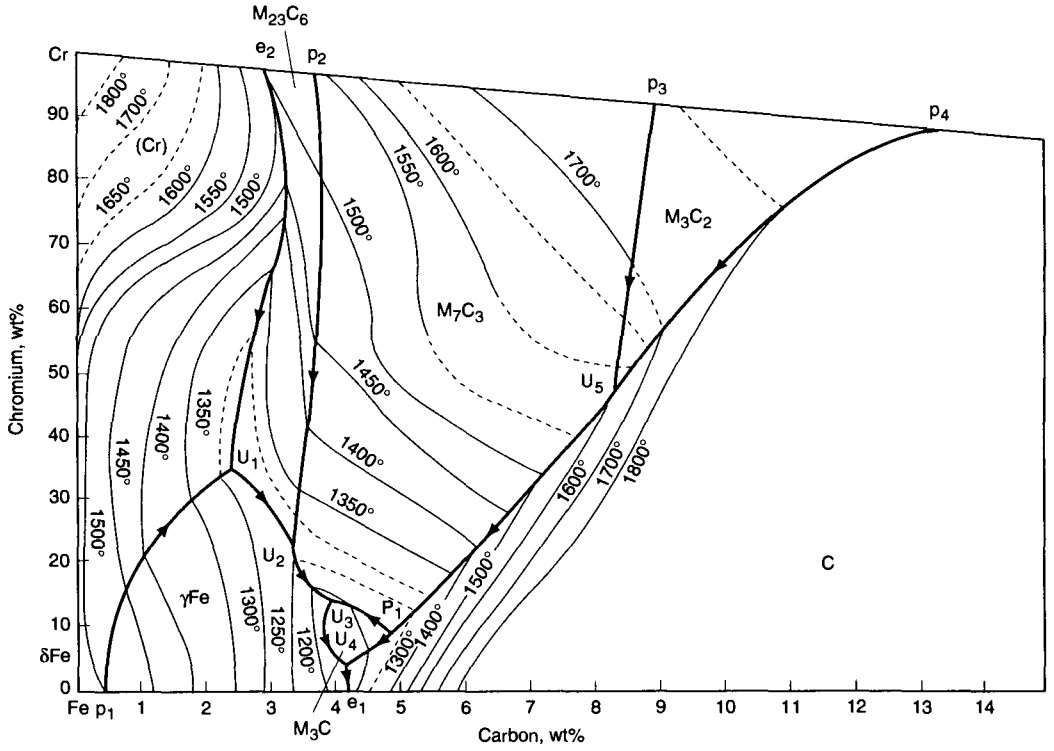

Fig. 4-27 Liquidus surface at iron-rich corner of the Fe-Cr-C system. Temperatures given in degrees centigrade. Source: Ref 41

38. J.-O. Andersson, A Thermodynamic Evaluation of the Fe-Cr-C System, *Metall. Trans. A*, Vol 19A, 1988, p 627–636
39. P. Gustafson, An Experimental Study and a Thermodynamic Evaluation of the Cr-Fe-W System, *Metall. Trans. A*, Vol 19A, 1988, p 2531–2546
40. K. Bungardt, E. Kunze, and E. Horn, Investigation of the Structure of the Iron-Chromium-Carbon System, *Arch. Eisenhüttenwes.*, Vol 29, 1958, p 193
41. G.V. Raynor and V.G. Rivlin, *Phase Equilibria in Iron Ternary Alloys*, Institute of Metals, London, 1988
42. *Handbook of Ternary Alloy Phase Diagrams*, P. Villars, A. Prince, and H. Okamoto, Ed., Vol 1-10, ASM International, 1995
43. J.R.T. Branco and G. Krauss, Heat Treatment and Microstructure of Tool Steels for Molds and Dies, *Tool Materials for Molds and Dies*, G. Krauss and H. Nordberg, Ed., Colorado School of Mines Press, 1987, p 94–117

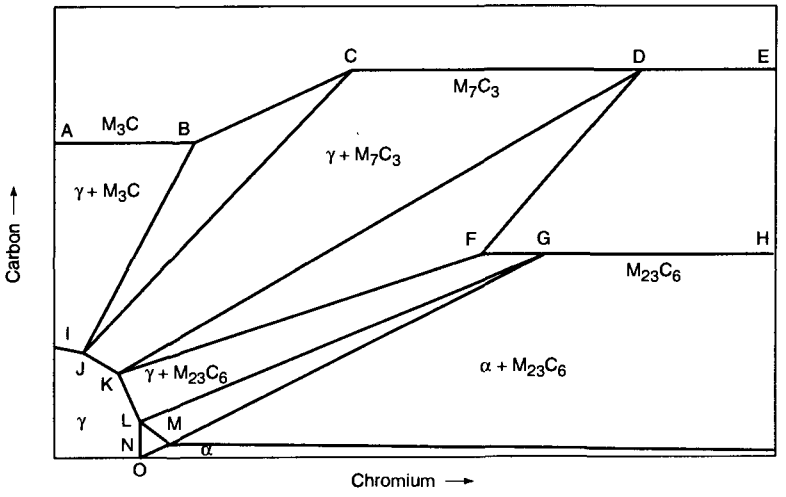

Fig. 4-28 Schematic isothermal section of the Fe-Cr-C system at 870 °C (1600 °F). See text for details. Source: Ref 6

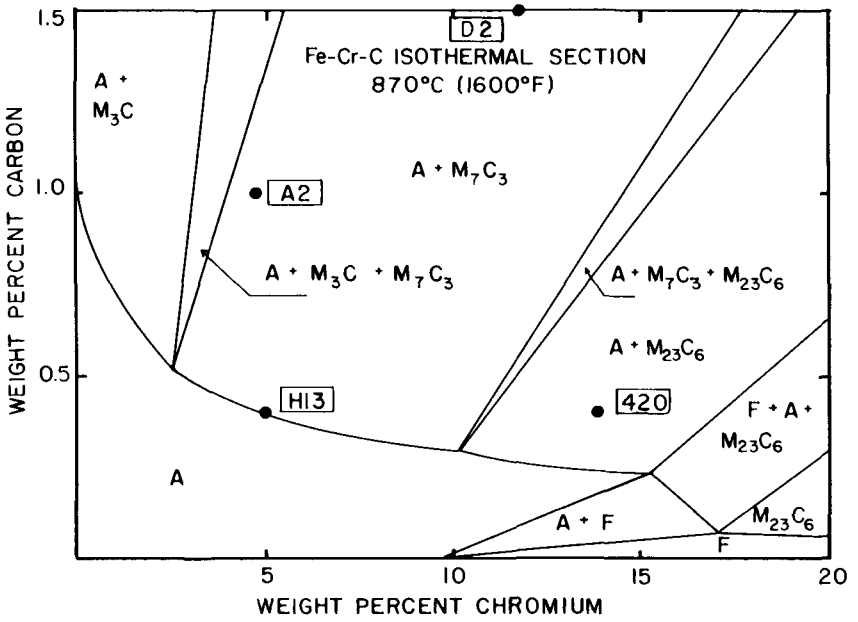

Fig. 4-29 Portion of the 870 °C (1600 °F) isothermal section of the Fe-Cr-C system with approximate compositions of H13, A2, D2, and 420 steels indicated. Source: Ref 6

Tool Steels: 5th Edition
George Roberts, George Krauss, Richard Kennedy, p 67-107
DOI:10.1361/toos1998p067

Copyright © 1998 ASM International®
All rights reserved.
www.asminternational.org

CHAPTER 5
Principles of Tool Steel Heat Treatment

This chapter describes how the phases outlined in Chapter 4 are arranged into desired microstructures during the heat treatment of tool steels. Figures 5-1 and 5-2 show schematic diagrams of the processing steps required to produce finished tool steel products (Ref 1, 2). The repeated cycles of heating to, and cooling from, the temperature ranges where various combinations of phases exist are emphasized. The primary processing associated with the melting, solidification, and breakdown stages of hot work has been described in Chapter 3. The final stages of processing include not only the final hardening heat treatment, but also the hot work and machining that produce the finished shapes and dimensions of tool steel products. The forming operations are performed before the final hardening heat treatment, since the very high final hardness of hardened tool steels makes them essentially unworkable. Only processes such as grinding with highly abrasive materials or electrodischarge machining (Ref 3) can be used to adjust dimensions of hardened tool steels.

Figure 5-3 shows, superimposed on the Fe-C diagram (Ref 4), the temperature ranges for the various heat treatment operations described in this chapter. The Fe-C diagram is used only as a base for discussion; as discussed in Chapter 4, the high carbon and alloy contents of tool steels significantly modify phase equilibria from those of the Fe-C system, and alloy carbides play a much greater role in the evolution of tool steel microstructures than in low-alloy carbon steels. Accommodations for these alloying effects are taken into account in the specific heat treatment temperatures recommended for the vari-

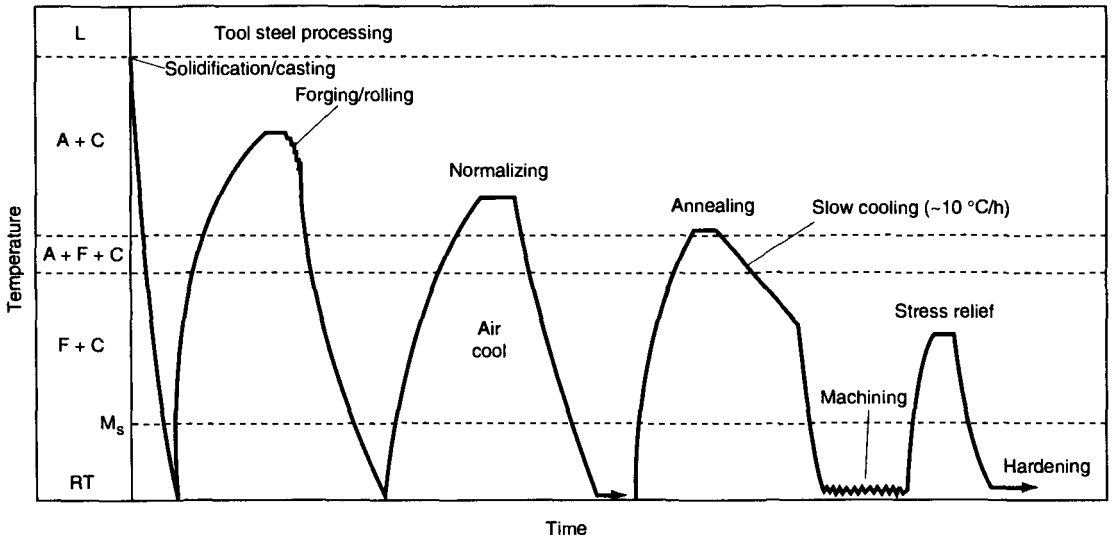

Fig. 5-1 Schematic diagram of tool steel processing and heat treatments prior to final hardening heat treatment. A, austenite; C, carbides; F, ferrite; M, martensite. After Ref 1 and 2

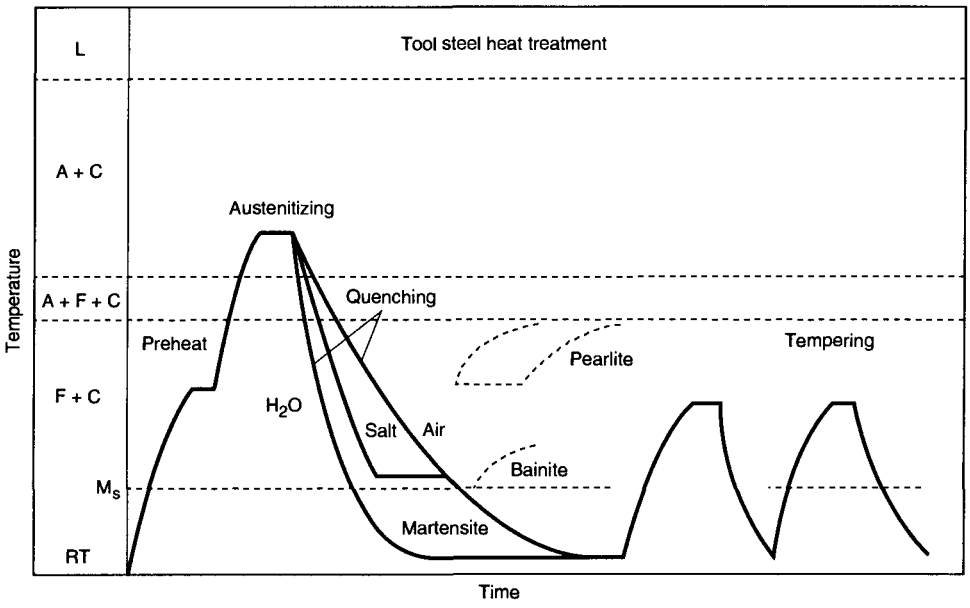

Fig. 5-2 Schematic diagram of tool steel heat treatment steps for final hardening. After Ref 1 and 2

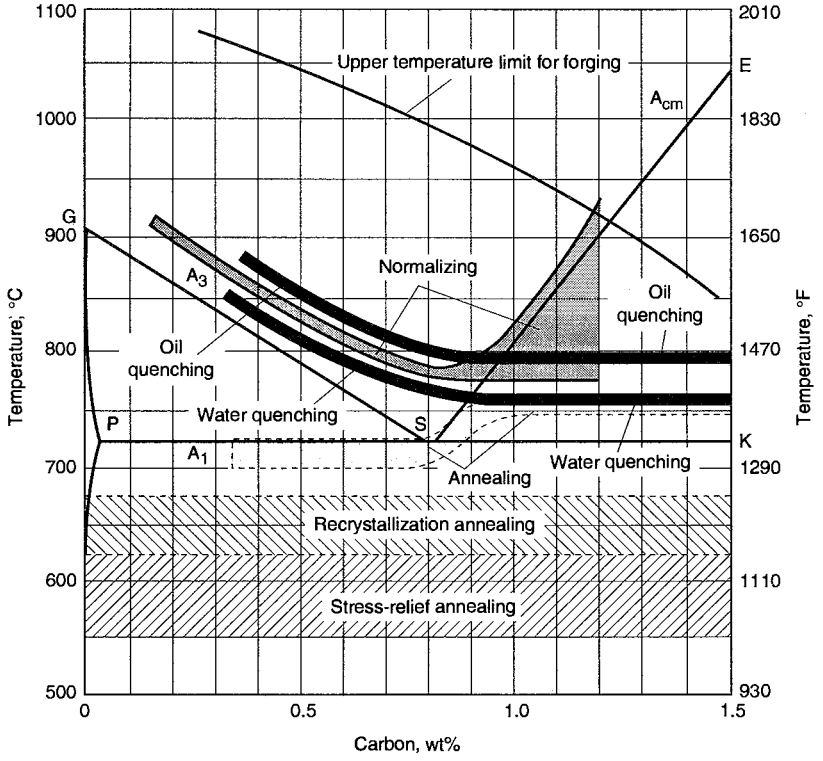

Fig. 5-3 Schematic diagram showing approximate temperature ranges, relative to the Fe-C phase diagram, for various carbor and tool steel heat treatments. Source: Ref 4

ous types and grades of tool steels, as presented elsewhere in this book.

Normalizing

This heat treatment is applied to tool steels that have been forged at high temperatures, as shown in Fig. 5-3. Forging deformation, depending on part geometry, may cause localized variations in microstructure and, because of the high temperatures used, may produce a coarse, austenitic grain structure. Normalizing is performed to produce more uniform, fine-grained microstructures for subsequent annealing and hardening heat treatments. Also, in tool steels with high stable carbide contents, the carbides may be preferentially aligned in the direction of hot work, and normalizing will help to produce more uniform distributions (Ref 4).

Normalizing heat treatments consist of heating to the cross-hatched temperature region shown in Fig. 5-3, then air cooling. As shown, the normalizing temperatures for hypereutectoid steels approach and sometimes exceed A_{cm} temperatures. Therefore, during heating to and holding at the normalizing temperature, austenite grains nucleate and grow from the ferrite-carbide microstructures stable at low temperatures. Considerable carbide dissolution, depending on alloy content, takes place during heating. During cooling, austenite then transforms to mixtures of ferrite and cementite. If the alloy content of a tool steel is low, cementite and pearlitic microstructures will form during air cooling, and the carbides in these structures will be spheroidized in subsequent annealing treatments. In hypereutectoid steels, where the microstructure is completely converted to austenite during normalizing, cementite networks will form on austenite grain boundaries on cooling prior to pearlite formation. An example of carbide network formation on austenitic grain boundaries in a low-alloy, high-carbon steel is shown in Fig. 5-4, and the fracture surface along the grain boundary carbides is shown in Fig. 5-5. The grain-boundary carbides grow by a ledge-type mechanism, and the fracture surface follows the stepped interfaces between the growing carbides and the austenite grains into which the carbides grow (Ref 5).

In tool steels with high alloy content, high hardenability may cause martensite to form during air cooling. Hardenability is the topic which relates alloying to the phase transformations that occur on cooling and is discussed in more detail later in this chapter. Although air hardening in tool steels with high hardenability is a beneficial characteristic during final hardening, martensite formation combined with the high austenitizing temperatures of normalizing may cause cracking, especially if carbide networks that provide pathways for brittle fracture are present. Therefore, air-hardening tool steels usually are not normalized. Table 5-1 (Ref 6) lists normalizing and annealing temperatures for the various classes and grades of tool steels; tool steels that are not normalized are identified.

Stress-Relief Heat Treatments

There are many effects and sources of residual stress in steels. Tensile surface residual stresses are detrimental and may cause cracking during fabrication or reduced resistance to fracture in service, whereas surface compressive stresses are generally beneficial and prevent cracking during manufacture and service. Short of cracking, residual stresses may cause distortion and undesired dimensional changes. A major source of residual stresses during heat treatment is expansion or contraction of surface microstructures at different times than interior microstructures because of differences in surface and interior cooling or heating rates. Control of residual

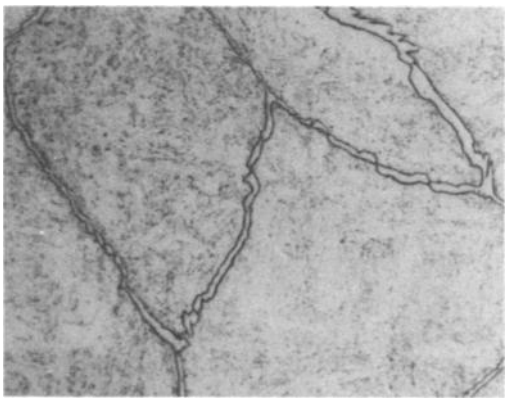

Fig. 5-4 Continuous network of cementite crystals that have formed on austenite grain boundaries in a hypereutectoid Fe-C-Cr alloy. Light micrograph. Source: Ref 5

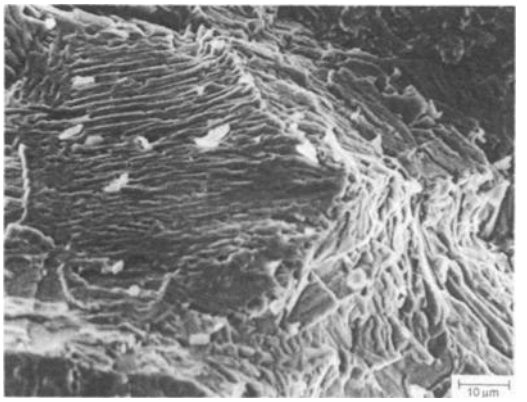

Fig. 5-5 Fracture ledges at interfaces of grain-boundary cementite in an Fe-1.12C-1.50Cr steel. SEM micrograph. Courtesy of T. Ando

Table 5-1 Normalizing and annealing temperatures for tool steels

Type	Normalizing treatment temperature(a) °C	°F	Annealing(b) Temperature °C	°F	Rate of cooling, max °C/h	°F/h	Hardness, HB
Molybdenum high-speed steels							
M1, M10	Do not normalize		815–870	1500–1600	22	40	207–235
M2	Do not normalize		870–900	1600–1650	22	40	212–241
M3, M4	Do not normalize		870–900	1600–1650	22	40	223–255
M6	Do not normalize		870	1600	22	40	248–277
M7	Do not normalize		815–870	1500–1600	22	40	217–255
M30, M33, M34, M36, M41, M42, M46, M47	Do not normalize		870–900	1600–1650	22	40	235–269
M43	Do not normalize		870–900	1600–1650	22	40	248–269
M44	Do not normalize		870–900	1600–1650	22	40	248–293
Tungsten high-speed steels							
T1	Do not normalize		870–900	1600–1650	22	40	217–255
T2	Do not normalize		870–900	1600–1650	22	40	223–255
T4	Do not normalize		870–900	1600–1650	22	40	229–269
T5	Do not normalize		870–900	1600–1650	22	40	235–277
T6	Do not normalize		870–900	1600–1650	22	40	248–293
T8	Do not normalize		870–900	1600–1650	22	40	229–255
T15	Do not normalize		870–900	1600–1650	22	40	241–277
Chromium hot-work steels							
H10, H11, H12, H13	Do not normalize		845–900	1550–1650	22	40	192–229
H14	Do not normalize		870–900	1600–1650	22	40	207–235
H19	Do not normalize		870–900	1600–1650	22	40	207–241
Tungsten hot-work steels							
H21, H22, H25	Do not normalize		870–900	1600–1650	22	40	207–235
H23	Do not normalize		870–900	1600–1650	22	40	212–255
H24, H26	Do not normalize		870–900	1600–1650	22	40	217–241
Molybdenum hot-work steels							
H41, H43	Do not normalize		815–870	1500–1600	22	40	207–235
H42	Do not normalize		845–900	1550–1650	22	40	207–235
High-carbon, high-chromium cold-work steels							
D2, D3, D4	Do not normalize		870–900	1600–1650	22	40	217–255
D5	Do not normalize		870–900	1600–1650	22	40	223–255
D7	Do not normalize		870–900	1600–1650	22	40	235–262
Medium alloy, air-hardening cold-work steels							
A2	Do not normalize		845–870	1550–1600	22	40	201–229
A3	Do not normalize		845–870	1550–1600	22	40	207–229
A4	Do not normalize		740–760	1360–1400	14	25	200–241
A6	Do not normalize		730–745	1350–1375	14	25	217–248
A7	Do not normalize		870–900	1600–1650	14	25	235–262
A8	Do not normalize		845–870	1550–1600	22	40	192–223
A9	Do not normalize		845–870	1550–1600	14	25	212–248
A10	790	1450	765–795	1410–1460	8	15	235–269
Oil-hardening cold-work steels							
O1	870	1600	760–790	1400–1450	22	40	183–212
O2	845	1550	745–775	1375–1425	22	40	183–212
O6	870	1600	765–790	1410–1450	11	20	183–217
O7	900	1650	790–815	1450–1500	22	40	192–217
Shock-resisting steels							
S1	Do not normalize		790–815	1450–1500	22	40	183–229(c)
S2	Do not normalize		760–790	1400–1450	22	40	192–217
S5	Do not normalize		775–800	1425–1475	14	25	192–229
S7	Do not normalize		815–845	1500–1550	14	25	187–223

(continued)

Table 5-1 (continued)

Type	Normalizing treatment temperature(a) °C	°F	Annealing(b) Temperature °C	°F	Rate of cooling, max °C/h	°F/h	Hardness, HB
Mold steels							
P2	Not required		730–815	1350–1500	22	40	103–123
P3	Not required		730–815	1350–1500	22	40	109–137
P4	Do not normalize		870–900	1600–1650	14	25	116–128
P5	Not required		845–870	1550–1600	22	40	105–116
P6	Not required		845	1550	8	15	183–217
P20	900	1650	760–790	1450–1500	22	40	149–179
P21	900	1650	Do not anneal				
Low-alloy special-purpose steels							
L2	870–900	1600–1650	760–790	1400–1450	22	40	163–197
L3	900	1650	790–815	1450–1500	22	40	174–201
L6	870	1600	760–790	1400–1450	22	40	183–212
Carbon-tungsten special-purpose steels							
F1	900	1650	760–800	1400–1475	22	40	183–207
F2	900	1650	790–815	1450–1500	22	40	207–235
Water-hardening steels							
W1, W2	790–925(d)	1450–1700(d)	740–790(e)	1360–1450(e)	22	40	156–201
W5	870–925	1600–1700	760–790	1400–1450	22	40	163–201

(a) Time held at temperature varies from 15 min for small sections to 1 h for large sizes. Cooling is done in still air. Normalizing should not be confused with low-temperature annealing. (b) The upper limit of ranges should be used for large sections and the lower limit for small sections. Time held at temperature varies from 1 h for light sections to 4 h for heavy sections and large furnace charges of high-alloy steel. (c) For 0.25 Si type, 183 to 207 HB; for 1.00 Si type, 207 to 229 HB. (d) Temperature varies with carbon content: 0.60 to 0.75 C, 815 °C (1500 °F); 0.75 to 90 C, 790 °C (1450 °F); 0.90 to 1.10 C, 870 °C (1600 °F); 1.10 to 1.40 C, 870 to 925 °C (1600 to 1700 °F). (e) Temperature varies with carbon content: 0.60 to 0.90 C, 740 to 790 °C (1360 to 1450 °F); 0.90 to 1.40 C, 760 to 790 °C (1400 to 1450 °F)

stresses during the various stages of hardening is a major consideration in all phases of the heat treatment of tool steels.

In tool steels, residual stress-relief treatments are most commonly performed following machining and grinding operations to shape a finished tool. These operations may introduce plastic deformation and high surface strains, typically in annealed, machinable ferrite-carbide microstructures, which on subsequent hardening may cause distortion and cracking. Grinding operations applied to hardened tools with tempered martensitic microstructures, or to tools that have been work hardened in service, may also cause cracking and high residual stresses before or during service (Ref 6). To maintain hardness, stress-relief treatments on reground tool steels should be performed at temperatures at or below the tempering temperatures used to produce the required hardness of the tool.

Stress-relief heat treatments, as shown in Fig. 5-3, are applied at temperatures where ferrite and carbides are stable, and therefore do not cause austenite formation and subsequent transformation. Often the objective of the stress relief is to reduce only the residual stresses introduced into the ferrite by cold work or machining, without causing significant changes in hardness. As a result, the stress relief is accomplished primarily by recovery mechanisms that reduce and rearrange the crystal defects introduced into ferrite by surface deformation. The defects by which plastic deformation of metal crystals is accomplished are known as dislocations. Dislocations are linear arrays of atoms displaced from equilibrium atom positions of perfect crystals and, if present in high densities, introduce work hardening and significant strain energy into a microstructure (Ref 7).

For highly strained surfaces, recrystallization—which eliminates the crystal defects by the nucleation of new, dislocation-free crystals and significantly lowers the cold-worked hardness—may occur during heating. Recrystallization requires an incubation time in order to develop the nuclei of the strain-free grains (Ref 7). In contrast, recovery mechanisms begin immediately as the stress-relief temperature is reached and stop short of recrystallization. Recovery rates are highest at the beginning of the stress-relief treatment and decrease with increasing time at temperature. Therefore, stress-relief heat treatments are generally of short duration (1 to 2 h) or, in larger sections, 1 h/25 mm (1 in.) of section thickness (Ref 4, 8).

The temperatures for stress-relief heat treatments are typically between 550 and 650 °C (1020 and 1200 °F) for plain carbon and low-alloy steels and between 600 and 750 °C (1110 and 1380 °F) for

hot-work and high-speed steels (Ref 4). As noted earlier, stress relief is also a function of time at temperature, but generally temperature has a much stronger effect on the kinetics of stress relief than does time. Studies showing the interrelationships of time and temperature on stress relief have been published (Ref 4, 9). Heavy sections should be cooled very slowly from stress-relief temperatures to at least 300 °C (570 °F) (Ref 4) and then air cooled. Otherwise, distortion and new residual stresses may be introduced due to uneven cooling of surfaces and interiors, especially at temperatures just below the stress-relief temperature where the flow stresses of the microstructure are low.

Annealing

Annealing heat treatments are designed to soften tool steel microstructures, primarily for the machining stages of manufacture, but also to provide microstructural uniformity for subsequent hardening heat treatments. The softening demonstrates the great versatility of carbon-base tool steels, which can be sequentially heat treated to produce machinable annealed microstructures with very low hardness followed by hardening to essentially unworkable microstructures of very high hardness. Table 5-1 lists annealing temperatures and resulting hardness ranges for the various types of tool steels and shows that, although many tool steels may not be normalized, almost all tool steels are subjected to annealing.

Figure 5-1 shows schematically the location of annealing in the manufacturing sequence for tool steels, and Fig. 5-3 shows that, in high-carbon steels, annealing temperatures are low in the austenite-carbide two-phase field. Very slow rates of furnace cooling from the annealing temperatures, from 8 to 22 °C/h (14 to 40 °F/h) depending on steel composition, as shown in Table 5-1, are also a necessary part of annealing. When a steel cools to 500 °C (930 °F), essentially all transformation is completed, and air cooling can be used to bring the steel to room temperature. Controlled-atmosphere furnaces, salt baths, and vacuum furnaces used to protect tool steels from oxidation and decarburization during annealing are described in Ref 10 and Chapter 6.

The microstructural objective of annealing is to produce dispersed, spherical carbides in a matrix of ferrite grains, a microstructure that is highly machinable compared to other microstructures formed in tool steels. Ferrite has low strength, and the continuous ferrite matrix easily deforms. Thus, with the assistance of the dispersed carbide particles, a spheroidized microstructure readily deforms and fractures in shear during chip formation in machining operations. Figure 5-6 shows the annealed microstructure of a high-carbon steel with spheroidized carbides of uniform size dispersed in ferrite, and Fig. 5-7 shows the annealed microstructure of a D2 tool steel with distributions of spheroidized carbides of two sizes. The larger particles are primary M_7C_3 carbides, which by virtue of the high alloy content of the D2 steel have formed during solidification and have been dispersed during hot working. The finer carbides, similar to those in Fig. 5-5, are a result of secondary carbide precipitation in austenite or spheroidization of carbides produced by the transformation of austenite to ferrite-carbide microstructures on cooling after earlier hot-work or normalizing heat treatments.

Several stages of microstructural change control the development of spheroidized carbide-ferrite microstructures during annealing: initiation of carbide spheroidization in ferrite during heating, austenite formation, spheroidization and coarsening of carbides in austenite, and transformation of the austenite on cooling to a matrix of ferrite with dispersed spherical carbides. Spheroidization is driven by the reduction of interfacial energy of carbide

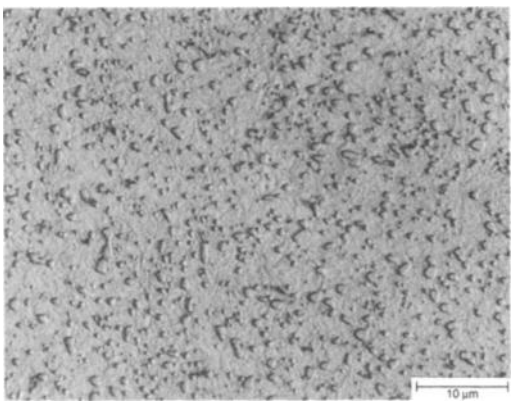

Fig. 5-6 Uniform distribution of spheroidized carbides in a 52100 steel. Light micrograph. Courtesy of K. Hayes

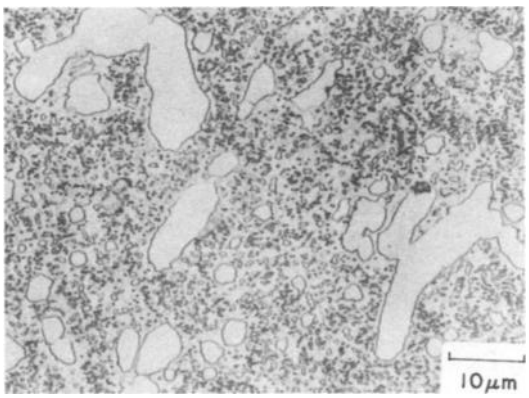

Fig. 5-7 Annealed microstructure of D2 tool steel showing distributions of coarse and fine spheroidized carbide particles. Light micrograph. Courtesy of J.R.T. Branco

particles in a matrix of ferrite or austenite. Spherical particles are the geometrical shapes which have minimum interfacial area per unit volume; therefore, to minimize interfacial energy, two-phase microstructures, given sufficient time, will evolve to form dispersions of spherical particles of the minority phase in a matrix of the majority phase. In steels, the first step in this process is the formation of spheroidized particles in ferrite-carbide microstructures present at the start of annealing (Ref 11).

The starting microstructure may consist of the lamellar or plate-shaped particles of cementite in pearlite that may have formed after cooling from a previous hot-working or normalizing operation. Alternatively, the starting microstructure may consist of bainite, another fine mixture of ferrite and carbides, or martensite. All the starting microstructures may also contain coarse primary or precipitated secondary carbides if the alloy content is high enough. Thus, the first step of spheroidization will produce a distribution of very fine spheroidized particles from the pearlitic, bainitic, or martensitic starting structures and, depending on alloy content, a distribution of coarser alloy carbide particles, much like that illustrated in Figure 5-7.

Austenite formation on heating to annealing temperatures is quite rapid. For example, in an AISI 52100 steel—a low-alloy, high-carbon steel containing nominally 1.0% C and 1.5% Cr—austenite formation was complete after 5 s at 850 °C (1560 °F) (Ref 12). In this study, the starting structure consisted of pearlite; as the austenite grains nucleated and grew, the lamellar carbides spheroidized and partially dissolved, leaving a dispersion of very fine cementite particles in austenite to start the balance of the annealing process.

When steel has reached an appropriate intercritical temperature (i.e., a temperature between A_1 and A_{cm} where austenite and carbides are stable), annealing proceeds by the replacement of fine carbide particles with fewer, larger particles in the austenite matrix, again a process of microstructural change driven by the reduction of interfacial energy. This process is often referred to as Ostwald ripening (Ref 13) and depends on the diffusion of carbon and alloying element atoms away from the small particles, through the austenitic matrix, to the larger particles. The dissolution of carbides that leads to coarsening thus depends on carbon diffusion and, for alloy carbides, on diffusion of the substitutional alloying elements (Ref 14, 15). Carbide dissolution and coarsening continue with increasing time at temperature and are accelerated by high-temperature annealing where diffusion coefficients are high. The study of carbide spheroidization in AISI 52100 steel showed that carbides on austenite grain boundaries coarsen most rapidly (Ref 12, 16), consistent with higher diffusion rates along grain boundaries in comparison to volume diffusion rates within grains (Ref 17).

Another key microstructural change associated with the development of spheroidized carbide-ferrite microstructures concerns the transformation of austenite on cooling from annealing temperatures. As the Fe-C diagram shows, the austenite must transform to a mixture of ferrite and carbides. In the absence of carbide particles, the austenite on slow cooling will transform to pearlite, a lamellar mixture of ferrite and cementite. However, if dispersed carbides are present, pearlite does not nucleate and grow; instead, further spheroidization and growth of the carbides take place as the austenite transforms to ferrite and additional carbides. It is this change in the transformation mechanism of the austenite which necessitates that annealing temperatures be kept low enough to ensure that sufficient spheroidized carbides are present at the start of cooling to nucleate additional spherical carbide growth on furnace cooling.

Hardening: Introductory Considerations

Hardening of tool steels, as shown in Fig. 5-2, is accomplished by three heat-treating steps: austenitizing, cooling or quenching for martensite formation, and tempering. Each heat treatment step produces major changes in microstructure, which when properly controlled lead to the final properties required for a given application. However, the microstructural changes contribute to and are accomplished within a framework of dimensional changes. These changes must also be understood and controlled in order to minimize distortion, residual stresses, and possibly cracking during the final stages of heat treatment. In view of the practical importance of dimensional changes, they are described in some detail here to provide background for the heat treatment considerations covered in subsequent sections.

Figure 5-8 shows the changes in dimensions that occur during the heating and cooling of a 1.0% C steel. Similar changes develop in all steels, but at temperatures that vary depending on chemical composition and type of steel. Thermal expansion occurs on heating to the Ac_1 temperature for the steel. At that point, contraction occurs as austenite, with its close-packed crystal structure, replaces ferrite, with its more open crystal structure (see Chapter 4). When the ferrite is completely replaced by austenite, thermal expansion again occurs with continued heating of austenite and any residual carbides.

On cooling, the austenite and carbide microstructure contracts. If the cooling rate is low, as is the case for annealing, the austenite starts to transform to ferrite and additional carbides at the Ar_1

temperature for the steel. The formation of the ferrite-carbide microstructure causes expansion, as shown by the dashed line in Fig. 5-8, and when austenite transformation to ferrite and cementite is complete, thermal contraction again occurs. If the transformation of ferrite-carbide microstructures is suppressed by rapid cooling or alloying, the austenite remains stable and continues to thermally contract, as shown by line 2 in Fig. 5-8. Eventually, at the M_s temperature for the steel, martensite forms, and significant low-temperature expansion occurs as the bct crystal structure of martensite replaces austenite. The densities and thermal expansion characteristics of tool steels are alloy dependent, and Table 5-2 lists these properties for selected tool steels.

The following sections describe the microstructural changes that are the objectives of the austenitizing, quenching, and tempering steps of tool steel hardening. Processing considerations related to the achievement of desired microstructures and the control of dimensional changes will also be discussed. The great variations of chemical composition of the various types of tool steels cause the microstructural changes to be accomplished at a variety of temperature ranges and heating and cooling conditions; the specific heat treatment parameters recommended for each class of tool steels are given in Table 5-3 and in later chapters.

Austenitizing for Hardening

Austenitizing for hardening is accomplished by heating the spheroidized carbide-ferrite microstructures of tool steels to an appropriate austenitizing temperature. Figure 5-3, and Fig. 5-9 which emphasizes hypereutectoid steels, show that austenitizing for hardening is performed at temperatures in the austenite-carbide two-phase field. As noted in Chapter 4, the use of the Fe-C diagram for alloyed tool steels is only approximate, and the austenite-carbide two-phase field may be considerably expanded to lower carbon contents and higher temperatures by the strong carbide-forming elements commonly used for tool steels. Except for the very highly alloyed high-speed tool steels, hardening temperatures for tool steels are generally in the same range as annealing temperatures, and the comments regarding carbide particle spheroidization, dissolution, and coarsening, as discussed earlier in terms of annealing, are also valid for austenitizing for hardening.

The very first consideration regarding the austenitizing of tool steels is the need for preheating many of the highly alloyed grades. As noted in the discussion relative to Fig. 5-8, an annealed tool steel microstructure will thermally expand on heating to the austenitizing temperature and will contract dur-

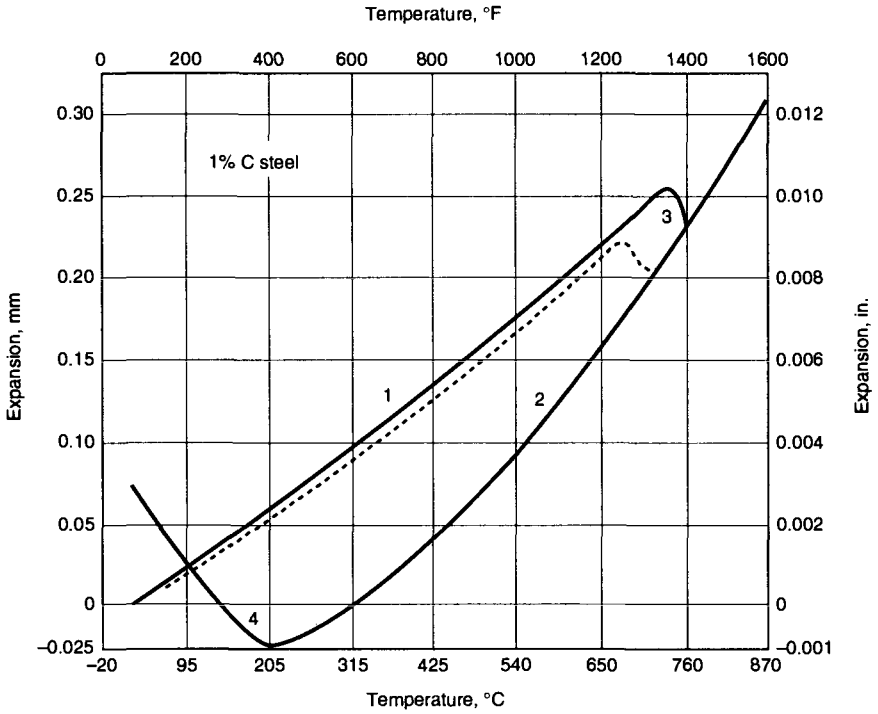

Fig. 5-8 Dilation of a 1% C steel on heating and either slow cooling (dashed line) or quenching (solid line)

ing austenite formation. If the temperature of a part is not uniform, as a result of temperature differences between the surface and interior, the dimensional changes occur at different times as a function of position, and localized volume changes may cause stresses to be generated. For example, rapidly expanding regions, by virtue of position and higher temperatures, will cause tensile stresses to be exerted on regions that have not expanded as rapidly. These stresses may cause plastic flow or distortion

Table 5-2 Density and thermal expansion of selected tool steels

	Density		Thermal expansion									
			µm/m K from 20 °C to					µin/in. °F from 70 °F to				
Type	g/cm^3	lb/in.^{3}	100 °C	200 °C	425 °C	540 °C	650 °C	200 °F	400 °F	800 °F	1000 °F	1200 °F
W1	7.84	0.282	10.4	11.0	13.1	13.8(a)	14.2(b)	5.76	6.13	7.28	7.64(a)	7.90(b)
W2	7.85	0.283	...	...	14.4	14.8	14.9	...	...	8.0	8.2	8.3
S1	7.88	0.255	12.4	12.6	13.5	13.9	14.2	6.9	7.0	7.5	7.7	7.9
S2	7.79	0.281	10.9	11.9	13.5	14.0	14.2	6.0	6.6	7.5	7.8	7.9
S5	7.76	0.280	...	...	12.6	13.3	13.7	...	...	7.0	7.4	7.6
S6	7.75	0.279	...	...	12.6	13.3	...	...	...	7.0	7.4	...
S7	7.76	0.280	...	12.6	13.3	13.7(a)	13.3	...	7.0	7.4	7.6(a)	7.4
O1	7.85	0.283	...	10.6(c)	12.8	14.0(d)	14.4(d)	...	5.9(c)	7.1	7.8(d)	8.0(d)
O2	7.66	0.277	11.2	12.6	13.9	14.6	15.1	6.2	7.0	7.7	8.1	8.4
O6	7.70	0.277	...	11.2	12.6	12.9	13.7	...	6.2	7.0	7.2	7.6
O7	7.8	0.282	...	...	...	...	...	...	...	...	...	...
A2	7.86	0.284	10.7	10.6(c)	12.9	14.0	14.2	5.96	5.91(c)	7.2	7.8	7.9
A6	7.84	0.283	11.5	12.4	13.5	13.9	14.2	6.4	6.9	7.5	7.7	7.9
A7	7.66	0.277	...	...	12.4.	12.9	13.5	...	...	6.9	7.2	7.5
A8	7.87	0.284	...	...	12.0	12.4	12.6	...	...	6.7	6.9	7.0
A9	7.78	0.281	...	...	12.0	12.4	12.6	...	...	6.7	6.9	7.0
A10	7.68	0.278	12.8	13.3	...	...	...	7.1	7.4	...	...	...
D2	7.70	0.278	10.4	10.3	11.9	12.2	12.2	5.8	5.7	6.6	6.8	6.8
D3	7.70	0.278	12.0	11.7	12.9	13.1	13.5	6.7	6.5	7.2	7.3	7.5
D4	7.70	0.278	...	...	12.4	...	...	...	...	6.9	...	...
D5	...	...	...	...	...	12.0	...	...	...	...	6.7	...
H10	7.81	0.281	...	...	12.2	13.3	13.7	...	...	6.8	7.4	7.6
H11	7.75	0.280	11.9	12.4	12.8	12.9	13.3	6.6	6.9	7.1	7.2	7.4
H13	7.76	0.280	10.4	11.5	12.2	12.4	13.1	5.8	6.4	6.8	6.9	7.3
H14	7.89	0.285	11.0	...	...	...	...	6.1	...	...	...	...
H19	7.98	0.288	11.0	11.0	12.0	12.4	12.9	6.1	6.1	6.7	6.9	7.2
H21	8.28	0.299	12.4	12.6	12.9	13.5	13.9	6.9	7.0	7.2	7.5	7.7
H22	8.36	0.302	11.0	...	11.5	12.0	12.4	6.1	...	6.4	6.7	6.9
H26	8.67	0.313	...	...	...	12.4	...	...	...	...	6.9	...
H42	8.15	0.295	...	...	...	11.9	...	...	...	...	6.6	...
T1	8.67	0.313	...	9.7	11.2	11.7	11.9	...	5.4	6.2	6.5	6.6
T2	8.67	0.313	...	...	...	...	...	...	...	...	...	...
T4	8.68	0.313	...	...	...	11.9	...	...	...	...	6.6	...
T5	8.75	0.316	11.2	...	...	11.5	...	6.2	...	...	6.4	...
T6	8.89	0.321	...	...	...	...	...	...	...	...	...	...
T8	8.43	0.305	...	...	...	...	...	...	...	...	...	...
T15	8.19	0.296	...	9.9	11.0	11.5	...	...	5.5(c)	6.1	6.4	...
M1	7.89	0.285	...	10.6(c)	11.3	12.0	12.4	...	5.9(c)	6.3	6.7	6.9
M2	8.16	0.295	10.1	9.4(c)	11.2	11.9	12.2	5.6	5.2(c)	6.2	6.6	6.8
M3, class 1	8.15	0.295	...	...	11.5	12.0	12.2	...	...	6.4	6.7	6.8
M3, class 2	8.16	0,295	...	...	11.5	12.0	12.8	...	...	6.4	6.7	7.1
M4	7.97	0.288	...	9.5(c)	11.2	12.0	12.2	...	5.3(c)	6.2	6.7	6.8
M7	7.95	0.287	...	9.5(c)	11.5	12.2	12.4	...	5.3(c)	6.4	6.8	6.9
M10	7.88	0.255	...	...	11.0	11.9	12.4	...	...	6.1	6.6	6.9
M30	8.01	0.289	...	...	11.2	11.7	12.2	...	...	6.2	6.5	6.8
M33	8.03	0.290	...	...	11.0	11.7	12.0	...	...	6.1	6.5	6.7
M36	8.18	0.296	...	...	...	...	...	...	...	...	...	...
M41	8.17	0.295	...	9.7	10.4	11.2	...	...	5.4	5.8	6.2	...
M42	7.98	0.288	...	...	...	...	...	...	...	...	...	...
M46	7.83	0.283	...	...	...	...	...	...	...	...	...	...
M47	7.96	0.288	10.6	11.0	11.9	...	12.6	5.9	6.1	6.6	...	7.0
L2	7.86	0.284	...	...	14.4	14.6	14.8	...	...	8.0	8.1	8.2
L6	7.86	0.284	11.3	12.6	12.6	13.5	13.7	6.3	7.0	7.0	7.5	7.6
P2	7.86	0.284	...	...	13.7	...	...	...	...	7.6	...	...
P5	7.80	0.282	...	...	...	...	...	...	...	...	...	...
P6	7.85	0.284	...	...	...	...	...	...	...	...	...	...
P20	7.85	0.284	...	...	12.8	13.7	14.2	...	...	7.1	7.6	7.9

(a) From 20 °C to 500 °C (70 °F to 930 °F). (b) From 20 °C to 600 °C (70 °F to 1110 °F). (c) From 20 °C to 260 °C (70 °F to 500 °F). (d) From 40 °C (100 °F)

Table 5-3 Hardening and tempering temperatures and procedures for tool steels

Type	Rate of heating	Hardening: Preheat temperature °C	Hardening: Preheat temperature °F	Hardening: Hardening temperature °C	Hardening: Hardening temperature °F	Time at temperature, min	Quenching medium(a)	Tempering temperature °C	Tempering temperature °F
Molybdenum high-speed steels									
M1, M7, M10	Rapidly from preheat	730–845	1350–1550	1175–1220	2150–2225(b)	2–5	O, A, or S	540–595(c)	1000–1100(c)
M2	Rapidly from preheat	730–845	1350–1550	1190–1230	2175–2250(b)	2–5	O, A, or S	540–595(c)	1000–1100(c)
M3, M4, M30, M33, M34	Rapidly from preheat	730–845	1350–1550	1205–1230(b)	2200–2250(b)	2–5	O, A, or S	540–595(c)	1000–1100(c)
M6	Rapidly from preheat	790	1450	1175–1205(b)	2150–2200(b)	2–5	O, A, or S	540–595(c)	1000–1100(c)
M36	Rapidly from preheat	730–845	1350–1550	1220–1245(b)	2225–2275(b)	2–5	O, A, or S	540–595(c)	1000–1100(c)
M41	Rapidly from preheat	730–845	1350–1550	1190–1215(b)	2175–2220(b)	2–5	O, A, or S	540–595(d)	1000–1100(d)
M42	Rapidly from preheat	730–845	1350–1550	1190–1210(b)	2175–2210(b)	2–5	O, A, or S	540–595(d)	950–1100(d)
M43	Rapidly from preheat	730–845	1350–1550	1190–1215(b)	2175–2220(b)	2–5	O, A, or S	540–595(d)	950–1100(d)
M44	Rapidly from preheat	730–845	1350–1550	1200–1225(b)	2190–2240(b)	2–5	O, A, or S	540–625(d)	1000–1160(d)
M46	Rapidly from preheat	730–845	1350–1550	1190–1220(b)	2175–2225(b)	2–5	O, A, or S	525–565(d)	975–1050(d)
M47	Rapidly from preheat	730–845	1350–1550	1180–1205(b)	2150–2200(b)	2–5	O, A, or S	525–595(d)	975–1100(d)
Tungsten high-speed steels									
T1, T2, T4, T8	Rapidly from preheat	815–870	1500–1600	1260–1300(b)	2300–2375(b)	2–5	O, A, or S	540–595(c)	1000–1100(c)
T5, T6	Rapidly from preheat	815–870	1500–1600	1275–1300(b)	2325–2375(b)	2–5	O, A, or S	540–595(c)	1000–1100(c)
T15	Rapidly from preheat	815–870	1500–1600	1205–1260(b)	2200–2300(b)	2–5	O, A, or S	540–650(d)	1000–1200(d)
Chromium hot-work steels									
H10	Moderately from preheat	815	1500	1010–1040	1850–1900	15–40(e)	A	540–650	1000–1200
H11, H12	Moderately from preheat	815	1500	995–1025	1825–1875	15–40(e)	A	540–650	1000–1200
H13	Moderately from preheat	815	1500	995–1040	1825–1900	15–40(e)	A	540–650	1000–1200
H14	Moderately from preheat	815	1500	1010–1065	1850–1950	15–40(e)	A	540–650	1000–1200
H19	Moderately from preheat	815	1500	1095–1205	2000–2200	2–5	A or O	540–705	1000–1300
Molybdenum hot-work steels									
H41, H43	Rapidly from preheat	730–845	1350–1550	1095–1190	2000–2175	2–5	O, A, or S	565–650	1050–1200
H42	Rapidly from preheat	730–845	1350–1550	1120–1220	2050–2225	2–5	O, A, or S	565–650	1050–1200
Tungsten hot-work steels									
H21, H22	Rapidly from preheat	815	1500	1095–1205	2000–2200	2–5	A or O	595–675	1100–1250
H23	Rapidly from preheat	845	1550	1205–1260	2200–2300	2–5	O	650–815	1200–1500

(continued)

(a) O, oil quench; A, air cool; S, salt bath quench; W, water quench; B, brine quench. (b) When the high-temperature heating is carried out in a salt bath, the range of temperatures should be about 15 °C (25 °F) lower than given in this line. (c) Double tempering recommended for not less than 1 h at temperature each time. (d) Triple tempering recommended for not less than 1 h at temperature each time. (e) Times apply to open-furnace heat treatment. For pack hardening, a common rule is to heat 1.2 min/mm (30 min/in.) of cross section of the pack. (f) Preferable for large tools to minimize decarburization. (g) Carburizing temperature. (h) After carburizing. (i) Carburized case hardness. (j) P21 is a precipitation-hardening steel having a thermal treatment that involves solution treating and aging rather than hardening and tempering. (k) Recommended for large tools and tools with intricate sections

Table 5-3 (continued)

Type	Rate of heating	Hardening: Preheat temperature °C	Hardening: Preheat temperature °F	Hardening: Hardening temperature °C	Hardening: Hardening temperature °F	Time at temperature, min	Quenching medium(a)	Tempering temperature °C	Tempering temperature °F
Tungsten hot-work steels (continued)									
H24	Rapidly from preheat	815	1500	1095–1230	2000–2250	2–5	O	565–650	1050–1200
H25	Rapidly from preheat	815	1500	1150–1260	2100–2300	2–5	A or O	565–675	1050–1250
H26	Rapidly from preheat	870	1600	1175–1260	2150–2300	2–5	O, A, or S	565–675	1050–1250
Medium-alloy, air-hardening cold-work steels									
A2	Slowly	790	1450	925–980	1700–1800	20–45	A	175–540	350–1000
A3	Slowly	790	1450	955–980	1750–1800	25–65	A	175–540	350–1000
A4	Slowly	675	1250	815–870	1500–1600	20–45	A	175–425	350–800
A6	Slowly	650	1200	830–870	1525–1600	20–45	A	150–425	350–800
A7	Very slowly	815	1500	955–980	1750–1800	30–60	A	150–540	300–1000
A8	Slowly	790	1450	980–1010	1800–1850	20–45	A	175–595	350–1100
A9	Slowly	790	1450	980–1025	1800–1875	20–45	A	510–620	950–1150
A10	Slowly	650	1200	790–815	1450–1500	30–60	A	175–425	350–800
Oil-hardening cold-work steels									
O1	Slowly	650	1200	790–815	1450–1500	10–30	O	175–260	350–500
O2	Slowly	650	1200	760–800	1400–1475	5–20	O	175–260	350–500
O6	Slowly	...	...	790–815	1450–1500	10–30	O	175–315	350–600
O7	Slowly	650	1200	790–830 845–885	W: 1450–1525 O: 1550–1625	10–30	O or W	175–290	350–550
Shock-resisting steels									
S1	Slowly	...	...	900–955	1650–1750	15–45	O	205–650	400–1200
S2	Slowly	650(f)	1200(f)	845–900	1550–1650	5–20	B or W	175–425	350–800
S5	Slowly	760	1400	870–925	1600–1700	5–20	O	175–425	350–800
S7	Slowly	650–705	1200–1300	925–955	1700–1750	15–45	A or O	205–620	400–1150
Mold steels									
P2	...	900–925(g)	1650–1700(g)	830–845(h)	1525–1550(h)	15	O	175–260	350–500
P3	...	900–925(g)	1650–1700(g)	800–830(h)	1475–1525(h)	15	O	175–260	350–500
P4	...	970–995(g)	1775–1825(g)	970–995(h)	1775–1825(h)	15	A	175–480	350–500
P5	...	900–925(g)	1650–1700(g)	845–870(h)	1550–1600(h)	15	O or W	175–260	350–500
P6	...	900–925(g)	1650–1700(g)	790–815(h)	1450–1500(h)	15	A or O	175–230	350–450
P20	...	870–900(h)	1600–1650(h)	815–870	1500–1600	15	O	480–595(i)	900–1100
P21(j)	Slowly	Do not preheat		705–730	1300–1350	60–180	A or O	510–550	950–1025
Low-alloy special-purpose steels									
L2	Slowly	...	...	W: 790–845 O: 845–925	W: 1450–1550 O: 1550–1700	10–30	O or W	175–540	350–1000
L3	Slowly	...	...	W: 775–815 O: 815–870	W: 1425–1500 O: 1500–1600	10–30	O or W	175–315	350–600
L4	Slowly	...	...	790–845	1450–1550	10–30	O	175–540	350–1000
Carbon-tungsten special-purpose steels									
F1, F2	Slowly	650	1200	790–870	1450–1600	15	W or B	175–260	350–500

(continued)

(a) O, oil quench; A, air cool; S, salt bath quench; W, water quench; B, brine quench. (b) When the high-temperature heating is carried out in a salt bath, the range of temperatures should be about 15 °C (25 °F) lower than given in this line. (c) Double tempering recommended for not less than 1 h at temperature each time. (d) Triple tempering recommended for not less than 1 h at temperature each time. (e) Times apply to open-furnace heat treatment. For pack hardening, a common rule is to heat 1.2 min/mm (30 min/in.) of cross section of the pack. (f) Preferable for large tools to minimize decarburization. (g) Carburizing temperature. (h) After carburizing. (i) Carburized case hardness. (j) P21 is a precipitation-hardening steel having a thermal treatment that involves solution treating and aging rather than hardening and tempering. (k) Recommended for large tools and tools with intricate sections

Table 5-3 (continued)

Type	Rate of heating	Hardening: Preheat temperature °C	Hardening: Preheat temperature °F	Hardening: Hardening temperature °C	Hardening: Hardening temperature °F	Time at temperature, min	Quenching medium(a)	Tempering temperature °C	Tempering temperature °F
Water-hardening steels									
W1, W2, W3	Slowly	565–650(k)	1050–1200(k)	760–815	1400–1550	10–30	B or W	175–345	350–650
High-carbon, high-chromium cold-work steels									
D1, D5	Very slowly	815	1500	980–1025	1800–1875	15–45	A	205–540	400–1000
D3	Very slowly	815	1500	925–980	1700–1800	15–45	O	205–540	400–1000
D4	Very slowly	815	1500	970–1010	1775–1850	15–45	A	205–540	400–1000
D7	Very slowly	815	1500	1010–1065	1850–1950	30–60	A	150–540	300–1000

(a) O, oil quench; A, air cool; S, salt bath quench; W, water quench; B, brine quench. (b) When the high-temperature heating is carried out in a salt bath, the range of temperatures should be about 15 °C (25 °F) lower than given in this line. (c) Double tempering recommended for not less than 1 h at temperature each time. (d) Triple tempering recommended for not less than 1 h at temperature each time. (e) Times apply to open-furnace heat treatment. For pack hardening, a common rule is to heat 1.2 min/mm (30 min/in.) of cross section of the pack. (f) Preferable for large tools to minimize decarburization. (g) Carburizing temperature. (h) After carburizing. (i) Carburized case hardness. (j) P21 is a precipitation-hardening steel having a thermal treatment that involves solution treating and aging rather than hardening and tempering. (k) Recommended for large tools and tools with intricate sections

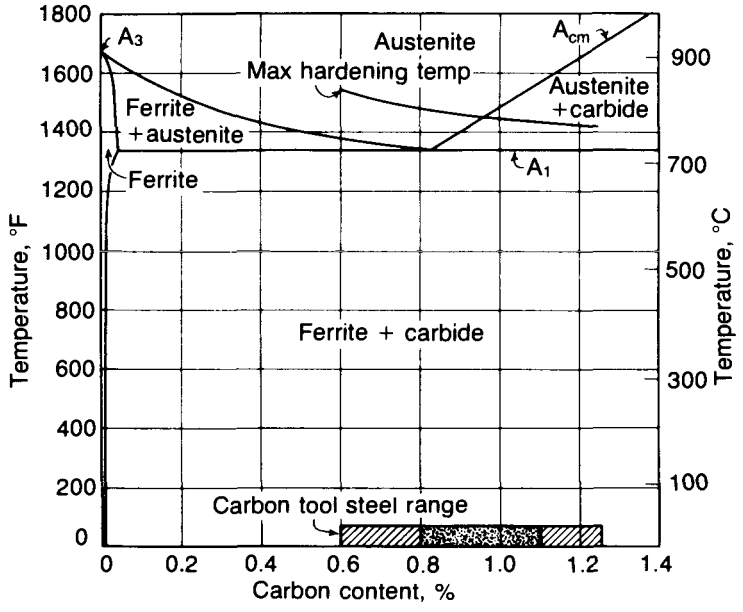

Fig. 5-9 Fe-C phase diagram showing maximum temperatures for austenitizing for hardening carbon tool steels

and, if high enough, may cause cracking, especially in highly alloyed tool steels with high carbide contents and low hot ductility and fracture resistance. Preheating establishes uniform temperature throughout a workpiece prior to heating to the final austenitizing temperature and minimizes the thermal shock and localized dimensional changes that would develop on heating a cold workpiece directly to the hardening temperature (Ref 4, 18).

Table 5-3 lists the recommended preheat temperatures for various grades of tool steels. Not all tools require preheating. For example, small parts in which temperature gradients on heating are minimal, and parts with simple geometries that would minimize stress concentrations due to section changes, may not require preheating. In contrast, high-speed tool steels hardened in salt baths may be subjected to two preheating steps (Ref 19). As shown schematically in Fig. 5-10, one of the preheat steps is performed below the lower critical temperature, prior to austenite formation, and the other is performed after austenite has formed, prior to heat-

ing to the final austenitizing temperature, which for high-speed steels is quite high. Preheating and final austenitizing are commonly accomplished in adjacent salt baths or furnaces set at the respective temperatures, but depending on production requirements and grade of steel, may also be performed in a single furnace (Ref 6). Figure 5-10 also shows that three tempering treatments, as discussed later in this chapter, can be applied to high-speed steels.

Austenitizing for hardening must accomplish several critical functions for the subsequent quenching and tempering heat treatment stages:

- Establish the volume fraction of undissolved alloy carbides that will contribute to wear resistance
- Adjust the chemistry of the austenite to provide the required M_S temperature, and thus a reasonable balance of martensite and austenite after quenching
- Adjust the chemistry of the austenite to provide the required hardenability in order to maximize the amount of martensite formed on quenching or cooling from the austenitizing temperature
- Adjust the chemistry of the austenite in order to dissolve sufficient alloying elements, which on quenching will be placed in supersaturation in the martensite and thus be available for precipitation and secondary hardening during tempering
- Control austenitic grain size to prevent coarsening and associated impaired fracture resistance

Remarkably, all of these very critical functions are accomplished during a single heating in the temperature ranges recommended for hardening the specific grades of tool steels. The key to successful austenitizing is to control the extent of alloy carbide dissolution as the tool steel composition approaches equilibrium at high temperatures. As alloy carbides dissolve, the alloying elements and carbon, which once made up the carbides, partition into the austenite. Thus, not only is the volume fraction of the carbides controlled, but also the chemistry of the austenite, which controls hardenability, M_S temperatures, retained austenite content, and secondary hardening potential.

Austenite Composition, M_S Temperatures, and Retained Austenite

The effect of austenite carbon content on M_S temperatures has been illustrated in Chapter 4. Alloying elements also strongly influence M_S temperatures, as shown in Eq 5-1 (Ref 20):

$$Ms(C) = 539 - 423C - 30.4\,Mn - 12.1\,Cr - 17.7\,Ni - 7.5\,Mo \quad \text{(Eq 5-1)}$$

Equation 5-1 was developed for steels containing up to 0.6% C, 4.9% Mn, 5% Cr, 5% Ni, and 5.4% Mo. Similar equations have been developed by other investigators (Ref 2). For example, Payson and Savage (Ref 21) have developed an equation that also includes factors for silicon and tungsten. Although Eq 5-1 has not been specifically developed for tool steels, it and similar equations invariably show the powerful effect of carbon on M_S temperatures and that all alloying elements commonly used in steels, with the possible exception of cobalt, lower M_S

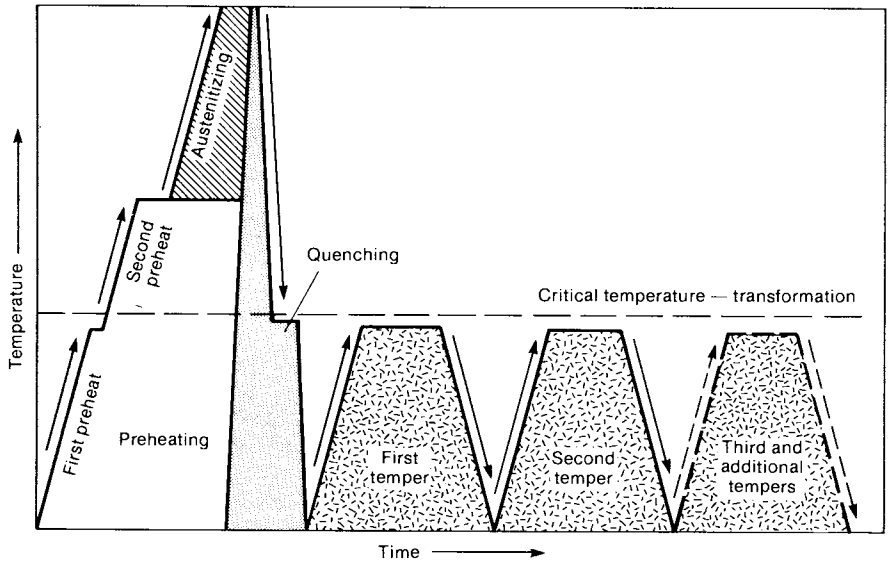

Fig. 5-10 Schematic diagram of high-speed tool steel hardening heat treatment steps. Two stages of preheating are shown.
Source: Ref 19

temperatures. As a result, in addition to carbon content, the higher the alloying element content of austenite, the lower the M_s temperatures and the greater the amount of retained austenite at room temperature. Thus, as austenitizing temperature is increased and the austenite composition is enriched with carbon and other alloying elements as carbides dissolve, less martensite is formed on cooling to room temperature. Figure 5-11 shows the effect of austenitizing temperature on M_s and retained austenite content in a 1.1% C-2.8% Cr steel (Ref 22). Austenitizing temperature has a strong effect on martensite transformation kinetics, and the data shown in Fig. 5-11 confirm the need in this steel to maintain relatively low intercritical austenitizing temperatures for hardening. At such temperatures, significant amounts of carbon and chromium are still combined in the form of spheroidized carbides, and almost complete transformation to martensite occurs on cooling to room temperature.

Figure 5-12 shows how variations in austenitizing temperature of A2 tool steel (1% C, 5% Cr, and 1% Mo) affect not only as-quenched hardness but also hardness levels achieved by subzero cooling and tempering (Ref 4). Again, the effects shown are a direct result of increasing austenitizing temperature and the enrichment of austenite as the alloy carbides dissolve. When the steel is austenitized at 950 °C (1740 °F), the recommended austenitizing temperature for A2 steel, the as-quenched hardness is a maximum because of almost complete transformation to martensite. Subzero cooling causes very little change in hardness because very little austenite is available to transform to martensite. After austenitizing at successively higher temperatures, retained austenite increases and as-quenched hardness decreases. Subzero cooling in these specimens effectively causes substantial amounts of retained austenite to transform to martensite and significantly increases hardness. With respect to tempering, the higher austenitizing temperatures cause greater dissolution of the alloy carbides and greater supersaturation of the alloying elements

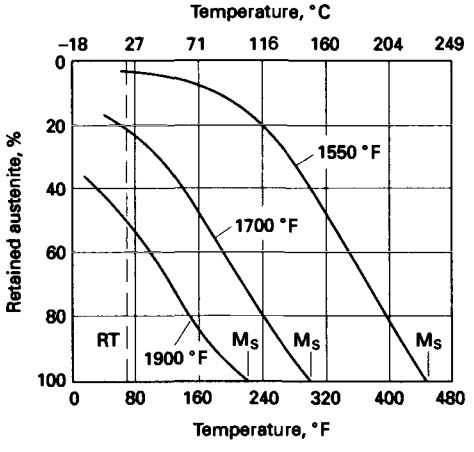

Fig. 5-11 Influence of austenitizing temperature on the martensite transformation kinetics of a tool steel containing 1.1% C and 2.8% Cr. Higher austenitizing temperatures lower M_s temperatures and increase the amount of austenite retained at room temperature. Source: Ref 22

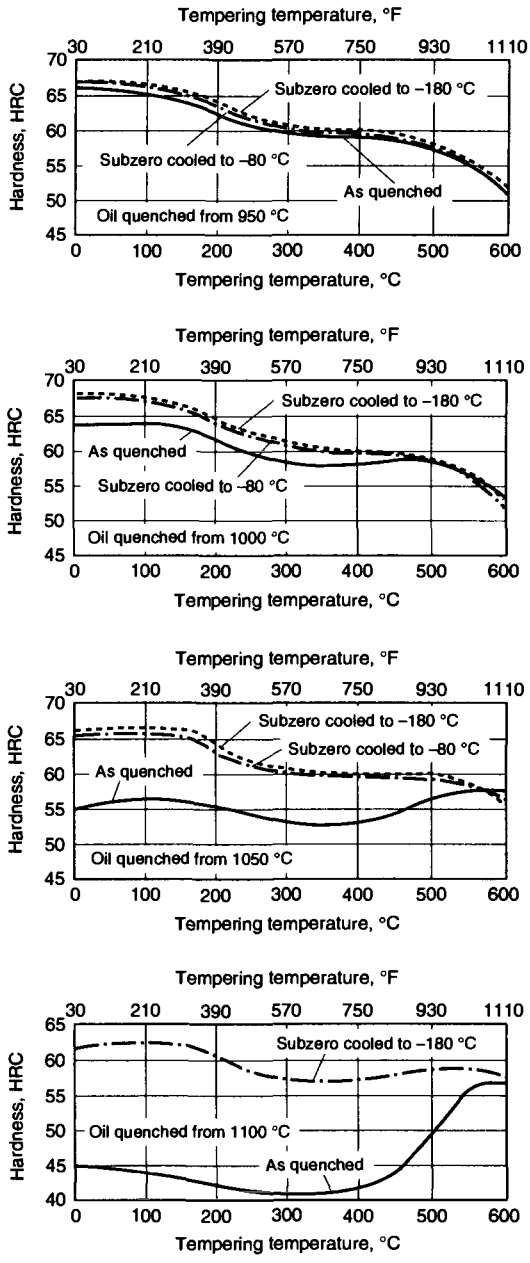

Fig. 5-12 Influence of austenitizing, subzero cooling, and tempering temperature on hardness of A2 tool steel. Source: Ref 4.

chromium and molybdenum in the martensite. Therefore, a more intense secondary hardening reaction at the higher tempering temperatures, where chromium and molybdenum are able to diffuse and precipitate as fine alloy carbides, occurs in the specimens austenitized at high temperatures.

Austenite Grain Size and Grain Growth

As austenitizing temperatures increase, austenite crystal sizes or grain sizes increase. Although the austenite transforms to martensite on quenching, features of the austenite grain structure are carried over into the tempered martensite. In particular, the segregation of impurity elements and carbide formation at coarse austenite grain boundaries may cause intergranular fracture and lower toughness of hardened steels. In order to recognize that it is the vestiges of the high-temperature austenite grain-boundary structure that affect properties in fully hardened tool steels with tempered martensitic microstructures, the high-temperature austenite grain boundaries revealed by etching or fracture at room temperature are sometimes referred to as prior-austenite grain boundaries.

Similar to spheroidization, the thermodynamic driving force for grain growth is reduction of interfacial energy, which in this case is the reduction of grain-boundary energy that accompanies the replacement of fine grains by coarser grains. The finest grains are always those that have formed just after complete austenitization following the nucleation, growth, and impingement of austenite grains during heating to and reaching the austenitizing temperature. Grain growth in the absence of particles begins immediately and continues with increasing time at temperature (Ref 7). However, in microstructures that contain second-phase particle distributions, grain growth is retarded by the particles.

In low-alloy carbon steels, fine austenite grain sizes are maintained by aluminum nitride precipitates that pin the austenite grain boundaries. Thus, grain growth does not begin immediately after austenite formation, and a stable fine grain size is maintained over a range of austenitizing temperatures and times. However, at higher temperatures or longer times, the aluminum nitrides coarsen and dissolve, and rapid austenite grain coarsening may occur. These fine-grained steels are the result of aluminum deoxidation or killing during melting, where some of the aluminum combines with oxygen and floats out in the slag and some of the aluminum remains in solution to eventually precipitate out as aluminum nitride particles. In tool steels, the carbides that coexist with austenite serve a similar function of grain size control. Equation 5-2 qualitatively relates a stable grain size, D, to characteristics of a particle distribution that restrains grain growth (Ref 23):

$$D = \frac{4r}{3f} \qquad \text{(Eq 5-2)}$$

where r is the radius of the particles and f is the volume fraction of particles. Modifications of Eq 5-2 have been developed (Ref 24), but the direct dependence of grain size on particle diameter and its inverse dependence on volume fraction remain the essential relationships of all modified grain size equations.

In aluminum-killed steels, the volume fraction of the aluminum nitride particles is very low, but the particles are very fine, and therefore a fine stable grain size is maintained. In tool steels, although carbide particles may be quite coarse, the volume fraction of carbides is high, and fine grain size is maintained by virtue of high carbide volume fractions. However, the carbide particle distributions are a function of temperature, and at high temperatures particles may coarsen and dissolve. In consequence, austenite grain sizes coarsen drastically as austenitizing temperatures increase and the particle distributions lose their effectiveness in controlling grain-boundary migration.

Figure 5-13 shows how austenite grain sizes in various tool steels increase with increasing austenitizing temperature. The grain sizes are plotted as a function of the grain size estimated from fracture surfaces by comparison to fracture surfaces of specimens with known grain sizes. The smaller the fracture grain size number, the finer the austenitic grain size. For each type of steel, there is a range of austenitizing temperatures where grain size is fine. However, consistent with the dissolution of carbides with increasing temperature, grain coarsening develops. Figure 5-11 shows that higher grain-coarsening temperatures, the temperatures at which

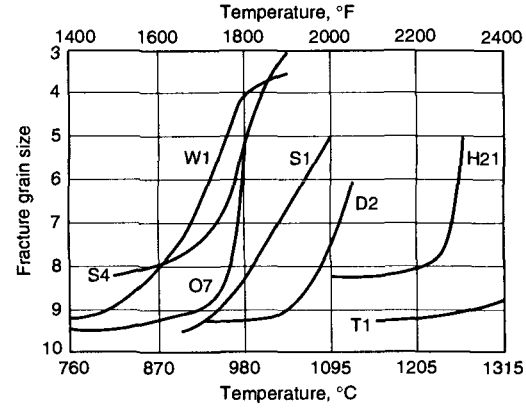

Fig. 5-13 Austenitic grain size as a function of austenitizing temperature for various tool steels

rapid, discontinuous grain growth occurs, correlate with the more highly alloyed tool steels, which have more stable carbides and higher volume fractions of carbides at high temperatures than do steels with lower alloy contents.

Discontinuous grain coarsening is observed in high-speed tool steels that have been doubly hardened—that is, reaustenitized and hardened after a previous austenitizing, quenching, and tempering cycle (Ref 25, 26). This type of coarsening was commonly observed, but the causes not understood, prior to the 1950s. Austenite grains grew so large that the shapes of the prior-austenite grains could be readily observed on fracture surfaces with the unaided eye, and the appearance of the intergranular fracture surfaces led to the term *fish-scale fracture* to describe the coarse-grained fracture phenomenon. Severe embrittlement accompanied the grain coarsening. Figure 5-14 shows an actual tracing of a very coarse grain, about 0.4 mm (0.016 in.) in diameter, from a polished and etched metallographic section of a specimen of 18-4-1 high-speed steel austenitized first at 1290 °C (2355 °F) and then reaustenitized at 1245 °C (2275 °F) (Ref 26). The discontinuous growth of this grain has replaced many fine grains the size of the small grains in the surrounding matrix. The cause of the coarsening was related to the rapid dissolution of the very fine carbides produced during previous hardening heat treatments. In contrast, grain coarsening did not occur in annealed specimens. The coarse carbides of the annealed microstructures resisted dissolution during the short-time, high-temperature austenitizing used for high-speed steels, leading to the recommendation that, if high-speed tool steels must be rehardened, they should be reannealed prior to the rehardening treatment.

Hardness and Hardenability

Hardness is the ability of a material to resist indentation and is measured by a variety of standardized tests that define the size, shape, and hardness of the indenter, and the load that is applied to create the indentation (Ref 27). Hardness values are then related to the length, width, or depth of the indentation. In hardened steels, hardness is most frequently measured with various loads on the Rockwell C scale (HRC), which uses a diamond cone indenter, or the Vickers hardness test (HV or DPH), which uses a diamond pyramid indenter. Table 5-4 gives equivalent hardness numbers for a number of hardness tests. The Rockwell C tests are valid only for measurements on higher-hardness materials and are not valid below 20 HRC. Vickers and Brinell (HB) hardness measurements are valid not only for the HRC range but also for softer materials such as tool steels in the annealed condition.

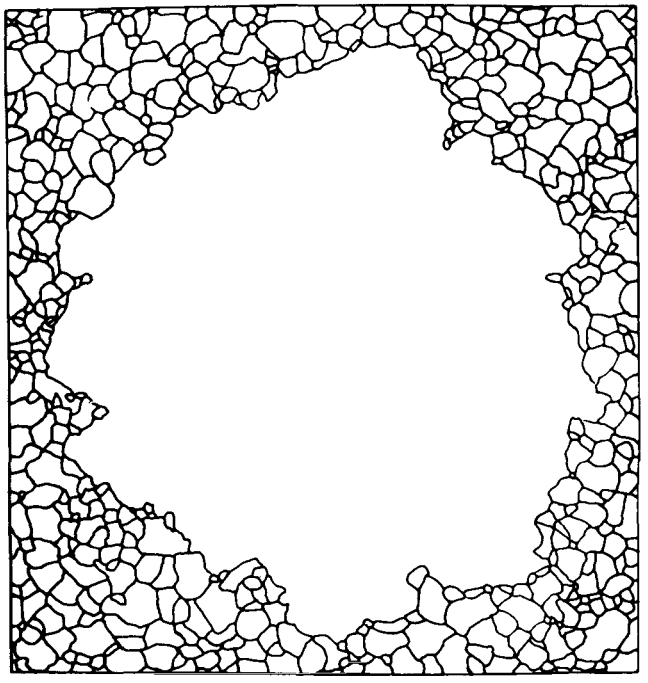

Fig. 5-14 Tracing of a very coarse austenite grain within a matrix of fine grains in a rehardened high-speed tool steel. 100×. Source: Ref 26

Table 5-4 Approximate equivalent hardness numbers and tensile strengths for steels(a)

Vickers hardness No.	Brinell hardness No. 3000 kg load, 10 mm ball: Standard ball	Brinell hardness No. 3000 kg load, 10 mm ball: Tungsten carbide ball	Rockwell hardness No. A scale, 60 kg load, Brale indenter	Rockwell hardness No. B scale, 100 kg load, 1/16 in diam ball	Rockwell hardness No. C scale, 150 kg load, Brale indenter	Rockwell hardness No. D scale, 100 kg load, Brale indenter	Rockwell superficial hardness No., superficial Brale indenter: 15N scale, 15kg load	30N scale, 30 kg load	45N scale, 45 kg load	Knoop hardness No., 500 g load and greater	Shore Scleroscope hardness No.	Tensile strength (approx.) 1000 psi	Vickers hardness No.
940	...	...	**85.6**	...	**68.0**	**76.9**	**93.2**	**84.4**	**75.4**	920	97	...	940
920	...	...	**85.3**	...	**67.5**	**76.5**	**93.0**	**84.0**	**74.8**	908	96	...	920
900	...	...	**85.0**	...	**67.0**	**76.1**	**92.9**	**83.6**	**74.2**	895	95	...	900
880	...	(767)	**84.7**	...	**66.4**	**75.7**	**92.7**	**83.1**	**73.6**	882	93	...	880
860	...	(757)	**84.4**	...	**65.9**	**75.3**	**92.5**	**82.7**	**73.1**	867	92	...	860
840	...	**(745)**	**84.1**	...	**65.3**	**74.8**	**92.3**	**82.2**	**72.2**	852	91	...	840
820	...	**(733)**	**83.8**	...	**64.7**	**74.3**	**92.1**	**81.7**	**71.8**	837	90	...	820
800	...	**(722)**	**83.4**	...	**64.0**	**73.8**	**91.8**	**81.1**	**71.0**	822	88	...	800
780	...	**(710)**	**83.0**	...	**63.3**	**73.3**	**91.5**	**80.4**	**70.2**	806	87	...	780
760	...	**(698)**	**82.6**	...	**62.5**	**72.6**	**91.2**	**79.7**	**69.4**	788	86	...	760
740	...	**(684)**	**82.2**	...	**61.8**	**72.1**	**91.0**	**79.1**	**68.6**	772	84	...	740
720	...	**(670)**	**81.8**	...	**61.0**	**71.5**	**90.7**	**78.4**	**67.7**	754	83	...	720
700	...	**(656)**	**81.3**	...	**60.1**	**70.8**	**90.3**	**77.6**	**66.7**	735	81	...	700
690	...	**(647)**	**81.1**	...	**59.7**	**70.5**	**90.1**	**77.2**	**66.2**	725	...	...	690
680	...	**(638)**	**80.8**	...	**59.2**	**70.1**	**89.8**	**76.8**	**65.7**	716	80	355	680
670	...	**(630)**	**80.6**	...	**58.8**	**69.8**	**89.7**	**76.4**	**65.3**	706	...	348	670
660	...	**620**	**80.3**	...	**58.3**	**69.4**	**89.5**	**75.9**	**64.7**	697	79	342	660
650	...	**611**	**80.0**	...	**57.8**	**69.0**	**89.2**	**75.5**	**64.1**	687	78	336	650
640	...	**601**	**79.8**	...	**57.3**	**68.7**	**89.0**	**75.1**	**63.5**	677	77	328	640
630	...	**591**	**79.5**	...	**56.8**	**68.3**	**88.8**	**74.6**	**63.0**	667	76	323	630
620	...	**582**	**79.2**	...	**56.3**	**67.9**	**88.5**	**74.2**	**62.4**	657	75	317	620
610	...	**573**	**78.9**	...	**55.7**	**67.5**	**88.2**	**73.6**	**61.7**	646	...	310	610
600	...	**564**	**78.6**	...	**55.2**	**67.0**	**88.0**	**73.2**	**61.2**	636	74	303	600
590	...	**554**	**78.4**	...	**54.7**	**66.7**	**87.8**	**72.7**	**60.5**	625	73	298	590
580	...	**545**	**78.0**	...	**54.1**	**66.2**	**87.5**	**72.1**	**59.9**	615	72	293	580
570	...	**535**	**77.8**	...	**53.6**	**65.8**	**87.2**	**71.7**	**59.3**	604	...	288	570
560	...	**525**	**77.4**	...	**53.0**	**65.4**	**86.9**	**71.2**	**58.6**	594	71	283	560
550	**(505)**	**517**	**77.0**	...	**52.3**	**64.8**	**86.6**	**70.5**	**57.8**	583	70	276	550
540	**(496)**	**507**	**76.7**	...	**51.7**	**64.4**	**86.3**	**70.0**	**57.0**	572	69	270	540
530	**(488)**	**497**	**76.4**	...	**51.1**	**63.9**	**86.0**	**69.5**	**56.2**	561	68	265	530
520	**(480)**	**488**	**76.1**	...	**50.5**	**63.5**	**85.7**	**69.0**	**55.6**	550	67	260	520
510	**(473)**	**479**	**75.7**	...	**49.8**	**62.9**	**85.4**	**68.3**	**54.7**	539	...	254	510
500	**(465)**	**471**	**75.3**	...	**49.1**	**62.2**	**85.0**	**67.7**	**53.9**	528	66	247	500
490	**(456)**	**460**	**74.9**	...	**48.4**	**61.6**	**84.7**	**67.1**	**53.1**	517	65	241	490

(continued)

(a) For carbon and alloy steels in the annealed, normalized, and quenched-and-tempered conditions; less accurate for cold-worked condition and for austenitic steels. The values in **boldface type** correspond to the values in the joint SAE-ASM-ASTM hardness conversions as printed in ASTM E 140, Table 1. The values in parentheses are beyond normal range and are given for information only.

Table 5-4 (continued)

Vickers hardness No.	Brinell hardness No. 3000 kg load 10 mm ball: Standard ball	Brinell hardness No. 3000 kg load 10 mm ball: Tungsten carbide ball	Rockwell hardness No.: A scale, 60 kg load, Brale indenter	Rockwell hardness No.: B scale, 100 kg load, 1/16 in diam ball	Rockwell hardness No.: C scale, 150 kg load, Brale indenter	Rockwell hardness No.: D scale, 100 kg load, Brale indenter	Rockwell superficial hardness No., superficial Brale indenter: 15N scale, 15kg load	30N scale, 30 kg load	45N scale, 45 kg load	Knoop hardness No., 500 g load and greater	Shore Scleroscope hardness No.	Tensile strength (approx.) 1000 psi	Vickers hardness No.
480	(448)	452	74.5	...	47.7	61.3	84.3	66.4	52.2	505	64	235	480
470	441	442	74.1	...	46.9	60.7	83.9	65.7	51.3	494	...	228	470
460	433	433	73.6	...	46.1	60.1	83.6	64.9	50.4	482	62	223	460
450	425	425	73.3	...	45.3	59.4	83.2	64.3	49.4	471	...	217	450
440	415	415	72.8	...	44.5	58.8	82.8	63.5	48.4	459	59	212	440
430	405	405	72.3	...	43.6	58.2	82.3	62.7	47.4	447	58	205	430
420	397	397	71.8	...	42.7	57.5	81.8	61.9	46.4	435	57	199	420
410	388	388	71.4	...	41.8	56.8	81.4	61.1	45.3	423	56	193	410
400	379	379	70.8	...	40.8	56.0	80.8	60.2	44.1	412	55	187	400
390	369	369	70.3	...	39.8	55.2	80.3	59.3	42.9	400	...	181	390
380	360	360	69.8	(110.0)	38.8	54.4	79.8	58.4	41.7	389	52	175	380
370	350	350	69.2	...	37.7	53.6	79.2	57.4	40.4	378	51	170	370
360	341	341	68.7	(109.0)	36.6	52.8	78.6	56.4	39.1	367	50	164	360
350	331	331	68.1	...	35.5	51.9	78.0	55.4	37.8	356	48	159	350
340	322	322	67.6	(108.0)	34.4	51.1	77.4	54.4	36.5	346	47	155	340
330	313	313	67.0	...	33.3	50.2	76.8	53.6	35.2	337	46	150	330
320	303	303	66.4	(107.0)	32.2	49.4	76.2	52.3	33.9	328	45	146	320
310	294	294	65.8	...	31.0	48.4	75.6	51.3	32.5	318	...	142	310
300	284	284	65.2	(105.5)	29.8	47.5	74.9	50.2	31.1	309	42	138	300
295	280	280	64.8	...	29.2	47.1	74.6	49.7	30.4	305	...	136	295
290	275	275	64.5	(104.5)	28.5	46.5	74.2	49.0	29.5	300	41	133	290
285	270	270	64.2	...	27.8	46.0	73.8	48.4	28.7	296	...	131	285
280	265	265	63.8	(103.5)	27.1	45.3	73.4	47.8	27.9	291	40	129	280
275	261	261	63.5	...	26.4	44.9	73.0	47.2	27.1	286	39	127	275
270	256	256	63.1	(102.0)	25.6	44.3	72.6	46.4	26.2	282	38	124	270
265	252	252	62.7	...	24.8	43.7	72.1	45.7	25.2	277	...	122	265
260	247	247	62.4	(101.0)	24.0	43.1	71.6	45.0	24.3	272	37	120	260
255	243	243	62.0	...	23.1	42.2	71.1	44.2	23.2	267	...	117	255
250	238	238	61.6	99.5	22.2	41.7	70.6	43.4	22.2	262	36	115	250
245	233	233	61.2	...	21.3	41.1	70.1	42.5	21.1	258	35	113	245
240	228	228	60.7	98.1	20.3	40.3	69.6	41.7	19.9	253	34	111	240
230	219	219	...	96.7	(18.0)	...	...	...	...	243	33	106	230
220	209	209	...	95.0	(15.7)	...	...	...	...	234	32	101	220
210	200	200	...	93.4	(13.4)	...	...	...	...	226	30	97	210
200	190	190	...	91.5	(11.0)	...	...	...	...	216	29	92	200

(continued)

(a) For carbon and alloy steels in the annealed, normalized, and quenched-and-tempered conditions; less accurate for cold-worked condition and for austenitic steels. The values in **boldface type** correspond to the values in the joint SAE-ASM-ASTM hardness conversions as printed in ASTM E 140, Table 1. The values in parentheses are beyond normal range and are given for information only.

Table 5-4 (continued)

Vickers hardness No.	Brinell hardness No. 3000 kg load 10 mm ball: Standard ball	Brinell hardness No. 3000 kg load 10 mm ball: Tungsten carbide ball	Rockwell hardness No. A scale, 60 kg load, Brale indenter	Rockwell hardness No. B scale, 100 kg load, 1/16 in diam ball	Rockwell hardness No. C scale, 150 kg load, Brale indenter	Rockwell hardness No. D scale, 100 kg load, Brale indenter	Rockwell superficial hardness No., superficial Brale indenter: 15N scale, 15kg load	30N scale, 30 kg load	45N scale, 45 kg load	Knoop hardness No., 500 g load and greater	Shore Scleroscope hardness No.	Tensile strength (approx.) 1000 psi	Vickers hardness No.
190	181	181	...	89.5	(8.5)	...	...	...	...	206	28	88	190
180	171	171	...	87.1	(6.0)	...	...	...	...	196	26	84	180
170	162	162	...	85.0	(3.0)	...	...	...	...	185	25	79	170
160	152	152	...	81.7	(0.0)	...	...	...	...	175	23	75	160
150	143	143	...	78.7	...	...	...	...	...	164	22	71	150
140	133	133	...	75.0	...	...	...	...	...	154	21	66	140
130	124	124	...	71.2	...	...	...	...	...	143	20	62	130
120	114	114	...	66.7	...	...	...	...	...	133	18	57	120
110	105	105	...	62.3	...	...	...	...	...	123	...	...	110
100	95	95	...	56.2	...	...	...	...	...	112	...	...	100
95	90	90	...	52.0	...	...	...	...	...	107	...	...	95
90	86	86	...	48.0	...	...	...	...	...	102	...	...	90
85	81	81	...	41.0	...	...	...	...	...	97	...	...	85

(a) For carbon and alloy steels in the annealed, normalized, and quenched-and-tempered conditions; less accurate for cold-worked condition and for austenitic steels. The values in **boldface type** correspond to the values in the joint SAE-ASM-ASTM hardness conversions as printed in ASTM E 140, Table 1. The values in parentheses are beyond normal range and are given for information only.

High hardness and microstructures that have high hardness are the major objectives of the final heat treatments applied to tool steels. Ideally, in plain carbon and low-alloy steels, the highest hardness is achieved by forming microstructures that consist entirely of martensite. A completely martensitic structure is unattainable, however, even if the transformation of austenite to nonmartensitic microstructures can be suppressed. This is due to the incorporation of second-phase particles, such as inclusions and carbide particles that are not dissolved during austenitizing. Also, as carbon content increases, the amount of retained austenite increases.

Figure 5-15 shows hardness as a function of carbon content for various microstructures that result from the transformation of austenite and various heat treatments of carbon steels (Ref 28, 29). The highest hardness of any steel is associated with martensitic microstructures (with qualifications, as discussed), and the effect of large amounts of retained austenite in high-carbon steels is indicated by the cross-hatched region. The lowest hardness is associated with microstructures consisting of ferrite and spheroidized carbides produced by the annealing treatments described earlier. If the austenite transforms to microstructures such as ferrite, pearlite, or bainite, hardness will be lower than that of a martensitic microstructure. Also, as indicated in Fig. 5-15, tempered martensitic microstructures have lower hardness than as-quenched martensitic microstructures. The latter observation holds for plain carbon and low-alloy steels. In highly alloyed tool steels, as discussed later, tempering may produce hardnesses that exceed even those of fully martensitic microstructures.

Hardness is related to chemical composition, crystal structure and perfection, and the size and distribution of the various phases that make up the microstructure. High hardness correlates with high resistance to slip and dislocation motion, high work-hardening rates, and high strengths. For example, Table 5-4 shows correlations of hardness with ultimate tensile strength. In martensite, the carbon-dependence of the high hardness of martensite is attributed to carbon atoms trapped in the octahedral interstitial sites of the martensitic crystal structure, as shown in Chapter 4 (Ref 30). Other contributing factors to the strength of martensite are the dislocation substructure of the martensite, dynamic interactions of carbon atoms with dislocations during strain hardening (Ref 31), and, in martensite tempered at low temperatures, the effect of fine transition carbide particles that precipitate from martensite supersaturated with carbon (Ref 32). Carbon, therefore, by its interaction with other structural elements of a martensitic microstructure, is the dominant factor controlling the strength of martensite. Substitutional alloying elements have a relatively small effect on the martensite strength.

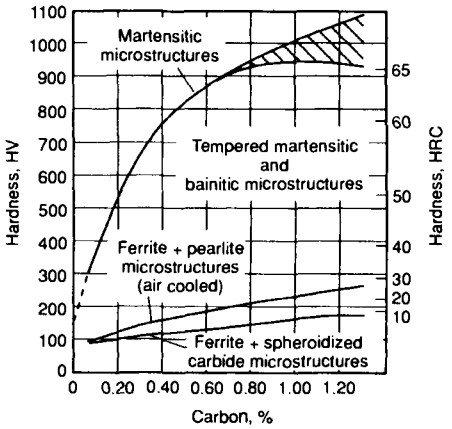

Fig. 5-15 Hardness of various microstructures as a function of carbon content in steels. The cross-hatched area indicates variations due to retained austenite. Source: Ref 28 and 29

Hardness, as discussed, is a measure of the strength of a microstructure and, in the context of heat-treated steels, is taken to be a measure of the strength of martensitic microstructures and the success of the hardening process. Hardenability refers to the ability of a given steel to form martensite, which in the context of heat-treated steels equates to the ability of a steel to form microstructures of the highest possible hardness. A comprehensive definition states: "Hardenability is the capacity of steel to transform partially or completely from austenite to some percentage of martensite at a given depth when cooled under some given conditions" (Ref 33). There are many parts to this definition. The reference to steel implies a given chemical composition and microstructural condition as produced by austenitizing. The incorporation of partial transformation to martensite leaves open the possibility of establishing hardenability criteria related to less than complete martensite formation. In this regard, the widely used Bain and Grossmann hardenability system assumes full hardening with only 50% martensite (Ref 34). Finally, the definition indicates that cooling conditions influence martensite formation. The latter consideration relates factors such as quenching media, quenching effectiveness, and section size to the diffusion-controlled transformations of austenite that compete with martensite formation.

In order to compare the hardenabilities of steels as a function of composition, the Bain and Grossmann system removes the variations due to cooling in various media by establishing the concept of the ideal diameter. The ideal diameter, D_I, of a steel is the diameter of a bar that hardens to 50% martensite in an ideal quench where the surface of the bar is assumed to cool instantly to the temperature of the quenching medium. Thus, the larger the ideal diameter, the higher the hardenability of the steel,

independent of the technological factors that affect quenching.

Hardenability is a function of carbon content, austenitic grain size, and alloy content, and Fig. 5-16 and 5-17 show how these parameters are used to calculate ideal diameters. First, an ideal diameter based on steel carbon content and austenitic grain size is selected from Fig. 5-16, and then multiplying factors for the amounts of the various alloying elements are selected from Fig. 5-17. The ideal diameter from Fig. 5-16 is then multiplied by the factor for each alloying element to determine the final D_I. Critical diameters—the size of bars that will harden to 50% martensite in a given quenching medium—can then be determined for various quench severities (Ref 2, 34). As the composition axes of Fig. 5-16 and 5-17 show, the Bain/Grossmann system for evaluating hardenability is applicable to medium-carbon steels with relatively low alloy contents.

Diffusion-Controlled Phase Transformations of Austenite

Hardenability is directly related to the diffusion-controlled transformations of austenite that compete with the transformation of austenite to martensite. These transformations include the transformation of austenite to proeutectoid ferrite and cementite, pearlite, and bainite. The atomic mechanisms by which these transformations proceed, and the microstructures and properties that result from the various phase transformations, have been the subject of continuous research, and the reader is referred to the literature for in-depth coverage of diffusion-controlled austenite transformations (Ref 35–39). Similarly, the coupling of the isothermal and continuous cooling kinetics of the various diffusion-controlled transformations to the hardenability of carbon steels has been the subject of extensive research, especially in medium-carbon, low-alloy hardenable steels (Ref 2, 33, 34, 40). This section briefly reviews some of these concepts and describes the microstructural appearance of the products of diffusion-controlled transformation of austenite. The role that diffusion-controlled phase transformations play relative to the hardenability of high-carbon and alloy tool steels is then emphasized.

The Fe-C phase diagram, Fig. 5-3, and the related discussion of normalizing heat treatments, show that in hypereutectoid steels—that is, steels with higher carbon content than the eutectoid carbon concentration—cementite first forms on austenite grain boundaries during cooling. Since the cementite forms prior to the eutectoid reaction, it is referred to as proeutectoid cementite. Similarly, in

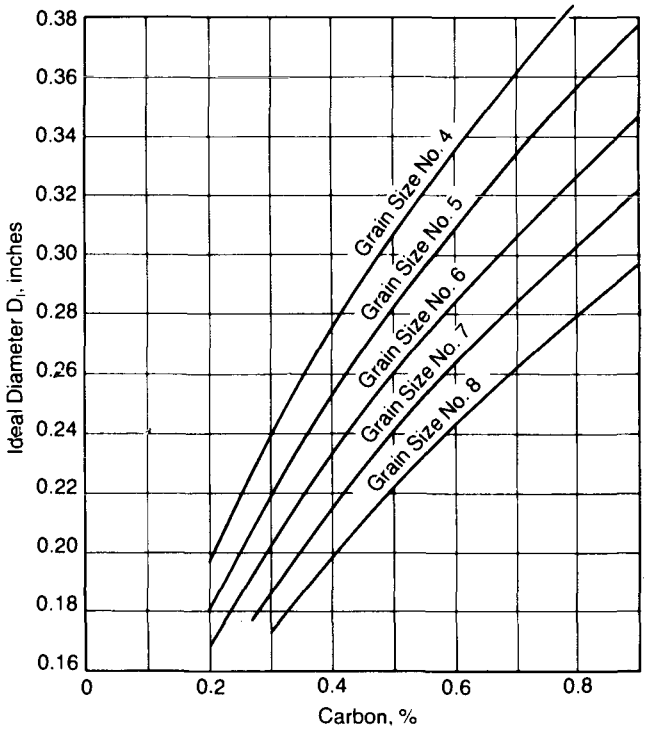

Fig. 5-16 Hardenability expressed as ideal critical diameter, as a function of austenite grain size and steel carbon content. Source: Ref 34

low-carbon, hypoeutectoid steels, proeutectoid ferrite forms on austenite grain boundaries during cooling prior to eutectoid transformation. Diffusion of carbon from the austenite to growing grain-boundary cementite is required because of the high carbon content of the cementite, and for proeutectoid ferrite formation, because of its very low solubility for carbon, carbon must diffuse away from the growing ferrite grains into the adjacent austenite.

As a result of the enrichment of the carbon in austenite adjacent to proeutectoid ferrite in hypoeutectoid steels and the depletion of carbon in the austenite adjacent to proeutectoid cementite in hypereutectoid steels, eventually the carbon content of the austenite—regardless of the carbon content of the starting austenite—approaches the eutectoid composition. At this point, with further removal of heat, the austenite transforms to a lamellar mixture of ferrite and cementite referred to as pearlite. This solid-state reaction in Fe-C alloys is written:

$$\text{Austenite (0.77C)} \leftrightarrow \text{Ferrite (0.02C)} + \text{Cementite (6.67C)} \qquad \text{(Eq 5-3)}$$

and occurs at 727 °C (1340 °F) under equilibrium conditions. Equation 5-3 shows that considerable partitioning of carbon by diffusion between the various phases is required for pearlite formation. Alloying will significantly change the equilibrium austenite compositions and temperatures for the eutectoid reaction, as has been shown in Chapter 4.

Figure 5-18 shows two light micrographs of pearlite microstructures. Figure 5-18(a) shows alternating ferrite (white) and cementite (gray) lamellae in the pearlitic microstructure of a 52100 steel, and Fig. 5-18(b) shows dark colonies of pearlite in a 4150 steel. In the latter micrograph, the ferrite and cementite lamellae are too closely spaced to be resolved in the light microscope; therefore, the pearlitic structure appears uniformly dark. Pearlite interlamellar spacing is a function of transformation temperature and decreases with decreasing temperature as undercooling enables more lamellae to be nucleated. As a result of the finer spacing and reduced diffusion distances, growth rates of pearlite increase with decreasing temperature despite the fact that carbon diffusion decreases with decreasing temperature.

If the transformation of austenite is suppressed to increasingly lower temperatures, the short-range iron atom diffusion at the austenite/pearlite interface that is required to transform the fcc austenitic crystal structure to crystal structures of ferrite and cementite is suppressed, and the mechanisms that form the characteristic morphology of spherical pearlite colonies can no longer operate. The result is formation of bainite, a nonlamellar mixture of ferrite and cementite. In contrast to the roughly spherical colonies of pearlite, bainite assumes a more regular, needlelike morphology.

Two morphologies of bainite in medium- and high-carbon steels are recognized. Upper bainite, (Fig. 5-19) forms in blocks of parallel ferrite crystals with intervening cementite crystals (Ref 41). Often, except for the general parallel morphology,

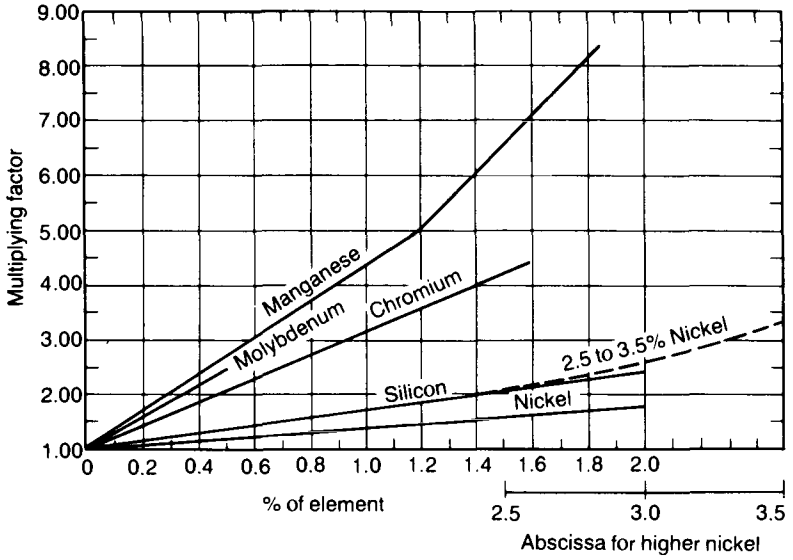

Fig. 5-17 Multiplying factors, used to determine ideal critical diameters of alloy steels, as a function of the concentration of various common alloying elements. Source: Ref 34

the ferrite and cementite crystals are too fine to be resolved in the light microscope. Lower bainite, as shown in Fig. 5-20 for a 1.1% C steel (Ref 42), consists of irregularly arranged ferrite needles or plates containing very fine cementite particles within the needles. Again, the fine carbides in lower bainite are not resolvable in the light microscope, and TEM (Fig. 5-20a) must be used to show the very fine intracrystalline carbides characteristic of lower bainite.

In summary, as the austenite transformation temperature decreases, or as cooling rates increase, the austenite transformation products shift from proeutectoid ferrite or cementite, to pearlite, to upper bainite, to lower bainite. The microstructures become finer with decreasing temperature, or with increasing cooling rates, as carbon diffusivity decreases. Consistent with the finer structures, hardnesses of the austenite transformation products tend to increase with decreasing transformation temperature. Eventually, if the diffusion-controlled transformations of austenite can be suppressed to low enough temperatures, either by rapid cooling or by alloying, diffusion effectively ceases and the austenite must transform to martensite by the diffusionless shear mechanism described in Chapter 4.

Transformation Diagrams, Jominy Curves, and Hardenability: General Considerations

Depending on alloy content, each steel has a unique set of kinetics, or time-temperature-dependent rates, at which austenite transforms to microstructures produced by the various diffusion-controlled transformations of austenite. These kinetics are empirically characterized by isothermal transformation (IT) and continuous cooling transformation (CCT) diagrams. Hardnesses of the microstructures produced by a range of cooling rates are determined by Jominy end-quench testing, and these results are used to produce hardenability bands for a given steel grade.

Figure 5-21 shows the interrelationships among the various approaches used to characterize diffusion-controlled transformations in medium-carbon, low-alloy steels (Ref 43). Isothermal transformation diagrams are experimentally determined by cooling austenite to temperatures below the A_3 or A_{cm} temperatures, and holding at those temperatures. Then the progress of the austenite transformation at constant temperatures as a function of time is followed by dilatometry or metallography. In order to use the metallographic method, specimens must be quenched from the temperature of interest after various times and examined to show the time-dependent increases in the amounts of proeutectoid ferrite or cementite, pearlite or bainite, depending on the temperature range transformation. The IT diagram in Fig. 5-21 is shown by the dashed curves, which mark the beginning and ending times for the various transformations at various temperatures.

Continuous cooling transformation diagrams are determined by cooling specimens at various rates from a given austenitizing temperature. Temperature and the dimensional changes that mark the volume increases caused by austenite transformation are monitored continuously as a function of cooling, and the hardnesses of fully transformed specimens, which often may consist of a mixture of microstructures, are often recorded on the diagrams.

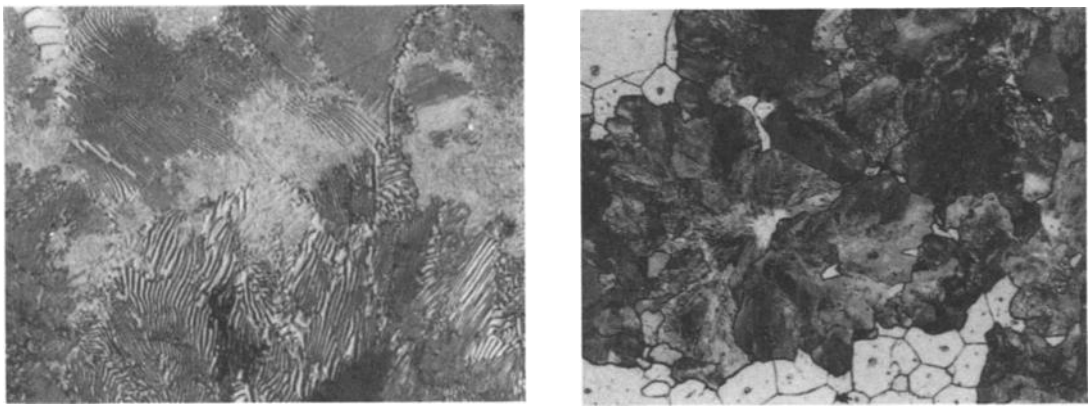

(a) (b)

Fig. 5-18 Pearlitic microstructures in 52100 steel (a) and 4150 steel (b). In the 52100 steel the roughly parallel lamellae of pearlite are resolved, but in the 4150 steel the interlamellar spacing is too fine to be resolved in the light microscope. Light micrographs. Courtesy of K. Hayes and F.A. Jacobs

The solid curves in Fig. 5-21 represent the CCT diagram. Also included are several cooling curves and the hardness values of the microstructures produced by those cooling rates. The CCT diagram is shifted to lower temperatures and longer times than the IT diagram because of reduced time at any temperature for the nucleation and growth of the diffusion-controlled transformation products.

The standardized Jominy end-quench test consists of quenching only one end of an austenitized 1 in. (25 mm) diam specimen with a column of water (Ref 44, 45) and then measuring hardness as a function of distance from the quenched end. As a result, a single specimen is subjected to a range of cooling rates, from that of water quenching to air cooling, and effectively all the microstructures of a large part of the CCT diagram are reproduced in a single specimen. Thus, the water-quenched end will have high hardness, corresponding to the martensitic microstructure characteristic of the carbon content of the steel, and the hardness will gradually decrease as mixtures of lower-strength microstructures successively replace martensite with increasing distance from the quenched end. Figure 5-21 demonstrates the relationship of Jominy testing to the CCT diagram.

Each grade of hardenable steel is manufactured to a specification that establishes the allowable range of chemical composition. Therefore, different heats of steel of a given grade will have somewhat different Jominy hardness profiles. The allowed ranges of hardness curves for a given grade of steel then make up hardenability bands, which specify allowable variations in hardenability for that grade. Figure 5-22 shows the hardenability curves for SAE/AISI 4140H steel (Ref 46). Extensive collections of hardenability curves exist for medium-carbon, plain carbon, and low-alloy steels (Ref 46), and an atlas of time-temperature IT and CCT diagrams for irons and steels has recently been published (Ref 47).

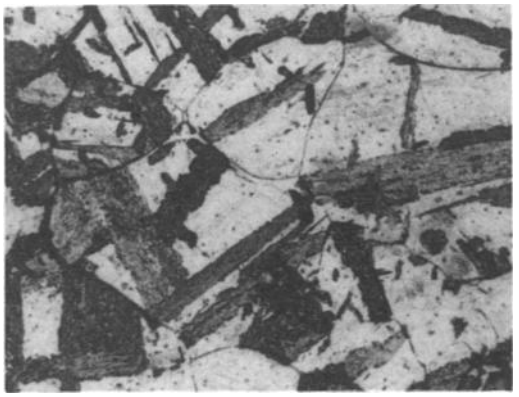

Fig. 5-19 Upper bainite colonies, which appear as dark-etching rectangular areas, in a 4150 steel. Each colony is composed of many parallel lathlike crystals of ferrite with cementite particles between the ferrite laths. Light micrograph. Courtesy of F.A. Jacobs

Transformation Diagrams, Jominy Curves, and Hardenability: Tool Steels

The high carbon and alloy concentrations of most tool steels cause significant differences in austenite transformation behavior and hardenability compared to those characteristics in the lower-carbon, lower-alloy steels described in the previous section. Figures 5-23 to 5-25 show IT diagrams for H-13,

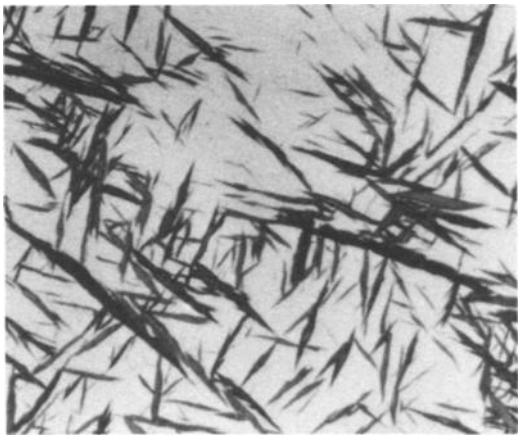

(a)

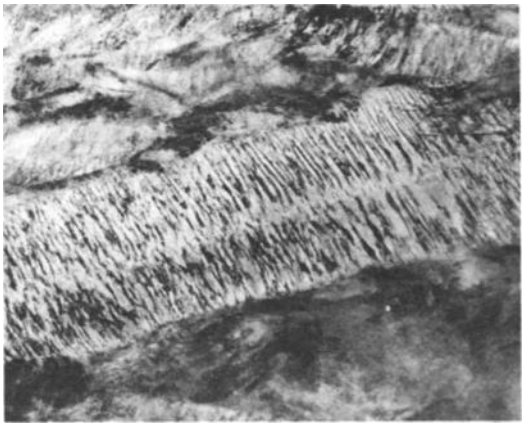

(b)

Fig. 5-20 Lower bainite in a 1.10% C steel. (a) Light micrograph showing shape and distribution of bainitic plates. (b) TEM micrograph showing fine carbide particles within a bainitic plate. Courtesy of M. Oka and H. Okamoto

A-10, and T1 tool steels, respectively (Ref 48, 49). The high alloy contents of these steels dramatically increase the times for isothermal transformation compared to low-alloy steels, and thus substantially increase hardenability. The need for the substitutional alloying elements, with their sluggish rates of diffusion, to partition between the various phases during austenite decomposition greatly increases the incubation times for detectable amounts of transformation products and substantially reduces the rates of the diffusion-controlled transformations.

Each of the tool steels shows three major regions of transformation. At high temperatures, proeutectoid cementite is the first transformation product, followed by a C-curve for pearlite formation or, in the case of the T1 steel, for the formation of a mixture of spheroidized ferrite and alloy carbide particles. At lower isothermal transformation temperatures, just above M_s there are C-curves for the time-dependent transformation of austenite to bainite. Finally, all the diagrams show the region of martensite formation and estimates of the amount of martensite formed as a function of temperature. At intermediate transformation temperatures, effectively no transformation occurs, even after many hours of holding.

The very high hardenability of the highly alloyed tool steels makes the results of Jominy testing uninformative, since the austenite transforms to martensite at all cooling rates achievable in a Jominy speci-

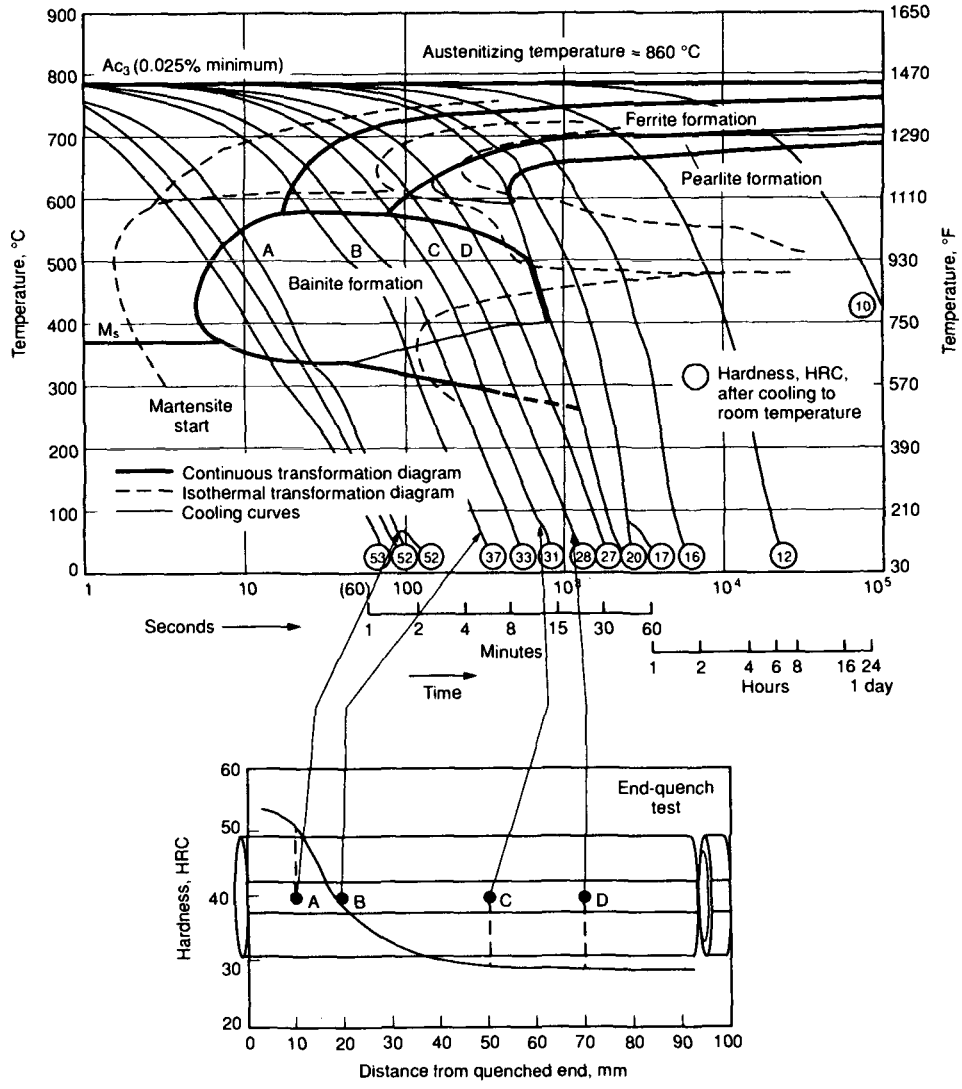

Fig. 5-21 IT and CCT diagrams, and the relationship of the CCT diagram to the Jominy end-quench test, for a 0.38C-0.99Cr-0.16Mo steel. Source: Ref 43

men. However, in tool steels of lower alloy content, Jominy curves do provide information. For example, Fig. 5-26 shows Jominy curves for an L2 special-purpose tool steel austenitized at three different temperatures. The higher the austenitizing temperature, the higher the hardness of the martensite and the better the hardenability. These changes correlate with increasing amounts of carbon and alloying elements taken into solution in austenite at the higher austenitizing temperatures as alloy carbides increasingly dissolve. The Jominy curves show that hardness increases as martensite is replaced by bainitic microstructures. However, specimens austenitized at higher temperatures show hardness peaks at distances from the quenched end associated with lower cooling rates. These hardness peaks are related to formation of pearlite with very fine interlamellar spacing.

Many IT diagrams for tool steels are given in the literature (Ref 47), but fewer CCT diagrams. Figure 5-27 shows examples of CCT diagrams for a hot-work die steel H13 austenitized at 1030 and 1100 °C (1885 and 2010 °F). The same transformation regions as in the IT diagram of H13 in Fig. 5-23 are shown; the major effect of austenitizing temperature is to change the kinetics of proeutectoid carbide formation. The higher austenitizing causes greater dissolution of carbides in the austenite and promotes grain-boundary carbide formation on cooling.

Jatczak (Ref 50) has extended the Bain and Grossmann system of characterizing hardenability by ideal critical diameters to high-carbon steels containing 0.60 to 1.10% C. A major difference in the factors that control hardenability in high-carbon steels, compared to medium-carbon steels, is the much greater role that undissolved carbides play in the high-carbon steels. When carbides are present, grain size variations as a function of austenitizing temperature are reduced, and hardenability is a function of the degree to which alloying elements are tied up with carbide particles. Figure 5-28 shows multiplying factors for carbon as a function of austenitizing temperature in high-carbon steels relative to medium-carbon steels. The multiplying factors increase with austenitizing temperature, but for a given temperature decrease with increasing carbon content because of increasing carbide stability. Figures 5-29 and 5-30 show the multiplying factors for high-carbon steels austenitized at 830 and 927 °C (1525 and 1700 °F), respectively. The lower austenitizing temperature is in the austenite-carbide

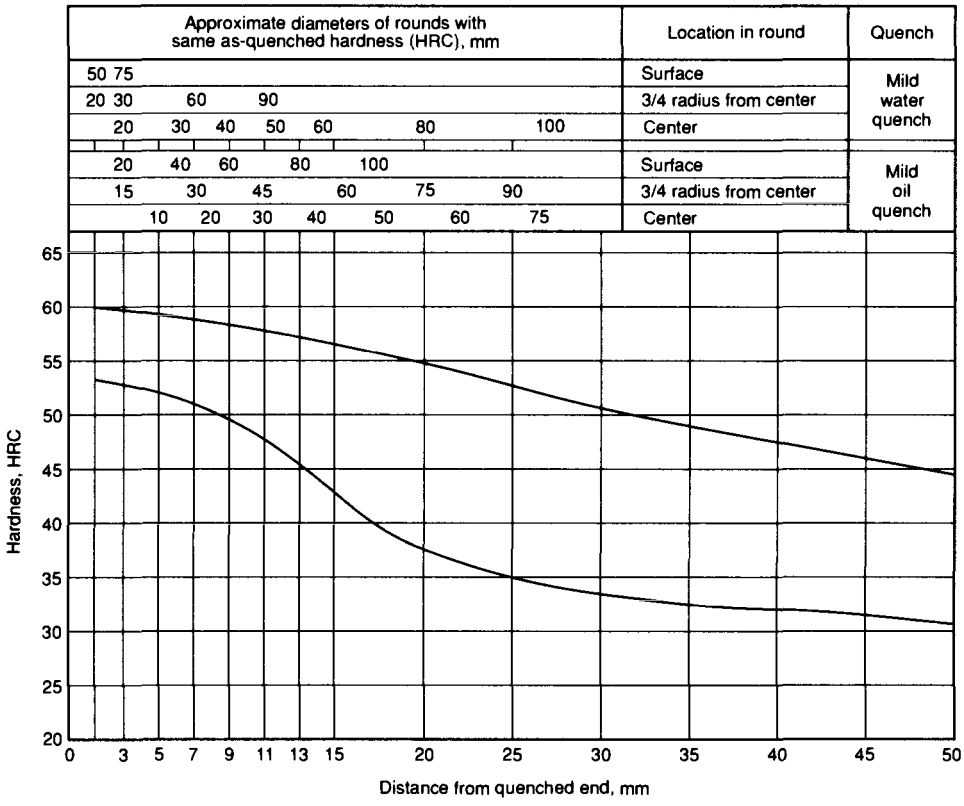

Fig. 5-22 Hardenability band for SAE/AISI 414OH steel. Maximum and minimum Jominy end-quench hardness curves are shown. Source: Ref 46

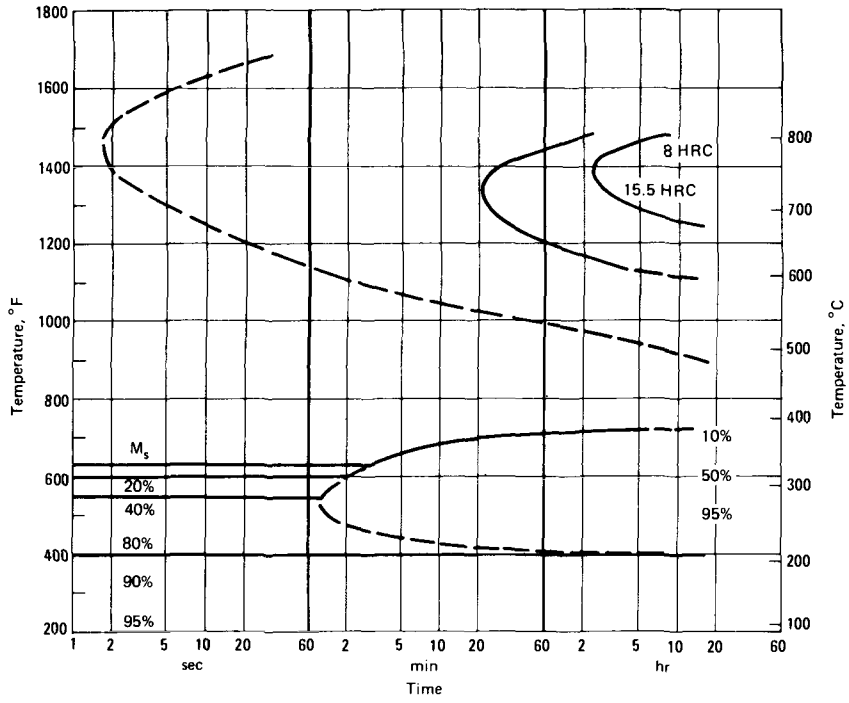

Fig. 5-23 IT diagram for H-13 tool steel containing 0.40% C, 1.0% Si, 5.0% Cr, 1.35% Mo, and 1.10% V and austenitized at 1850 °C (3360 °F). Source: Crucible Steel, Ref 48

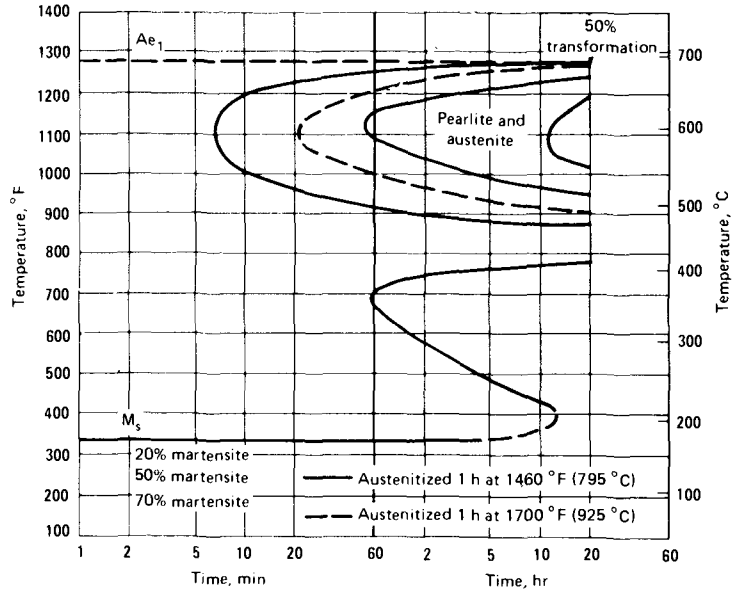

Fig. 5-24 IT diagram for A10 tool steel containing 1.36% C, 1.81% N, 0.15% Cr, and 1.41% Mo and austenitized at 795 and 925 °C (1460 and 1700 °F) as shown. Source: Ref 48

two-phase field and is frequently used to reduce retained austenite content and improve toughness in high-carbon tool and bearing steels, while the higher austenitizing temperature is commonly used for carburizing, and specimens may be directly quenched from this temperature. Figures 5-29 and 5-30 show the effectiveness of molybdenum in promoting hardenability; in view of its strong carbide-forming tendency, its effectiveness is quite sensitive to austenitizing temperature. Silicon in molybdenum-containing steels, as indicated by the curves identified by Si* in Fig. 5-29 and 5-30, is also very

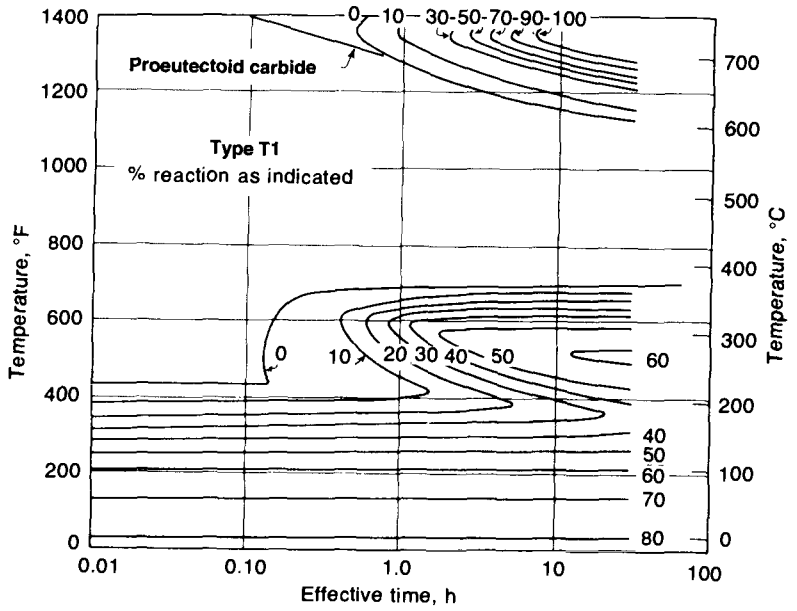

Fig. 5-25 IT diagram for T1 high-speed steel. Source: Ref 49

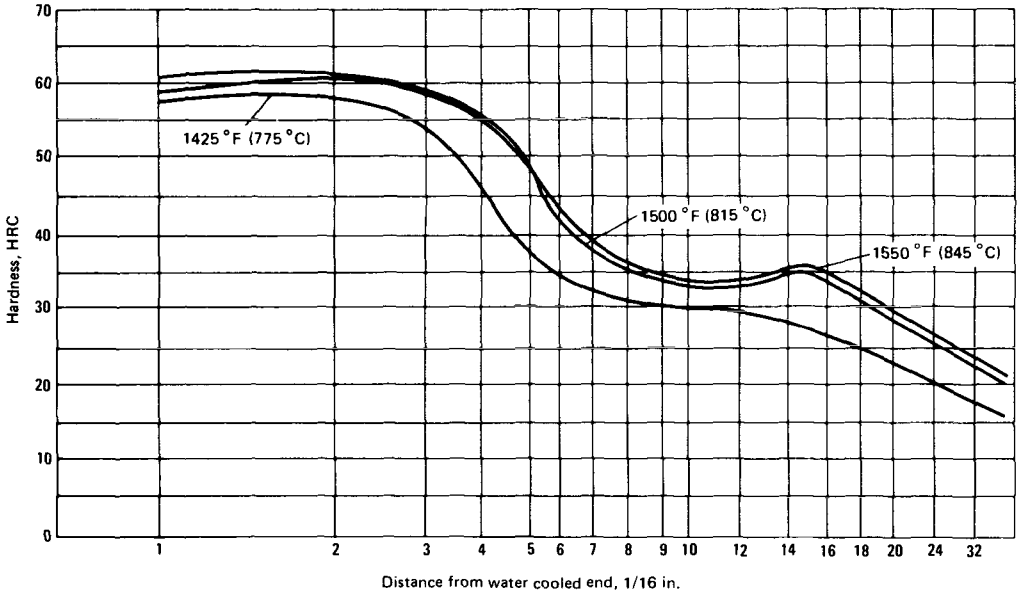

Fig. 5-26 Jominy end-quench curves for L2 tool steel containing 0.50% C, 0.80% Cr, and 0.20% V after austenitizing at three temperatures as shown. Source: Teledyne VASCO, Ref 48

effective in promoting hardenability, especially in steels austenitized at 925 °C (1700 °F).

Jatczak has also studied the hardenability of highly alloyed tool steels that are capable of air hardening (Ref 51). Despite such high hardenability, in very heavy sections of air-hardenable steels cooling rates could be so slow that some nonmartensitic transformation products of low hardness might form. To evaluate the hardenability of such deep-hardening steels, Jatczak developed an air hardenability test bar, 1in. (25 mm) in diam, which is partially inserted into a 6 in. (152 mm) diam bar (Fig. 5-31). The entire assembly is austenitized and cooled in still air; the cooling rates achieved range

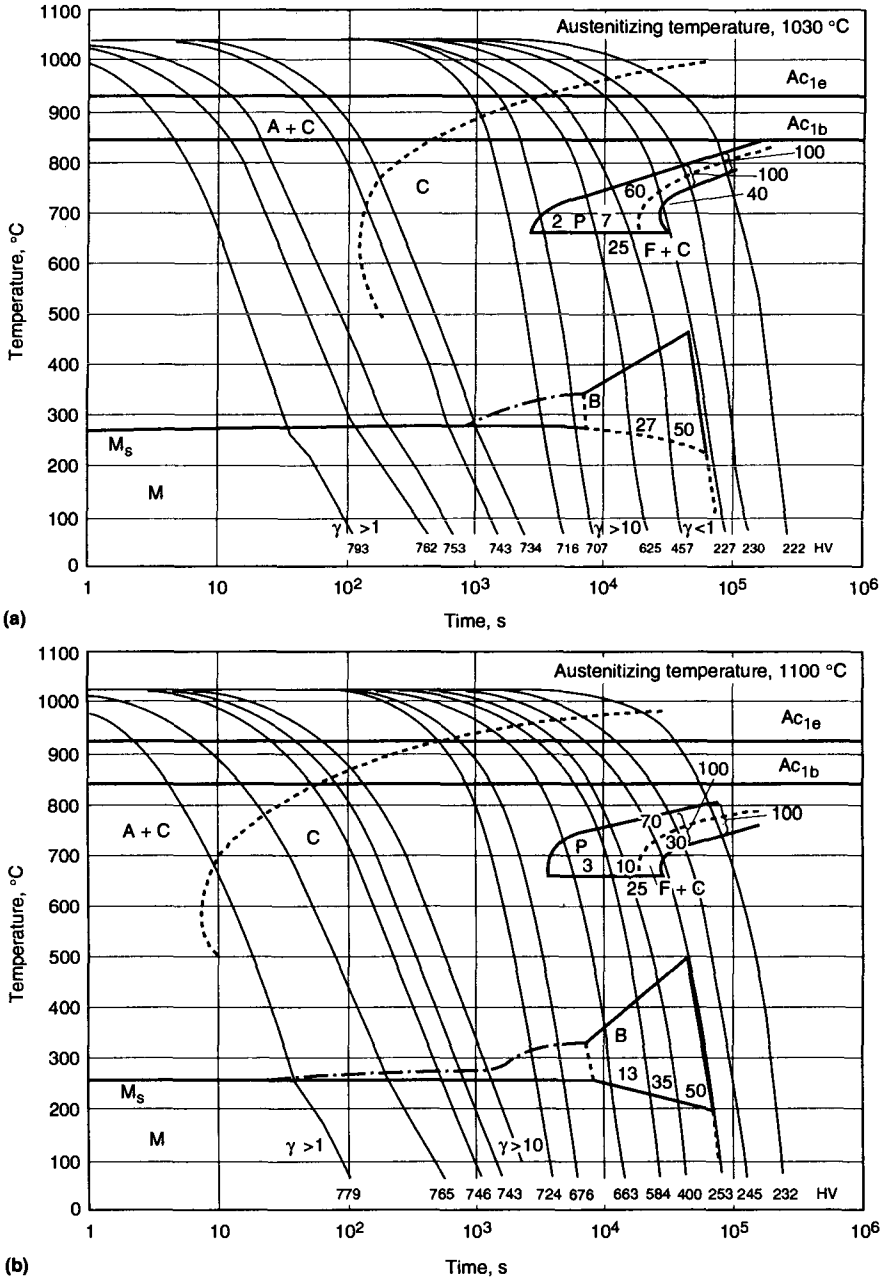

Fig. 5-27 CCT diagrams for H-13 tool steel austenitized at 1030 °C (1885 °F) (a) and 1100 °C (2010 °F) (b). Source: Ref 4 (from Atlas Zur Wärmebehandlung der Stähle

from essentially that of the air-cooled end of a standard Jominy test to very low rates in the portion of the test bar inserted in the large round. Figure 5-32 shows the results of testing four air-hardenable cold-work die steels by the air-hardenability test. The significant differences in the hardenability of these steels would not be detectable by standard Jominy testing.

Martensite Transformation Kinetics and Stabilization

The transformation of austenite to martensite in steels, to a first approximation, is a function only of decreasing temperature. Such time-independent transformation kinetics are referred to as athermal; that is, they occur without thermal activation, in contrast to thermally activated diffusion-controlled transformations. Equation 5-4 describes the athermal formation of martensite:

$$f = 1 - \exp - (1.10 \times 10^{-2} \Delta T) \qquad \text{(Eq 5-4)}$$

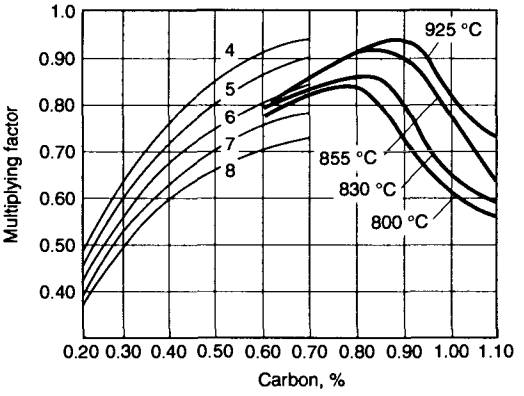

Fig. 5-28 Multiplying factors for carbon as a function of austenitizing temperature for high-carbon steels compared to low-carbon steels. Source: Ref 50

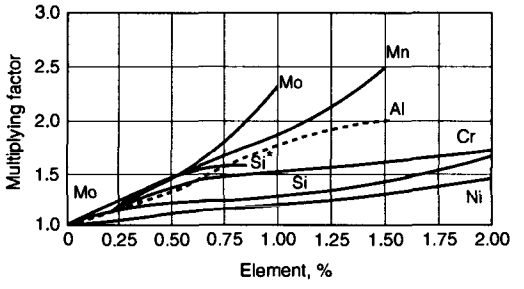

Fig. 5-29 Multiplying factors for alloying elements in high-carbon steels quenched from 830 °C (1525 °F). See text for discussion of Si*. Source: Ref 50

where f is the volume fraction of martensite and ΔT is the undercooling below M_s in degrees centigrade (Ref 52). Thus, when the M_s temperature is known or can be calculated—for example, from Eq 5-1—only the temperature to which the steel is quenched, independent of time, determines the amount of martensite formed.

Figure 5-33 shows the amounts of austenite and martensite formed as a function of temperature for a low-alloy tool steel. The solid curves represent the progress of martensite formation during continuous cooling from two austenitizing temperatures, 845 and 1010 °C (1550 and 1850 °F). The M_s for the specimen austenitized at 1010 °C (1850 °F) is lower than that of the specimen austenitized at 845 °C (1550 °F), because of, as discussed earlier, the greater dissolution of carbides and the corresponding enrichment of the austenite with carbon and other carbide-forming elements. The lower M_s temperature, as shown by Eq 5-1, results in a smaller amount of martensite in the 1010 °C (1850 °F) specimen at room temperature, compared to the amount in the specimen austenitized at 845 °C (1550 °F). However, further cooling below room temperature of both specimens causes additional transformation of austenite to martensite.

The dashed line in Fig. 5-33 shows that if cooling is interrupted by quenching to 70 °C (160 °F) and holding for 30 min. before continued cooling, the martensitic transformation ceases until some lower temperature is reached. This phenomenon, a retardation of the athermal transformation kinetics of austenite to martensite, is known as stabilization and occurs during slow cooling (for example, during oil quenching as compared to water quenching) or when cooling is interrupted. Figure 5-34, presenting another example of stabilization, shows that the effect of interrupted cooling is a function of time at the hold temperature (Ref 53). The mechanism of stabilization has been attributed to stress relaxation or strain aging (i.e., the diffusion of carbon atoms to potential sites of martensite plate nucleation) during isothermal holding (Ref 54, 55). A study involving

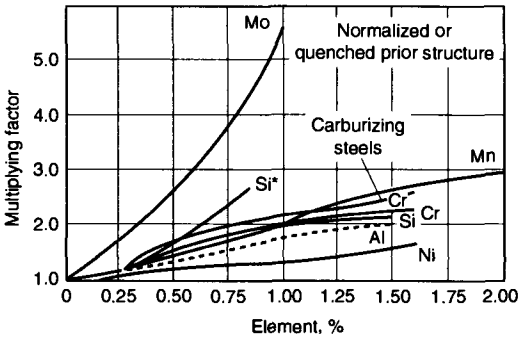

Fig. 5-30 Multiplying factors for alloying elements in high-carbon steels quenched from 927 °C (1700 °F). See text for discussion of Si*. Source: Ref 50

an Fe-19Ni-0.5C alloy showed that stabilization develops over an aging temperature range of 300 to −78 °C (570 to −108 °F) and concluded that several mechanisms must be responsible for stabilization over this temperature range (Ref 55).

Although athermal transformation of austenite to martensite is the dominant mode of martensite formation in steels, isothermal transformation is also sometimes observed. In Fe-Ni-Cr and Fe-Ni-Mn alloys, which have M_s temperatures below room temperature, the isothermal transformation of austenite to martensite occurs as a function of time with C-curve kinetics, as shown in Fig. 5-35 (Ref 56). The isothermal transformation in these alloys is attributed to the thermal activation of small martensite nucleation sites or embryos for the nucleation of stable martensite crystals (Ref 57, 58).

Measurements and models of martensite transformation kinetics, primarily in alloys with subzero M_s temperatures, have recently been comprehensively reviewed by Raghavan (Ref 59). This author also describes a third type of transformation kinetics, termed burst kinetics, where large amounts of transformation occur at a single temperature. This type of kinetics occurs in Fe-Ni and Fe-Ni-C alloys with subzero M_s temperatures and is dependent on the dynamic nucleation of martensite plates by other plates, a process termed autocatalysis.

Isothermal martensite formation has also been documented in high-carbon steels. Okamoto and Oka (Ref 60, 61) have characterized the morphology, crystallography, and isothermal transformation kinetics of two types of martensite in steels containing 1.10 to 1.8% C. Based on morphology, one type is identified as thin plate isothermal martensite (TIM) and the other as lenticular isothermal martensite (LIM). The TIM may become the nucleus of lower bainite, which is then termed lower bainite with midrib (LBm), or the nucleus of LIM, depending on the transformation temperature. Figure 5-36 shows an IT diagram that identifies the kinetics and transformation temperature ranges for the various bainitic and martensitic transformation products in an Fe-1.80C alloy (Ref 60).

Tempering

Tempering, the final heat treatment step applied to tool steels, is defined as the heating of a martensitic or hardened steel to some temperature below the A_1 temperature; this step produces the final structure and mechanical properties of a hardened steel. The preceding austenitizing and quenching steps of hardening are designed to produce the as-quenched microstructures that can be tailored by tempering to produce the desired performance of a given tool steel. As-quenched microstructures consist of martensite and retained austenite, produced by cooling through the M_s from the austenitizing temperature, and alloy carbides retained during austenitizing. The martensite is unstable, in view of the high dislocation density or twin substructure formed as a result of the shear transformation from austenite, and is supersaturated with respect to both carbon and alloying elements at whatever levels were produced in the austenite after chemical partitioning between the austenite and retained carbides during austenitizing.

In carbon and low-alloy steels, the primary purpose of tempering is to raise the toughness and fracture resistance of hardened steels from the very low values characteristic of as-quenched martensite. In more highly alloyed tool steels, tempering can be used not only to increase hardness but also to produce a dispersion of stable alloy carbides resistant to coarsening during exposure to heating. Such coarsening would lower hardness and limit tool life during high-speed machining or high-temperature forging.

Figure 5-37 shows schematically hardness as a function of tempering temperature, assuming a con-

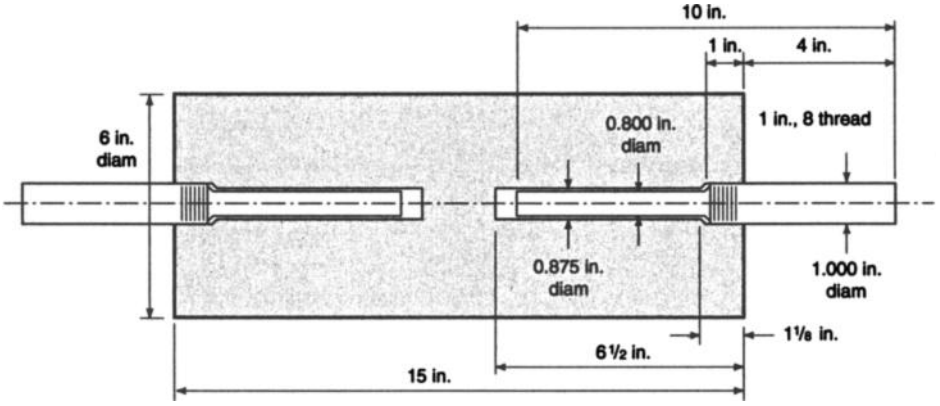

Fig. 5-31 Air-hardenability test bar developed by Jatczak. Source: Ref 51

stant time, or as a function of a tempering parameter that includes both tempering temperature and time as variables for four classes of tempering behavior. Class 1 behavior is typical of carbon and low-alloy steels. Hardness decreases continuously with increasing tempering; concurrently, toughness increases—except in certain temperature ranges where embrittlement phenomena develop (Ref 2).

Air-hardenability data

Type	Heat no.	Grain size	C	Mn	P	S	Si	Cr	Nu + Cu	Mo	V	Norm temp °F	Quench temp °F
A6	△	8-9	.71	2.12			.42	.96	.23	1.27	.025	Anneal	1600
A2	○	9	1.03	.63			.29	5.37	.26	1.00	–	in.	1750
D2	●	7	1.53	.36			.26	12.01	–	.89	.67	in.	1850
A10	□	8-9	1.36	1.84			1.14	.28	1.93	1.41	–	in.	1475
A4	▲	9	.96	2.05			.24	2.09	–	1.12	–	in.	1550

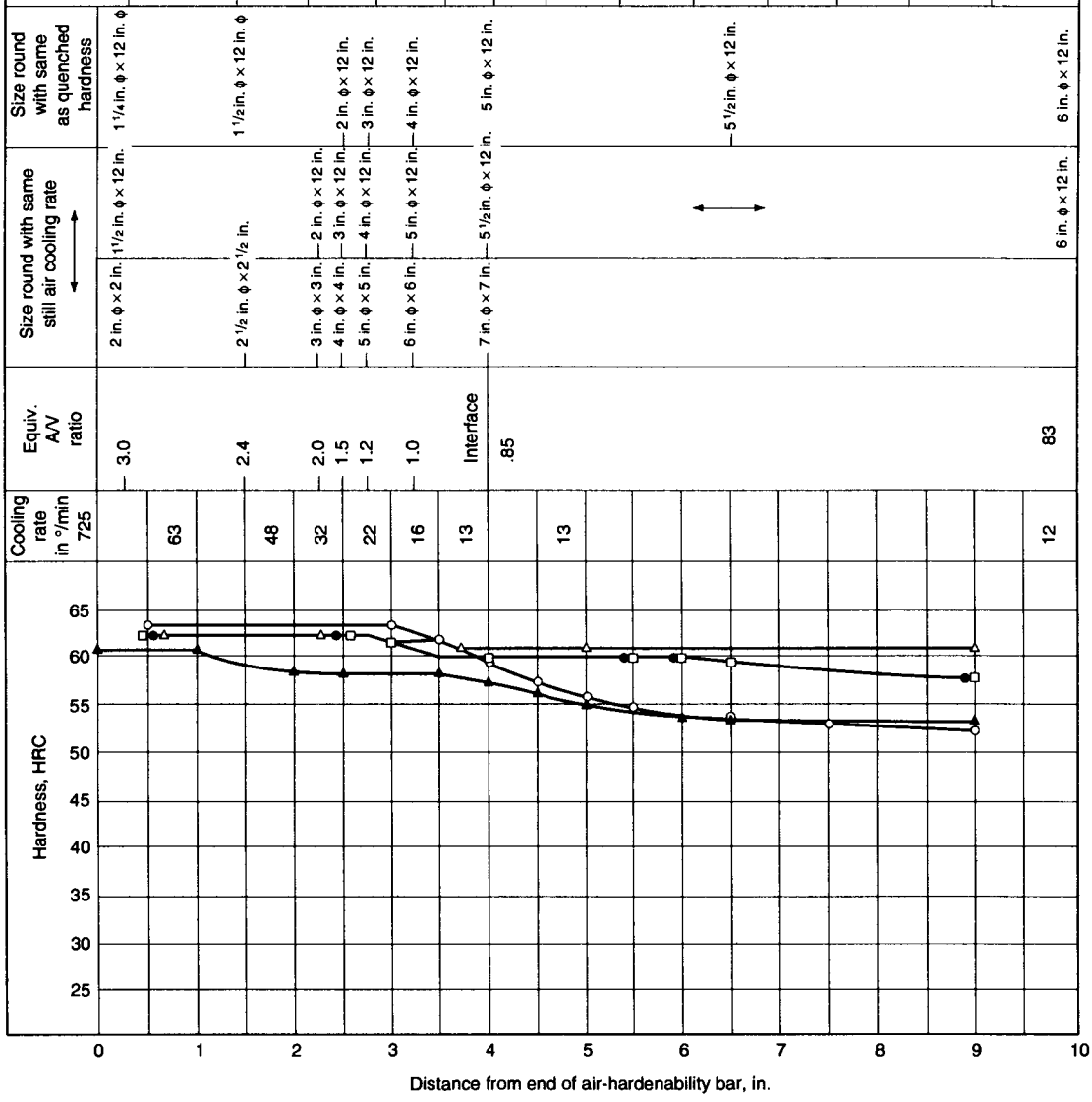

Fig. 5-32 Results of air-hardenability testing of four air-hardening cold-work die steels. Source: Ref 51

Class 2, 3, and 4 tempering behaviors are associated with various grades of alloy tool steels. Class 2 represents the medium- to high-alloy cold-work die steels in which carbide precipitation and accompanying softening are retarded by the alloy additions.

Many steels with low to medium alloy additions have curves between those shown for classes 1 and 2. Class 3 tempering behavior is typical of the highly alloyed high-speed steels that undergo secondary hardening, a precipitation hardening associ-

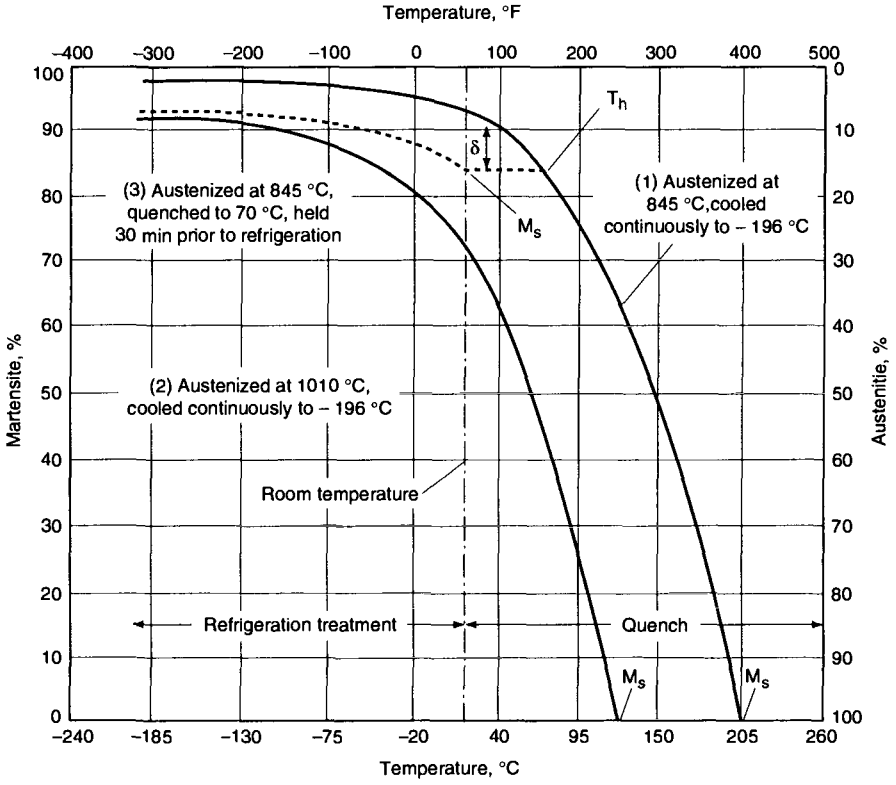

Fig. 5-33 Martensite transformation diagram for a low-alloy tool steel

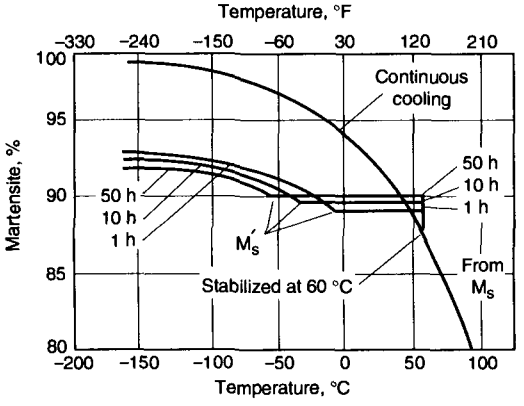

Fig. 5-34 Retardation of martensite transformation as a function of holding time at 60 °C (140 °F) in a 1.1C-0.2Si-0.3Mn steel. Source: Ref 53

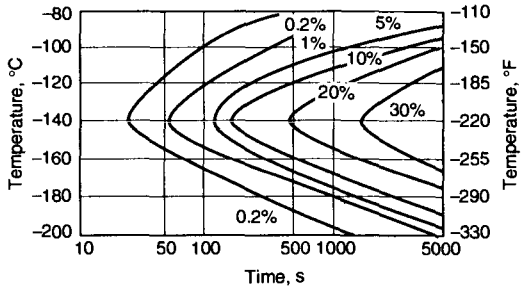

Fig. 5-35 IT curves for martensite formation in an Fe-23Ni-3.6Mn alloy. Curves are identified by the percentage of martensite formed. Source: Ref 56

ated with the precipitation of alloy carbides in tempered martensite. The precipitation of high densities of fine alloy carbides not only retards softening but may also increase hardness to levels equal to or exceeding those in the untempered condition. Class 4 behavior is representative of medium- to high-alloy hot-work die steels in which secondary hardening develops, but the overall hardness is lower than class 3 because of the lower carbon content of these steels.

The high defect density and supersaturation of as-quenched martensite provide the thermodynamic driving forces for a number of time-temperature-dependent microstructural changes during tempering. Also, retained austenite is unstable below A_1 and must therefore transform during tempering. Eventually, the most stable structure that can be developed by tempering is a spherical dispersion of coarse carbides in a matrix of ferrite. However, before this state is reached, many finer dispersions of carbides develop in tempered martensite. The finer dispersions are a result of kinetic limitations associated with short diffusion distances related to low temperatures or the low diffusivity of alloying elements. In order of increasing tempering temperature, assuming a constant time of tempering, the following microstructural changes evolve:

- Carbon atom rearrangement in martensite crystals (A1, . . .)
- Transition iron carbide precipitation in martensite crystals (T1)
- Transformation of retained austenite (T2)
- Cementite precipitation and lowering of martensite tetragonality to produce a bcc ferritic matrix of tempered martensite (T3)
- Precipitation of alloy carbides (T4)

These microstructural changes, and the mechanisms by which they develop, have been of great interest relative to their importance in creating the final service microstructures of hardened steels.

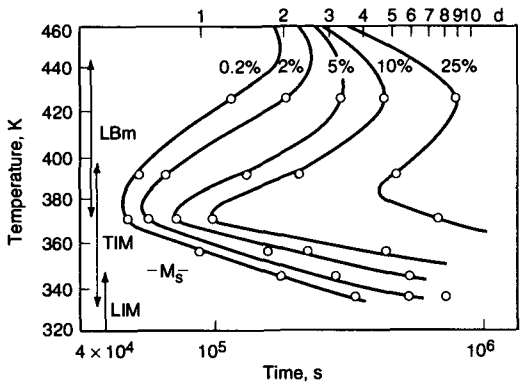

Fig. 5-36 IT curves for LIM, TIM, and LBm in an Fe-1.80C steel. Source: Ref 60

Consequently, there are a number of good reviews and summaries of tempering reactions and structures (Ref 62–67). The remainder of this section briefly reviews selected aspects of the changes that evolve during tempering.

Carbon atom rearrangement may take the form of carbon atom segregation to dislocations and martensite crystal boundaries, clustering of small groups of carbon atoms, development of modulated clusters of carbon atoms on {102} crystal planes of martensite, or the long-period ordering of carbon atoms. These changes occur around room temperature (in the range of –40 to 100 °C (–40 to 210 °F) and are due to the ability of the small interstitial carbon atoms to diffuse at these temperatures. However, despite the ability to diffuse, the diffusion distances in this temperature range are very short, and the resulting structures due to carbon rearrangement are very fine. High-resolution TEM and electron diffraction have been used to identify the structures produced by carbon atom rearrangement, and electrical resistivity changes have been used to follow the kinetics of the rearrangements.

The carbon atom rearrangements occur at temperatures below commercial tempering temperature ranges. Therefore, it has been suggested that the various rearrangements be referred to as aging reactions (A1, A2, . . .) (Ref 65) in order to distinguish them from the tempering reactions or stages (T1, T2, . . .) that are commercially used to adjust microstructure and properties during tempering. The base for characterizing and classifying the various tempering reactions in hardened carbon steels was es-

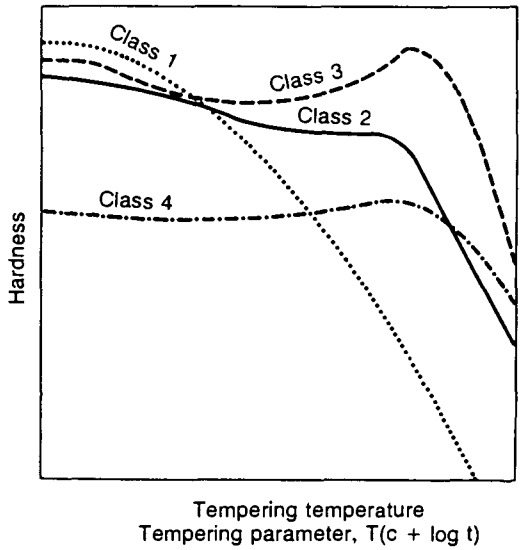

Fig. 5-37 Schematic diagram of hardness versus tempering temperature (assuming constant time at each temperature) or versus a time-temperature tempering parameter for four major types of tempering response in tool steels

tablished by a series of papers written by Cohen and colleagues in the 1950s (Ref 68–71).

The first stage of tempering, T1, consists of the precipitation of transition carbide particles at temperatures between 100 and 200 °C (210 and 390 °F). The crystal structure of the transition carbide was first identified as hexagonal, and the carbide was termed epsilon-carbide (ε-carbide) in order to differentiate it from cementite or θ-carbide (Ref 72). More recently, the crystal structure of the transition carbide was identified as orthorhombic and termed eta-carbide (η-carbide) (Ref 73). The diffraction patterns that identify the diffracting crystal planes of structure can be readily indexed as either hexagonal or orthorhombic, and identification of the structure must be resolved by future work.

The transition carbides precipitate within martensite crystals as rows of very fine particles, only 2 to 4 nm in size. Not all of the carbon supersaturation of the martensite is relieved by the transition carbide precipitation, and the martensitic matrix is estimated to retain about 0.25 wt% C in solution. The first stage of tempering improves toughness, but hardness decreases only slightly from that of as-quenched martensite. High hardness and strength are maintained because the low tempering temperatures limit the size of the transition carbide particles and cause little change in the dislocation substructure of the as-quenched martensite. The transition carbides have been estimated to have compositions between $Fe_{2.4}C$ (Ref 72) and Fe_2C (Ref 73); no substitutional alloying elements, because of their very sluggish diffusion in the temperature range of the first stage, are associated with the formation of the transition carbides.

The second stage of tempering, T2, consists of the transformation of retained austenite to mixtures of ferrite and cementite, and for tempering times on the order of 1 h, occurs in carbon and low-alloy steels at temperatures between 200 and 350 °C (390 and 660 °F). This diffusion-controlled reaction is characterized by an activation energy of 113 kJ/mol (27 kcal/mol), consistent with the activation energy for the diffusion of carbon in austenite. The carbides formed are much coarser than the transition carbides and are responsible for a decrease in toughness referred to as tempered martensite embrittlement (Ref 2).

In highly alloyed tool steels, the retained austenite is much more stable than in low-alloy steels. As a result, the diffusion-controlled transformation of retained austenite is shifted to higher tempering temperatures. Figure 5-38 shows hardness changes and changes in the amount of retained austenite in A2 tool steel as a function of tempering temperature (Ref 74); it is apparent that some austenite is retained to quite high temperatures. Similar to hardened carbon and low-alloy steels, the more highly alloyed austenite may transform to bainitic mixtures of carbides and ferrite. However, depending on alloying, another mechanism of austenite transformation during tempering of tool steels consists of austenite transformation to martensite on cooling after tempering.

Figure 5-39 shows length changes as a function of tempering temperature, obtained by dilatometric analysis, of an M2 tool steel heated three times to tempering temperatures of either 540 or 570 °C (1000 or 1060 °F) (Ref 75, 76). Prior to tempering, this steel contained about 30 vol% retained austenite. Strong indications of the volume changes associated with martensite formation are noted after cooling from the first tempering treatment, only small indications during the second tempering, and no indications after the third tempering. Martensite formation after tempering is attributed to alloy carbide precipitation in the austenite during tempering for secondary hardening. As a result of the reduced carbon and alloy content of the retained austenite, M_s temperatures increase and martensite forms on cooling to room temperature.

Whether the austenite transforms to coarse carbides at the tempering temperature or to untempered martensite on cooling after tempering, either condition increases the sensitivity of a tool steel to brittle fracture. As a result, double and triple tempering treatments are applied to secondary-hardening tool steels, either to spheroidize coarse carbides or to temper the untempered martensite formed after the first or second tempering treatments.

The third stage of tempering, T3, consists of the precipitation of cementite. As more carbon combines with iron in the form of cementite, eventually complete relief of the carbon supersaturation of the martensitic matrix is achieved. The tetragonality of

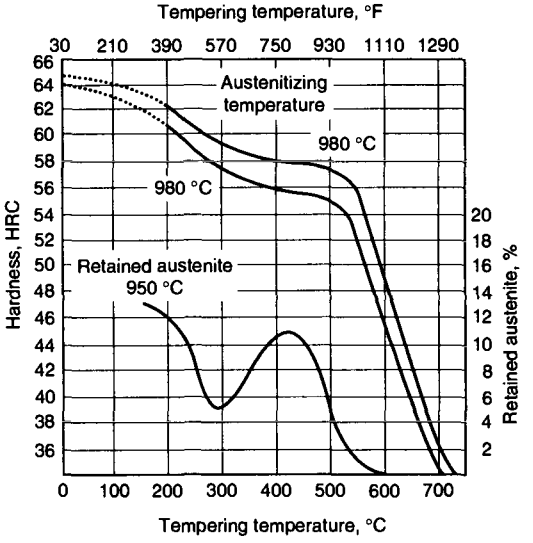

Fig. 5-38 Hardness and retained austenite as a function of tempering in A2 tool steel. Source: Ref 74

the martensite thus is eliminated, and the crystal structure of the martensite becomes cubic. Although the tempered martensitic matrix is now effectively ferrite, it is still referred to as tempered martensite because of its martensitic origin and the fact that the martensitic crystals retain their lath or plate shape to very late stages of tempering. In low-alloy steels, once the ferrite and cementite structure has formed, coarsening continues with increasing tempering. Eventually a spheroidized microstructure, with very low hardness and very high toughness, is produced. Accompanying cementite formation and coarsening, the martensitic crystals coarsen and the high dislocation density of the martensite is substantially reduced by recovery, and by recrystallization, if at high tempering temperatures there are sufficient residual dislocations to provide the necessary strain energy for recrystallization (Ref 66, 67).

All alloying elements, depending on type and amount, retard microstructural coarsening and thus the rate of softening during tempering (Ref 77). However, in highly alloyed tool steels, secondary hardening dramatically reverses the softening typical of low-alloy steels. This reversal is caused by the precipitation of fine alloy carbides in the tempered martensitic matrix. Figure 5-40 shows the sequence of alloy carbide types that develops in two tool steels with various alloying element contents (Ref 78). Prior to the tempering conditions that produce the secondary hardening peak, cementite has formed, as expected from the progress of the third stage of tempering. At low and intermediate tempering temperatures, the substitutional alloying elements do not have sufficient mobility to form carbide particles. At tempering temperatures above 500 °C (930 °F), alloying elements are able to diffuse, albeit only over short diffusion distances because of the low alloy element diffusion coefficients even in this temperature range.

The limited diffusivity of the substitutional alloying elements initially keeps the precipitated carbide particles fine, and thus the characteristic secondary-hardening hardness peaks develop. At higher tempering temperatures, however, diffusion accelerates, and the first-precipitated alloy carbides are replaced by others. These rapidly coarsen and hardness rapidly falls. Tungsten, vanadium, molybdenum, and chromium are the strong carbide-forming elements most commonly used to achieve secondary hardening and must be dissolved in austenite during austenitizing in order to be incorporated during quenching into martensite with sufficient supersaturation for secondary hardening during tempering. Figure 5-41 shows the effect of systematic variations of the strong carbide-forming elements on secondary hardening of a base 0.5% C steel (Ref 79).

The secondary-hardening alloy carbides form as very small disks or needles on specific crystallographic habit planes within the martensitic matrix (Ref 80). Figure 5-42 shows an example of very fine alloy carbide precipitate particles in a highly mag-

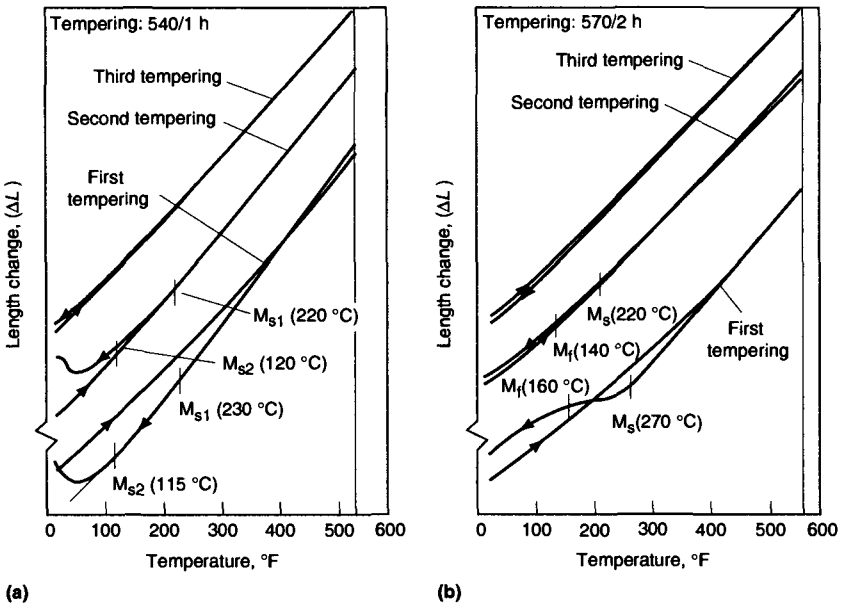

Fig. 5-39 Dilatometric changes as a function of three successive tempering steps in an M2 tool steel. Specimens were cooled after tempering three times (1 h) at 540 °C (1000 °F) (a) and three times (2 h) at 570 °C (1060 °F) (b). Source: Ref 75

nified martensite lath in tempered H13 tool steel. Depending on the dominant alloying elements, the alloy carbides go through sequences of carbides of increasing stability, as shown in Fig. 5-40.

In chromium-rich steels the sequence of carbides is M_3C to M_7C_3 to $M_{23}C_6$, whereas in molybdenum- and tungsten-rich steels the sequence is M_3C to M_2C to M_6C. The more stable carbides tend to coarsen rapidly and to lower hardness and performance. Carbides with multiple alloying elements have high stability and resistance to coarsening. Manganese and nickel have relatively little effect on tempering resistance, but cobalt (which in itself is not a carbide former), when combined with molybdenum and tungsten, enhances secondary hardening and promotes hardness retention to higher temperatures. The cobalt may reduce the rate of recovery of the martensitic substructure, thereby providing nucleation sites for more and finer alloy carbide particles for secondary hardening (Ref 81).

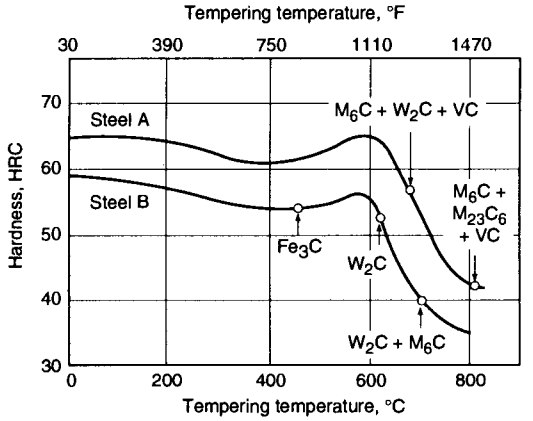

Fig. 5-40 Sequence of alloy carbide formation in two steels. Steel A contains 0.8% C, 18% W, 4% Cr, 2% V, and 10% Co; steel B contains 0.8% C, 9% W, 3% Cr, and 3% Co. Source: Ref 78

Each tool steel has its recommended tempering conditions for optimum performance. These temperatures, together with recommended austenitizing temperatures, are listed in Table 5-3. In order to prevent cracking, tempering should be performed as soon as possible after quenching, and heating to tempering temperatures should be slow to ensure uniform temperature distribution within a tool. Table 5-5 presents approximate heating times to attain various temperatures in parts of various sizes and geometries. Slow cooling in still air after tempering is recommended to minimize development of residual stresses.

REFERENCES

1. J.R.T. Branco and G. Krauss, Heat Treatment and Microstructure of Tool Steels for Molds and Dies, *Tool Materials for Molds and Dies,* G. Krauss and H. Nordberg, Ed., Colorado School of Mines Press, 1987, p 94–117
2. G. Krauss, *Steels: Heat Treatment and Processing Principles,* ASM International, 1990
3. Abrasives for Grinding Operations, *ASM Specialty Handbook: Tool Materials,* J.R. Davis, Ed., ASM International, 1995, p 101–115
4. K.-E. Thelning, *Steel and Its Heat Treatment,* 2nd ed., Butterworths, London, 1984
5. T. Ando and G. Krauss, The Isothermal Thickening of Cementite Allotriomorphs in a 1.5Cr-1C Steel, *Acta Metall.,* Vol 29, 1981, p 351–363
6. B.A. Becherer and T.J. Witheford, Introduction to Heat Treating of Tool Steels, *Heat Treating,* Vol 4, *ASM Handbook,* ASM International, 1991, p 711–725
7. W.C. Leslie, *The Physical Metallurgy of Steels,* McGraw-Hill, 1981
8. H. Ohtani, Processing—Conventional Heat Treatments, *Constitution and Properties of Steels,* F.B.

Table 5-5 Approximate heating times recommended to attain tempering temperatures

Tempering temperature		Time required to reach furnace temperature(a): In hot air oven without circulation(b)						In circulating air oven or an oil bath(c)					
		Cubes or spheres		Squares or cylinders		Average flats		Cubes or spheres		Squares or cylinders		Average flats	
°C	°F	min/mm	min/in.	min/mm	min/in.	min/mm	min/in.	min/mm	min/in.	min/mm	min/in.	min/mm	min/in.
120	250	1.2	30	2.2	55	3.2	80	0.6	15	0.8	20	1.2	30
150	300	1.2	30	2.0	50	3.0	75	0.6	15	0.8	20	1.2	30
175	350	1.2	30	2.0	50	2.8	70	0.6	15	0.8	20	1.2	30
205	400	1.0	25	1.8	45	2.6	65	0.6	15	0.8	20	1.2	30
260	500	1.0	25	1.6	40	2.4	60	0.6	15	0.8	20	1.2	30
315	600	1.0	25	1.6	40	2.2	55	0.6	15	0.8	20	1.2	30
370	700	0.8	20	1.4	35	2.0	50	0.6	15	0.8	20	1.2	30
425	800	0.8	20	1.2	30	1.8	45	0.6	15	0.8	20	1.2	30
≥480	≥900	0.8	20	1.2	30	1.6	40	0.6	15	0.8	20	1.2	30

(a) Data are given in minutes per millimeter, and in minutes per inch of diameter or thickness, with furnace maintained at the temperature indicated in column 1. Data may be used as a guide for charges of irregular shapes and quantities by estimating total size of charge and applying the above allowance to the number of inches from outside to center of charge. (b) Times indicated are for tools with dark or scaled surfaces. If surfaces or finish ground, or otherwise brightened, twice as much time should be allowed in a still hot air oven. No extra allowance need be made for bright surfaces in a circulating oven or in an oil bath. (c) Oil baths are usually not used above 205 °C (400 °F).

Pickering, Ed., Vol 7, *Materials Science and Technology*, VCH Publishing, Weinheim, Germany, 1992, p 147–181

9. A.H. Rosenstein, Interpretation of Stress Relaxation Data for Stress-Relief Application, *J. Mater.*, Vol 6 (No. 2), 1971, p 265–281
10. B.A. Becherer, Processes and Furnace Equipment for Heat Treating of Tool Steels, *Heat Treating*, Vol 4, *ASM Handbook*, ASM International, 1991, p 726–733
11. S. Chattopadhyay and C.M. Sellars, Quantitative Measurements of Pearlite Spheroidization, *Metallography*, Vol 10, 1977, p 89–105
12. K.R. Hayes, "The Effect of Intercritical Heating and Phosphorus on Austenite Formation and Carbide Distribution of AISI 52100 Steel," M.S. thesis, Colorado School of Mines, 1984
13. R.A. Oriani, Ostwald Ripening of Precipitates in Solid Matrices, *Acta Metall.*, Vol 12, 1964, p 1399–1409

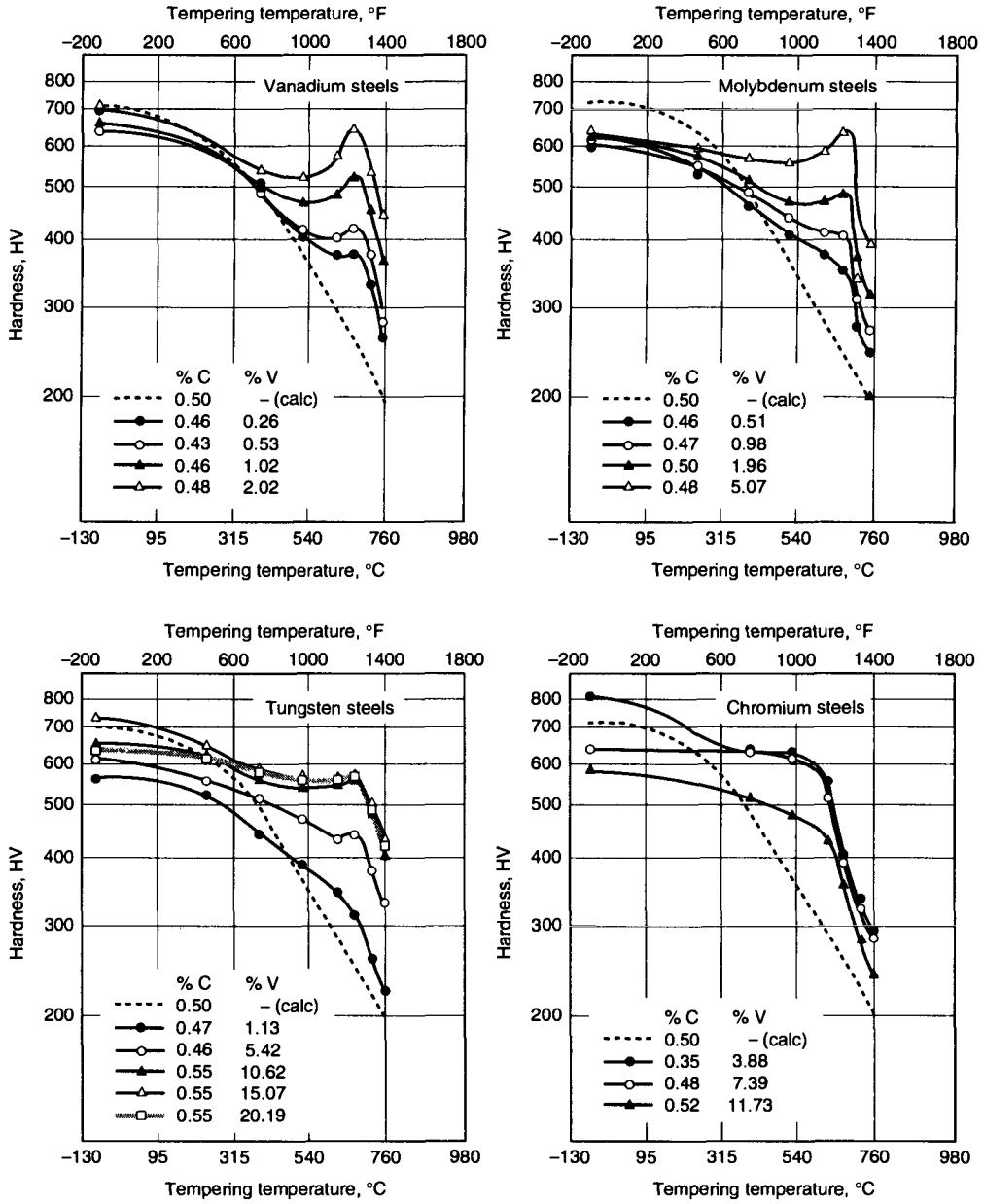

Fig. 5-41 Secondary hardening due to alloy carbide precipitation as produced by increasing additions of vanadium, molybdenum, tungsten, and chromium in 0.5% C steel. Source: Ref 79

14. J. Agren, Kinetics of Carbide Dissolution, *Scand. J. Metall.*, Vol 19, 1990, p 2–8
15. P. Malecki and E.W. Langer, Dissolution of Cementite with Alloying Elements in Austenite, *Scand. J. Metall.*, Vol 19, 1990, p 182–186
16. E.L. Brown and G. Krauss, Retained Carbide Distribution in Intercritically Austenitized 52100 Steel, *Metall. Trans. A*, Vol 17A, 1986, p 31–36
17. M.V. Speight, Growth Kinetics of Grain-Boundary Precipitates, *Acta Metall.*, Vol 16, 1968, p 133–135
18. W. Wilson, *Metallurgy and Heat Treatment of Tool Steels*, McGraw-Hill, London, 1975
19. Wrought High-Speed Tool Steels, *ASM Specialty Handbook: Tool Materials*, J.R. Davis, Ed., ASM International, 1995, p 10–20
20. K.W. Andrews, Empirical Formulae for the Calculation of Some Transformation Temperatures, *J. Iron Steel Inst.*, Vol 203, 1965, p 721–727
21. P. Payson and C.H. Savage, Martensite Reactions in Alloy Steels, *Trans. ASM*, Vol 33, 1944, p 261–275
22. W.J. Harris, Jr., and M. Cohen, Stabilization of the Austenite-Martensite Transformation, *Trans. AIME*, Vol 180, 1949, p 447–470
23. C. Zener, referenced by C.S. Smith, *Trans. TMS-AIME*, Vol 175, 1948, p 15
24. T. Gladman, On the Theory of the Effect of Precipitate Particles on Grain Growth in Metals, *Proc. R. Soc.(London) A*, Vol 294, 1966, p 298–309
25. E. Kula and M. Cohen, Grain Growth in High Speed Steel, *Trans. ASM*, Vol 46, 1954, p 727–758
26. A.H. Grobe, G.A. Roberts, and D.S. Chambers, Discontinuous Grain Growth in High Speed Steel, *Trans. ASM*, Vol 46, 1954, p 759–788
27. H.E. Boyer and T.L. Gall, Ed., *Metals Handbook Desk Edition*, American Society for Metals, 1985
28. E.C. Bain and H.W. Paxton, *Alloying Elements in Steels*, 2nd ed., American Society for Metals, 1961
29. G. Krauss, Microstructures, Processing, and Properties of Steels, *Properties and Selection: Iron, Steels, and High-Performance Alloys*, Vol 1, ASM International, 1990, p 126–139
30. M. Cohen, The Strengthening of Steel, *Trans. TMS-AIME*, Vol 224, 1962, p 638–656
31. W.C. Leslie and R.J. Sober, The Strength of Ferrite and of Martensite as Functions of Composition, Temperature and Strain Rate, *Trans. ASM*, Vol 60, 1967, p 459–484

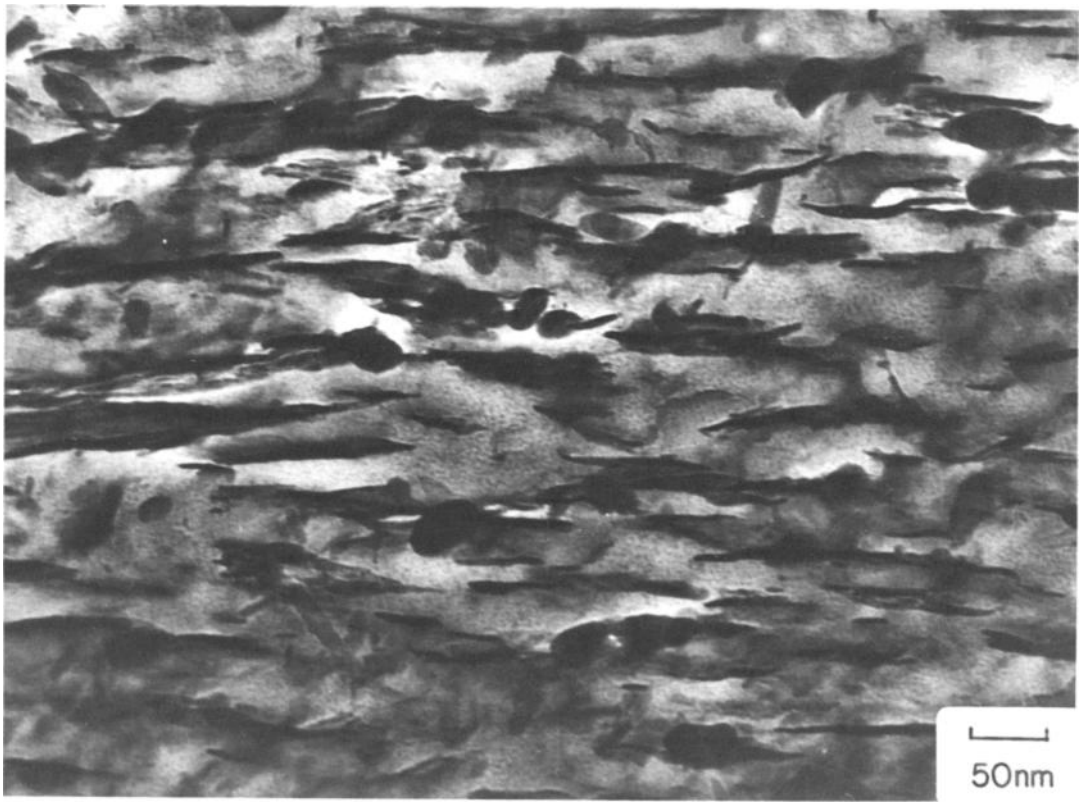

Fig. 5-42 Fine alloy carbide particles (thin, black linear features) in a lath or single crystal of martensite in H13 tool steel tempered 100 h at 530 °C. TEM micrograph. Courtesy of J.R.T. Branco

32. G. Krauss, Heat Treated Martensitic Steels: Microstructural Systems for Advanced Manufacture, *Iron Steel Inst. Jpn. Int.*, Vol 35 (No. 4), 1995, p 349–359
33. C.A. Siebert, D.V. Doane, and D.H. Breen, *The Hardenability of Steel*, American Society for Metals, 1977
34. M.A. Grossmann and E.C. Bain, *Principles of Heat Treatment*, American Society for Metals, 1964
35. V.F. Zackay and H.I. Aaronson, Ed., *Decomposition of Austenite by Diffusional Processes*, Interscience, New York, 1962
36. H.I. Aaronson, Ed., *Phase Transformations*, American Society for Metals, 1970
37. H.I. Aaronson, D.E. Laughlin, R.F. Sekerka, and C.M. Wayman, Ed., *Solid-Solid Phase Transformations*, TMS-AIME, 1982
38. A.R. Marder and J.I. Goldstein, Ed., *Phase Transformations in Ferrous Alloys*, TMS-AIME, 1984
39. Symposium on Atomistic Mechanisms of Nucleation and Growth in Solids, *Metall. Mater. Trans. A*, Vol 27A, 1996, p 1431–1689
40. D.V. Doane and J.S. Kirkaldy, Ed., *Hardenability Concepts with Applications to Steel*, TMS-AIME, 1978
41. F.A. Jacobs, "Combined Effects of P and C on Hardenability and Phase Transformation Kinetics in 41xx Steels," M.S. thesis, Colorado School of Mines, 1982
42. H. Okamoto and M. Oka, Lower Bainite with Midrib in Hypereutectoid Steels, *Metall. Trans. A*, Vol 17A, 1986, p 1113–1120
43. *Atlas zür Warmebehandlung der Stahle*, Vol 1–4, Max-Planck-Institüt für Eisenforschung, in cooperation with the Verein Deutscher Eisenhüttenleute, Verlag Stahleisen, Dusseldorf, 1954–1976
44. W.E. Jominy and A.L. Boegehold, *Trans. ASM*, Vol 26, 1938, p 574
45. ASTM Method A 255 and SAE Standard J406
46. Hardenability of Carbon and Low-Alloy Steels, *Properties and Selection: Irons, Steels, and High-Performance Alloys*, Vol 1, ASM International, 1990, p 451–570
47. G.F. Vander Voort, Ed., *Atlas of Time-Temperature Diagrams for Irons and Steels*, ASM International, 1991
48. H. Chandler, Ed., *Heat Treater's Guide: Practices and Procedures for Irons and Steels*, 2nd ed., ASM International, 1995
49. M. Cohen, M.P. Gordon, and R.S. Rose, The Kinetics of Austenite Decomposition in High Speed Steel, *Trans. ASM*, Vol 31, 1943, p 161
50. C.F. Jatczak, Hardenability in High Carbon Steels, *Metall. Trans.*, Vol 4, 1973, p 2267–2277
51. C. F. Jatczak, Assessment of Hardenability in Deep Hardening Steels, *Hardenability Concepts with Applications to Steel*, D.V. Doane and J.S. Kirkaldy, Ed., TMS-AIME, 1978, p 334–346
52. D.P. Koistinen and R.E. Marburger, A General Equation Prescribing the Extent of the Austenite-Martensite Transformation in Pure Iron-Carbon Alloys and Plain Carbon Steels, *Acta Metall.*, Vol 7, 1959, p 59–60
53. M. Cohen, Retained Austenite, *Trans. ASM*, Vol 41, 1949, p 35
54. K.R. Kinsman and J.S. Shyne, Thermal Stabilization of Austenite in Iron-Nickel-Carbon Alloys, *Acta Metall.*, Vol 15, 1967, p 1527–1543
55. R. Brook, T.K. Sanyal, and G. White, Thermal Stabilization of Austenite in a High-Nickel Steel, *Metall. Trans. A*, Vol 8A, 1977, p 1449–1452
56. C.H. Shih, B.L. Averbach, and M. Cohen, Some Characteristics of the Isothermal Martensitic Transformation, *Trans. TMS-AIME*, Vol 203, 1955, p 183–187
57. V. Raghavan and M. Cohen, Measurement and Interpretation of Isothermal Martensitic Kinetics, *Metall. Trans.*, Vol 2, 1971, p 2409–2418
58. S.R. Pati and M. Cohen, Nucleation of the Isothermal Martensitic Transformation, *Acta Metall.*, Vol 17, 1969, p 189–199
59. V. Raghavan, Kinetics of Martensitic Transformations, *Martensite*, G.B. Olson and W.S. Owen, Ed., ASM International, 1992, p 197–225
60. H. Okamoto and M. Oka, Kinetics and Crystallography of Isothermal Martensite Transformation in Hypereutectoid Steels, *Proc. Int. Conf. Martensitic Transformations*, Japan Institute of Metals, Tokyo, 1986, p 276–281
61. M. Oka and H. Okamoto, Isothermal Transformations in Hypereutectoid Steels, *Proc. Int. Conf. Martensitic Transformations*, Japan Institute of Metals, Tokyo, 1986, p 271–275
62. G.R. Speich and W.C. Leslie, Tempering of Steel, *Metall. Trans.*, Vol 3, 1972, p 1043–1054
63. Y. Imai, Phases in Quenched and Tempered Steels, *Trans. Jpn. Inst. Met.*, Vol 16, 1975, p 721–734
64. The Peter G. Winchell Symposium on the Tempering of Steel, *Metall. Trans. A*, Vol 14A, 1983, p 991–1145
65. G. Krauss, Tempering and Structural Change in Ferrous Martensitic Structures, *Phase Transformations in Ferrous Alloys*, A.R. Marder and J.I. Goldstein, Ed., TMS-AIME, 1984, p 101–123
66. G. Krauss and P.E. Repas, Ed., *Fundamentals of Aging and Tempering in Bainitic and Martensitic Steel Products*, Iron and Steel Society, 1992
67. G.R. Speich and K.A. Taylor, Tempering of Ferrous Martensites, *Martensite*, G.B. Olson and W.S. Owen, Ed., ASM International, 1992, p 243–275
68. C.S. Roberts, B.L. Averbach, and M. Cohen, The Mechanism and Kinetics of the First Stage of Tempering, *Trans. ASM*, Vol 45, 1953, p 576–604
69. B.S. Lement, B.L. Averbach, and M. Cohen, Microstructural Changes on Tempering Iron-Carbon Alloys, *Trans. ASM*, Vol 46, 1954, p 851–881
70. F.E. Werner, B.L. Averbach, and M. Cohen, The Tempering of Iron-Carbon Martensite Crystals, *Trans. ASM*, Vol 49, 1957, p 823–841
71. B.S. Lement, B.L. Averbach, and M. Cohen, Further Study of Microstructural Changes on Tempering Iron-Carbon Alloys, *Trans. ASM*, Vol 47, 1955, p 291–319

72. K.H. Jack, Structural Transformations in the Tempering of High Carbon Martensitic Steel, *J. Iron Steel Inst.*, Vol 169, 1951, p 26–36
73. Y. Hirotsu and S. Nagakura, Crystal Structure and Morphology of the Carbide Precipitated from Martensitic High Carbon Steel during the First Stage of Tempering, *Acta Metall.*, Vol 20, 1972, p 645–655
74. Data Sheets: Cold Work Tool Steel, Uddeholm Steel Division, Hagfors, Sweden
75. A. Kulmburg, E. Kaiser, and S. Wilmes, Rationalisierungsmoglichkeiten beim Anlassen von Schnellarbeitsstahlen, *Härt.-Tech. Mitt.*, Vol 42 (No. 3), 1987, p 133–138
76. A. Kulmburg, E. Kaiser, and F. Korntheuer, Vorgange beim Anlassen von Warm- und Kaltarbeitsstahlen, *Härt.-Tech. Mitt.*, Vol 44 (No. 2), 1989, p 3–7
77. R.A. Grange, C.R. Hibral, and L.F. Porter, Hardness of Tempered Martensite in Carbon and Low-Alloy Steels, *Metall. Trans. A*, Vol 8A, 1977, p 1775–1785
78. H.W. Rayson, Tool Steels, *Constitution and Properties of Steels*, F.B. Pickering, Ed., VCH Publishing, 1992, p 581–640
79. W. Crafts and J.L. Lamont, Secondary Hardening of Tempered Martensitic Alloy Steel, *Trans. TMS-AIME*, Vol 180, 1949, p 471
80. R.W.K. Honeycombe and H.K.D.H. Bhadeshia, *Steels: Microstructure and Properties*, 2nd ed., Edward Arnold, London, 1995
81. V.K. Chandhok, J.P. Hirth, and E.J. Dulis, Effect of Cobalt on Tempering Tool and Alloy Steels, *Trans. ASM*, Vol 56, 1963, p 677–692

Tool Steels: 5th Edition
George Roberts, George Krauss, Richard Kennedy, p 109-123
DOI:10.1361/toos1998p109

Copyright © 1998 ASM International®
All rights reserved.
www.asminternational.org

CHAPTER 6
Practical Aspects of Tool Steel Heat Treatment

Heat treatment of tool steels is as important as the selection of the grade itself. Machine tools or production dies made from tool steels should never have their rigid metallurgical requirements compromised or outweighed by cost considerations. These requirements involve control of the surface condition and chemistry, the temperature (often up to 1315 °C, or 2400 °F), the time at a given temperature, and the heating and cooling rates. Special attention must be paid to these requirements in the design, construction, and operation of furnaces used to heat treat tool steels, especially those used for hardening, where metallurgical factors become all-important. Attempting to reduce production costs by bypassing heat treatment steps will yield an end product that fails to meet tool life expectations and does not justify its high initial expense.

Furnaces for heat treatment of tool steels include ceramic-lined salt bath furnaces, vacuum furnaces, controlled-atmosphere furnaces, and fluidized-bed furnaces.

Salt Bath Furnaces

Molten salts of various compositions are well adapted to all operations in the heat treatment of tool steels. Salt bath heating is the predominant method of hardening high-speed tool steels, providing excellent results for tools that cannot be ground after hardening or that require an excellent surface condition and sharp edges.

Table 6-1 lists various salt bath compositions and processing temperatures for heat treatment of tool steels. With correct operating conditions, tools can be heat treated without carburization, decarburization, or scaling. The surface will be fully hard with a minimum of distortion. Three types of salt baths are generally used:

- *Preheating bath:* minimizes thermal shock, equalizes temperature, and minimizes the amount of time required at the high-temperature stage
- *High-temperature bath:* serves as the austenitizing step

Table 6-1 Typical compositions and recommended working temperature ranges of salt mixtures used in heat treating of tool steels

Salt mixture	Composition, %						Melting point		Working range	
No.	$BaCl_2$	NaCl	KCl	$CaCl_2$	$NaNO_3$	KNO_3	°C	°F	°C	°F
Austenitizing salts (high heat)										
1	98–100	...	...	...	...	...	950	1742	1035–1300	1895–2370
2	80–90	10-20	...	...	...	...	870	1598	930–1300	1705–2370
Preheat salts										
3	70	30	...	...	...	...	335	635	700–1035	1290–1895
4	55	20	25	...	...	...	550	1022	590–925	1095–1700
Quench and temper salts										
5	30	20	...	50	...	...	450	842	500–675	930–1250
6	...	...	...	...	55–80	20–45	250	482	285–575	545–1065

- *Quenching bath:* equalizes the temperature and ensures a clean surface after heat treatment

Most tools that are heat treated in salt baths are fully hard from surface to core, regardless of the section thickness. Distortion and residual stress are minimized due to temperature uniformity.

Heat treatment in salt baths is accomplished by conduction, with the molten salt providing a ready source of heat as required. Although steels come in contact with heat through the tool surfaces, the core of a tool rises in temperature at approximately the same rate as its surface. Heat is quickly drawn to the core from the surface. Salt baths provide heat at a rate equal to the heat absorption rate of the total tool. Convection or radiation heating methods are unable to maintain the rate of heating necessary to reach equilibrium with the rate of heat absorption. The ability of a salt bath to supply heat at a rapid rate enhances the uniformity of properties and the resultant tool quality. Heat-treating times are shortened, as well. For example, a bar 25 mm (1 in.) in diameter can be heated to temperature equilibrium in 4 min in a salt bath, whereas 20 to 30 min would be required to obtain the same properties in convection or radiation furnaces.

Salt baths are efficient; about 93 to 97% of the electric power consumed goes directly into heating. Tool steels that are heat treated in salt baths typically are processed in ceramic-lined furnaces with submerged or immersed electrodes containing chloride-based salts. More detailed information on the salt bath furnaces described here can be found in Ref 1.

Immersed-Electrode Salt Bath Furnaces. Ceramic-lined furnaces with immersed (over-the-side) electrodes (Fig. 6-1) have greatly extended the useful range and capacity of molten salt equipment compared to externally heated pot furnaces. The most important of these advances are that:

- The electrodes can be replaced without bailing out the furnace.
- Immersed electrodes allow more power capacity to be put into the furnace, thus increasing production.
- Immersed electrodes permit easy start-up when the bath is solid. A simple gas torch is used to melt a liquid path between the two electrodes, which allows the electrodes to pass current through the salt to obtain operating temperatures.

However, immersed-electrode furnaces are not as energy-efficient as submerged-electrode furnaces (discussed below). The area in which the immersed electrodes enter the salt bath allows additional heat loss through increased surface area. In the submerged-electrode furnaces shown in Table 6-2 (furnaces A and B), the surface area of the salt bath, A, is smaller than the surface area of the salt bath plus the surface area of the immersed electrodes, A + B, in the immersed-electrode furnaces (furnaces C, D, and E). Placing a

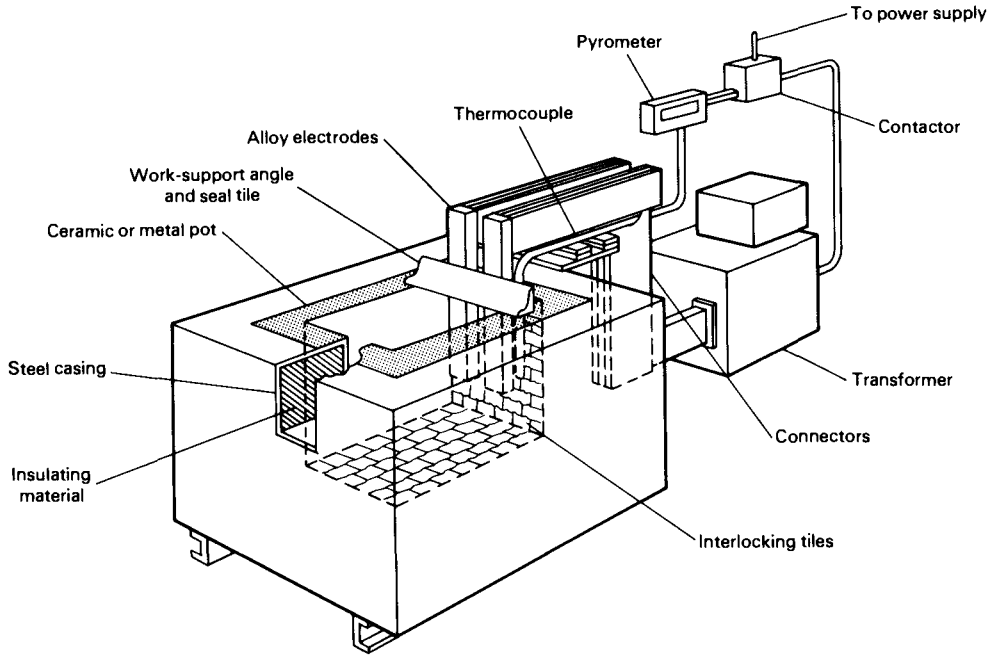

Fig. 6-1 Internally heated salt bath furnace with immersed electrodes and ceramic tiles

good cast ceramic and fiber-insulated cover over the bath and electrodes can reduce surface radiation losses up to 60%.

Immersed-electrode furnaces are lined with superduty fireclay brick. Approximately 130 mm (5 in.) of castable and insulating brick then surrounds the fireclay brick on five sides. Figure 6-1 is a schematic drawing of an immersed-electrode furnace with interlocking tiles and removable electrodes. The removable electrodes enter the furnace from the top, and a seal tile is located in front of the electrodes to protect them from exposure to air at the air/bath interface. This protection helps prolong electrode life. Table 6-2 compares the service lives of electrodes and refractories for some basic furnace designs.

Submerged-electrode salt bath furnaces have the electrodes placed beneath the working depth for bottom heating (Fig. 6-2). Many submerged-electrode furnaces are designed for specific production requirements and are equipped with patented features that offer certain economical and technical advantages. General characteristics of submerged-electrode furnaces include:

- *Maximum work space with minimum bath area:* The electrodes do not occupy any portion of the bath surface, so they come in contact only with the salt. Consequently, bath size is smaller, and electrode life increases many times over by incorporating unidirectional wear and eliminating excessive deterioration at the air/bath interface.
- *Circulation-convection currents:* Bottom heating provides more uniform bath temperatures and bath movement through the use of natural convection currents.
- *Triple-layer ceramic wall construction:* The temperature gradients through the wall cause any salt penetrating the wall to solidify before it can pene-

Table 6-2 Service life of electrodes and refractories

Operating temperature		Service life, years	
°C	°F	Electrodes	Refractories
Submerged-electrode furnaces			
Furnace A			
535–735	1000–1350	15–25	15–25
735–955	1350–1750	6–12	6–12
955–1175	1750–2150	5–7	5–7
1010–1285	1850–2350	2–4	2–4
Furnace B			
535–735	1000–1350	10–20	10–20
735–955	1350–1750	4–8	4–8
955–1175	1750–2150	3–4	3–4
1010–1285	1850–2350	1–3	1–3
Immersed-electrode furnaces			
Furnace C			
535–735	1000–1350	2–4(a)	4–5
735–955	1350–1750	1–2(a)	2–3
955–1175	1750–2150	½–1(a)	1–2
1010–1285	1850–2350	¼–½(a)	1½
Furnace D			
535–735	1000–1350	2–4(a)	4–5
735–955	1350–1750	1–2(a)	2–3
955–1175	1750–2150	½–1(a)	1–2
1010–1285	1850–2350	¼–½(a)	1½
Furnace E			
535–735	1000–1350	2–4(a)	4–5
735–955	1350–1750	1–2(a)	2–3
955–1175	1750–2150	½–1(a)	1–2
1010–1285	1850–2350	¼–½(a)	1½

Note: Service life estimates are based on the assumption that proper rectification of chloride salts is being done, as well as routine unit maintenance and care. (a) Hot leg only

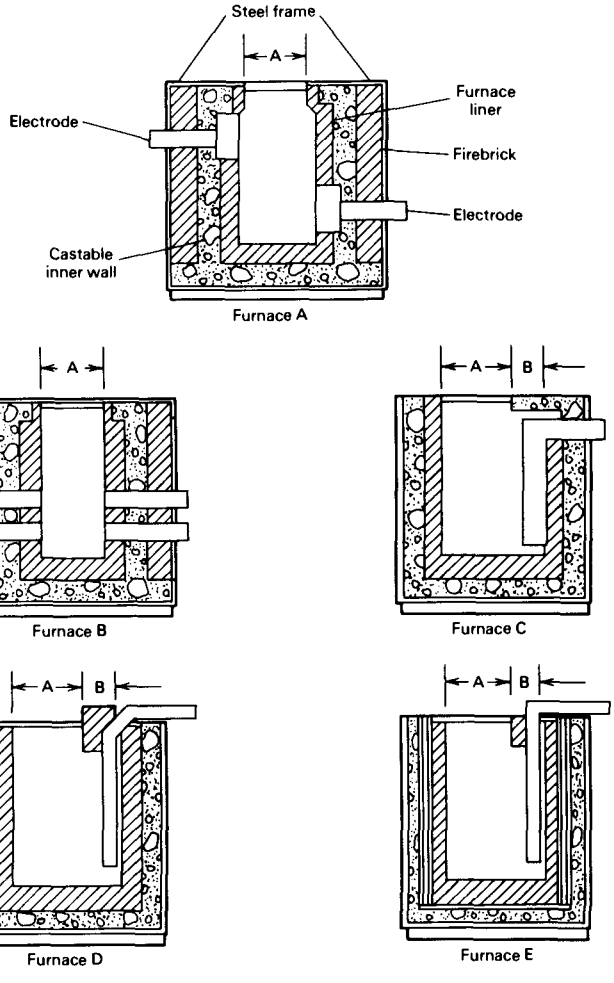

trate the cast refractory material that forms the center portion of the wall. The design requires from 5 to 8% of the initial salt charge to fill the ceramic pot. By comparison, in some designs 140 to 150% of the initial charge is needed to seal the ceramic walls of furnaces built with two layers of ceramic brick, backed up and supported by a steel plate. Salt penetrates the ceramic walls of any furnace and distorts the geometry of the walls. Reducing the amount of salt allowed to penetrate the ceramic walls aids in maintaining dimensions and in promoting a longer furnace life.

- *Electrode placement:* Enclosing the electrode in a clear rectangular box, free of any protruding obstructions, eliminates potential hazards to operating personnel during cleaning. Any sludge formed in the furnace is removed easily.

Automatic Heat Treating of Tool Steels. Figure 6-3 illustrates three heat-treating arrangements for production heat treatment of tool steels. Table 6-3 gives relative process times and temperatures for heat treating, and Table 6-4 gives process times for twist drills. The systems are equipped for cycles ranging from less than 1 min to 10 min. The parts are suspended on tong-type fixtures and are carried through the process by a chain conveyor on carrier bars. To facilitate rapid transfer of the tool steels, rotary transfer arms are placed between the preheat and high-heat units and between the high-heat and

Table 6-3 Relative process times and temperatures for automated heat treating of tool steels

Process stage	Operating temperature		Total time in furnace(a)
	°C	°F	
First preheat	650–870	1200–1600	X
Second preheat	760–1040	1400–1900	X
High heat	1010–1290	1850–2350	X
Isothermal quench	540–705	1000–1300	X
Air cool	Room temperature	Room temperature	6X, 12X, 24X
Wash, hot water	80–95	180–200	6X
Rinse, hot water	80–95	180–200	X

(a) See Table 6-4 for drill sizes and times in the high heat indicated by an "X" in this table.

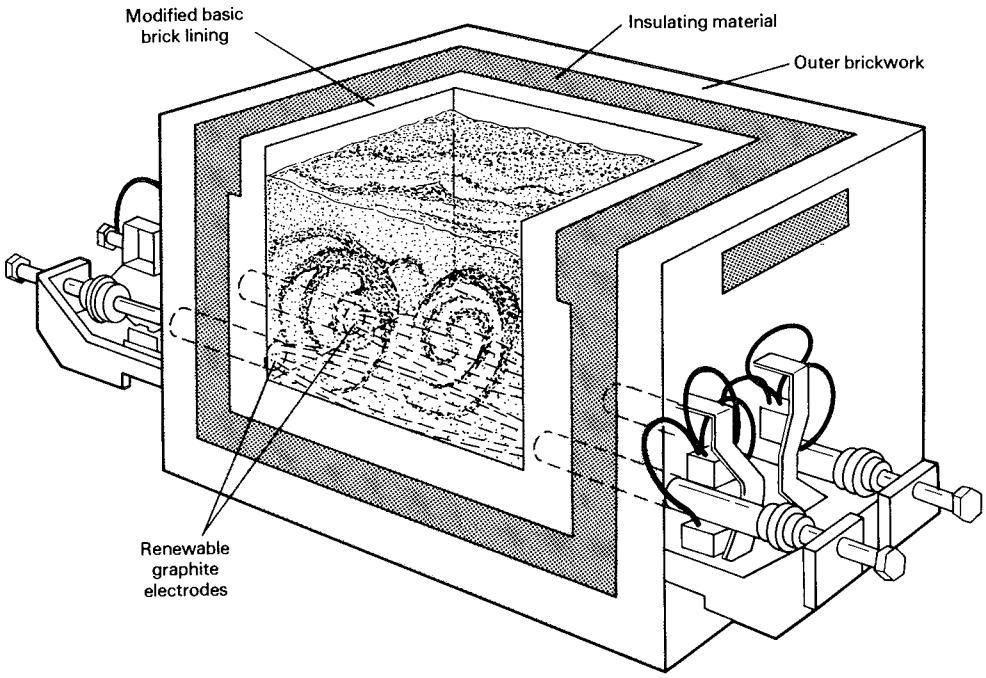

Fig. 6-2 Internally heated salt bath furnace with submerged electrodes. This furnace has a modified brick lining for use with carburizing salts.

quench units. Transfer-arm placement is chiefly governed by the production rate; however, transfer arms are always required between the high-heat and the quench units to satisfy metallurgical conditions. The lines also have areas above the furnaces to accommodate air cooling of the tools. In special cases, lines will be made with a station for an isothermal nitrate quench after the neutral salt quench. This additional stage allows rapid reduction of the temperature of the tools and reduces the air cooling time from 24× to 6× the time at the high-heat temperature. *Caution: Even if as little as 600 ppm of nitrate salts is allowed to enter the high-heat furnace, extreme surface damage can be done to the tool being heat treated.*

Rectification of Salt Baths. Neutral salts used for austenitizing steel become contaminated with soluble oxides and dissolved metals during use, due to a reaction between the chloride salts and the oxide layers present on fixtures and workpieces. The buildup of resulting oxides and dissolved metals renders the bath oxidizing and decarburizing toward steel, so the bath must be rectified periodically.

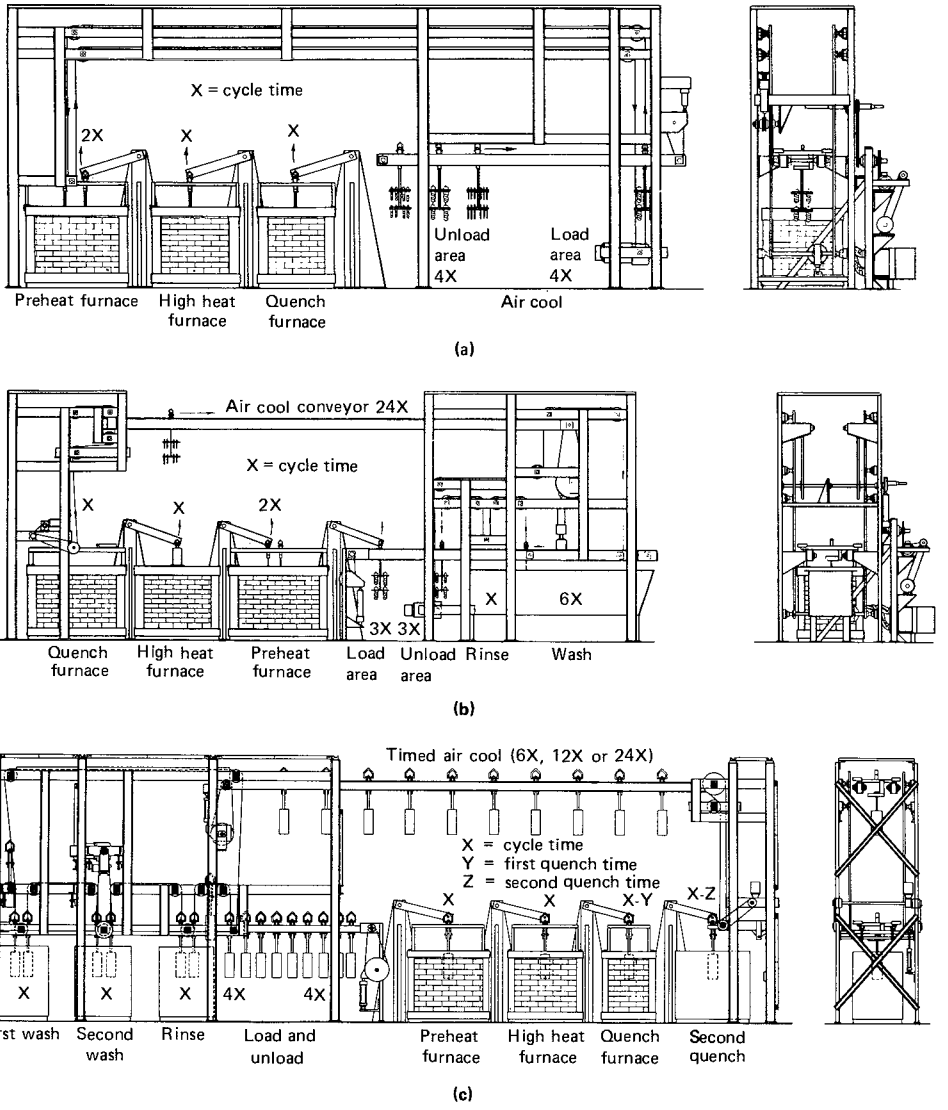

Fig. 6-3 Process designs for automated salt bath furnaces for heat treating of high-speed tool steels. Installations can be custom designed to meet specific customer requests. (a) Does not include a wash and rinse operation. (b) Similar to (a) but includes a wash and rinse operation that necessitates relocation of the load and unload operations. (c) Similar to (b) but includes a second quench and a variation in wash cycles specified by the customer

Baths of salts such as mixtures No. 1 and 2 in Table 6-1 can be rectified with silica, methyl chloride, or ammonium chloride. The higher the temperature of operation, the more frequent the need for rectification. Baths in which the electrodes protrude above the surface require daily rectification with either ferrosilicon or silicon carbide. Baths operated above 1080 °C (1975 °F) require rectification at least once a day, with more frequent rectification certainly recommended.

During rectification of a bath, the silica combines with the dissolved metallic oxides to form silicates. Although these silicates settle out as a viscous sludge that can be removed, sufficient soluble silicates can remain to cause the bath to become decarburizing. Any sludge or salts obtained as a by-product of the heat treatment must be disposed of in accordance with federal, state, and local regulations.

More effective methods of rectifying salt baths are to bubble methyl chloride through the bath or submerge ammonium chloride pellets in a perforated cage in the bath. The ammonium chloride pellets react with the oxides to regenerate the original neutral salt without sludge formation or bath thickening.

To remove dissolved metals from high-temperature baths, graphite rods are introduced at operating temperature. The graphite reduces any metallic oxides to metals that adhere to the rod. The metal can be scraped off and the rod reused.

To control the decarburizing tendency of high-temperature baths, test specimens should be hardened frequently by quenching them in oil or brine. A file-soft surface indicates the need for more rectification. This test may be supplemented by analysis of the bath. High-heat baths containing more than 0.5% BaO are likely to be decarburizing to steel.

The following method can be used to rectify austenitizing baths such as salt mixtures No. 2 and 3 in Table 6-1:

1. Add 57 g (2 oz) of boric acid for each 45 kg (100 lb) of salt after every 4 h of operation.
2. Insert a 75 mm (3 in.) graphite rod into the bath for 1 h for every 4 h of operation.

Table 6-4 Time cycles for heat treating of twist drills

Diameter		
mm	in.	Time
2.54–4.78	0.100–0.188	1 min, 30 s
4.80–8.08	0.189–0.318	1 min, 40 s
8.10–12.90	0.319–0.508	1 min, 50 s
12.93–18.24	0.509–0.718	2 min, 1 s
18.26–23.32	0.719–0.918	2 min, 20 s
23.34–38.10	0.919–1.500	2 min, 40 s
102 mm (4 in.) diam cups		6 min
64 mm (2½ in.) diam end mills		7 min
76 mm (3 in.) diam end mills		10 min

Pieces in high heat on smaller diameters

2.54 mm (0.100 in.) = 160 pieces/tong = 480 pieces in bath = 1.2 kg (2.6 lb)
4.78 mm (0.188 in.) = 85 pieces/tong = 255 pieces in bath = 3.5 kg (7.65 lb)
6.50 mm (0.256 in.) = 63 pieces/tong = 188 pieces in bath = 5.6 kg (12.3 lb)
8.08 mm (0.318 in.) = 25 pieces/tong = 75 pieces in bath = 3.9 kg (8.6 lb)
12.90 mm (0.508 in.) = 16 pieces/tong = 48 pieces in bath = 8.3 kg (18.2 lb)

Controlled-Atmosphere Furnaces

An atmosphere should be selected that will protect the surface of tool steel against the addition or the depletion of carbon during heat treatment. It is desirable to choose one that requires no adjustment of composition to suit various steels. An ammonia-based atmosphere containing 25 vol% N_2 and 75 vol% H_2 (class 601 of the American Gas Association, or AGA) meets this requirement and has the advantage of being sufficiently reducing to prevent oxidation of high-chromium steels. In the range of dew points generally found in this gas, –40 to –50 °C (–40 to –60 °F), there is no serious depletion of carbon, because the decarburizing action is slow and any loss of carbon at the surface is partially replaced by diffusion from the interior. For applications in which high superficial hardness is important, a carburized surface can be obtained by the addition of about 1% methane to the atmosphere. Although an ammonia-based atmosphere costs more than an endothermic gas atmosphere, this seldom becomes important, because tool heat-treating furnaces generally are comparatively small and thus require a correspondingly small quantity of gas.

Endothermic-based atmospheres are often used to protect tool steel during heat treatment. Table 6-5 lists suggested ranges of dew point for an AGA class 302 endothermic atmosphere when used for hardening some common tool steels. Relatively short heating times for hardening small tools allow treatment to be carried out with the theoretical carbon balance of the atmosphere varying over a rather wide range. However, for the hardening of large die sections, the particular composition of the die steel being treated requires careful control of the atmosphere if carburization or decarburization is to be avoided during the relatively long heat-treating cycle. More detailed information on the atmospheres used to heat treat steels can be found in Ref 2.

Vacuum Furnaces

One of the most important considerations when heat treating tool steels is that the treatment must be

accomplished with minimal change of the workpiece surface. An excellent method is to minimize the exposure to air during heat treatment by minimizing or reducing the quantity of air in a vessel, as with creating a partial vacuum. Vacuum furnaces with pressures of 26 Pa to 1.3 mP (200 to 0.01 μm Hg) are possible with the sophisticated pumping equipment integral to vacuum furnaces.

Vacuum furnaces have historically been popular with heat-treating processes such as brazing, sintering, and outgassing. More recently, vacuum furnaces have become predominant for hardening of selected tool steels. One reason for their widespread use is the freedom from environmental problems they afford the user: In contrast to salt bath heat treating, they eliminate disposal problems. Another reason is their flexibility. Vacuum furnaces can be designed for operating temperatures in excess of 2760 °C (5000 °F), and they can be programmed to run an almost limitless variety of stress relieving, preheating, hardening, and quenching cycles. Design of computer hardware and software can allow these steps to be programmed individually or sequentially to enhanceproductivity.

Hot-Wall Vacuum Furnaces. Until recently, vacuum furnaces were inhibited by technical considerations from being used for hardening of tool steels. The early designs were hot-wall furnaces, which had two limitations. First, the retort in which the vacuum was developed lost considerable strength when it was heated and tended to collapse. Second, the retort had limited capability for the type of quenching techniques required by tool steels. Because of the demand of the heat-treating industry for higher temperatures, lower pressures, rapid heating and cooling capabilities, and higher production rates, hot-wall vacuum furnaces have essentially become obsolete (with the exception of low-pressure chemical vapor deposition and ion-nitriding processes).

Cold-Wall Vacuum Furnaces. Vacuum furnaces now incorporate a heating unit inside a vacuum chamber that is of double-wall construction. Between the two walls, water or coolant is circulated for effective cooling of the vacuum chamber, enabling high-temperature operation. These cold-wall vacuum furnaces have been designed by various manufacturers and offer countless variations in size, pumping capacity, heating capacity, quenching method, speed, computerization, and so on.

In cold-wall furnaces, the electric heating elements are located inside the retort. The heating elements can be made of a refractory metal, such as tungsten, molybdenum, or tantalum or from graphite rods or cloth. Properties of these materials are compared in Table 6-6. The heating elements are surrounded by refractory metal baffles that provide insulation and direct radiant reflection. Centered or positioned within the furnace is a refractory metal hearth on which a fixtured or basketed workload can be positioned.

Single-Chamber Vacuum Furnaces. A simple vacuum furnace consists of one chamber in which the workpiece is both heated and cooled (Fig. 6-4). Cooling (quenching) is accomplished by backfilling or blowing inert gas across the workpieces. In order to quench rapidly enough to obtain the desired microstructure of tool steel, it is necessary to increase the pressure of the quench gas (usually nitrogen). This is accomplished by high-velocity, high-pressure blowers that have reported

Table 6-5 Ranges of endothermic-atmosphere dew point for hardening of tool steels

Data compiled for short times at temperature; furnace dew point; AGA class 302 (39.8 N_2-20.7CO-38.7H_2-0.8CH_4) atmosphere

Steel	Furnace temperature(a)		Dew point range	
	°C	°F	°C	°F
W2, W3	800	1475	7 to 13	45 to 55
S1	925	1700	4 to 7	40 to 45
S2	870	1600	4 to 16	40 to 60
O1	800	1475	7 to 12	45 to 55
O2	775	1425	7 to 12	45 to 55
O7	855	1575	–4 to 2	25 to 36
D2, D4	995	1825	–7 to –1	20 to 30
D3, D6	955	1750	–7 to –1	20 to 30
H11, H12, H13	1010	1850	2 to 7	35 to 45
T1	1290	2350	–18 to –12	0 to 10
M1	1205	2200	–15 to –12	5 to 10
F2, F3	830	1525	–5 to 1	23 to 34

(a) Approximate midrange of austenitizing temperatures for the specific types of tool steels

Table 6-6 Characteristics of heating elements used in vacuum furnaces

Material	Melting point		Upper operating temperature limit		Vapor pressure at 1600 °C (2910 °F)		Vapor pressure at 1800 °C (3270 °F)	
	°C	°F	°C	°F	Pa	torr	Pa	torr
Molybdenum	2617	4743	1705	3100	1.3×10^{-6}	10^{-8}	1.3×10^{-4}	10^{-6}
Tantalum	2996	5425	2500	4530	1.3×10^{-9}	10^{-11}	1.3×10^{-7}	10^{-9}
Tungsten	3410	6170	2800	5070	1.3×10^{-11}	10^{-13}	1.3×10^{-9}	10^{-11}
Graphite	3700	6700	2500	4530	1.3×10^{-11}	10^{-13}	1.3×10^{-8}	10^{-10}

cooling gas pressures of up to 60 kPa (6 bar). The cooling rate required varies, depending on the type of steel used and the size and shape of the workpiece.

In evaluating vacuum heat treatment, it is also necessary to consider flow patterns and furnace load. A variety of vacuum furnace designs have been developed that produce a wide range of cooling rates by varying gas pressures, gas velocities, and gas flow patterns. In some cases, gas quenching may not be adequate to achieve the necessary cooling rate for a component, and other quenching methods may need to be considered (i.e., salt bath, fluidized bed, or oil quenching).

Multiple-chamber vacuum furnaces (integrated quench furnaces) are designed to improve throughput or enhance quench rate. While vacuum furnaces typically have thermocouples available at several locations in the furnace, as well as on the surface of the load or within the confines of the load itself, multiple-chamber furnaces (Fig. 6-5) allow nearly continuous hardening of components. In such systems, three chambers of modules exist:

- A purge (loading chamber)
- A multiple-zone heating chamber
- A quench chamber

A loaded tray automatically moves into the purge chamber where decompression begins. Once the vacuum level is similar to the level in the heating chamber, the tray or basket is moved through an insulated door for heating. Heating is accomplished by transfer through multiple preheating zones and one final high-heat zone. Meanwhile, another tray has moved into the purge chamber. Once the preprogrammed time interval has elapsed in the high-heat zone, the basket is transferred to the final quench chamber for immersion. Ultimately, the basket is transported from the quench chamber through a door to an unloading tray. Additional information on multiple-chamber vacuum furnaces is available in Ref 3.

Vacuum Furnace Kinetics. The suitability of a vacuum furnace to harden a particular component is governed by many factors, not the least of which is the quenching capability. With gas quenching, the effects of gas variables such as pressure, velocity,

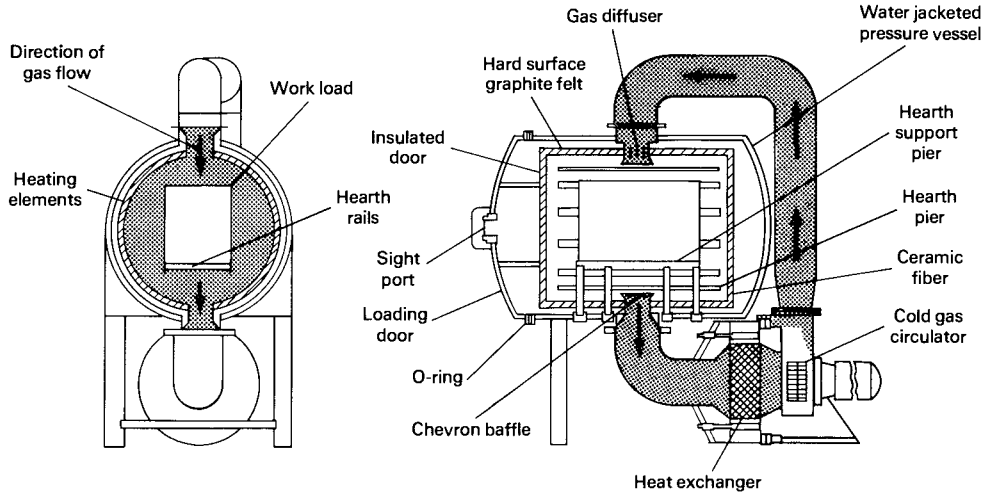

Fig. 6-4 Schematic of a single-chamber batch-type pressure-quench vacuum furnace

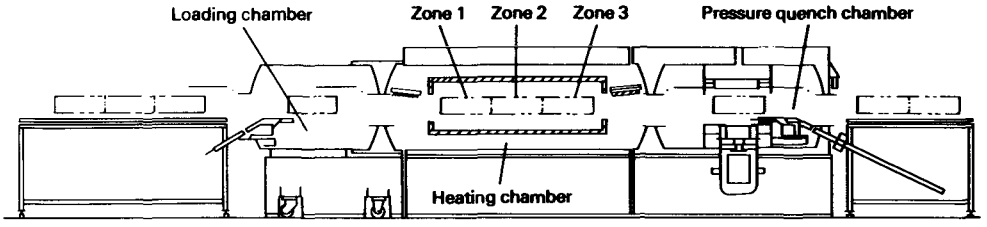

Fig. 6-5 Schematic of a typical in-line multiple-chamber vacuum furnace

and flow patterns are significant. Fundamentally, in the cooling of any steel, the process is limited by:

- *Gas parameters* that control the rate of heat transfer from the surface of the component (surface thermal resistance)
- *Component parameters* that control the rate of heat transfer within the component from the center to the surface of the workpiece (component thermal resistance effect)

In general, gas parameters predominate in determining the cooling rate in large-diameter components (greater than 250 mm, or 10 in.). Both types of parameters must be taken into consideration.

Gas Parameters. The gas parameter constituent of heat removal is described by Eq 6-1:

$$Q = hA \cdot \Delta T \qquad \text{(Eq 6-1)}$$

where Q is the heat removal rate, h is the heat transfer coefficient, A is the surface area of the component, and ΔT is the temperature difference between the component and the gas.

During the initial cooling period, the gas temperature has only a minor effect on the workpiece. After this initial cooling period, however, the component cooling rate becomes increasingly sensitive to changes in gas temperature, with the cooling rate decreasing as the gas temperature increases. Two important features of furnace design that affect gas temperature are:

- *Heat exchanger type, location, and size,* which control the bulk gas temperature into the furnace
- *Flow distribution,* which controls the local gas temperature around the workpiece

High gas temperatures usually occur only in the initial cooling period of a workpiece, when the effect of gas temperature is minimal, as discussed previously.

The effect of the heat-transfer coefficient, h, on the cooling rate of a 25 mm (1 in.) diam slug is shown in Fig. 6-6. The heat-transfer coefficient for a given gas is related to local gas velocity, V, and gas pressure, P, as follows:

$$h = C(VP)^m \qquad \text{(Eq 6-2)}$$

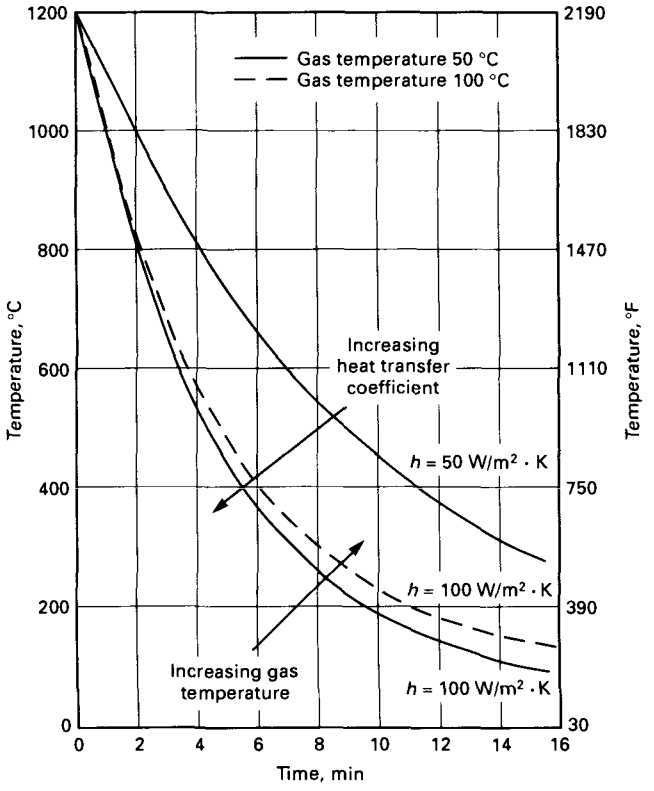

Fig. 6-6 Plot of temperature vs. time showing the effect of gas temperature and heat-transfer coefficient, h, on the cooling of 25 mm (1 in.) diam steel slugs. Source: Ref 4

where m and C are constants that depend on the furnace type, component size, and workload configuration. Equal increases in either V or P have the same effect on h and hence on the cooling rate of a component.

The effect of increased gas velocity on cooling is shown in Fig. 6-7. Local gas velocities were increased around the components (25 mm, or 1 in. in diam) by increasing the gas flow rate from 2.1 to 3.5 m^3/s (4400 to 7500 ft^3/min). The effect of increased gas pressures on the cooling of similar components is shown in Fig. 6-8.

Two practical considerations when increasing either gas velocity or pressure are that:

- High-pressure vacuum furnaces are required to be designed and built to stringent safety regulations.
- Increases in both gas velocity and pressure affect the design of the blower and the power required to recirculate the gases. (For example, doubling the gas velocity increases the blower power by a factor of eight, while doubling the gas pressure increases the blower power only by a factor of two.)

The heat-transfer coefficient is also a function of the gas properties. Figure 6-9 shows the effect of four gases on the cooling of 25 mm (1 in.) diam slugs. Nitrogen is usually the gas of choice because:

- Hydrogen is explosive and must be used with extreme care.
- Helium is expensive.
- Argon gives poor cooling rates.

It is evident that the cooling rates of steel components are determined not only by gas parameters such as gas temperature, gas velocity, and gas pressure but also by the physical properties of the gas itself (i.e., conductivity, density, and viscosity). In practice, gas velocity and gas pressure are the most significant factors in controlling component cooling rates.

Component Parameters. Component size, shape, and material properties control the rate of heat transfer from the center of the material core to the surface of the material. Material properties (i.e., density, specific heat, and thermal conductivity) vary only marginally from one steel to another and hence are considered constants for the purpose of this discussion. Component size and shape can vary greatly.

The effect of diameter on cooling is shown in Fig. 6-10. At the surface of the component, the

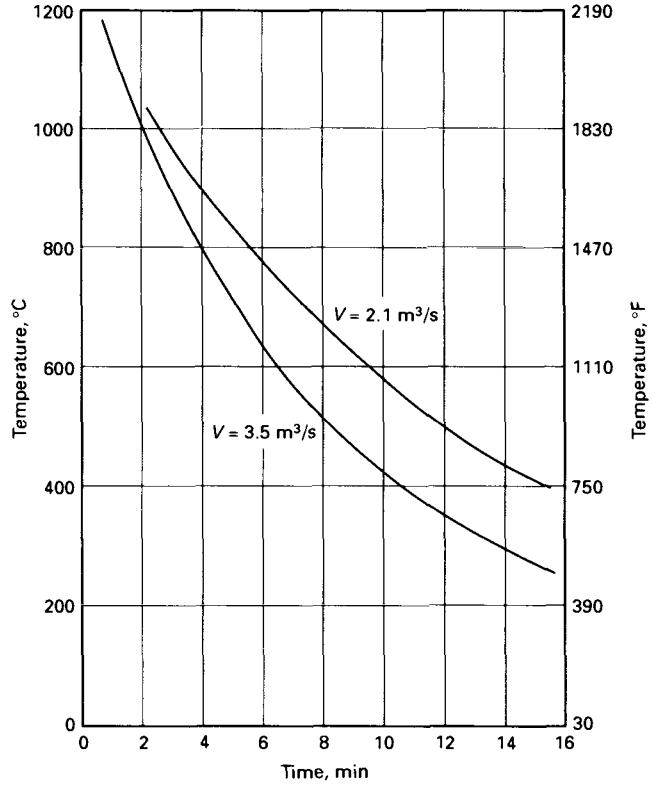

Fig. 6-7 Plot of temperature vs. time showing the effect of local gas velocity, V, on the cooling of 25 mm (1 in.) diam steel slugs. Slugs are cooled with 105 kPa (15 psig) N_2 quench gas. Load size is 836.4 kg (1844 lb). Source: Ref 4

cooling rate is inversely proportional to the component diameter (e.g., increasing the diameter by a factor of two decreases the cooling rate by a factor of two). The temperature at the center of the component lags behind the temperature at the surface of the component. This effect is more clearly shown in Fig. 6-11, where the ratio of surface temperature and center temperature is plotted over a wide range of diameters and values of h. At low values of h, gas parameters predominate over the cooling rate, and only negligible differences exist between the temperature at the surface of the component and the temperature at the center. As h increases, component parameters begin to restrict the cooling rate of the component, and large differences begin to develop between the temperature at the surface and the temperature at the center. These temperature differences can cause distortion and cracking in large-diameter components.

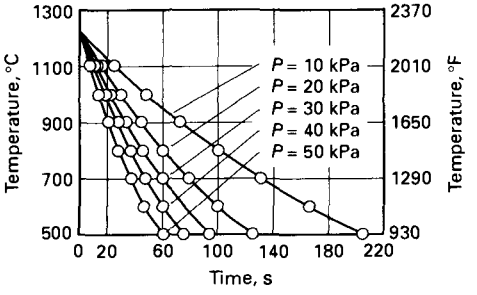

Fig. 6-8 Plot of temperature vs. time showing the effect of nitrogen gas pressure, P, on the cooling of M2 tool steel slugs, 25 mm (1 in.) diam by 48 mm (1⅞ in.) long. Source: Ref 4

The center cooling rate of the component is usually of more interest. Figure 6-12 is a graph of the variation in center cooling rate in M2 tool steel over the temperature range 1200 to 600 °C (2190 to 1110 °F) for a range of values of h. For a large-diameter component (e.g., 250 mm, or 10 in.), the center cooling rate increases only marginally with large increases in h, compared to increases in a small-diameter component. For such components, even fast oil or salt quenching (where h is approximately 1000 to 5000 W/m^2 · K, or 200 to 900 Btu/ft^2 · h · °F) may not provide the center cooling rate required to develop the desired steel hardness.

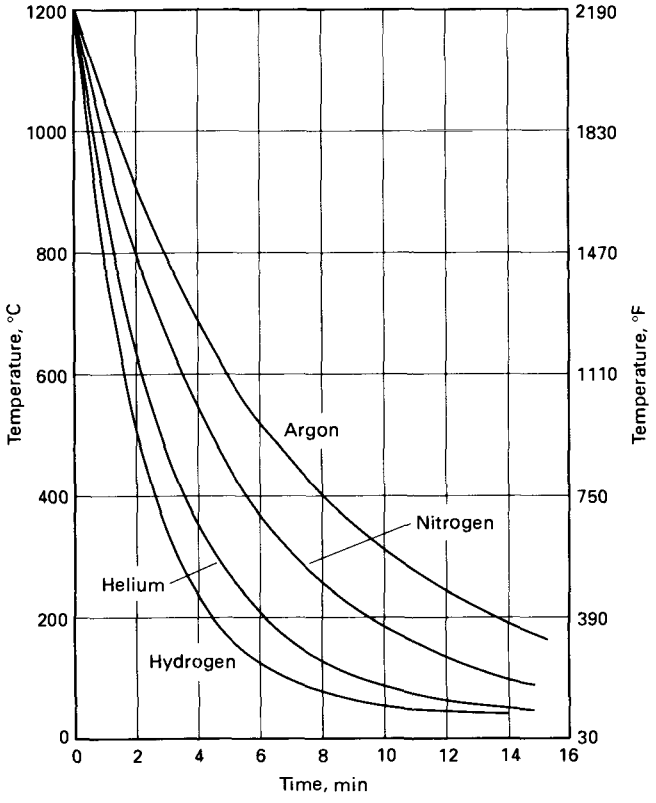

Fig. 6-9 Plot of temperature vs. time showing the effect of selected gases on the cooling of 25 mm (1 in.) diam tool steel slugs. Source: Ref 4

From this discussion of how component parameters affect cooling rates, two important conclusions can be drawn:

- High values of h can cause large variations in temperature between the center and surface of components, particularly as the diameter increases, that may result in cracking and/or distortion.
- Even high values of h may not be able to cool the center of large-diameter components fast enough to harden them adequately.

Fluidized-Bed Furnaces

Fluidized-bed furnaces use a solid, rather than a liquid or gas, for heat transfer. In general, the furnace is composed of a layer of small, mobile particles of an inert refractory (for example, aluminum oxide or silica sand) in a container that is heated and fluidized by a flowing stream of gas. Objects to be heat treated are immersed directly into the bed of particles. More detailed information on both the principles of fluidized-bed heat treating and the types of furnaces used can be found Ref 5.

A fluid bed results when a gas is passed upward through a bed of small solid particles at a rate fast enough to lift these particles and create turbulence. This motion of particles, similar to that of a fluid, is shown in Fig. 6-13. When gas is forced upward through small holes in a supporting plate, two forces meet to raise the particles: the buoyancy of the gas and the retarding force known as aerodynamic drag.

Most fluidized-bed furnaces are used at temperatures below 1095 °C (2000 °F), although some manufacturers have furnaces capable of temperatures through 1205 °C (2200 °F). The temperature limitation is related to exposure damage (wear and tear on the retort materials). Fluidized beds have been designed to perform a wide variety of heat-treating tasks, including stress relieving, preheating, hardening, quenching, annealing, and tempering, as well as a variety of surface treatments, such as carburizing, nitriding, and steam tempering. This discussion deals primarily with aspects of neutral hardening of tool steels.

Heat transfer with fluidized-bed furnaces is particularly good and offers characteristics approaching those of molten salt bath furnaces. Heating properties of the fluidized bed can be adjusted

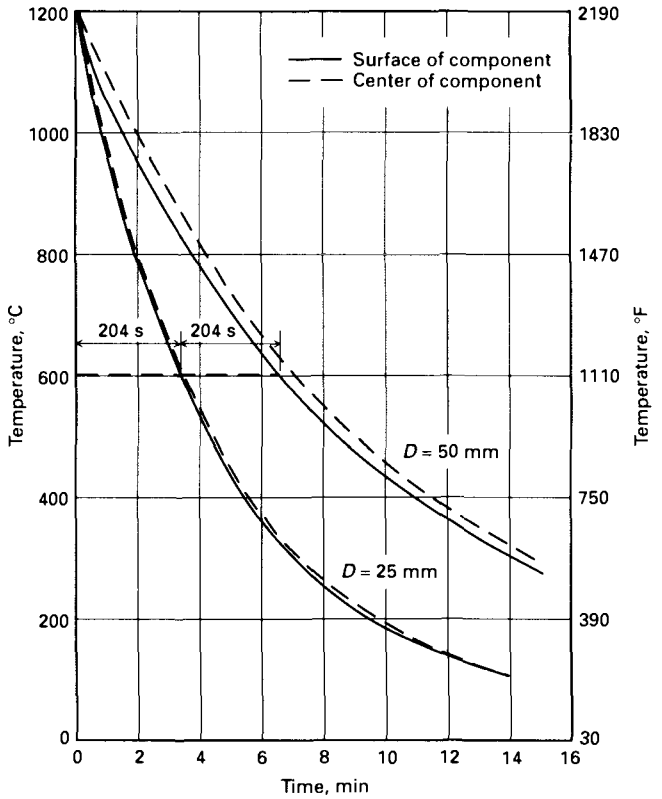

Fig. 6-10 Plot of temperature vs. time showing the effect of varying diameter, D, on the cooling of tool steels slugs. Source: Ref 4

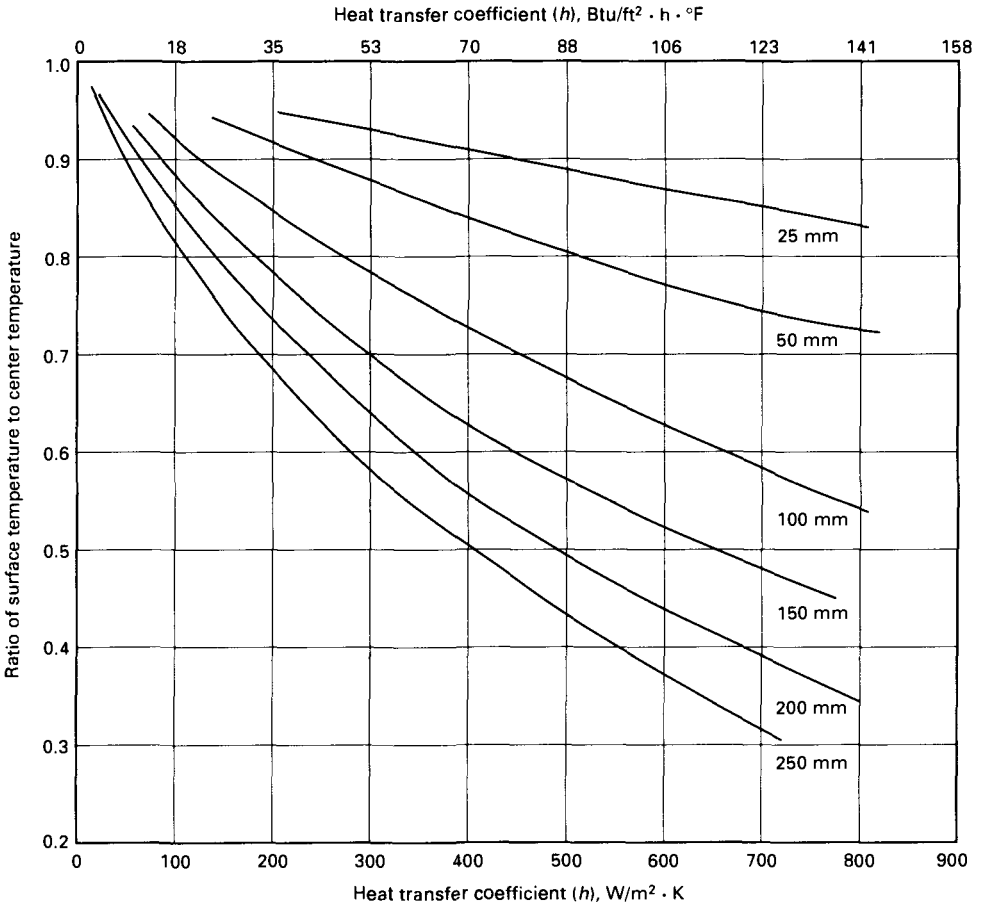

Fig. 6-11 Plot of surface-to-center temperature ratio vs. the heat-transfer coefficient, h, to show the effect of varying tool steel slug diameters ranging from 25 to 250 mm (1 to 10 in.). Source: Ref 4

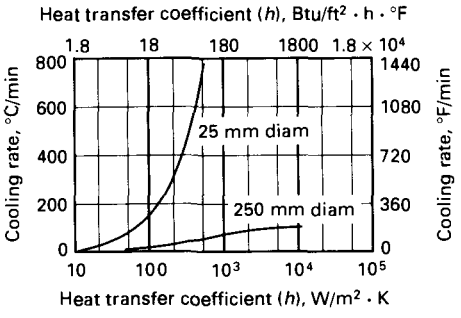

Fig. 6-12 Plot of cooling rate at the center of the slug vs. the heat-transfer coefficient, h, of M2 tool steel to show the effect of varying diameters over the temperature range of 1200 to 600 °C (2190 to 1110 °F). Source: Ref 4

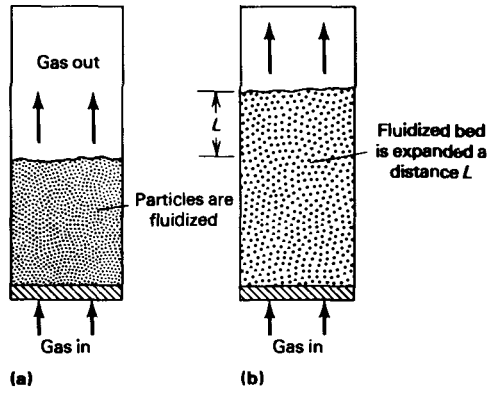

Fig. 6-13 Schematic showing the principle of the fluidized-bed furnace. (a) Initially, the gas flows upward through the permeable base to agitate the particles as the pressure is gradually increased. (b) Eventually, the gas flow is sufficient to lift the small particles of refractory materials and to transform the particle movement into a violent, turbulent motion. Although the particles are actually solid, the fluidized bed simulates the motion of a liquid. Source: Ref 6

through a wide range, because many parameters can be varied. Some of the major variable parameters are:

- *Particle properties:* size, shape, bulk density, and absolute density
- *Properties of the gas used to fluidize the bed:* density, viscosity, heat capacity, and thermal conductivity
- *System properties:* flow of gas through the bed, total weight of the particles in a given bed, cross section and shape of the retort or bed container, and type of permeable plate used to support the particles

One of the major attributes of the fluidized bed is the high rate at which heat can be transferred from the bed of particles to an immersed object. Coefficients of heat transfer on the order of 400 to 740 $W/m^2 \cdot K$ (70 to 130 $Btu/ft^2 \cdot h \cdot °F$) are possible. This heat flow rate is two to ten times higher than that provided by normal convection or radiation. In addition, the rate of heat transfer in the full bed is relatively independent of the temperature level and the emissivity of the immersed object. The turbulence of the fluidized bed is important in mixing and can effectively minimize thermal gradients within the bed.

Figure 6-14 illustrates the nature of heat-transfer in a fluidized bed. Under curve 1, the bed is nonfluidized in a static state, with low heat-transfer rates that increase only slightly with velocity. After the minimum fluidization velocity (V_{mf}) is reached, h increases rapidly over a comparatively narrow velocity range (curve 2). At a certain optimum velocity (V_{opt}), the heat-transfer coefficient reaches a maximum (h_{max}) and then tends to diminish as the fluidized bed attains more gaslike properties (curve 3).

The actual heat-transfer rate experienced in a fluidized bed depends on the fluidizing gas velocity and its thermal conductivity, the size, density, and thermophysical properties of the bed particles, and the geometry and structural design features of the furnace. Besides velocity, particle size is the most important of these parameters: h rises as particle diameter decreases. The parameters result in values of h as high as 570 $W/m^2 \cdot K$ (100 $Btu/ft^2 \cdot h \cdot °F$), similar to that obtained in liquid baths and up to five times that obtained in a conventional open-fired furnace. Figure 6-15 compares the heating rate in a fluidized-bed furnace with that in other typical modes of heating.

Fluidized-bed heat-treating furnaces are manufactured by several suppliers and are available in three fundamental configurations. Two of the configurations are fluidized by the products of combustion and are known as internally fired and externally fired types. For the third configuration, known as the indirectly heated type, fluidization and heating are accomplished independently.

The indirectly heated type is most often used for neutral hardening and therefore is more applicable to tool steel heat treating. Because the heating and fluidization modes are independent of each other, this type of furnace is used where special atmospheres are required. Literally any gas can be used for fluidization, and this type of furnace can accommodate a wide range of processes, including carburizing, carbonitriding, steam treating, and bright annealing. An example of an indirectly heated fluidized-bed furnace is shown in Fig. 6-16. The furnace shown is heated electrically, but a fluidized-bed furnace may also be fuel fired (simply by replacing the electric elements on the outside with a suitable burner system) or both fuel fired and electrically heated. In special configurations, furnaces may also be cooled to operate at subambient temperatures.

Fluidized-bed particles are similar in some respects to salt baths and can provide a supporting neutral environment. The fluidized particles do not collect on the work surface, so no dragout or subsequent cleaning is required. The aluminum oxide or silica oxide particles can become contaminated, but they are not typically considered an environmental hazard, unlike the lead and salt compounds used in other heat-treating methods. However, the

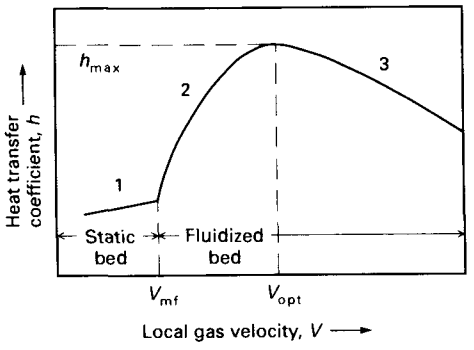

Fig. 6-14 Heat-transfer coefficient, h, rises with the increase in velocity of the fluidized bed until a peak value, h max, is reached at the optimum velocity, V_{opt}. Source: Ref 7

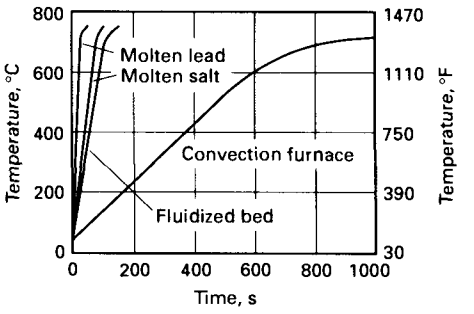

Fig. 6-15 Fluidized-bed heating compared with conventional immersion heating (molten salt and molten lead baths) and convection heating for 16 mm (5/8 in.) diam steel bars. Source: Ref 7

workpiece may be exposed to surface contamination upon removal from the high-temperature bed (e.g., it may become decarburized during transfer to a quenching media). Especially if multiple fluidized-bed furnaces or a combination of furnaces is used, potential contamination must be considered in the layout of the heat-treating department.

Acknowledgement

The information in this chapter is largely taken from B.A. Becherer, Processes and Furnace Equipment for Heat Treating of Tool Steel, *Heat Treating*, Vol 4, *ASM Handbook*, ASM International, 1991, p 726–733.

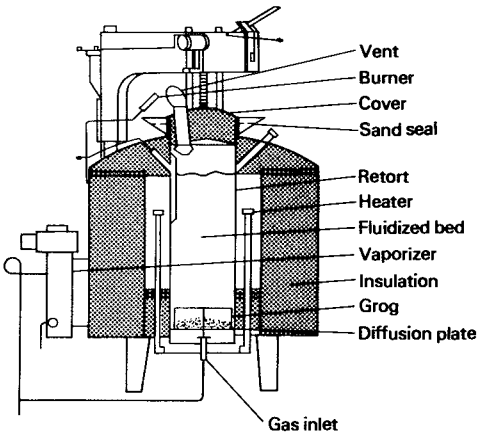

Fig. 6-16 Schematic of an indirectly heated fluidized-bed heat-treating furnace. The gas enters the furnace from the supply line on bottom left. Source: Ref 8

References

1. Salt Bath Equipment, *Heat Treating*, Vol 4, *ASM Handbook*, ASM International, 1991, p 475–483
2. Furnace Atmospheres, *Heat Treating*, Vol 4, *ASM Handbook*, ASM International, 1991, p 542–567
3. Heat Treating in Vacuum Furnaces and Auxiliary Equipment, *Heat Treating*, Vol 4, *ASM Handbook*, ASM International, 1991, p 492–509
4. E.J. Radcliffe, Gas Quenching in Vacuum Furnaces: A Review of Fundamentals, *Ind. Heat.*, Nov 1987, p 34–39
5. Fluidized-Bed Equipment, *Heat Treating*, Vol 4, *ASM Handbook*, ASM International, 1991, p 484–491
6. J.D. Stauffer and C.O. Pederson, Principles of the Fluid Bed, *Met. Prog.*, April 1961, p 78–82
7. A. Fennell, Continuous Heat Treating with Fluidized Beds, *Ind. Heat.*, Sept 1981, p 36–38
8. J.E. Japka, Fluidized-Bed Furnace Heat Treating Applications for the Die Casting Industry, *Die Cast. Eng.*, May–June 1983, p 22–26

Tool Steels: 5th Edition
George Roberts, George Krauss, Richard Kennedy, p 125-140
DOI:10.1361/toos1998p125

Copyright © 1998 ASM International®
All rights reserved.
www.asminternational.org

CHAPTER 7
Water-Hardening Tool Steels

Table 7-1 lists compositions of the water-hardening grades of tool steel in current use. The water-hardening steels are either essentially plain carbon steels or very low-alloy carbon steels. As a result, the water-hardening tool steels are the least expensive of tool steels and require strict control of processing and heat treatment to achieve good properties and performance. Carbon content is the primary factor determining properties and heat treatment response, and the Fe-C phase diagram can be used almost directly to evaluate temperature ranges of phase stability and processing.

The low alloy content of the water-hardening tool steels yields few alloy carbides and, therefore, lower wear resistance compared to more highly alloyed tool steels. Hardenability also is low, and severe brine or water quenching is required to produce martensitic microstructures (hence the term *water hardening* to describe this type of steel). Despite rapid quenching, the water-hardening tool steels may harden only to shallow depths. In some applications, such as cold header dies, shallow hardening is beneficial in that it provides a hard surface and a lower-strength, tougher core. Other applications of water-hardening tool steels include shear blades, blanking dies, reamers, threading dies, taps, twist drills, lathe tools, coining dies, woodworking tools, and cutlery.

General Processing and Performance Considerations

The carbon tool steels are used because high hardness can be achieved if quenching is rapid enough to produce fully martensitic microstructures, at least at the surface of hardened tools. Fig. 7-1 shows that the hardness of as-quenched martensitic steels is strongly dependent on carbon content, especially for low- and medium-carbon steels. At carbon contents within the range used for W1 and W2 tool steels, maximum hardness for martensitic microstructures can be achieved (Ref 1, 2). In order to preserve hardness in these carbon steels, tempering is generally performed at low temperatures. Fig. 7-1 also shows the hardness ranges expected for carbon steels quenched to martensite and tempered between 150 and 200 °C (300 and 390 °F). Another reason for low tempering temperatures is that, without significant alloying additions, softening develops rapidly in the water-hardening steels at higher tempering temperatures.

Although hardness provides a good measure of strength and wear resistance of tool steels, it gives no information on toughness or fracture resistance. Fig. 7-2 shows a map of the types of fracture that develop in low-temperature-tempered (LTT) martensitic steels as a function of carbon content. The diagram is based on fracture that results from tensile loading or from loading under bending conditions where high tensile stresses are applied to the

Table 7-1 Composition limits for water-hardening tool steels

AISI type	UNS No.	Composition(a), %							
		C	Mn	Si	Cr	Ni	Mo	W	V
W1	T72301	0.70–1.50(b)	0.10–0.40	0.10–0.40	0.15 max	0.20 max	0.10 max	0.15 max	0.10 max
W2	T72302	0.85–1.50(b)	0.10–0.40	0.10–0.40	0.15 max	0.20 max	0.10 max	0.15 max	0.15–0.35
W5	T72305	1.05–1.15	0.10–0.40	0.10–0.40	0.40–0.60	0.20 max	0.10 max	0.15 max	0.10 max

(a) 0.20% max Cu, 0.025% max P, and 0.025% max S. (b) Specified carbon ranges are designated by suffix numbers.

surfaces of tool steel components. Also, the diagram assumes that the martensitic microstructures were produced by quenching from above A_{cm} temperatures. Under these conditions, as-quenched and LTT martensitic microstructures in steel have high susceptibility to quench embrittlement (Ref 3), a brittle, intergranular form of fracture where cracks follow paths along prior-austenite grain boundaries. When tool steels are intercritically austenitized between A_{cm} and A_1 temperatures or subjected to compressive loading, as in many of the applications listed above for the water-hardening tool steels, overload fractures develop primarily in shear through the microstructure of carbides and tempered martensite.

Low alloy content, low resistance to softening during heating or tempering, and the tendency to brittle fracture establish the performance and manufacturing parameters for water-hardening tool steels. Table 7-2 lists some of the properties and processing factors for W1, W2, and W5 tool steels. Performance factors are rated on a scale of 1 to 10, where 1 and 10, respectively, represent low and high performance in the various categories. For example, wear resistance and hot hardness are rated low, consistent with negligible alloying element content, which translates to the absence of high-hardness alloy carbides and low resistance to softening during heating. Low alloy content also is reflected in low hardenability and shallow (S) hardening.

The susceptibility to brittle intergranular fracture strongly influences the processing of water-hardening tool steels and accounts for their low rating with respect to safety on hardening. As noted in the discussion of Fig. 7-2, sensitivity to intergranular fracture develops in fully austenitized steels. The low intergranular fracture resistance is related to phosphorus segregation and cementite formation at austenite grain boundaries during hardening heat treatments (Ref 3–5) and is associated with quench crack formation during heat treatment, as well as brittle fracture in service. Quench embrittlement is avoided in hypereutectoid carbon tool steels by austenitizing intercritically at temperatures between 760 and 845 °C (1400 and 1550 °F). The carbides retained at these temperatures lower the carbon content of austenite and maintain a fine austenitic grain

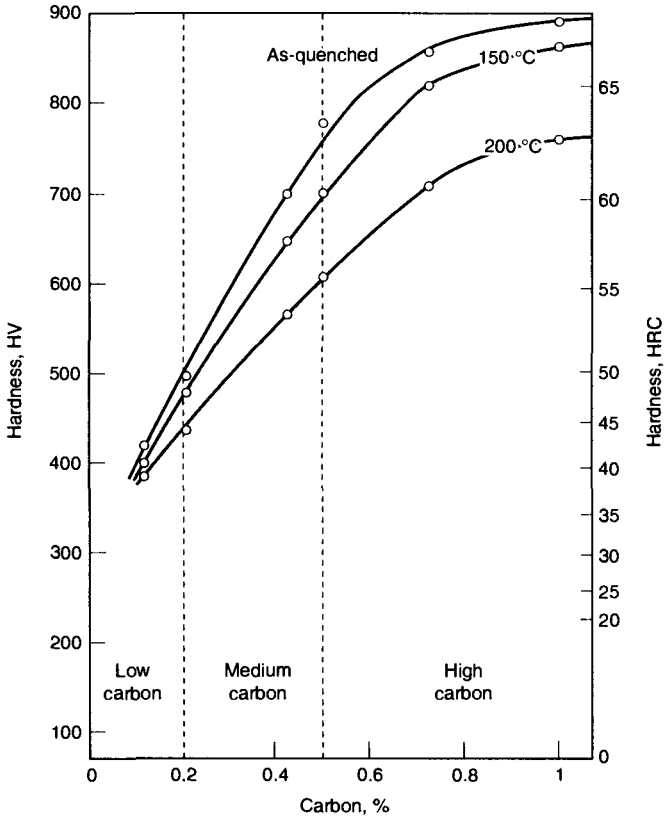

Fig. 7-1 Hardness as a function of carbon content for as-quenched and low-temperature-tempered hardened steels. Source: Ref 1, adapted from Ref 2

structure. As a result, the tendency to form grain-boundary cementite is reduced, and grain-boundary phosphorus segregation is diluted because of high grain-boundary area. Thus, with proper control of hardening temperatures, the sensitivity to intergranular fracture is reduced, and moderate toughness, limited by resistance to transgranular ductile or shear fractures, can be achieved in applications for water-hardening tool steels (Ref 5).

Plain carbon steels are among the easiest tool steels to forge. Recommended forging temperatures of 980 to 1065 °C (1800 to 1950 °F), as shown in Table 7-2, place the carbon tool steels in the single-phase austenite field. Therefore, no excess carbides, which might decrease forgeability, are present during forging. Prolonged holding at forging temperatures should be avoided in order to minimize decarburization and scaling. The best forging temperature for a given steel depends on carbon content. The lower the carbon content, the higher the forging temperature. For example, a 0.70% C steel may be forged at 1050 °C (1925 °F), whereas 950 °C (1825 °F) is best for a steel containing 1.20% C. Recommended finishing temperatures similarly depend on carbon content, decreasing from 815 °C (1500 °F) for 0.70% C steel to 790 °C (1450 °F) for a 1.20% C steel. After forging, pieces may be air cooled.

Although normalizing is not absolutely necessary, forgings can be normalized from a temperature above A_{cm} and air cooled. As discussed in Chapter 5, a normalizing treatment will develop a more uniform, fine-grained austenite structure, but will tend to form a microstructure of pearlite and grain-boundary cementite. Annealing is necessary after forging or normalizing or after cold working. Benefits of annealing include lower hardness for machining, relief of residual stresses induced by mechanical working, and development of a structure that will respond uniformly to hardening. The best microstructure for machining of carbon tool steels consists of a fine distribution of carbides in ferrite or a mixture of pearlite and spheroidized carbides in ferrite (Ref 6). Too coarse a spheroidized microstructure is not good for machinability and will increase the time during hardening required for dissolution of carbide particles to the level required for good hardenability.

Hardening and Microstructure of Water-Hardening Tool Steels

As noted in the previous section, the high hardness of water-hardening tool steels is obtained by intercritical austenitizing and rapid quenching to form martensite. In addition to the beneficial effects of intercritical austenitizing on elimination of quench cracking and quench embrittlement, maintaining austenitizing temperatures between A_1 and A_{cm} also reduces retained austenite, which if present in large amounts would substantially reduce hardness and wear resistance. The carbides that are retained during intercritical austenitizing reduce the

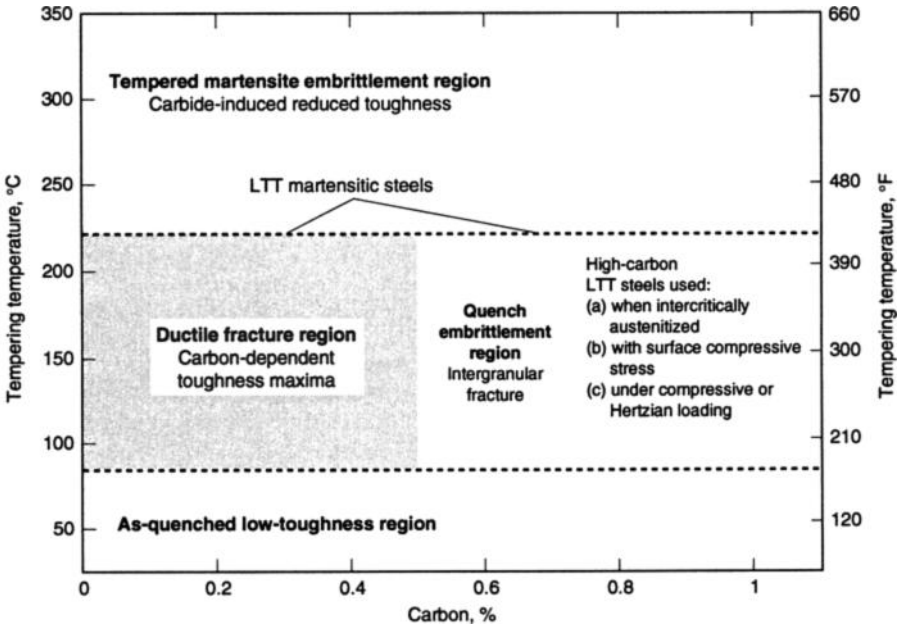

Fig. 7-2 Types of fracture as a function of carbon content and tempering temperature in carbon steels. Source: Ref 1

carbon content of the coexisting austenite. As a result, M_s temperatures are increased relative to a fully austenitized structure, and more martensite forms (i.e., less austenite is retained) on quenching to room temperature.

Fig. 7-3 shows examples of the microstructures formed by austenitizing a W1 tool steel, containing 0.94% C and 0.21% Mn, above and below A_{cm} (Ref 7). When the steel was austenitized at 790 °C (1450 °F), as shown in Fig. 7-3(a), the hardened microstructure consisted of very fine tempered martensite (dark) and spheroidized carbides (white). No retained austenite was resolvable in the light microscope. In contrast, the microstructure of a specimen quenched from an austenitizing temperature of 855 °C (855 °F) consisted of coarse plates of tempered martensite (dark) and retained austenite (white) (Fig. 7-3b). Although the carbides and retained austenite in the two microstructures both appear white, they are distinguished by their shapes: The carbides are present as spherical particles, or oblong particles with curved boundaries, and the retained austenite is present as geometrically shaped or triangular patches between the martensite plates.

The microstructure in Fig. 7-3(b) is considered to be a result of overheating during austenitizing. A consequence of heating above A_{cm} is that, without the grain-boundary pinning effects of undissolved carbide particles, grain size increases rapidly. Thus, the conditions for austenite grain-boundary embrittlement are enhanced, and quench cracking is more likely. Fig. 7-4 shows the results of an early study that related the incidence of quench cracking in carbon tool steel to austenitic grain size: The coarser the grain size, the higher the incidence of quench-cracked pieces (Ref 8).

Quench cracking is the result of tensile stresses developed during the through-hardening of carbon and low-alloy steels. The tensile stresses develop because the exterior of a part transforms to martensite before the interior. When the interior eventually transforms to martensite, the resulting expansion causes tensile stresses in the hardened surface. If an embrittling condition that lowers the cohesive strength of the microstructure exists—as, for example, the combined effect of phosphorus segregation and cementite formation in a coarse-grained austenite—and if the quenching stresses exceed that cohesive strength, cracking will occur. However, if surface tensile stresses can be reduced or even be made compressive, cracking may not occur. Carburized steels, with thin, hardened high-carbon case microstructures and soft low-carbon core microstructures formed by transformation well above surface M_s temperatures, are examples of heat-treated components that develop surface compressive stresses and in which quench cracking is eliminated (Ref 9).

Table 7-2 Performance factors and processing information for water-hardening tool steels

Factor	W1	W2	W5
Major factors			
Wear resistance(a)	2–4	2–4	3–4
Toughness(b)	3–7	3–7	3–7
Hot hardness	1	1	1
Minor factors			
Usual working hardness, HRC	58–65	58–65	58–65
Depth of hardening	S	S	S
Finest grain size at full hardness, Shepherd standard	9	9	9
Surface hardness as-quenched, HRC	65–67	65–67	65–67
Core hardness (25 mm, or 1 in., diam round), HRC	38–43	38–43	38–43
Manufacturing factors			
Availability	4	4	2
Cost	1	1	1
Machinability	9	9	9
Quenching medium	W	W	W
Hardening temperature, °C (°F)	760–845 (1400–1550)	760–845 (1400–1550)	760–845 (1400–1550)
Dimensional change on hardening	H	H	H
Safety on hardening	L	L	L
Susceptibility to decarburization	L	L	L
Approximate hardness as-rolled or forged, HB	275	275	275
Annealed hardness, HB	159–202	159–202	163–202
Annealing temperature, °C (°F)	740–790 (1360–1450)	740–790 (1360–1450)	740–790 (1360–1450
Tempering range, °C (°F)	150–345 (300–650)	150–345 (300–650)	150–345 (300–650)
Forging temperature, °C (°F)	980–1065 (1800–1950)	980–1065 (1800–1950)	980–1065 (1800–1950)

Note: Ratings are explained in Chapter 2. (a) Wear resistance increases with increasing carbon content. (b) Toughness decreases with increasing carbon content and depth of hardening.

Hardenability of Water-Hardening Tool Steels

The hardenability of water-hardening tool steels is low because little or no alloying elements are available to slow the diffusion-controlled transformations of austenite during cooling. Fig. 7-5 shows an IT diagram for a W1 tool steel. The curves for the start and finish of the diffusion-controlled transformations follow a single C-curve. The nose of the C-curve represents the most rapid transformation of austenite, and at the temperatures around the nose, transformation is initiated and completed within seconds. Therefore, quenching must be very severe to prevent diffusion-controlled transformation of austenite to transformation products other than martensite.

Above the nose of the C-curve, austenite transforms to pearlite, and below the nose austenite transforms to various forms of bainite. These decomposition products of austenite have been described in Chapter 5, and Fig. 7-6 shows various cementite-ferrite microstructures formed in a carbon steel as revealed by high-resolution light microscopy. Pearlite colonies appear as dark nodules, upper bainite appears as fine, featherlike regions, and lower bainite appears as dark-etching plates or needles. The single C-curve and short transformation times for diffusion-controlled transformation of austenite in carbon tool steels are in sharp contrast to the well-separated, double C-curves and very long transformation times for diffusion-controlled transformation of austenite in more highly alloyed tool steels.

The relatively low hardenability of water-hardening tool steels results in only partial hardening of sections of any size. For example, Fig. 7-7 shows the partial penetration of high-hardness martensite in a 19 mm (0.75 in.) diam round bar of brine-quenched W1 tool steel. Depth of hardness penetration, to the distance from the surface where hardness drops below a given value (for example, 55 HRC as defined in Fig. 7-7), has been used as a measure of hardenability for shallow-hardening steels. Figures 7-8 and 7-9 show the effects of small amounts of alloying elements on hardenability in terms of depth of hardness penetration for bars of 25 and 19 mm (1 and 0.75 in.) diam, respectively. Figure 7-8 shows the effects of small combined amounts of manganese, silicon, chromium, and nickel on hardenability of brine-quenched 1% C steels, and Fig.

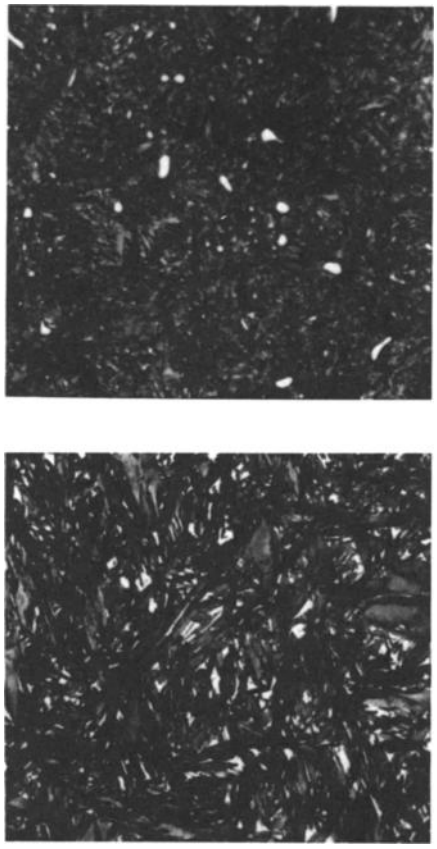

Fig. 7-3 Microstructures of W1 tool steel containing 0.94% C and 0.21% Mn. (a) Austenitized at 790 °C (1450 °F), brine quenched and tempered at 165 °C (325 °F). (b) Austenitized at 855 °C (1575 °F), brine quenched and tempered at 165 °C (325 °F)

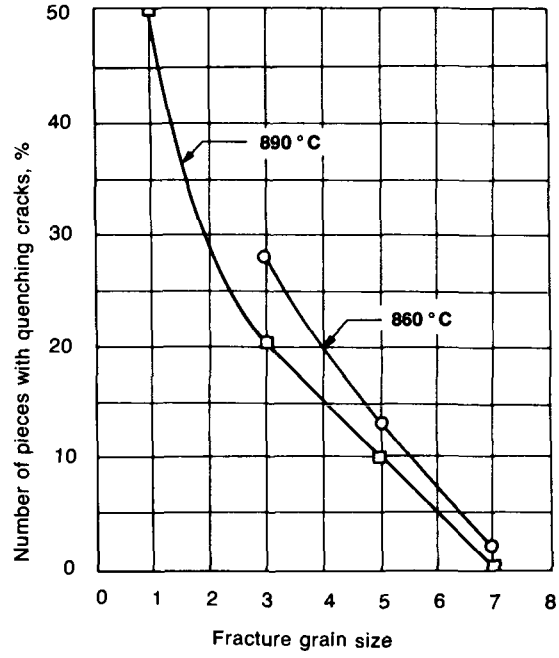

Fig. 7-4 Quench crack severity as a function of grain size for carbon tool steel austenitized at two temperatures. Source: Ref 8

7-9 shows the effects of manganese plus silicon amounts on hardenability of high-carbon steels with two modest levels of chromium.

Hardenability of high-carbon W-type steels has also been evaluated by determining ideal diameters according to the method of Grossmann (Ref 10–12). Table 7-3 lists critical diameters for brine-quenched high-carbon steels containing about 1.0% C with low alloy contents (Ref 11), Table 7-4 shows the effects of manganese, silicon, and chromium variations on ideal critical diameters of 1.27% C steels, and Table 7-5 shows the effect phosphorus variations on hardenability of 1.0% C tool steels. Phosphorus, an undesirable residual element because of the role it plays in quench cracking and quench embrittlement, has been found to increase hardenability of medium- and high-carbon steels (Ref 13, 14).

Hardenability has also been discussed in Chapter 5, along with the work of Jatczak (Ref 12), which shows the important effect of austenitizing above and below A_{cm} on the hardenability of high-carbon steels. Fig. 7-10 also shows the effect of austenitizing temperature on the hardenability of water-hardening tool steels (Ref 15). The section size that will harden to 60 HRC on oil quenching increases with increasing austenitizing temperature for three arbitrary classifications of hardenability, based on control of minor alloying additions as discussed above. Increasing hardenability with increasing austenitizing temperature is consistent with increased solution of carbides and increased grain size.

Tempering of Water-Hardening Tool Steels

As-quenched martensitic specimens have very low toughness and high residual stresses. Therefore, hardened carbon tool steels should be tempered immediately after hardening, preferably before the tool reaches room temperature, in order to prevent cracking and increase toughness. The as-quenched hardness of water-hardening tool steels drops rapidly as a function of tempering temperature. Fig. 7-11 shows hardness changes as a function of tempering temperature for tempering times between ½ and 2 h for a 1% C tool steel. The approximate temperature ranges of the three stages of tempering, as described in Chapter 5, are shown. In view of the absence of alloying elements in carbon tool steels, all microstructural changes are dependent primarily on carbon atom diffusion to form the various distributions of carbides within the matrix tempered martensite. Therefore, tempered microstructures coarsen rapidly, and hardness decreases accordingly.

Hardness changes are also a function of tempering time. Figure 7-12 shows hardness changes as a function of time at various tempering temperatures for a W1 tool steel (Ref 16). At a given temperature, hardness at first decreases rapidly from that of as-quenched martensite but then decreases much

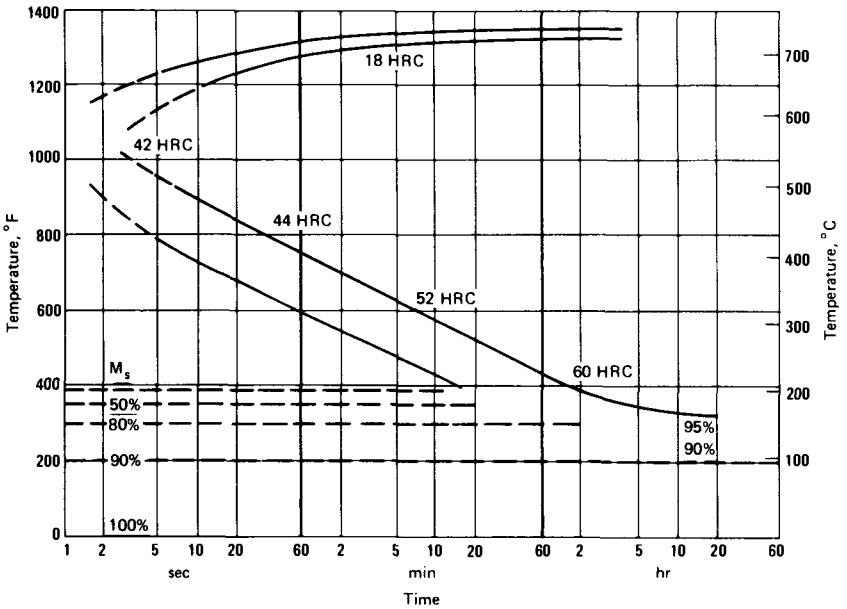

Fig. 7-5 IT diagram for W1 tool steel containing 1.14% C, 0.22% Mn, and 0.61% Si and austenitized at 790 °C (1455 °F)

more slowly with increasing time. These observations reinforce the rule that temperature is a much more important parameter than time with respect to the tempering process.

Austenitizing temperature and alloying, within the narrow range applied to water-hardening tool steels, also affect hardness and microstructural changes during tempering. Figure 7-13 shows tempering curves for shallow-hardening, medium-hardening, and deep-hardening groups of water-hardening tool steels. The more highly alloyed steels show better resistance to softening during tempering. Higher austenitizing temperatures, which put more carbon in solution in the austenite, and conse-

Table 7-3 Compositions and hardenabilities of W-type tool steels

Heat	Composition, %							Critical diameter for brine quench (H = 5.0)			
								Calculated		Observed (approx.)	
No.	C	Mn	Si	Cr	Ni	V	Mo	mm	in.	mm	in.
1	1.02	0.09	0.03	0.05	0.02	0.03	0.03	3.8	0.15	<12.7	<0.5
2	1.03	0.28	0.15	0.04	0.02	...	nil	8.9	0.35	<12.7	<0.5
3	1.07	0.15	0.09	0.05	0.10	...	nil	5.1	0.20	<12.7	<0.5
4	1.07	0.34	0.22	0.10	0.03	...	nil	11.4	0.45	<12.7	<0.5
5	1.00	0.24	0.17	0.09	0.07	...	0.01	11.4	0.45	12.7	0.5
6	1.09	0.26	0.26	0.17	0.20	...	nil	11.4	0.45	12.7	0.5
7	1.04	0.29	0.16	0.15	0.14	...	0.03	12.7	0.50	15.2	0.6
8	1.00	0.31	0.28	0.13	0.07	...	0.03	15.2	0.60	17.8	0.7
9	0.97	0.46	0.29	0.17	0.05	...	nil	20.3	0.80	20.3	0.8
10	0.99	0.36	0.31	0.15	0.17	...	0.03	19.1	0.75	20.3	0.8
11	0.98	0.50	0.37	0.23	0.12	...	0.03	22.9	0.90	25.4	1.0
12	0.94	0.45	0.36	0.21	0.16	...	nil	25.4	1.0	25.4	1.0

Note: Ideal critical diameters calculated using data of Jatczak and Devine (Ref 11) and converted to critical diameter for $H = 5.0$ according to curves of Grossman (Ref 10)

Table 7-4 Effect of manganese, silicon, and chromium on the hardenability of 1.27% C steels

Heat designation	Composition, %					Penetration, 19 mm (0.75 in.) diam round in 1/64 in.		Ideal critical diameter, mm (in.)			
						790 °C (1450 °F)	870 °C (1600 °F)	Observed, 790 °C (1450 °F)	Calculated (1)	Calculated (2)	Calculated (3)
	C	Mn	Si	Cr	Other						
A	1.26	0.13	0.04	0.02	(a)	5	5½	16.3 (0.64)	10.7 (0.42)	11.2 (0.44)	8.1 (0.32)
B	1.26	0.31	0.27	0.09	(b)	8	14	18.8 (0.74)	20.1 (0.79)	6.1 (0.24)	17.8 (0.70)
C	1.30	0.40	0.27	0.29	(c)	13	Through	20.6 (0.81)	20.6 (0.81)	36.3 (1.43)	25.4 (1.00)

(a) 0.010% S, 0.010% P. (b) 0.010% S, 0.018% P. (c) 0.010% S, 0.016% P, 0.02% Mo

Table 7-5 Effect of phosphorus on the hardness penetration in 1% C tool steels

Composition, %							Depth of hardened case in 255 mm (1 in.) diam brine quenched from 775 °C (1430 °F)	
C	Mn	Si	Cr	Ni	S	P	mm	in.
1.01	0.34	0.24	0.26	0.27	0.012	0.014	5.59	0.220
...	...	...	...	...	...	0.040	7.11	0.280
1.00	0.31	0.28	0.17	0.18	0.015	0.015	4.06	0.160
...	...	...	...	...	...	0.040	5.08	0.200

Source: Ref 14

quently higher carbon in the martensite, produce microstructures with somewhat higher hardness than do lower austenitizing temperatures.

Hardness of carbon tool steels, as described above, decreases slowly with increasing tempering in the first stage and then more rapidly. The hardness decreases are continuous, except for the very beginning of stage 1, where hardness may increase slightly in high-carbon steels due to very fine-scale transition carbide precipitation (Fig 7-12) (Ref 17). Evaluation techniques other than hardness measurements, however, show that some properties, especially those related to fracture, are not continuous in the tempering temperature range used for the water-hardening steels. In high-strength, low-toughness, high-carbon martensitic steels tempered at low temperatures, very small surface flaws initiate tensile fracture; as a result, tensile testing is not reliable. Mechanical property changes must therefore be assessed by less notch-sensitive techniques such as torsion or compression testing.

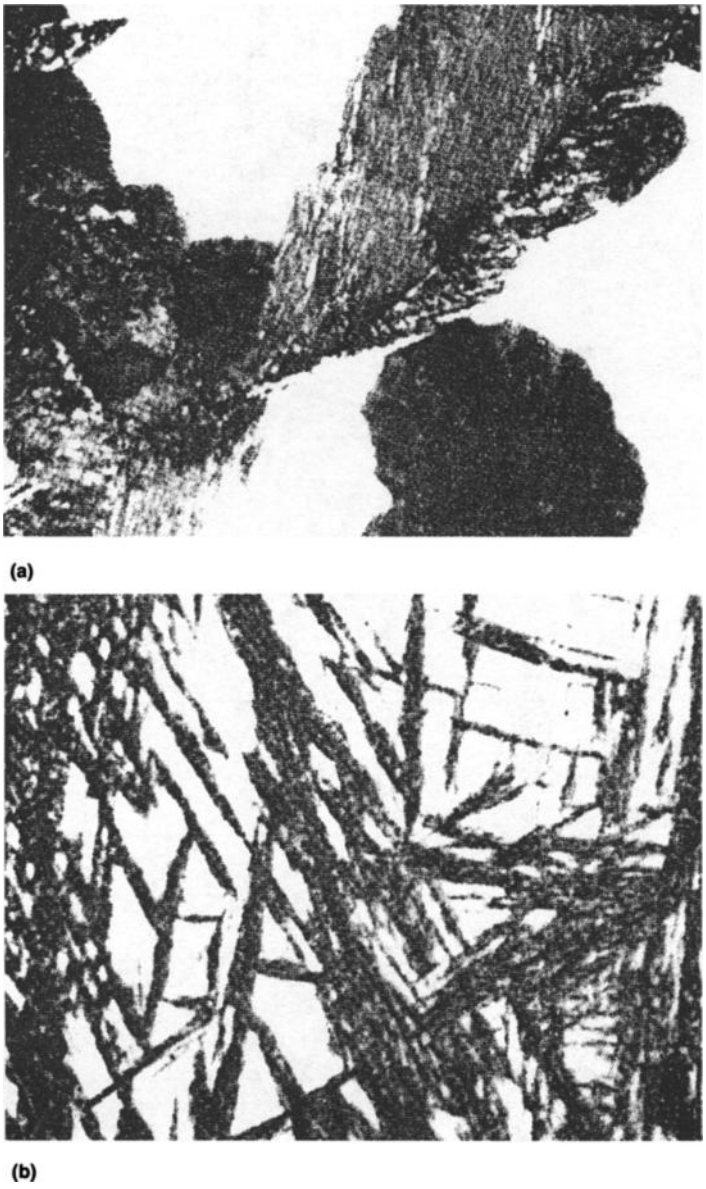

Fig. 7-6 Microstructures of water-hardening tool steels. (a) Upper bainite (fine, feathery structure) and pearlite (dark nodules). (b) Lower bainite and retained austenite. Courtesy of J.R. Vilella

Figure 7-14 shows a series of torsion stress-strain curves for a 1.1% C steel quenched from 790 °C (1450 °F) and tempered at various temperatures (Ref 18). Tempering between 150 and 200 °C (300 and 390 °F) improves strength and ductility compared to as-quenched specimens, but tempering at 250 °C (480 °F) lowers ductility even though strength is decreased. Torsion impact testing (Fig. 7-15) shows a similar maximum in fracture resistance between 150 and 200 °C (300 and 390 °F) and a sharp drop in specimens tempered around 260 °C (500 °F) (Ref 19). The peak in torsion impact strength is a function of austenitizing temperature, and Fig. 7-16 shows that the low-temperature peak in torsional strength is shifted to higher tempering temperatures with increasing austenitizing temperatures. These changes represent complex interactions between the mechanisms of plastic deformation as affected by carbon in solution and transition carbide formation in martensite, and the mechanisms of fracture associated with larger carbides that contribute to the initiation and propagation of torsional shear fractures. These interactions have been discussed relative to LTT medium-carbon martensitic steels (Ref 1, 20, 21), but are largely unexplored in high-carbon hardened steels.

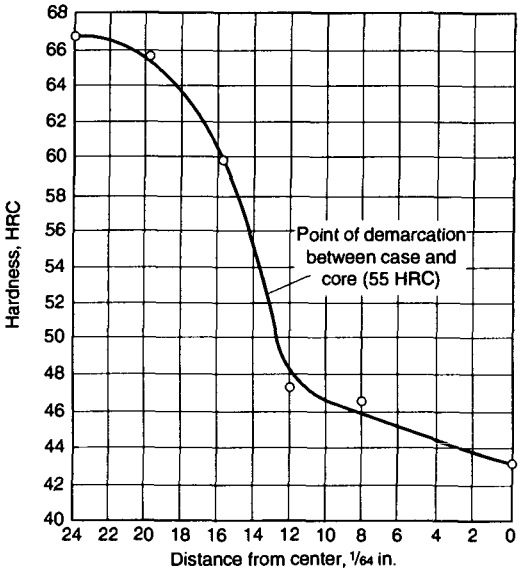

Fig. 7-7 Hardness profile of a 19 mm (0.75 in.) diam bar of brine-quenched W1 steel containing 1.06% C, 0.27% Si, 0.36% Mn, 0.010% S, 0.015% P, and 0.05% Cr. Data from Teledyne VASCO

The decrease in toughness of hardened steels tempered in the range of 250 to 350 °C (480 to 660 °F) has been referred to as tempered martensite embrittlement (Ref 22). In medium-carbon steels, tempered martensite embrittlement may take several forms, ranging from intergranular fracture to transgranular cleavage and ductile fracture, depending on the phosphorus and carbon content of the steel. All of the mechanisms have been linked to the formation of carbides during the second and beginning third stage of tempering, and the effect of embrittlement is more severe the greater the toughness of the steel in the unembrittled condition. In high-carbon hardened steels, which have inherently low toughness even if tempered below the embrittlement range, tempered martensite embrittlement tends to maintain that low toughness, rather than substantially decrease toughness.

Figures 7-17 and 7-18 show the Charpy V-notch (CVN) impact toughness and fracture toughness, respectively, of a low-alloy 52100 steel containing 1% and 1.5% Cr (Ref 5). This steel is closer in composition to the low-alloy L-type tool steels discussed in Chapter 8, but similar fracture behavior is expected in water-hardening steels austenitized be-

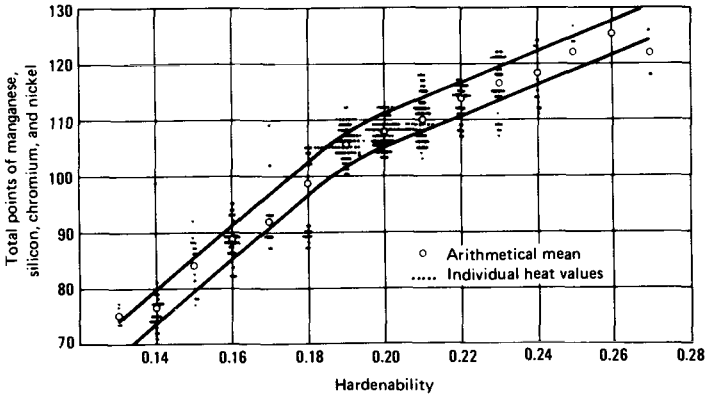

Fig. 7-8 Effect of total manganese, silicon, chromium, and nickel contents on the depth of hardness penetration in 25 mm (1 in.) diam bars of steels containing 1% C and brine quenched from 790 °C (1455 °F)

low their A_{cm} temperature. The 52100 specimens were intercritically austenitized at 850 °C (1560 °F); therefore, the hardened microstructures consisted of spheroidized carbides dispersed in a matrix of tempered martensite. All fracture surfaces consisted of microvoids formed around the spheroidized carbide particles, and thus the fracture is classified as ductile. Nevertheless, toughness is very low, whether measured by impact loading in CVN specimens or by static loading of precracked specimens during fracture toughness testing. The low-toughness ductile fracture is attributed to the high-carbon tempered martensitic matrix and the high density of closely spaced carbide particles. The slight decrease in toughness after tempering between 200 and 300 °C (390 and 570 °F) was attributed to the formation of additional void-nucleating particles during the second stage of tempering. Phosphorus content had a relatively small effect on specimens tempered at low temperatures but a greater effect after high-tem-

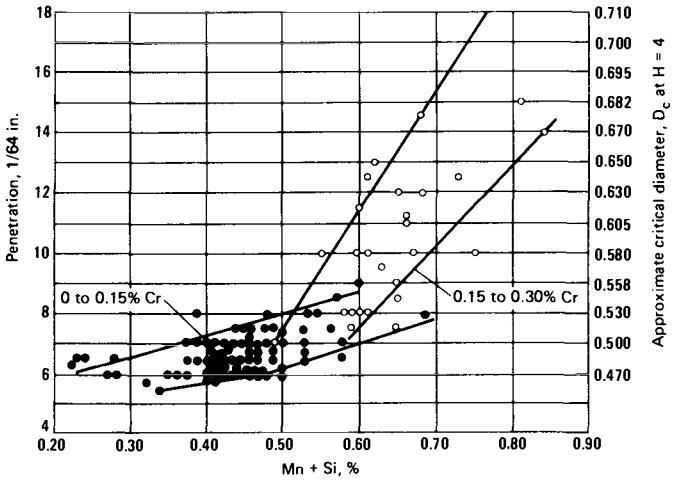

Fig. 7-9 Depth of hardness penetration as a function of manganese, silicon, and chromium contents of 19 mm (0.75 in.) diam bars of steels containing 1 to 1.10% C, 0.02 to 0.04% Ni, 0.010 to 0.015% S, and 0.012 to 0.016% P. Specimens were brine quenched from 790 °C (1455 °F). Data from Teledyne VASCO

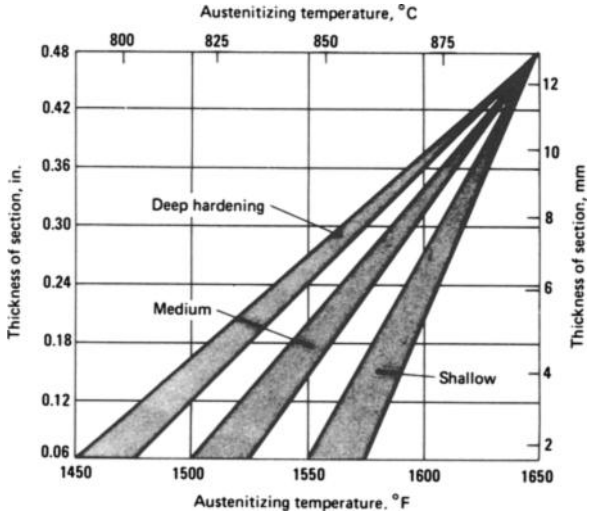

Fig. 7-10 Thickness of sections that harden to 60 HRC as a function of austenitizing temperature for W-type tool steels with various levels of hardenability

perature tempering, during which phosphorus atoms could diffuse to carbide interfaces and lower carbide/matrix interfacial fracture resistance.

Specimens of the 52100 steels austenitized above A_{cm} at 965 °C (1770 °F) were embrittled by phosphorus segregation and cementite formation at austenite grain boundaries, and in the compact tension fracture toughness tests, unstable crack propagation occurred by brittle intergranular fracture in the as-quenched condition and after tempering at all temperatures up to 300 °C (570 °F). The specimens austenitized at 965 °C (1770 °F) also were sensitive to quench cracking, and all quenched CVN specimens showed quench cracks in the specimen notches. Figure 7-19 compares the transgranular fracture surface of a 52100 specimen austenitized at 850 °C (1560 °F) to the largely intergranular fracture surface of a 52100 specimen austenitized at 965 °C (1770 °F). Both specimens were tempered at 200 °C 390 °F) for 1 h.

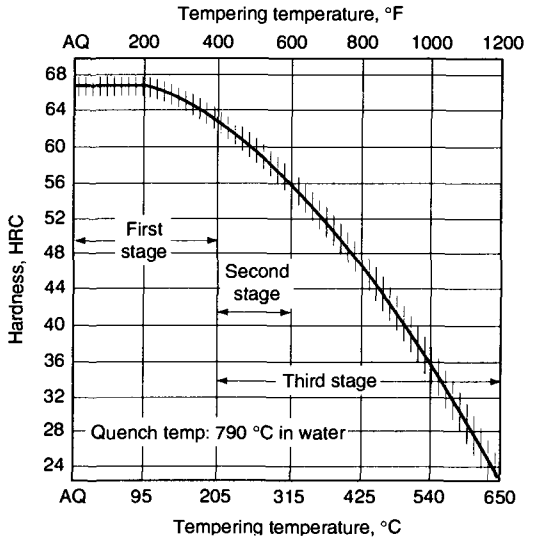

Fig. 7-11 Hardness as a function of tempering temperature for 1% C tool steels. Tempering times between ½ and 2 h. AQ, as quenched. Data from Teledyne VASCO

The transformations and microstructural changes that develop during tempering of martensite, in addition to changing mechanical properties, cause dimensional changes. Figure 7-20 shows the relative length changes that occurred as a function of time during tempering of a W1 tool steel containing 1.07% C at a number of temperatures (Ref 23). During low-temperature tempering, the specimens contract as the tetragonality of the high-carbon as-quenched martensite is reduced by transition carbide precipitation. At tempering temperatures of 120 °C (250 °F) and higher, the contraction is reversed, and specimens begin to expand as retained austenite, with its close-packed crystal structure, transforms to bainitic mixtures of ferrite and cementite. The dimensional changes associated with the transformation of the retained austenite shift to shorter times with increasing tempering temperature. This response to tempering is shown clearly in Fig. 7-21.

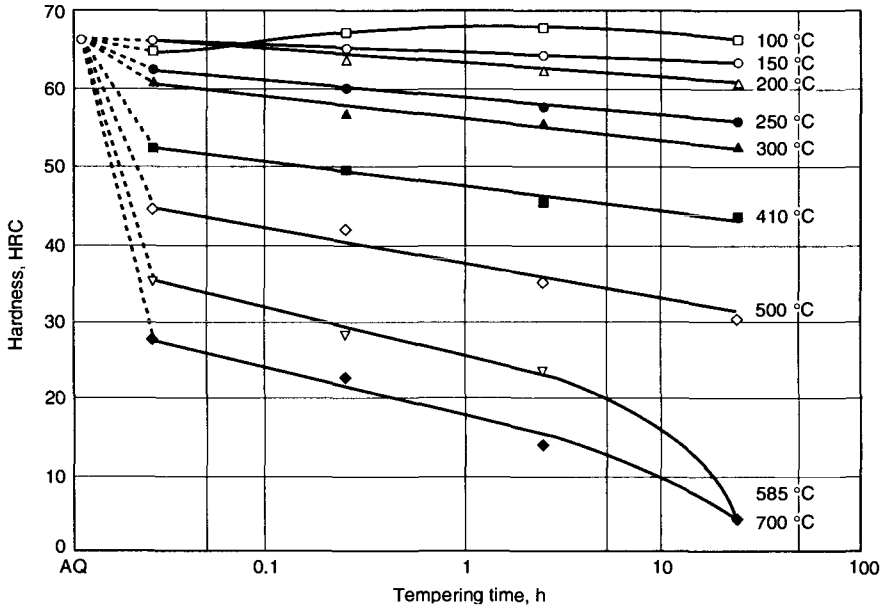

Fig. 7-12 Hardness as a function of tempering time at various temperatures for W1 steel containing 0.98% C, 0.30% Mn, and 0.30% Si. Specimens were hardened by brine quenching after 1 h at 870 °C (1600 °F) and cooling to −70 °C (−95 °F). Source: Ref 16

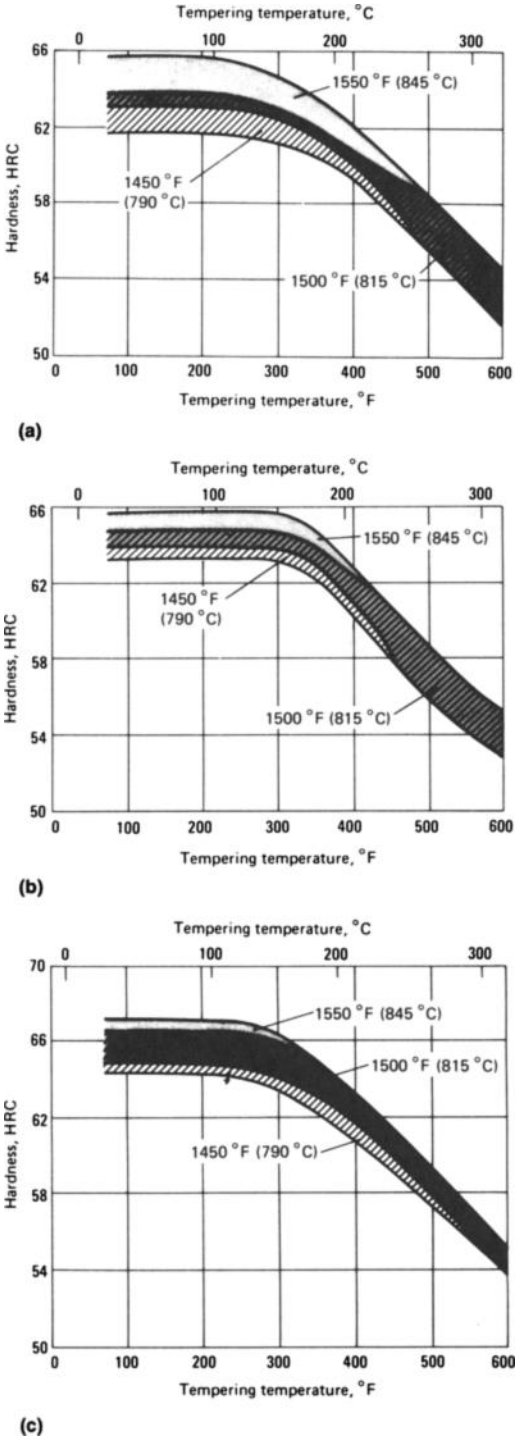

Fig. 7-13 Hardness as a function of tempering time for water-hardening tool steels quenched from temperatures shown. (a) Shallow-hardening steels: 0.90 to 1.00% C, 0.18 to 0.22% Mn, 0.20 to 0.22% Si, 0.18 to 0.22% V. (b) Medium-hardening steels: 0.90 to 1.00% C, 0.25% Mn, no alloying elements. (c) Deep-hardening steels: 0.90 to 1.00% C, 0.30 to 0.35% Mn, 0.20 to 0.25% Si, 0.23 to 0.27% Cr

The gradual contraction of hardened specimens at room temperature, as shown in Figure 7-20, is of considerable practical importance. The gradual change in dimensions at low temperatures, often termed aging, is a serious concern in accurate measuring tools where dimensional stability is of prime importance. The dimensional instability may be reduced by tempering at high temperatures, but this approach decreases hardness and, consequently, wear resistance. Lement et al. (Ref 24) have studied the effect of various tempering heat treatments, including refrigeration and double tempering, on dimensional changes at room temperature for times up to 1 year. The results are shown in Table 7-6. For a hardness level of 65 HRC, a simple 1 h temper at 150 °C (300 °F) is just as effective in minimizing dimensional changes as more complex heat treatments. Repeated cycles of low-temperature tempering at 150 °C (300 °F) and cooling in dry ice at –76 °C (–105 °F) have also been suggested to stabilize dimensions of tools and gages (Ref 25).

REFERENCES

1. G. Krauss, Heat Treated Martensitic Steels: Microstructural Systems for Advanced Manufacture, *Iron Steel Inst. Jpn. Int.*, Vol 35, 1995, p 349–359
2. R.A. Grange, C.R. Hribal, and L.F. Porter, Hardness of Tempered Martensite in Carbon and Low-Alloy Steels, *Metall. Trans. A*, Vol 8A, 1977, p 1775–1785
3. R.S. Hyde, "Quench Embrittlement and Intergranular Oxide Embrittlement Effects on Bending Fatigue Initiation of Gas-Carburized Steel," Ph.D. thesis, Colorado School of Mines, 1994
4. H.M. Obermeyer and G. Krauss, Toughness and Intergranular Fracture of a Simulated Carburized Case in EX-24 Type Steel, *J. Heat Treat.*, Vol 1 (No. 3), 1980, p 31–39
5. D.L. Yaney, "The Effects of Phosphorus and Tempering on the Fracture of AISI 52100 Steel", M.S. thesis, Colorado School of Mines, 1981
6. J.V. Emmons, Effect of Structure on the Machining of Tool Steel, *Trans. ASST*, Vol 2, 1921–22, p 1100
7. *Atlas of Microstructures*, Vol 7, *Metals Handbook*, 8th ed., American Society for Metals, 1972
8. R. Arpi, Quality of Tool Steel as Evaluated by Fracture Method, *Jernkontorets Ann.*, Vol 115, 1931, p 75
9. D.P. Koistinen, The Distribution of Residual Stresses in Carburized Cases and Their Origin, *Trans. ASM*, Vol 50, 1958, p 227–241
10. M.A. Grossmann, Hardenability Calculated from Chemical Composition, *Trans. AIME*, Vol 150, 1942, p 227
11. C.F. Jatczak and R.Q. Devine, Jr., Calculation of Hardenability in High Carbon Alloy Steels, *Trans. ASM*, Vol 47, 1955, p 748
12. C.F. Jatczak, Hardenability in High Carbon Steels, *Metall. Trans.*, Vol 4, 1973, p 2267–2277

13. F.A. Jacobs and G. Krauss, The Effects of Phosphorus and Carbon on the Hardenability of 41xx Type Steels, *J. Heat Treat.*, Vol 2, 1981, p 139–146
14. G.R. Barrow and G. Soler, Hardenability Control of a 1% Carbon Steel, *Trans. ASM*, Vol 31, 1943, p 943
15. H. Chandler, Ed., *Heat Treater's Guide: Practices and Procedures for Irons and Steels*, 2nd ed., ASM International, 1995
16. J.H. Hollomon and L.D. Jaffe, Time-Temperature Relations in Tempering High Carbon Steels, *Trans. AIME*, Vol 162, 1945, p 223
17. D.L. Williamson, K. Nakazawa, and G. Krauss, A Study of the Early Stages of Tempering in an Fe-1.2% C Alloy, *Metall. Trans. A*, Vol 10A, 1979, p 1351–1363
18. O.V. Greene and R.D. Stout, The Stress-Strain Characteristics of the Torsion Impact Test, *Trans. ASM*, Vol 28, 1940, p 277
19. F.R. Palmer and G.V. Luerssen, *Tool Steel Simplified*, 3rd ed., Carpenter Steel Co., 1960
20. W.C. Leslie and R.J. Sober, The Strength of Ferrite and of Martensite as a Function of Composition, Temperature, and Strain Rate, *Trans. ASM*, Vol 60, 1967, p 459–484
21. G. Krauss, Carbon-Dependent Fracture of As-Quenched Martensite, *Displacive Phase Transformations and Their Applications in Materials Engineering*, TMS, 1996
22. G. Krauss, *Steels: Heat Treatment and Processing Principles*, ASM International, 1990
23. B.L. Averbach and M. Cohen, The Isothermal Decomposition of Martensite and Retained Austenite, *Trans. ASM*, 41, 1949, p 1024
24. B.S. Lement, B.L. Averbach, and M. Cohen, The Dimensional Stability of Steel, Part IV: Tool Steels, *Trans. ASM*, Vol 41, 1949, p 1061
25. W.P. Boyle, Aging Tools and Gauges, *Steel*, Vol 109 (No. 12), 1941, p 71

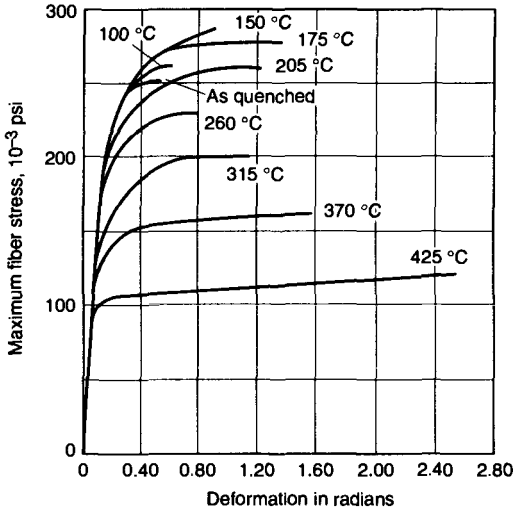

Fig. 7-14 Torsion stress-strain curves for 1.1% C tool steel quenched from 790 °C (1450 °F) and tempered at the various temperatures shown. Source: Ref 18

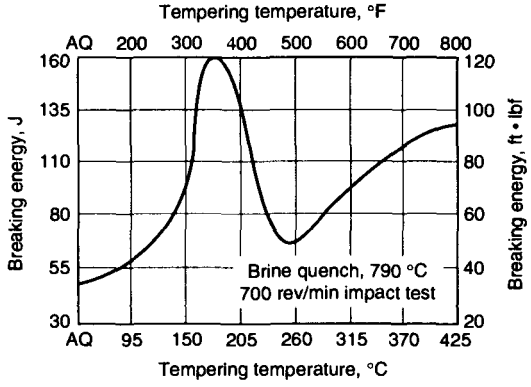

Fig. 7-15 Effect of tempering temperature on torsion impact values of quenched 1.10% C steels. Source: Ref 19

Table 7-6 Effect of heat treatment of W1 steel on dimensional stability at room temperature

Thermal treatment, °C (°F)				Total change in length on aging at 20 °C (68 °F), μm/m or μin./in.		
First temper	Refrigeration	Second temper	Hardness, HRC	1 month	3 months	1 year
150 (300), 1 h	None	None	65	–3	–6	–10
150 (300), 1 h	–86 (–123)	None	65.5	–8	–10	–14
150 (300), 1 h	–196 (–321)	None	65.5	–10	–14	–17
150 (300), 1 h	–86 (–123)	150 (300), 1 h	65.5	–10	–10	–14
150 (300), 1 h	–196 (–321)	150 (300), 1 h	65.5	–8	–11	–16
175 (350), 1 h	None	None	64.5	–3	–6	–10
205 (400), 1 h	None	None	63	–2	–3	–7
260 (500), 1 h	None	None	61.5	–2	–3	–3
None	–196 (–321)	150 (300), 1 h	67.5	–4	–9	–13
None	–196 (–321)	175 (350), 1 h	66	–4	–8	–9
None	–196 (–321)	205 (400), 1 h	63.5	–3	–5	–6
None	–196 (–321)	260 (500), 1 h	59.5	–3	–5	–5

Note: All specimens were initially hardened by water quenching from 790 °C (1450 °F). Source: Ref 24

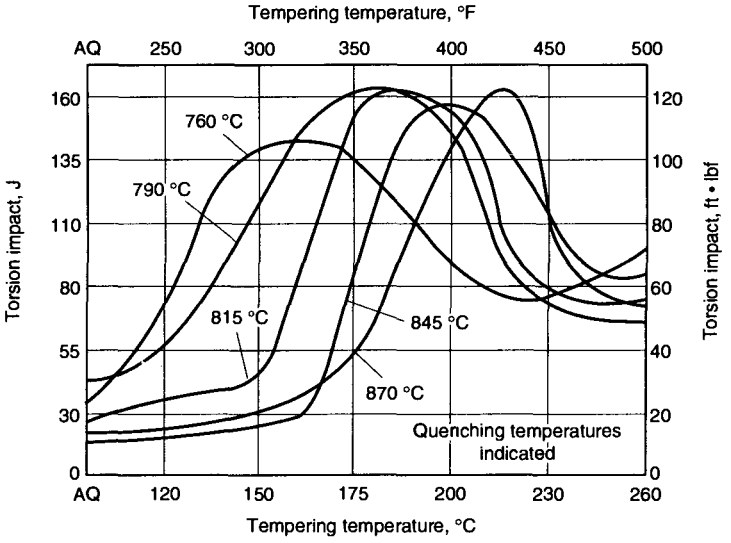

Fig. 7-16 Torsion impact energy absorbed as a function of tempering temperature for 1% C tool steel austenitized at various temperatures as shown. Source: Ref 19

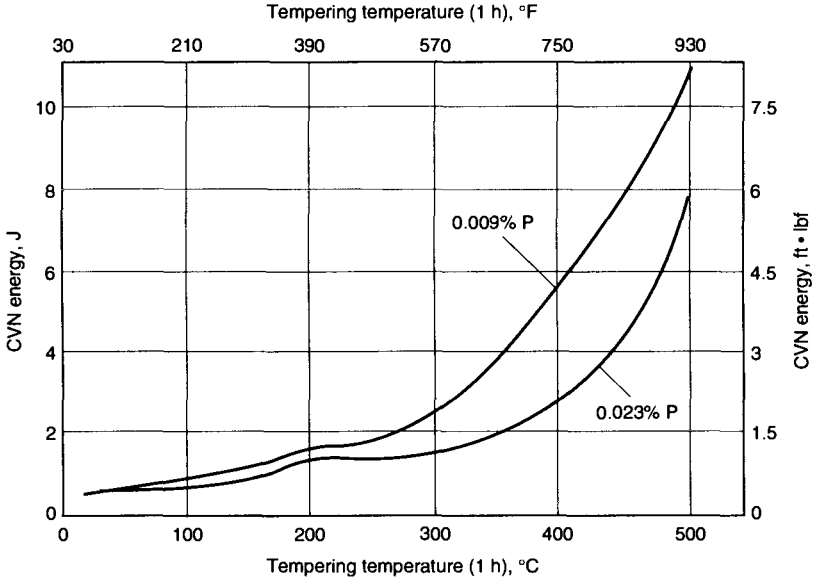

Fig. 7-17 CVN energy absorbed as a function of tempering temperature for 52100 steel with two levels of phosphorus. Austenitized at 850 °C (1560 °F). Source: Ref 5

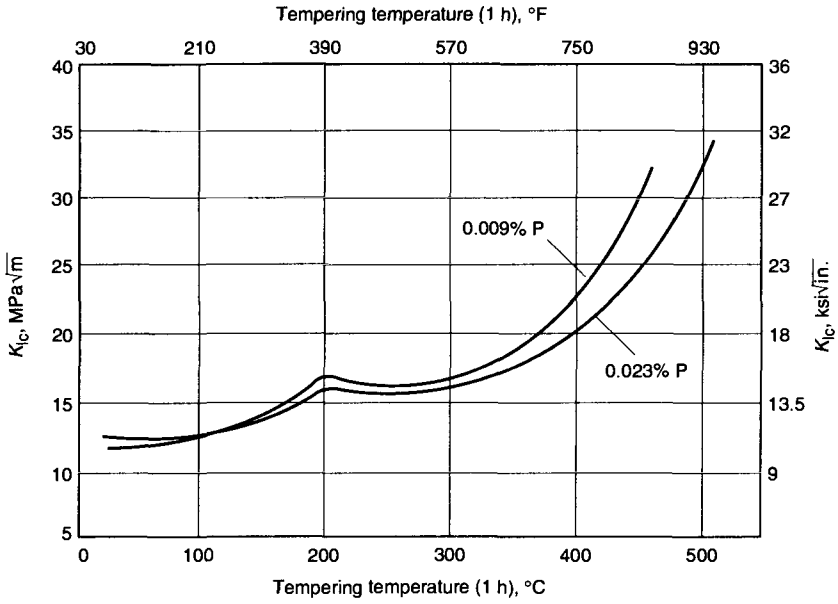

Fig. 7-18 Fracture toughness as a function of tempering temperature for 52100 steel with two levels of phosphorus. Austenitized at 850 °C (1560 °F). Source: Ref 5

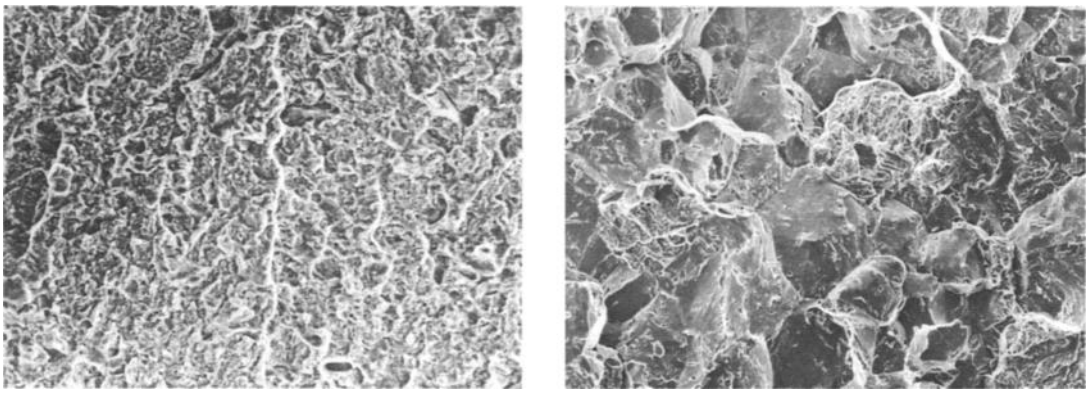

(a) (b)

Fig. 7-19 Fracture surfaces of hardened 52100 steel after austenitizing at 850 °C (1560 °F) (a) and 965 °C (1770 °F) (b). Source: Ref 5

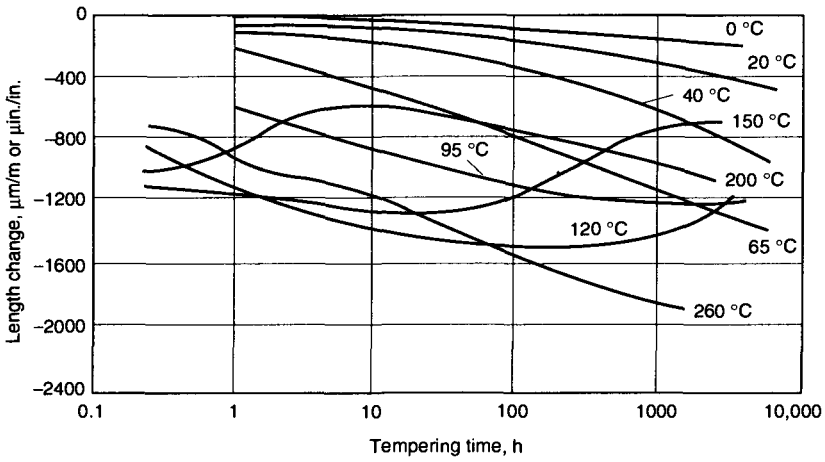

Fig. 7-20 Relative length changes on tempering W1 tool steel containing 1.07% C. Tempering time is considered to begin 1.5 h after hardening. Source: Ref 23

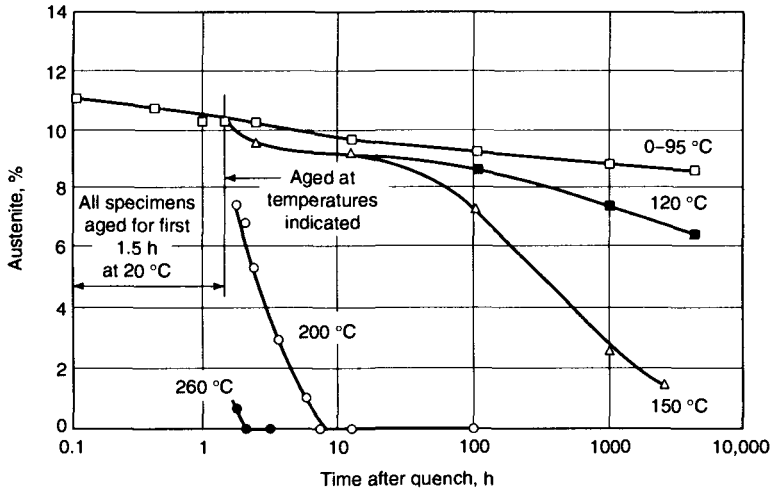

Fig. 7-21 Effect of tempering temperature on the isothermal transformation of retained austenite. Source: Ref 23

Tool Steels: 5th Edition
George Roberts, George Krauss, Richard Kennedy, p 141-163
DOI:10.1361/toos1998p141

Copyright © 1998 ASM International®
All rights reserved.
www.asminternational.org

CHAPTER 8
Low-Alloy Special-Purpose Tool Steels

The low-alloy special-purpose tool steels, designated as group L steels in the AISI classification system, are similar to the water-hardening tool steels but have somewhat greater alloy content. The higher alloy content increases wear resistance, or tool life, and also increases hardenability relative to the water-hardening steels. In view of their higher hardenability, for most applications the L steels can be oil quenched, a factor that minimizes dimensional changes during hardening. Parts with simple shapes or heavy sections made from L-type steels (for example, rolling-mill rolls) can be water or brine quenched. At one time at least seven grades of L steels were used in varying amounts (Ref 1), but currently only types L2 and L6, with various carbon levels, are manufactured and used. The fourth edition of *Tool Steels* includes considerable information about the L-type tool steels that are no longer used.

Table 8-1 lists the compositions of the L2 and L6 tool steels, and Table 8-2 provides processing and performance information for these steels. This chapter will discuss the metallurgy of the L steels in the order presented in these tables: first the chromium-alloyed L steels with carbon contents above 0.65%, then the chromium-alloyed steels with carbon contents below 0.65%, and finally the nickel-alloyed L6 steels. Applications for the L steels include tools such as precision gages, cold-heading dies, swaging dies, rock drills, shears, woodworking tools, punches and dies, drills, broaches, and cutlery. Nontool uses include bearings, bearing races, and small- to medium-size rolls.

Low-Alloy Chromium Tool Steels with High Carbon Content

Chromium, the major alloying element added to L2 tool steels, affects hardenability and tempering resistance; the higher the chromium content, the better the hardenability and the better the resistance to softening during tempering. Figure 8-1 shows hardness-penetration curves for brine-quenched 38 mm (1.5 in.) diam rounds of 1.10% C steels austenitized at two temperatures. The steels with higher chromium contents harden to deeper depths than the lowest-chromium steel. Although hardness decreases for all the steels with increasing distance into the rounds, indicating bainite formation, the higher hardness of the higher-chromium steels at a given location correlates with bainite-martensite mixtures with a higher martensite content than in the lowest-chromium steel. The higher austenitizing temperature, 815 °C (1500 °F) versus 790 °C (1450 °F), shows the beneficial effect of increased chromium and carbon in austenite solution on hardenability. The effect of chromium on increasing depth of hardening has been applied in bearing manufacture. Table 8-3 shows how chromium content can be adjusted to provide the proper hardenability for through-hardened bearings of different sizes (Ref 2).

Table 8-1 Compositions of low alloy L-type tool steels

		Nominal composition, mass %						
AISI type	UNS No.	C	Mn	Si	Cr	V	Ni	Mo
L2, high carbon	T61202	0.65–1.10	0.10–0.90	0.50 max	0.70–1.20	0.10–0.30	...	...
L2, medium carbon	T61202	0.45–0.65	0.10–0.90	0.25	0.70–1.20	0.10–0.30	...	0.25 max(a)
L6	T61206	0.65–0.75	0.25–0.80	0.25	0.60–1.20	0.20–0.30 (a)	1.25–2.00	0.50 max(a)

(a) optional

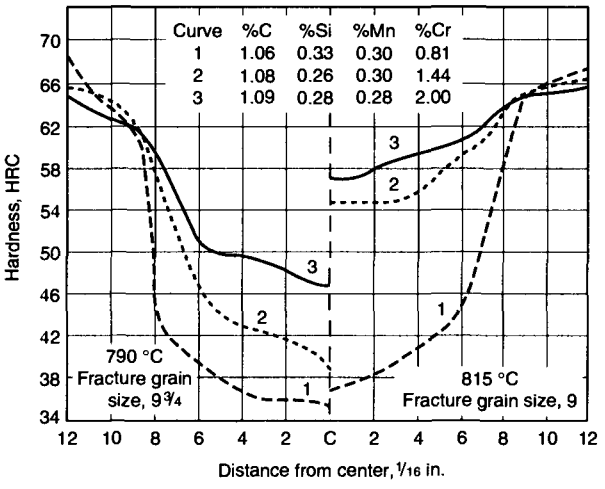

Fig. 8-1 Hardness-penetration curves for 38 mm diam by 100 mm (1½ by 4 in) round bars of 1.10% C steels with 0.81, 1.44, and 2.00% Cr, brine quenched from 790 and 815 ° C (1450 and 1500 °F) Courtesy of R.A. Frost, Teledyne VASCO

Table 8-2 Performance factors and processing information for low-alloy special-purpose tool steels

Factor	L1, high carbon	L2, medium carbon		L6
Major factors				
Wear resistance(a)	2–3	1	1	3
Toughness(b)	4–6	7	7	6
Hot hardness	2	2	2	2
Minor factors				
Usual working hardness, HRC	45–63	45–60	45–62	45–62
Depth of hardening	M	M	M	M
Finest grain size at full hardness,Shepherd standard	9	9	8½	8
Surface hardness as-quenched, HRC	58–67	64–61	56–62	58–63
Core hardness (25 mm or 1 in., diam round), HRC	54–60	47–58	54–58	58–62
Manufacturing factors				
Availability	2	2	2	2
Cost	1	1	1	1
Machinability	8	8	8	7
Quenching medium	W, O	W, O	W, O	O
Hardening temperature, °C (°F)	760–815 (1400–1500)	790–925 (1450–1700)	800–885 (1475–1625)	760–790 (1400–1450)
Dimensional change on hardening	H	H	M	M
Safety on hardening	L	L	M	M
Susceptibility to decarburization	M	M	M	M
Approximate hardness as-rolled or forged, HB	350	300	300	400
Annealed hardness, HB	163–202	163–202	163–207	183–255
Annealing temperature, °C (°F)	760–815 (1400–1500)	790–830 (1450–1525)	790–830 (1450–1525)	760–790 (1400–1450)
Tempering range, °C (°F)	175–540 (350–1000)	175–540 (350–1000)	175–595 (350–1000)	175–540 (350–1000)
Forging temperature, °C (°F)	980–1095 (1800–2000)	980–1095 (1800–2000)	980–1095 (1800–2000)	980–1095 (1800–2000)

Note: Ratings are explained in Chapter 2. (a) Wear resistance increases with increasing carbon content. (b) Toughness decreases with increasing carbon content and depth of hardening.

Vanadium, also an alloying element added to L2 tool steels, actually reduces hardenability somewhat, if the steels are austenitized at low temperatures. Figure 8-2 shows reduced hardness penetration in steels, with about the same carbon and chromium contents, when vanadium is added. This effect is related to the very strong carbide-forming ability of vanadium and to the fact that at low austenitizing temperatures, around 800 °C (1475 °F), vanadium carbides do not dissolve. Finely dispersed vanadium carbide particles thus maintain a very fine austenitic grain size, which reduces hardenability (see Chapter 4). The strong carbide-forming characteristics of vanadium and the associated fine austenitic grain sizes, however, are desirable because they increase fracture resistance and resist grain coarsening during overheating.

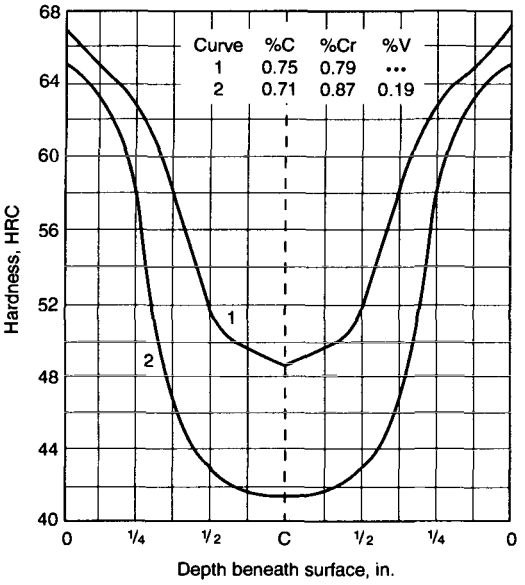

Fig. 8-2 Hardness-penetration curves for 40 mm diam by 150 mm (1½ by 6 in.) round bars of L2 tool steel with and without vanadium, brine quenched from 800 ° C (1475 °F). Data from Teledyne VASCO

Table 8-3 Chromium content required for through-hardening of listed sizes

Ball diameter		
mm	in.	Cr, %
3.2–16	⅛–⅝	0.75–1.05
16–29.8,	⅝–1 3/16	1.05–1.35
>29.8	>1 3/16	1.35–1.65

Due to their relatively low alloy content, the L-type tool steels are readily forged (typically between 980 and 1095 °C, or 1800 and 2000 °F) and may be air cooled after forging. Annealing is performed at relatively low temperatures, as listed in Table 8-2, in order to produce a very fine dispersion of carbides in ferrite for subsequent hardening.

Hardening of the high-carbon L_2 tool steels is dependent on austenitizing and the transformations that occur during cooling. Table 8-4 shows examples of hardening temperatures for selected grades of L2 steels. The somewhat better hardenability of the L steels compared to the water-hardening steels makes possible adequate martensite formation by oil quenching in most applications, but in some cases water quenching may be required for sufficient depth of hardening. Table 8-4 shows that austenitizing temperatures for water quenching are lower than those for oil quenching, consistent with the fact that more severe water quenching can accomplish hardening without the benefits of the enhanced carbon and chromium solution that occurs at higher austenitizing temperatures. Water quenching, however, must be used with care because of the increased possibility that the higher surface tensile stresses generated by more severe quenching will cause quench cracking. The latter precaution applies especially to the L2 grades with higher hardenability by virtue of high manganese contents within the specification range.

The L-type tool steels have austenite transformation characteristics typical of low-alloy steels; namely, the transformation kinetics as a function of temperature are characterized by a single C-curve as compared to the two well-separated C-curves for transformations in the highly alloyed tool steels. Figure 8-3 shows an IT diagram for a 1% C steel containing 1.21% Cr (Ref 3). As discussed in Chapter 4, Jominy end-quench testing relates austenite transformation kinetics to the hardness of the microstructures formed by continuous cooling. Figures 8-4 to 8-7 show Jominy end-quench curves for various L2 steel compositions. The effects of carbon content between 0.70 and 1.00% and chromium contents of 0.80 and 1.40% are shown for a constant vanadium content of 0.2%. The effect of austenitizing at three temperatures also is shown for each grade.

Table 8-4 Typical compositions and hardening temperatures for L2-type steels

Typical composition, %				Hardening temperature, °C (°F)			
				Water quench		Oil quench	
C	Mn	Cr	V				
0.70	0.25	0.80	0.20	775–815	1425–1500	815–860	1500–1575
0.80–1.00	0.25	0.80	0.20	760–805	1400–1480	800–845	1475–1550
1.00	0.25	1.40	0.20	760–805	1400–1480	815–870	1500–1600

The higher the austenitizing temperature, the higher the hardness of the fully martensitic microstructures that form at the quenched end of the Jominy specimens and the greater the distance from the quenched end to which high hardness is maintained. The carbide that forms in the L steels during annealing is cementite, which incorporates a limited amount of chromium in its crystal structure (Ref 4). At the higher austenitizing temperatures, as the carbides dissolve, increasing amounts of chromium and carbon go into solution in the austenite, producing the changes shown on the Jominy curves. Figure 8-8 shows similar effects of hardening temperature on hardness profiles of brine-quenched 89 mm (3.5 in.) diam rounds of an L2 steel and illustrates the relatively shallow hardening of the L steels in heavy sections. A unique aspect of the L2 steel Jominy curves is the small hardness peak, at cooling rates slower than those at which bainite form, associated with the formation of pearlite with very fine interlamellar ferrite-cementite spacing (Ref 5, 6).

Figure 8-9 shows a CCT diagram for a 1.0% C steel alloyed with manganese, nickel, chromium, and molybdenum (Ref 7). Although this grade is no longer produced, the diagram illustrates the pro-

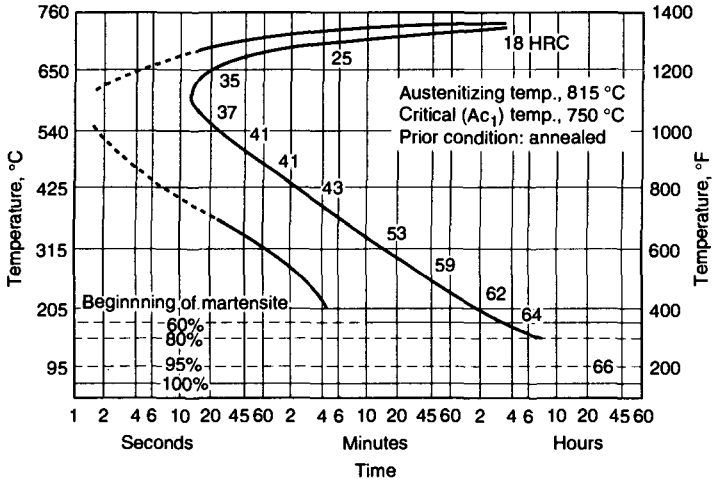

Fig. 8-3 IT diagram for decomposition of austenite in an L-type tool steel containing 1.01% C, 0.50% Mn, 0.30% Si, and 1.21% Cr. Specimens were austenitized for 30 min at 815 °C (1500 °F). Source: Ref 3

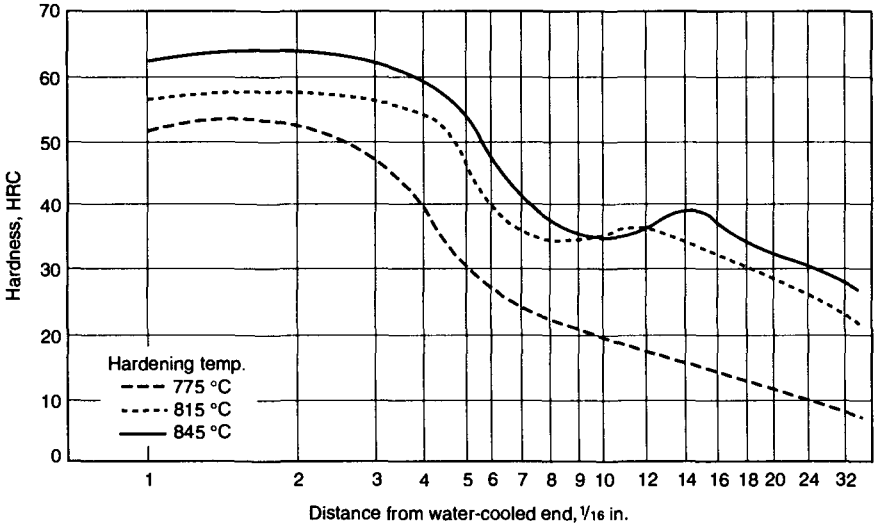

Fig. 8-4 Jominy end-quench curves for L2 tool steel, containing 0.7% C, 0.80% Cr, and 0.20% V, after quenching from three hardening temperatures. Data from Teledyne VASCO

gression of microstructures from martensite through pearlite as cooling rate decreases for this type of steel (Ref 8). Carbides retained after austenitizing are a constant component of all the transformed microstructures.

If hardenability is adequate, and with appropriate cooling rates and section sizes, the austenite of the low-alloy L-type tool steels transforms to martensitic microstructures. The martensite transformation kinetics, tempering, and associated dimensional changes have been extensively studied as a result of sponsorship of Cohen and colleagues at the Massachusetts Institute of Technology by manufacturers of gage blocks (Ref 9-16). Much of this work has been summarized in a book by Lement (Ref 16).

The amount of martensite formed in a low-alloy steel during a continuous quench to room temperature is a function only of the M_s temperature of the austenite from which it forms. The athermal martensite transformation during continuous cooling and the stabilization of the transformation during interrupted cooling have been described in Chapter 5. The M_s temperature is in turn directly related to the composition of the austenite as determined by alloy composition and austenitizing temperature.

Figure 8-10 shows the effect of austenitizing temperature on M_s temperatures in 1.1% C steels without chromium and with two levels of chromium (Ref.14). Again, the strong effect of carbide dissolution as a function of temperature is shown. This

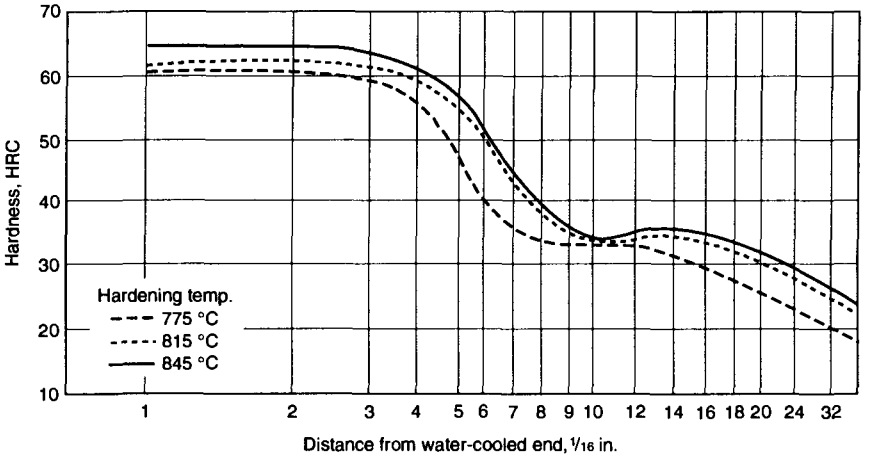

Fig. 8-5 Jominy end-quench curves for L2 tool steel, containing 0.80% C, 0.80% Cr, and 0.20% V, after quenching from three hardening temperatures. Data from Teledyne VASCO

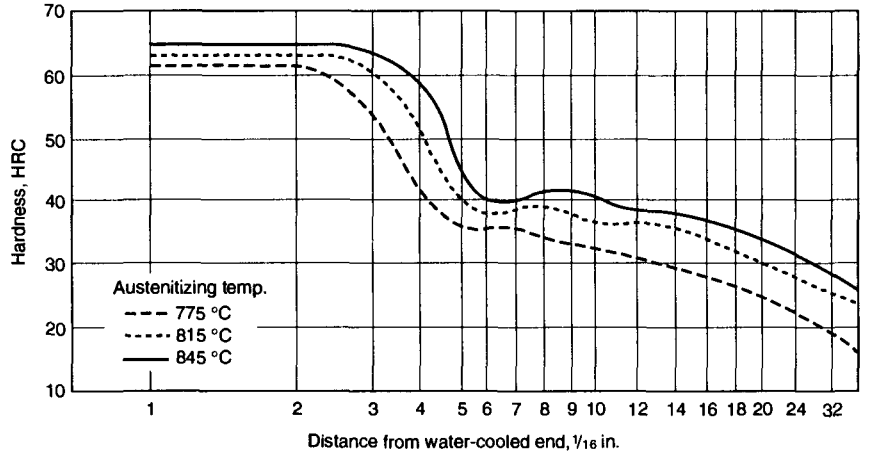

Fig. 8-6 Jominy end-quench curves for L2 tool steel, containing 0.92% C, 0.80% Cr, and 0.20%V, after quenching from three hardening temperatures. Data from Teledyne VASCO

effect was related earlier to increased hardenability; here, another effect of chromium and carbon dissolved in austenite is noted— namely, lower M_s temperatures. As a result, less martensite forms on reaching room temperature, and more austenite is retained. For example, Table 8-5 shows that the amount of retained austenite increases as increased austenitizing temperature dissolves more carbides in 1.1% C steels with varying amounts of chromium. In view of martensite athermal formation kinetics, retained austenite present at room temperature can be transformed by refrigeration. However, arrested cooling— which causes stabilization and reduces the rate of martensite formation when cooling is resumed— must be taken into account.

Differences in cooling rate also affect martensite transformation kinetics. Slower cooling rates lower the rate of martensite transformation and result in higher amounts of retained austenite on cooling to a given temperature. Table 8-6 shows the effect of various cooling schedules on the amount of retained austenite formed in an L2 tool steel (Ref 17), and Fig. 8-11 compares the hardness of transformed microstructures and the amount of retained austenite formed during water and oil quenches as a function of austenitizing temperature (Ref 10). Independent of cooling media, the amount of retained austenite increases rapidly in specimens austenitized above 845 °C (1550 °F) and approaches a maximum in specimens austenitized above 1010 °C (1850 °F), the temperature above which significant grain coarsening also develops.

Retained austenite in as-quenched specimens of L-type tool steels is not stable at room temperature and transforms to martensite with increasing time at room temperature. Figure 8-12 shows the isothermal transformation of retained austenite as a function of time at room temperature for L2 steel containing 1.0% C, 1.56% Cr, and 0.20% V and quenched in various media to produce various as-quenched amounts of retained austenite (Ref 13). The expansion created by the transformation of retained austenite to martensite creates stress; therefore, tempering soon after quenching is recommended to prevent the development of this additional source of stress after quenching.

Tempering of the low-alloy, high-carbon L2-type tool steels causes a continuous decrease in hardness with increasing tempering temperature, and higher chromium contents reduce the rate of softening, as shown in Fig. 8-13. At tempering temperatures below 200 °C (390 °F), the first stage of tempering (i. e., transition carbide precipitation in martensite crystals) constitutes the major change in microstructure. Hardness remains relatively high, or may even increase slightly, toughness increases, residual stresses decrease, and specimen dimensions contract. Figure 8-14 shows that retained austenite is stable in the first stage of tempering (Ref 18).

The second stage of tempering (i.e., the transformation of retained austenite to carbide-ferrite microstructures) proceeds rapidly with tempering at temperatures above 200 °C (390 °F) in the low-alloy L2-type steels (Fig. 8-14). Hardness drops rapidly and toughness is reduced. A beneficial effect, however, of the elimination of retained austenite is increased dimensional stability under service stresses in applications such as gages and ball and roller bearings (Ref 19). If retained austenite is present in these applications, it may transform, by stress- or strain-controlled mechanisms (Ref 20), to martensite with attendant increases in part dimensions.

Figure 8-15 shows the dimensional changes that occur as a function of tempering time and temperature in a low-alloy L2 tool steel containing 1.0 % C, 1.5 % Cr, and 0.2 % V. The slight expansion at room temperature and below is attributed to isothermal transformation of retained austenite to martensite. At higher tempering temperatures there is an overall contraction that correlates with the decrease in

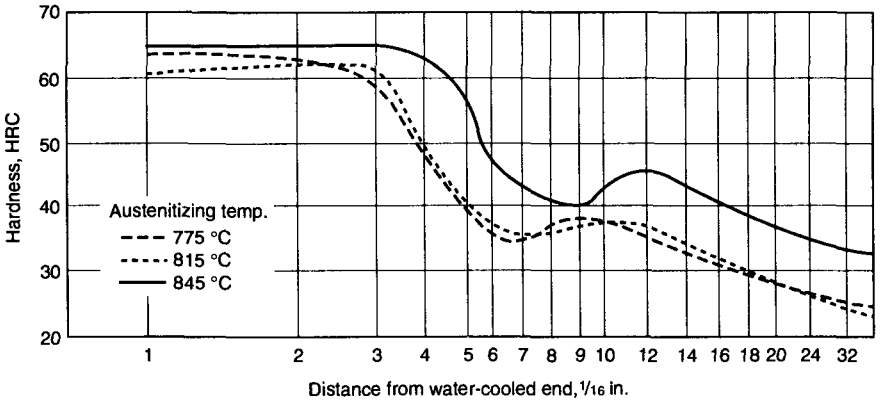

Fig. 8-7 Jominy end-quench curves for L2 tool steel, containing 1.00% C, 1.40% Cr, and 0.20% V, after quenching from three hardening temperatures. Data from Teledyne VASCO

tetragonality of the martensite as transition carbides precipitate and relieve the carbon supersaturation of the martensite. At higher temperatures, the initial contraction period is followed by expansion, as retained austenite transforms to ferrite and carbides in the second stage of tempering. The diffusion-controlled transformation of the retained austenite is a function of time and temperature, and at the lower tempering temperatures requires considerable time for initiation. The dimensional changes associated with austenite transformation go through a maximum with increasing tempering temperature, and at higher temperatures are overwhelmed by the contraction associated with third-stage formation of ferrite and cementite and the complete elimination of tetragonality in the tempered martensite.

The dimensional changes shown in Fig. 8-15 are based on changes produced only during tempering of as-quenched hardened microstructures. The hardening process results in an expansion relative to the spheroidized annealed structure of ferrite and carbides, and to obtain the over-all change in dimensions on hardening and tempering, this length change, estimated to be +1500 micro-in./in. for L2 type steels with 1.0% C, should be added to the changes shown in Fig. 8-15.

Torsional impact strength of high-carbon L-type steels as a function of tempering temperature is shown in Fig. 8-16 (Ref 21). Included for comparison is a curve for a plain carbon water-hardening steel. All the steels show a maximum in torsional impact strength when tempered between 150 and

Table 8-5 Effect of austenitizing temperature and chromium content on retained austenite and undissolved carbides in 1.1% C steels

	845 °C (1550 °F)		925 °C (1700 °F)	
Chromium content, %	Retained austenite, %	Undissolved carbide, %	Retained austenite, %	Undissolved carbide, %
0	16	0.5	20	0
1.5	7	4.5	22	1.6
2.8	2	6.9	21	3.5

(a) All specimens were brine quenched to 25°C (77 °F)

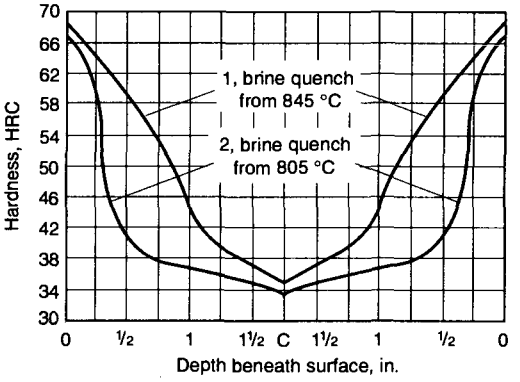

Fig. 8-8 Effect of quenching temperature on the hardness-penetration curves for 90 mm (3½ in.) diam round bars of an L2 tool steel containing 1.0%C, 1.40%Cr, and 0.20% V. Data from Teledyne VASCO

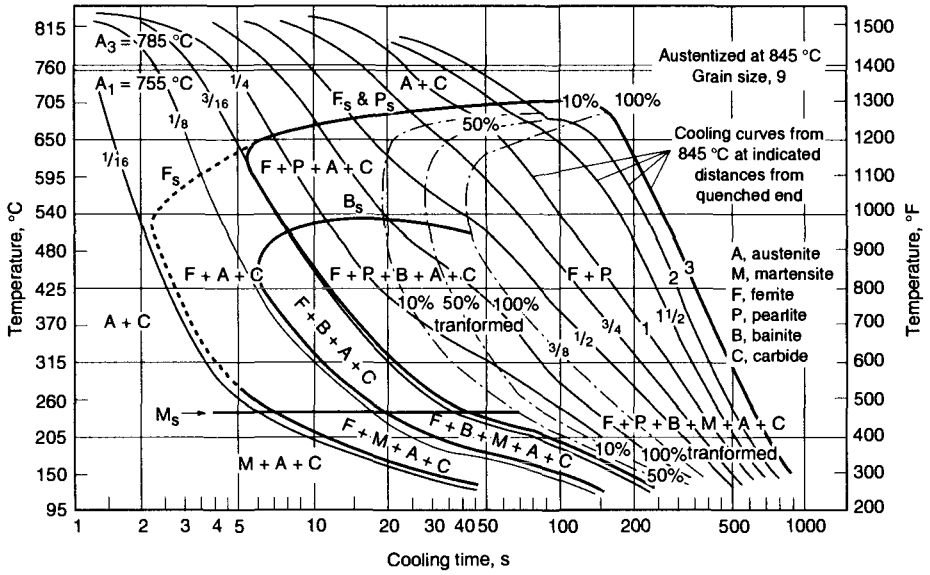

Fig. 8-9 CCT diagram for an L-type steel containing 1.06% C, 0.33% Mn, 0.32% Si, 0.11% Ni, 1.44% Cr, and 0.03% Mo. Source: Ref 7

200 °C (300 and 390 °F), but then show a marked decrease in toughness when tempered at temperatures above this range. This decrease in toughness, formerly referred to as 260 °C (500 °F) embrittlement, is now termed tempered martensite embrittlement. The major cause for the drop in toughness is the introduction of coarse carbide particles during the second stage of tempering. Tempered martensite embrittlement also reduces CVN impact toughness and fracture toughness, as described for a 52100 steel in Chapter 7.

Figure 8-17 shows static torsion curves for high-carbon L-type steels with and without addition of vanadium. The vanadium-containing steel shows better ductility than the steel without vanadium, and both steels show a decrease in ductility in specimens tempered in the tempered martensite embrittlement range.

The comments that have been made here with regard to the increase in toughness with tempering in the first-stage temperature range are based on specimens properly hardened at intercritical austenitizing temperatures as noted in Table 8-2 for the various L tool steels. Austenitizing for hardening at temperatures above A_{cm} (i.e., overheating on heat treatment) will cause grain coarsening and associated phosphorus segregation and cementite formation at austenite grain boundaries. Such embrittled grain boundaries are then extremely sensitive to intergranular fracture during quenching or in service, as discussed in earlier chapters.

Low-Alloy Chromium Tool Steels with Medium Carbon Content

The medium carbon content (between 0.45 and 0.6 %) of these L2 tool steels makes possible good combinations of high strength and toughness in hardened and tempered conditions. As Table 8-2 shows, the toughness of the medium-carbon L2 steels is much improved relative to the high-carbon L2 steels, but wear resistance is reduced. Other medium-carbon types of tool steels, such as L6, which contains nickel as described below, and the medium-carbon S-type tool steels alloyed with silicon and tungsten may have comparable toughness but may be less favored than the medium-carbon L2 grades for various reasons. For example, the nickel-containing steels are less machinable, the silicon-

Table 8-6 Effect of cooling rate in the martensite transformation range on retained austenite in an L2-type steel

Quenching treatement	Retained austenite, %
Water quenched to 20 °C (68 °F)	5.8
Oil quenched to 20 °C (68 °F)	7.0
Salt quenched to 230 °C (450 °F), water quenched to 20 °C (68 °F)	6.1
Salt quenched to 230 °C (450 °F), oil quenched to 20 °C (68 °F)	6.2
Salt quenched to 230 °C (450 °F), air cooled to 20°C (68 °F)	10.6

(a) Composition: 1.0% C, 1.5% Cr, 0.2% V; austenitized at 845 °C (1500 °F); 4.0% undissolved carbide. Source: Ref 17

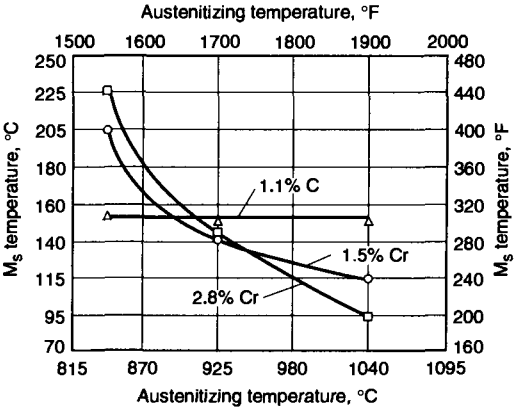

Fig. 8-10 Effect of austenitizing temperature and chromium content on the M_s temperature of 1.1% C steels. Source: Ref 14

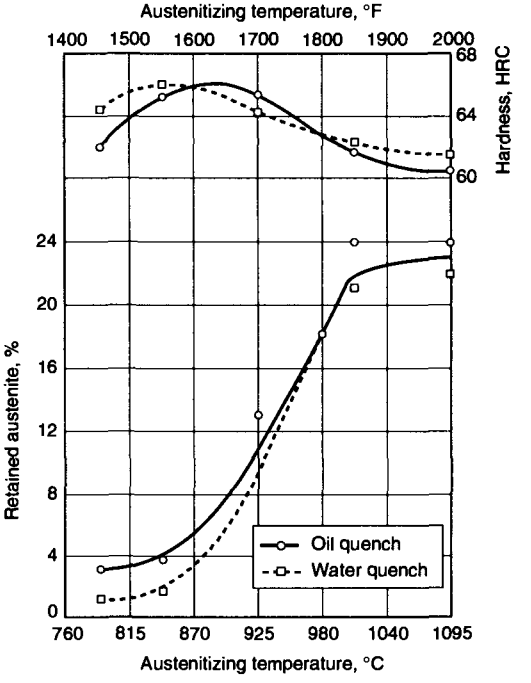

Fig. 8-11 Effect of austenitizing temperature and quenching medium on retained austenite content and as-quenched hardness of an L2 steel containing 1.04% C, 1.54% Cr, and 0.20% V. Source: Ref 10

containing steels are more susceptible to decarburization, and the tungsten-containing steels, although they have better wear resistance and hot hardness, are more expensive.

Forging temperatures for the medium-carbon L2 steels are listed in Table 8-2. Forging is readily accomplished, with finishing temperatures down to 845 °C (1550 °F) allowable with the application of reasonable care. Somewhat slower rates of heating to forging temperatures than those used for plain carbon steels may be used to prevent cracking. The medium-carbon L2 steels can be air cooled after forging, and furnace cooling from the annealing temperature range listed in Table 8-2 should result in well-annealed microstructures with annealed hardness values in the listed range.

For hardening, the medium-carbon L2 steels have relatively low sensitivity to austenitizing temperature. The A_{cm} temperature is reduced relative to the high-carbon grades of L2 tool steel; therefore, the dissolution of carbides plays a reduced role in hardenability. Also, vanadium additions maintain fine austenitic grain sizes at austenitizing temperatures up to 925 °C (1700 °F). Figure 8-18 shows the relatively flat hardness and fine grain size as a function of austenitizing temperature for an L2 steel containing 0.45% C.

Figure 8-19 shows an IT diagram for an L2 steel containing 0.50% C. Two overlapping C-curves, one for ferrite and pearlite, the other for bainite, are apparent. Pearlitic hardenability (i.e., resistance to pearlite formation) is higher than bainitic hardenability; therefore, the formation of a proeutectoid constituent or bainite limits hardenability. When molybdenum is added to this grade of steel, the shift between pearlite and bainite C-curves is accentuated, as shown in Fig. 8-20 and 8-21 (Ref 22, 23). Jominy end-quench curves for L2 steels with 0.50 and 0.60% C are shown in Fig. 8-22 and 8-23, respectively. Higher carbon content raises the hardness of the martensite formed at the water-quenched end, according to Fig. 7-1, and maintains higher hardness at greater distances, corresponding to slower cooling rates, from the quenched end.

Hardness as a function of tempering temperature is shown in Fig. 8-24 for a number of medium-carbon L2-type steels. In the vanadium-containing grades, increasing carbon content maintains higher hardness through the first stage of tempering. At higher tempering temperatures, hardness decreases continuously but at a lower rate with increasing carbon content. Additions of molybdenum cause significant retardation of softening at high temperatures.

The L2 tool steels with medium carbon content at and below 0.50% C have limited sensitivity to quench embrittlement, as would be expected from Fig. 7-2. As a result, tensile testing can be applied to evaluate mechanical properties of hardened and tempered specimens. Table 8-7 compares the mechanical properties of two medium-carbon L2 steels, almost identical in composition except for vanadium content. After tempering at 425 °C (800 °F), the vanadium-containing steel shows not only higher strength and hardness, but also increased ductility relative to the vanadium-free steel. Other sets of mechanical properties for medium-carbon L2 steels are listed in Table 8-8 as a function of tempering temperature and heat treatment parameters, such as quench media and austenitizing temperature. Oil quenching of 0.45% C L2 steels reduces strength, but increases ductility compared to water quenching. Higher carbon content increases strength, but reduces ductility, even in oil-quenched specimens.

Elevated-temperature mechanical properties of an L2 steel containing 0.50% C are listed in Table 8-9. Only tests at temperatures at or below the tempering temperature applied to the steel prior

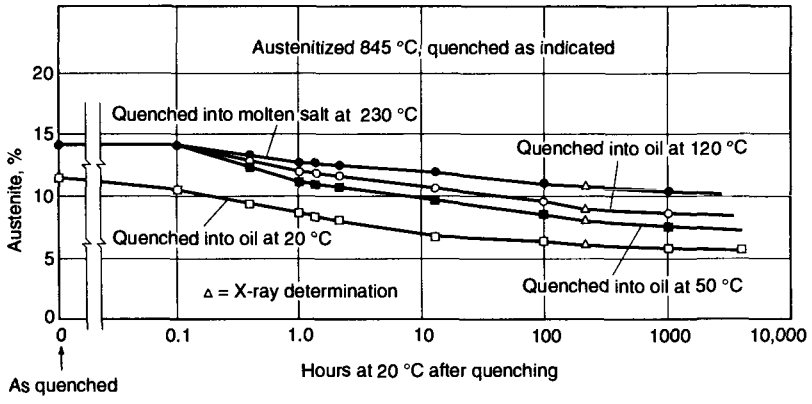

Fig. 8-12 Isothermal decomposition of austenite at room temperature in an L2 steel, containing 1.0% C, 1.56% Cr, and 0.20% V, after different quenching treatments. Specimens quenched to temperatures above room temperature were held at temperature for 5 min and air cooled. Source: Ref13

to testing yield stable properties; otherwise, as shown, the specimens lose strength and soften rapidly.

Various measurements of toughness as a function of tempering temperature are shown in Fig. 8-25 to 8-27. All the medium-carbon L2 steels show an increase in toughness from the as-quenched condition to LTT maxima around 200 °C (390 °F). Tempering at higher temperatures, between 315 and 425 °C (600 and 800 °F), produces a minimum in toughness referred to as tempered martensite embrittlement. This embrittlement is related to the formation of additional, coarse carbides by the transformation of austenite in the second stage of tempering (Ref 26). The additional carbides provide sites for microvoid nucleation under stress conditions that cause ductile, shear fractures. Under tensile loading conditions, if phosphorus content is on the high side of specification limits, an intergranular fracture mode of tempered martensite embrittlement may develop (Ref 26, 27).

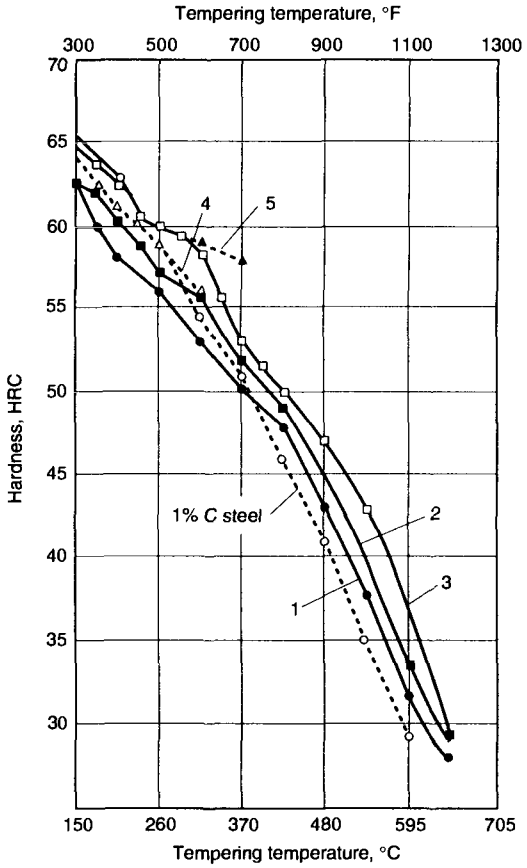

The energy absorbed in the various tests includes that associated with the plastic deformation, prior to fracture, of microstructures consisting of tempered martensite crystals and retained austenite, as well as the energy absorbed in the fracture process at various particle dispersions. Fine-scale, difficult-to-resolve changes in the fine structure of martensite, retained austenite, and particle dispersions, as affected by alloy content, austenitizing temperature, quench rate, and tempering temperature, must account for the variations in the toughness values shown in Fig. 8-25 to 8-27, both at the maxima and at the minima in toughness produced by tempering the medium-carbon L2 steels at low temperatures. The fine-scale differences in microstructures and their effect on deformation and fracture have not been fully evaluated at this time; therefore, experience and empirical measurements of properties and toughness must continue to suffice as guidelines for the selection of various tool steel grades and heat treatments.

The good combinations of strength and toughness of the medium-carbon L2 steels make them desirable for applications requiring good fracture and shock resistance. Applications have included wrenches, jack screws, shear blades, chisels, rivet sets, gears, driveshafts, gripper dies, drop-forging dies, springs, spindles, and arbors. Heavier applications may require more alloying for increased hardenability, and in view of the relatively low wear and tempering resistance of these steels, applications that require wear performance are best limited to short-run, less demanding service.

Low-Alloy Chromium Tool Steels Containing Nickel

The L6 grade of low-alloy tool steels contains nickel in addition to chromium. Nickel is an

	Composition, %						Hardening temperature		Hardening	
Curve	C	SI	Mn	Mo	Cr	V	°C	°F	medium	Specimen size
1	0.70	0.25	0.20	...	0.80	0.20	795	1460	Water	1 (diam) × 1¼ in.
	0.80	0.25	0.20	...	0.80	0.20	780	1430	Water	1 (diam) × 1¼ in.
2	0.92	0.25	0.20	...	0.80	0.20	775	1425	Water	1 (diam) × 1¼ in.
3	1.03	0.25	0.32	...	1.41	1.19	805	1480	Brine	1 (diam) × 1¼ in.
4	1.00		0.35	0.30	1.20	...	830	1525	Oil	1 (diam) × 1½ in.
5	0.97	1.60	1.56	...	2.85	...	845	1550	Oil	4⅝ (diam) × 8 in.

Fig. 8-13 Hardness as a function of tempering temperature for various L-type steels. Curves 1, 2, 3, and 5, Teledyne VASCO; curve 4, Crucible Steel Co.

austenite-stabilizing element and thus lowers the A_1 and A_3 critical temperatures and extends the temperature range of austenite stability. Also, nickel is not a carbide-forming element; therefore, it goes into solid solution in austenite and ferrite and provides solid-solution strengthening to those phases. In contrast, chromium is a ferrite-stabilizing and carbide-forming alloying element in steels. The effects of nickel make the L6 steels slightly less machinable than the L2 steels without nickel, as well as lower the annealing and hardening temperatures somewhat compared to those used in the chromium steels.

The hardenability of L6 tool steel is good, and all grade variations can be oil quenched. Hot hardness and softening resistance during tempering are low; thus, the L6 steels are not used for elevated-temperature service. Relatively high carbon content provides good low-temperature wear resistance. Typical tool applications are woodworking saws and knives, shear blades, blanking dies, punches, and press-brake dies. Nontool uses include spindles, clutch parts, gears, and ratchets.

Forging of the L6 steels is readily accomplished in the temperature range of 980 to 1090 °C (1800 to 2000 °F), with finishing temperatures as low as 845 °C (1550 °F). The molybdenum-containing variety of L6 tool steels has high hardenability; therefore, this grade of steel should be cooled from forging temperatures at rates slower than those of air cooling. Again, because of high hardenability, L6 steels should not be normalized, but should be annealed after forging and before hardening.

The L6 steels, as noted above, are oil hardening, and as Fig. 8-28 shows, the molybdenum-containing grade can even be hardened by cooling with an air blast. Figure 8-28 also shows that austenite grain coarsening is not severe up to austenitizing temperatures of about 955 °C (1750 °F). The L6 steels show no pronounced tendency to decarburize on hardening, and virtually any type of hardening furnace is adequate. When hardening large or intricate sections, it is advisable to heat slowly through the critical temperature range, 650 to 760 °C (1200 to 1400 °F).

Figure 8-29 shows an IT diagram for an L6 steel. Well-developed pearlite and bainite C-curves are present, and pearlite formation substantially lags bainite formation. These transformation characteristics result in good hardenability, as shown in

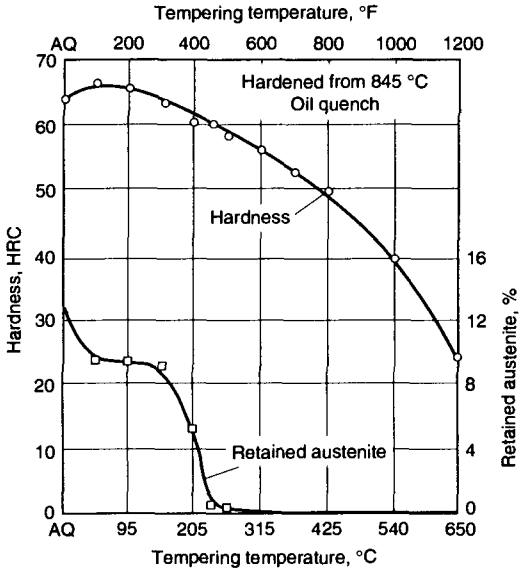

Fig. 8-14 Hardness and retained austenite as a function of tempering temperature in a high-carbon L-type tool steel. Source: Ref 18

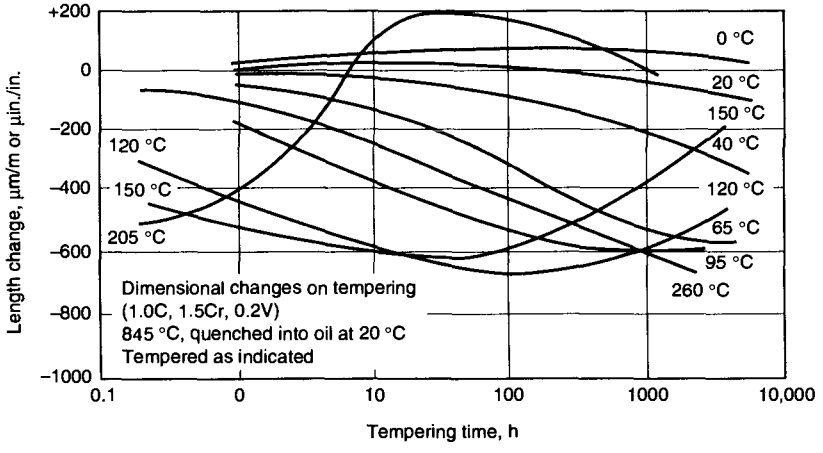

Fig. 8-15 Length changes on tempering a high-carbon L2 tool steel. Tempering time is considered to begin 1.5 h after quenching. Source: Ref 13

Table 8-7 Mechanical properties of medium-carbon L2 steels with and without vanadium(a)

Property	Steel A(b)	Steel B(c)
Tensile strength, Mpa (ksi)	1523 (220.9)	1605 (232.8)
Yield point, Mpa (ksi)	1384 (200.7)	1546 (224.2)
Yield-tensile ratio	0.911	0.963
Elongation, %	9.6	10.4
Reduction of area, %	35.9	43.1
Hardness, HV	457	481
Izod impact, J(ft·lbf)	16.3 (12.0)	16.3 (12.0)

(a) Oil quenched from 840 °C (1545 °F); tempered at 425 °C (800 °F). (b) Composition: 0.49% C, 0.76% Mn, 0.21% Si, 1.07% Cr. (c) Composition: 0.50% C, 0.79% Mn, 0.31% Si, 0.98% Cr, 0.20% V

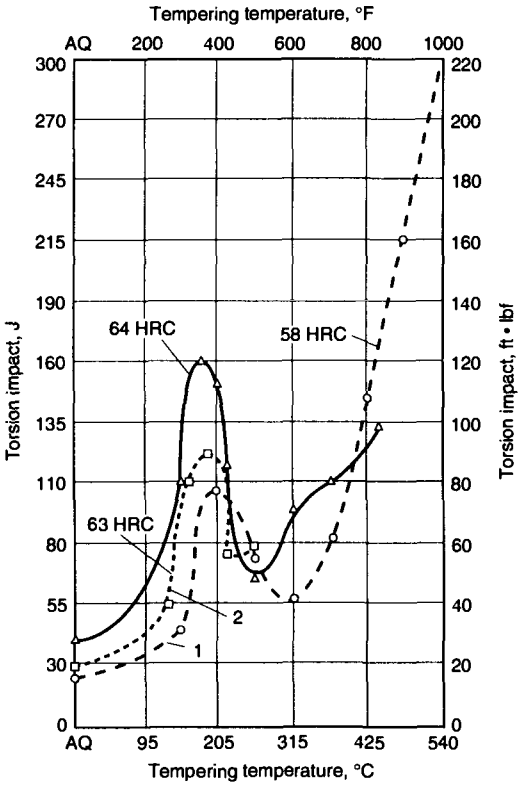

Curve	Composition % C	Cr	V	Hardening temperature °C	°F	Hardening medium
1	0.70	0.80	0.20	800	1475	Water
2	1.03	1.50	...	805	1480	Brine
3	1.06	...	...	790	1450	Brine

Fig. 8-16 Torsional impact energy absorbed as a function of tempering temperature for high-carbon L-type steels. Curve 1, Bethlehem Steel Co.; curves 2 and 3, Ref 21

the Jominy end-quench curves of Fig. 8-30. The increased hardenability with increasing austenitizing temperature reflects significant carbide dissolution and increasing availability of carbon, chromium, and molybdenum in austenite solution for good hardenability on quenching.

The effect of tempering on the hardness of L6-type steels is shown in Fig. 8-31. Hardness decreases continuously with increasing tempering, and the L6 grade with molybdenum shows the best tempering resistance. For wood-cutting saws, a tempered hardness of 45 to 50 HRC has been found desirable, whereas most other applications require hardness in the range of 58 to 62 HRC, as obtained by LTT.

Impact strength as a function of tempering temperature as determined by several testing techniques is shown in Fig. 8-32. The torsion impact test shows a low-temperature maximum in toughness, but the unnotched Izod and Charpy impact tests show only an increase in toughness with increasing temperature, even in the tempered martensite embrittlement range. The excellent torsional ductility of as-quenched and quench-and-tempered L6 tool steel is shown in Fig. 8-33. However, Table 8-10 shows that ductility as measured by tensile testing is low in specimens tempered at low temperatures, but increases with increasing tempering temperatures above 315 °C (600 °F).

Figure 8-34 shows the dimensional changes that develop on tempering of an L6 tool steel (Ref 28). The curves show the changes relative to the expansion that occurred during hardening and the formation of as-quenched martensite. At low temperatures where transition carbides precipitate and lower the tetragonality of the martensitic crystal structure, the specimens contract. Expansion develops at higher tempering temperatures where austenite transforms to bainite. After transformation of retained austenite, contraction again develops as the remaining tetragonality of the tempered martensite is relieved.

References

1. G.A. Roberts and R.A. Cary, *Tool Steels*, 4th ed., American Society for Metals, 1980
2. H.G. Freeland, Ball Steel, *Trans. ASST*, Vol 2, 1921–22, p 898
3. P. Payson and J.L. Klein, The Hardening of Tool Steels, *Trans. ASM*, Vol 31, 1943, p 218
4. L.R. Woodyatt and G. Krauss, Iron-Chromium-Carbon System at 870C, *Metall. Trans. A*, Vol 7A, 1976, p 983–989
5. F. Munoz del Corral, "Jominy Hardenability Curves with Anomalies," Inst. Hierro y Acero, Spec. No. 6, April 1952, p 432
6. T. Kawai, Anomaly Shapes of Jominy Hardenability Curves, *Tetsu-to-Hagané* (J. Iron Steel Inst. Jpn.), Vol 38, 1953, p 1159

7. R.C. Hess and D.J. Blickwede, Cooling Transformation Diagrams for AISI 4024 and 52100, *Met. Prog.*, Vol 74, July 1958, p 96B
8. D.J. Blickwede and R.C. Hess, Heat Treatment Diagram for AISI 52100, *Met. Prog.*, Vol 72, July 1957, p 96B
9. S.G. Fletcher and M. Cohen, The Dimensional Stability of Steel, Part I: Subatmospheric Transformation of Retained Austenite, *Trans. ASM*, Vol 34, 1945, p 216
10. S.G. Fletcher, B.L. Averbach, and M. Cohen, The Dimensional Stability of Steel, Part II: Further Experiments on Subatmospheric Transformations, *Trans. ASM*, Vol 40, 1948, p 703
11. B.L. Averbach, M. Cohen, and S.G. Fletcher, The Dimensional Stability of Steel, Part III: Decomposi-

Table 8-8 Tensile properties of L2 type steels after tempering at various temperatures

Tempering temperature		Tensile strength		Yield strength				
°C	°F	MPa	ksi	MPa	Ksi	Elongation in 50 mm (2 in.), %	Reduction of area, %	Hardness, HRC
L2 (0.50% C, 0.80% Cr, 0.20% V) oil quenched from 860 °C (1575 °F) (Ref 24)								
315	600	1655	240	...	...	5	10	42
370	700	1379	200	...	...	10	30	38
425	800	1158	168	...	...	14	45	33.5
480	900	965	140	...	...	17	55	29
540	1000	814	118	...	...	20	62	23.5
595	1100	690	100	...	...	22	66	215 HB
650	1200	586	85	...	...	24	68	187 HB
705	1300	517	75	...	...	25	70	160 HB
L2 (0.45% C, 0.55% Mn, 0.95% Cr, 0.20% V) water quenched from 925 °C (1700 °F) (Bethlehem Steel Co.)								
	None	2137	310	...	...	...	...	...
150	300	2117	307	...	...	...	...	...
205	400	2075	301	...	...	...	...	...
260	500	2000	290	1710	248	8	31	...
315	600	1806	262	1613	234	8	33	...
370	700	1634	237	1517	220	9	35	...
425	800	1510	219	1407	204	10	37	...
480	900	1413	205	1324	192	11	39	...
540	1000	1331	193	1241	180	12	40	...
595	1100	1255	182	1151	167	14	42	...
650	1200	1020	148	924	134	17	46	...
L2 (0.50% C, 1.30% Cr, 0.20% V) water quenched from 860 °C (1575 °F) (Bethlehem Steel Co.)								
150	300	1862	270	1793	260	4	4	55
205	400	2000	290	1793	260	...	17	54
260	500	1903	276	1717	249	9	25	52
315	600	1772	257	1607	233	...	30	51
370	700	1634	237	1503	218	10	...	49
425	800	1496	217	1379	200	...	...	47
480	900	1358	197	1241	180	11	40	41
540	1000	1220	177	1124	163	12	...	40
595	1100	1083	157	1000	145	15	49	37
650	1200	945	137	876	127	19	54	30
705	1300	807	117	745	108	22	61	20
L2 (0.50% C, 0.70% Mn, 1.00% Cr, 0.20% V) oil quenched from 860 °C (1575 °F) (Ref 25)								
205	400	2055	298	1813	263	1	5	58
260	500	2069	300	1813	263	4	12	56
315	600	1951	283	1724	250	7	27	54
370	700	1772	257	1620	235	10	37	52
425	800	1586	230	1489	216	11	42	50
480	900	1407	204	1345	195	12	44	45
540	1000	1255	182	1207	175	13	46	41
595	1000	1151	167	1083	157	16	47	38
(0.53% C, 0.54% Mn, 0.66% Cr, 0.33% Mo) oil quenched from 845 °C (1550 °F) (Allegheny Ludlum Industries)								
204	400	2275	330	1758	255	5	6.5	57
315	600	1889	274	1627	236	6.5	28.0	52
425	800	1600	232	1434	208	9.7	36.6	46
540	1000	1269	184	1124	163	12.2	45.8	39
650	1200	958	139	855	124	18.0	56.4	32

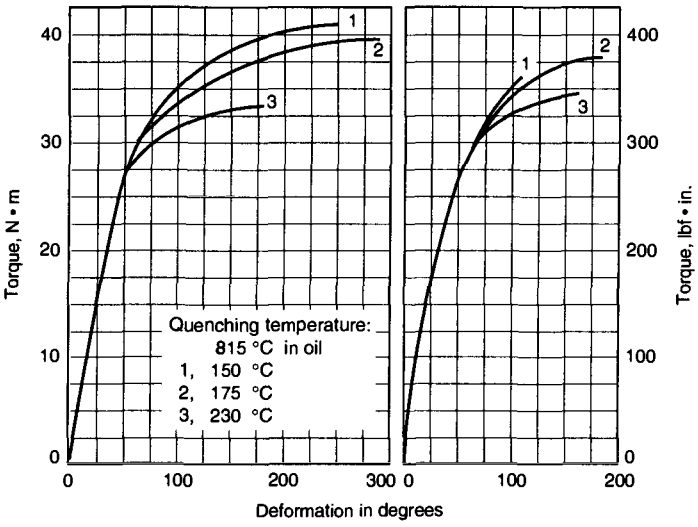

Fig. 8-17 Comparison of static torsion torque deformation curves for L-type steels with (left) and without (right) vanadium after tempering at three temperatures. Data from Teledyne VASCO

tion of Martensite and Austenite at Room Temperature, *Trans. ASM*, Vol 40, 1948, p 728

12. B.S. Lement, B.L. Averbach, and M. Cohen, The Dimensional Stability of Steel, Part IV: Tool Steels, *Trans. ASM*, Vol 41, 1949, p 1061
13. B.L. Averbach and M. Cohen, The Isothermal Decomposition of Martensite and Retained Austenite, *Trans. ASM*, Vol 41, 1949, p 1024
14. W.J. Harris and M. Cohen, Stabilization of the Austenite-Martensite Transformation, *Trans. AIME*, Vol 180, 1949, p 447
15. R.W. Balluffi, M. Cohen, and B.L. Averbach, The Tempering of Chromium Steels, *Trans. ASM*, Vol 43, 1951, p 497
16. B.L. Averbach and M. Cohen, X-ray Determination of Retained Austenite by Integrated Intensities, *Trans. AIME*, Vol 176, 1948, p 401
17. B.S. Lement, *Distortion in Tool Steels*, American Society for Metals, 1959
18. D.A. Hay, A.B. Jones, L.Schetky, and B.L. Averbach, "An Investigation of Spin Axis Instrument Bearings," Progress Report No. 2, U.S. Navy, Bureau of Ships, 1957
19. E.B. Mikus, T.J. Hughel, J.M. Gerty, and A.C. Knudsen, The Dimensional Stability of a Precision Ball Bearing Material, *Trans. ASM*, Vol 52, 1960, p 307
20. G.B. Olson, Transformation Plasticity and the Stability of Plastic Flow, *Deformation, Processing, and Structure*, G. Krauss Ed., American Society for Metals, 1984, p 391–424
21. G.V. Luerssen and O.V. Greene, The Torsion Impact Test, *Proc. ASTM*, Vol 33 (Part II), 1933, p 315
22. E.A. Loria, Isothermal Transformation of Austenite in Two Alloy Steels, *Trans. ASM*, Vol 41, 1949, p 1248
23. A.R. Troiano, "Final Report on Investigation of the Metallographic and Physical Properties of New Types of Gun Steels," OSRD Report No. 3513, Serial No. M-239, April 1944

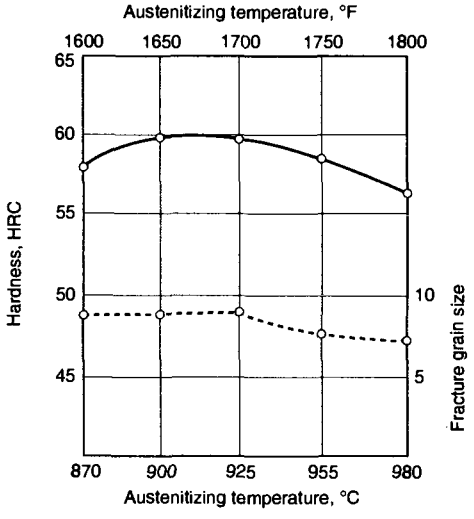

Fig. 8-18 Effect of austenitizing temperature on as-quenched hardness and fracture grain size of a medium-carbon L2 tool steel containing 0.45% C, 0.55% Mn, 0.95% Cr, and 0.20% V. All specimens were oil quenched. Data from Bethlehem Steel Company

24. *Alloy Digest*, Engineering Alloys Digest, Inc., 1956
25. *Alloy Digest*, Engineering Alloys Digest, Inc., 1957
26. G. Krauss, *Steels: Heat Treatment and Processing Principles*, ASM International, 1990, p 231–236
27. G. Krauss and C.J. McMahon, Jr., Low-Toughness and Embrittlement Phenomena in Steels, *Martensite*, G.B. Olson and W.S. Owen, Ed., ASM International, 1992, p 295–321
28. F.R. Palmer and G.V. Luerssen, *Tool Steel Simplified, 3rd ed., Carpenter Steel Co., 1960*

Table 8-9 Elevated temperature tensile properties of L2 tool steel(a)

Hardness before testing, HRC	Testing temperature °C	Testing temperature °F	Tensile strength MPa	Tensile strength ksi	Yeld strength (0.2 % offset) MPa	Yeld strength (0.2 % offset) ksi	Elogation in 50mm (2 in.), %	Reduction of area, %	Hardness after testing, HRC
Tempered at 315 °C (600 °F)									
53.8	260	500	1851.3	268.5	1620	235	12.0	40.5	52.0
53.8	315	600	1643.8	238.4	1438.3	208.6	13.0	46.5	52.0
54.3	425	800	1225.2	177.7	1099.1	159.4	13.6	55.8	48.7
53.5	540	1000	834	121	748.1	108.5	21.0	69.0	43.2
54.5	650	1200	338	49	303	44	86.2	93.5	36.0
Tempered at 425 °C (800 °F)									
50.3	260	500	1598.3	231.8	1398.3	201.5	9.1	22.7	47.5
50.3	315	600	1492.8	216.5	1327.3	192.5	11.8	39.0	47.0
49.7	425	800	1207	175	1079.8	156.6	12.5	55.0	45.5
49.8	540	1000	838.4	121.6	724	105	16.0	64.8	42.5
49.3	650	1200	328.2	47.6	287.5	41.7	60.5	88.4	35.0
Tempered at 540 °C (1000 °F)									
45.5	260	500	1389.3	201.5	1160.4	168.3	9.1	31.3	42.0
45.5	315	600	1327.3	192.5	1114.9	161.7	10.7	36.4	41.5
46.0	425	800	1121.1	162.6	992.2	143.9	12.0	49.5	41.2
45.3	540	1000	835.7	121.2	767.4	111.3	19.0	70.9	40.2
45.0	650	1200	293.7	42.6	283.4	41.1	62.7	89.6	35.7

(a) Composition: 0.50% C, 0.70% Mn, 1.00% Cr, 0.20% V; oil quenched from 870°C (1600 °F); tempered at indicated temperatures. Source: Ref 25

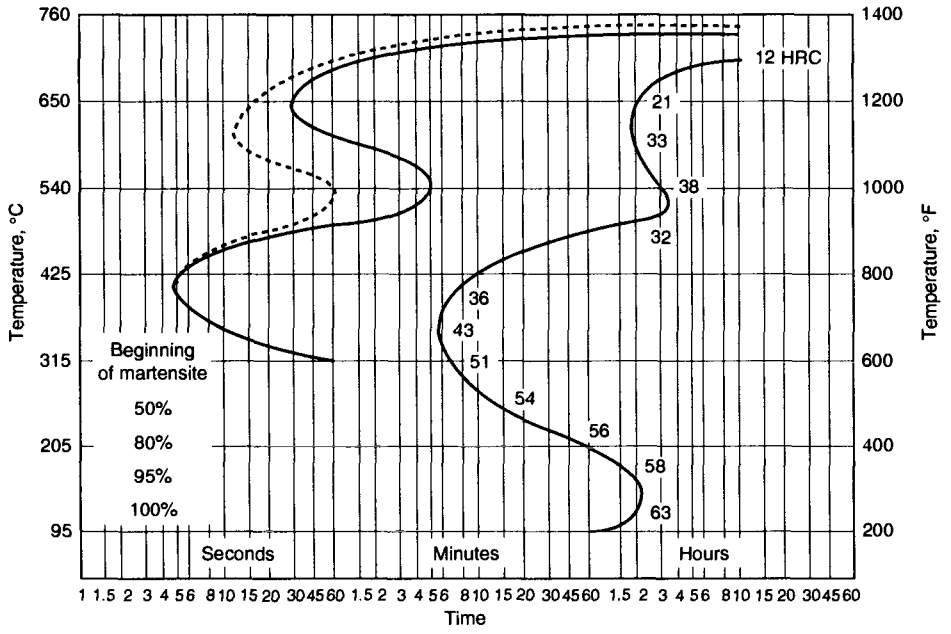

Fig. 8-19 IT diagram for L2 tool steel containing 0.50% C, 0.80% Mn, 1.00% Cr, and 0.20% V. Data from Crucible Steel Co.

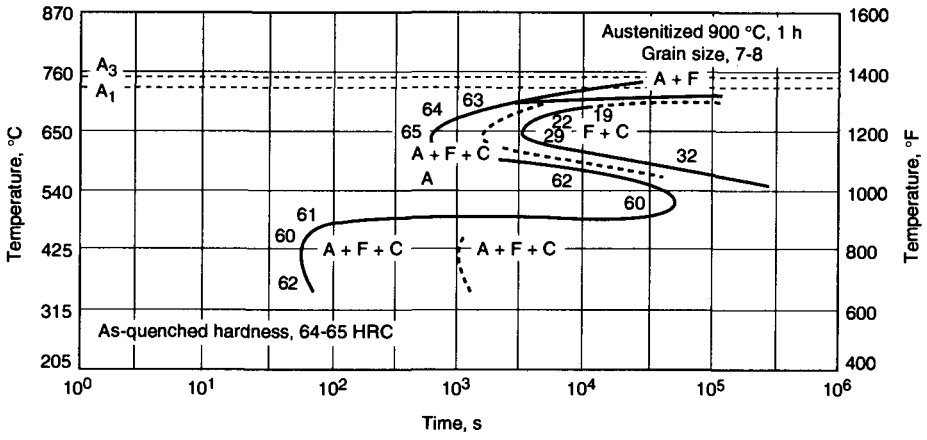

Fig. 8-20 IT diagram for an L2 steel containing 0.59% C, 0.96% Mn, 1.06% Cr, 0.54% Mo, and 0.12% V. Source: Ref 22

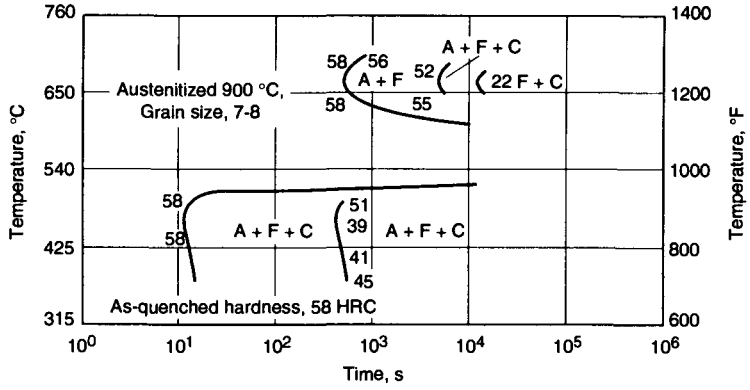

Fig. 8-21 IT diagram for L-type steel containing 0.39% C, 1.10% Mn, 1.00% Cr, 0.56% Mo, and 0.12% V. Source: Ref 23

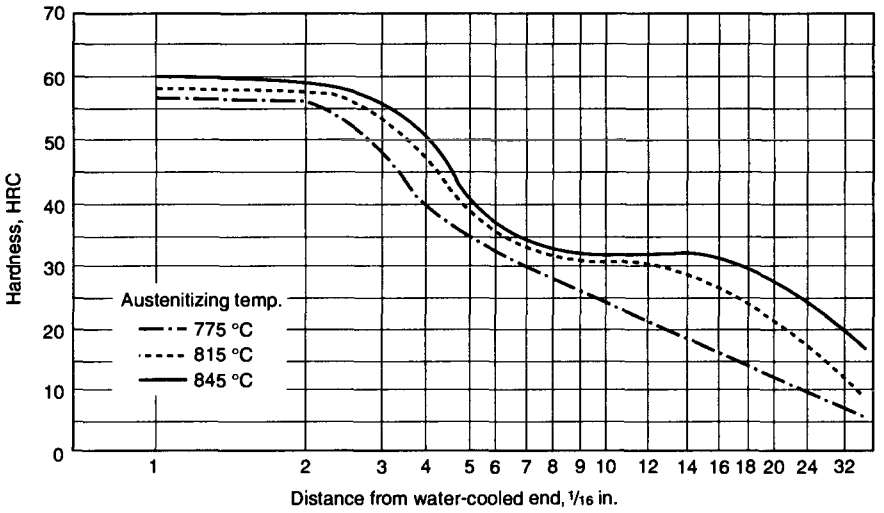

Fig. 8-22 Jominy end-quench curves for L2 steel, containing 0.50% C, 0.80% Cr, 0.20% V, after quenching from three different austenitizing temperatures. Data from Teledyne VASCO

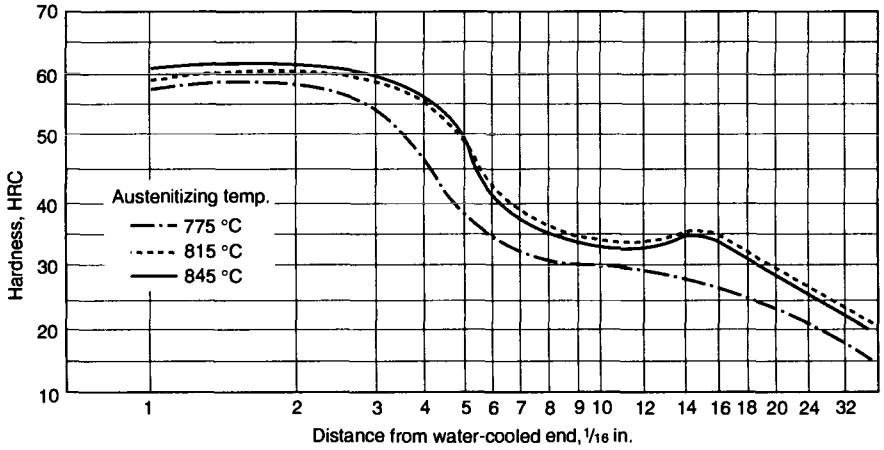

Fig. 8-23 Jominy end-quench curves for L2 steel, containing 0.60% C, 0.80% Cr, and 0.20% V, after quenching from three different austenitizing temperatures. Data from Teledyne VASCO

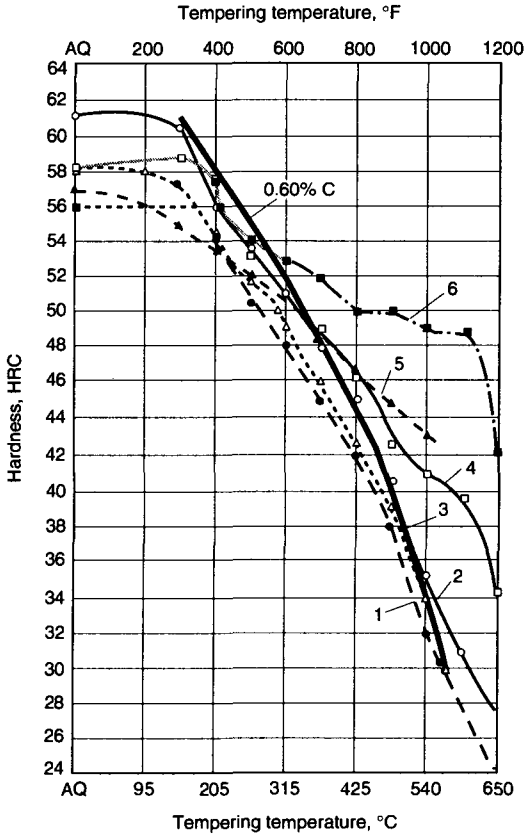

Curve	Composition, %					Hardening temperature		Hardening medium
	C	Mn	Cr	Mo	V	°C	°F	
1	0.50	0.20	0.80	...	0.20	815	1500	Water
2	0.60	0.20	0.80	...	0.20	800	1475	Water
3	0.50	0.70	1.00	...	0.20	815	1500	Water
4	0.55	0.55	0.65	0.35	...	870	1600	Oil
5	0.43	0.85	1.15	0.50	...	900	1650	Oil
6	0.45	...	1.60	1.10	0.25	900	1650	Oil

Fig. 8-24 Effect of tempering temperature on a number of medium-carbon L-type steels. Curves 1 and 2, Teledyne VASCO; curve 3, Universal-Cyclops Steel Corp.; curve 4, Allegheny Ludlum Industries; curves 5 and 6, Vulcan Kidd Steel Division

Table 8-10 Tensile properties of L6 tool steel(a)

Tempering temperature		Tensile strength		Elongation in 50 mm (2 in.), %	Reduction of area, %	Hardness, HRC
°F	°C	MPa	Ksi			
205	400	2055	298	1.3	2.0	57
315	600	2004.72	290.75	4.3	9.3	53.5
425	800	1591.02	230.75	8.5	24.7	47
540	1000	1341.97	194.63	12.5	34.0	42
650	1200	966.2	140.13	18.8	47.2	32

(a) Composition: 0.68% C, 0.60% Mn, 0.65% Cr, 1.40% Ni, 0.20% Mo; austenitizing temperature 815 °C (1500 °F); oil quenched, tempered 2h. Source: Allegheny Ludlum Steel Corp.

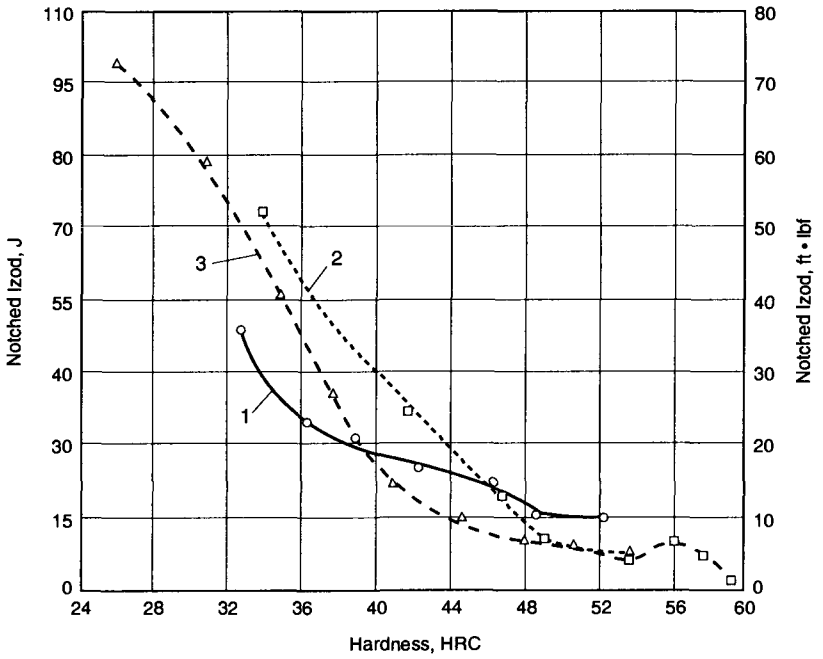

Curve	Composition, %					Hardening temperature		Hardening medium
	C	Mn	Cr	Mo	V	°C	°F	
1	0.50	0.70	1.00	...	0.20	885	1625	Oil
2	0.55	0.55	0.65	0.35	...	870	1600	Oil
3	0.43	0.85	1.15	0.50	...	855	1575	Oil

Fig. 8-25 Notched Izod impact energy absorbed versus tempered hardness for medium-carbon L2 steels. Curve 1, Ref 25; curve 2, Allegheny Ludlum Industries; curve 3, Teledyne VASCO

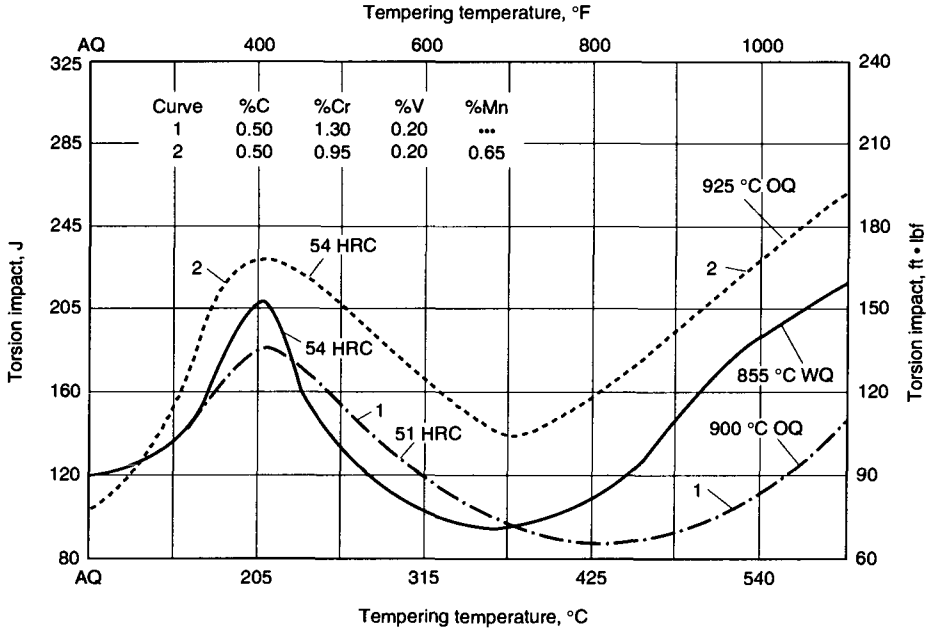

Fig. 8-26 Effect of tempering temperature on the torsion impact properties of L2 steels containing 0.50% C after different hardening treatments. Specimens were 6.25 mm (0.250 in.) diam rounds broken at a speed of 1200 rev/min. Data from Bethlehem Steel Co.

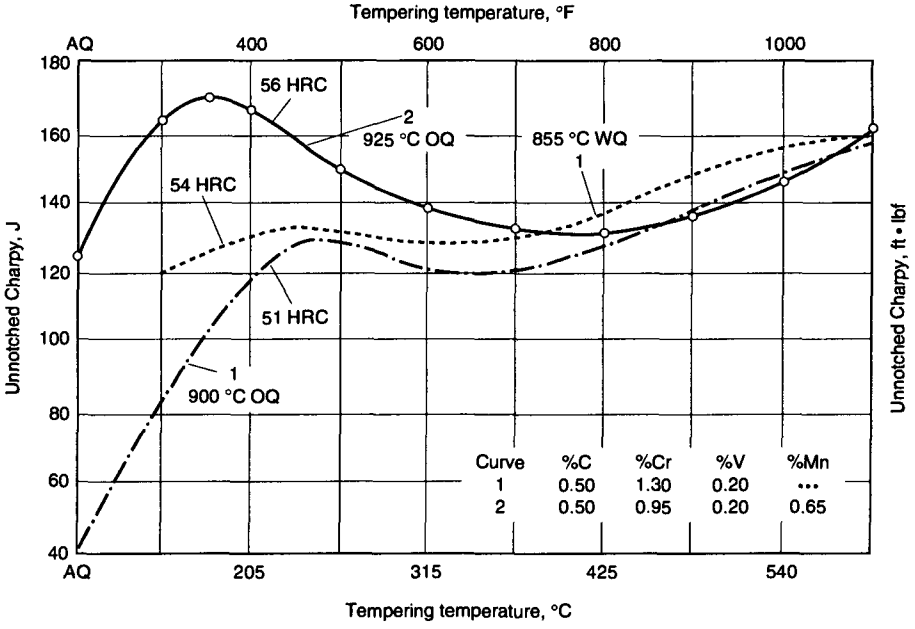

Fig. 8-27 Effect of tempering temperature on unnotched Charpy energy absorbed for L2 steels with 0.50% C after different hardening treatments. Data from Bethlehem Steel Co.

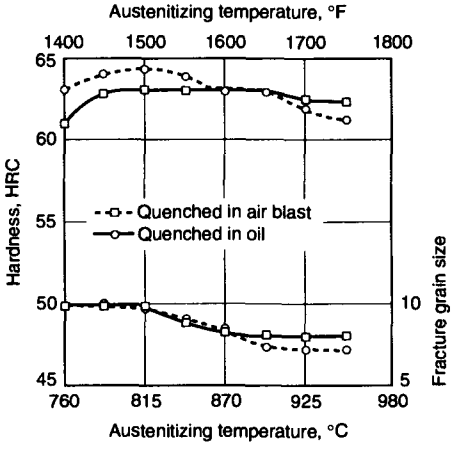

Fig. 8-28 As-quenched hardness and fracture grain size for 25 mm diam by 125 mm (1 by 5 in.) bars of L6 steel, containing 0.75% C, 0.75% Mn, 0.90% Cr, 1.75% Ni, and 0.35% Mo, as a function of austenitizing temperature and quenching in oil or air. Data from Bethlehem Steel Co.

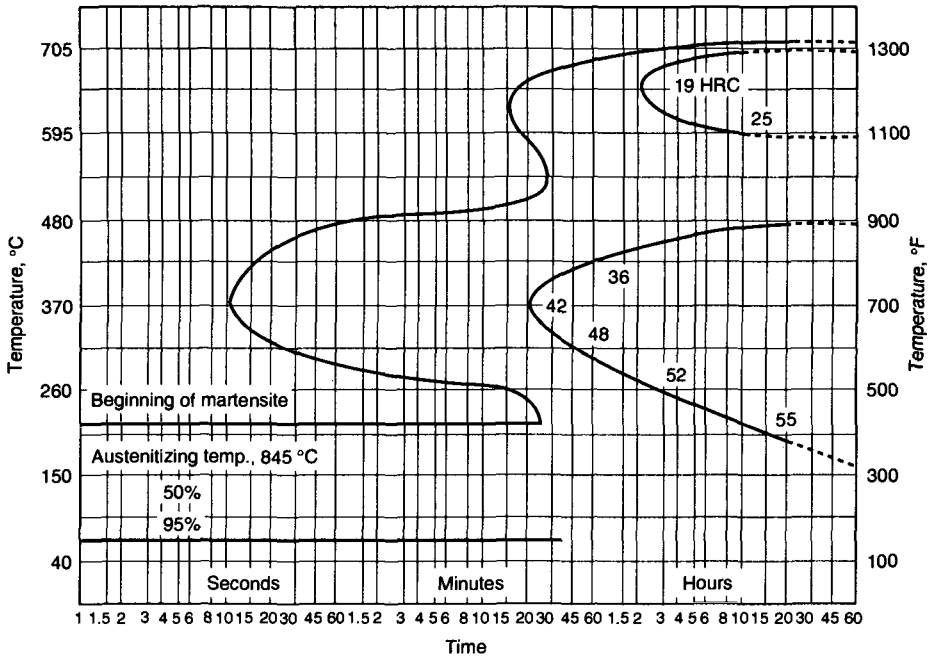

Fig. 8-29 IT diagram for an L6 tool steel containing 0.75% C, 0.60% Mn, 0.80% Cr, 1.25% Ni, 0.25% Mo, and 0.15% V. Data from Crucible Steel Co.

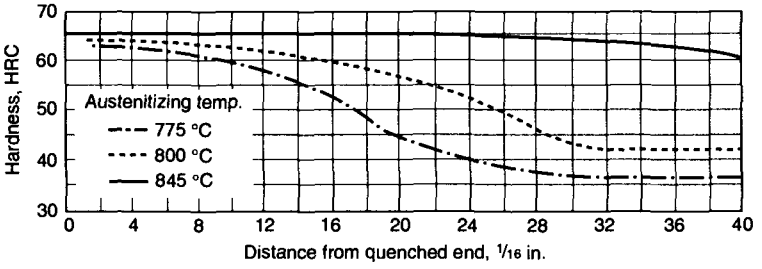

Fig. 8-30 Jominy end-quench curves for L6 tool steel containing 0.70% C, 0.55% Mn, 0.85% Cr, 1.40% Ni, and 0.25% Mo after austenitizing at three different temperatures. Data from Teledyne VASCO

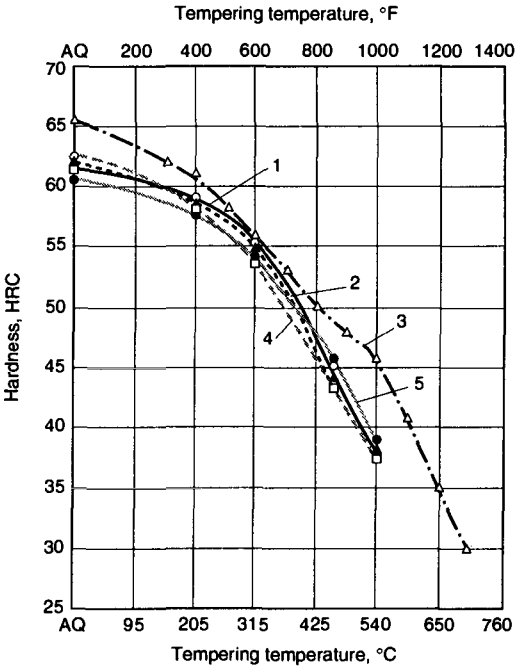

Curve	Composition C	Mn	Cr	Ni	Mo	Hardening temperature °C	°F	Hardening medium
1	0.90	0.35	0.30	1.40	...	815	1500	Oil
2	1.00	0.40	0.65	1.40	...	815	1500	Oil
3	0.75	0.75	0.90	1.75	0.35	815	1500	Oil
4	0.75	0.35	...	2.60	...	815	1500	Oil

Fig. 8-31 Hardness as a function of tempering temperature for various nickel-containing L6-type steels. Curves 1, 2, 4, and 5, Jessop Steel Co.; curve 3, Bethlehem Steel Co.

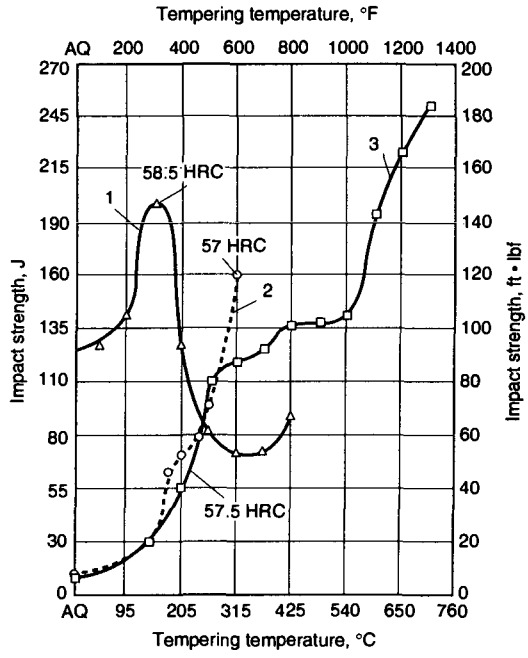

Curve	Composition C	Mn	Cr	Ni	Mo	Hardening temperature °C	°F	Hardening medium
1	0.75	0.35	1.00	1.75	...	830	1525	Oil
2	0.68	0.60	0.65	1.40	0.20	815	1500	Oil
3	0.75	0.75	0.90	1.75	0.35	845	1550	Oil

Fig. 8-32 Effect of tempering temperature on impact energy absorbed by L6-type steels. Curve 1, torsion impact, Ref 27; curve 2, unnotched Izod impact test, Allegheny Ludlum Industries; curve 3, unnotched, Bethlehem Steel Co.

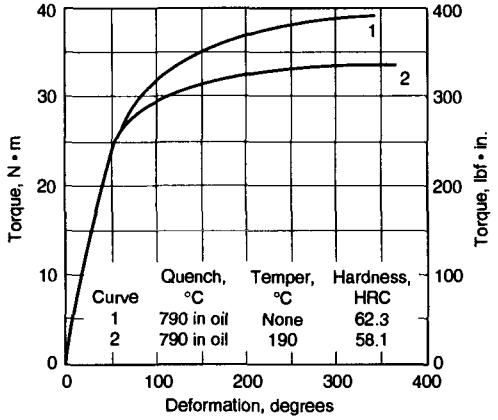

Fig. 8-33 Static torsion tests on quenched and quenched-and-tempered L6 steel containing 0.70% C, 0.55% Mn, 0.85% Cr, 1.40% Ni, and 0.25% Mo. Data from Teledyne VASCO

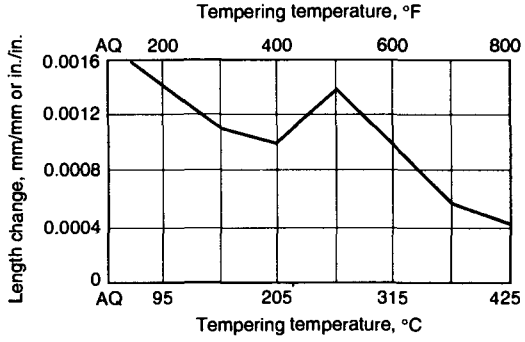

Fig. 8-34 Length change as a function of tempering temperature for a 20 mm (¾ in.) diam specimen of L6 steel containing 0.75% C, 0.35% Mn, 1.00% Cr, 1.75% Ni. Source: Ref 28

Tool Steels: 5th Edition
George Roberts, George Krauss, Richard Kennedy, p 165-179
DOI:10.1361/toos1998p165

Copyright © 1998 ASM International®
All rights reserved.
www.asminternational.org

CHAPTER 9
Shock-Resisting Tool Steels

The shock-resisting tool steels, designated as group S steels in the AISI classification system, have been developed to produce good combinations of high hardness, high strength, and high toughness or impact fracture resistance. Table 9-1 lists the compositions of the currently used S-type steels. Besides manganese, chromium, and molybdenum, which are commonly added to tool steels to provide hardenability and tempering resistance, silicon is a major addition unique to the S-type steels. Silicon provides tempering resistance and also produces, in some tempered conditions, a microstructure with reduced sensitivity to fracture. Tungsten is also added in significant amounts in the S1 grade. Table 9-2 presents performance and processing information regarding the S-type steels.

Silicon-containing hardened steels were originally developed for springs and are still widely used for spring applications where good fatigue resistance is required. Combinations of high hardness and toughness make the S-type steels applicable to chisel, punch, and die applications. As shown in Table 9-1, carbon content in the S tool steels is maintained around 0.5%, a level which makes possible the development of a high-strength tempered martensitic microstructure without the incorporation of coarse carbides that would lower toughness. The effects of silicon are described in the next section.

Alloying Effects of Silicon

Silicon contents of up to 0.3% are common in all types of steels as a result of the use of silicon for deoxidation during steelmaking. Additions of silicon above 0.3% are made in the S-type tool steels primarily to provide resistance to softening during tempering and to maintain a fracture-resistant microstructure. Silicon is a ferrite-stabilizing element in steels; therefore, A_1 and A_3 critical temperatures are raised, necessitating higher hardening temperatures. Silicon also promotes decarburization of steels and oxidizes readily when exposed to air or atmospheres containing partial pressures of oxygen. A well-known effect of silicon in this regard is the intergranular formation of silicon oxides at the surface of carburized steels during gas carburizing (Ref 1). Decarburization will lower wear and fatigue resistance; it should be avoided by atmosphere control during heat treatment or, if necessary, removed by grinding or polishing.

Silicon is not a carbide-forming element in steels, but instead promotes graphite formation or graphitization during lengthy, high-temperature exposure, especially in higher carbon steels. Graphitization in the S-type steels is not a major problem because of their medium carbon contents and additions of strong carbide-forming elements that also assist in preventing graphitization.

Table 9-1 Composition limits of shock-resisting tool steels

AISI type	No.	Composition(a), %							
		C	Mn	Si	Cr	Ni	Mo	W	V
S1	T41901	0.40–0.55	0.10–0.40	0.15–1.20	1.00–1.80	0.30 max	0.50 max	1.50–3.0	0.15–0.30
S2	T41902	0.40–0.55	0.30–0.50	0.90–1.20	...	0.30 max	0.30–0.60	...	0.50 max
S5	T41905	0.50–0.65	0.60–1.00	1.75–2.25	0.50 max	...	0.20–1.35	...	0.35 max
S6	T41906	0.40–0.50	1.20–1.50	2.00–2.50	1.20–1.50	...	1.20–1.50	...	0.30–0.40
S7	T41907	0.45–0.55	0.20–0.90	0.20–1.00	3.00–3.50	...	1.30–1.80	...	0.20–0.30(b)

(a) 0.25% max Cu, 0.03% max P, and 0.03% max S. (b) Optional

Figure 9-1 shows the positive effect of increasing silicon content on the tempering resistance of steels containing 0.6% C and 0.8% Mn (Ref 2). This effect is related to the fact that silicon is a non-carbide-forming element and its solubility in cementite is very low. Therefore, the nucleation and growth of cementite in the second and early third stages of tempering is severely retarded because silicon must diffuse away from regions of cementite formation (Ref 3). The very low solubility of silicon in cementite and its rejection from cementite to high concentrations at cementite-ferrite interfaces has been directly confirmed by an atom probe study (Ref 4).

The fact that cementite formation during tempering is suppressed by silicon has two effects: Dispersions of fine transition carbides in martensitic crystals persist to higher tempering temperatures, and retained austenite also remains stable to higher tempering temperatures. The effect of high silicon additions on austenite retention rather than cementite formation has also been documented in bainitic transformations; bainitic microstructures in high-silicon steels consist of ferrite and austenite rather than ferrite and cementite (Ref 5, 6).

The high toughness of the silicon-containing S-type steels may be related to the retardation of the second stage of tempering. In particular, prevention of the decomposition of retained austenite would prevent the formation of coarse cementite particles associated with tempered martensite embrittlement and reduced fracture resistance (Ref 7). The addition of silicon for increased tempering resistance to promote toughness has also been effectively used in the design of ultrahigh-strength structural steels (Ref 8, 9). An example of such a steel is 300M, a high-silicon (1.45 to 1.8%) modification of 4340 steel that contains nominally 0.4% C, 0.8% Cr, 1.8% Ni, and 0.25% Mo.

Shock-Resisting Steels Containing Tungsten

The S1 steels are also referred to as tungsten chisel steels because of their wide use in shock-resisting tools, such as chisels, shear blades, forming dies, and rock drills. The tungsten addition also permits S1 steels to be used for hot-working operations. The alloying, except for the lower carbon

Table 9-2 Performance factors and processing information for shock-resisting tool steels

Factor	S1 (0.45% C)	S1 (0.55% C)	S2	S5	S6
Major factors					
Wear resistance	4	4	2	2	2
Toughness	8	8	8	8	8
Hot hardness	5	5	2	3	3
Minor factors					
Usual working hardness, HRC	50–58	50–58	50–60	50–60	50–56
Depth of hardening	M	M	M	M	M
Finest grain size at full hardness, Shepherd standard	8	8	8	9	8
Surface hardness as-quenched, HRC	55–58	55–58	61–63	61–63	56–58
Core hardness (25 mm, or 1 in., diam round), HRC	55–58	55–58	56–60	58–62	56–58
Manufacturing factors					
Availability	3	3	3	3	2
Cost	2	2	1	1	1
Machinability	8	8	8	8	8
Quenching medium	O	O	W	O	O
Hardening temperature, °C (°F)	900–980 (1650–1800)	900–980 (1650–1800)	845–900 (1550–1650)	870–925 (1600–1700)	915–955 (1675–1750)
Dimensional change on hardening	M	M	H	H	H
Safety on hardening	M	M	L	M	M
Susceptibility to decarburization	M	M	H	H	H
Approximate hardness as-rolled or forged, HB	400	400	425	425	400
Annealed hardness, HB	183–223	183–223	183–217	192–223	192–223
Annealing temperature, °C (°F)	790–815 (1450–1500)	790–815 (1450–1500)	760–790 (1400–1450)	760–800 (1400–1475)	790–815 (1450–1500)
Tempering range, °C (°F)	205–650 (400–1200)	205–650 (400–1200)	150–425 (300–800)	150–425 (300–800)	150–425 (300–800)
Forging temperature, °C (°F)	1010–1120 (1850–2050)	1010–1120 (1850–2050)	1010–1120 (1850–2050)	1010–1120 (1850–2050)	1010–1120 (1850–2050)

Note: Ratings are explained in Chapter 2.

content of the S1 steel, is similar to the oil-hardening O7 cold-work tool steel. Compared to the other S-type steels, S1 has slightly better impact toughness and wear resistance, primarily because of its tungsten content. Tungsten is not particularly effective in increasing hardenability, however, and the deep hardening of S1 steels is due to chromium, silicon, manganese, or molybdenum additions.

The S1 steels can be forged at temperatures as high as 1120 °C (2050 °F). Slow heating to the forging temperature is recommended to minimize thermal gradients, but prolonged soaking at forging temperatures is not recommended because of the potential for decarburization. After forging, parts should be cooled slowly, and in large tools, normalizing at 900 °C (1650 °F) is advisable prior to annealing. For best machinability, and to minimize the danger of cracking, parts should be annealed after forging or normalizing.

The S1 steels have sufficient hardenability for hardening by quenching in oil from temperatures between 815 and 950 °C (1500 and 1750 °F). The moderate cooling rates of oil quenching minimize distortion and reduce susceptibility to quench cracking. However, precautions should be taken to minimize decarburization on hardening. If an atmosphere furnace or neutral salt bath is not available, pack hardening in a carbon-containing material is adequate to minimize decarburization. Also, preheating between 650 and 760 °C (1200 and 1400 °F) helps to reduce time at austenitizing temperatures and consequently the time for decarburization.

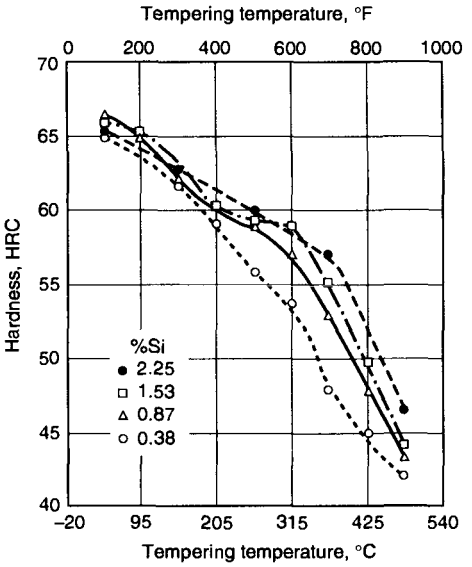

Fig. 9-1 Effect of silicon on the tempered hardness of 0.6C-0.8Mn steels hardened at 870 °C (1600 °F), water quenched, cooled to –195 °C (–320 °F), and tempered for 2 h at the temperatures shown. Source: Ref 2

The amount of carbon dissolved in austenite, which is a function of steel carbon content and austenitizing temperature, determines the maximum hardness obtainable on hardening S1-type steels. Figure 9-2 shows surface hardness as a function of austenitizing temperature for several S1 steels. A comparison of curves 2 and 3 for the same steel quenched in oil and water shows that water quenching produces consistently higher hardness at lower hardening temperatures. Also, comparison of curves 1 and 4 shows that higher steel carbon content translates directly to higher hardness. Vanadium additions maintain fine austenitic grain sizes up to austenitizing temperatures of 955 °C (1750 °F).

Isothermal transformation diagrams for S1 steels without and with silicon additions are shown in Fig. 9-3 and 9-4, respectively. The diagrams cannot be compared directly because different austenitizing temperatures were used, but both show that hardenability is limited by bainite formation. The flat Jominy end-quench curves shown in Fig. 9-5 for three heats of a low-silicon S1 steel demonstrate the good hardenability of this steel type. Figure 9-6 illustrates the effect of carbon content on hardness profiles through S1 steel bars of various diameters;

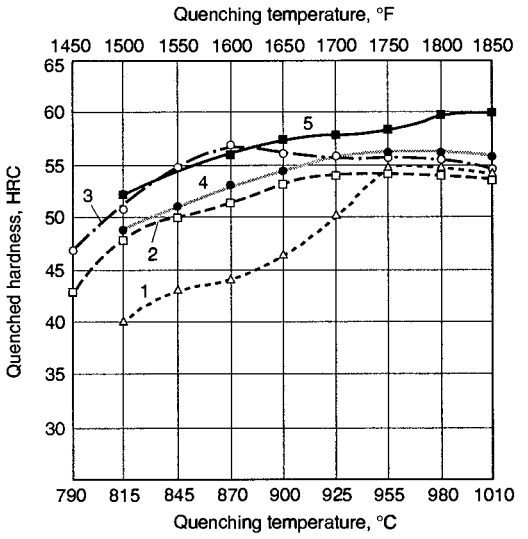

Curve	Composition, % C	Si	W	Cr	V	Quenching medium	Specimen size
1	0.43	...	2.00	1.30	0.25	Oil	⅞ (diam) × 3 in.
2	0.45	...	2.41	1.50	...	Oil	1 (diam) × 5 in.
3	0.45	...	2.41	1.50	...	Water	1 (diam) × 5 in.
4	0.55	...	2.00	1.35	0.25	Oil	...
5	0.52	0.85	2.25	1.30	0.25	Oil	⅞ (diam) × 2½ in.

Fig. 9-2 Effect of hardening temperature on the surface hardness of various S1 steels. Curves 1 and 5, Allegheny Ludlum Industries; Curves 2 and 3, Bethlehem Steel Co.; curve 4, Latrobe Steel Co.

the higher-carbon steel has consistently higher hardness for a given size of bar than does the lower-carbon steel.

The effects of silicon, molybdenum, and vanadium on hardenability of S1 steels are shown in the Jominy end-quench curves of Fig. 9-7 (Ref 10 ,11). Carbon, manganese, chromium, and tungsten were held roughly constant in the subject set of steels. The silicon addition without either molybdenum or vanadium strongly promotes hardenability. When the latter elements are present, even greater increases in hardenability are observed.

Figures 9-8 and 9-9 show hardness as a function of tempering temperature for a number of S1-type steels. Both compare the tempering resistance of the S1 steels to that of a plain carbon steel containing 0.5% carbon; the rate of softening of the S1 steels is substantially lower than that of the plain carbon steel. The increased tempering resistance of the various S1 steels is related to both silicon content and the content of the carbide-forming elements. Shock-resisting tools manufactured from S1 tool steels are usually tempered to 54 to 57 HRC and when used for hot work are tempered to 44 to 52 HRC.

Toughness of as-quenched S1 steels increases to a low-temperature-tempering (LTT) maximum after tempering between 150 and 260 °C (300 and 500 °F), and then drops from this maximum after tempering in the tempered martensite embrittlement temperature range of 315 to 425 °C (600 to 800 °F), as discussed in earlier chapters. Figures 9-10 and 9-11 show these changes in toughness as a function of temperature as determined by various types of toughness testing. The results of unnotched Charpy tests (Fig. 9-10) show better impact performance for a high-silicon S1 steel, whereas notched impact testing (Fig. 9-11) shows lower toughness for a high-silicon steel, compared to steels with lower silicon contents. The notched Izod tests indicate low toughness even in the high-silicon specimens tempered below the tempered martensite embrittlement range.

A decrease in Charpy impact toughness due to silicon content was also found by Koshiba and Kuno (Ref 10). Figure 9-12 shows their results for hardened S1 steels tempered at 400 °C (750 °F) and tested at temperatures up to 500 °C (930 °F). Toughness reaches a plateau for testing temperatures above 205 °C (400 °F) and increasing silicon content lowered toughness at all testing temperatures. Toughness is related to the plastic deformation that precedes fracture as well as to the brittle or ductile mechanisms of fracture. Since silicon retards the formation of crack-enhancing carbides, perhaps the role silicon plays in strengthening and strain hardening of the matrix microstructure of tempered martensite and retained austenite accounts for the reduced toughness observed in the higher-silicon steels.

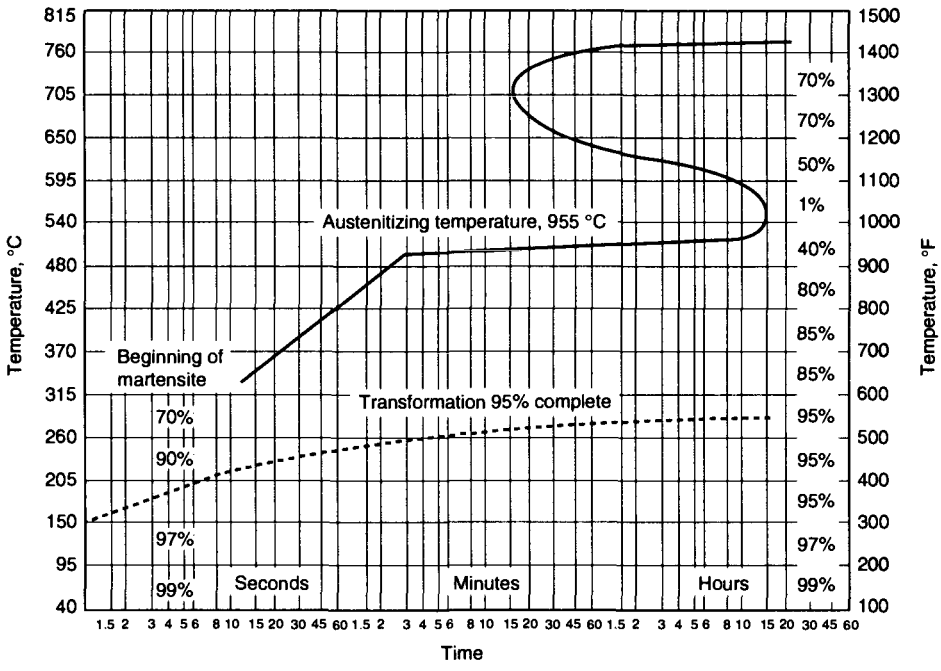

Fig. 9-3 IT diagram for an S1 steel containing 0.50% C, 2.75% W, 1.25% Cr, and 0.20% V. The amount of transformation after 30 h is shown on the right-hand side. Data from Crucible Steel Co.

Figure 9-13 shows the results of static torsion testing on the ultimate torsional strength and deformation of an S1 steel. These data show that torsional ductility, similar to other measurements of toughness, also reaches a peak and then decreases. Since this steel was not alloyed with silicon, the decrease in ductility can be attributed to the formation of carbide particles during the second stage of tempering.

The effect of tempering temperature on the room-temperature tensile properties of S1 steels is shown in Fig. 9-14. Carbon level significantly influences the mechanical properties, with higher carbon content increasing ultimate tensile and yield strengths and lowering ductility. Reduction of area, which is related to strain hardening and the amount of post-uniform necking deformation in tensile specimens, shows the greatest sensitivity to carbon content in the S1 steels. This observation is consistent with other work (Ref 12) where specimens of LTT steels, even though they were able to plastically deform and fail by ductile fracture mechanisms, exhibited characteristically low necking deformation and reduction of area if they contained 0.5% C.

Mechanical properties as a function of tempering temperature, as determined by bend testing, are presented in Fig. 9-15 (Ref 13). The effect of elevated temperatures on tensile properties is shown in Fig. 9-16. Little improvement in ductility and little change in strength are noted at temperatures below 315 °C (600 °F).

Shock-Resisting Tool Steels without Tungsten

Performance factors and recommended processing temperatures for the S-type tool steels without tungsten are listed in Table 9-2. Without the tungsten additions, wear resistance and hot hardness are lower, but the combination of medium carbon and high silicon content provides comparable high toughness ratings for the S-type steels with and without tungsten. Without carbide-stabilizing additions of tungsten, susceptibility to decarburization and graphitization increases as discussed earlier, and precautions should be taken to minimize soaking prior to forging and to provide surface protection during annealing. The S-type steels should always be annealed after forging.

Hardenability of the S-type steels is generally good and, depending on the level of alloying and section size, either water or oil quenching may be applied. Figure 9-17 shows the effects of austenitizing temperature on the surface hardness of oil- and water-quenched specimens for S-type steels with varying levels of carbon content. Although the hardenability of these steels is higher than plain carbon steels, they are only mildly susceptible to cracking during hardening by water quenching. Figures 9-18

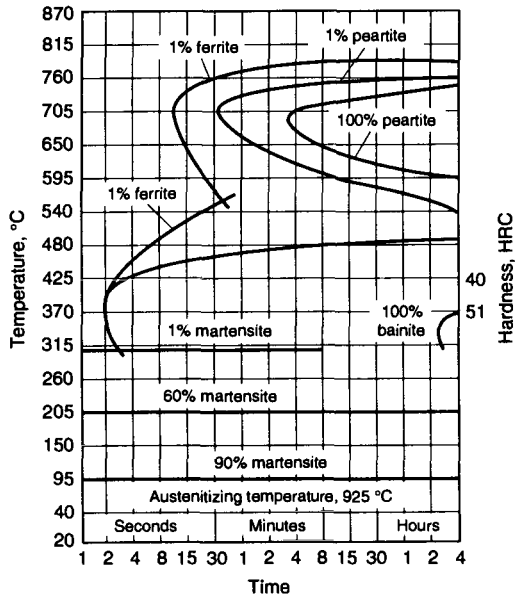

Fig. 9-4 IT diagram for an S1 steel containing 0.50% C, 0.25% Mn, 0.75% Si, 2.50% W, 1.25% Cr, and 0.20% V. Data from Uddeholm Company of America, Inc.

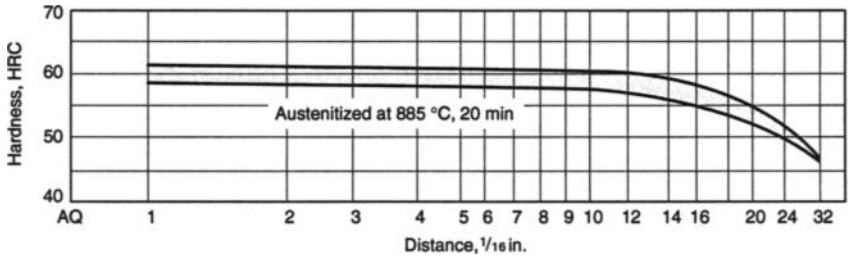

Fig. 9-5 Jominy end-quench curves for three heats of an S1 steel containing 0.53% C, 0.28% Si, 0.20% Mn, 2.00% W, 1.65% Cr, and 0.25% V. AQ, as quenched. Data from Teledyne VASCO

and 9-19 show Jominy end-quench hardenability bands for various sets of S-type steels, demonstrating differences in hardenability effected by various combinations of alloying elements. In Fig. 9-18, band 1 was based on 27 heats, band 2 on 5 heats, and band 3 on 4 heats. Molybdenum additions are especially effective in increasing hardenability (Fig. 9-18), but vanadium, if specimens are austenitized at temperatures where vanadium carbides maintain a very fine austenite grain size, contributes to lower hardenability (Fig. 9-19).

Isothermal transformation diagrams for various shock-resisting tool steels are shown in Fig. 9-20 to 9-23. With increasing contents of silicon and other alloying elements, the diffusion-controlled transformations to pearlite and bainite are increasingly re-

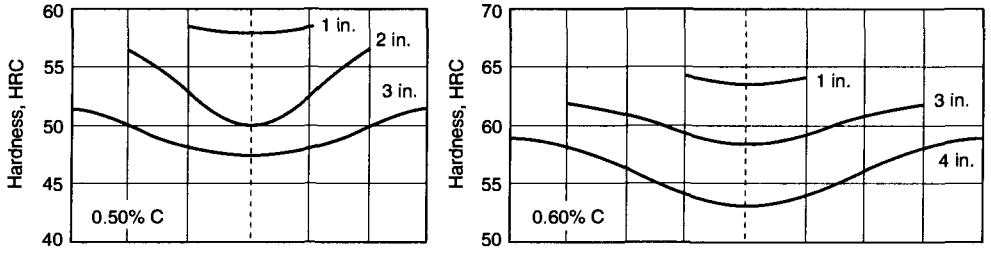

0.50% C

Austenitized at 925 °C, oil quenched
Specimen sizes:
1 (dam) × 3 in.
2 (diam) × 5 in.
3 (diam) × 6 in.

Composition, %				
C	Si	W	Cr	V
0.50	0.95	2.25	1.25	0.25

0.60% C

Austenitized at 925 °C, oil quenched
Specimen sizes:
1 (diam) × 3 in.
3 (diam) × 6 in.
4 (diam) × 6 in.

Composition, %				
C	Si	W	Cr	V
0.60	0.95	2.25	1.25	0.25

Fig. 9-6 Hardness profiles through various size rounds of S1 steel with two levels of carbon. Data from Columbia Tool Steel Co.

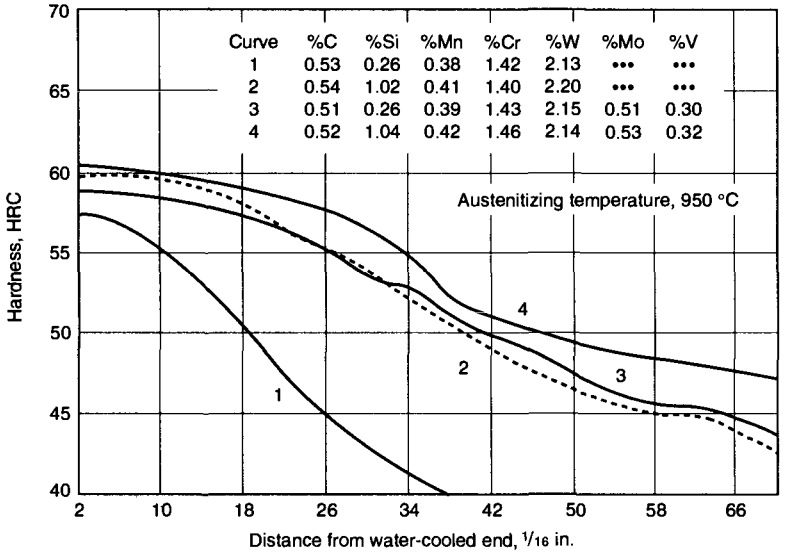

Fig. 9-7 Effect of silicon, molybdenum, and vanadium on Jominy end-quench curves for S1-type tool steels. Source: Ref 10, 11

tarded and controlled by diverging C-curve kinetics. These changes in transformation behavior are consistent with increasing hardenability and deeper hardening of the more highly alloyed S-type steels.

The effect of alloying on hardness changes as a function of tempering for various S-type steels is shown in Fig. 9-24 through 9-27. Resistance to softening is significantly higher in the silicon steels than in plain carbon steels of comparable carbon content. As discussed, silicon retards the formation of cementite during the second and early third stages of tempering, thereby increasing the temperature range of stability of the fine microstructure produced in the first stage of tempering. Increased high-temperature resistance to tempering is provided by alloying elements such as chromium, molybdenum, and vanadium, which tend to form fine alloy carbides at higher temperatures.

The effects of tempering on toughness of S-type steels are shown in Fig. 9-28 to 9-30. The strong effect of carbon content on toughness under conditions of bending or tensile loading is evident in the results of unnotched Charpy tests (Fig. 9-28). The very low toughness of the high-carbon steel is consistent with the sensitivity to quench embrittlement and intergranular fracture as discussed relative to Fig. 7-2. Torsional impact testing, which is not influenced by intergranular fracture, provides a testing approach sensitive to the shear resistance of tempered specimens with microstructures consisting of dispersed carbides in a matrix of tempered martensite. Figure 9-29 shows the torsional impact energy absorbed as a function of testing temperature for various S-type steels (Ref 14). High silicon content shifts the low-temperature maxima in toughness and the reduced toughness associated with tempered martensite embrittlement to higher tempering temperatures. These shifts in toughness are consistent with the ability of silicon to prevent the formation of coarse cementite particles that would reduce ductile fracture resistance. Figure 9-30 illustrates the effects of carbon on hardness and notched impact toughness as a function of tempering temperature for two S5 steels. Lower carbon increases toughness at the expense of hardness.

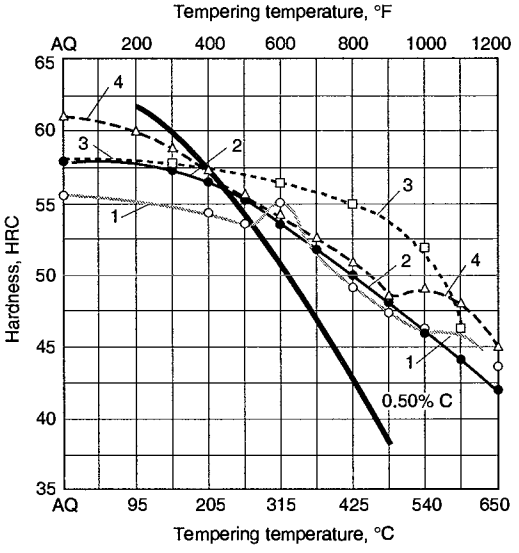

Curve	Composition, % C	W	Cr	V	Quenching temperature °C	°F
1	0.43	2.00	1.30	0.25	955	1750
2	0.53	2.00	1.65	0.25	900	1650
3	0.50	2.75	1.25	0.20	925	1700
4	0.55	2.50	1.50	0.35	925	1700

Fig. 9-8 Hardness as a function of tempering temperature for various S1 tungsten chisel steels. Curve 1, Allegheny Ludlum Industries; curve 2, Teledyne VASCO; curve 3, Crucible Steel Co.; curve 4, Carpenter Steel Co.

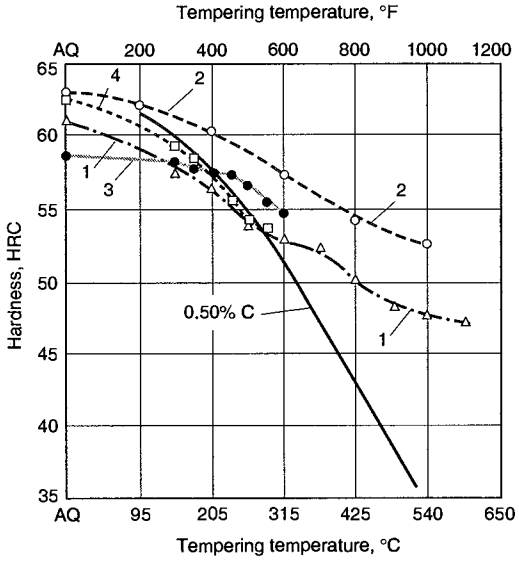

Curve	Composition, % C	Si	W	Cr	V	Hardening temperature °C	°F	Hardening medium
1	0.50	0.75	2.50	1.15	0.20	955	1750	Oil
2	0.58	0.95	2.25	1.25	0.25	925	1700	Oil
3	0.50	...	1.00	1.00	...	870	1600	Oil
4	0.50	...	1.00	1.00	...	815	1500	Water

Fig. 9-9 Hardness as a function of tempering temperature for various S1 tungsten chisel steels. Curve 1, Bethlehem Steel Co.; curve 2, Columbia Tool Steel Co.; curves 3 and 4, Vulcan-Kidd Steel Division of H.K. Porter Co.

Tensile properties of some hardened S-type steels are listed in Table 9-3 as a function of tempering temperature and heat treatment. After low-temperature tempering, yield and ultimate strengths are very high, but ductility, as measured by reduction of area, is low.

References

1. R. Chatterjee-Fischer, Internal Oxidation during Carburizing and Heat Treating, *Metall. Trans. A*, Vol 9A, 1978, p 1553-1560

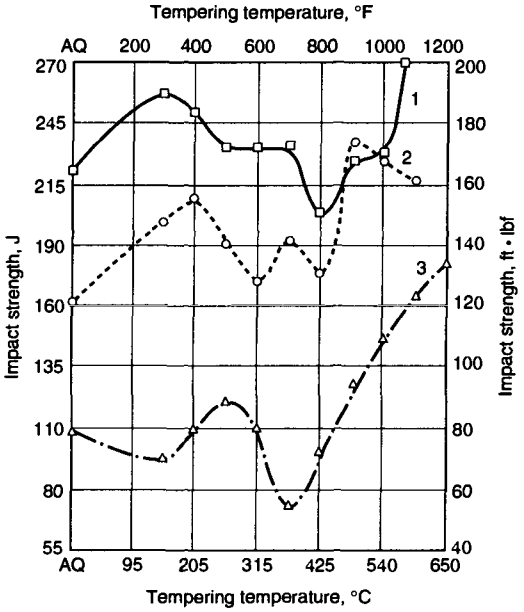

Curve	Test	Composition, % C	Si	W	Cr	V	Quenching temperature °C	°F	Quenching medium
1	Unnotched Charpy	0.50	0.75	2.50	1.15	0.20	955	1750	Oil
2	Unnotched Charpy	0.45	...	2.40	1.50	0.25	925	1700	Oil
3	Torsion impact	0.45	...	2.40	1.50	0.25	925	1700	Oil

Fig. 9-10 Impact energy absorbed as a function of tempering temperature during unnotched Charpy and torsion impact testing of S1 steel specimens. Data from Bethlehem Steel Co.

Table 9-3 Tensile properties of silicon tool steels

Tempering temperature		S5 (0.55% C) Water quenched at 830 °C (1525 °F) 61 HRC					S5 (0.55% C) Oil quenched at 870 °C (1600 °F) 61 HRC					S4 (0.63% C) Water quenched at 870 °C (1600 °F) 61 HRC				
		Yield strength		Tensile strength		Reduction	Yield strength		Tensile strength		Reduction	Yield strength		Tensile strength		Reduction
°C	°F	MPa	ksi	MPa	ksi	of area, %	MPa	ksi	MPa	ksi	of area, %	MPa	ksi	MPa	ksi	of area, %
150	300	1862	270	2206	320	18	...	...	2220	322	...	...	...	1620	235	...
205	400	1869	271	2137	310	...	1944	282	2344	340	20	...	...	2137	310	...
260	500	1820	264	2062	299	...	1910	277	2344	340	...	...	...	2331	338	...
315	600	1744	253	1979	287	20	1855	269	2255	327	...	...	...	2275	330	...
370	700	1655	240	1862	270	...	1793	260	2089	303	...	1793	260	2131	309	19
425	800	1558	226	1731	251	...	1710	248	1896	275	...	1448	210	1641	238	28
480	900	1448	210	1586	230	...	1586	230	1710	248	30	1241	180	1400	203	32
540	1000	1303	189	1434	208	29	1379	200	1517	220	...	1076	156	1241	180	37
595	1100	1255	182	1248	181	...	1269	184	1338	194	38	924	134	1089	158	40
650	1200	931	135	1048	152	40	1089	158	1172	170	43	793	115	958	139	45
705	1300	690	100	848	123	50	883	128	1000	145	52	690	100	848	123	54

Data from Bethlehem Steel Co.

2. A.G. Allten and P. Payson, The Effect of Silicon on the Tempering of Martensite, *Trans. ASM*, Vol 45, 1953, p 498
3. W.S. Owen, The Effect of Silicon on the Kinetics of Tempering, *Trans. ASM*, Vol 46, 1954, p 812-829
4. S.J. Barnard, G.D.W. Smith, A.J. Garratt-Reed, and J. Vander Sande, Atom Probe Studies: (1) The Role of Silicon in the Tempering of Steel, and (2) Low Temperature Chromium Diffusivity in Bainite, *Solid-Solid Phase Transformations*, H.I. Aaronson, D.E. Laughlin, R.F. Sekerka, and C.M. Wayman, Ed., TMS-AIME, 1982, p 881-885
5. H.K.D.H. Bhadeshia, *Bainite in Steels*, Institute of Materials, London, 1992, p 73
6. H.K.D.H. Bhadeshia and D.V. Edmonds, The Bainite Transformation in a Silicon Steel, *Metall. Trans. A*, Vol 10A, 1979, p 895-907
7. G. Krauss, *Steel: Heat Treatment and Processing Principles*, ASM International, 1990, p 231-236
8. F.B. Pickering, The Properties of Tool Steels for Mould and Die Applications, *Tool Materials for Molds and Dies*, G. Krauss and H. Nordberg, Ed., Colorado School of Mines Press, 1987, p 3-32
9. F.B. Pickering, *Physical Metallurgy and the Design of Steels*, Applied Science, Essex, U.K., 1978
10. S. Koshiba and T. Kuno, Effect of Silicon on the Properties of Shock-Resisting Silicon-Chromium-Tungsten Tool Steel, *Nippon Kinzoku Gakkai Si*, Vol 20, 1956, p 129
11. S. Koshiba and T. Kuno, Effect of Molybdenum and Vanadium Additions on Silicon-Chromium-Tungsten Steels for Shock-Resisting Tools, *Tetsu-*

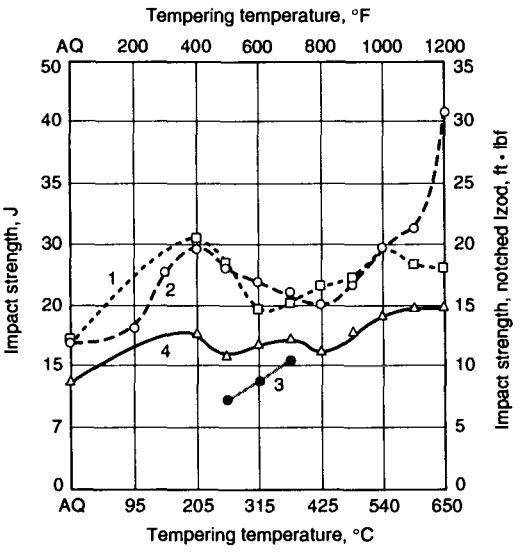

Curve	Composition, %					Quenching temperature		Quenching medium
	C	Si	W	Cr	V	°C	°F	
1	0.43	0.29	2.00	1.30	0.25	955	1750	Oil
2	0.50	...	2.50	1.40	0.25	955	1750	Oil
3	0.55	0.25	2.75	1.25	0.20	955	1750	Oil
4	0.52	0.85	2.25	1.30	0.25	955	1750	Oil

Fig. 9-11 Impact energy absorbed as a function of tempering temperature during notched Izod testing of S1 steel specimens. Curves 1 and 4, Allegheny Ludlum Industries; curve 2, Teledyne Firth Sterling; curve 3, Crucible Steel Co.

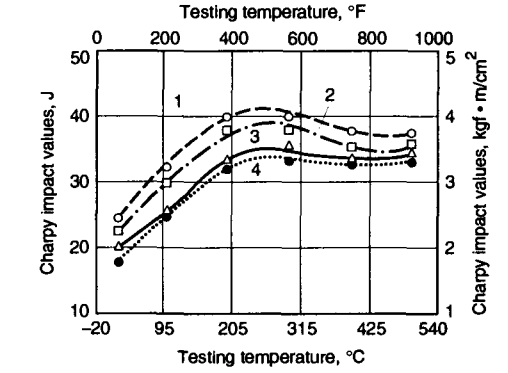

Curve	Composition, %						
	C	Si	Mn	W	Cr	Mo	V
1	0.51	0.26	0.39	2.15	1.43	0.51	0.30
2	0.54	0.51	0.41	2.25	1.50	0.52	0.29
3	0.54	0.78	0.38	2.17	1.47	0.49	0.32
4	0.52	1.04	0.42	2.14	1.46	0.53	0.32

Fig. 9-12 Effect of testing temperature on impact energy absorbed during Charpy testing of S1 steels hardened from 950 °C (1740 °F), oil quenched, and tempered at 400 °C (750 °F). Source: Ref 10

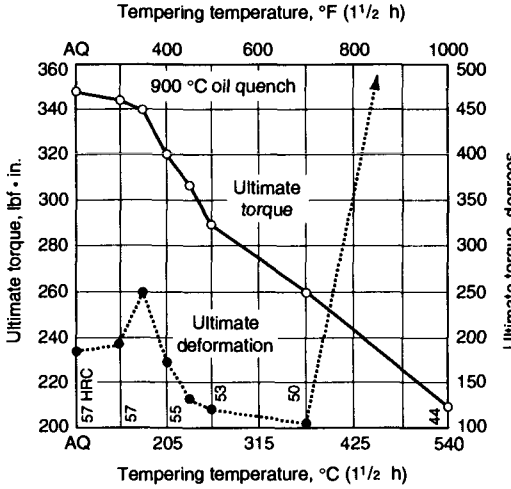

Fig. 9-13 Effect of tempering temperature on the static torsion properties of S1-type steel containing 0.50% C, 2.00% W, 1.65% Cr, and 0.25% V. Data from Teledyne VASCO

to-Hagané, (J. Iron Steel Inst. Jpn.), Vol 43, 1957, p 142
12. G. Krauss, Heat Treated Martensitic Steels: Microstructural Systems for Advance Manufacture, *Jpn. Iron Steel Inst. Int.*, Vol 35 (No. 4), 1995, p 349-359
13. J.C. Hamaker, V.C. Strang, and G.A. Roberts, Bend:Tensile Relationships for Tool Steels at High Strength Levels, *Trans. ASM*, Vol 49, 1957, p 550
14. F.R. Palmer and G.V. Luerssen, *Tool Steel Simplified*, Carpenter Steel Co. 1960

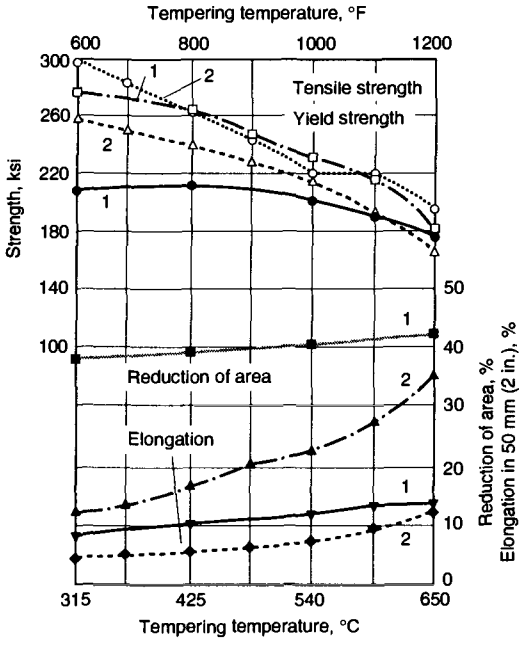

Curve	Composition, % C	Si	W	Cr	V	Quenching temperature °C	°F	Quenching medium
1	0.43	0.29	2.00	1.30	0.25	955	1750	Oil
2	0.50	0.25	1.98	1.68	0.24	900	1650	Oil

Fig. 9-14 Mechanical properties as a function of tempering temperature for tungsten-containing S1 steel specimens. Curve 1, Allegheny Ludlum Industries; curve 2, Teledyne VASCO

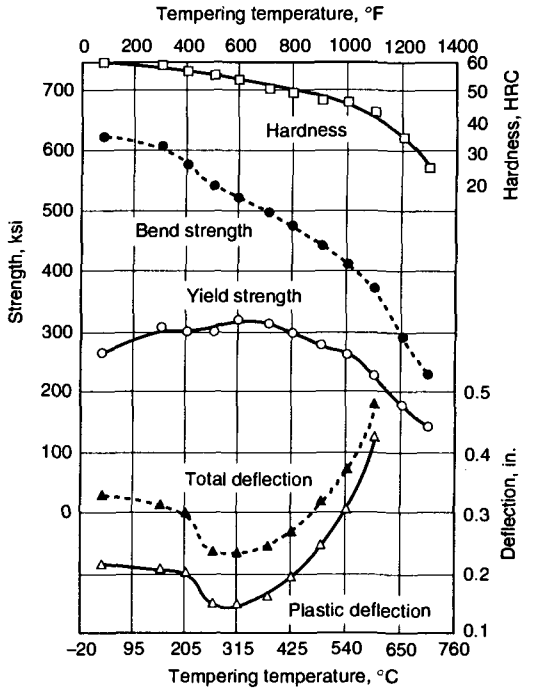

Fig. 9-15 Effect of tempering temperature on properties determined by bend testing of S1 steel specimens, containing 0.50% C, 1.98% W, 1.68% Cr, and 0.24% V, oil quenched from 900 °C (1650 °F) and tempered for 2 h at the temperatures shown. Source: Ref 13

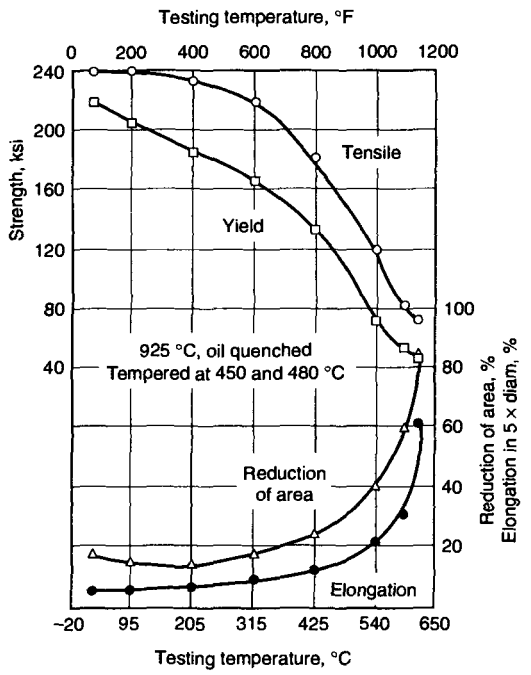

Fig. 9-16 Elevated-temperature tensile properties of an S1 steel, containing 0.50% C, 0.75% Si, 2.50% W, 1.25% Cr, and 0.20% V, as a function of test temperature. Data from Uddeholm Company of America Inc.

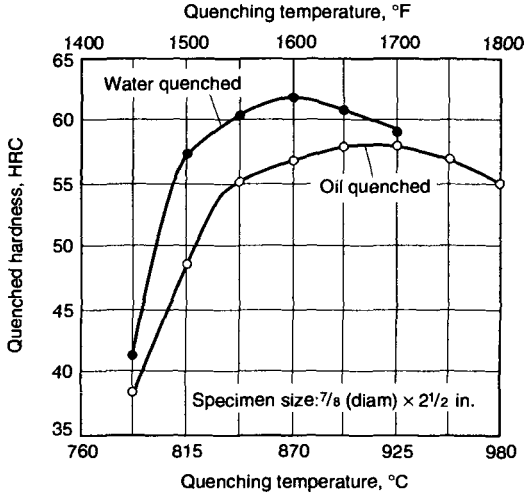

(a)

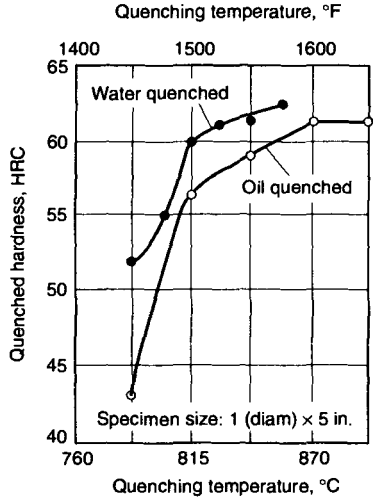

(b)

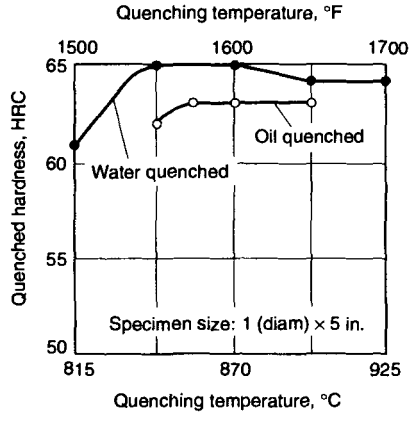

(c)

Fig. 9-17 Surface hardness of as-quenched rounds of various silicon tool steels as a function of austenitizing temperature and quenching medium. (a) 0.46% C, 1.60% Si, 0.80% Mn, and 0.40% Mo. Courtesy of Allegheny Ludlum Industries. (b) 0.55% C, 2.30% Si, 0.80% Mn, 0.50% Mo, and 0.25% V. Courtesy of Bethlehem Steel Co. (c) 0.63% C, 1.95% Si, and 0.78% Mn. Data from Bethlehem Steel Co.

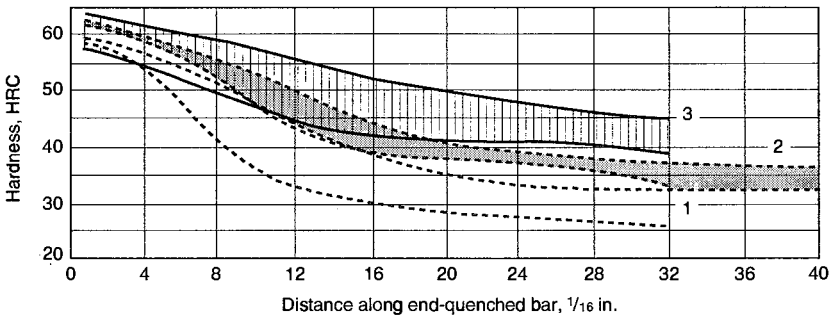

Curve	Composition, %						Quenching temperature	
	C	Si	Mn	Cr	Mo	V	°C	°F
1	0.55	2.00	0.85	0.25	...	0.20	855	1575
2	0.50	1.60	0.70	...	0.40	0.12	870	1600
3	0.55	2.00	0.90	0.25	1.20	0.25	855	1575

Fig. 9-18 Jominy end-quench hardenability bands for various silicon tool steels. Bands 1 and 3, Teledyne VASCO; band 2, Allegheny Ludlum Industries

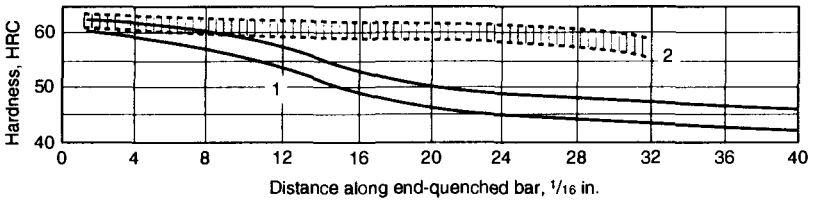

Curve	Composition, %						Quenching temperature	
	C	Si	Mn	Cr	Mo	V	°C	°F
1	0.60	2.00	0.85	0.25	0.25	0.20	870	1600
2	0.57	1.90	0.85	0.25	0.33	...	855	1575

Fig. 9-19 Jominy end-quench bands of S5 tool steel with and without vanadium addition. Band 1, Allegheny Ludlum Industries; band 2, Teledyne VASCO

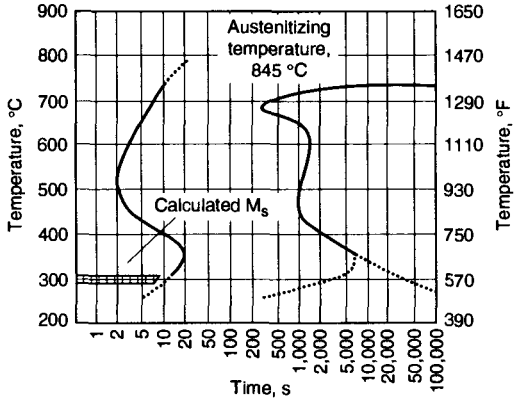

Fig. 9-20 IT diagram for S2 tool steel containing 0.5% C, 0.40% Mn, 1.00% Si, and 0.5% Mo. Data from Carpenter Steel Co.

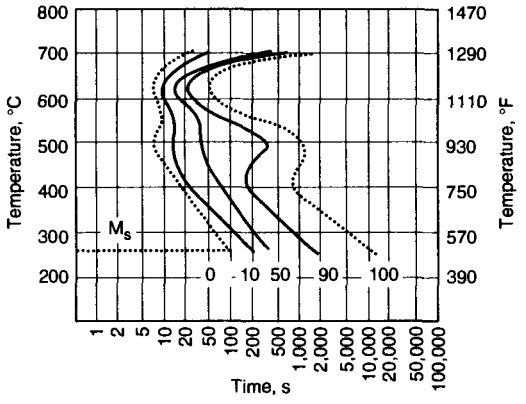

Fig. 9-21 IT diagram for S4 tool steel containing 0.55% C, 0.87% Mn, and 1.74% Si

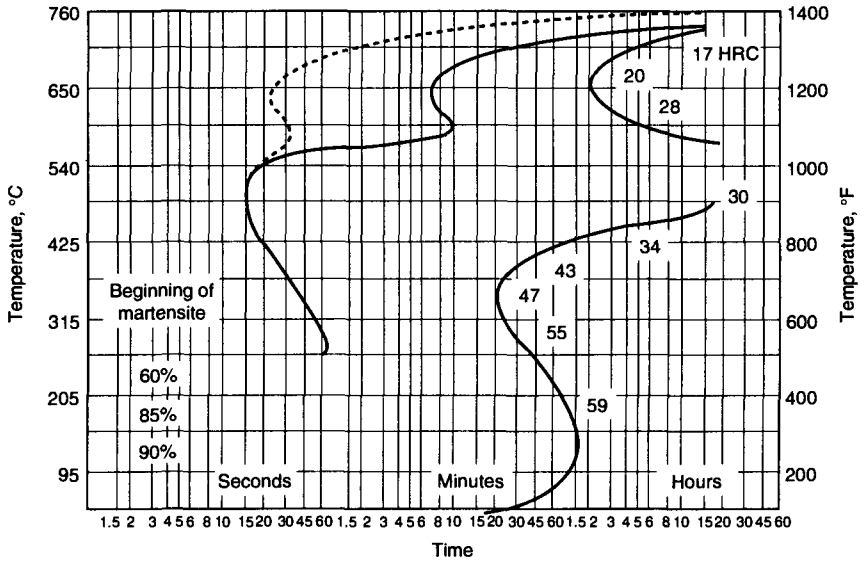

Fig. 9-22 IT diagram for S5 tool steel containing 0.6% C, 0.75% Mn, 1.90% Si, 0.25% Cr, and 0.30% Mo. Specimens austenitized at 900 °C (1650 °F). Data from Crucible Steel Co.

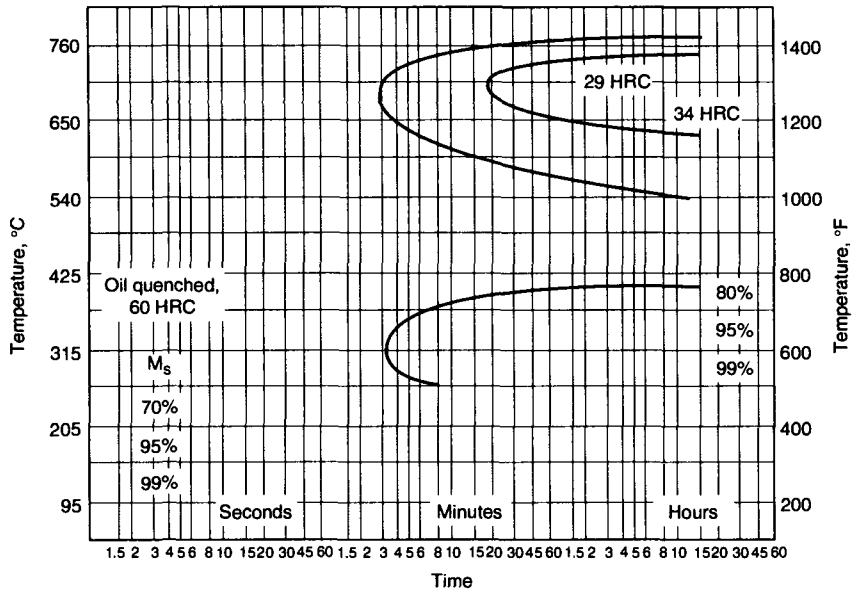

Fig. 9-23 IT diagram for S6 tool steel containing 0.43% C, 1.35% Mn, 2.25% Si, 1.35% Cr, 0.40% Mo, and 0.30% V. Specimens austenitized at 925 °C (1700 °F). Data from Crucible Steel Co.

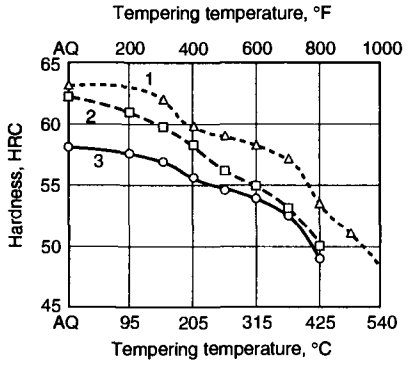

Curve	Composition, % C	Mn	Si	Mo	V	Quenching temperature °C	°F	Quenching medium
1	0.65	0.50	1.10	0.50	0.20	885	1625	Oil
2	0.50	0.45	1.10	0.50	0.20	855	1575	Water
3	0.50	0.45	1.10	0.50	0.20	900	1650	Oil

Fig. 9-24 Hardness as a function of tempering temperature for S-type silicon tool steels. Data from Universal-Cyclops Steel Corp.

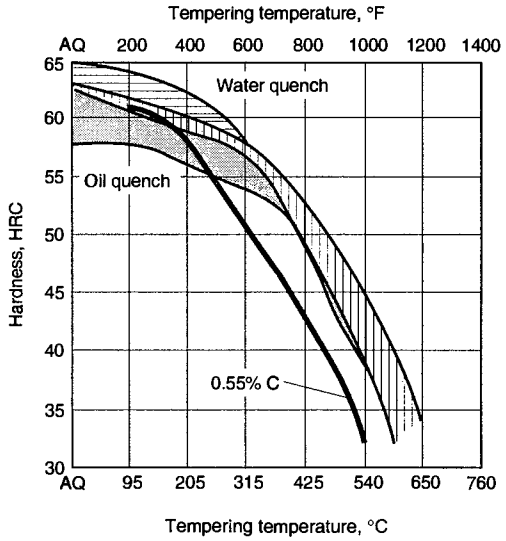

Fig. 9-25 Hardness as a function of tempering temperature for S-type silicon tool steels (0.54 to 0.60 % C, 0.75 to 0.92% MN, 1.90 to 2.00% Si, 0.00 to 0.25% V, and 0.00 to 0.34% Cr) and plain carbon steel (0.55% C). Water quench, 845 to 900 °C (1550 to 1650 °F); oil quench, 870 to 955 °C (1600 to 1750 °F). Combined data from Teledyne VASCO, Vulcan-Kidd Steel Division of H.K. Porter Co., Crucibile Steel Co., and Bethlehem Steel Co.

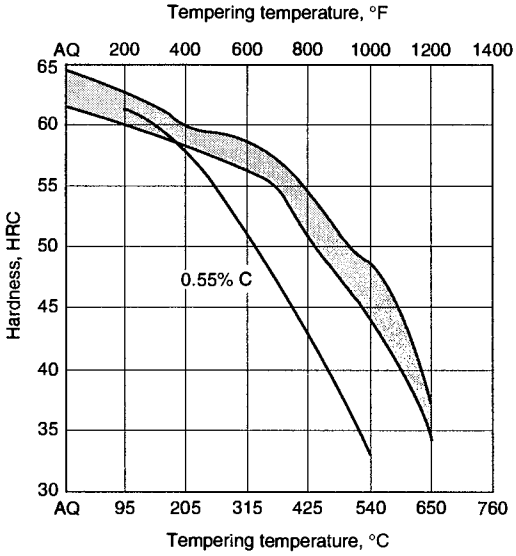

Type	Composition, % C	Mn	Si	V	Mo	Cr	Quenching temperature °C	°F	Quenching medium
S5	0.50	0.70	1.60	0.00	0.25	0.00	870	1600	Oil or
S5	0.60	0.85	2.00	0.20	0.40	0.28	900	1650	Water

Fig. 9-26 Hardness as a function of tempering temperature for S5 silicon tool steels and plain carbon steel containing 0.55% C. Combined data from Teledyne VASCO, Bethlehem Steel Co., and Allegheny Ludlum Industries

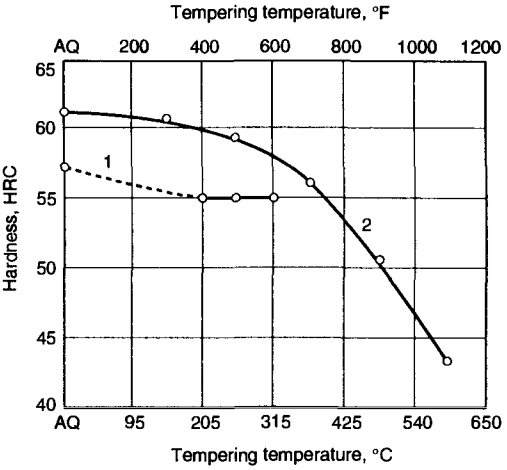

Curve	Composition, % C	Mn	Si	Mo	V	Cr	Quenching temperature °C	°F	Quenching medium
1	0.43	1.35	2.25	0.40	0.30	1.35	925	1700	Oil
2	0.55	0.97	1.95	1.07	0.25	0.29	870	1600	Oil

Fig. 9-27 Hardness as a function of tempering temperature for S6-type silicon tool steels. Curve 1, Crucible Steel Co.; curve 2, Teledyne VASCO

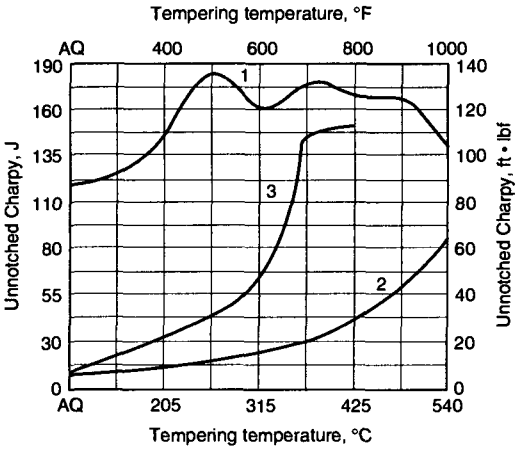

Curve	Composition, %				Quenching temperature		Quenching medium
	C	Si	Mn	Mo	°C	°F	
1	0.55	2.30	0.80	0.50	870	1600	Oil
2	0.63	1.95	0.78	...	845	1550	Water
3	0.63	1.95	0.78	...	870	1600	Oil

Fig. 9-28 Impact energy absorbed during unnotched Charpy testing of S-type silicon tool steels. Data from Bethlehem Steel Co.

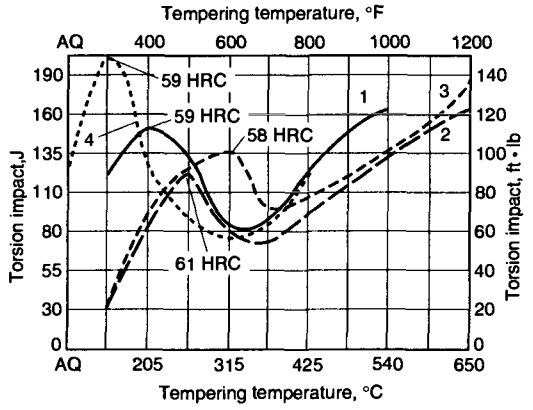

Curve	Composition, %				Quenching temperature		Quenching medium
	C	Si	Mo	V	°C	°F	
1	0.55	2.30	0.50	0.25	870	1600	Oil
2	0.63	1.95	...	...	845	1550	Water
3	0.63	1.95	...	...	870	1600	Oil
4	0.50	1.00	0.50	...	845	1550	Brine

Fig. 9-29 Impact energy absorbed during torsion testing of S-type silicon tool steels subjected to various austenitizing and quenching treatments. Curves 1 to 3, Bethlehem Steel Co.; curve 4, Ref 14

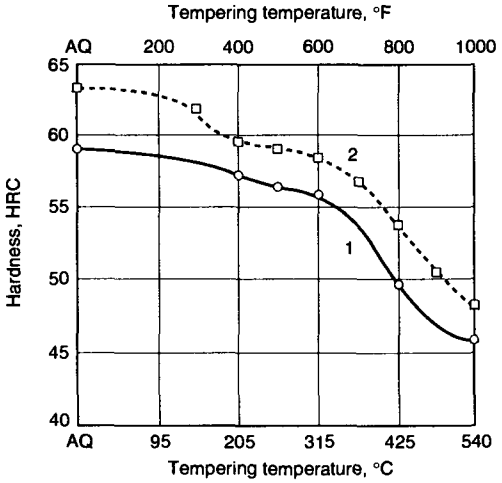

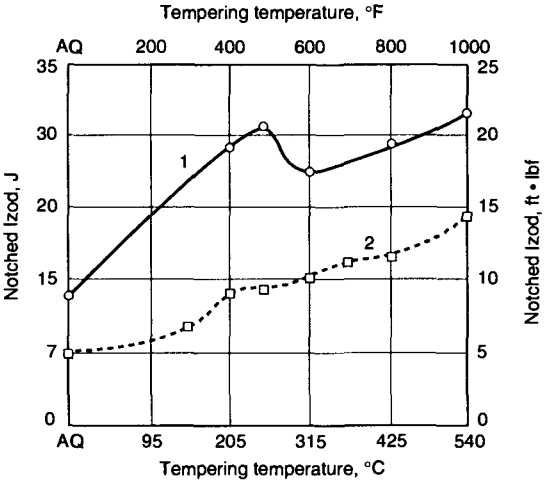

Curve	Composition, %						Quenching temperature		Quenching medium
	C	Mn	Si	Cr	Mo	V	°C	°F	
1	0.50	0.70	1.60	...	0.40	0.12	870	1600	Oil
2	0.60	0.85	2.00	0.25	0.25	0.20	885	1625	Oil

Fig. 9-30 Hardness and notched Izod impact energy absorbed as a function of tempering temperature for S5 tool steels with two levels of carbon content. Data from Allegheny Ludlum Industries

Tool Steels: 5th Edition
George Roberts, George Krauss, Richard Kennedy, p 181-192
DOI:10.1361/toos1998p181

Copyright © 1998 ASM International®
All rights reserved.
www.asminternational.org

CHAPTER 10
Oil-Hardening Cold-Work Tool Steels

The oil-hardening cold-work tool steels, designated as group O steels in the AISI classification system, derive their high hardness and wear resistance from high carbon and modest alloy contents. The high carbon content makes possible the formation of martensite of high hardness, and the alloying elements provide sufficient hardenability to make possible hardening of sections of reasonable size by oil quenching. Alloy content is insufficient to provide the alloy carbides necessary for cutting at high speeds or hot-working applications; therefore, the O-type steels are restricted to cold-work applications.

Table 10-1 lists the nominal compositions of the various O-type tool steels, and Table 10-2 ranks the performance and lists processing temperature data for the steels. The high carbon content of the O-type steels makes possible austenitizing for hardening at relatively low intercritical temperatures where austenite and carbides coexist. The reduced carbon content of the austenite is still sufficient to provide martensite of high hardness and good hardenability, but fine grain size is maintained by the undissolved carbides, and the low hardening temperatures and oil quenching provide relative freedom from cracking of intricate sections.

Combinations of alloying elements other than carbon provide various levels of hardenability, as well as special characteristics. For example, the high silicon content of O6 tool steel causes graphite formation, which enhances machinability and may serve as a solid lubricant for improved die life, and the high tungsten content of O7 tool steel provides carbide-containing microstructures that maintain very sharp cutting edges and high wear resistance for applications such as roll turning tools, paper and woodworking knives, and tools for finishing purposes.

Microstructures

Figure 10-1 shows light micrographs of typical microstructures produced during various processing stages for some O-type tool steels. Spheroidized carbide particles dispersed in a matrix of ferrite, produced by annealing an O2 tool steel at 725 °C (1335 °F) and furnace cooling, are shown in Fig. 10-1(a). Figure 10-1(b) shows the microstructure of an O1 tool steel austenitized at 815 °C (1500 °F), oil quenched, and tempered at 220 °C (430 °F) to produce a hardness of 58.5 HRC. Spheroidized carbides (white), retained as a result of intercritical austenitizing, are dispersed in a dark-etching matrix of tempered martensite. This matrix consists of crystals of martensite, very fine transition carbides within the martensite crystals, and retained austenite, all of which are too fine to be resolved in the light microscope.

If an O-type steel is austenitized above A_{cm}, the upper critical temperature, all carbides dissolve and the austenite takes into solution all the carbon and alloying elements in the steel. Consequently,

Table 10-1 Composition limits of oil-hardening cold-work steels

		Composition, %							
AISI type	UNS No.	C	Mn	Si	Cr	Ni	Mo	W	V
O1	T31501	0.85–1.00	1.00–1.40	0.50 max	0.40–0.60	0.30 max	...	0.40–0.60	0.30 max
O2	T31502	0.85–0.95	1.40–1.80	0.50 max	0.50 max	0.30 max	0.30 max	...	0.30 max
O6	T31506	1.25–1.55(b)	0.30–1.10	0.55–1.50	0.30 max	0.30 max	02.0–0.30	...	...
O7	T31507	1.10—1.30	1.00 max	0.60 max	0.35–0.85	0.30 max	0.30 max	1.00–2.00	0.40 max

(a) 0.25% max Cu, 0.03% max P, and 0.03% max S. (b) Contains free graphite in the microstructure

austenitic grain size increases, M_s temperature decreases, and a high sensitivity to intergranular fracture and quench cracking develops. Figure 10-1(c) shows the microstructure that develops when an O1 tool steel is overheated by austenitizing at 980 °C (1795 °F), oil quenching, and tempering at 220 °C (425 °F). The black-etching plates of tempered martensite and high volume fraction of retained austenite (white) that mark an overheated condition are now readily resolved. Typical distributions of graphite in O6 tool steel are shown in Fig. 10-2.

Processing Prior to Hardening

All the O-type steels are somewhat sensitive to cracking if rapidly heated to forging temperatures; therefore, preheating to about 650 °C (1200 °F) is good practice. The minimum permissible forging temperature for manganese types is 815 °C (1500 °F) and for tungsten-chromium types is 870 °C (1600 °F). Forging below these temperatures may result in center bursts or surface cracking. Although slightly air hardening, forged O-type steel tools may be generally air cooled from forging temperatures—except for small or intricately shaped parts, which should be cooled in an insulating material. Normalizing, except for large parts, is ordinarily unnecessary, but forged parts should always be annealed before hardening.

Manganese grades of O-type tool steels require slightly lower temperatures for annealing than tungsten-chromium types (Table 10-2) and should be cooled at slower rates, about 11 °C/h (20 °F/h), than tungsten-chromium grades, which may be cooled at about 28 °C/h (50 °F/h). Parts should always be protected from decarburization during annealing.

The following isothermal schedule has been used for annealing O1 and O2 tool steels:

1. Hold 4 h at 730 °C (1350 °F).
2. Heat to 780 °C (1440 °F) and hold 2 h.
3. Cool to 670 °C (1275 °F) and hold 6 h.
4. Cool in air.

Depending on the size of the charge and thermal inertia of the annealing furnace, an isothermal annealing cycle may sometimes prove more rapid than conventional annealing. As described, the development of a well-spheroidized, annealed microstructure takes considerable time, especially for the tungsten-containing O-type steels.

Table 10-2 Performance factors and processing information for oil-hardened cold-work tool steels

Factor	O1	O2	O6	O7
Major factors				
Wear resistance	4	4	3	5
Toughness	3	3	3	3
Hot Hardness	3	3	2	3
Minor factors				
Usual working hardness, HRC	57–62	57–62	58–63	58–64
Depth of hardening	M	M	M	M
Finest grain size at full hardness, Shepherd standard	9	9	9	9
Surface hardness as-quenchd, HRC	61–64	61–64	65–67	61–64
Core hardness (25 mm, or 1in., diam round), HRC	59–61	59–61	50–55	59–61
Manufacturing factors				
Availability	4	3	2	2
Cost	1	1	1	1
Machinability	8	8	9	7
Quenching medium	O	O	O	W, O
Hardening temperature, °C (°F)	790–815 (1450–1500)	760–800 (1400–1475)	790–815 (1450–1500)	790–885 (1450–1625)
Dimensional change on hardening	M	M	M	M
Safety on hardening	H	H	M	M
Susceptibilty to decarburization	M	M	M	M
Approximate hardness as-rolled or forged, HB	325	325	375	325
Annealed hardness, HB	183–212	183–212	183–217	192–217
Annealing temperature, °C (°F)	760–790 (1400–1450)	745–775 (1375–1425)	775 (1425)(a)	790–815 (1450–1500)
Tempering range, °C (°F)	150–260 (300–500)	150–260 (300–500)	150–315 (300–600)	165–290 (325–550)
Forging temperature, °C (°F)	980–1065 (1800–1950)	980–1050 (1800–1925)	980–1065 (1800–1950)	980–1095 (1800–2000)

Note: Ratings are explained in Chapter 2. (a) Temperature shown is that which would be used if annealing for reworking after hardening and tempering were necessary.

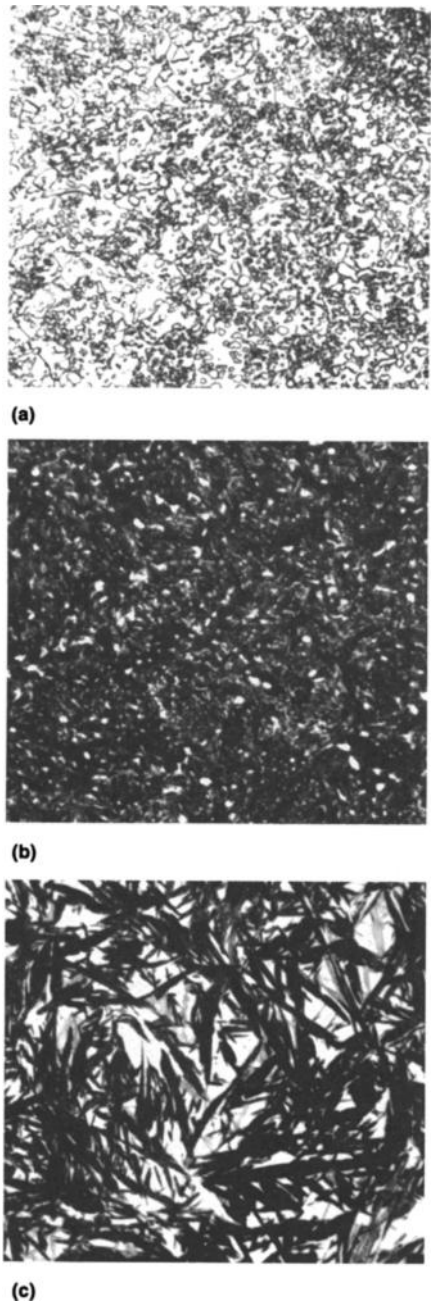

Fig. 10-1 Microstructures of oil-hardening tool steels. Light micrographs. Nital etch. (a) Spheroidized carbides in a ferrite matrix of O2 tool steel annealed at 725 °C (1335 °F). (b) Spheroidized carbides in a matrix of tempered martensite in O1 tool steel austenitized at 815 °C (1500 °F), oil quenched, and tempered at 220 °C (430 °F) to a hardness of 58.5 HRC. (c) Retained austenite and plate martensite in O1 tool steel austenitized at 980 °C (1795 °F), oil quenched, and tempered at 220 °C (430 °F)

Hardenability and Hardening

Figure 10-3 shows an IT curve for an O1 tool steel (Ref 1). The transformation of austenite to proeutectoid cementite/pearlite and bainitic microstructures is not separated into two well-defined temperature ranges, consistent with the moderate alloy content of the O1 steel. Manganese stabilizes austenite, lowers A_1 temperatures, and thus makes possible the low hardening temperatures recommended for some O-type steels. Increasing hardening temperatures result in increasing amounts of retained austenite in quenched parts (Ref 2), a severe example of which is shown in Fig. 10-1(c). Table 10-3 lists the amounts of retained austenite measured by x-ray diffraction in specimens of some O-type steels subjected to various heat treatment cycles (Ref 3). Refrigeration to –196 °C (–321 °F) effectively reduces, but does not entirely eliminate, retained austenite. Also, air cooling of the O1 tool steel through the martensite formation range results in greater amounts of retained austenite due to stabilization.

Figure 10-4 shows the effect of austenitizing temperature on the as-quenched hardness of O-type steels. Maximum hardness of the O2 steel, containing only manganese and a little molybdenum, is attained at temperatures as low as 760 °C (1400 °F), whereas the chromium and tungsten-chromium grades do not attain maximum hardness before hardening temperatures above 845 °C (1550 °F) are reached. The O7-type steels are usually hardened by oil quenching, but parts of simple shape may be water quenched safely. In O7 steels with low chromium contents and without molybdenum, water quenching is necessary to harden parts thicker than 25 mm (1 in.). Water quenching also allows the use of lower austenitizing temperatures for hardening, since the more rapid cooling makes up for some of the loss of hardenability due to alloying elements incorporated in retained alloy carbide particles.

Figures 10-5 and 10-6 show Jominy end-quench curves for O1 and O7 tool steels, respectively. The O1 steel exhibits significantly deeper hardening capacity than does the O7 steel. The O1 steel also shows marked improvement in hardenability when austenitized at higher temperatures, in contrast to the much milder effect of austenitizing temperature on hardenability of the O7 steel. The stability of the tungsten carbides in the O7 steel accounts for its lower hardenability at a given austenitizing temperature, as well as the lower sensitivity of hardenability to austenitizing temperature. The lower hardenability of the O7 steels significantly limits the size of part that can be hardened. For example, through-hardening of O1 steel bars 63.5 mm (2.5 in.) in diameter can be accomplished by oil quenching from 800 °C (1475 °F), but only bars with

diameters of less than 16 mm (0.625 in.) would be through-hardened in an O7 steel oil quenched from 815 °C (1500 °F). The O6 tool steels, which contain silicon and therefore some graphite, also contain additions of manganese and molybdenum and are relatively deep hardening.

Tempering

Figure 10-7 presents hardness as a function of tempering temperature for several O-type steels. The O7 chromium-tungsten grades have higher tempering resistance than the O1 and O2 steels. With

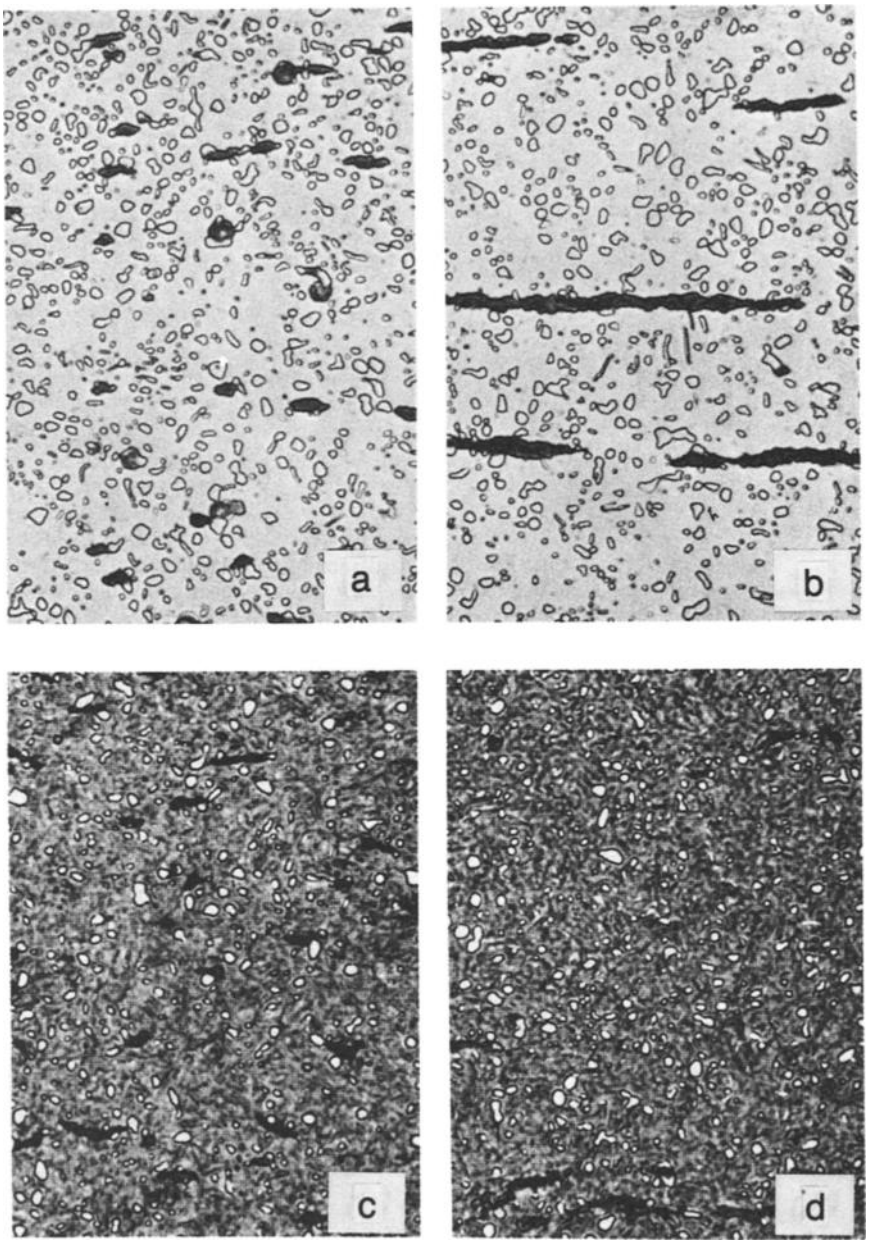

Fig. 10-2 Typical distributions of graphite (black features) in O6 tool steel. Light micrographs, 1000x. Nital etch. (a) Annealed microstructure, transverse section. (b) Annealed microstructure, longitudinal section. (c) Hardened microstructure, transverse section. (d) Hardened microstructure, longitudinal section

molybdenum, the tempering resistance of O1 and O2 tool steels is about the same, but without the molybdenum, the O2 steel softens somewhat more rapidly than does O1 steel. Despite these differences, all the O-type steels soften continuously with increasing tempering; therefore, to preserve high hardness the O-type steels are tempered at low temperatures, typically between 150 and 260 °C (300 and 500 °F).

Figures 10-8 to 10-12 show measurements of toughness, determined by various experimental approaches, as a function of tempering temperature for hardened O-type steels. Figure 10-8 compares unnotched impact toughness at constant hardness values for three O-type steels. Compared to the O2 and O7 steels, the O1 steel shows the best impact toughness at high hardness.

All the measurements of toughness show a small maximum in specimens tempered between 150 and 260 °C (300 and 500 °F), the tempering temperature range where high hardness is maintained. Toughness then decreases as specimens are tempered in the tempered martensite embrittlement range, where coarse carbide particles are produced by the decomposition of retained austenite (Ref 5). Higher tempering temperatures produce large increases in toughness, or ductility, as shown by increases in ultimate deformation measured in static torsion tests (Fig. 10-11 and 10-12). The substantial increases in toughness obtained by high-temperature tempering, however, are accompanied by significant decreases in hardness and strength in the moderately alloyed O-type tool steels.

Bend strengths and maximum deflections obtained during bend testing as a function of tempering temperature are shown for O1 and O7 tool steels in Fig. 10-13 and 10-14, respectively. The bend strength increases from that of the as-quenched state

Table 10-3 Retained austenite in O1 and O7 tool steels at room temperature and after refrigerating at –196° C (–321 °F)

	Austenitizing treatment			Retained austenite, % (a)			
	Temperature						
Type	°C	°F	Time, min	Treatment A(b)	Treatment B(b)	Treatment C(b)	Treatment D(b)
O1	790	1450	30	8.5	5.5	10.5	11
O7	870	1600	30	13.5	6.5	...	...

(a) Determined by x-ray measurements. (b) Treatment A, oil quenched to 20 °C (68 °F); treatment B, oil quenched to 20 °C (68° F) and cooled to –196 °C (–321 °F); treatment C, oil quenched to 50 °C (125 °F) and air cooled to 20 °C (68 °F); treatment D, salt quenched to 230 °C (450 °F) and air cooled to 20 °C (68 °F)

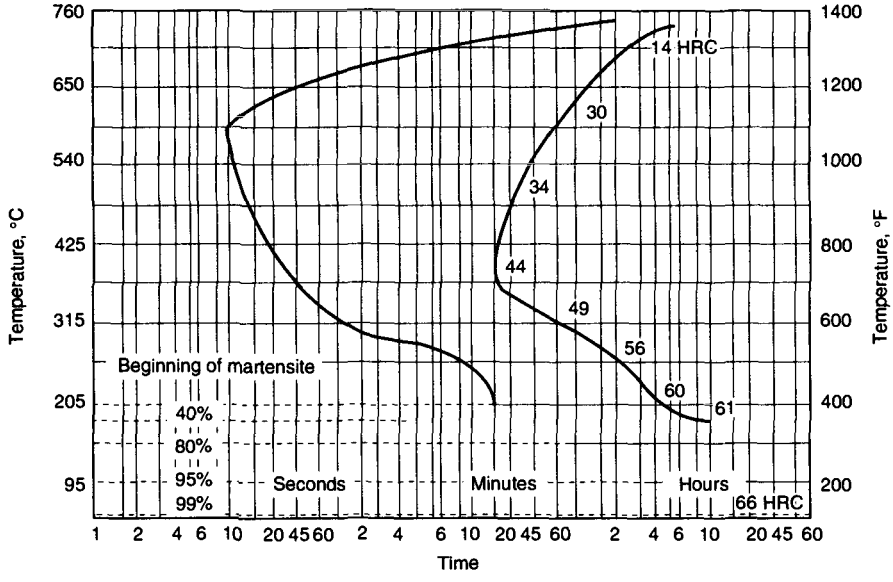

Fig. 10-3 IT diagram for O1 tool steel, containing 0.85%C, 1.18% Mn, 0.26% Si, 0.50% Cr, and 0.44% W, after austenitizing at 790 °C (1450 °F) for 1 h. Critical (Ac_1) temperature: 745 °C (1370 °F). Prior condition: annealed. Source: Ref 1

to a maximum after tempering of around 315 °C (600 °F), then drops with increasing tempering temperature as bend ductility increases. Table 10-4 lists tensile properties and hardness of O1 and O7 tool steels as a function of tempering temperature. Specimens tempered below 425 °C (800 °F) are too notch sensitive to provide reliable results, but as Table 10-4 shows, mechanical properties can be determined for specimens tempered at 425 °C (800 °F) and higher. The very low values of elongation and reduction of area of the O7 tool steel tempered at the lower temperatures reflect low fracture resistance and the absence of necking.

Figures 10-15 and 10-16 show the dimensional changes that occur during tempering of O-type steels. The magnitudes of the dimensional changes depend on specimen size and dimension measured, but all specimens show an increase due to hardening from the annealed state, as best shown in Fig. 10-16. The dimensions of as-quenched specimens contract as martensite loses its tetragonality in the first stage of tempering. Figure 10-16 shows that O1 and O7 steel specimens hardened at 845 °C (1550 °F) and 900 °C (1650 °F), respectively, undergo much more expansion on hardening than an O1 specimen hardened at 790 °C (1450 °F). This observation is explained by the greater solution of carbon in austenite at the higher austenitizing temperatures and the subsequent greater tetragonality of the martensite that forms from that austenite. Also, it follows that the greater the tetragonality of the as-quenched martensite, the greater the contraction in specimen dimensions as tetragonality is relieved during the first and third stages of tempering.

Following the initial contraction on tempering, specimen dimensions expand as retained austenite with its close-packed crystal structure transforms to ferrite and cementite with more open crystal structures during the second stage of tempering. The expansion is greatest in specimens that retain more austenite because of exposure to high austenitizing temperatures for hardening, as demonstrated in Fig. 10-16. Therefore, if an absolute minimum in dimensional change is required, O2 tool steel, which can be hardened from low austenitizing temperatures that minimize both martensite tetragonality and retained austenite content, may be selected.

Selection and Applications

By far the most popular oil-hardening steel is the O1 grade. O1 tool steel can be hardened from a relatively low austenitizing temperature, has sufficient hardenability to produce adequate depth of hardening and surface hardness in all but the very largest tools, is not sensitive to grain growth on overheating, has slightly higher toughness than the other oil-hardening steels, and is the most widely available of the O-type steels.

As noted in the previous section, O2 tool steel exhibits the lowest dimensional changes on heat treatment. Type O6 tool steel, by virtue of graphite distribution in its microstructure, provides good machinability for the fabrication of intricate dies, and type O7 is the most wear resistant of the oil-hardening tool steels and may be preferred for tooling applications for longer production runs.

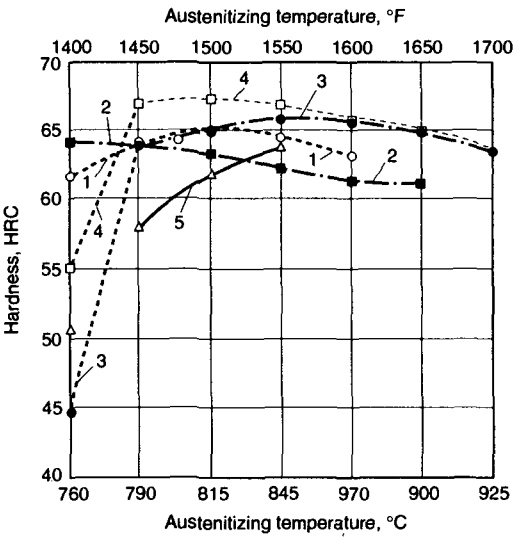

Curve	Type	Composition, % C	Mn	W	Cr	Mo	V	Quenching medium	Specimen size
1	O1	0.90	1.10	0.50	0.50	...	...	Oil	1 (diam) × 2 in.
2	O2	0.90	1.55	...	...	0.30	...	Oil	1 (diam) × 3 in.
3	O7	1.25	0.30	1.40	0.40	...	0.20	Oil	1 (diam) × 2 in.
4	O7	1.25	0.30	1.40	0.40	...	0.20	Water	1 (diam) × 2 in.
5	...	1.05	0.70	0.50	1.60	...	...	Oil	1 (diam) × 3 in.

Fig. 10-4 Effect of austenitizing temperature on as-quenched hardness of oil-hardening cold-work die steels. Curves 1 to 4, Allegheny Ludlum Industries; curve 5, Columbia Tool Steel Co.

All the oil-hardening cold-work tool steels are used for similar applications, including:

Taps	Hobs	Slitting saws
Reamers	Thread-rolling dies	Circular cutters
Broaches	Master tools	Drills
Blanking dies	Punches	Coining dies
Forming dies	Burnishing tools	Cold-trimming dies
Gages	Knurling tools	Plastic molds
Small shear blades	Feed rolls	Drawing dies

References

1. P. Payson and J. Klein, The Hardening of Tool Steels, *Trans. ASM*, Vol 31, 1943, p 218
2. E.C. Bain and M.A. Grossmann, The Nature of Oil Hardening, Nondeforming Tool Steels, *Trans. ASST*, Vol 10, 1926, p 883
3. B.S. Lement, B.L. Averbach, and M. Cohen, The Dimensional Stability of Steel, Part IV: Tool Steels, *Trans. ASM*, Vol 41, 1949, p 1061
4. F.R. Palmer and G.V. Luerssen, *Tool Steel Simplified*, Carpenter Steel Co., 1960
5. G. Krauss, *Steels: Heat Treatment and Processing Principles*, ASM International, 1990
6. J.C. Hamaker, V.C. Strang, and G.A. Roberts, Bend Tensile Relationships for Tool Steels at High Strength Levels, *Trans. ASM*, Vol 49, 1957, p 550

Table 10-4 Tensile properties of O1 and O7 tool steels

Tempering temperature		Hardness,	Tensile strength		Yield strength (0.2% offset)		Elongation in 50 mm	Reduction of
°C	°F	HRC	MPa	KSI	MPa	KSI	(2 in.), %	area, %
Type O1(a)								
425	800	50	1710	248	1538	223	8.0	17
480	900	47	1496	217	1358	197	8.5	19
540	1000	44	1269	187	1165	169	9.5	22
595	1100	39	1096	159	979	142	12.0	28
650	1200	31	917	133	814	118	17.0	33
705	1300	22	772	112	634	92	27.0	44
Type O7(b)								
425	800	54.2	1875	272	1800	261	0.6	0.3
480	900	52.1	1779	258	1641	238	0.8	1.3
540	1000	50.4	1634	237	1510	219	1.0	0.8
595	1100	46.8	1441	209	1276	185	2.1	2.6
650	1200	40.2	1110	161	1020	148	5.2	9.2
705	1300	30.9	883	128	821	119	9.3	12.3

(a) Composition: 0.89 C, 1.10 Mn, 0.47 Cr, 0.41 W, 0.22 V; oil quenched. Source: Bethlehem Steel Co. (b) Composition: 1.17 C, 1.52 W, 0.75 Cr, 0.26 Mo, 0.16 V; 1600 °F; oil-quenched. Source: Ref 6

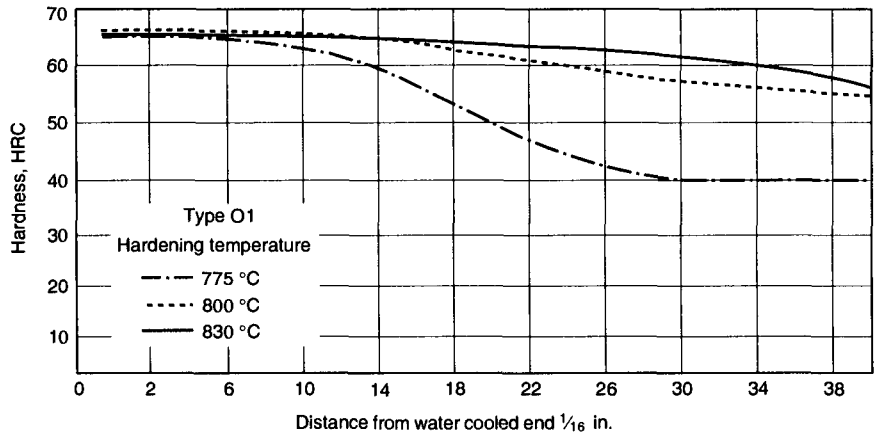

Fig. 10-5 Jominy end-quench hardenability curves for O1 tool steel containing 0.95% C, 0.30% Si, 1.20% Mn, 0.50% W, 0.50% Cr, and 0.20% V, hardened from three different austenitizing temperatures. Data from Teledyne VASCO

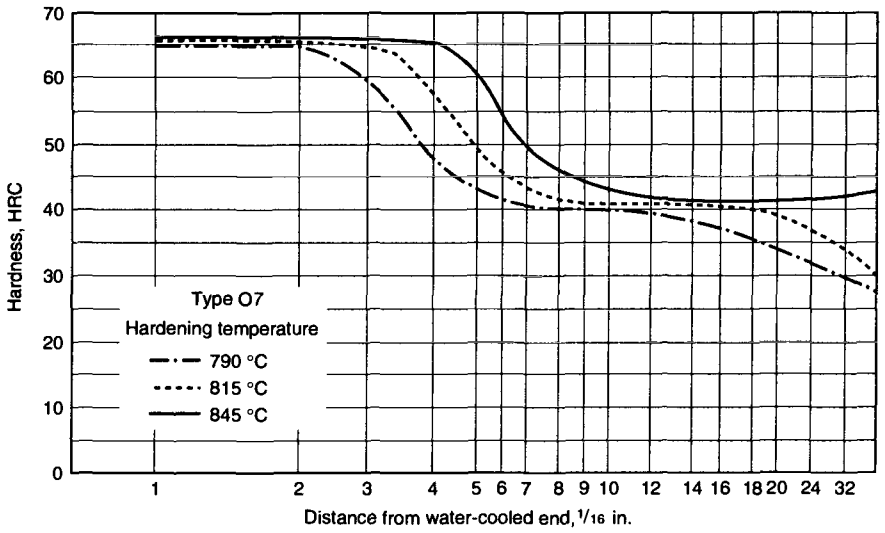

Fig. 10-6 Jominy end-quench hardenability curves for O7 tool steel containing 1.20% C, 0.30% Mn, 0.26% Si, 0.70% Cr, 0.25% Mo, 1.56% W, and 0.20% V. Data from Teledyne VASCO

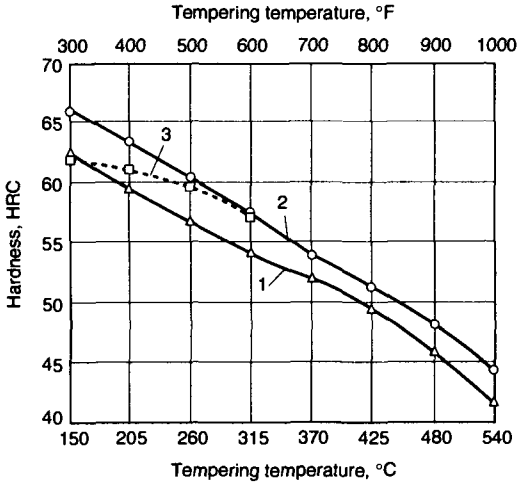

Curve	Type	Composition, %						Hardening temperature		Hardening medium
		C	Mn	W	Cr	Mo	V	°C	°F	
1	O1	0.95	1.20	0.50	0.50	...	0.20	790	1450	Oil
	O2	0.90	1.55	...	...	0.30	...	790	1450	Oil
2	O7	1.20	0.25	1.60	0.70	0.25	0.20	800	1475	Water
3	...	1.05	0.70	0.50	1.60	...	...	845	1550	Oil

Fig. 10-7 Effect of tempering temperature on the hardness of oil-hardening cold-work die steels. Curves 1 and 2, Teledyne VASCO; curve 3, Columbia Tool Steel Co.

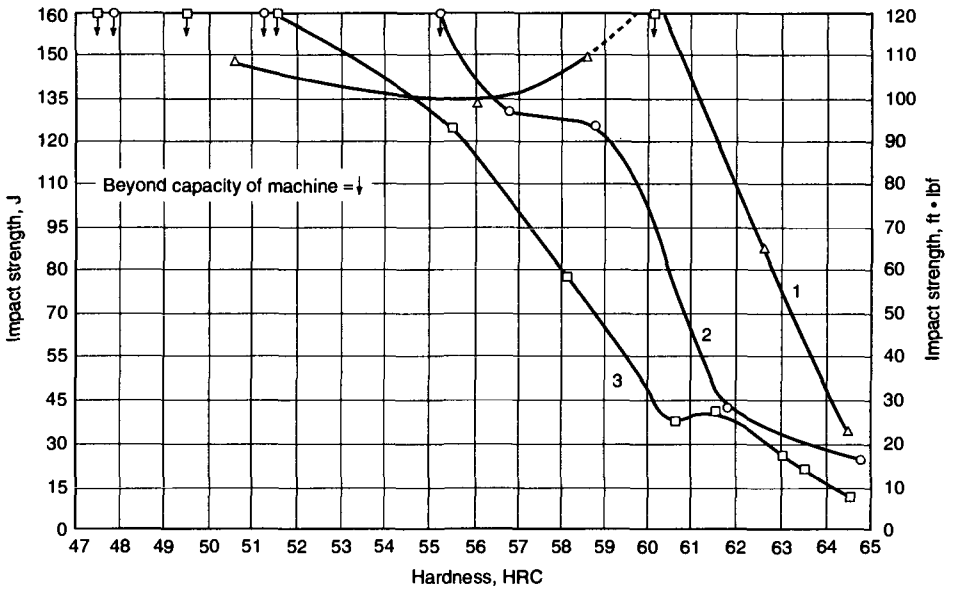

Curve	Type	Composition, %						Hardening temperature		Hardening medium
		C	Mn	W	Cr	Mo	V	°C	°F	
1	O1	0.90	1.10	0.50	0.50	...	...	800	1475	Oil
2	O2	0.90	1.55	...	...	0.30	...	775	1425	Oil
3	O7	1.25	0.30	1.40	0.40	...	0.20	900	1650	Oil

Fig. 10-8 Unnotched Izod impact strength as a function of tempered hardness level for O-type tool steels. Note that in the usual working hardness range (57 to 64 HRC), type O1 has the highest impact strength. Data from Allegheny Ludlum Industries

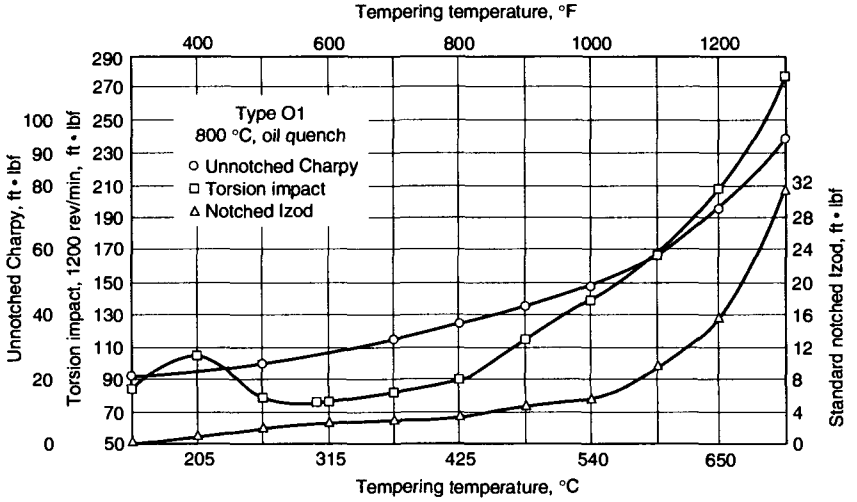

Fig. 10-9 Effect of tempering temperature on toughness ratings of O1 tool steel containing 1.2% Mn. Data from Bethlehem Steel Co.

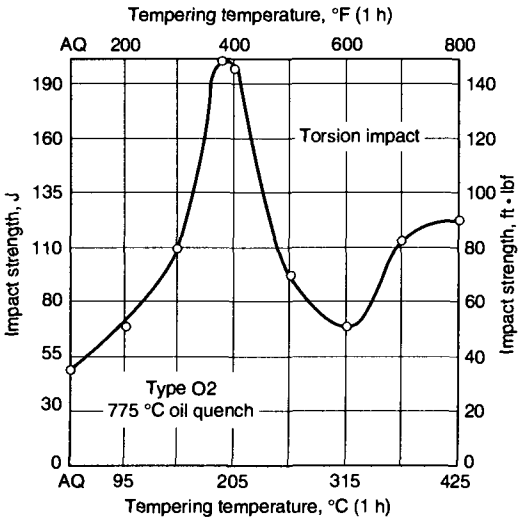

Fig. 10-10 Effect of tempering temperature on torsion impact strength of O2 tool steel containing 1.60% Mn. AQ, as quenched. Source: Ref 4

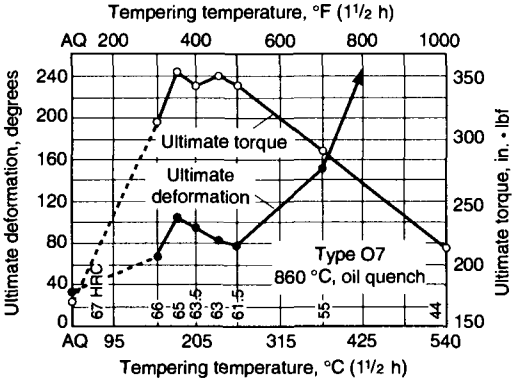

Fig. 10-12 Results of static torsion tests of type O7 tool steel containing 1.6% W as a function of tempering temperature. The hardness before testing is noted along the abscissa. Data from Teledyne VASCO

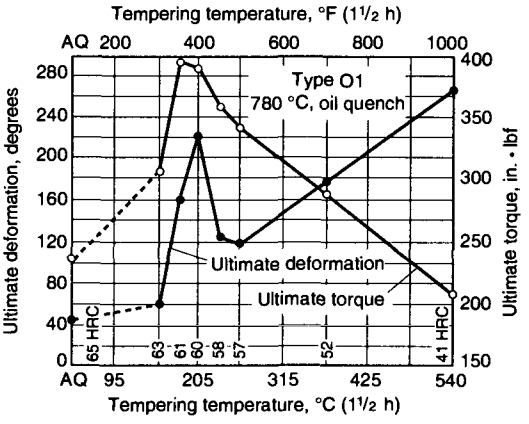

Fig. 10-11 Results of static torsion tests of O1 tool steel containing 1.2% Mn as a function of tempering temperature. The hardness before testing is noted along the abscissa. Data from Teledyne VASCO

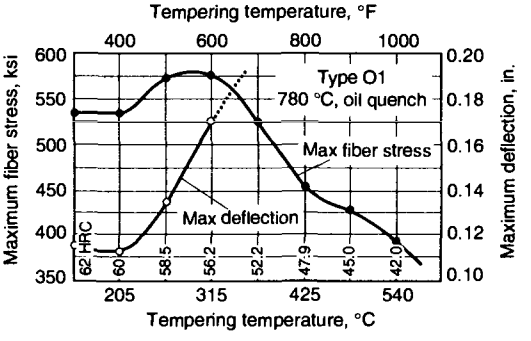

Fig. 10-13 Maximum fiber stress and maximum deflection obtained in bend testing samples of O1 tool steel containing 1.2% Mn as a function of tempering temperature. Hardness values are noted along the abscissa. Data from Teledyne VASCO

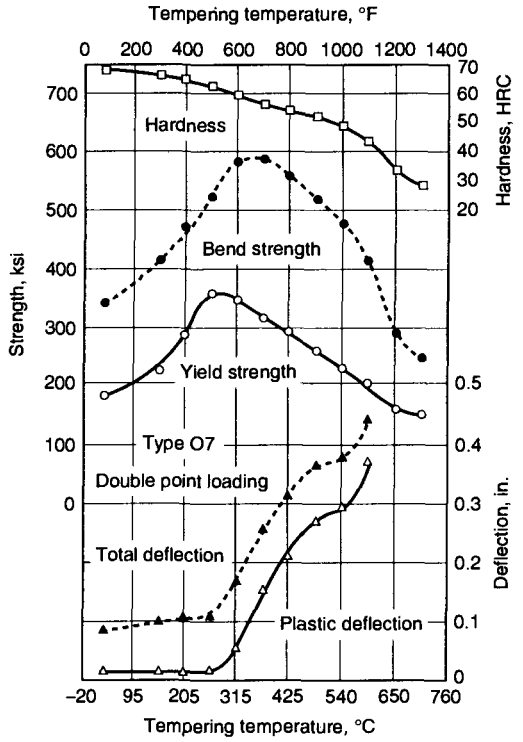

Fig. 10-14 Effect of tempering on the double-point bend test properties of O7 tool steel. Specimens were oil quenched from 870 °C (1600 °F) and tempered for 2 h at various temperatures. Source: Ref 6

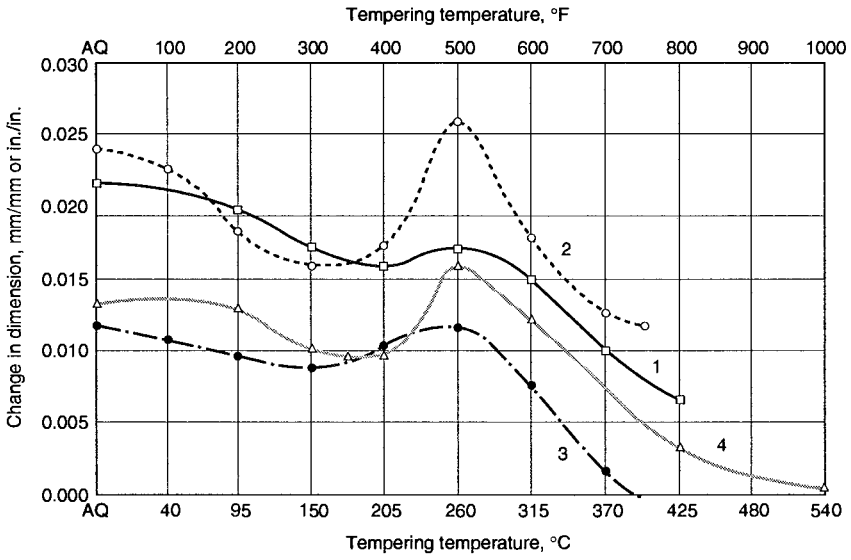

Curve	Hardening temperature °C	Hardening temperature °F	Hardening medium	Specimen size	Dimension measured
1	815	1500	Oil	1 × 2 × 6 in.	Average of three principal dimensions
2	800	1470	Oil	2 (diam) × 2 in	Length
3	800	1470	Oil	⅜ (diam) × 2 in	Length
4	790	1450	Oil	1 (diam) × 5 in	Length

Fig. 10-15 Dimensional changes in O1 tool steel as a function of tempering temperature. Curve 1, Latrobe Steel Co.; curves 2 and 3, Uddeholm Company of America, Inc.; curve 4, Allegheny Ludlum Industries

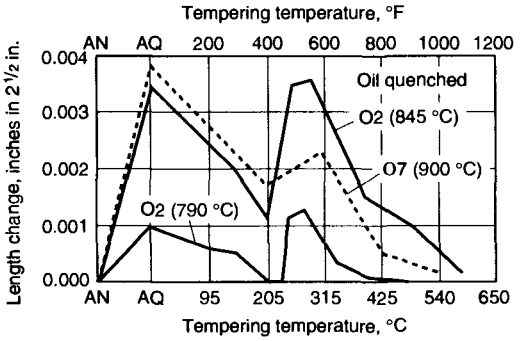

Fig. 10-16 Length changes as a function of tempering temperature for O1 and O7 tool steels quenched from indicated temperatures. AN, Annealed; AQ, as quenched. Data from Ref 2 and Allegheny Ludlum Industries

Tool Steels: 5th Edition
George Roberts, George Krauss, Richard Kennedy, p 193-202
DOI:10.1361/toos1998p193

Copyright © 1998 ASM International®
All rights reserved.
www.asminternational.org

CHAPTER 11
Air-Hardening, Cold-Work Tool Steels

The air-hardening cold-work tool steels, designated as group A steels in the AISI classification system, achieve their processing and performance characteristics with combinations of high carbon and moderately high alloy content. The high alloy content is sufficient to provide not only air-hardening capability, but also a distribution of large alloy carbide particles superimposed on the microstructures developed by heat treatment processing. The alloy carbides have very high hardness relative to martensite and cementite, as discussed in terms of tool steel alloy design in Chapter 4, and thus contribute to enhanced wear resistance of A-type steels compared to tool steels of lower alloy content. Although the alloy content is high and the A-type steels have good temper resistance with demonstrated secondary hardening, their hot hardness relative to other even more highly alloyed tool steels is not sufficient for high-speed machining or hot-work applications; as a result, the A-type tool steels are still largely used for cold-work applications.

Table 11-1 presents the nominal chemical compositions of the A-type tool steels, and Table 11-2 lists processing and performance information. A major processing advantage of these steels, compared to tool steels that must be water or oil quenched, is that air hardening produces minimum distortion and very high safety and resistance to cracking during hardening. Various combinations of manganese, chromium, and molybdenum contents make possible the air-hardening capability of the A-type steels. Table 11-1 shows that many of these steels are alloyed with about 5% Cr, but others, such A4, A6, and A10, have high manganese contents and lower chromium contents. The latter adjustment in composition permits the use of lower austenitizing temperatures for hardening, which in turn further reduces dimensional changes and minimizes undesirable surface reactions such as decarburization during hardening.

Silicon is a major alloying element in the A8, A9, and A10 steels and helps to promote toughness, as discussed for the S-type steels in Chapter 9. Also, in combination with the high carbon contents of A10 steel, silicon promotes graphite formation. The graphite content of A10 steel makes it highly machinable in the annealed condition, and in the hardened condition, the graphite contributes to galling and seizing resistance at tool steel die/workpiece interfaces. Type A7 is the most highly alloyed of the A-type tool steels, and earlier merited a classification of its own as a special wear-resistant cold-work die steel (Ref 1). The tungsten and high vanadium contents of A7 steels, combined with high carbon

Table 11-1 Composition limits of air-hardening, medium-alloy cold-work steels

AISI	UNS	Composition, %								
type	No.	C	Mn	Si	Cr	Ni	Mo	W	V	Co
A2	T30102	0.95–1.05	1.00 max	0.50 max	4.75–5.50	0.30 max	0.90–1.40	...	0.15–0.50	...
A3	T30103	1.20–1.30	0.40–0.60	0.50 max	4.75–5.50	0.30 max	0.90–1.40	...	0.80–1.40	...
A4	T30104	0.95–1.05	1.80–2.20	0.50 max	0.90–2.20	0.30 max	0.90–1.40	...	...	...
A6	T30106	0.65–0.75	1.80–2.50	0.50 max	0.90–1.20	0.30 max	0.90–1.40	...	...	...
A7	T30107	2.00–2.85	0.80 max	0.50 max	5.00–5.75	0.30 max	0.90–1.40	0.50–1.50	3.90–5.15	...
A8	T30108	0.50–0.60	0.50 max	0.75–1.10	4.75–5.50	0.30 max	1.15–1.65	1.00–1.50	...	...
A9	T30109	0.45–0.55	0.50 max	0.95–1.15	4.75–5.50	1.25–1.75	1.30–1.80	...	0.80–1.40	...
A10	T30110	1.25–1.50(b)	1.60–2.10	1.00–1.50	...	1.55–2.05	1.25–1.75	...	...	...

(a) 0.25% max Cu, 0.03% max P, and 0.03% max S. Where specified, sulfur may be increased to 0.06 to 0.15% to improve machinability. (b) Contains free graphite in the microstructure

Table 11-2 Performance factors and processing information for air-hardening, medium-alloy, cold-work tool steels

Factor	A2	A3	A4	A6	A7	A8	A9	A10
Major factors								
Wear resistance	6	7	5	4	9	4	4	3
Toughness	4	3	4	5	1	8	8	3
Hot hardness	5	5	4	4	6	6	6	3
Minor factors								
Usual working hardness,HRC	57–62	58–63	54–62	54–60	58–66	48–57	40–56	55–62
Depth of hardening	D	D	D	D	D	D	D	D
Finest grain size at full hardness, Shepherd standard	8½	8½	8½	8½	8½	8	8	8
Surface hardness as-quenched, HRC	63–65	63–65	61–63	60–62	64–66	60–62	55–57	60–63
Core hardness (25 mm, or 1 in., diam round), HRC	63–65	63–65	61–63	60–62	64–66	60–62	55–57	60–63
Manufacturing factors								
Availability	4	1	1	2	2	2	2	2
Cost	1	1	1	1	3	1	1	2
Machinability	8	8	6	6	1	8	7	8
Quenching medium	A	A	A	A	A	A	A	A
Hardening temperature, °C (°F)	925–980 (1700–1800)	970–995 (1775–1825)	815–870 (1500–1600)	830–870 (1525–1600)	925–980 (1700–1800)	980–1010 (1800–1850)	970–1010 (1775–1850)	790–815 (1450–1500)
Dimensional change on hardening	L	L	L	L	L	L	L	L
Safety on hardening	H	H	H	H	H	H	H	H
Susceptibility to decarburization	H	H	H	H	H	H	H	M
Approximate hardness as-rolled or forged, HB	500	500	500	500	550	500	500	425
Annealed hardness, HB	202–229	212–235	202–248	217–248	235–262	192–228	197–235	235–269
Annealing temperature, °C (°F)	845–870 (1550–1600)	815–845 (1500–1550)	740–760 (1360–1400)	730–745 (1350–1375)	870–900 (1600–1650)	815–845 (1500–1550)	790–830 (1450–1525)	775 (1425)(a)
Tempering range, °C (°F)	175–540 (350–1000)	175–565 (350–1050)	150–425 (300–800)	150–425 (300–800)	150–540 (300–1000)	480–650 (900–1200)	480–650 (900–1200)	150–425 (300–800)
Forging temperature, °C (°F)	1010–1095 (1850–2000)	1010–1095 (1850–2000)	1010–1095 (1850–2000)	1040–1120 (1900–2050)	1040–1150 (1900–2100)	1040–1150 (1900–2100)	1040–1150 (1900–2100)	980–1050 (1800–1925)

Note: Ratings are explained in Chapter 2. (a) Temperature shown is that which would be used if annealing for reworking after hardening and tempering were necessary.

content, produce high volume fractions of alloy carbides; these promote very high wear resistance and good hot hardness, but low toughness.

Microstructures

Figure 11-1 shows light micrographs of A7 tool steel microstructures after annealing and after hardening and tempering. The most apparent microstructural features are distributions of two sizes of carbides. The larger carbides, often considered to be massive on a microstructural scale, are primary alloy carbides that do not dissolve even during high-temperature hot working or austenitizing of A-type steels. They are present because of the high content of strong alloy carbide-forming elements such as chromium and molybdenum, and in the case of the A7 steel, vanadium. The smaller carbides are the secondary carbides formed at lower temperatures by austenite decomposition to ferrite-carbide microstructures, annealing, or tempering, and spheroidization of the carbides in those microstructures. Figure 11-1(a) shows a high density of smaller, secondary carbides that have been spheroidized by lengthy annealing. Many of the smaller carbides are dissolved during austenitizing for hardening, as shown in Figures 11-1(b) and (c), but the massive primary carbide distribution is largely unchanged by hardening.

The matrices in which the resolvable carbides are distributed consist of ferrite in the annealed microstructure (Fig. 11-1a) and tempered martensite in the hardened microstructures Fig. 11-1b and c). Details of the tempered martensitic microstructure are too fine to be resolved in the light microscope, but transmission electron microscopy shows that the microstructure consists of plate-shaped martensitic crystals within a matrix of retained austenite. An example of this type of microstructure in a hardened A2 tool steel was shown earlier in Fig. 4-21.

Processing Prior to Hardening

Table 11-2 shows processing temperature ranges for forging and annealing. Preheating at temperatures about 650 to 675 °C (1200 to 1250 °F) reduces soaking time and the time for decarburization, to which the A-type steels are highly susceptible because of their high carbon content. The chromium A-type steels should not be forged below 900 °C (1650 °F), but the manganese types may be safely forged at temperatures as low as 815 °C (1500 °F). In view of the air-hardening ability of the A-type steels, they should be slowly cooled in insulating materials after forging to at least 205 °C (400 °F). Also, because of air hardening, the A-type steels should not be normalized after forging but should be annealed before machining or hardening.

Hardenability and Hardening

The alloy content of the A-type tool steels severely retards the transformation of austenite to ferrite-carbide microstructures. Figure 11-2 shows an IT diagram for an A2 steel austenitized at 1010 °C (1850 °F). Two well-defined C-curves, one for pearlite and the other for bainite, characterize the austenite decomposition. Substantial times are re-

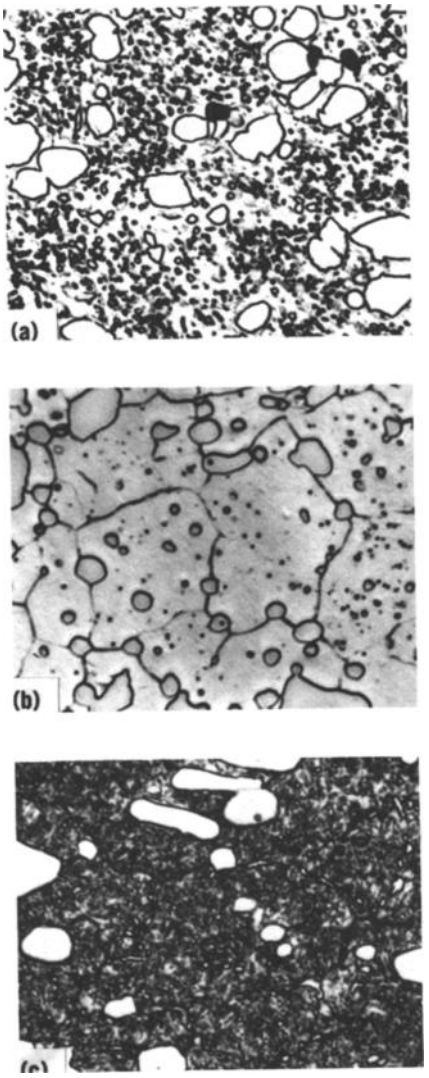

Fig. 11-1 Microstructures of A7 tool steel. Light micrographs, 1000x, nital etch. (a) Massive and smaller spheroidized carbides in a ferritic matrix in a specimen box annealed at 900 °C (1650 °F) and cooled at 25 °C/h (45 °F/h). (b) Carbides in a matrix of tempered martensite in a specimen austenitized at 955 °C (1750 °F), air cooled, and tempered at 150 °C (300 °F). (c) Carbides in a matrix of tempered martensite in a specimen austenitized at 955 °C (1750 °F), air cooled, and tempered at 315 °C (600 °F)

quired to initiate the transformations, consistent with the air hardening.

The air-hardening characteristics of A-type steels make evaluation of their hardenabilities by Jominy end-quench testing insensitive to differences in heat treatment or alloying. As a result, Jatczak (Ref 3) has developed a test to evaluate differences in hardenabilities of deep-hardening steels subjected to slow cooling rates equivalent to those characteristic of cooling in very heavy sections of steel. This test has been described in Chapter 5 and, as shown in Fig. 5-32, is capable of evaluating differences in the hardenabilities of deep-hardening A-type steels. Generally, the as-quenched hardness of the chromium A-type steels, air cooled from 950 °C (1740 °F) should be 63 to 65 HRC, and hardenability should be sufficient to fully harden a 50 by 150 by 250 mm (2 by 6 by 10 in.) block.

The A-type tool steels are susceptible to decarburization during austenitizing for hardening, and significant decarburization will lower the surface hardness of hardened parts. Tools should be heated in vacuum, or in salt baths, fluidized beds, or furnaces with neutral or slightly carburizing atmospheres; packing in appropriate compounds such cast iron chips or charcoal is also used to protect surfaces from the loss of carbon. Too high a protective carbon potential, however, will lead to carburization and associated low surface hardness because of excessive retained austenite. The rate of decarburization increases with both time and temperature; and decarburization can also be minimized by preheating, which will minimize soaking time at high austenitizing temperatures where decarburization most rapidly develops.

Proper control of austenitizing is critical for the achievement of optimum hardened microstructures and properties in the air-hardened cold-work tool steels. Too low an austenitizing temperature will leave too high a content of carbon and alloying elements incorporated in alloy carbides, lowering hardenability and reducing hardness because of the formation of nonmartensitic microstructures during air cooling. Too high an austenitizing temperature will cause too high a content of carbon and alloying elements to dissolve in austenite, lowering M_s temperatures and reducing hardness because of excessive retained austenite in the hardened microstructures. These effects of austenitizing produce parabolic curves of as-quenched hardness versus austenitizing temperature, as shown in Fig. 11-3 for several A-type steels. The A2 steel with 5% Cr addition requires a higher austenitizing temperature to produce peak as-cooled hardness, whereas the steels with major additions of manganese develop peak hardness after austenitizing at lower temperatures. Figure 11-4 shows hardness as a function of carbon content for air-cooled A4 steels austenitized at various temperatures. For medium carbon contents, the effect of austenitizing on hardness and hardenability is relatively low because all the carbon and alloying elements are put into solution at low austenitizing temperatures. In the high-carbon steels, the effect of austenitizing temperature is much greater; higher temperatures are required to dissolve the higher quantities of carbides present in these steels after annealing. The results shown in Fig. 11-4 led to the development of A6 steel, which has just sufficient carbon to attain 62 HRC after

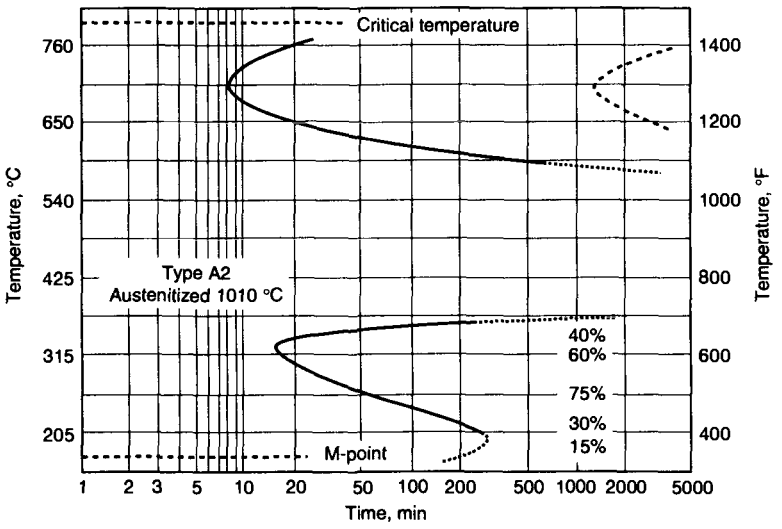

Fig. 11-2 IT diagram for air-hardening A2 steel, containing 0.97% C, 0.48% Mn, 0.40% Si, 4.58% Cr, 1.04% Mo, and 0.25% V, after austenitizing for 1 h at 1010 °C (1850 °F). Source: Ref 2

hardening at the relatively low austenitizing temperature of 875 °C (1575 °F) (Ref 4).

Substantial amounts of austenite can be retained in A-type steels after austenitizing at high temperatures, as increasing amounts of carbon and alloying elements dissolve and produce austenite with low M_s temperatures. Figure 11-5 shows amounts of retained austenite as a function of austenitizing temperature for A2 and A6 steels (Ref 5, 6). The strong effect of carbon and chromium, relative to manganese, on the temperature dependence and amount of austenite retained is demonstrated. Cooling rate, due to stabilization of the martensitic transformation on slower cooling, has a real but much smaller effect on the amount of retained austenite than does austenitizing temperature. Earlier, in Fig. 5-12, another set of data showing the effect of austenitizing temperature on as-cooled hardness of A2 tool steel was presented (Ref 7). The low hardness of A2 specimens austenitized at higher temperatures, due to retained austenite, was substantially increased by refrigeration or high-temperature tempering as the retained austenite transformed to martensitic or bainitic microstructures during those treatments.

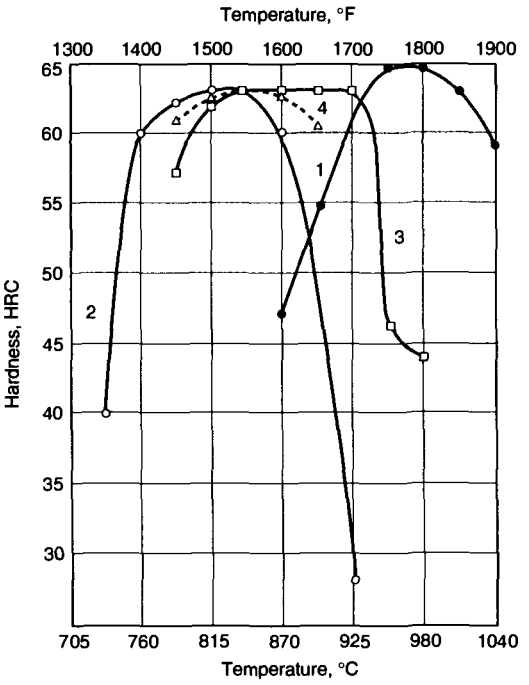

Curve	Type	Composition, % C	Mn	Cr	Mo	V	Specimen size
1	A2	1.00	0.50	5.00	1.00	0.20	1 (diam) × 2 in.
2	...	1.00	3.00	1.00	1.00	...	1 (diam) × 1 in.
3	...	0.95	2.00	2.20	1.10	...	...
4	A6	0.70	2.00	1.00	1.35	...	...

Fig. 11-3 Effect of austenitizing temperature on the surface hardness of A-type steels. Specimens were air cooled from the austenitizing temperatures. Curves 1 and 2, Allegheny Ludlum Industries; curve 3, Bethlehem Steel Co.; curve 4, Universal-Cyclops Steel Corp.

Tempering

Figure 11-6 shows hardness as a function of tempering temperature for an A2 steel austenitized for hardening at three temperatures, an O2 steel, and a plain carbon steel containing 1% C. The tempering

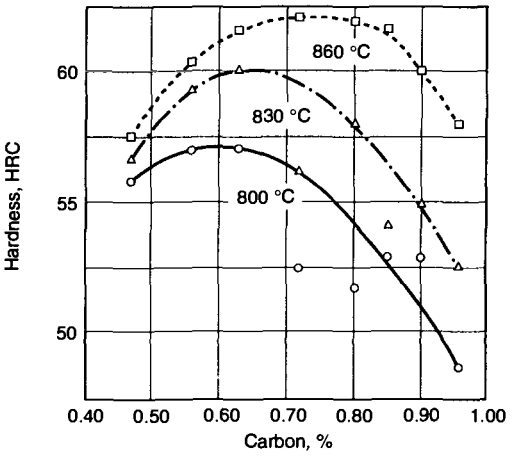

Fig. 11-4 Effect of carbon content and austenitizing temperature on the center hardness of 100 mm (4 in.) diam bars of A4 tools steel air cooled from the hardening temperature. Source: Ref 4

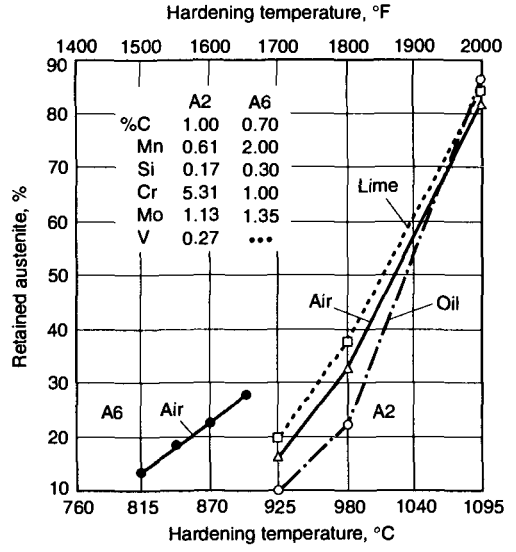

Fig. 11-5 Retained austenite as a function of austenitizing temperature for air-cooled A6 tool steel and A2 steel cooled in different media. Source: Ref 5, 6

resistance of the A2 steel is much higher than that of the plain carbon and O2 steel, and a definite but small secondary hardening peak develops in the A2 steel after tempering at about 510 °C (950 °F). The hardness increase due to secondary hardening is highest in specimens hardened at the highest austenitizing temperature. In those specimens, the supersaturation of the martensite with carbon and alloying elements is higher than in specimens austenitized at lower temperatures; consequently, the precipitation of alloy carbides at the higher tempering temperatures is most intense. Fig. 11-7 presents additional tempering curves for A-type steels and shows that resistance to softening during tempering is best in the steels with the higher chromium content.

The microstructure and hardness changes caused by tempering are a function of time and temperature. Most often, as in this book, changes due to tempering are plotted only as a function of temperature, and time at temperature is assumed constant at 1 or 2 h. Figure 11-8 plots hardness of an A2 steel austenitized at several temperatures as a function of a time-temperature parameter developed by Hollomon and Jaffe (Ref 8) and extended to tool steels by Roberts et al. (Ref 9). The fact that logarithm of time is used in the parameter reflects the fact that time has a smaller effect on tempering changes than does temperature. For a given hardness corresponding to a given value of the parameter, if time is known or estimated, the temperature to achieve that hardness can be calculated. Ideally, the parameter assumes a single mechanism of microstructural change that causes hardness to change as a function of time and temperature, an assumption that is not valid for tool steels where several mechanisms of change may operate depending on the stage of tempering. The use of the tempering parameter should be effective when applied to time-temperature regimes where a single mechanism of hardness change predominates.

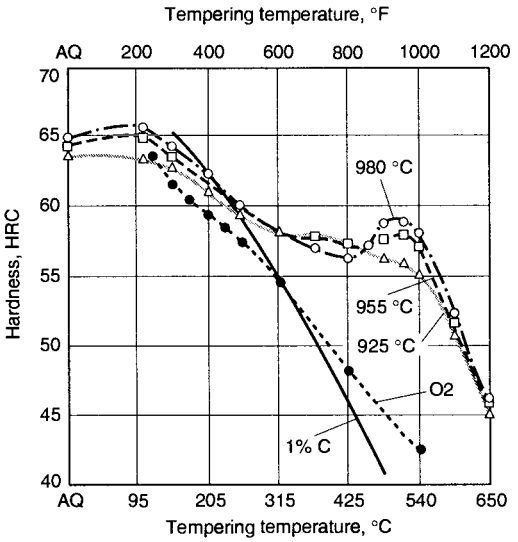

Fig. 11-6 Effect of tempering temperature on the hardness of A2 tool steel, containing 1.00% C, 0.60% Mn, 5.25% Cr, 1.10% Mo, and 0.25% V, after air cooling from various austenitizing temperatures. Data from Universal-Cyclops Steel Corp. Shown for comparison are curves for O2 tool steel and a 1.0% C steel. AQ, as quenched

As noted earlier, the retained austenite content of hardened air-hardening steels may be quite high. The retained austenite is thermodynamically unstable at temperatures below the A_1 and, as discussed in Chapter 5, must transform to more stable combinations of phases during what is known as the second stage of tempering. In carbon and low-alloy steels, retained austenite transformation occurs by a single, well-defined reaction at temperatures between 200 and 300 °C (390 and 570 °F). In highly alloyed tool steels, austenite transformation may take place in two stages, each with its own set of kinetics. Figure 11-9 shows IT curves for retained austenite in an A2 steel (Ref 5). The apparent high-temperature transformation of retained austenite in high-alloy tool steels during tempering may be complicated by the fact that the austenite not only transforms at temperature, but also transforms to martensite on cooling to room temperature from the tempering temperature (Ref 10). Such changes during tempering are detrimental to toughness and sometimes necessitate additional tempering steps. The kinetics of retained austenite transformation on tempering A-type tool steels is very much a function of austenitizing temperature for hardening, with the higher austenitizing temperatures producing more stable, highly alloyed retained austenite that transforms sluggishly during tempering.

The effect of tempering on properties other than hardness of A-type tool steels is shown in Fig. 11-10 to 11-13. Static torsion tests (Fig. 11-10) show that the torsional strength of a fully hardened A2 steel peaks after tempering at about 150 °C (300 °F) and exceeds that of an O1 tool steel in all tempered conditions. Moreover, torsional ductility, as measured by ultimate deformation, does not drop during low-temperature tempering of the A2 steel, while it does show the characteristic drop in the O1 steel. Figure 11-11, however, shows a minimum in torsional impact energy absorbed in hardened A2 specimens tempered around 260 °C (500 °F) (Ref 11). The generally good unnotched impact fracture energy of A2 tool steel tempered to retain high hardness is shown in Fig. 11-12. Limited mechanical property data obtained by tensile testing of A2 and A6 tool steels is shown in Table 11-3, and fatigue performance of an A6 steel hardened and double tempered to 60 HRC is shown in Fig. 11-13.

The dimensional changes caused by hardening and tempering A-type tool steels are shown in Fig.

Table 11-3 Mechanical properties of A2 and A6 tool steels

Tempering temperature		Hardness,	Tensile properties						Unnotched Charpy impact strength	
			Ultimate strength		Yield strength		Elongation in 50 mm	Reduction of area,		
°C	°F	HRC	MPa	ksi	MPa	ksi	(2 in.), %	%	J	ft · lbf
A2(a)										
540	1000	54.1	1858.2	269.5	...	...	...	...	...	...
595	1100	46.7	1603.8	232.6	1269	184	5.0	13.9	...	...
A6(b)										
175	350	59.7	2137	310	...	...	0.5	1.0	117	86
315	600	55.5	2016.8	292.5	1822.3	264.3	1.0	2.2	163	120
480	900	51.0	1751	254	1510	219	2.5	7.4	170	125

(a) Hardened from 945 °C (1730 °F). Source: Teledyne VASCO. (b) Hardened from 845 °C (1550 °F). Source: Universal Cyclops Steel Corp.

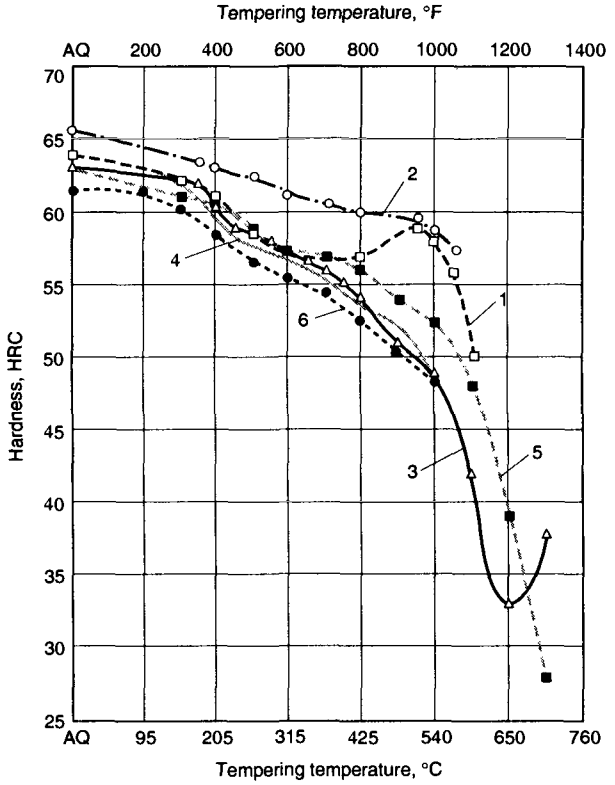

Curve	Type	Composition, %					Hardening temperature		Hardening medium
		C	Mn	Cr	Mo	V	°C	°F	
1	...	0.80	0.70	5.25	1.15	0.25	980	1800	Air
2	...	1.25	0.50	5.25	1.15	1.00	980	1800	Air
3	...	1.00	3.00	1.00	1.00	...	815	1500	Air
4	A4	1.00	2.00	0.90	0.90	...	845	1550	Air
5	...	0.95	2.00	2.20	1.10	...	845	1550	Air
6	A6	0.70	2.00	1.00	1.35	...	845	1550	Air

Fig. 11-7 Effect of tempering temperature on the hardness of air-hardening cold-work die steels after air cooling from indicated temperatures. Curves 1 and 2, Braeburn Alloy Steel Co.; curve 3, Allegheny Ludlum Industries; curve 4, Vulcan-Kidd Steel Division of H.K. Porter Co.; curve 5, Bethlehem Steel Co.; curve 6, Carpenter Steel Co.

11-14 and 11-15. In carbon tool steels the increase in volume due to hardening may be 0.7% of the as-annealed volume, but the volume changes are reduced in tool steels alloyed with chromium. Scott and Gray (Ref 12) measured an expansion of 0.001 in./in. in all directions of a fully hardened steel containing 1% C and 5% Cr, and showed (Fig. 11-14) essentially continuous contraction of the dimensions in a hardened A2 steel with increasing tempering temperature. The expansion expected from the transformation of retained austenite in this case apparently slowed the rate of contraction but was not sufficient to cause significant increases in specimen dimensions. In contrast, Fig. 11-15 shows a sharp expansion in dimensions when two other A-type tools steels are tempered above 205 °C (400 °F), a temperature above which retained austenite transformation typically begins during tempering.

As discussed, retained austenite may be a significant component of the hardened microstructures of A-type steel, and can be controlled by austenitizing, refrigeration, and tempering. For a given hardened structure, transformation of retained austenite during tempering is accomplished at temperatures where hardness may be significantly reduced and where the transformation of the austenite may cause significant dimensional changes (Fig. 11-15). Transformation of retained austenite by refrigeration, therefore, eliminates a source of mechanical and dimensional stability, either during tempering or in service where deformation may cause the transformation of austenite to martensite (Ref 13-16). In fact, the expansion that accompanies subzero transformation of austenite to martensite can be used to salvage tools that are undersize after conventional hardening. Subzero cooling, however, may increase susceptibility to cracking. Also, maximum transformation of austenite, and hence maximum expansion, during subzero cooling is achieved only by continuous cooling; an intermediate tempering treatment stabilizes retained austenite and may render subsequent refrigeration relatively ineffective.

The air-hardening tool steels can be used for all the applications listed for the oil-hardening tool steels at the end of Chapter 10. In comparison to the O-type steels, the higher hardenability of the A-type steels which makes possible air hardening, provides the great advantages of reduced distortion and increased safety during hardening heat treatments.

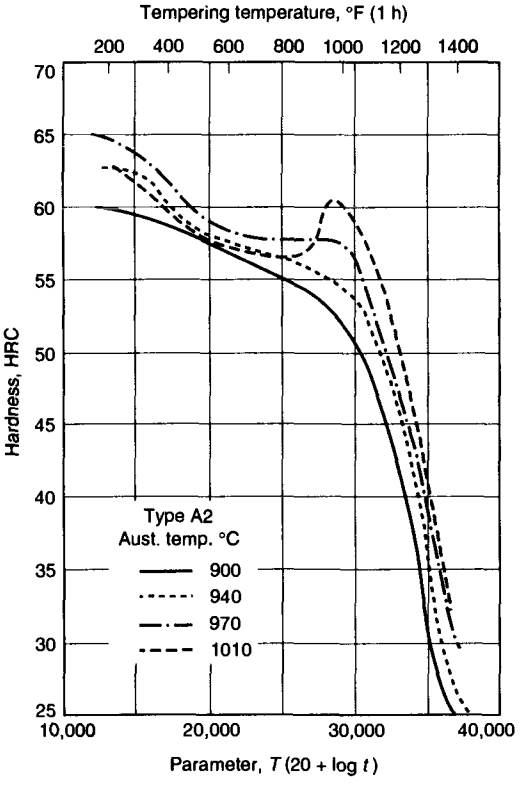

Fig. 11-8 Master tempering curves for A2 tool steel, containing 1.01% C, 0.70% Mn, 5.36% Cr, 10.6% Mo, and 0.26% V, hardened by air cooling from various temperatures. *T* is absolute temperature (°F + 460); *t* is time in hours. Data from Teledyne VASCO

REFERENCES

1. G.A. Roberts and R.A. Cary, *Tool Steels,* 4th ed., American Society for Metals, 1980
2. P. Payson and J. Klein, The Hardening of Tool Steels, *Trans. ASM,* Vol 31, 1943, p 218
3. C.F. Jatczak, Assessment of Hardenability in Deep Hardening Steels, *Hardenability Concepts with Applications to Steel,* D.V. Doane and J.S. Kirkaldy, Ed., TMS-AIME, 1978, p 334–346
4. C.B. Post, Air-Hardening Tool and Die Steels, *Iron Age,* 24 Nov 1949, p 63
5. O. Zmeskal and M. Cohen, The Tempering of Two High Carbon-High Chromium Steels, *Trans. ASM,* Vol 31, 1943, p 380
6. C.F. Jatczak, O.A. Pfouts, and D.J. Girardi, Air-Hardening Graphitic Steel Lowers Tool and Die Costs, *Tool Eng.,* Aug 1959, p 63
7. K.-E. Thelning, *Steel and Its Heat Treatment,* 2nd ed., Butterworths, London, 1984
8. J.H. Hollomon and L.D. Jaffe, Time-Temperature Relations in Tempering Steel, *Trans. AIME,* Vol 162, 1945, p 223
9. G.A. Roberts, A.H. Grobe, and C.F. Moersch, Jr., The Tempering of High-Alloy Tool Steels, *Trans. ASM,* Vol 39, 1947, p 521
10. A. Kulmburg, F. Korntheuer, E. Kaiser, and H.P. Fauland, The Processes during Tempering of Tool Steels, *New Materials, Processes, Experiences for Tooling,* H. Berns, M. Hofmann, L.-A. Norstrom, K. Rasche, and A.-M. Schindler, Ed., MAT SEARCH, Andelfingen, Switzerland, 1992, p 529–536

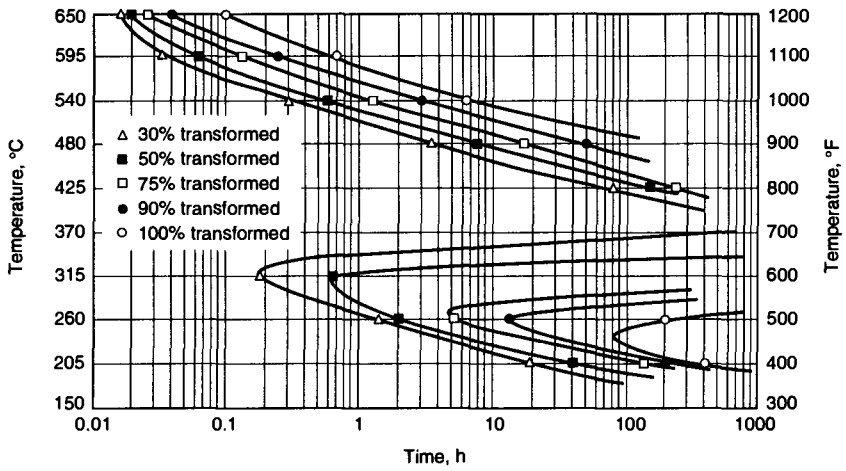

Fig. 11-9 Transformation curves for retained austenite in an air-hardening A2 tool steel containing 1.00% C, 0.61% Mn, 0.17% Si, 5.31% Cr, 0.27% V, and 1.13% Mo, air cooled from 980 °C (1800 °F). Source: Ref 5

11. F.R. Palmer and G.V. Luerssen, *Tool Steel Simplified,* 3rd ed., Carpenter Steel Co., 1960
12. H. Scott and T.H. Gray, Dimensional Changes on Hardening High-Chromium Tool Steels, *Trans. ASM,* Vol 29, 1941, p 503
13. L.E. Gippert and G.M. Butler, Jr., Changes in Size and Toughness of High-Carbon Chromium Steels Due to Subzero Treatments, *Trans. ASM,* Vol 39, 1947, p 549
14. B.S. Lement, *Distortion in Tool Steels,* American Society for Metals, 1959
15. B.L. Averbach, S.A. Kulin, and M. Cohen, The Effect of Plastic Deformation on Solid Reactions, Part II: The Effect of Applied Stress and Strain on the Martensite Transformation, *Cold Working of Metals,* American Society for Metals, 1949
16. G.B. Olson, Transformation Plasticity and the Stability of Plastic Flow, *Deformation, Processing and Structure,* G. Krauss, Ed., American Society for Metals, 1984, p 391–424

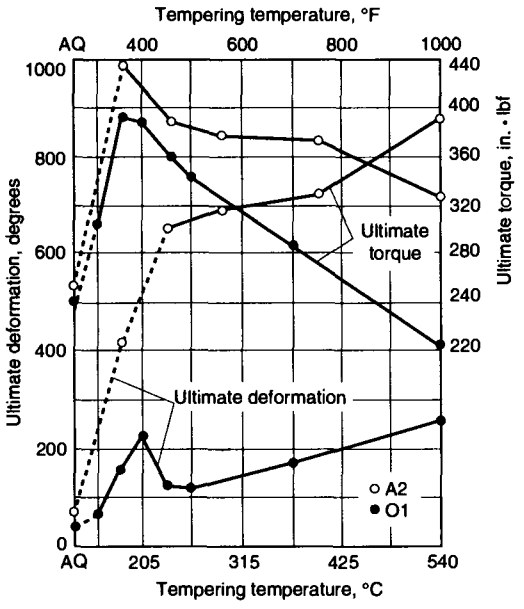

Fig. 11-10 Comparison of static torsion properties of an A2 tool steel and O1 manganese oil-hardening tool steel after quenching to produce maximum hardness in each steel and tempering at the indicated temperatures. Data from Teledyne VASCO

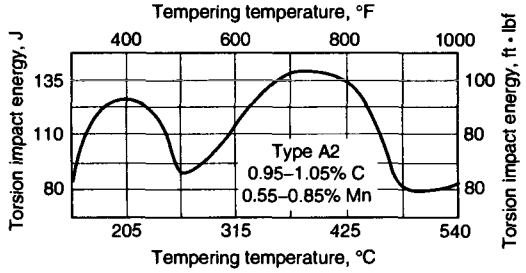

Fig. 11-11 Effect of tempering temperature on the torsion impact energy for an A2 steel air cooled from 970 °C (1775 °F). Source: Ref 11

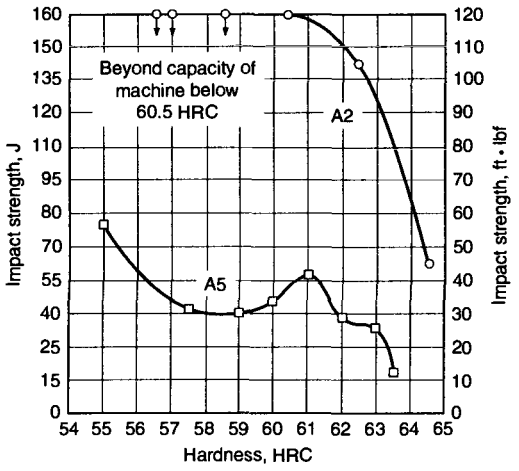

Fig. 11-12 Unnotched Izod impact strength as a function of tempered hardness for A2 steel hardened from 955 °C (1750 °F) and A5 (A4 with 3% Mn) steel hardened from 815 °C (1500 °F). Specimens were tempered for 1 h to indicated hardness levels. Data from Allegheny Ludlum Industries

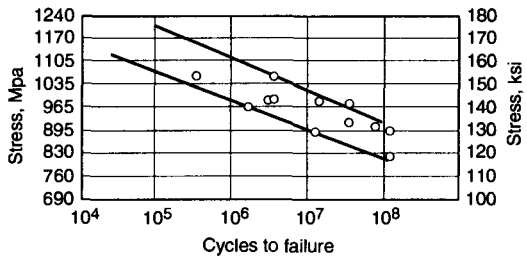

Fig. 11-13 Rotating beam fatigue performance of A6 tool steel hardened by air cooling from 845 °C (1550 °F) and double tempering for 2 h at 175 °C (350 °F). Approximate hardness, 60 HRC. Data from Universal-Cyclops Steel Corp.

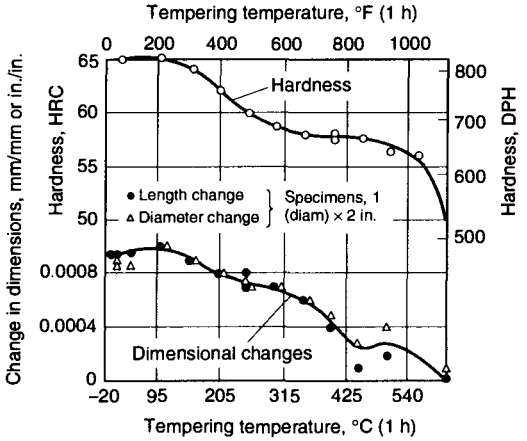

Fig. 11-14 Effect of tempering temperature on the hardness and dimensional changes of A2 tool steel after cooling from 945 °C (1730 °F). The steel contained 1.00% C, 0.65% Mn, 0.30% Si, 5.20% Cr, 1.00% Mo, and 0.25% V. Source: Ref 12

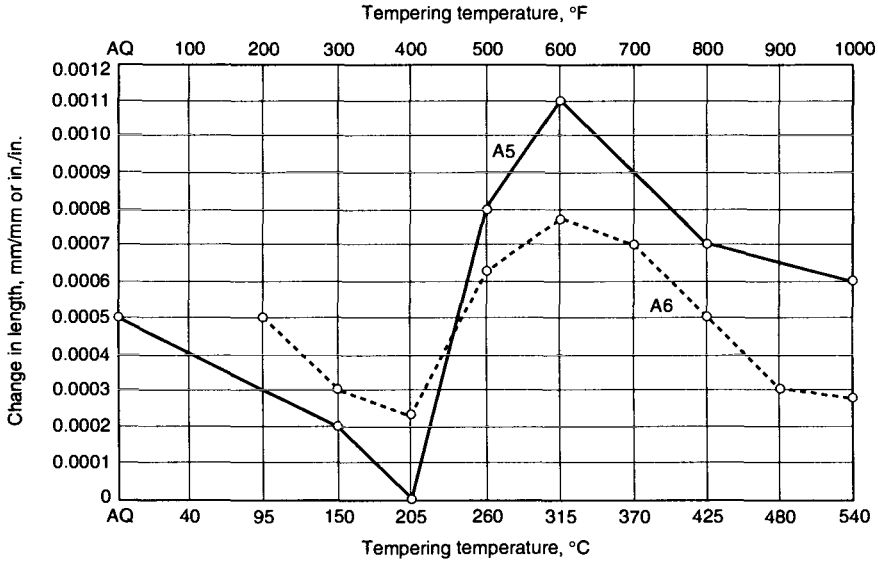

Fig. 11-15 Length change produced on tempering A5 (A4 with 3% Mn) tool steel air cooled from 815 °C (1500 °F) and A6 tool steel air cooled from 845 °C (1550 °F). Data from Allegheny Ludlum Industries and Carpenter Steel Co.

Tool Steels: 5th Edition
George Roberts, George Krauss, Richard Kennedy, p 203-217
DOI:10.1361/toos1998p203

Copyright © 1998 ASM International®
All rights reserved.
www.asminternational.org

CHAPTER 12
High-Carbon, High-Chromium, Cold-Work Tool Steels

The high-carbon, high-chromium tool steels, designated as group D steels in the AISI classification system, are the most highly alloyed cold-work steels. Chromium, at a nominal concentration of 12%, is the major alloying element, but molybdenum, vanadium, nickel, manganese, tungsten, and cobalt may be added in significant amounts to the various grades of D-type steels. Table 12-1 presents the nominal compositions of the currently used D steels, and performance and processing information is listed in Table 12-2. In view of their high carbon and alloy contents, all the D steels are deep hardening. Except for D3 steel, which does not contain molybdenum and contains an addition of tungsten, the D-type steels are hardenable by air cooling from austenitizing temperatures used for hardening and thus have very low susceptibility to distortion and cracking during hardening. Type D3 tool steels are oil quenched.

The D-type tool steels were first developed as possible substitutes for high-speed steels used for cutting tools but were found to have insufficient hot hardness and tended to be too brittle for machining applications (Ref 1–3). Nevertheless, the high carbon and alloy contents produce large volume fractions of high-hardness alloy carbides, which provide excellent wear resistance for cold-work applications. A number of early studies have evaluated and optimized the content of the carbides formed by the strong carbide-forming elements added to the group D steels (Ref 4-9). As discussed in Chapter 4 with respect to alloy design of tool steels, the Fe-Cr-C system and its carbide equilibria have received considerable attention (Ref 10). Type D7, the high-carbon, high-vanadium modification of D2 steel, develops the highest volume fraction of alloy carbides and the best wear resistance of the D-type steels. The high chromium content of the D-type steels is not sufficient to provide the level of corrosion resistance characteristic of stainless steel, because much of the chromium is incorporated in alloy carbides. However, the D-type steels do have excellent oxidation resistance at high temperatures, and the high chromium content of the D steels provides appreciable resistance to staining after tools are hardened and polished.

Microstructure

Solidification of the high-chromium cold-work steels causes considerable segregation of alloying elements. The first crystals to solidify are richest in iron, and carbon, chromium, and other elements are rejected to interdendritic or intercellular liquid regions where the alloy carbides eventually form. Hot

Table 12-1 Composition limits of high-carbon, high-chromium cold-work tool steels

AISI	UNS	Composition(a), %								
Type	No.	C	Mn	Si	Cr	Ni	Mo	W	V	Co
D2	T30402	1.40–1.60	0.60 max	0.60 max	11.00–13.00	0.30 max	0.70–1.20	...	1.10 max	...
D3	T30403	2.00–2.35	0.60 max	0.60 max	11.00–13.50	0.30 max	...	1.00 max	1.00 max	...
D4	T30404	2.05–2.40	0.60 max	0.60 max	11.00–13.00	0.30 max	0.70–1.20	...	1.00 max	...
D5	T30405	1.40–1.60	0.60 max	0.60 max	11.00–13.00	0.30 max	0.70–1.20	...	1.00 max	2.50–3.50
D7	T30407	2.15–2.50	0.60 max	0.60 max	11.50–13.50	0.30 max	0.70–1.20	...	3.80–4.40	...

(a) 0.25% max Cu, 0.03% max P, 0.03% max S. Where specified, sulfur may be increased to 0.06 to 0.15% to improve machinability

work breaks up the segregated solidification structure, but because the alloy carbides are stable during high-temperature hot working, they are elongated by the hot work. Figure 12-1 shows the carbide dispersions in the wrought and annealed microstructure of a high-carbon, high-chromium steel. The longitudinal section, parallel to the hot-rolling direction, shows the elongated shape of the primary carbides, while the section transverse to the rolling direction shows that the cross sections of the primary carbides are roughly equiaxed. Similar to the A-type steels, a dispersion of finer spheroidized secondary carbides also exists, a result of the lower-temperature heat treatment processing of the D-type steels.

Figure 12-2 shows the microstructure of a hardened high-carbon, high-chromium steel. Primary and secondary carbides residual from austenitizing and prior-austenite grain boundaries are clearly visible. Many of the smaller carbides in the annealed structure have dissolved during austenitizing, but the relatively high volume fraction of residual carbides pins austenite grain boundaries, helps to maintain a fine austenitic grain size, and eventually contributes to the wear resistance of the steels. The matrix consists of tempered martensite and retained austenite, which is difficult to etch because of the high chromium content and, even if etched, is too fine to be resolved in the light microscope.

Processing Prior to Hardening

Table 12-2 lists the temperature ranges for forging and annealing of the D-type steels. Care must be taken to limit forging temperatures because the high-carbon, high-chromium steels may be partially molten at 1150 °C (2100 °F). These steels also have exceptionally low heat conductivity and absorb heat very slowly. Therefore, temperature gradients that may cause cracking during heating or cooling can readily develop. In order to minimize cracking on heating for forging or hardening, preheating at 650 to 700 °C (1200 to 1300 °F) is necessary. The D-type steels containing about 1% V have the narrowest forging temperature range, and forging below 870 °C (1600 °F) generally is not recommended. Because of their deep-hardening

Table 12-2 Performance factors and processing information for high-carbon, high-chromium cold-work tool steels

Factor	D2	D3	D4	D5	D7
Major factors					
Wear resistance	8	8	8	8	9
Toughness	2	1	1	2	1
Hot hardness	6	6	6	7	6
Minor factors					
Usual working hardness, HRC	58–64	58–64	58–64	58–63	58–66
Depth of hardening	D	D	D	D	D
Finest grain size at full hardness, Shepherd standard	7½	7½	7½	7½	7½
Surface hardness as-quenched, HRC	61–64	64–66	64–66	61–64	64–68
Core hardness (25 mm, or 1 in., diam round), HRC	61–64	64–66	64–66	61–64	64–68
Manufacturing factors					
Availability	4	4	3	2	2
Cost	3	3	3	3	3
Machinability	3	2	2	3	1
Quenching medium	A	O	A	A	A
Hardening temperature, °C (° F)	980–1025 (1800–1875)	925–980 (1700–1800)	970–1010 (1775–1850)	980–1025 (1800–1875)	1010–1065 (1850–1950)
Dimensional change on hardening	L	L	L	L	L
Safety on hardening	H	M	H	H	H
Susceptibility to decarburization	H	H	H	H	H
Approximate hardness as-rolled or forged, HB	550	400	550	550	550
Annealed hardness, HB	217–255	217–255	217–255	223–255	235–269
Annealing temperature, °C (°F)	870–900 (1600–1650)	870–900 (1600–1650)	870–900 (1600–1650)	870–900 (1600–1650)	870–900 (1600–1650)
Tempering range, °C (°F)	205–540 (400–1000)	205–540 (400–1000)	205–540 (400–1000)	205–540 (400–1000)	150–540 (300–1000)
Forging temperature, °C (°F)	1010–1095 (1850–2000)	1010–1095 (1850–2000)	1010–1095 (1850–2000)	1010–1095 (1850–2000)	1065–1150 (1950–2100)

Note: Ratings are explained in Chapter 2.

characteristics, the D-type steels should be slowly cooled after forging and should not be normalized.

Forgings should always be annealed before machining or hardening. The high-carbon, high-chromium steels are annealed at 870 to 900 °C (1600 to 1650 °F) and slowly cooled at rates not to exceed 28 °C/h (50 °F/h) to 540 °C (1000 °F). Other heat treatments that have been used to anneal D-type steels include cooling from 870 to 900 °C (1600 to 1650 °F) to 540 °C (1000 °F) and reheating to 760 to 790 °C (1400 to 1450 °F), or isothermal annealing at 775 °C (1425 °F) for 4 to 6 h after first heating at 900 °C (1650 °F) for 2 h.

Hardenability and Hardening

The high hardenability and deep-hardening characteristics of the D-type steels are consistent with severe retardation of diffusion-controlled transformations of austenite by high alloy element content. Figure 12-3 (Ref 11) and Fig. 12-4 show IT diagrams for D2 and D4 tool steels. As is typical for highly alloyed tool steels, the pearlitic and bainitic transformations are displaced to long times and have well-separated C-curve kinetics. Thus, in properly austenitized specimens, air cooling is sufficient for the formation of high-hardness martensitic microstructures through relatively heavy sections. For example, D2 steel austenitized at 1010 °C (1850 °F) can be fully hardened to 62 to 64 HRC throughout a 75 by 150 by 250 mm (3 by 6 by 10 in.) block by air cooling. Molybdenum is especially effective in suppressing pearlite formation and is a common addition at nominally 1% for all the D-type steels except D3. Without molybdenum, the transformation of austenite to pearlite accelerates, and, as is the case in heavier sections of D3, oil quenching is required to form martensitic microstructures without softer pearlitic or bainitic constituents.

Hardening consists of three stages: heating to the austenitizing temperature, holding at the austenitizing temperature, and cooling or quenching. As noted, the ability to harden the D-type steels by air cooling provides the great benefit of minimizing distortion and dimensional changes during martensite formation. However, to prevent cracking and fully exploit the dimensional stability of the D-type steels, they must also be heated slowly and uniformly to austenitizing temperatures. Preheating at 650 to 705 °C (1200 to 1300 °F) is highly recommended, especially in view of the low thermal conductivity of these high-chromium tool steels. Tools should be heated in neutral atmospheres to maintain surface carbon contents.

Proper austenitizing of the high-carbon, high-chromium tool steels is critical for the production of hardened microstructures of high hardness. Figure

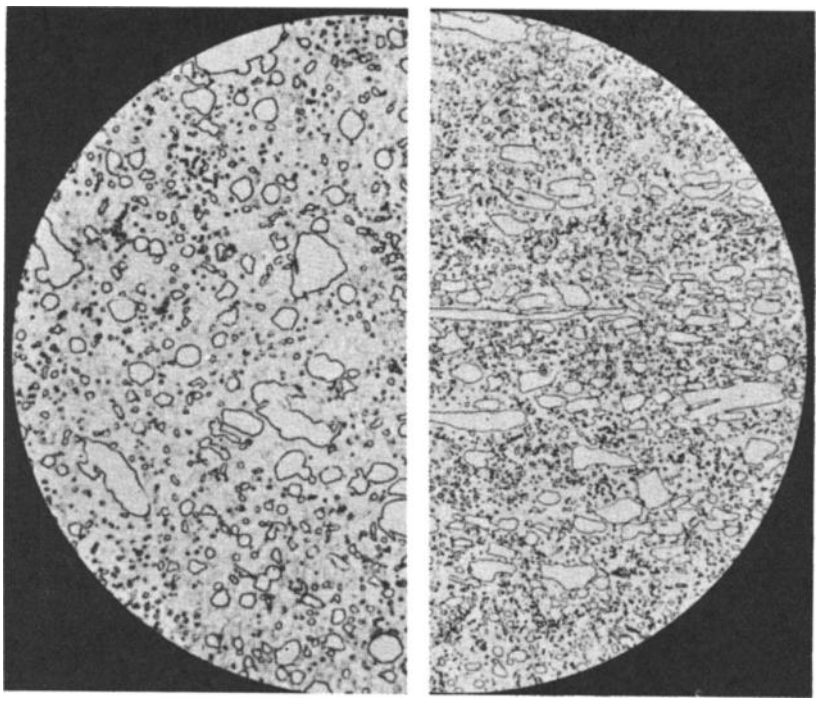

Fig. 12-1 Light micrographs showing annealed microstructure of high-carbon, high-chromium D-type tool steel. (Left) Transverse section, 1000×. (Right) Longitudinal section, 500×

12-5 shows as-quenched hardness as a function of austenitizing temperature for several D-type tool steels quenched in air or oil. Each steel has an optimum temperature range for achieving maximum hardness. This temperature is determined by the optimum solution of the alloy carbides in annealed microstructures, similar to that shown in Fig. 12-1, with increasing austenitizing temperature. At

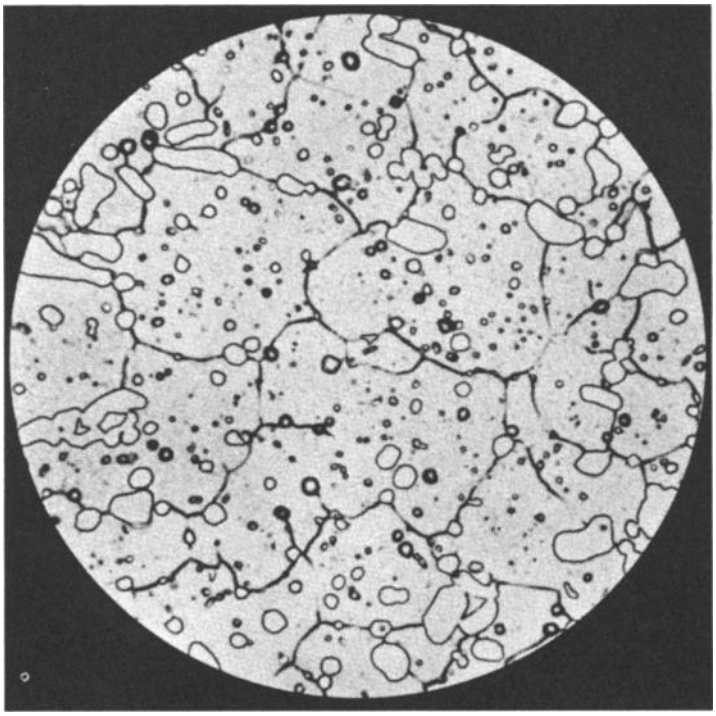

Fig. 12-2 As-quenched, hardened microstructure of high-carbon, high-chromium D-type tool steel. Light micrograph, 100×. Courtesy of R. Patterson, Teledyne VASCO

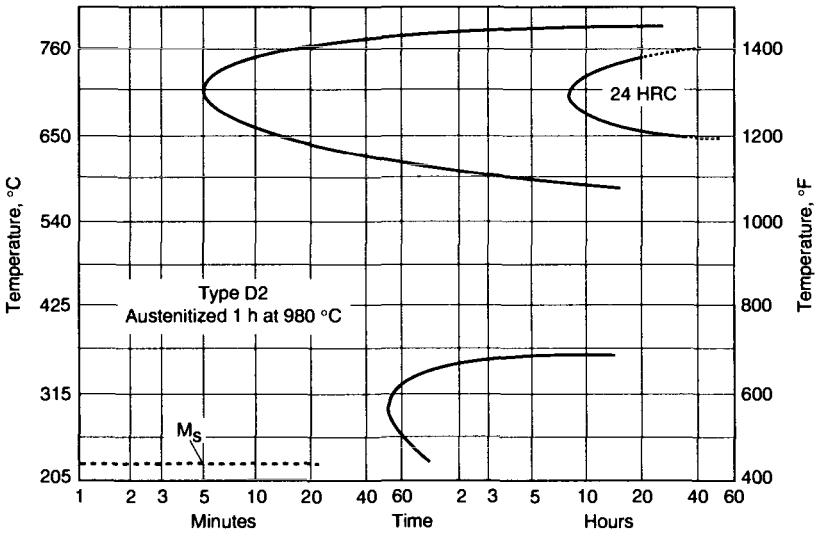

Fig. 12-3 IT diagram for D2 tool steel, containing 1.55% C, 0.27% Mn, 0.45% Si, 11.34% Cr, 0.53% Mo, and 0.24% V, austenitized at 980 °C (1800 °F). Source: Ref 11

low austenitizing temperatures, insufficient carbides have dissolved, the hardenability of the matrix austenite is too low, and nonmartensitic microstructures with low hardness form on cooling. At high austenitizing temperatures, too many carbides dissolve, the alloy content of the matrix austenite is too high, and excessive austenite with low hardness is retained in hardened microstructures.

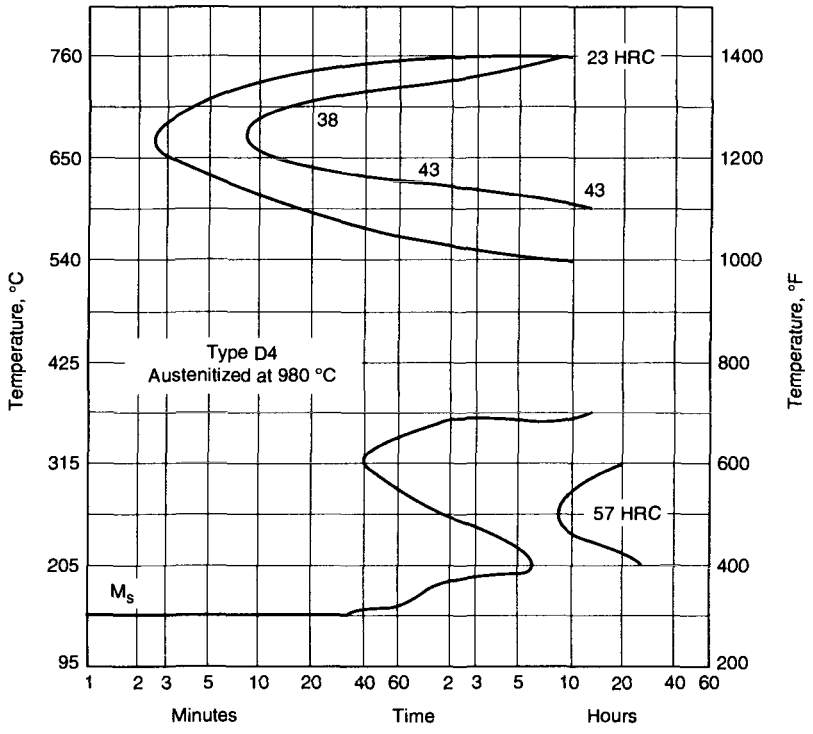

Fig. 12-4 IT diagram for D4 tool steel, containing 2.25% C, 11.50% Cr, 0.80% Mo, and 0.20% V, austenitized at 980 °C (1800 °F). Data from Crucible Steel Co.

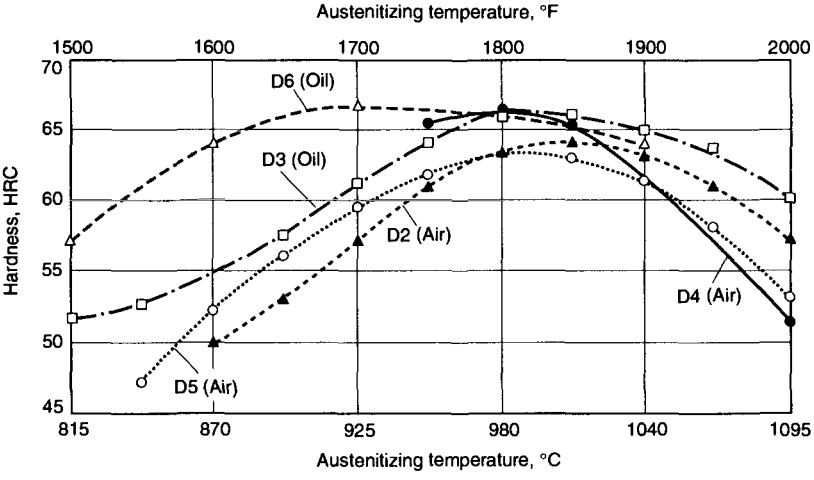

Fig. 12-5 As-quenched hardness as a function of austenitizing temperature for hardening of several D-type steels. Specimens were oil quenched or air cooled as indicated. Data from Teledyne VASCO, Allegheny Ludlum Industries, Columbia Tool Steel Co., Latrobe Steel Co., and Bethlehem Steel Co.

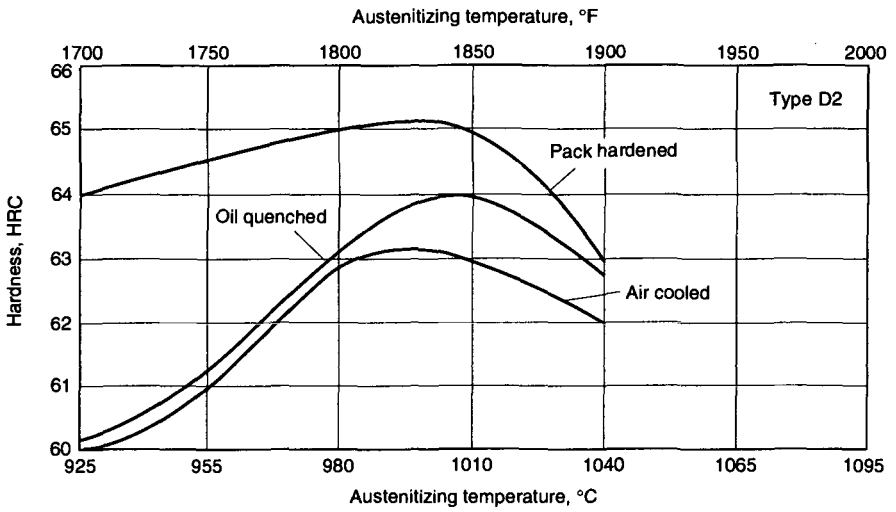

Fig. 12-6 As-quenched hardness as a function of austenitizing temperature and heat treatment conditions for D2 tool steel

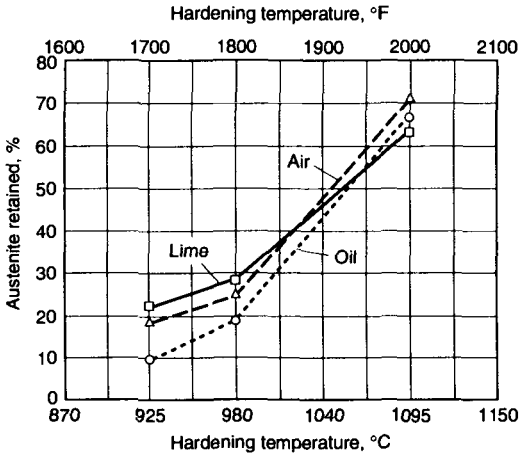

Fig. 12-7 Retained austenite in hardened microstructures of D2 tool steel as a function of austenitizing temperature for hardening and cooling media. Source: Ref 12

Figure 12-6 shows the effect of austenitizing temperature, cooling media, and pack hardening on the as-quenched hardness of D2 tool steel. The pack-hardened specimens were packed in a carburizing compound during austenitizing, and the resultant increased surface carbon content produced the highest martensitic hardness of all the steels after austenitizing at all temperatures. The air-quenched and oil-quenched specimens develop martensitic microstructures with about the same hardness after austenitizing to temperatures of about 980 °C (1800 °F). At higher austenitizing temperatures, as-quenched microstructures in air-cooled specimens, which cool at slower rates than the oil-quenched specimens, are sensitive to stabilization of the martensitic transformation. As a result, the air-cooled specimens retain more austenite and show lower as-quenched hardness than do the oil-quenched specimens.

Figure 12-7 shows the amount of austenite retained in hardened microstructures as a function of austenitizing temperature and cooling media in a D2 tool steel (Ref 12). Specimens cooled at the slower rates in lime and air show higher retained austenite, consistent with the stabilization of martensitic transformation by slower cooling. As noted earlier, the considerable increase in retained austenite in specimens of D2 tool steel cooled from high austenitizing temperatures is a result of alloy carbide dissolution and the enrichment of austenite with carbon, chromium, and other carbide-forming elements. The highly alloyed austenite not only has very high hardenability, but also is highly stable with respect to martensite formation. Table 12-3 lists the amounts of the various microstructural components in D2 tool steel oil quenched from various temperatures. As the volume fraction of carbides decreases with increasing temperature, martensite volume fraction falls steeply, and the microstructure is dominated by retained austenite.

Austenitic grain size of D-type tool steels does not coarsen very rapidly at typical hardening temperatures. This beneficial characteristic is a result of the considerable volume fraction of coarse carbides that do not dissolve during austenitizing. The carbides pin grain boundaries and maintain a fine, relatively uniform grain size according to Eq 5-2 (see Chapter 5). However, if the high-chromium steels are subjected to two austenitizing and hardening cycles, the possibility of discontinuous austenite grain coarsening exists.

Figure 12-8 shows austenitic grain size as a function of austenitizing temperature for D2 tool steel

subjected to single and double austenitizing treatments. High intercept grain size numbers indicate fine grain sizes. A second hardening treatment may (1) refine austenitic grain size developed in the second austenitizing treatment, if the initial austenitizing temperature is held at or below 980 °C (1800 °F) or (2) severely coarsen the austenitic grain size if the first austenitizing treatment is above 980 °C (1800 °F). Several principles explain the various grain growth phenomena. First, a double cycle of hardening requires the nucleation of a very fine austenitic grain structure during austenitizing of the tempered martensite produced in the first cycle. Second, whether or not the austenite grains coarsen is a function of the size and volume fraction of the carbide particles that serve to retard grain-boundary motion. The pinning particles present during the second austenitizing tend to be finer than those typically present in an annealed structure at the start of a first hardening cycle. Although the finer particles initially retard grain growth very effectively, they also dissolve more readily at higher temperature, therefore setting the stage for discontinuous grain coarsening at higher austenitizing temperatures.

The above work regarding the effect of rehardening treatments was driven by the severe grain coarsening observed in rehardened high-speed tool steels, which are typically austenitized at very high temperatures (Ref 14, 15). The high-carbon, high-chromium D-type steels are not austenitized at the same high temperatures used for high-speed tool steels, and therefore, the potential for severe grain coarsening in the D-type steels serves primarily as a reminder to maintain strict upper limits on austenitizing temperature if rehardening should be required.

Table 12-3 Amounts of microconstituents in D2 tool steel as a function of austenitizing temperature

Austenitizing temperature(a)		Volume, %		
°C	°F	Martensite	Austenite	Carbide
1040	1900	79	7	14
1065	1950	65	22	13
1095	2000	33	55	12
1120	2050	5	85	10
1135	2075	2	88	10
1150	2100	2	88	10

(a) Specimens austenitized 30 min at temperature and quenched into oil. Composition: 1.60% C, 11.95% Cr, 0.33% Mn, 0.32% Si, 0.79% Mo, 0.25% V, 0.18% P, and 0.010% S. Source: Ref 13

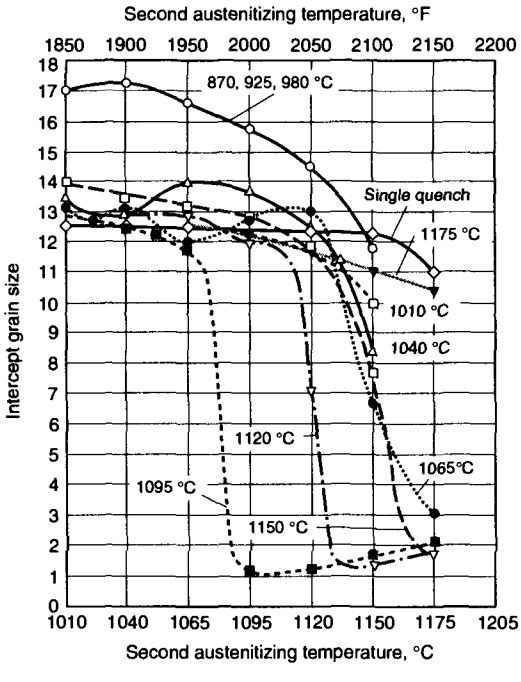

Fig. 12-8 Austenitic grain size as a function of second austenitizing temperature of D2 steel after quenching from first austenitizing temperatures as indicated. The austenite grain size as a function of austenitizing temperature for specimens "single quenched" from a single austenitizing treatment are also shown. Data from Teledyne VASCO

Tempering

Figures 12-9 and 12-10 show hardness changes as a function of tempering temperature, and Fig. 12-11 and 12-12 (Ref 16) show hardness changes as a function of a time-temperature tempering parameter, as described in Chapter 11, for various D-type steels in various heat-treated conditions. All the high-carbon, high-chromium cold-work steels show a strong resistance to softening during tempering, and in some heat-treated conditions show a pronounced secondary hardening peak. Steels designed to simulate the matrix compositions of D-type steels without carbides (i.e., matrix steels) indicate that the tempering resistance of the matrix is due to the stability of M_3C carbides rather than to the precipitation of chromium-rich M_7C_3 carbides (Ref 4, 17–21).

The strongest response to secondary hardening is in specimens that have been austenitized at higher temperatures where more carbon and alloying elements have been taken into solution and thus are available for precipitation at high tempering temperatures. However, as discussed above, high-temperature austenitizing also causes large amounts of austenite to be retained in as-quenched structures. The retained austenite significantly lowers the hardness of as-quenched specimens, and since the retained austenite in the highly alloyed D-type steels is quite stable, hardness remains low

until the secondary hardening temperature range is reached.

Figure 12-13 shows curves for the transformation of retained austenite in a D2 steel during tempering. In contrast to the A-type cold-work steels with lower chromium contents, no appreciable transformation of retained austenite occurs during low-temperature tempering in the temperature range of 260 to 315 °C (500 to 600 °F). At secondary hardening temperatures, in addition to isothermal transformation of retained austenite to mixtures of ferrite and carbides, precipitation of alloy carbides in the austenite may further reduce the stability of untransformed austenite and make possible martensite or bainite formation on cooling from the tempering temperature to room temperature.

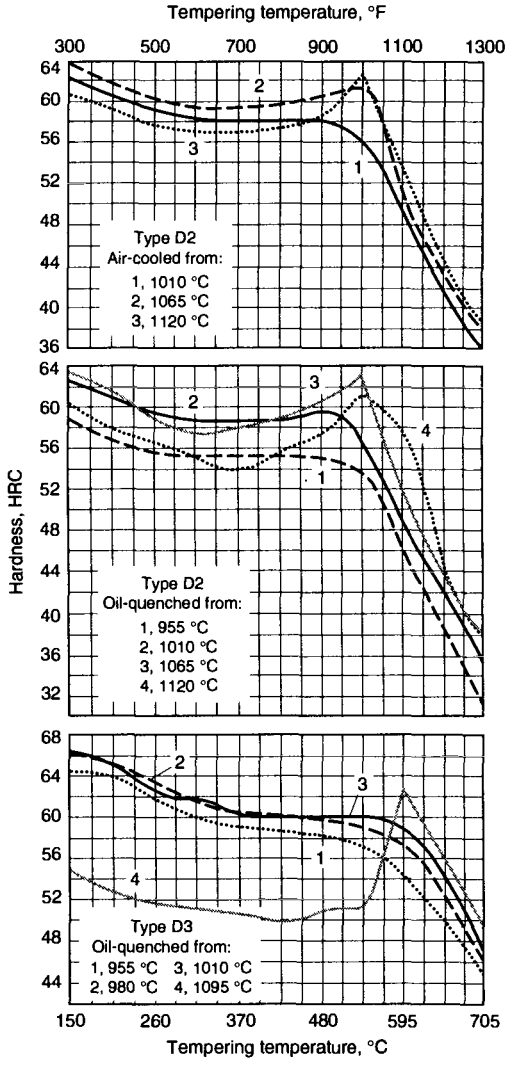

Fig. 12-9 Hardness as a function of tempering temperature for D2 and D3 tool steels subjected to various austenitizing and cooling conditions. Source: Ref 3

The toughness and fracture resistance of hardened high-carbon, high-chromium cold-work tool steels is low. In the as-quenched condition, low toughness is caused by a microstructure consisting of high-carbon martensite, which strain hardens at very high rates, and a high density of coarse, undissolved carbides, which serve as fracture initiation sites. Residual stresses developed on quenching will also contribute to low fracture resistance but will be minimized by air cooling. Tempering will lower residual stresses and increase toughness and the plasticity of the martensite. However, tempering causes the transformation of retained austenite, which introduces additional carbides at various stages of tempering of the D-type steels. This may increase sensitivity to fracture.

Figures 12-14 to 12-19 show various evaluations of the toughness, ductility, and mechanical properties of D-type steels. Toughness, under conditions of torsional loading or unnotched impact bending (Ref 22), is generally adequate and improved by tempering, depending on alloy content and heat treatment conditions. Toughness would be substantially reduced in impact bending tests with notches, which cause substantial stress concentration and high triaxial stresses at their roots. Tempering at temperatures that cause the decomposition of retained austenite are associated with minima in toughness, the phenomenon referred to as tempered martensite embrittlement in medium-carbon steels. As best shown in Fig. 12-14, the high alloy content of the D-type steels may introduce several of these minima and, compared to lower alloy steels, cause the minima to occur after tempering at higher temperatures. Figures 12-14, 12-17, and 12-18 show that the toughness minima due to retained austenite transformation occur after tempering at about 480 °C (900 °F).

In most comparisons of toughness and ductility of the high-carbon D3 steel versus the lower-carbon D2 steels (Fig. 12-15 to 12-17), the toughness of the D2 steel is better, consistent with somewhat lower carbon contents of its martensite and lower densities of retained alloy carbides.

The compressive strengths of hardened D-type cold-work steels tempered at low temperatures are high and generally correlate directly with hardness, as shown in Fig. 12-19. Table 12-4 lists compressive strengths measured for several D-type steels quenched to maximum hardness and tempered at low temperatures. The mechanical properties of the D-type tool steels, because of the elongation of the primary alloy carbides by hot work as demonstrated in Fig. 12-1, are anisotropic (Ref 23). Strength and ductility as measured by tension, compression, and bend tests are a maximum in the direction parallel to the rolling direction and a minimum in the direction transverse to the rolling direction.

The dimensional changes resulting from the hardening of the high-carbon, high-chromium tool steels are very small (Ref 24–26). For example, Scott and Gray (Ref 25) have indicated an expansion of only 0.1% of the annealed volume after hardening an 11% Cr alloy by air cooling. Hardening temperatures on the high side of the recommended range, which result in considerable retained austenite, may in fact cause overall specimen shrinkage.

The dimensional changes on hardening D-type steels may be markedly dependent on direction, with greater extension in the rolling direction than in the transverse direction. Again, this directionality is related to the primary alloy carbide distribution as related to solidification and hot work. Figure 12-20 shows longitudinal and transverse dimensional changes as a function of forging reduction of a D3 steel (Ref 27). Air cooling of the D-type steels minimizes distortion, but considerable distortion may develop if temperature gradients develop during heat treatment (Ref 28). Sachs and Jay (Ref 29) have investigated the effects of various forging techniques on carbide particle size, dendritic cell size, and distor-

Table 12-4 Compressive strengths of high-carbon, high-chromium steels after hardening to maximum hardness and tempering at temperatures noted

Steel	Tempering temperature, °C	Tempering temperature, °F	Hardness, HRC	Ultimate compressive, MPa	Ultimate compressive, ksi
D2	175	350	61.5	3841	557
	230	450	59.5	3641	528
D3	175	350	63.5	3634	527
	230	450	61.5	3290	477

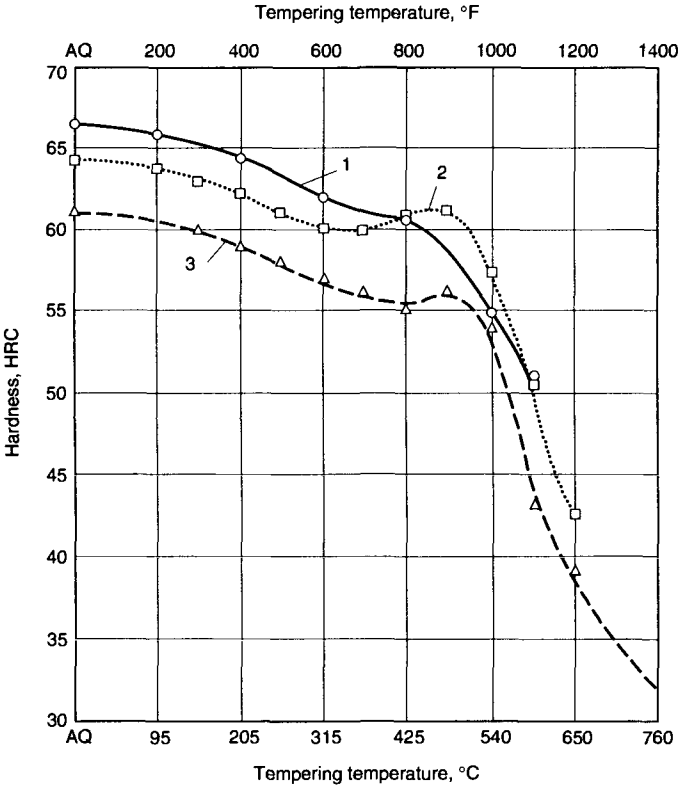

Curve	Type	Composition, % C	Si	Cr	W	Mo	V	Ni	Co	Hardening Temperature, °C	°F	Hardening Medium
1	...	2.10	0.85	11.50	0.75	...	...	...	...	925	1700	Oil
2	D5	1.50	0.50	12.25	...	0.85	...	...	3.10	1010	1850	Air
3	...	.085	...	11.50	...	0.45	0.30	1.00	...	1010	1850	Air

Fig. 12-10 Hardness as a function of tempering temperature for D-type tool steels hardened as shown. Data from Columbia Tool Steel Co., Latrobe Steel Co., and Bethlehem Steel Co.

tion of D3 steel and found that variations in forging techniques, including upset forging, have relatively little effect on distortion.

Figure 12-21 shows the effects of tempering on dimensional changes of several D-type steels. Consistent with the microstructural changes that evolve

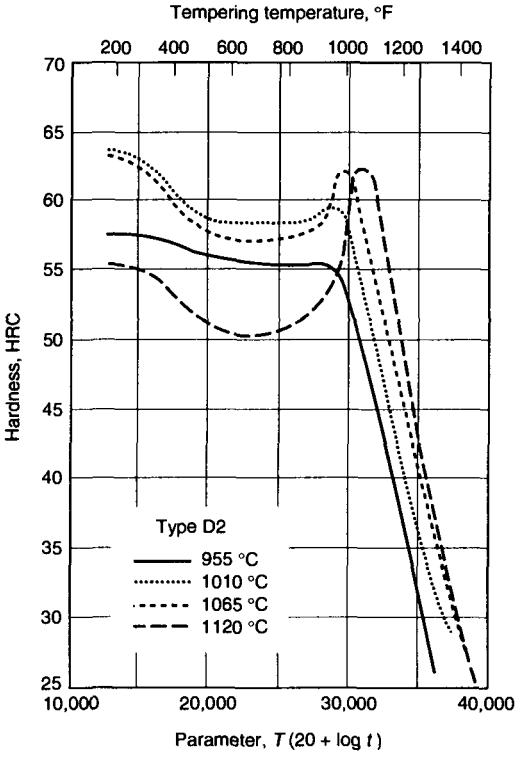

Fig. 12-11 Hardness as a function of temperature-time tempering parameter for D2 steels austenitized as shown. T is absolute temperature (°F + 460); t is time in hours. Data from Teledyne VASCO

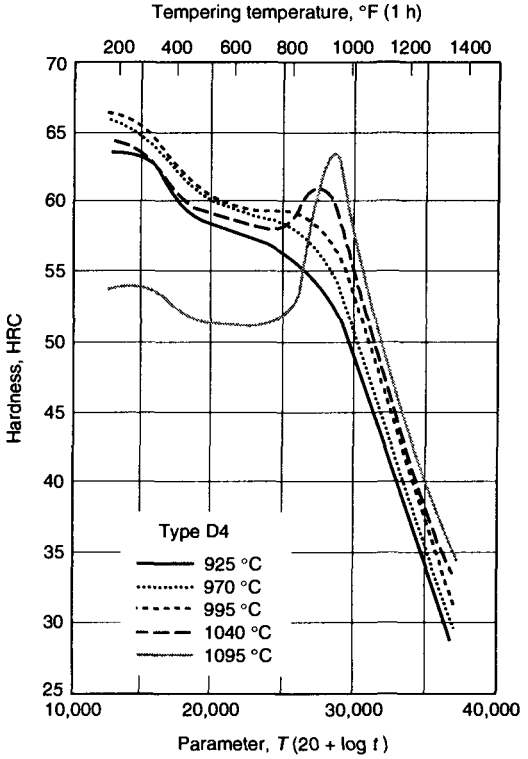

Fig. 12-12 Hardness as a function of temperature-time tempering parameter for D4 steels austenitized as shown. T is absolute temperature (°F + 460); t is time in hours. Data from Teledyne VASCO

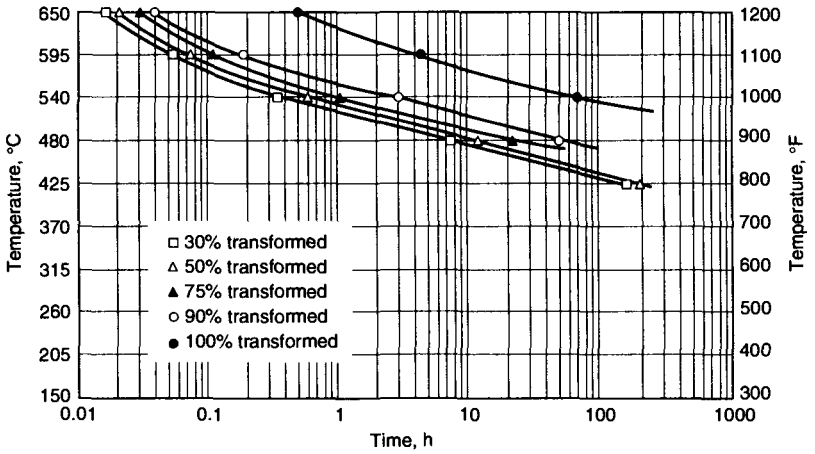

Fig. 12-13 Transformation curves for austenite retained in hardened D2 tool steel. Source: Ref 12

with increasing tempering, an initial contraction occurs as the tetragonality of the martensite crystal structure decreases in the first stage of tempering. The expansion due to the transformation of retained austenite in the second stage of tempering begins at about 425 °C (800 °F). The latter tempering temperature is significantly higher than that which initiates austenite transformation and expansion in tool steels with lower alloy content. The intensity of the expansion depends on alloying and hardening

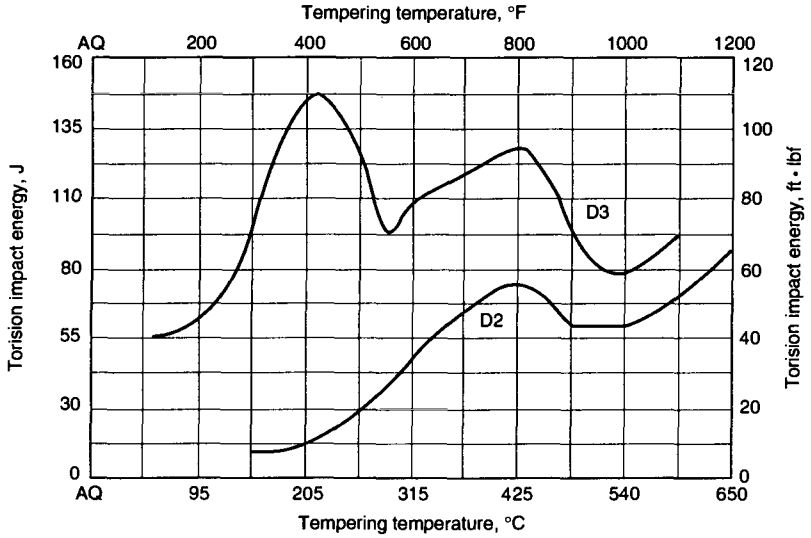

Type	Composition, %					Quench temperature		Quench medium
	C	Cr	Mo	V	Ni	°C	°F	
D2	1.60	13.00	0.75	0.27	...	980	1800	Air
D3	2.10	12.50	...	...	0.50	970	1775	Oil

Fig. 12-14 Torsional impact energy absorbed by D2 and D3 tool steel specimens as a function of tempering temperature. Absolute magnitudes of impact energy are not comparable because of testing variations. Curve for D2, Bethlehem Steel Co.; curve for D3, Ref 22

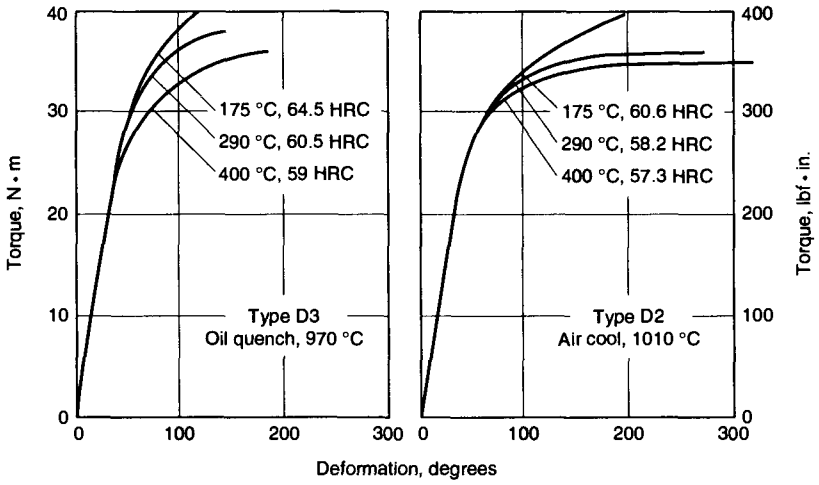

Fig. 12-15 Comparison of ductility in static torsion tests of D3 (left) and D2 (right) tool steels quenched to maximum hardness and tempered at the three temperatures shown. Data from Teledyne VASCO

temperature, and for the data shown in Fig. 12-21, is highest for a D5 steel containing cobalt and hardened at a relatively high temperature.

Refrigeration treatments can be applied to high-carbon, high-chromium tool steels to transform retained austenite and thereby increase hardness, im-

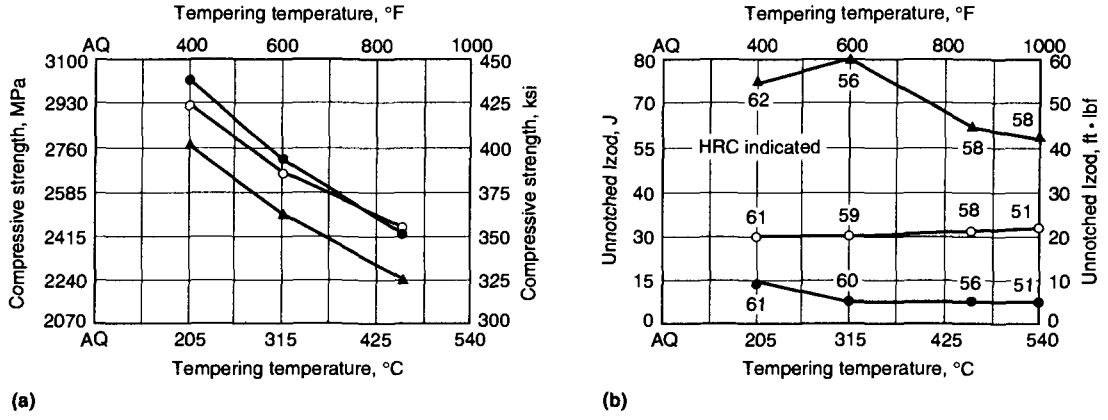

Symbol	Type	Composition, % C	Cr	Mo	V	Austenitizing temperature °C	°F	Quench medium
▲	D2	1.55	12.0	0.80	0.25	1010	1850	Air
○	D3	2.10	12.0	...	1.0	980	1800	Oil
●	D3	2.40	11.5	...	...	955	1750	Oil

Fig. 12-16 Compressive strength (a) and energy absorbed in unnotched Izod specimens (b) as a function of tempering. Source: Ref 1

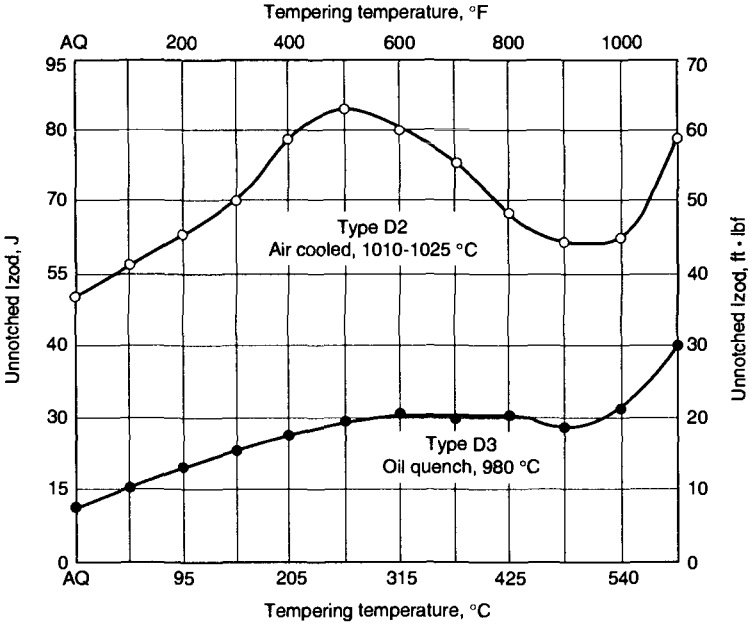

Fig. 12-17 Energy absorbed by unnotched Izod D2 and D3 tool steel specimens as a function of tempering temperature. Data from Jessop Steel Co., Allegheny Ludlum Industries, and Teledyne Firth-Sterling Steel Co.

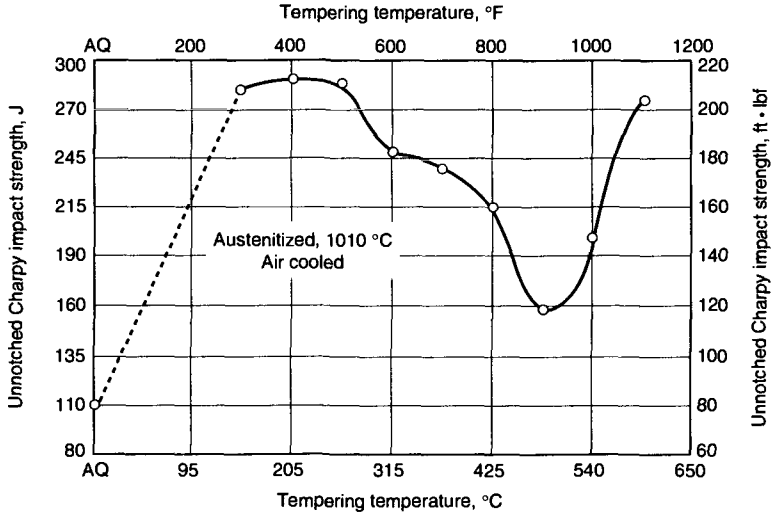

Fig. 12-18 Unnotched Charpy impact energy absorbed by hardened high-carbon, high-chromium tool steel specimens (0.85% C, 11.50% Cr, 1.00% Ni, 0.45% Mo, and 0.30% V) as a function of tempering temperature. Data from Bethlehem Steel Co.

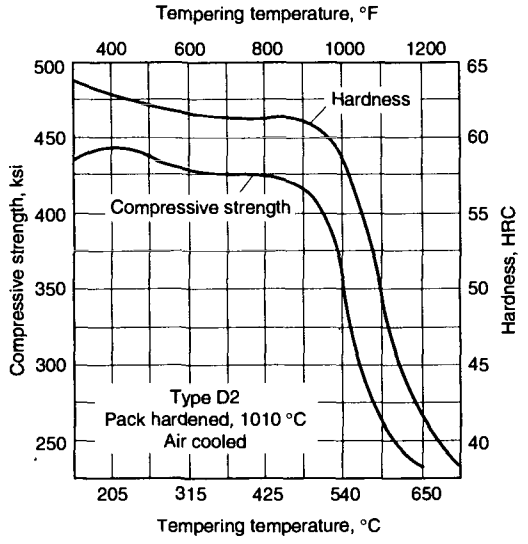

Fig. 12-19 Effect of tempering temperature on the hardness and compressive strength of a D2 tool steel hardened as shown. Data from Bethlehem Steel Co.

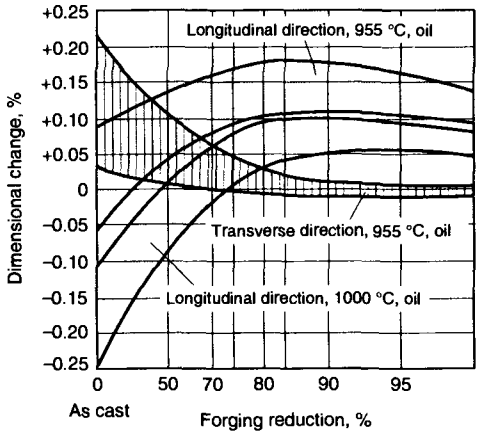

Fig. 12-20 Dimensional changes during hardening of D3 tool steel as a function of forging reduction. Data were obtained from 20 mm (0.8 in.) cylindrical specimens from square and round bars subjected to various amounts of forging reduction. *Source:* Ref 27

prove dimensional stability, or salvage undersize parts (Ref 30-32). For extreme dimensional stability at room temperature, the following heat-treating cycles after hardening have proved beneficial for D2 tool steel (Ref 31):

Cycle 1

1. Cool continuously to –196 °C (–321 °F).
2. Hold 1 h at 345 °C (650 °F); oil quench.

Hardness: 63 HRC

Cycle 2

1. Cool continuously to –196 °C (–321 °F).
2. Hold 1 h at 510 °C (950 °F); oil quench.
3. Repeat steps 1 and 2 three times.
4. Hold 1 h at 230 °C (450 °F); air cool.

Hardness: 59.5 HRC

Selection and Applications

The high-carbon, high-chromium D-type steels are divided into two major groups according to carbon content. The high-carbon types—D3, D4, and D7—have the greatest wear resistance but the lowest toughness. The lower carbon types—D2 and D5—have reasonably high wear resistance and are slightly tougher than the D types containing 2% or more carbon. Type D5 has slightly better hot hardness than D2 but is otherwise very similar, and the two steels can be used interchangeably.

If long production runs are expected, one of the higher-carbon steels may be selected in preference to D2. The higher-carbon types, however, are more difficult to machine. If the greater dimensional changes accompanying oil quenching can be tolerated, the oil-hardening D3 steel offers the advantage of better surface condition since a combination of lower hardening temperature and liquid quenching should result in minimum surface decarburization and scaling.

The D-type steels are widely used for blanking and cold-forming punches and dies. Type D2 is sometimes used for hot trimming of forgings, but primarily the high-carbon, high-chromium steels are used for cold-work applications. Typical applications include:

Blanking dies	Spinning tools
Burnishing tools	Slitting cutters
Coining dies	Knurls
Deep-drawing dies	Broaches
Wire-drawing dies	Cold-extrusion dies
Forming dies	Wear plates
Gages	Mandrels
Thread-rolling dies	Crimping dies
Lathe centers	Hot-swaging dies
Punches	Lamination dies
Forming and bending rolls	Cutlery
Trimming dies	Shear blades

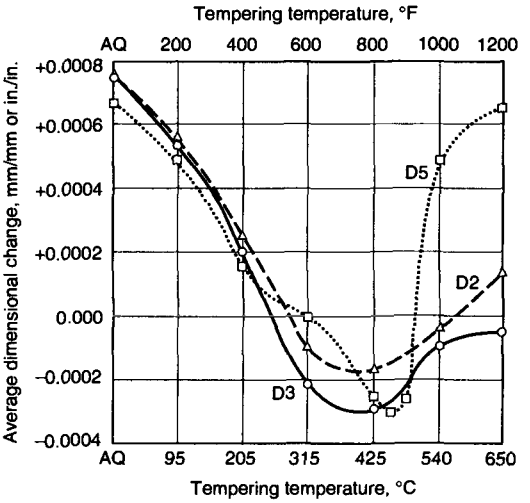

Type	Hardening temperature °C	Hardening temperature °F	Hardening medium
D2	...	...	...
D3	955	1750	Oil
D5	1010	1850	Air

Fig. 12-21 Average dimensional changes of D2, D3, and D5 tool steels after hardening and as a function of tempering temperature. Values reported are the average change of three principal dimensions in a block 25 by 50 by 150 mm (1 by 2 by 6 in.) in size. Data from Latrobe Steel Co.

REFERENCES

1. W.H. Wills, Practical Observations on High-Carbon High-Chromium Tool Steels, *Trans. ASM*, Vol 23, 1935, p 469
2. W.H. Wills, Further Study of High-Carbon High-Chromium Tool Steels, *Trans. ASM*, Vol 25, 1937, p 1013
3. J.P. Gill, High-Carbon High-Chromium Steels, *Trans. ASST*, Vol 15, 1929, p 387
4. K. Kuo, Carbides in Chromium, Molybdenum and Tungsten Steels, *J. Iron Steel Inst.*, Vol 173, 1953, p 363
5. T. Sato, T. Nishzawa, and K. Murai, Study on Carbides in Commercial Special Steels by Electrolytic Isolation, Part 5: On Carbides in Several Cold Work Steels, *Tetsu-to-Hagané (J. Iron Steel Inst. Jpn.)*, Vol 42, 1956, p 565
6. L.P. Tarasov, The Microhardness of Carbides in Tool Steels, *Met. Prog.*, 1948, p 846
7. K. Bungardt, E. Kunze, and E. Horn, Investigation of the Structure of the Iron-Chromium-Carbon System, *Arch. Eisenhüttenwes.*, Vol 29, 1958, p 193
8. N. Yamanaka and K. Kusaka, Influence of Vanadium and Molybdenum on the Properties of Air-Hardening Die Steel Containing 1.5 pct Carbon and 12.0 pct Chromium, *Tetsu-to-Hagané (J. Iron Steel Inst. Jpn.)*, Vol 41, 1955, p 613
9. S. Koshiba and S. Nagashima, Effect of Tungsten on the High-Carbon High-Chromium Die Steel, *Tetsu-to-Hagane (J. Iron Steel Inst. Jpn.)*, Vol 39, 1953, p 119
10. G.V. Raynor and V.G. Rivlin, *Phase Equilibria in Iron Ternary Systems*, Institute of Metals, London, 1988
11. P. Payson and J. Klein, The Hardening of Tool Steels, *Trans. ASM*, Vol 31, 1943, p 218
12. O. Zmeskal and M. Cohen, The Tempering of Two High-Carbon High-Chromium Steels, *Trans. ASM*, Vol 31, 1943, p 380
13. B.L. Averbach, S.A. Kulin, and M. Cohen, The Effect of Plastic Deformation on Solid Reactions, Part II: The Effect of Applied Stress on the Martensite Reaction, *Cold Working of Metals*, American Society for Metals, 1949
14. E. Kula and M. Cohen, Grain Growth in High Speed Steel, *Trans. ASM*, Vol 46, 1954, p 727-758

15. A.H. Grobe, G.A. Roberts, and D.S. Chambers, Discontinuous Grain Growth in High Speed Steel, *Trans. ASM,* Vol 46, 1954, p 759-788
16. G.A. Roberts, A.H. Grobe, and C.F. Moersch, Jr., The Tempering of High Alloy Tool Steels, *Trans. ASM,* Vol 39, 1947, p 521
17. T. Sato, Y. Honda, and T. Nishizawa, Study on Carbides in Practical Steels by Electrolytic Isolation, Part II: On Carbides in High-Carbon High-Chromium Die Steel, *Tetsu-to-Hagané (J. Iron Steel Inst. Jpn.),* Vol 42, 1956, p 1118
18. W. Crafts and J.L. Lamont, Secondary Hardening of Tempered Martensitic Alloy Steel, *Trans. AIME,* Vol 180, 1949, p 471
19. S.Z. Bokshtein, Carbide Phase during Tempering of Alloy Steels, *Zh. Tekh. Fiz.,* Vol 19 (No. 5), 1949, p 532
20. R.W. Balluffi, M. Cohen, and B.L. Averbach, The Tempering of Chromium Steels, *Trans. ASM,* Vol 43, 1951, p 497
21. E.C. Roberts, N.J. Grant, and M. Cohen, Creep-Tempering Relationships in Hardened 4.5 pct Chromium Steels, *Trans. ASM,* Vol 47, 1955, p 650
22. F.R. Palmer and G.V. Luerssen, *Tool Steel Simplified,* 3rd ed., Carpenter Steel Co., 1960
23. L.J. Klinger, C.C. Choe, and G. Sachs, Flow and Fracture Characteristics of a Die Steel at High Hardness Levels, *Trans. AIME,* Vol 185, 1949, p 927
24. E. Ameen, Dimensional Changes of Tool Steels during Quenching and Tempering, *Trans. ASM,* Vol 28, 1940, p 472
25. H. Scott and T.H. Gray, Dimensional Changes on Hardening High-Chromium Tool Steels, *Trans. ASM,* Vol 29, 1941, p 503
26. G.M. Butler, Study of Dimensional and Other Changes in Various Die Steels due to Heat Treatment, *Trans. ASM,* Vol 30, 1942, p 191
27. J. Frehser, Anisotropic Dimensional Changes on Heating Ledeburitic Chromium Tool Steels, *Arch. Eisenhüttenwes.,* Vol 24, 1953, p 483
28. K. Sachs, A Study of the Distortion of High-Carbon High-Chromium Die Steels, *J. Iron Steel Inst.,* Vol 189, 1958, p 216
29. K. Sachs and G.T.F. Jay, The Distortion of High-Carbon High-Chromium Die Steels, *J. Iron Steel Inst.,* Vol 191, 1959, p 353
30. L.E. Gippert and G.M. Butler, Jr., Changes in Size and Toughness of High-Carbon High-Chromium Steels due to Subzero Treatments, *Trans. ASM,* Vol 39, 1947, p 549
31. B.S. Lement, B.L. Averbach, and M. Cohen, The Dimensional Stability of Steel, Part IV: Tool Steels, *Trans. ASM,* Vol 41, 1949, p 1061
32. B.S. Lement, *Distortion in Tool Steels, American Society for Metals, 1959*

Tool Steels: 5th Edition
George Roberts, George Krauss, Richard Kennedy, p 219-250
DOI:10.1361/toos1998p219

Copyright © 1998 ASM International®
All rights reserved.
www.asminternational.org

CHAPTER 13
Hot-Work Tool Steels

Steels for hot-work applications, designated as group H steels in the AISI classification system, have in common the capacity to resist softening during long or repeated exposures to high temperatures needed to hot work or die cast other materials. The H-type steels are subdivided into three classes that sort according to the alloying approach used to impart high hot hardness: chromium hot-work steels, which contain nominally 5% Cr and significant amounts of other elements including silicon, molybdenum, and vanadium; tungsten hot-work steels; and molybdenum hot-work steels. Multiple alloying elements are also added to the tungsten and molybdenum hot-work steels, and the performance of these steels is generally somewhat better than the chromium steels. Table 13-1 lists the compositions of the three groups of hot-work steels, and Table 13-2 ranks performance and processing information.

All tool and die steels for hot-work applications should have these general characteristics:

- *Resistance to deformation at working temperatures.* This characteristic more than any other distinguishes hot-work tool steels from other tool steels, which may have higher heat-treated room-temperature hardness, and thus provide better performance for cold-work applications, but which soften rapidly at hot-working temperatures.
- *Resistance to shock.* Good resistance to mechanical and thermal shock and good notch toughness are required to prevent cracking and catastrophic fail-

Table 13-1 Composition limits for hot-work tool steels

AISI	UNS	Composition(a), %								
Type	No.	C	Mn	Si	Cr	Ni	Mo	W	V	Co
Chromium hot-work steels										
H10	T20810	0.35–0.45	0.25–0.70	0.80–1.20	3.00–3.75	0.30 max	2.00–3.00	...	0.25–0.75	...
H11	T20811	0.33–0.43	0.20–0.50	0.80–1.20	4.75–5.50	0.30 max	1.10–1.60	...	0.30–0.60	...
H12	T20812	0.30–0.40	0.20–0.50	0.80–1.20	4.75–5.50	0.30 max	1.25–1.75	1.00–1.70	0.50 max	...
H13	T20813	0.32–0.45	0.20–0.50	0.80–1.20	4.75–5.50	0.30 max	1.10–1.75	...	0.80–1.20	...
H14	T20814	0.35–0.45	0.20–0.50	0.80–1.20	4.75–5.50	0.30 max	...	4.00–5.25	...	...
H19	T20819	0.35–0.45	0.20–0.50	0.20–0.50	4.00–4.75	0.30 max	0.30–0.55	3.75–4.50	1.75–2.20	4.00–4.50
Tungsten hot-work steels										
H21	T20821	0.26–0.36	0.15–0.40	0.15–0.50	3.00–3.75	0.30 max	...	8.50–10.00	0.30–0.60	...
H22	T20822	0.30–0.40	0.15–0.40	0.15–0.40	1.75–3.75	0.30 max	...	10.00–11.75	0.25–0.50	...
H23	T20823	0.25–0.35	0.15–0.40	0.15–0.60	11.00–12.75	0.30 max	...	11.00–12.75	0.75–1.25	...
H24	T20824	0.42–0.53	0.15–0.40	0.15–0.40	2.50–3.50	0.30 max	...	14.00–16.00	0.40–0.60	...
H25	T20825	0.22–0.32	0.15–0.40	0.15–0.40	3.75–4.50	0.30 max	...	14.00–16.00	0.40–0.60	...
H26	T20826	0.45–0.55(b)	0.15–0.40	0.15–0.40	3.75–4.50	0.30 max	...	17.25–19.00	0.75–1.25	...
Molybdenum hot-work steels										
H42	T20842	0.55–0.70(b)	0.15–0.40	...	3.75–4.50	0.30 max	4.50–5.50	5.50–6.75	1.75–2.20	...

(a) 0.25% max Cu, 0.03% max P, and 0.03% max S; where specified, sulfur may be increased to 0.06 to 0.15% to improve machinability. (b) Available in several carbon ranges

Table 13-2 Performance factors and processing information for hot-work tool steels

Factor	H10	H11	H12	H13	H14	H19	H21	H22	H23	H24	H25	H26
Major factors												
Wear resistance	3	3	3	3	4	5	4	5	5	5	4	6
Toughness	9	9	9	9	6	6	6	5	5	5	6	4
Hot hardness	6	6	6	6	7	7	8	8	8	8	8	8
Minor factors												
Usual working hardness, HRC	39–56	38–55	38–55	40–53	40–54	40–55	40–55	36–54	38–48	40–55	35–45	50–58
Depth of hardening	D	D	D	D	D	D	D	D	D	D	D	D
Finest grain size at full hardness, Shepherd standard	8	8	8	8	8	8½	9	9	7	9	9	9
Surface hardness as-quenched, HRC	52–59	53–55	53–55	51–54	53–57	48–57	45–63	48–56	34–40	52–56	33–46	51–59
Core hardness (25 *mm*, or 1 in., diam round), HRC	52–59	53–55	53–55	51–54	53–56	48–57	45–63	48–56	34–40	52–56	33–46	51–59
Manufacturing factors												
Availability	3	4	4	4	3	2	4	2	2	2	2	3
Cost	1	1	1	1	2	2	4	4	4	4	4	4
Machinability	8	8	8	8	7	6	6	6	4	6	6	5
Quenching medium	A, O	A	A	A	A	A, O	A, O	A, O	S, O, A	A, O	A, O	S, O, A
Hardening temperature, °C (°F)	1010–1040 (1850–1900)	995–1025 (1852–1875)	995–1025 (1825–1875)	995–1040 (1825–1900)	1010–1065 (1850–1950)	980–1205 (1800–2200)	1095–1205 (2000–2200)	1095–1205 (2000–2200)	1205–1275 (2200–2325)	1040–1230 (1900–2250)	1150–1260 (2100–2300)	1175–1260 (2150–2300)
Dimensional change on hardening	L	L	L	L	L	L	M	M	M	M	M	M
Safety on hardening	H	H	H	H	H	H	M	M	M	M	M	M
Susceptibility to decarburization	H	H	H	H	H	H	M	H	H	M	M	M
Approximate hardness as-rolled or forged, HB	500	500	500	500	500	500	450	450	450	500	450	500
Annealed hardness, HB	192–229	192–229	192–229	192–229	207–235	202–241	207–235	207–235	213–255	202–248	207–235	212–241
Annealing temperature, °C (°F)	870–900 (1600–1650)	845–900 (1550–1650)	845–900 (1550–1650)	845–900 (1550–1650)	870–900 (1600–1650)	870–900 (1600–1650)	870–900 (1600–1650)	870–900 (1600–1650)	870–900 (1600–1650)	870–900 (1600–1650)	870–900 (1600–1650)	870–900 (1600–1650)
Tempering range, °C (°F)	540–650 (1000–1200)	540–650 (1000–1200)	540–650 (1000–1200)	540–650 (1000–1200)	565–650 (1000–1200)	565–675 (1050–1250)	595–675 (1100–1250)	595–675 (1100–1250)	650–815 (1200–1500)	565–650 (1050–1200)	565–650 (1050–1200)	565–650 (1050–1200)
Forging temperature, °C (°F)	1040–1120 (1900–2050)	1065–1150 (1950–2100)	1065–1150 (1950–2100)	1065–1150 (1950–2100)	1065–1175 (1950–2150)	1095–1205 (2000–2200)	1065–1175 (1950–2150)	1065–1175 (1950–2150)	1040–1175 (1900–2150)	1065–1150 (1950–2100)	1065–1175 (1950–2150)	1065–1175 (1950–2150)

Note: Ratings are explained in Chapter 2.

ure. For this reason, the carbon contents of the H steels are maintained at low or medium levels.

- *Resistance to high-temperature wear.* Resistance to erosion or wear at hot-working temperatures, often referred to as "washing," is important for long tool and die life, and is generally improved by selection of alloying and microstructures that have higher hot hardness but lower toughness.
- *Resistance to heat treatment distortion.* Distortion and dimensional changes during production must be minimized, especially for intricate dies. Higher-alloy steels with hardenability sufficient to permit hardening by air cooling provide the best resistance to distortion during heat treatment.
- *Machinability* of hot-work tool steels must be enhanced by attention to primary processing and annealing and cannot be enhanced by additions that develop distributions of inclusions or other second-phase particles used to promote machinability in other steels. Such second-phase particles lower impact strength and fatigue resistance.
- *Resistance to heat checking.* Repeated exposure to cycles of heating and stress causes networks of fine, shallow cracks to develop in hot-work steels. This condition is referred to as heat checking and is the principal factor limiting the life of hot-work tool steels used for die-casting dies. Factors that affect heat checking are discussed later in this chapter.

Selection of the best hot-work tool steel for a given application depends on matching manufacturing and performance requirements to the steel and heat treatment that provide the best combination of properties for those requirements. Selection is largely influenced by the temperatures developed in dies, the manner of applying load in the application, and the manner of cooling the die. The hot hardness of carbon and low-alloy steels diminishes rapidly after heating to 230 °C (450 °F); the hot hardness of the chromium die steels does not vary materially until temperatures of 425 °C (800 °F) are reached; and the tungsten hot-work steels retain considerable hardness up to 620 °C (1150 °F). The last temperatures represent the approximate working limits for the chromium and tungsten groups of hot-work steels. Table 13-3 lists the as-heat-treated hardness and hot hardness of some chromium and tungsten hot-work tool steels and illustrates the higher temper resistance and hot hardness of the tungsten hot-work steels.

If it is necessary to water-cool dies to keep operating temperatures low, and thus eliminate undue softening, chromium hot-work steels are preferred to tungsten grades because of their greater resistance to cracking. Certain tungsten types, however, can be water cooled if the die design permits continuous circulation of water. In no instance should tungsten hot-work tool steels containing high levels of chromium be subjected to rapid heating and cooling cycles. Where extreme shock is likely to be encountered during operation, low-carbon H-type steels are preferred.

Figure 13-1 shows a heat treatment processing schematic for hot-work tool steels (Ref 1). Considering the high austenitizing temperatures used to harden H-type steels, several preheating stages are recommended. Air cooling and hot bath cooling (a technique that provides somewhat faster cooling rates than air cooling) are indicated. As noted, hardened tools and dies should be tempered before reaching room temperature. For optimum toughness and to prolong the life of hot-work tools and dies, multiple tempering is recommended. After initial tempering at secondary hardening temperatures, the embrittling effects of coarse carbide structures, formed by the transformation of retained austenite, are mitigated by subsequent tempering steps.

Several other general comments concerning the use of hot-work tool steels can be made. The tight black scale formed during heat treatment should be left on tools unless it is excessive or is combined with either surface carburization or decarburization. This scale is very resistant to abrasion and helps to hold die lubricant, thus assisting in wear prevention. Ground and polished tools tend to gall and seize. If grinding and polishing after heat treatment are necessary, tools may be reheated to just below the tempering temperature in order to reform a protective oxide coating. Such a coating, however, is less effective than the original one formed during hardening.

To minimize thermal shock, tools and dies should be preheated carefully before beginning a hot-working operation. Tool life can be extended by keeping tools and dies warm during prolonged periods of downtime. Proper cooling of tools and dies prevents local overheating and enables operation at lower, more uniform temperatures. In die-casting dies, internal cooling by circulating water is common. In forging dies, cooling can be accomplished with a water or oil spray, or with an air blast. The latter method is the mildest, whereas water spraying is the most severe. These cooling methods also serve to remove from tools and dies the loose scale formed on hot metal during fabrication. Care must be taken to prevent corrosion when tools are stored after heat

Table 13-3 Room-temperature and hot hardness of some hot-work tool steels(a)

Steel type	Hardness at room temperature after tempering 2 h at indicated temperature		Hot hardness	
	595 °C (1100 °F)	650 °C (1200 °F)	595 °C (1100 °F)	650 °C (1200 °F)
H12	392	328	192	108
H21	529	437	280	211
H26	588	505	405	276

(a) Mutual indentation values converted to HB.

treatment. Small rust spots soon become pits when a tool is placed in service.

Chromium Hot-Work Steels

The chromium hot-work tool steels are the most widely used for forging and die-casting applications. Originally developed for die casting of aluminum alloys, the alloy design objectives for the steels included air-hardening capability from relatively low austenitizing temperatures, little movement during hardening, minimum scaling tendency during air cooling, resistance to erosion by aluminum, resistance to thermal fatigue or heat checking, and reasonable alloy content and cost (Ref 2). The outstanding characteristics of H11 and other chromium hot-work steels are their high toughness and shock resistance. Although their hot hardness is lower than that of the other types of hot-work steels, the high shock resistance of the chromium H-type steels makes them preferable for most hot-work operations, especially when dies must be cooled with water or other flushing media. Typical applications include die-casting dies for aluminum, zinc, and magnesium castings, forging dies and inserts, punches, piercers and mandrels for hot work, hot-extrusion tooling, shear blades for hot work, and all types of dies for hot work. Some of the chromium H-type steels have been used for structural parts that require ultrahigh strength (Ref 3).

The relatively low carbon and alloy content of the chromium hot-work steels makes them highly forgeable in the temperature ranges listed in Table 13-2. Forging should not be attempted below 870 °C (1600 °F), and preheating at 700 to 815 °C (1300 to 1500 °F) prior to forging is recommended for large pieces. The chromium H-type steels have high hardenability and thus should be furnace cooled after forging. Although the chromium H steels generally are not subjected to normalizing heat treatments, normalizing has been used to improve the transverse ductility of large forgings (Ref 4). During forging and annealing heat treatments, hot-work tool steels should be protected from carburization and decarburization. To minimize distortion on hardening, stress-relief anneals, as shown in Fig. 13-1, may be applied before finish machining and hardening.

Isothermal transformation diagrams for some chromium hot-work steels are shown in Fig. 13-2 to 13-5 (Ref 5). The IT diagrams are qualitatively similar to CCT diagrams, and an example of the latter has been presented earlier in Fig. 5-27. Combined with chromium, molybdenum (~1% content) strongly retards the diffusion-controlled transformations of austenite in the chromium H-type steels. Typical of other highly alloyed tool steels, the pearlitic and bainitic transformation temperature ranges are well separated. However, because of the relatively low carbon content of the chromium H-type steels, the hardness of the pearlitic transformation products tends to be low and the M_s temperatures relatively high. The latter characteristic means that if cooling rates are sufficient to avoid pearlite and bainite formation, hardened microstructures will consist primarily of martensite with little retained austenite.

Despite the medium carbon contents of the chromium hot-work steels, the proeutectoid phase that forms is an alloy carbide, reported to be a vanadium-rich MC carbide containing moderate amounts of molybde-

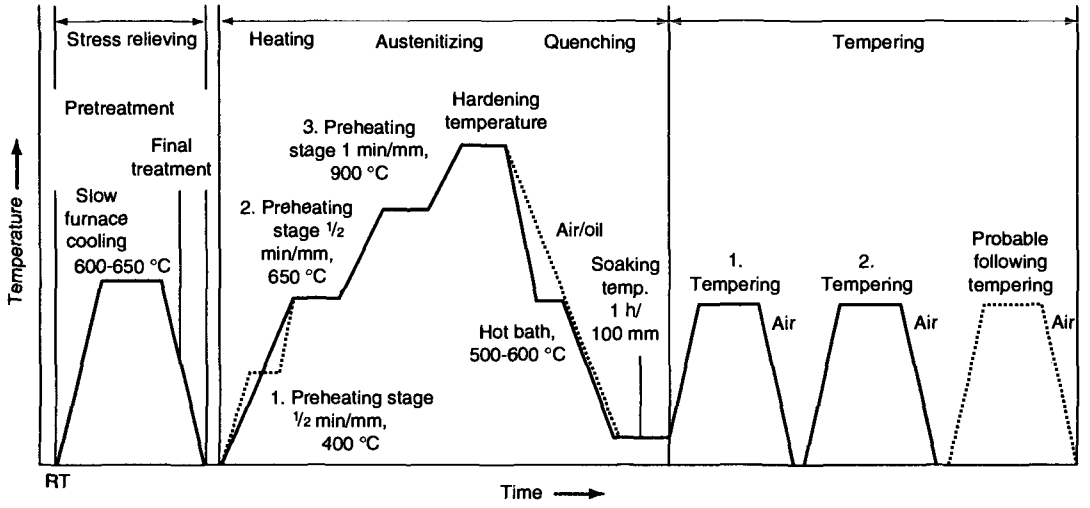

Fig. 13-1 Schematic of the heat treatment steps for hardening hot-work tool steels with hardening temperatures higher than 900 °C (1650 °F). Source: Ref 1

num and chromium and small but significant amounts of silicon and iron (Ref 6). The temperature ranges for the carbide formation are shown by the dashed lines in the IT diagrams of Fig. 13-2 to 13-5. While the pearlite transformation is quite sluggish, carbide formation can initiate at very short times or relatively rapid cooling rates. The carbide particles nucleate on austenite grain boundaries and

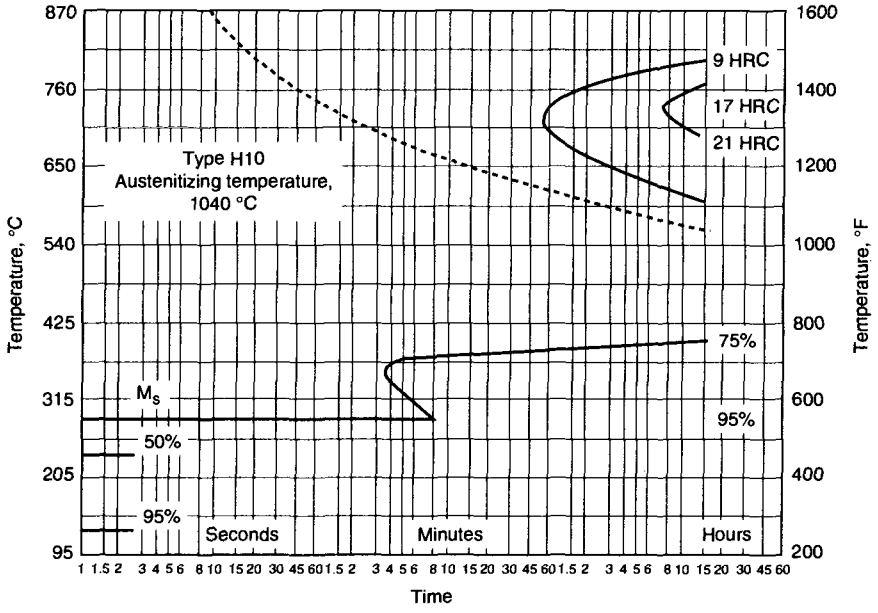

Fig. 13-2 IT diagram for H10 steel containing 0.40% C, 1.00% Si, 0.55% Mn, 3.25% Cr, 2.50% Mo, and 0.33% V. Courtesy of Crucible Steel Co.

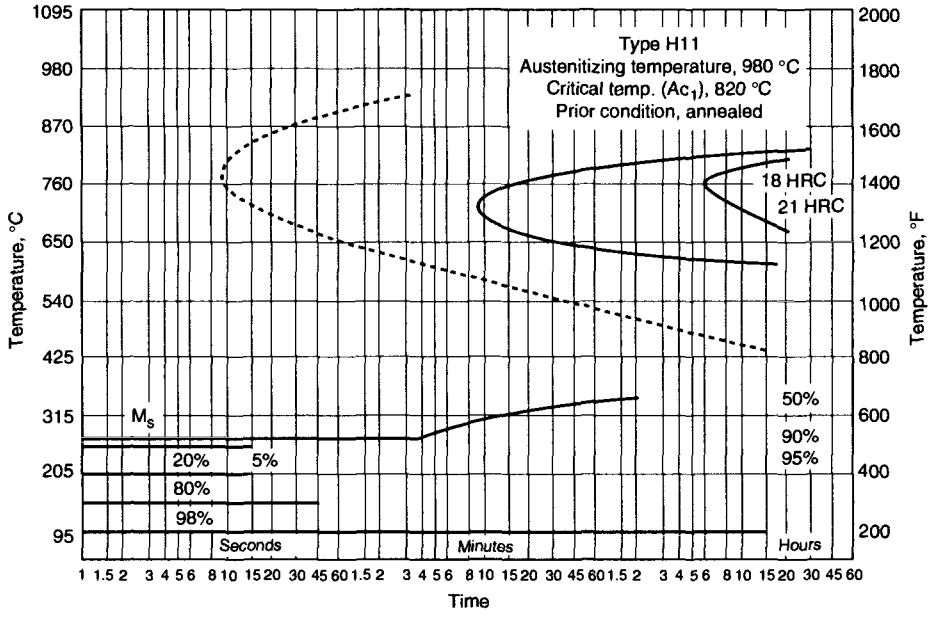

Fig. 13-3 IT diagram for H11 steel containing 0.38% C, 0.50% Mn, 1.08% Si, 0.30% Ni, 5.00% Cr, 1.35% Mo, and 0.40% V. Source: Ref 5

never grow to any substantial thickness, especially during continuous air cooling. Nevertheless, the grain-boundary carbide networks increase the susceptibility of the H-type steels to brittle intergranular fracture and are the reason that the steels are not normalized. Grain-boundary carbide formation on cooling is enhanced by austenitizing at high temperatures in the hardening range, where austenitic

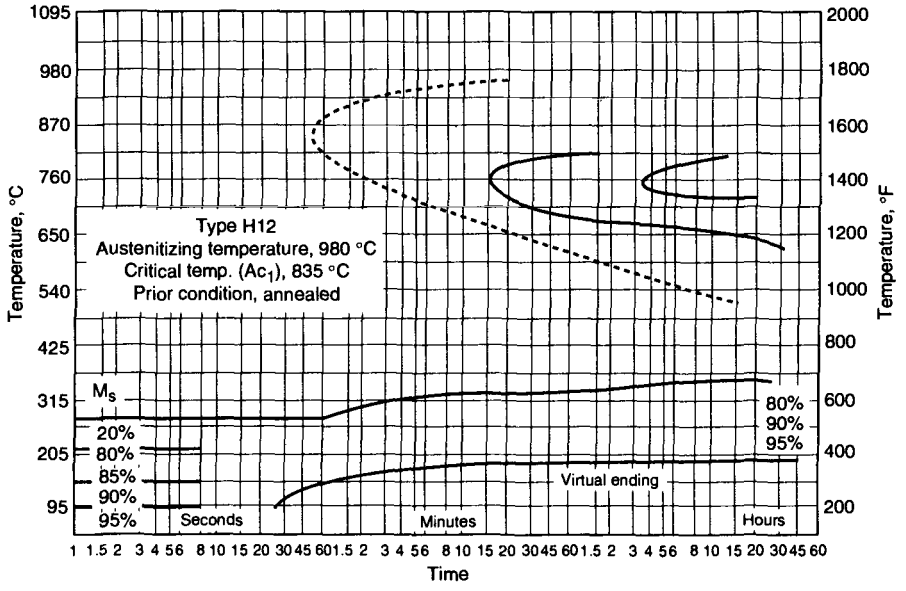

Fig. 13-4 IT diagram for H12 tool steel with the composition shown. Source: Ref 5

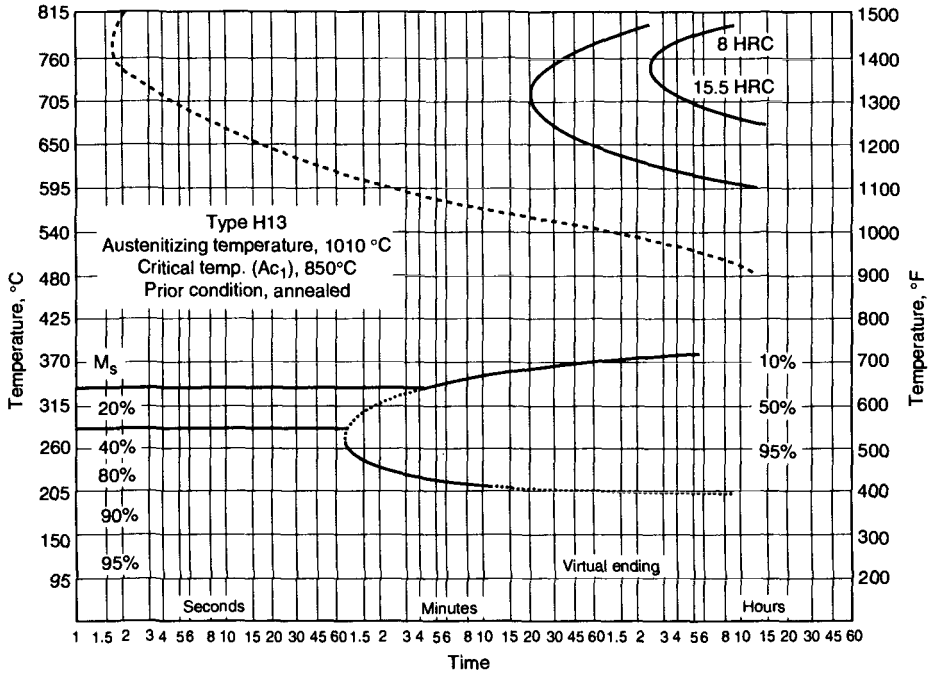

Fig. 13-5 IT diagram for H13 steel containing 0.40% C, 1.05% Si, 5.00% Cr, 1.35% Mo, and 1.10% V. Courtesy of Crucible Steel Co.

grain size coarsens and more carbon goes into solution as the alloy carbides dissolve. In addition to carbide formation, hardenability and the kinetics of the other diffusion-controlled isothermal and continuous cooling transformations of austenite are influenced by austenitizing temperature, as discussed below.

All of the chromium hot-work steels have high hardenability. Figure 13-6 shows Jominy end-quench curves for chromium steels with and without molybdenum and shows the strong effect of molybdenum in promoting martensite formation to the large distances from the quenched end which correspond to slow cooling rates that would be expected in heavy sections of steel. Vanadium and tungsten additions have relatively little influence on hardenability because, at most austenitizing temperatures in the recommended range, a substantial fraction of these elements is incorporated in stable alloy carbides.

Figure 13-7 shows the effect of austenitizing temperature on the hardness of air-cooled chromium hot-work steels. At low austenitizing temperatures, as-cooled hardness is low because of reduced hardenability associated with an austenite matrix impoverished in alloying elements. Branco (Ref 7) estimates that annealed H11/H13 steels contain about 3.5 to 4.5 wt% coarse carbides produced during annealing and preceding stages of processing. The carbides have various crystal structures and compositions and contain a large fraction of the alloying elements needed for hardenability and eventual secondary hardening.

Dissolution of alloy carbides entering the austenitizing process after annealing is continuous with increasing austenitizing temperature and time, as illustrated in Fig. 13-8 for an H13 tool steel (Ref 6). Relative to the annealed starting structure, the volume fraction of carbides has decreased to about 2% after austenitizing at 1025 °C (1875 °F) and to about 1% after austenitizing at 1105 °C (2025 °F). At the lower austenitizing temperatures, three types of carbides, residual from annealing and earlier processing, are present: vanadium-rich MC, molybdenum/iron-rich M_6C, and chromium/iron-rich M_7C_3. After austenitizing at the higher temperatures, around 1100 °C (2010 °F), only vanadium-rich MC carbides remain and the other types of carbides have completely dissolved (Ref 6, 7). Accompanying the dissolution of the alloy carbides with increasing austenitizing temperature, austenitic grain size also increases. Figure 13-9 shows the gradual increase in austenitic grain size with increasing austenitizing temperature for an H13 steel (Ref 6). Time at austenitizing temperature has relatively little effect on grain size at conventionally used hardening temperatures.

Although the chromium hot-work tool steels have high hardenability, their hardenability is insufficient to produce fully martensitic structures in the heavy dies used for casting of aluminum and other metals. Schmidt (Ref 6) has studied the effects on microstructure and properties of H13 steel of extremes in cooling rates in air cooled specimens 12.5 mm (0.5 in.) in size and in specimens subjected to cooling rates that simulate cooling rates at midradius locations of air-cooled bars 150 and 300 mm (6 and 12 in.) in diameter. Figure 13-10 shows the various cooling rates superimposed on CCT curves generated by Nilsson et al. (Ref 8) for H13 tool steel austenitized at 1030 and 1080 °C (1885 and 1975 °F); the heavy sections transform to bainite rather than martensite.

The smaller air-cooled specimens transform fully to lath martensite, as has been illustrated in Fig. 4-20, while the specimens cooled at the slower rates transform to mixtures of upper and lower bainite. The two types of bainite were oriented in light-etching and dark-etching bands, consistent with alloy element variations produced by ingot solidification and hot work. Light-etching bands contained mixtures of martensite and lower bainite and were consistently higher in hardness than dark-etching bands

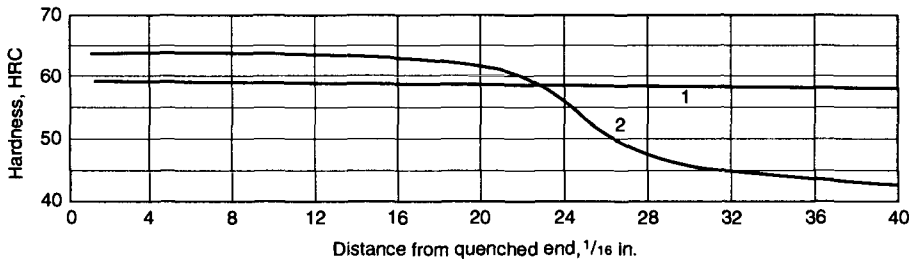

Curve	Type	Composition, %					Austenitizing temperature	
		C	Si	Cr	W	Mo	°C	°F
1	H12	0.35	0.92	4.76	1.42	1.45	1010	1850
2	...	0.96	0.29	3.93	...	...	1010	1850

Fig. 13-6 Jominy end-quench hardenability curves for chromium hot-work tool steels. Courtesy of Teledyne VASCO

consisting of upper bainite. The light-etching bands were found to be richer in chromium and molybdenum than the dark-etching bands, consistent with the higher hardenability and hardness of these regions (Ref 6).

Figure 13-11 shows as-quenched hardness as a function of austenitizing temperature for the three sets of H13 specimens cooled as shown in Fig. 13-10. The high hardness of the smaller air-cooled specimens is consistent with their fully martensitic structures and increases significantly with increasing austenitizing temperature as more carbon is dissolved in the austenite and is consequently trapped in the martensite on cooling. Increasing amounts of retained austenite would be expected in the specimens austenitized at the higher temperatures, but the amounts are not large enough to lower hardness as is the case for higher-carbon, more highly alloyed tool steels such as the high-carbon, high-chromium cold-work steels. The hardness of the bainitic microstructures in the specimens cooled at rates simulating those in heavy, air-cooled sections is significantly lower than that of the martensitic microstructures and is relatively insensitive to austenitizing temperature.

The chromium hot-work tool steels have good resistance to softening during tempering, a characteristic that translates to good performance during hot-work applications. Hardness as a function of a time-temperature tempering parameter for an H11 steel and as a function of tempering temperature for several chromium H-type steels is shown in Fig.

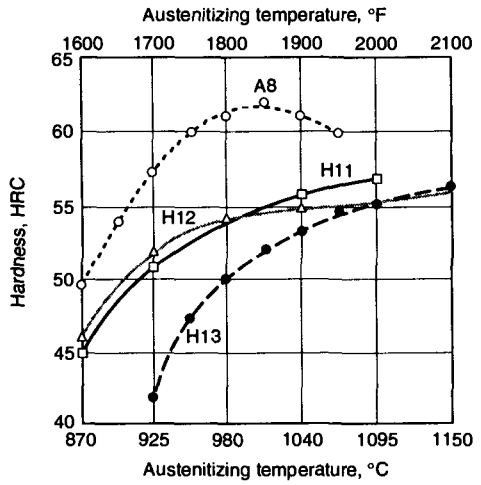

Type	Composition, % C	Si	Cr	W	Mo	V	Specimen size
H11	0.38	1.00	5.25	...	1.35	0.50	1 (diam) × 3 in.
H12	0.35	1.00	5.00	1.30	1.60	0.30	...
H13	0.40	1.00	5.25	...	1.20	1.00	...
A8	0.55	0.95	5.00	1.20	1.20	...	...

Fig. 13-7 Effect of austenitizing temperature on hardness of chromium hot-work tool steels. Data from Columbia Tool Steel Co. and Latrobe Steel Co.

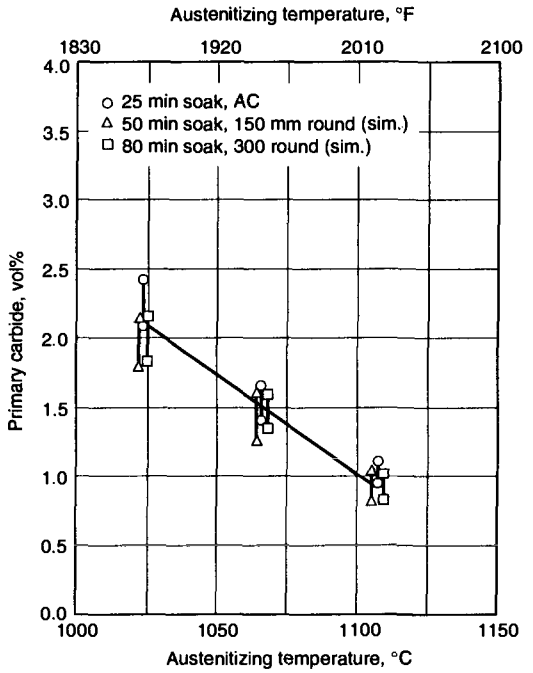

Fig. 13-8 Volume percent of primary carbides in H13 tool steel as a function of austenitizing temperature for specimens soaked at various times. Source: Ref 6

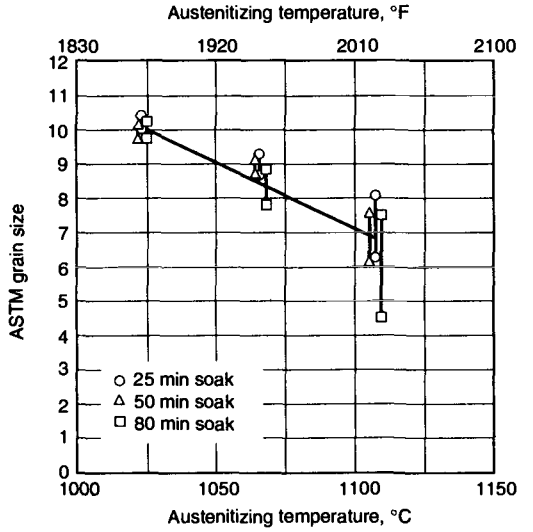

Fig. 13-9 Austenite grain size (as measured by ASTM grain size number) in H13 tool steel as a function of austenitizing temperature for specimens soaked for various times. Source: Ref 6

13-12 and 13-13, respectively. The tempering curves start at moderate hardness levels, consistent with the as-quenched martensitic hardness of medium-carbon steels and are relatively flat as a function of tempering temperature. Small hardness peaks at around 540 °C (1000 °F) indicate that the hardness is maintained by secondary hardening. The key element for the secondary hardening and tempering resistance is vanadium, which is dissolved during austenitizing for hardening and which at peak tempered hardness precipitates as very fine particles of vanadium-rich MC carbides in martensite laths (Ref 7). Figure 13-14 shows the strong effect of vanadium additions on maintaining hardness in chromium hot-work steels at high testing temperatures. Other carbides precipitate—namely, cementite, which forms from interlath retained austenite at tempering temperatures below the aging peak, and chromium-rich M_7C_3 and molybdenum-rich M_6C carbides, which form during overaging (Ref 6). The carbides other than the vanadium-rich MC carbides coarsen rapidly and do not contribute significantly to strengthening. As hardness decreases with increasing testing temperature, impact toughness increases (Fig. 13-15).

The chromium hot-work steels are usually double tempered to working hardness in the range of 44 to 50 HRC. Where extreme shock or heavy stresses are encountered, hardness may be lowered to 40 to 44 HRC. Tempering to these hardness ranges corresponds to an overaged or overtempered condition, beyond that which produces peak hardness. Tempering beyond peak hardness is performed to avoid the minimum in toughness that develops when the chromium hot-work steels are tempered at temperatures that produce peak strengthening. Figure 13-16 shows the minimum in H13 steel as a function of tempering time and temperature. The sharpest decrease in impact toughness is associated with peak hardness after tempering for several hours at 500 °C

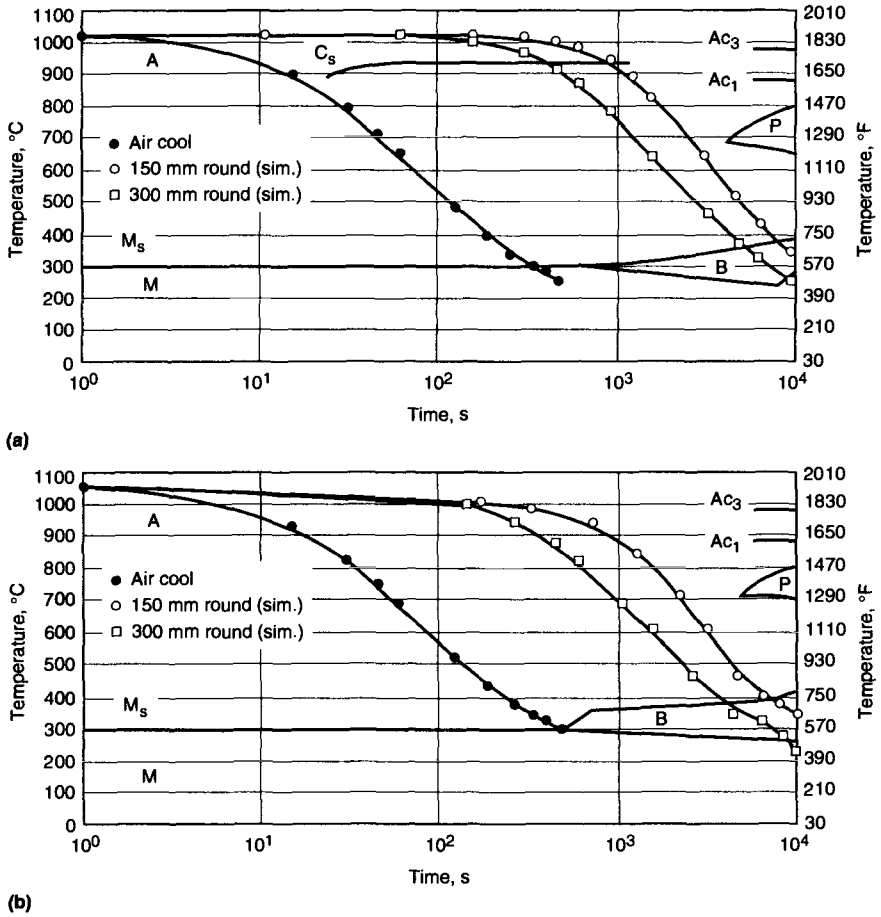

Fig. 13-10 Cooling curves for H13 specimens 12.5 mm (0.5 in.) in size (air cool) and midradius locations in 150 and 300 mm (6 and 12 in.) diam rounds superimposed on CCT diagrams for H13 steel cooled from 1030 °C (1885 °F) (a) and 1080 °C (1975 °F) (b). A, austenite; B, bainite; C, cementite; M, martensite; P, pearlite. CCT diagrams, Ref 8; cooling curves, Ref 6

(930 °F); at lower tempering temperatures the minimum takes longer to develop.

The fracture surfaces of embrittled specimens of H13 tool steel tempered to peak hardness consist of transgranular cleavage (Fig. 13-17). The cleavage fracture is attributed to a combination of two microstructural features: (1) coarse interlath carbides, which initiate cleavage, and (2) very fine, dense MC carbide intralath precipitation, which severely limits its dislocation motion and plasticity (Ref 9). The interlath and intralath carbide formation processes are diffusion-dependent reactions and, therefore, as shown in Fig. 13-16, are dependent on time and temperature to create the structures most sensitive to cleavage fracture. The interlath carbides form from austenite retained between martensite laths and have plate-shaped morphologies similar to those that cause the transgranular cleavage form of tempered martensite embrittlement in low-alloy steels such as 4340 steel (Ref 10). In the low-alloy steels, interlath carbides are formed by tempering at temperatures between 250 and 400 °C (480 and 750 °F). In the case of the H13 steel, high silicon and alloy contents defer the decomposition of the retained austenite to higher tempering temperatures. Overaging spheroidizes the interlath carbides, coarsens the intralath carbides, and increases dislocation mobility, thereby reestablishing conditions for ductile fracture.

Tempering of bainitic structures formed during slow cooling of heavy sections of chromium H-type steels also produces significant secondary hardening. Figure 13-18, from the study by Schmidt (Ref 6), shows the effect of austenitizing temperature and starting microstructure on the tempering response of H13 steel. Air-cooled small specimens (12.5 mm, or 0.5 in.), as discussed earlier, developed fully martensitic microstructures of high as-quenched hardness. The positive increment in hardness produced by increasing austenitizing temperatures persists over the entire range of tempering temperatures. The bainitic structures, formed by cooling at rates that simulate cooling in 150 and 300 mm (6 and 12 in.) rounds, harden significantly on tempering relative to their low as-quenched hardness, and eventually reach hardness levels comparable to those of the tempered martensitic microstructures. The high secondary-hardening response of the bainitic structures, similar to the explanation for martensitic microstructures, is attributed to the precipitation of vanadium-rich MC carbides in the bainite (Ref 6). This explanation is consistent with the fact that the bainitic microstructures form at low temperatures, as demonstrated in the CCT diagrams of Fig. 13-10, and therefore consist of mixtures of ferrite and iron carbides, since the temperature at which bainite forms is too low for alloy carbide formation. Thus, the vanadium that has dissolved during austenitizing is available for precipitation during high-temperature tempering. The resulting enhanced alloy carbide precipitation, especially in

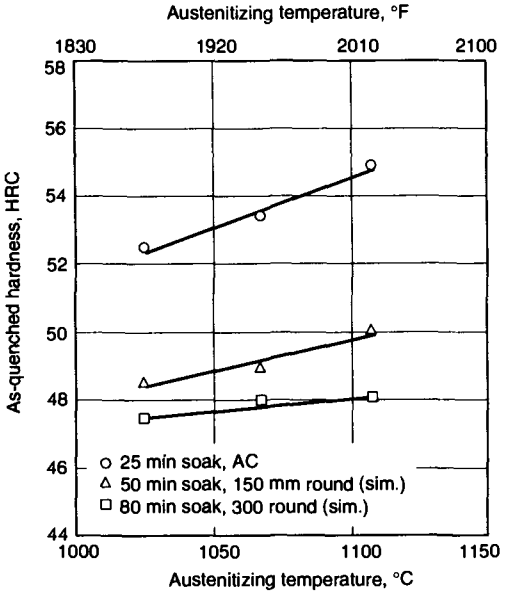

Fig. 13-11 As-quenched hardness of H13 steel as a function of austenitizing temperature for specimens cooled at rates simulating air-cooled 12.5 mm (0.5 in.) specimens, 150 mm (6 in.) diam rounds, and 300 mm (12 in.) diam rounds. Source: Ref 6

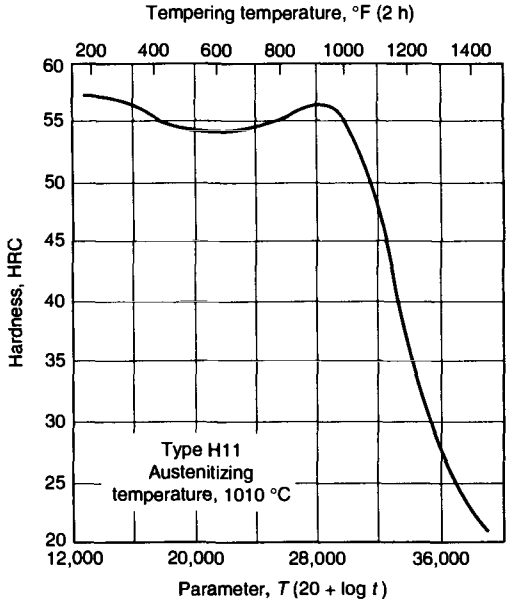

Fig. 13-12 Hardness as a function of time-temperature parameter for H11 steel containing 0.40% C, 0.92% Si, 5.09% Cr, 1.34% Mo, and 0.52% V. Source: Ref 3

specimens austenitized at high temperatures, has also been related to cleavage fracture of bainitic specimens tempered above peak aging temperatures (Ref 11, 12).

Impact toughness of fully heat-treated (i.e., austenitized), quenched-and-tempered H13 specimens with martensitic and bainitic microstructures is presented in Fig. 13-19 (Ref 6), showing the effect of variations in austenitizing temperature, cooling rate (which controls microstructure), tempering temperature, and test temperature. The impact toughness measured at the higher test temperature of 425 °C (800 °F), which represents conditions under which the chromium hot-work steels are expected to operate, is always higher than the toughness measured at room temperature. The fracture surfaces of specimens tested at the higher temperatures were characterized by microvoid coalesence and thus were dependent on the arrays of particles that initiate microvoids. These particles are coarser in bainitic microstructures. Also, the effect of tempering temperature, as discussed earlier, is shown in the curves with the specimens tempered at 540 °C (1000 °F), close to the conditions that produce peak hardness, having much lower toughness compared to specimens tempered at the higher temperatures.

For martensitic microstructures, Fig. 13-19 shows that increased austenitizing temperature lowers room-temperature impact toughness in specimens tempered at temperatures of 595 and 620 °C (1100 and 1150 °F), which are above those that produce peak hardness. This decrease in toughness is associated with a transition to intergranular fracture along prior-austenite grain boundaries in the specimens austenitized at the higher temperatures (Ref 6); the increased intergranular fracture is consistent with the greater susceptibility to carbide formation on austenitic grain boundaries in specimens austenitized at higher temperatures.

Figure 13-19 shows that specimens cooled at the slower rates which produce bainitic microstructures have significantly lower impact toughness than more rapidly cooled specimens with martensitic microstructures. The lower impact toughness of the tempered bainitic microstructures, even in specimens tempered at 620 °C (1150 °F), was associated with fracture surfaces characterized by 100% cleavage (Ref 6). The cleavage fracture is similar to that shown in Fig. 13-17 for tempered-martensite-embrittled martensitic specimens and may be related to similar arrays of coarse interlath carbides in matrix structures that have been precipitation hardened to high hardness. In the case of the tempered martensitic specimens, the interlath carbides are produced by the transformation of retained austenite during tempering, while in the bainitic specimens the interlath carbides are formed by carbon rejection from ferrite as a result of austenite-to-bainite transformation during slow cooling.

Other measures of mechanical performance of the chromium hot-work steels include tensile properties and the results of fatigue testing. Table 13-4 lists tensile properties of chromium H-type steels as a function of testing temperature. The H11 data show that relatively little decrease in strength and no decrease in hardness occur at testing temperatures below 540 °C (1000 °F). The fatigue performance of H11 in rotating-beam fatigue testing is shown in Fig. 13-20 (Ref 13, 14) and in cantilever bending fatigue testing in Fig. 13-21 (Ref 15). Compared to 4340 steel heat treated to the same high tensile strength, the H11 steel shows better fatigue resistance (Fig. 13-20). The specimens subjected to the cantilever bend testing were tempered to a peak hardness of 51 HRC by tempering at 500 °C (930 °F) and an overaged hardness of 48 HRC by tempering at 600 °C (1110 °F). The results of the fatigue testing show little effect of tempering on fatigue performance. Fracture toughness of the two tempered conditions of the H11 steel was measured from the size

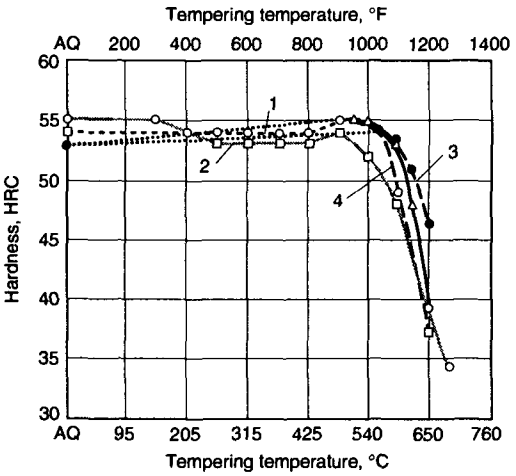

Curve	Type	Composition, % C	Si	Cr	W	Mo	V	Hardening temperature °C	°F	Specimen size
1	H12	0.37	1.00	5.00	1.25	1.45	0.35	1010	1850	1 (diam) × 3 in.
2	H13	0.40	1.00	5.25	...	1.25	1.05	1010	1850	1 (diam) in.
3	...	0.38	1.00	3.50	1.25	1.00	1.00	1040	1900	...
4	H10	0.40	1.00	3.25	...	2.50	0.33	1010	1850	4 × 4 × 4 in.

Fig. 13-13 Hardness as a function of tempering temperature for various chromium hot-work die steels air cooled from hardening temperatures. AQ, as quenched. Data from Bethlehem Steel Co., Braeburn Alloy Steel Corp., and Crucible Steel Co.

and shape of the fatigue cracks at instability and the maximum applied stresses applied during cantilever beam testing. Figure 13-22 shows that the fracture toughness of the overaged specimens was higher than that of the peak-aged specimens, consistent with the impact toughness measurements discussed earlier.

The average dimensional changes produced by heat treatment of three chromium hot-work tool steels are shown in Fig. 13-23. Little change is caused by tempering until an expansion consistent with retained austenite transformation develops after tempering at temperatures above 480 °C (900 °F). The results reported in Fig. 13-23 are average values, and depending on anisotropy residual from processing, dimensional changes at various orientations to the rolling direction may vary from the average (Ref 16).

Heat Checking and Thermal Fatigue of H11/H13 Tool Steels. A network of fine cracks, referred to as heat checking, develops in the widely used chromium hot-work steels during exposure to repeated fluctuations in temperature and stress. Heat checking has long been known as a major factor limiting life during hot-work applications, especially the life of die-casting dies used to cast metals with relatively high melting points, such as aluminum, magnesium, and brass (Ref 17). As a result, effort is ongoing to define the alloying, manufacturing, and heat-treating conditions that provide the best resistance to heat checking (Ref 6, 18–29).

The cracks in a heat-checked array initiate and grow in transgranular and intergranular paths through the microstructure and are filled with oxides (Ref 21). Softening of the tool steel surface accompanies crack formation (Ref 21, 24). Examples of heat checking of various degrees of severity are shown in Fig. 3-24. These examples are the basis of the scale developed by Uddeholm to rank the damage associated with heat checking (Ref 20). The scale assigns numbers to both the size of the leading or largest cracks and the various distributions of the network cracks, as shown in the parallel columns of photographs. The overall heat-checking damage is rated by a summation of the two numbers. With

Table 13-4 Tensile properties of chromium-molybdenum hot-work tool steels at elevated temperatures(a)

Testing temperature		Tensile strength		Yield strength (0.2% offset)		Elongation 50 mm (2 in.), %	Reduction of area, %	Room-temperature hardness, HRC	
								Before testing	After testing
°C	°F	MPa	ksi	MPa	ksi				
H11(b)									
Room		1806	262	1482	215	10.0	35.8	50	50
150	300	1689	245	1358	197	10.1	36.1	50	50
260	500	1600	232	1345	195	9.8	34.5	50	50
345	650	1579	229	1317	191	10.0	35.2	50	50
425	800	1510	219	1289	187	11.4	38.7	50	50
480	900	1427	207	1145	166	12.2	38.9	50	50
540	1000	1241	180	965	140	11.0	35.4	50	50
595	1100	979	142	724	105	12.8	46.2	50	47
650	1200	586	85	434	63	18.9	66.6	50	41
H13(c)									
480	900	1531	222	...	...	9	37	52	...
540	1000	1413	205	...	...	11	43	52	...
595	1100	1193	173	...	...	15	49	52	...
650	1200	814	118	...	...	22	59	52	...
H12(d)									
400	750	1703	247	...	...	12	36	53	...
540	1000	1482	215	...	...	12	41	53	...
650	1200	531	77	...	...	32	83	53	...
760	1400	124	18	...	...	71	97	53	...
H12(e)									
540	1000	1358	197	1086.7	157.6	10	55	50	...
620	1150	593.7	86.1	396.5	57.5	24	71	49.5	...

(a) Data from Teledyne VASCO, Allegheny Ludlum Industries, and Universal-Cyclops Steel Corp. (b) Composition: 0.40% C, 0.92% Si, 5.09% Cr, 1.34% Mo, 0.52% V. Heat treatment: 1010°C (1850 °F) and air cooled, then double tempered, 2½ h at 570 °C (1060 °F). (c) Composition: 0.40% C, 1.00% Si, 5.25% Cr, 1.15% Mo, 1.00% V. Heat treatment: austenitized at 1010 °C (1850 °F) and oil quenched, then tempered 2 h at 565 °C (1050 °F). (d) Composition: 0.33% C, 0.85% Si, 5.00% Cr, 1.25% W, 1.45% Mo, 0.23% V. Heat treatment: austenitized at 1050 °C (1925 °F) and oil quenched, then tempered 2 h at 565 °C (1050 °F). (e) Austenitized at 980 °C (1800 °F), air cooled, then tempered 1½ h at 565 °C (1050 °F).

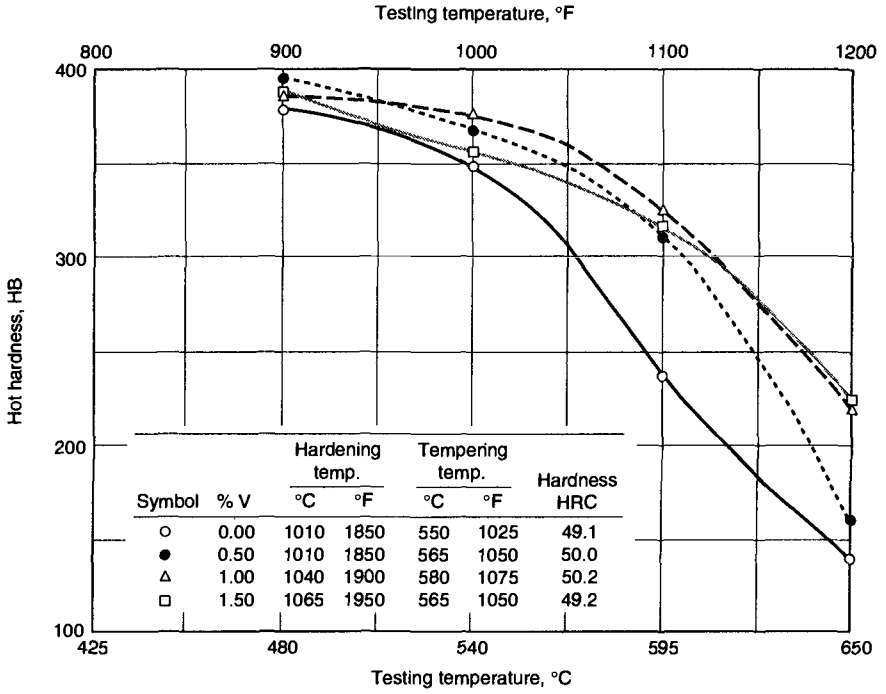

Fig. 13-14 Effect of vanadium on the hot hardness of chromium hot-work steel with a base composition of 0.33% C, 5% Cr, 0.80% Si, and 1.35% Mo. All specimens were double tempered for 2 h periods. Courtesy of Teledyne VASCO

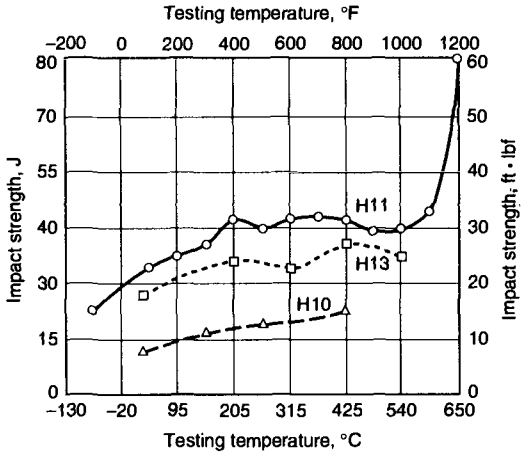

increasing numbers of thermal cycles, the severity of checking increases and the depth of cracking increases. Generally, depth of cracking correlates with the heat-checking ratings, and the ratings can be used to estimate grinding depths required to remove the heat-checking crack networks, which, if they become too coarse, negatively influence the surface finish of die castings made in a heat-checked die.

The fine cracks are caused by the alternating stresses that develop when the die surface is heated to temperatures higher than the die interior (Ref 21). When liquid metal contacts the die surface, compressive surface stresses are developed as the die surface expands and is restrained by the cooler interior of the die. As the metal casting solidifies and cools, the surface contracts and tensile stresses are established. Low thermal expansion coefficients and good thermal conductivity help to minimize the

Type	Composition, % C	Si	Cr	Mo	V	Hardening temperature °C	°F	Hardening medium	Tempered hardness, HRC
H10	0.40	1.00	3.25	2.50	0.33	...	...	...	56.5
H11	0.40	0.92	5.09	1.34	0.52	1010	1850	Air	51.0
H13	0.40	1.00	5.25	1.15	1.00	1010	1850	Oil	52.5

Fig. 13-15 CVN impact toughness of various chromium H-type steels as a function of testing temperature. Note that the as-tempered hardness of the steels varied. Data from Ref 3, Allegheny Ludlum Industries and Crucible Steel Co.

thermal gradients and stresses, but these properties vary over narrow limits for the hot-work steels and microstructures used for die casting (Ref 22). If the temperature differences are high enough, the alternating cycles of compression and tension are sufficient to cause plastic flow and eventual crack formation (Ref 21, 23). Generally, dies for aluminum casting are preheated as a means to reduce the temperature gradients between die surfaces and die interiors, thereby reducing the magnitude of the cyclic stresses that lead to cracking. The higher operating temperatures of preheated dies also increase tool steel toughness and fracture resistance, as has been shown in Fig. 13-15 and 13-19 (Ref 6).

Good heat-checking resistance in chromium hot-work steels is produced by heat-treated microstructures that have good hot hardness and good toughness. Figure 13-25 shows the dependence of heating checking, as rated by the Uddeholm scale, on hardness and unnotched impact energy of H13 steel (Ref 24). Heat-checking resistance is increased by high hardness and high impact toughness, as provided by tempered martensitic microstructures. Bainitic microstructures have lower strength and toughness and therefore are expected to have lower heat-checking resistance.

As discussed earlier relative to Fig. 13-11, higher austenitizing temperatures produce higher as-quenched hardness, especially in specimens with martensitic microstructures. Wallace et al. (Ref 19, 21) have shown that higher hardness produced by high-temperature austenitizing correlates with improved heat-checking resistance. Figure 13-26 shows that thermal fatigue crack area is very much reduced by austenitizing at higher temperatures and heat treating to higher hardness. The improved fatigue crack resistance develops despite the fact that toughness is also decreased by high-temperature austenitizing (Ref 19, 21). However, the latter factor limits the exploitation of high austenitizing temperatures to about 1065 °C (1950 °F), since the low toughness of steels austenitized above that temperature may result in gross brittle fracture of die-casting dies.

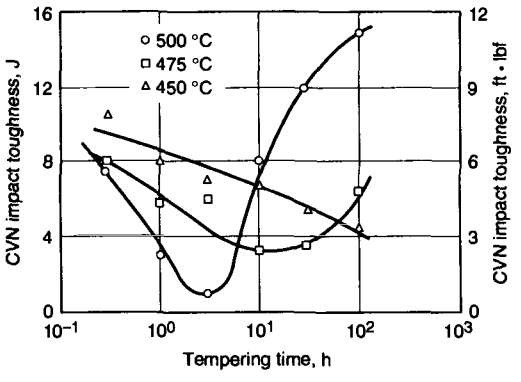

Fig. 13-16 CVN energy absorbed at room temperature for H13 specimens as a function of time at various tempering temperatures. Source: Ref 9

A properly heat-treated hot-work tool steel has the optimum distribution of fine carbides in a matrix of tempered martensite for good hot hardness. However, other critical components of the microstructure are coarse nonmetallic inclusions, such as oxides and sulfides, and coarse alloy carbides introduced during solidification and elongated by hot work (Ref 22, 26). Inclusion particles and coarse alloy carbides are sites of fracture initiation and will lower resistance to heat checking and gross fracture of even properly heat-treated hot-work tools and dies. Moreover, inclusions, especially sulfides, and coarse alloy carbide arrays, together with residual alloy segregation, elongated in the hot-rolling direction will produce nonuniform mechanical behavior (Ref 22). In particular, transverse mechanical properties may be significantly reduced.

Recognition of the detrimental effects of coarse particles has driven the development of new melting and processing approaches, as described in Chapter 3. In particular, vacuum degassing, ladle metallurgy, argon oxygen decarburization, electroslag remelting, vacuum arc remelting, and powder metallurgy approaches to the manufacture of tool steels have greatly improved the quality, cleanliness, and uniformity of hot-work tool steels. Consequently, distortion and cracking during heat treatment have been significantly reduced and tool and die performance significantly enhanced with respect to heat-checking and catastrophic fracture resistance of premium grades of chromium H-type steels (Ref 19, 22, 25-27).

Stable hardened and tempered microstructures that maintain high hardness and resist softening at operating stresses and temperatures are essential for good heat-checking resistance. As a result, it is imperative to maintain proper alloy composition and microstructure at the surface of hot-work tools and dies during processing, and especially to take care to minimize surface decarburization or carburization during austenitizing for hardening. The North American Die Casting Association has published an excellent guide for all aspects of heat treatment of H13 steel for die casting (Ref 25). Preferred furnaces for austenitizing include vacuum furnaces, sealed quench or controlled-atmosphere furnaces with inert gas, hydrogen, or hydrocarbon atmospheres, or salt baths with salts formulated to prevent oxidation and decarburization. The use of packing materials such as charcoal or cast iron chips is discouraged because of the inability to control surface carbon by this approach.

Other processing approaches that may affect the heat-checking performance of chromium H-type steels are the use of electrodischarge machining (EDM) and surface-hardening techniques. The

EDM process is used to shape mold and die components after hardening heat treatment and is capable of producing complex geometries that could not be produced by other machining techniques (Ref 29).

The EDM process works by melting away the tool material, thus creating a brittle as-cast surface layer subjected to high tensile residual stresses, a hard, untempered layer of martensite, and a softened layer

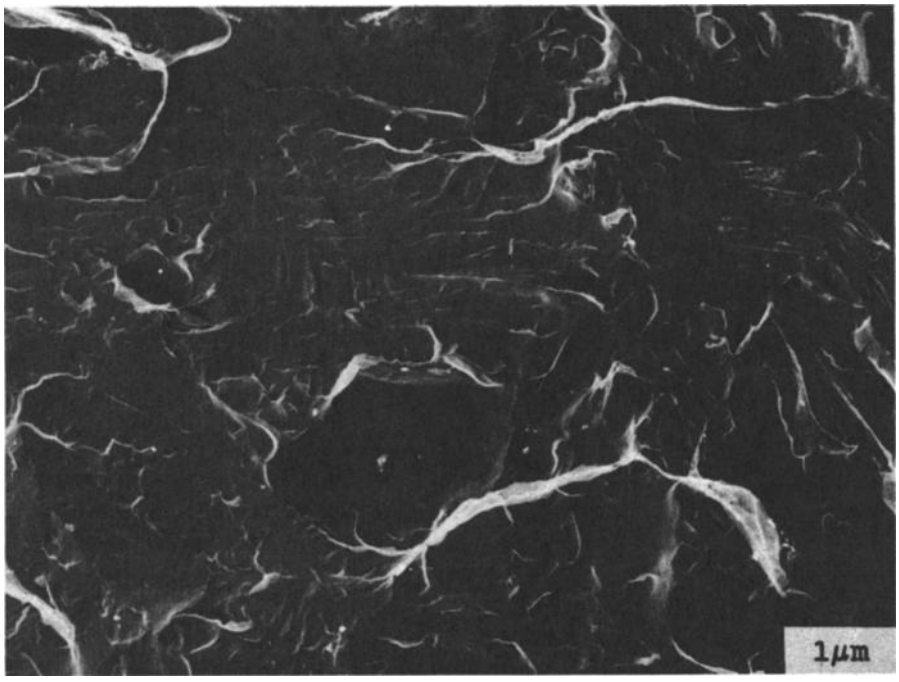

Fig. 13-17 Cleavage fracture on overload fracture surface of H13 steel CVN specimen tempered at 500 °C (930 °F) for 3 h. TEM carbon replica. Source: Ref 9

of overtempered martensite (Ref 28, 29). Centa and Wallace (Ref 28) have shown that these changes in the surface microstructure of hardened H13 steel cause significant reductions in thermal fatigue and heat-checking resistance. Polishing or mechanical abrasion to remove the as-cast surface layer not only removes the brittle surface structures but also replaces surface tensile stresses with compressive stresses, thereby improving resistance to thermal cracking (Ref 28, 29). With respect to other means of surface preparation, others have found that milling and heavy shot peening, perhaps because of the hardening introduced by cold work, increase resistance to thermal fatigue (Ref 24).

Surface modification treatments that increase the surface hardness of tool steels offer another approach to enhancing heat-checking resistance. Eliasson and Sandberg (Ref 24) have shown that nitriding and coating of H13 steel with high-hardness layers of TiN/TiC by chemical vapor deposition (CVD) significantly increase resistance thermal fatigue compared to that of untreated surfaces. Figure 13-27 shows that the improvement by surface modification is largely in prevention of thermal crack initiation; once cracks have been initiated, crack propagation is rapid. The improved resistance to crack initiation was related to increased surface resistance to softening in the coated steels during thermal cycling.

Tungsten Hot-Work Steels

The compositions of the tungsten hot-work tool steels, also designated as group H steels in the AISI classification system, are listed in Table 13-1, and processing and performance ratings are given in Table 13-2. Tungsten H-type steels were historically the first high-alloy steels used for hot-work tooling. They contain from 9 to 19% W, low carbon, and moderate amounts of chromium and vanadium. The high-tungsten H26 grade is in fact a low-carbon modification of 18-4-1 (T1) high-speed steel.

The tungsten hot-work steels have greater hot hardness than any class of hot-work steels and therefore have excellent resistance to softening and washing of dies during hot-work operations. However, the same high-carbide-containing microstructures that provide hot hardness also cause the tungsten steels to have lower toughness and higher susceptibility to brittle fracture. In order to offset this low fracture resistance, tungsten hot-work tool steel alloy design incorporates low carbon content. Despite this low content, tungsten H-type steels have lower resistance to thermal shock than do the chromium hot-work steels and cannot be rapidly cooled with water during operation without danger of breakage.

Tungsten die steels are used where maximum hot strength and resistance to softening at elevated temperatures are the principal requirements, and resistance to shock, while important, is a secondary consideration. Within this general characterization, the various types of tungsten hot-work steels offer various combinations of elevated-temperature wear or erosion resistance and toughness, depending on carbon and alloy content and heat treatment as described below. Typical applications for the tungsten H-type steels include extrusion dies for brass, bronze, and steel, hot-press dies, dummy blocks, hot-swaging and drawing dies, shear blades for hot work, and hot punches.

Tungsten is a strong ferrite-stabilizing and carbide-forming element in steels; as a result, ferrite exists over a significant range of compositions at

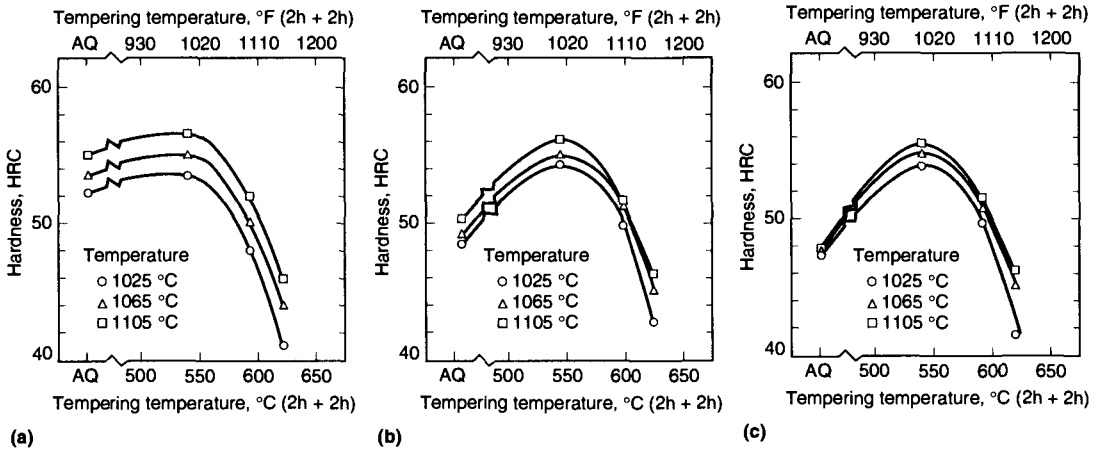

Fig. 13-18 Hardness as a function of tempering temperature for H13 steel austenitized at various temperatures. (a) Air-cooled 12.5 mm (0.5 in.) specimens. (b) Simulated air cooling at midradius of 150 mm (6 in.) diam rounds. (c) Simulated air cooling at midradius of 300 mm (12 in.) diam rounds. Source: Ref 6

high temperatures. Figure 13-28 shows an isothermal section of the Fe-W-C system at 1200 °C (2190 °F) as developed by the pioneering studies of Takeda (Ref 30). Considerable more recent work on the phases, phase equilibria, and phase diagrams of the Fe-W-C system is summarized in Ref 31. The isothermal section of Fig. 13-28 provides guidelines for the phase equilibria that exist at temperatures close to the hardening temperatures for the tungsten H-type steels; superimposed on the diagram are contents of iron, tungsten, and carbon of some of the steels. Actual boundaries of the phase fields will be shifted by other alloying elements. For example, chromium and vanadium also stabilize ferrite and are also incorporated into alloy carbides. Therefore, in tungsten steels with multiple alloying elements, more ferrite may be retained during austenitizing treatments for hardening than indicated by only the Fe-W-C diagrams. The ferrite will reduce the amount of austenite that transforms to martensite on quenching and thus contributes to low hardness in hardened tools. In order to reduce ferrite stability, the austenite-stabilizing elements nickel and cobalt were added to some of the tungsten hot-work tool steels developed earlier, but which are no longer widely used (Ref 32).

A number of carbide phases are stable in the Fe-W-C system. A major alloy carbide in tungsten

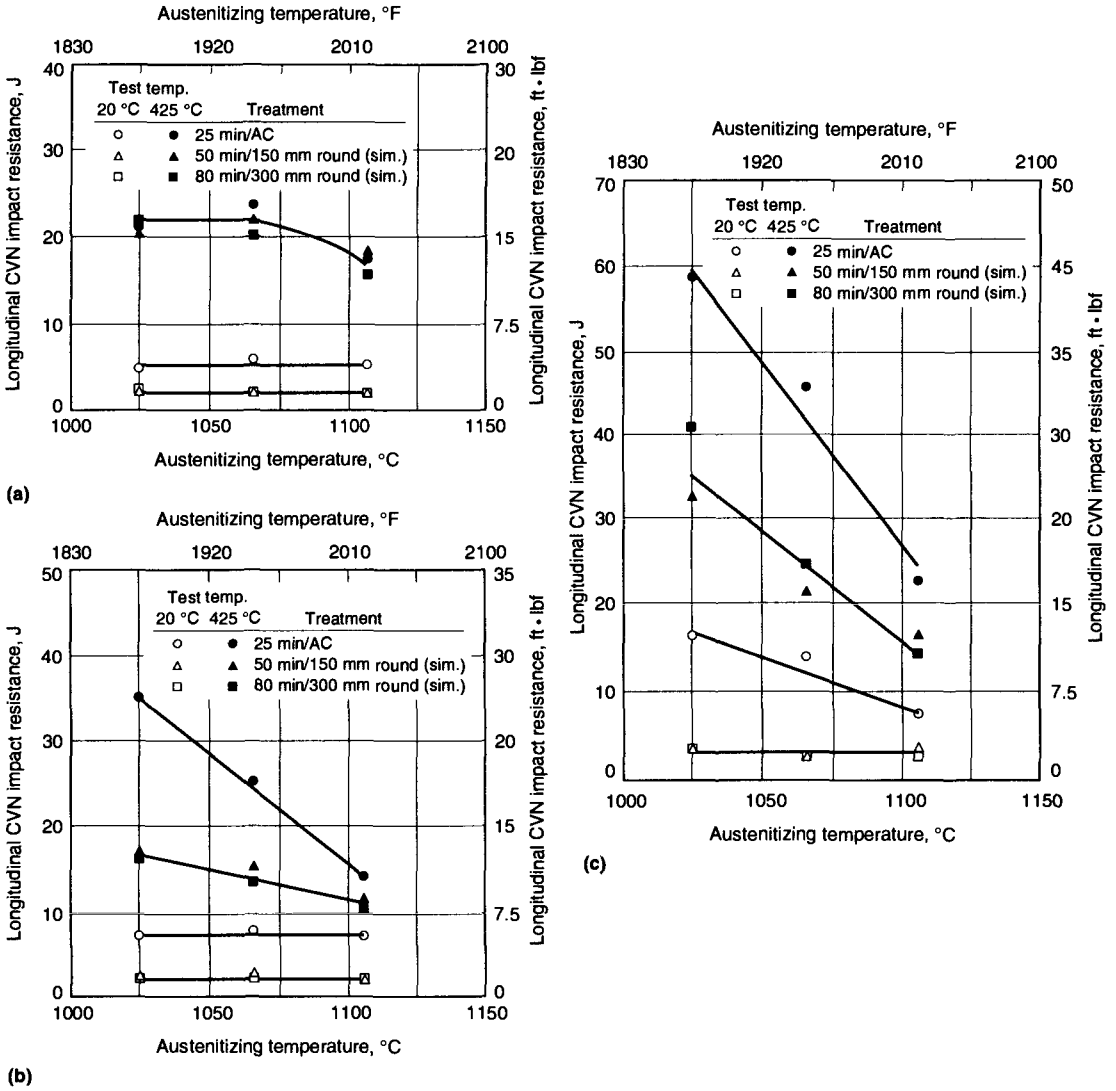

Fig. 13-19 CVN toughness of H13 steel as a function of austenitizing temperature. Specimens cooled at various rates and tested at room temperature or 425 °C (800 °F) after double tempering for 2 h periods at (a) 540 °C (1000 °F), (b) 595 °C (1100 °F), and (c) 620 °C (1150 °F). Source: Ref 6

hot-work steels is M_6C, which exists over the approximate composition range of Fe_4W_2C to Fe_3W_3C and is stable at both hardening and tempering temperatures. The binary carbide W_2C has also been reported to form on tempering. The $M_{23}C_6$ carbide is not stable in the Fe-W-C system, but appears as a metastable phase in the tungsten hot-work tool steels, perhaps because chromium is also present as an alloying element (Ref 33). The $M_{23}C_6$ carbides may coexist with M_6C carbides in some of the lower-tungsten-containing H-type steels at temperatures in the ranges used for tempering.

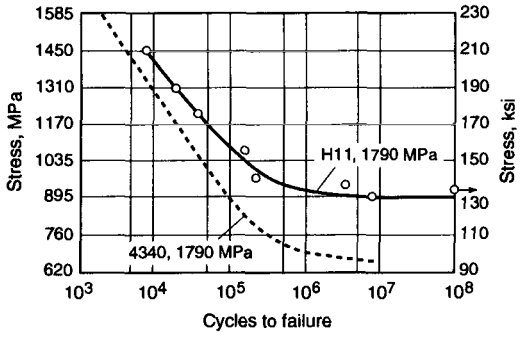

Fig. 13-20 Stress versus cycles to failure of H11 and 4340 steels, both heat treated to 1790 MPa (260 ksi) ultimate tensile strength. Source: Ref 13, 14

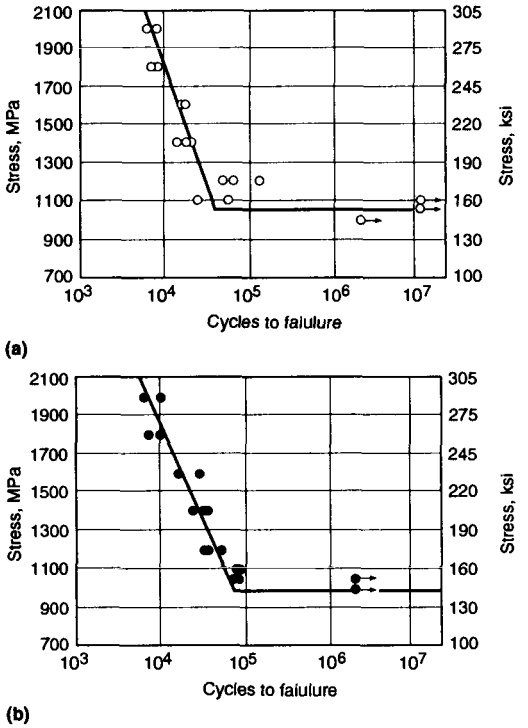

Fig. 13-21 Stress versus cycles to failure of H11 tool steel subjected to cantilever bend specimen fatigue testing. (a) Tempered at 500 °C (930 °F), peak hardness. (b) Tempered at 600 °C (1112 °F), overaged. Source: Ref 15

The low carbon content of the tungsten hot-work steels makes them more readily forgeable than high-speed steels. Preheating to 790 to 845 °C (1450 to 1550 °F), before heating to the starting forging temperature, should be performed. Finishing temperatures should be not lower than 870 °C (1600 °F). The tungsten hot-work tool steels are air hardening and thus should be slow cooled after forging. Forgings should not be normalized and should always be annealed before machining or hardening. Annealing should be performed in neutral atmospheres. Because of their relatively low carbon contents, the tungsten hot-work steels are highly sensitive to carburization if carbon-containing packing materials are used during annealing. Stress relieving at temperatures between 595 and 675 °C (1100 and 1250 °F) prior to final machining helps to reduce distortion on subsequent hardening.

Typical IT diagrams for some tungsten H-type steels are shown in Fig. 13-29 to 13-31 (Ref 5). Well-separated C-curves for the transformation of austenite to pearlite and bainite are characteristic features of the diagrams. Preceding the sluggish transformation to pearlite at the higher temperatures is the formation of proeutectoid carbide, as indicated by the dashed lines in Fig. 13-29 and 13-30. The proeutectoid carbide in the tungsten hot-work steels was not considered to have any major effect on mechanical properties (Ref 5). The bainite transformations are relatively rapid compared to the pearlitic transformations, and in heavier sections, mixtures of bainite and martensite would be expected after hardening. The relatively low carbon contents of the tungsten hot-work steels means that M_s temperatures are high and that only small

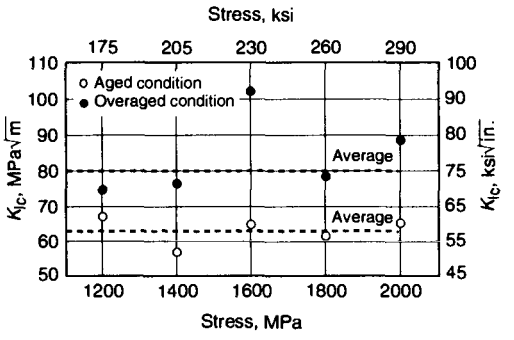

Fig. 13-22 Fracture toughness of hardened H11 steel tempered to peak hardness at 500 °C (930 °F) and overaged at 600 °C (1110 °F). The K_I values were calculated from the size and shape of fatigue cracks at instability at various maximum applied stresses. Source: Ref 15

amounts of austenite will be retained within hardened microstructures.

Figures 13-32 and 13-33 show as-quenched hardness as a function of austenitizing temperature for some tungsten hot-work steels. Unlike many of the tool steels discussed to this point, the increasing hardness with increasing austenitizing temperature is due not only to the solution of alloy carbides and the corresponding increase in carbon and alloy content of the austenite. As mentioned earlier, ferrite coexists with the austenite and alloy carbides during austenitizing of the tungsten steels, especially at the lower austenitizing temperatures. This ferrite is stable to room temperature and does not contribute to hardening, which is achieved only by transformation of austenite to martensite. The low as-quenched hardness of the low-carbon H25 steel (Fig. 13-33) is directly attributable to high retained ferrite content.

The tungsten H-type steels are relatively deep hardening and readily through-harden in 25 mm (1 in.) sections on air cooling. Larger sections require more rapid cooling, and more rapid cooling approaches that have been used include:

- Direct quenching in warm oil at about 65 °C (150 °F)
- Interrupted oil quenching during which tools are quenched in oil until the surface becomes black and then are air cooled to room temperature
- Quenching in molten salt at 540 to 595 °C (1000 to 1100 °F) and then air cooling to room temperature. This approach is shown schematically in Fig. 13-1
- Cooling in an air blast

To reduce distortion, tools should be preheated at 815 to 900 °C (1500 to 1650 °F) before heating to the final hardening temperature. High austenitizing temperatures promote rapid solution of carbides, and it is not necessary to soak tungsten hot-work steels extensively at hardening temperatures. As soon as parts have reached a uniform temperature throughout, they can be quenched. For maximum hot hardness, the high side of the hardening temperature range should be used, and for maximum toughness, the low side of the range should be used. Parts should be tempered as soon as possible after quenching. To reduce the danger of cracking, slow heating to the tempering temperature is recommended. Double, or even triple, tempering should be applied for maximum toughness and microstructural stability.

Figure 13-34 shows hardness as a function of tempering temperature for an H21 steel austenitized at three different temperatures. With increasing austenitizing temperature, not only does as-quenched hardness increase, but so do the peak tempered hardness and the maximum temperatures

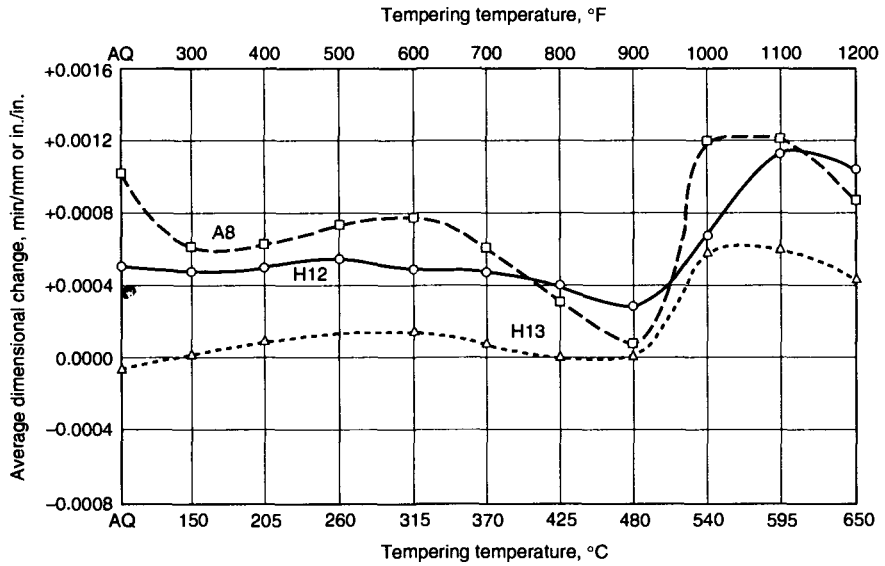

Type	Composition, %						Hardening temperature		Hardening medium
	C	Si	Cr	Mo	W	V	°C	°F	
H12	0.35	1.00	5.00	1.60	1.30	0.30	1010	1850	Air
H13	0.40	1.00	5.00	1.20	...	1.00	...	...	...

Fig. 13-23 Effect of tempering temperature on dimensional changes in chromium hot-work tool steels. Values represent the average dimensional change in three principal directions of a block 25 by 50 by 150 mm (1 by 2 by 6 in.) in size. Courtesy of Latrobe Steel Co.

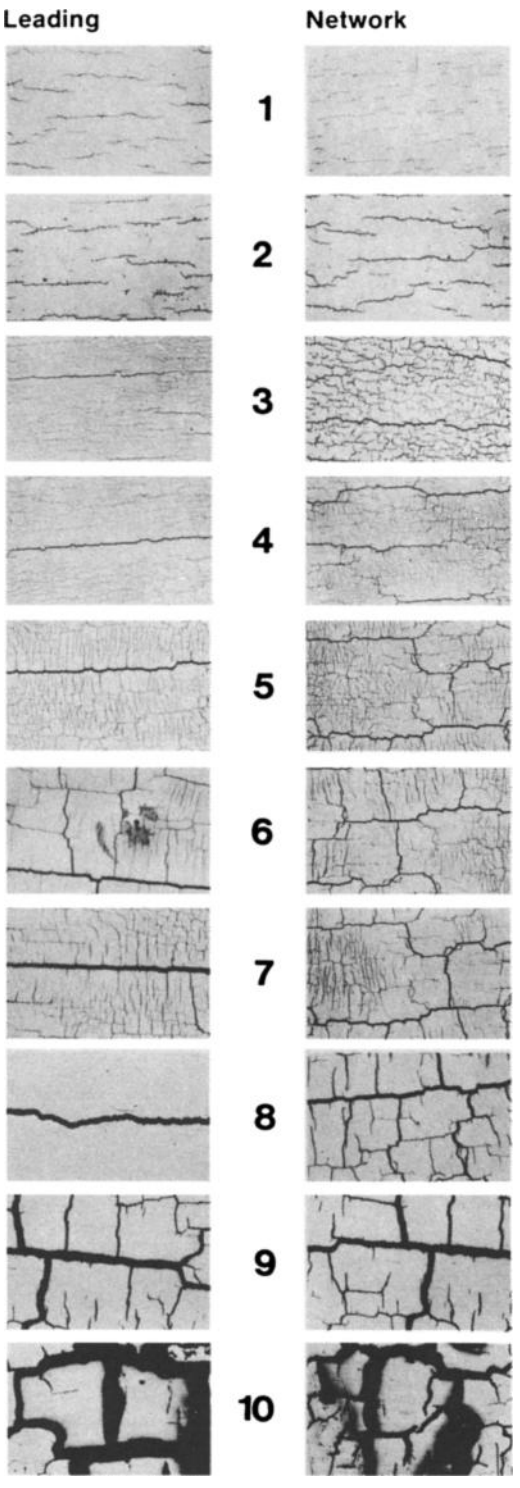

Fig. 13-24 Uddeholm heat-checking scale. Photographs (actual size) in the left column represent leading, largest cracks, and in the right column represent severity of crack networks. Added ratings from both columns give final rating of heat checking.

that resist softening. This behavior is consistent with increased supersaturation of as-quenched martensite with carbon and alloying elements and the associated greater intensity of secondary hardening in specimens that are austenitized at the higher temperatures. Alloy carbides that have been identified to form on tempering an H21 steel include W_2C, M_6C, and $M_{23}C_6$, with W_2C being the carbide primarily associated with peak hardness (Ref 34, 35). Figures 13-35 and 13-36 show additional curves of hardness as a function of tempering temperature for various tungsten hot-work steels (Ref 36, 37). The curves emphasize the major effect of alloy carbon content on as-quenched and tempered hardness.

Tempering temperatures corresponding to the maximum temperature expected in service should be selected for tungsten steels expected to encounter temperatures not over 650 to 700 °C (1200 to 1300 °F). If this is not done, during operation the die working surface tends to soften more rapidly than the body of the die. The resulting surface stresses that develop may lead to premature failure. Since the tungsten hot-work steels develop maximum hardness at tempering temperatures between 565 and 595 °C (1050 and 1100 °F), there should seldom be a need to temper them below this temperature range. If softer dies are required, a tempering temperature above that which produces peak hardness should be selected. Such increased tempering will not only lower hardness but also relieve internal stresses and increase toughness.

The tungsten hot-work steels retain a considerable portion of their hardness at elevated temperatures. Figure 13-37 compares elevated-temperature hardness of H21 and H24 steels, heat treated to two initial conditions, as a function of testing temperature. The specimens with the higher initial hardness retain higher hardness throughout most of the temperature range, and the H24 steel, with its higher tungsten content, has better hot hardness than does the H21 steel in similar initial conditions.

Figures 13-38 to 13-40 present impact toughness as a function of tempering temperature for various tungsten hot-work steels in various heat-treated conditions. Figure 13-38 shows that the high hardening temperatures that produce the highest hardness and softening resistance have the lowest room-temperature impact toughness. There is a pronounced decrease in toughness after tempering at temperatures that produce peak hardness, and microstructural changes similar to those discussed relative to the chromium hot-work tool steels are most probably responsible for this decrease. Tempering above the temperatures that produce peak hardness substantially increases impact toughness, as best shown in Fig. 13-40. Also, similar to the chromium hot-work steels, tempered martensitic microstructures in the tungsten hot-work steels have better toughness than tempered bainitic microstructures (Fig. 13-39).

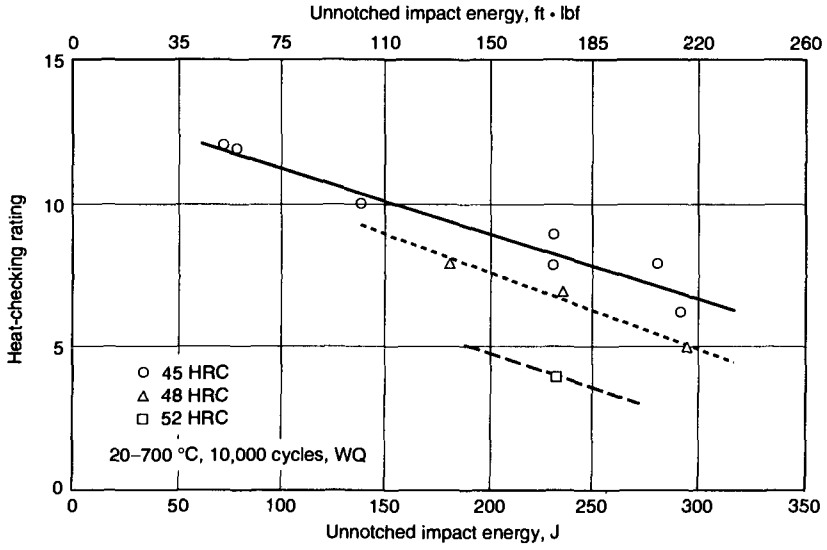

Fig. 13-25 Heat-checking resistance (lower readings indicate higher resistance) as a function of unnotched impact toughness and hardness of H13 steel. Source: Ref 24

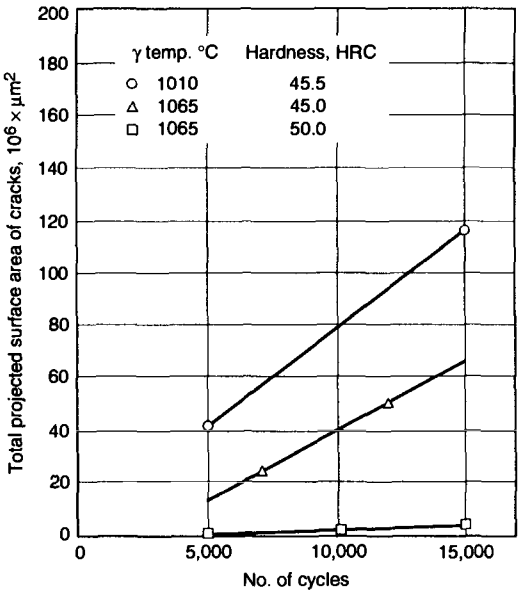

Fig. 13-26 Surface area of thermal cracking as a function of thermal cycles for H13 steel austenitized and heat treated to various levels of hardness. Source Ref 19, as reproduced in Ref 6

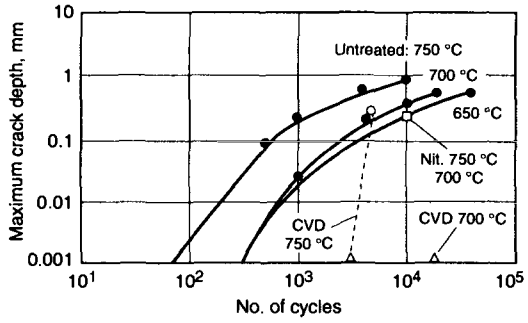

Fig. 13-27 Maximum crack depth versus number of thermal cycles for H13 type steels in untreated, nitrided, or CVD-coated conditions. Top temperature in thermal cycles was between 650 and 750 °C (1200 and 1380 °F). Source: Ref 24

Although the room-temperature impact toughness of the tungsten hot-work steels is low, the toughness at hot-working temperatures is significantly higher. Figure 13-41 shows this increase in toughness as function of testing temperature for H21 and H22 steels heat treated to the same hardness. Also compared is the effect of microstructure produced by changing the rate of cooling after austenitizing. In the H21 steel, tempered martensitic microstructures outperform bainitic microstructures, but in the H22 steel, with inherently lower toughness, microstructural differences in matrix microstructures play a smaller role in fracture resistance. The temperature dependence of toughness provides an important reason to preheat dies prior to use and to maintain them at temperature during operation. If hot-working impact loads are applied to cold dies, the dies may crack immediately because of their low room-temperature toughness; preheating will increase toughness and produce satisfactory performance.

Many hot-work dies are used in a hardness range of 42 to 45 HRC. Figure 13-42 shows the combinations of austenitizing temperatures and tempering temperatures that will produce this hardness level in an H21 steel. Also shown are the results of measurements of ductility (ultimate deformation) and toughness (ultimate torque) obtained from static torsion tests. The torsional properties are low for specimens austenitized and tempered at combinations of low austenitizing and tempering temperatures, increased to a maximum at an austenitizing temperature of 1065 °C (1950 °F) and a tempering temperature of 620 °C (1150 °F), and then decreased rapidly for combinations of higher austenitizing and tempering temperatures.

Table 13-5 shows elevated-temperature tensile properties of some tungsten steels. Increasing carbon content within a given grade, as shown for example by the H21 steel with 0.28% C and 0.35% C, raises hot strength. Increasing tungsten content, as shown by comparison of the properties of the H21 and H22 steels, lowers hot ductility.

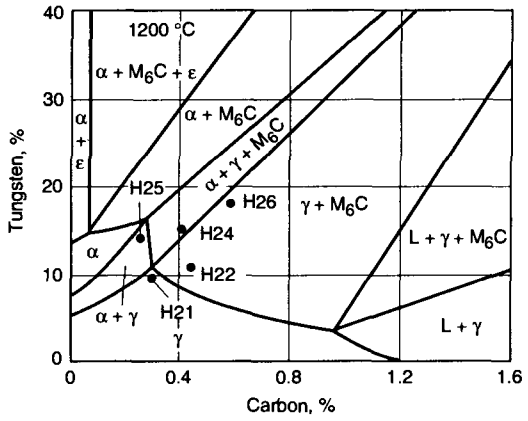

Fig. 13-28 Isothermal section of Fe-W-C diagram at 1200 °C (2190 °F). Nominal compositions of tungsten, carbon, and iron for some tungsten hot-work steels are plotted. Source: Ref 30

Molybdenum Hot-Work Steel

Table 13-1 presents the composition of H42 tool steel, the single molybdenum hot-work tool steel still widely used. As a result of wartime shortages of tungsten, a number of molybdenum hot-work steels were developed (Ref 32), but gradually the use of these steels has declined. The properties of these steels for hot-work applications were intermediate to the chromium and tungsten hot-work tool steels discussed earlier, and the availability of H42 offers a roughly comparable alternative to the tungsten steels when cost is considered.

H42 steel contains nominally 5% Mo, 6% W, 2% V, and 4% Cr and is available in several carbon ranges. The high content of carbide-forming elements controls hardening and makes possible high hardness as

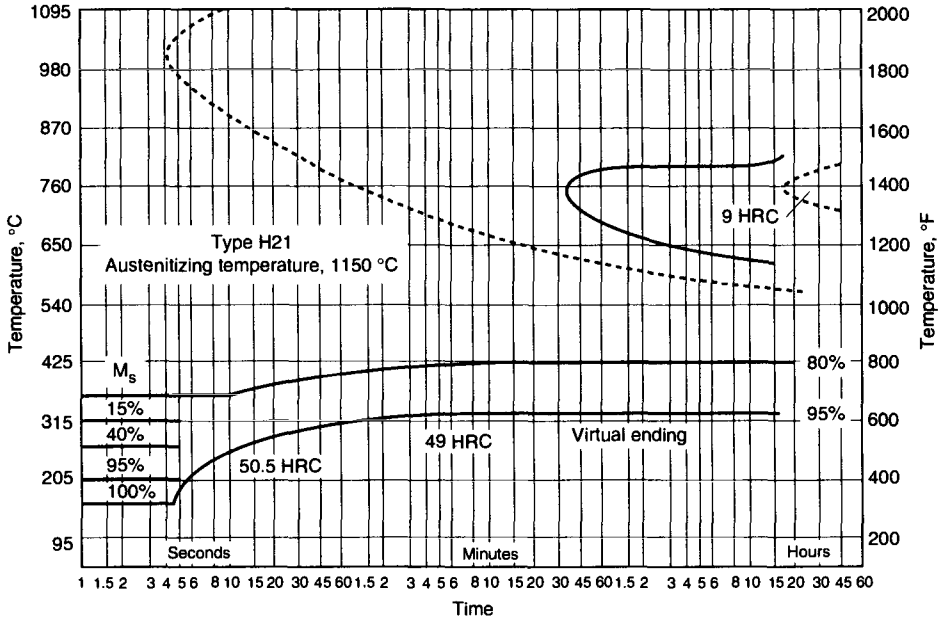

Fig. 13-29 IT diagram for H21 steel containing 0.30% C, 3.25% Cr, 9.00% W, and 0.25% V, and after austenitizing at 1150 °C (2100 °F). Source: Ref 5

a result of secondary hardening during tempering. Preheating at 760 to 815 °C (1400 to 1500 °F) prior to heating to forging temperatures is recommended, and because of the high hardenability and air-hardening capability of H42 steel, forgings should be slow cooled and should not be normalized. Molybdenum hot-work steels are highly susceptible to decarburization and must be protected during annealing and hardening heat treatments.

Figure 13-43 shows as-quenched hardness as a function of austenitizing temperature for some molybdenum hot-work steels. Relatively high austenitizing temperatures are required to provide high as-quenched hardness and a good base for secondary hardening during tempering. For hardening, preheating in two stages, the first at 540 to 650 °C (1000 to 1200 °F) and the second at 845 to 870 °C (1555 to 1600 °F), is recommended to reduce thermal shock. In view of the high optimal austenitizing temperatures, carbide dissolution and the adjustment of austenite chemistry are quite rapid, and holding times should be short, on the order of 2 to 5 min.

The effect of tempering temperature on the hardness of several molybdenum hot-work steels is shown in Fig. 13-44 and 13-45 (Ref 38). The combination of alloying elements and proper heat treatment of the H42 steel provides superior hardness relative to some of the other molybdenum hot-work steels that are no longer widely used. Immediately after reaching 50 °C (120 °F), tools should be tempered at temperatures of 565 to 650 °C (1050 to 1200 °F), which are on the high side of those which produce maximum secondary hardening. Double

Table 13-5 Tensile properties of tungsten hot-work tool steels at elevated temperatures

Testing temperature		Tensile strength		Yield strength (0.2% offset)		Elongation in 50 mm	Reduction	Initial room-temperature hardness,
°C	°F	MPa	ksi	MPa	ksi	(2 in.), %	of area, %	HRC
H21(a)								
25	80	1379	200	1193	173	8	30	43
425	800	1138	165	952	138	11	23	42
480	900	1048	152	896	130	14	43	42
540	1000	889	129	765	111	11	29	41
595	1100	938	136	627	91	6	12	44
650	1200	745	108	586	85	4	9	43
H21(b)								
25	80	1675	243	1482	215	12	37	50
205	400	1579	229	1310	190	12	42	50
315	600	1531	222	1241	180	11	42	50
425	800	1517	220	1207	175	10	40	50
540	1000	1448	210	1124	163	9	32	50
650	1200	896	130	586	85	5	15	50
H22(c)								
25	80	1310	190	1103	160	9	21	42
425	800	1138	165	986	143	8	17	43
480	900	1055	153	896	130	8	22	43
540	1000	938	136	807	117	6	14	43
595	1100	827	120	731	106	5	6	43
650	1200	641	93	552	80	4	10	42
H22(d)								
400	750	1644.5	238.5	...	...	3.5	17.0	52 (est)
540	1000	1542.76	223.75	...	...	5.5	16.2	52 (est)
650	1200	904.97	131.25	...	...	5.5	24.5	52 (est)
760	1400	221	32	...	...	35.5	89.8	52 (est)
H24(e)								
400	750	1853.03	268.75	...	...	3.0	5.8	53.5 (est)
540	1000	1556.55	225.75	...	...	1.5	5.0	53.5 (est)
650	1200	862	125	...	...	1.0	5.5	53.5 (est)
760	1400	218.92	31.75	...	...	23.0	78.9	53.5 (est)

(a) Composition: 0.28% C, 8.65% W, 3.34% Cr, 0.26% V. Specimens hardened by quenching at a rate equivalent to the center cooling rate of an air-cooled 100 by 100 by 100 mm (4 by 4 by 4 in.) block and tempered to the indicated hardness level. Source: Ref 5. (b) Composition: 0.35% C, 9.35% W, 3.25% Cr, 0.50% V. Specimens quenched in oil from 1175 °C (2150 °F) and tempered at 625 °C (1160 °F) to 50 HRC. Source: Bethlehem Steel Co. (c) Composition: 0.38% C, 11.64% W, 1.95% Cr, 0.31% V. Specimens treated as in (a). (d) Composition: 0.38% C, 12% W, 3% Cr, 0.45% V. Specimens quenched in air from 1175 °C (2150 °F) and tempered 2 h at 595 °C (1100 °F). Source: Allegheny Ludlum Industries. (e) Composition: 0.45% C, 14% W, 3.5% Cr, 0.70% V. Specimens treated as in (d).

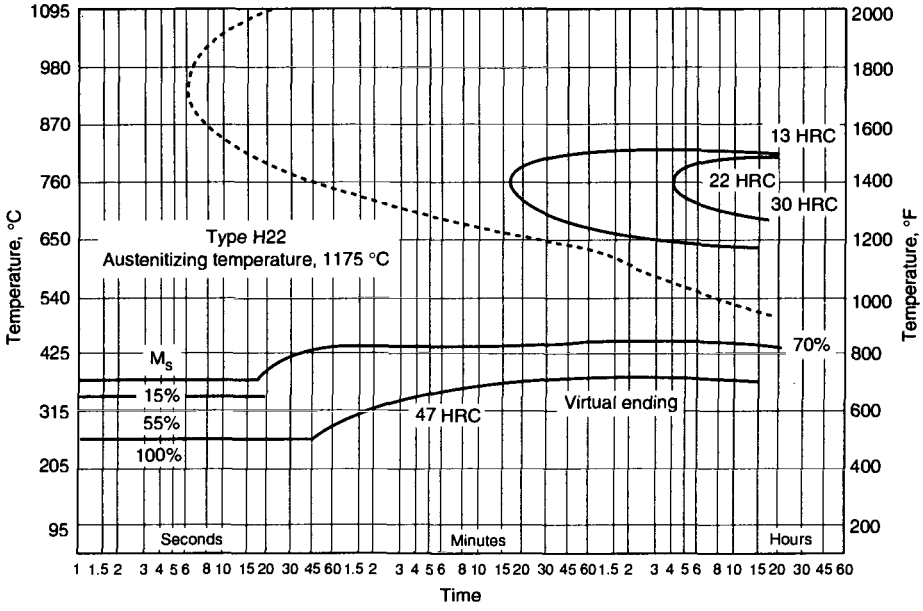

Fig. 13-30 IT diagram for H22 steel containing 0.40% C, 2.00% Cr, 11.50% W, and 0.35% V, and after austenitizing at 1175 °C (2150 °F). Source: Ref 5

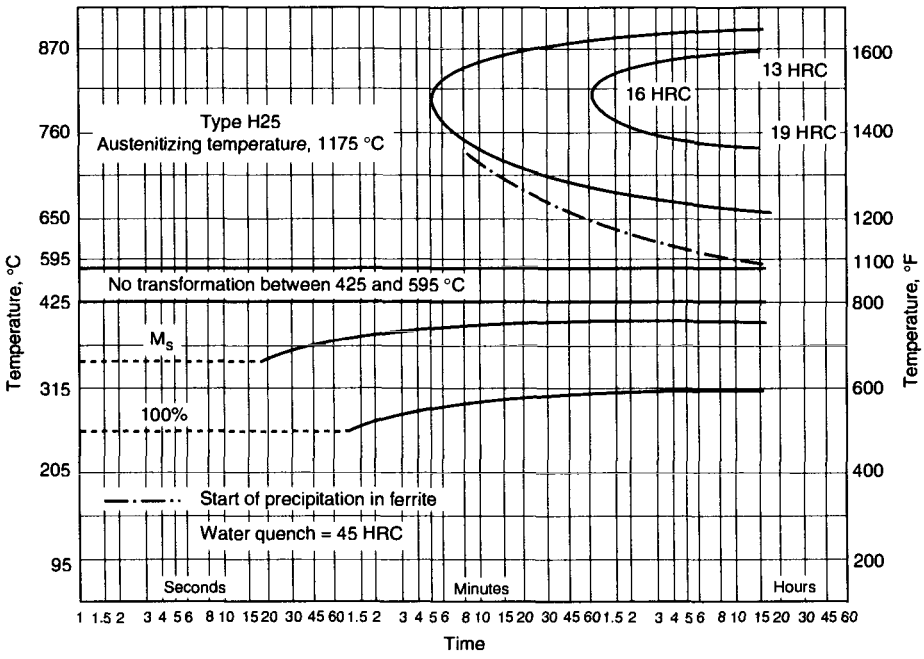

Fig. 13-31 IT diagram for H25 steel containing 0.25% C, 4.00% Cr, 15.00% W, and 0.50% V, and austenitized at 1175 °C (2150 °F). The structure of this alloy at 1175 °C consists of about 70% austenite and 30% ferrite. Courtesy of Crucible Steel Co.

tempering is essential and triple tempering is beneficial.

REFERENCES

1. I. Schruff, Comparison of Properties and Characteristics of Hot-Work Tool Steels, *Thyssen Edelstahl Tech. Ber.*, Vol 16, 1990, p 32-44
2. S. Tour, Steels for Die-Casting Dies, *Trans. AIME*, Vol 116, 1935, p 242
3. J.C. Hamaker, Jr., Die Steel Useful for Ultra High-Strength Structural Requirements, *Met. Prog.*, Dec 1956, p 93
4. G.A. Roberts and J.C. Hamaker, Jr., U.S. Patent 2,893,902, 7 July 1959
5. P. Payson and A.E. Nehrenberg, The Metallography and Properties of High Alloy Hot Work Steels, *AISI Yearbook*, American Iron and Steel Institute, 1948, p 540
6. M.L. Schmidt, Effect of Austenitizing Temperature on Laboratory Treated and Large Section Sizes of H-13 Tool Steels, *Tool Materials for Molds and Dies*, G. Krauss and H. Nordberg, Ed., Colorado School of Mines Press, 1987, p 118–164
7. J.R.T. Branco, "Development of Nb Modified AISI H13/H11 Type Tool Steels," Ph.D. thesis, Colorado School of Mines, 1989
8. H. Nilsson, O. Sandberg, and W. Roberts, The Influence of Austenitization Temperature and the Cooling Rate after Austenitization on the Mechanical Properties of the Hot-Work Tool Steels H11 and H13, *Tools for Die Casting*, Uddeholm/Swedish Institute for Metals Research, Stockholm, 1983, p 51–69
9. J.R.T. Branco and G. Krauss, Toughness of H11/H13 Hot Work Die Steels, *New Materials Processes Experiences for Tooling*, H. Berns, M. Hofmann, L.-A. Norstrom, K. Rasche, and A.-M. Schindler, Ed., MAT SEARCH, Andelfingen, Switzerland, 1992, p 121–134
10. J.P. Materkowski and G. Krauss, Tempered Martensite Embrittlement in SAE 4340 Steel, *Metall. Trans. A*, Vol 10A, 1979, p 1643–1651
11. J. Akerman, "The Effect of Cooling Rate after Austenitization on the Properties of Hot-Work Tool Steels H-11 and H-13—A Literature Review," Report No. 1500, Swedish Institute for Metals Research, Stockholm, Nov 1980
12. P. Sommer et al., Einfluss von Chemischer Zusammansetzung und Gefuge auf die Ubergangstemperatur der Kerbschlagszahigkeit warmfester Stahle, *Arch. Eisenhüttenwes.*, Vol 48 (No. 10), 1977, p 535–539

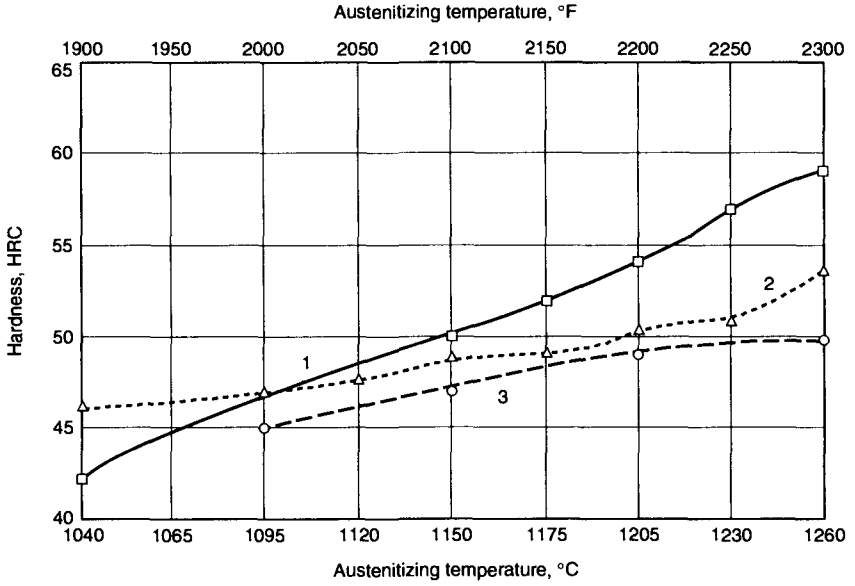

Curve	Type	Composition, % C	Cr	W	V	Ni	Quench medium	Specimen size
1	H21	0.35	3.25	9.35	0.50	...	Air	1 (diam) × 5 in.
2	H22	0.38	3.00	12.00	0.45	...	Air	1 (diam) × 2 in.
3	...	0.30	2.75	9.75	...	1.65	Air	3¾ (diam) × 3¼ in.

Fig. 13-32 As-quenched hardness as a function of austenitizing temperature for tungsten hot-work steels. Data from Bethlehem Steel Co., Vulcan-Kidd Division of H.K. Porter Co., and Allegheny Ludlum Industries

13. J.C. Hamaker, Jr. and E.J. Vater, "Carbon: Strength Relationships in 5 Per Cent Chromium Ultra High-Strength Steels," Reprint No. 80, ASTM, 1960
14. H.N. Cummings, F.B. Stulen, and W.C. Schulte, Relation of Inclusions to the Fatigue Properties of SAE 4340 Steel, *Trans. ASM*, Vol 49, 1957, p 482
15. K. Peters, unpublished research, Colorado School of Mines, 1991
16. B.S. Lement, *Distortion in Tool Steels*, American Society for Metals, 1959, 173 p
17. G.A. Roberts and A.H. Grobe, Service Failures of Aluminum Die-Casting Dies, *Met. Prog.*, Vol 69 (No. 2), 1956, p 58
18. H. Nordberg and W. Roberts, Ed., *Tools for Die Casting*, Uddeholm/Swedish Institute for Metals Research, Stockholm, 1983
19. J.F. Wallace, Effect of Selected Processing on Compositional Factors on the Failure of H-13 Steel as Dies for Aluminum Die Casting, *Die Tech '84*, American Die Casting Institute, 1984, p 6–37
20. S. Malm and J. Tidlund, Increased Life for Die Casting Dies, Paper No. G-T79-051, *Trans. 10th Int. Die Casting Congress*, Society of Die Casting Engineers, 1979, p 173–186
21. J.C. Benedyk, D.J. Moracz, and J.F. Wallace, Thermal Fatigue Behavior of Die Materials for Aluminum Die Casting, Paper No. 111, *Trans. 6th Int. Die Casting Congress*, Society of Die Casting Engineers, 1970, p 187–206
22. W. Roberts and L.-A. Norstrom, Premium Die Steel and Heat Treatment Solutions for the 1990s, Paper No. G-T87-009, *Trans. 14th Int. Die Casting Congress*, Society for Die Casting Engineers, 1987, p 1–12
23. M.A.H. Howes, A Study of Thermal Fatigue Mechanisms, *Thermal Fatigue of Materials and Components*, D.A. Spera and D.F. Mowbray, Ed., STP 612, ASTM, 1976, p 86–105
24. L. Eliasson and O. Sandberg, Effect of Different Parameter on Heat-Checking Properties of Hot-Work Tool Steels, *New Materials and Processes for Tooling*, H. Berns, H. Nordberg, and H.-J. Fleischer, Ed., Verlag Schurmann & Klagges KG, Bochum, Germany, 1989, p 3–14
25. Heat Treatment of H13 Die Casting Tool Steel, North American Die Casting Association, 1988
26. H.-J. Becker, K.-D. Fuchs, E. Haberling, and K. Rasche, Microstructure and Technological Properties of Hot Work Tool Steels for Pressure Die Casting Dies, Paper No. G-T89-053, *Trans. 15th Int. Die Casting Congress*, North American Die Casting Association, 1989, p 1–7
27. E. Kogler, R. Breitler, and A. Schindler, Die Steel Quality and Life Requirements for Aluminum Die Casting Dies, Paper No. G-T89-052, *Trans. 15th*

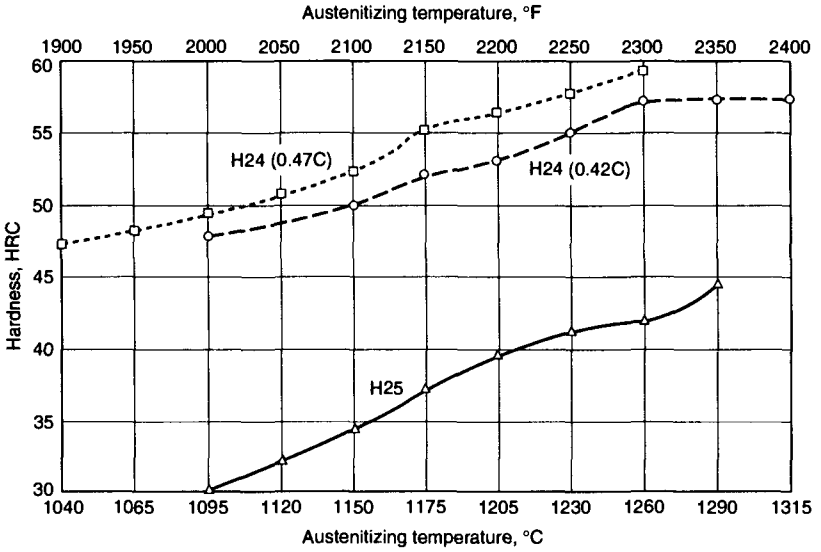

Type	Composition, %				Hardening medium	Specimen size
	C	Cr	W	V		
H24	0.42	3.50	14.00	0.30	Air	1 (diam) × 5 in.
H24	0.47	3.50	14.00	0.70	Air	1 (diam) × 2 in.
H25	0.25	4.00	15.00	0.50	Oil	...

Fig. 13-33 As-quenched hardness as a function of austenitizing temperature in tungsten hot-work steels with various carbon contents. Data from Latrobe Steel Co., Bethlehem Steel Co., and Allegheny Ludlum Industries

Int. Die Casting Congress, North American Die Casting Association, 1989, p 1-14
28. L.L. Centa and J.F. Wallace, Effect of Electro-Discharge Machining on the Surface and Sub-Surface Microstructure of H-13 Steel, Paper No. G-T89-032, *Trans. 15th Int. Die Casting Congress,* North American Die Casting Association, 1989, p 1–13
29. C.J. Dorsch and H.P. Nichols, The Effects of EDM on the Surface of Hardened H-13 Die Components, Paper No. G-T89-031, *Trans. 15th Int. Die Casting Congress,* North American Die Casting Association, 1989, p 1–6
30. S. Takeda, Metallographic Investigation of the Ternary Alloys of the Iron-Tungsten-Carbon System, *Tech. Rep. Sendai,* Vol 9, 1930, p 483; Vol 10, 1931, p 42
31. G.V. Raynor and V.G. Rivlin, C-Fe-W System, *Phase Equilibria in Iron Ternary Alloys,* Institute of Metals, London, 1988, p 200–212
32. G.A. Roberts and R.A. Cary, *Tool Steels,* 4th ed., American Society for Metals, 1980
33. K. Kuo, Carbides in Chromium, Molybdenum, and Tungsten Steels, *J. Iron Steel Inst.,* Vol 173, 1953, p 363
34. K. Kuo, Carbide Precipitation, Secondary Hardening, and Red Hardness of High Speed Steel, *J. Iron Steel Inst.,* Vol 174, 1953, p 223
35. T. Sato, T. Nishizawa, and K. Murai, On Carbides in W-Cr-V Hot-Work Die Steels (Study on Carbides in Commercial Steels by Electrolytic Isolation—VI), *Tetsu-to-Hagané (J. Iron Steel Inst. Jpn.),* Vol 44, 1958, p 1378
36. G.A. Roberts, A.H. Grobe, and C.F. Moersch, Jr., The Tempering of High Alloy Tool Steels, *Trans. ASM,* Vol 39, 1947, p 521
37. G.H. Grobe and G.A. Roberts, Effect of Carbon Content on 18-4-1 High Speed Steel, *Trans. ASM,* Vol 45, 1953, p 475
38. R.B. Corbett, J.A. Succop, and A. Feduska, Alpha-Molybdenum Hot-Work Die Steels, *Trans. ASM,* Vol 46, 1954, p 1599

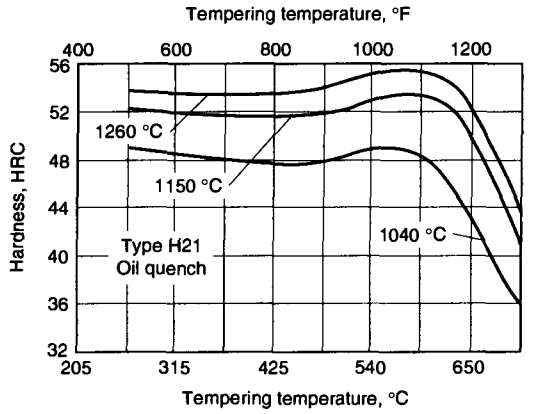

Fig. 13-34 Hardness as a function of tempering temperature for H21 steel austenitized at various temperatures. Courtesy of Teledyne VASCO

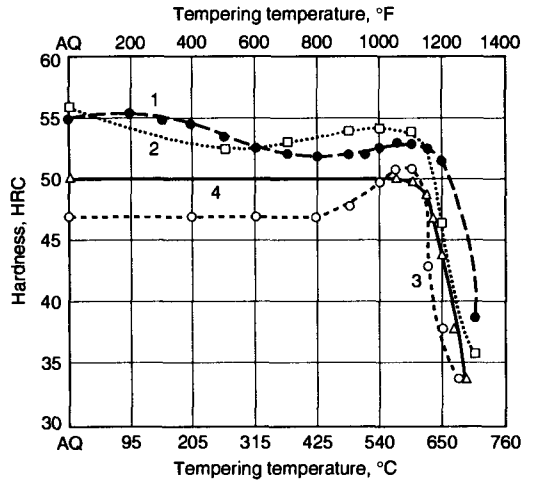

Curve	Type	Composition, %						Hardening temperature		Hardening medium	Specimen size
		C	W	Cr	V	Ni	Co	°C	°F		
1	H20	0.35	9.25	2.00	0.50	...	...	1175	2150	Oil	½ (diam) × ⅝ in.
2	H22	0.38	12.00	3.00	0.45	...	...	1205	2200	Oil	1 (diam) × 1 in.
3	...	0.30	9.75	2.75	...	1.65	...	1150	2100	Air	3¾ (diam) × 3¼ in.
4	...	0.30	12.00	2.50	0.40	...	3.60	1175	2150	Oil	...

Fig. 13-35 Hardness as a function of tempering temperature for several tungsten hot-work steels. Data from Vulcan Kidd Division of H.K. Porter Co., Allegheny Ludlum Industries, and Braeburn Alloy Steel Corp.

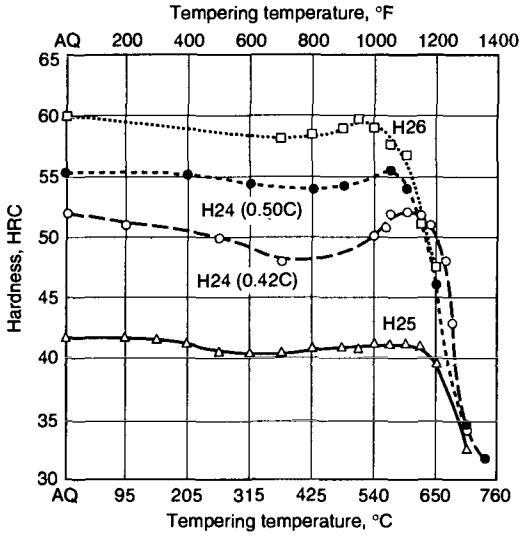

Type	Composition, %					Hardening temperature		Hardening medium	Specimen size
	C	W	Cr	V	Mo	°C	°F		
H24	0.42	14.00	3.50	0.30	...	1175	2150	Air	1 (diam) × 2½ in.
H24	0.50	14.50	3.00	0.50	...	1150	2100	Oil	3 (diam) × ½ in.
H25	0.26	14.30	3.60	0.40	...	1175	2150	Oil	½ (diam) × ⅝ in.
H26	0.58	18.26	4.04	0.99	0.36	1205	2200	Oil	½ in. cube

Fig. 13-36 Hardness as a function of tempering temperature for tungsten hot-work steels with varying carbon content. Data from Ref 36, Bethlehem Steel Co. and Teledyne VASCO

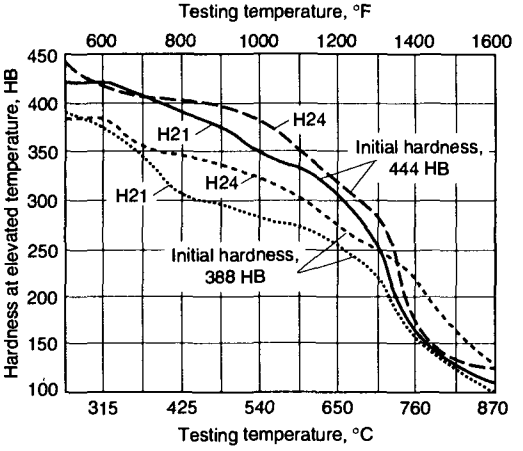

Type	Composition, %				T_{max}		Quench medium
	C	W	Cr	V	°C	°F	
H21	0.40	8.75	3.50	0.20	1260	2300	Oil
H24	0.45	15.00	2.75	0.40	1260	2300	Oil

Fig. 13-37 Elevated-temperature hardness as a function of test temperature for H21 and H24 steel heat treated to initial room-temperature hardnesses of 444 and 388 HB. Courtesy of Crucible Steel Co.

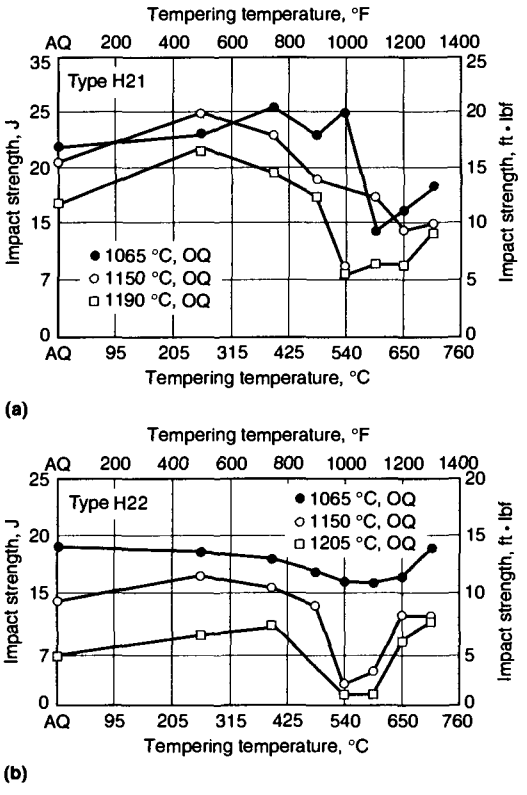

Fig. 13-38 Impact toughness determined by notched Izod specimen testing for H21 and H22 steels as a function of tempering temperature. Courtesy of Allegheny Ludlum Industries

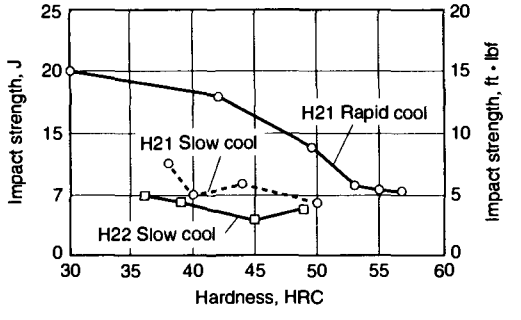

Fig. 13-39 CVN impact toughness as a function of tempered hardness for H21 and H22 steels. Rapid cooling accomplished by cooling in still air; slow cooling accomplished by furnace cooling to simulate cooling in center of an air-cooled block 100 by 100 by 100 mm (4 by 4 by 4 in.) in size. Source: Ref 5

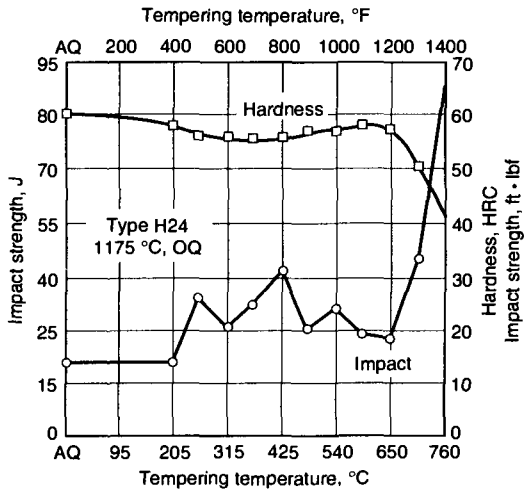

Fig. 13-40 Unnotched Izod impact toughness and hardness as a function of tempering temperature for H24 steel. Courtesy of Allegheny Ludlum Industries

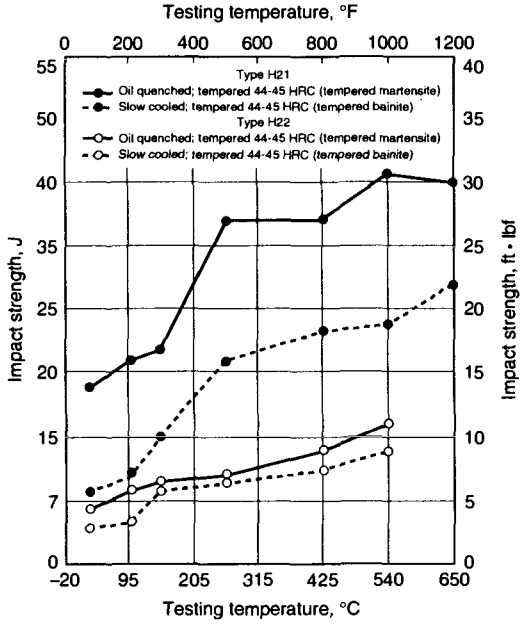

Fig. 13-41 CVN impact toughness as a function of testing temperature for H21 and H22 steels hardened from 1175 °C (2150 °F) and oil quenched or cooled at a slow rate to simulate air cooling in the center of a 100 by 100 by 100 mm (4 by 4 by 4 in.) block. Source: Ref 5

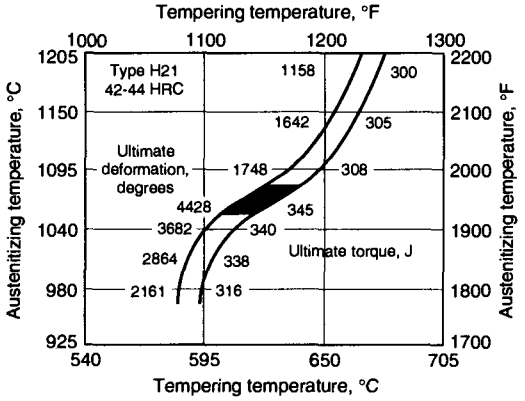

Fig. 13-42 Combinations of quenching temperature and tempering temperature to produce a hardness of 42 to 55 HRC in H21 steel. Torsional ductility and toughness are given by values of ultimate deformation (left size of band) and ultimate torque (right side of band). Courtesy of Teledyne VASCO

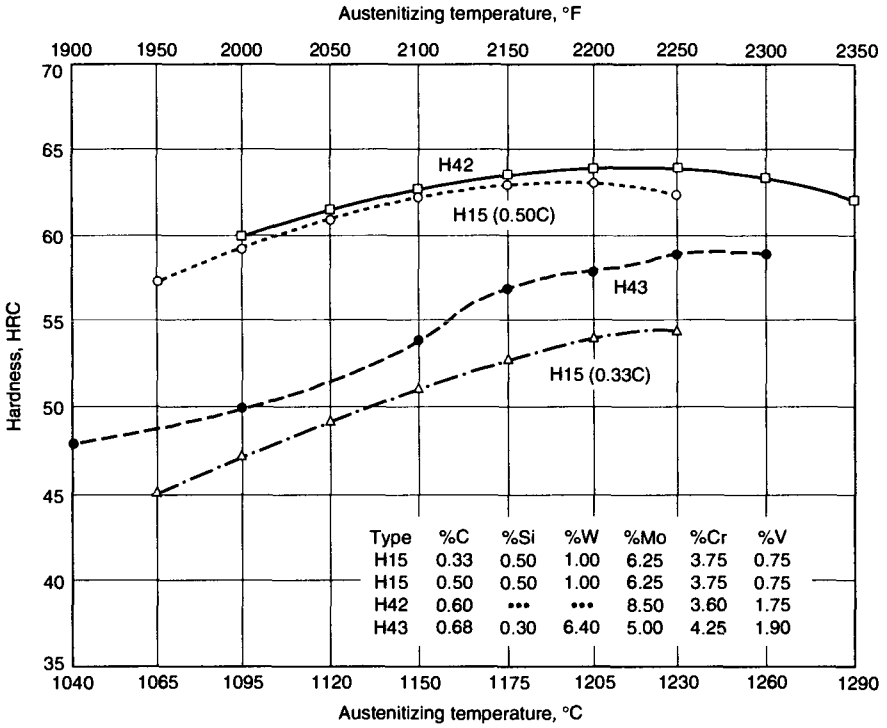

Fig. 13-43 As-quenched hardness of molybdenum hot-work steels as a function of austenitizing temperature. Specimens were oil quenched from indicated temperatures. Data from Latrobe Steel Co. and Bethlehem Steel Co.

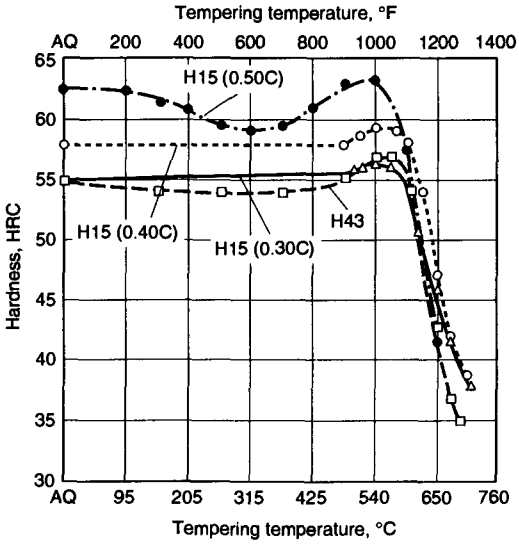

Type	Composition, %						Specimen size	Hardening temperature		Hardening medium
	C	Si	Mo	W	Cr	V		°C	°F	
H15	0.30	0.60	6.25	1.00	3.50	0.75	1 in. cube	1230	2250	Oil
H15	0.40	0.60	6.25	1.00	3.50	0.75	1 in. cube	1230	2250	Oil
H15	0.50	0.50	6.25	1.00	3.75	0.75	...	1175	2150	Oil
H43	0.60	...	8.50	...	3.60	1.75	1 (diam) × 2 in.	1205	2200	Air

Fig. 13-44 Hardness as a function of tempering temperature for molybdenum hot-work steels. Data from Universal-Cyclops Steel Corp., Latrobe Steel Co., and Bethlehem Steel Co.

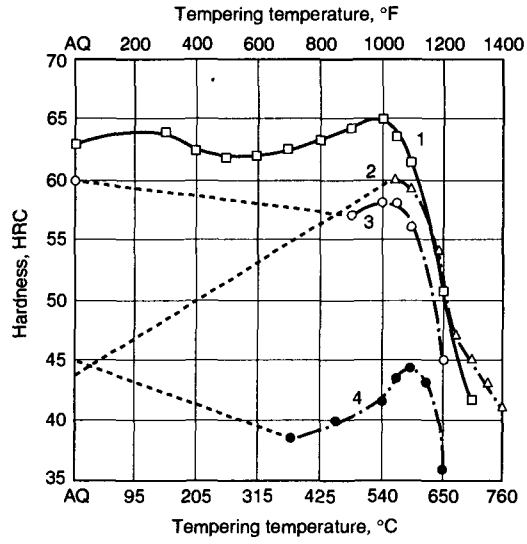

Curve	Type	Composition, %							Hardening temperature		Hardening medium
		C	Cr	W	Mo	V	Ni	Co	°C	°F	
1	H42	0.59	3.83	5.31	4.81	1.59	...	...	1230	2250	Oil
2	...	0.10	3.50	4.00	5.00	0.50	...	25.00	955	1750	Air
3	...	0.62	3.75	1.70	8.70	1.00	...	...	1150	2100	Oil
4	...	0.22	...	...	2.95	...	2.80	...	1040	1900	Water

Fig. 13-45 Hardness as a function of tempering temperature for molybdenum hot-work steels. Data from Teledyne VASCO, Atlas Steels, Ltd., and Ref 38

Tool Steels: 5th Edition
George Roberts, George Krauss, Richard Kennedy, p 251-290
DOI:10.1361/toos1998p251

Copyright © 1998 ASM International®
All rights reserved.
www.asminternational.org

CHAPTER 14
High Speed Steels

High-speed tool steels have in common the ability to maintain high hardness at elevated temperatures: typically, 52 HRC at 540 °C (1000 °F) and 48 HRC at 595 °C (1100 °F). Thus, as the term *high-speed* implies, these steels are primarily used for cutting tools that generate considerable heat during high-speed machining of steels and other metals. In addition to excellent hot hardness, sometimes referred to as red hardness because of the ability of the high-speed steels to resist softening even when red hot, the high-speed steels possess a number of unique alloying and processing features. These features include sufficient alloy and carbon content to provide excess alloy carbides in heat-treated tools, hardening at temperatures close to or at their melting points, hardening with fine austenitic grain sizes, deep hardening by cooling in still air, and prominent secondary hardening during tempering.

The high-speed steels are designated as group M or group T steels in the AISI classification system, depending on whether the major alloying approach is based on molybdenum or tungsten. Table 14-1 lists the compositions of the various molybdenum and tungsten high-speed steels and Tables 14-2 (a) and (b) list processing information and rank the properties and performance of the steels. Steels M50 and M52 have been included in the tables; as noted, however, they are considered to be intermediate high-speed steels and do not have all the features common to high-speed steels. In particular, hardening temperatures are lower, there is a tendency toward grain coarsening, and red hardness is lower in the intermediate high-speed steels compared to the other high-speed steels.

As described in Chapter 1, the era of alloying and high-speed steels was initiated by Mushet's development of an air-hardening, high-carbon, tungsten-containing steel in 1868. That development, combined with the discoveries by Taylor and White in the 1890s that very high-temperature hardening and high-temperature tempering conferred remarkable benefits to tool steels used for high-speed machining, established the basis for modern high-speed steel alloy development, processing, and application. By 1910, production and use of the high-speed steel containing 18% W, 4% Cr, and 1% V (18-4-1) was firmly established. The 18-4-1 steel was effectively the same steel as the T1 steel listed in Table 14-1, and many modifications of tungsten-base high-speed steels followed its commercial adoption. However, shortages of tungsten during World War II spurred the development and commercial acceptance of the molybdenum and molybdenum-tungsten grades.

The group T and M high-speed steels have effectively the same performance, and today, because of cost advantages, the molybdenum high-speed steels are much more widely used than the tungsten high-speed steels. The difference in cost is based in part on the fact that the atomic weight of molybdenum is about one-half that of tungsten; therefore, on a weight basis, less molybdenum than tungsten is required to provide equivalent performance. Molybdenum and tungsten atoms have similar atomic radii and form similar carbides. A replacement of 1.6 to 2.0 wt% W with only 1 wt% Mo has been found to produce markedly similar microstructure and properties in high-speed tool steels.

The large number of high-speed steels listed in Table 14-1 represents a number of choices based on performance and alloy modifications within the two major groups. The alloying modifications are based not only on tungsten and molybdenum contents, but also on carbon content, the total content of carbide-forming elements (including tungsten, molybdenum, chromium, and vanadium), and cobalt content. For example, if T1 steel is taken as the base for the tungsten group of high-speed steels, increases in carbon and vanadium lead to T2 steel. Cobalt additions provide for several of the other grades of tungsten steels, and the T15 steel is alloyed at a substantially increased level of vanadium, somewhat reduced tungsten, and high carbon content.

Table 14-1 Composition limits of high-speed tool steels

AISI type	UNS No.	Composition(a), % C	Mn	Si	Cr	Ni	Mo	W	V	Co
Molybdenum high-speed steels										
M1	T11301	0.78–0.88	0.15–0.40	0.20–0.50	3.50–4.00	0.30 max	8.20–9.20	1.40–2.10	1.00–1.35	...
M2	T11302	0.78–0.88 0.95–1.05	0.15–0.40	0.20–0.45	3.75–4.50	0.30 max	4.50–5.50	5.50–6.75	1.75–2.20	...
M3, class 1	T11313	1.00–1.10	0.15–0.40	0.20–0.45	3.75–4.50	0.30 max	4.75–6.50	5.00–6.75	2.25–2.75	...
M3, class 2	T11323	1.15–1.25	0.15–0.40	0.20–0.45	3.75–4.50	0.30 max	4.75–6.50	5.00–6.75	2.75–3.75	...
M4	T11304	1.25–1.40	0.15–0.40	0.20–0.45	3.75–4.75	0.30 max	4.25–5.50	5.25–6.50	3.75–4.50	...
M7	T11307	0.97–1.05	0.15–0.40	0.20–0.55	3.50–4.00	0.30 max	8.20–9.20	1.40–2.10	1.75–2.25	...
M10	T11310	0.84–0.94 0.95–1.05	0.10–0.40	0.20–0.45	3.75–4.50	0.30 max	7.75–8.50	...	1.80–2.20	...
M30	T11330	0.75–0.85	0.15–0.40	0.20–0.45	3.50–4.25	0.30 max	7.75–9.00	1.30–2.30	1.00–1.40	4.50–5.50
M33	T11333	0.85–0.92	0.15–0.40	0.15–0.50	3.50–4.00	0.30 max	9.00–10.00	1.30–2.10	1.00–1.35	7.75–8.75
M34	T11334	0.85–0.92	0.15–0.40	0.20–0.45	3.50–4.00	0.30 max	7.75–9.20	1.40–2.10	1.90–2.30	7.75–8.75
M35	T11335	0.82–0.88	0.15–0.40	0.20–0.45	3.75–4.50	0.30 max	4.50–5.50	5.50–6.75	1.75–2.20	4.50–5.50
M36	T11336	0.80–0.90	0.15–0.40	0.20–0.45	3.75–4.50	0.30 max	4.50–5.50	5.50–6.50	1.75–2.25	7.75–8.75
M41	T11341	1.05–1.15	0.20–0.60	0.15–0.50	3.75–4.50	0.30 max	3.25–4.25	6.25–7.00	1.75–2.25	4.75–5.75
M42	T11342	1.05–1.15	0.15–0.40	0.15–0.65	3.50–4.25	0.30 max	9.00–10.00	1.15–1.85	0.95–1.35	7.75–8.75
M43	T11343	1.15–1.25	0.20–0.40	0.15–0.65	3.50–4.25	0.30 max	7.50–8.50	2.25–3.00	1.50–1.75	7.75–8.75
M44	T11344	1.10–1.20	0.20–0.40	0.30–0.55	4.00–4.75	0.30 max	6.00–7.00	5.00–5.75	1.85–2.20	11.00–12.25
M46	T11346	1.22–1.30	0.20–0.40	0.40–0.65	3.70–4.20	0.30 max	8.00–8.50	1.90–2.20	3.00–3.30	7.80–8.80
M47	T11347	1.05–1.15	0.15–0.40	0.20–0.45	3.50–4.00	0.30 max	9.25–10.00	1.30–1.80	1.15–1.35	4.75–5.25
M48	T11348	1.42–1.52	0.15–0.40	0.15–0.40	3.50–4.00	0.30 max	4.75–5.50	9.50–10.50	2.75–3.25	8.00–10.00
M62	T11362	1.25–1.35	0.15–0.40	0.15–0.40	3.50–4.00	0.30 max	10.00–11.00	5.75–6.50	1.80–2.10	...
Tungsten high-speed steels										
T1	T12001	0.65–0.80	0.10–0.40	0.20–0.40	3.75–4.50	0.30 max	...	17.25–18.75	0.90–1.30	...
T2	T12002	0.80–0.90	0.20–0.40	0.20–0.40	3.75–4.50	0.30 max	1.0 max	17.50–19.00	1.80–2.40	...
T4	T12004	0.70–0.80	0.10–0.40	0.20–0.40	3.75–4.50	0.30 max	0.40–1.00	17.50–19.00	0.80–1.20	4.25–5.75
T5	T12005	0.75–0.85	0.20–0.40	0.20–0.40	3.75–5.00	0.30 max	0.50–1.25	17.50–19.00	1.80–2.40	7.00–9.50
T6	T12006	0.75–0.85	0.20–0.40	0.20–0.40	4.00–4.75	0.30 max	0.40–1.00	18.50–21.00	1.50–2.10	11.00–13.00
T8	T12008	0.75–0.85	0.20–0.40	0.20–0.40	3.75–4.50	0.30 max	0.40–1.00	13.25–14.75	1.80–2.40	4.25–5.75
T15	T12015	1.50–1.60	0.15–0.40	0.15–0.40	3.75–5.00	0.30 max	1.00 max	11.75–13.00	4.50–5.25	4.75–5.25
Intermediate high-speed steels										
M50	T11350	0.78–0.88	0.15–0.45	0.20–0.60	3.75–4.50	0.30 max	3.90–4.75	...	0.80–1.25	...
M52	T11352	0.85–0.95	0.15–0.45	0.20–0.60	3.50–4.30	0.30 max	4.00–4.90	0.75–1.50	1.65–2.25	...

(a) 0.25% max Cu, 0.03% max P, and 0.03% max S. Where specified, sulfur may be increased to 0.06 to 0.15% to improve machinability.

The M group of high-speed steels can be divided into two subgroups, one based primarily on molybdenum additions with limited tungsten, and the other based on molybdenum plus substantial tungsten additions. The molybdenum subgroup includes the M1, M7, and M10 steels, and the molybdenum-tungsten subgroup includes the M2, M3, and M4 steels. Three of these steels, M1, M2, and M10, together with T1, are very similar in properties and cutting performance and can be used interchangeably for many applications. Each of the M subgroups also includes modifications with cobalt, and the most highly alloyed types are capable of achieving superhigh hardness of 69 to 70 HRC after tempering. The effects of each of the alloying elements and carbon content on the processing, microstructures, and properties of high-speed steels are described in detail in this chapter.

Solidification of High-Speed Steels

High-speed tool steels are complex, multicomponent alloy systems in which microstructures are very dependent on the kinetics of solidification and solid-state reactions and the nonuniform distributions of phases that accompany these reactions. Following Hoyle (Ref 1), the best way to rationalize the microstructural changes that occur during the processing of high-speed tool steels is to consider vertical sections through the multicomponent systems that make up these steels. The vertical sections plot regions of phase stability as a function of temperature and carbon content but do not give the compositions of the coexisting phases or the configuration of the phases. Nevertheless, the vertical sections indicate when various phases must form during processing, and this information together with other observations provides a good understanding of the evolution of microstructure in high-speed steels. Figure 14-1 shows a vertical section through the Fe-W-Cr-C system at 18% W and 4% Cr as developed by several investigators (Ref 2–5) and serves as the base to characterize phase relationships in T1-type high-speed steels. Figure 14-2 shows a vertical section through the Fe-W-Mo-Cr-V-C system at 6% W, 5% Mo, 4% Cr, and 2% V (Ref 6) and serves as the base for M2-type high-speed steels.

Table 14-2(a) Performance factors and processing information for T-type high-speed tool steels

Factor	T1	T2	T4	T5	T6	T8	T15
Major factors							
Wear resistance	7	8	7	7	8	8	9
Toughness	3	3	2	1	1	2	1
Hot hardness	8	8	8	9	9	8	9
Minor factors							
Usual working hardness, HRC	63–65	63–66	63–65	63–65	63–65	63–65	64–68
Depth of hardening	D	D	D	D	D	D	D
Finest grain size at full hardness, Shepherd standard	9½	9½	9½	9½	9½	9½	9½
Surface hardness as-quenched, HRC	64–66	65–67	63–66	64–66	64–66	64–66	65–68
Core hardness (25 mm, or 1 in., diam round), HRC	64–66	65–76	63–66	64–66	64–66	64–66	65–68
Manufacturing factors							
Availability	4	4	4	4	2	3	3
Cost	4	4	5	5	5	5	5
Machinability	5	5	3	2	1	3	1
Quenching medium	S, O, A	S, O, A	S, O, A	S, O, A	S, O, A	S, O, A	S, O, A
Hardening temperature, °C (°F)	1260–1300 (2300–2375)	1260–1300 (2300–2375)	1260–1300 (2300–2375)	1275–1300 (2325–2375)	1275–1300 (2325–2375)	1260–1300 (2300–2375)	1205–1260 (2200–2300)
Dimensional change on hardening	M	M	M	M	M	M	M
Safety on hardening	M	M	L	L	L	L	L
Susceptibility to decarburization	M	M	H	H	H	H	H
Approximate hardness as-rolled or forged, HB	525	525	575	575	575	575	575
Annealed hardness, HB	217–255	223–255	228–269	235–285	248–302	228–255	214–277
Annealing temperature, °C (°F)	870–900 (1600–1650)	870–900 (1600–1650)	870–900 (1600–1650)	870–900 (1600–1650)	870–900 (1600–1650)	870–900 (1600–1650)	870–900 (1600–1650)
Tempering range, °C (°F)	540–595 (1000–1100)	540–595 (1000–1100)	540–595 (1000–1100)	540–595 (1000–1100)	540–595 (1000–1100)	540–595 (1000–1100)	540–650 (1000–1200)
Forging temperature, °C (°F)	1065–1175 (1950–2150)	1065–1175 (1950–2150)	1065–1175 (1950–2150)	1065–1175 (1950–2150)	1065–1175 (1950–2150)	1065–1175 (1950–2150)	1065–1175 (1950–2150)

Note: Ratings are explained in Chapter 2.

Table 14-2(b) Performance factors and processing information for M-type high-speed tool steels

Factor	M1	M2	M3, class 1	M3, class 2	M4	M7	M10	M30	M33	M34	M35	M36	M41	M42	M43	M44	M46	M47	M50(a)	M52(a)
Major factors																				
Wear resistance	7	7	8	8	9	8	7	7	8	8	7	7	8	8	8	8	8	8	6	6
Toughness	3	3	3	3	3	3	3	2	1	1	2	1	1	1	1	1	1	1	3	3
Hot hardness	8	8	8	8	8	8	8	8	9	9	8	9	9	9	9	9	9	9	6	6
Minor factors																				
Usual working hardness, HRC	63–65	63–65	63–66	63–66	63–66	63–66	63–65	63–65	63–65	63–65	63–65	63–65	66–70	66–70	66–70	66–70	66–69	66–70	61–63	62–64
Depth of hardening	D	D	D	D	D	D	D	D	D	D	D	D	D	D	D	D	D	D	D	D
Finest grain size at full hardness, Shepherd standard	9½	9½	9½	9½	9½	9½	9½	9½	9½	9½	9½	9½	9½	9½	9½	9½	9½	9½	8½	8½
Surface hardness as-quenched, HRC	64–66	64–66	64–66	64–66	65–67	64–66	64–66	64–66	64–66	64–66	64–66	64–66	63–65	63–65	63–65	63–65	63–65	63–65	63–65	63–65
Core hardness (25 mm, or 1 in., diam round), HRC	64–66	64–66	64–66	64–66	65–67	64–66	64–66	64–66	64–66	64–66	64–66	64–66	63–65	63–65	63–65	63–65	63–65	63–65	63–65	63–65
Manufacturing factors																				
Availability	4	4	3	3	3	4	4	2	1	1	1	2	2	3	2	2	2	2	2	2
Cost	3	4	4	4	4	3	3	4	5	5	4	5	5	5	5	5	5	5	3	3
Machinability	6	5	4	4	3	5	6	3	2	2	3	2	2	2	2	2	2	2	6	5
Quenching medium	S, O, A	S, O, A	S, O, A	S, O, A	S, O, A	S, O, A	S, O, A	S, O, A	S, O, A	S, O, A	S, O, A	S, O, A	S, O, A	S, O, A	S, O, A	S, O, A	S, O, A	S, O, A	S, O, A	S, O, A
Hardening temperature °C (°F)	1175–1220 (2150–2225)	1190–1230 (2175–2250)	1205–1230 (2200–2250)	1205–1230 (2200–2250)	1205–1230 (2200–2250)	1175–1220 (2150–2225)	1175–1220 (2150–2225)	1205–1230 (2200–2250)	1205–1230 (2200–2250)	1205–1230 (2200–2250)	1220–1245 (2225–2275)	1220–1245 (2225–2275)	1190–1215 (2175–2220)	1160–1190 (2125–2175)	1150–1175 (2100–2150)	1200–1225 (2190–2240)	1190–1220 (2175–2225)	1175–1205 (2150–2200)	1065–1120 (1950–2050)	1150–1175 (2100–2150)
Dimensional change on hardening	M	M	M	M	M	M	M	M	M	M	M	M	M	M	M	M	M	M	L	L
Safety on hardening	L	L	L	L	L	L	L	L	L	L	L	L	L	L	L	L	L	L	M	M
Susceptibility to decarburization	H	H	H	H	H	H	H	H	H	H	H	H	H	H	H	H	H	H	M	M
Approximate hardness as-rolled or forged, HB	525	525	550	550	575	525	525	575	575	575	575	575	575	575	...	...	...	...	575	575
Annealed hardness, HB	207–235	212–241	223–255	223–255	223–255	217–255	207–255	235–269	235–269	233–269	235–269	235–269	241–269	235–269	248–269	244–285	235–269	235–269	207–235	207–235
Annealing temperature, °C (°F)	815–870 (1500–1600)	870–900 (1600–1650)	870–900 (1600–1650)	870–900 (1600–1650)	870–900 (1600–1650)	815–870 (1500–1600)	815–870 (1500–1600)	870–900 (1600–1650)	870–900 (1600–1650)	870–900 (1600–1650)	870–900 (1600–1650)	870–900 (1600–1650)	870–900 (1600–1650)	870–900 (1600–1650)	870–900 (1600–1650)	870–900 (1600–1650)	870–900 (1600–1650)	870–900 (1600–1650)	815–830 (1500–1525)	815–830 (1500–1525)

(continued)

Note: Ratings are explained in Chapter 2. (a) Intermediate high-speed steel

Table 14-2(b) (continued)

Factor	M1	M2	M3, class 1	M3, class 2	M4	M7	M10	M30	M33	M34	M35	M36	M41	M42	M43	M44	M46	M47	M50(a)	M52(a)
Manufacturing factors (continued)																				
Tempering range, °C (°F)	540–595 (1000–1100)	540–595 (1000–1100)	540–595 (1000–1100)	540–595 (1000–1100)	540–595 (1000–1100)	540–595 (1000–1100)	540–595 (1000–1100)	540–595 (1000–1100)	540–595 (1000–1100)	540–595 (1000–1100)	540–595 (1000–1100)	540–595 (1000–1100)	540–595 (1000–1100)	510–595 (950–1100)	510–595 (950–1100)	540–625 (1000–1160)	525–565 (975–1050)	525–595 (975–1100)	510–550 (950–1025)	525–550 (975–1025)
Forging temperature, °C (°F)	1040–1150 (1900–2100)	1040–1150 (1900–2100)	1040–1150 (1900–2100)	1040–1150 (1900–2100)	1040–1150 (1900–2100)	1040–1150 (1900–2100)	1040–1150 (1900–2100)	1040–1150 (1900–2100)	1040–1150 (1900–2100)	1040–1150 (1900–2100)	1040–1150 (1900–2100)	1040–1150 (1900–2100)	1065–1150 (1950–2100)	1065–1150 (1950–2100)	1040–1150 (1900–2100)	1040–1150 (1900–2100)	1040–1150 (1900–2100)	1040–1150 (1900–2100)	1065–1120 (1950–2050)	1065–1120 (1950–2050)

Note: Ratings are explained in Chapter 2. (a) Intermediate high-speed steel

Superimposed on the vertical sections, the horizontal cross-hatched region in Fig. 14-1 shows the normal range of carbon variations in tungsten high-speed steels, and the vertical line AB in Fig. 14-2 shows a typical carbon concentration for an M2 steel. In these compositions, starting from the liquid phase, dendritic or branched crystals of δ-ferrite nucleate and grow in the liquid upon cooling. Figure 14-3 shows an example of a primary dendrite with its axis normal to the figure in an as-cast M2 steel (Ref 7). The dendritic crystal is cross-shaped and the liquid surrounding the dendrite has solidified as eutectic microstructures, as described below. The ferrite crystals are primarily iron-rich, and the other alloying elements are rejected into the surrounding liquid. With further cooling, the steel enters the three-phase ferrite-liquid-austenite phase field, and austenite forms around the ferrite dendrites. Finally, the remaining interdendritic liquid, highly enriched in the strong alloy carbide-forming elements, solidifies as eutectic structures consisting of colonies of closely spaced austenite and alloy carbide crystals. During these final stages of solidification, four phases—δ-ferrite, austenite, carbide, and liquid—coexist. Eventually, solidification is complete and the ferrite is replaced by austenite, leaving a microstructure that consists of austenite and alloy carbides. Subsequent hot-work reductions and austenitizing heat treatments for hardening are performed in this phase field.

The interdendritic eutectic microstructures in as-cast high-speed microstructures may take several morphologies and consist of various alloy carbides, depending on steel composition and solidification conditions. The primary alloy carbide in high-speed steels is M_6C or η-carbide, where M, the metal component, may consist of tungsten, molybdenum, and iron. Vanadium is typically present in MC carbides, and tungsten and molybdenum may be present in M_2C carbides. These carbides are described in more detail in the next section. Figure 14-4 shows examples of feathery (austenite plus M_6C and MC carbides), herringbone (austenite plus M_6C car-

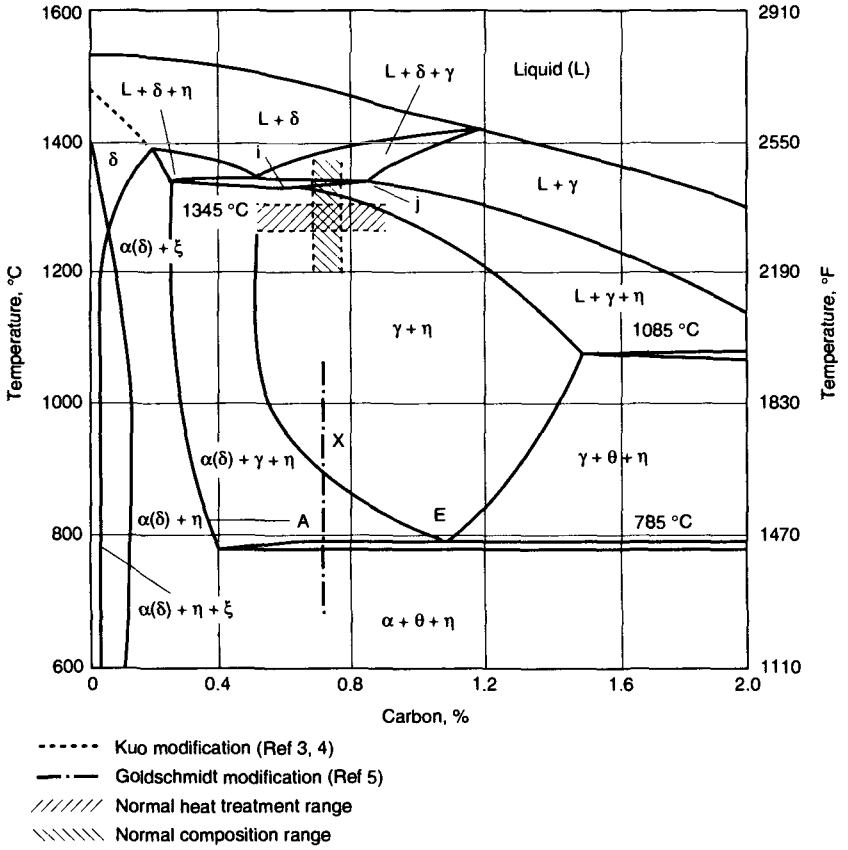

Fig. 14-1 Phase diagram for T1-type high-speed steel based on 18W-4Cr section through the quaternary Fe-W-Cr-C system. Source: Ref 1, based on work from Ref 2 to 5

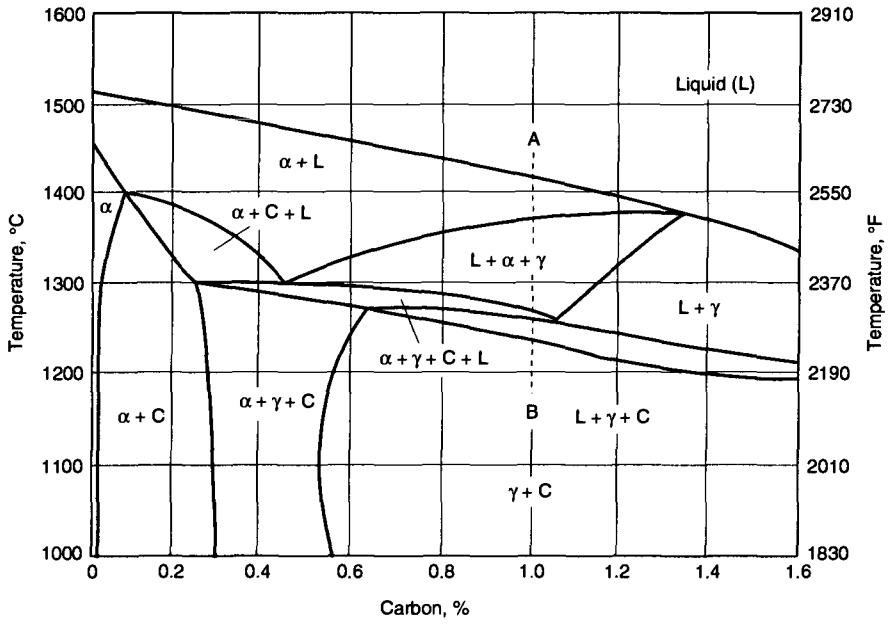

Fig. 14-2 Phase diagram for M2-type high-speed steel based on the 6W-5Mo-4Cr-2V section through the Fe-W-Mo-Cr-V-C system. C, carbide. Source: Ref 1, based on work from Ref 6

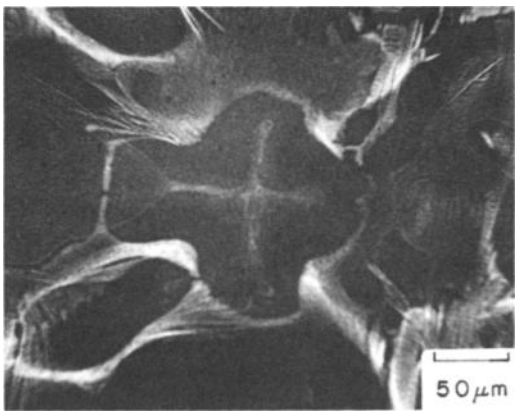

Fig. 14-3 Microradiograph showing primary dendrite with axis normal to the plane of polish in an M2 high-speed steel. Source: Ref 7

bides), and blocky (austenite plus MC carbides) interdendritic eutectic morphologies in an as-cast M2 high-speed steel (Ref 7).

Hot Work and Annealing

The concentration of the alloying elements in the interdendritic eutectic colonies constitutes a very nonuniform structure unsuitable for hardening of high-speed steels. The dendritic and interdendritic regions increase in size as solidification rates decrease, and to minimize the associated heterogeneity in structure and composition, the size of high-speed ingots is limited to square sections of 300 to 400 mm (12 to 16 in.) on a side. New primary processing approaches, such as spray deposition and powder production and consolidation, which involve solidification at very high rates, have the capability to significantly reduce segregation and improve uniformity of high-speed steels (Ref 1). However, in ingots the only way to improve uniformity is to apply substantial amounts of hot work at high temperatures.

Figure 14-5 shows how hot reduction alters the solidification structure of a high-speed steel. At moderate reductions, the as-cast network of interdendritic eutectic colonies is elongated in the direction of rolling in a still-interconnected pattern, sometimes referred to as a "hooky" pattern. After substantial amounts of hot work, the combined action of high temperature and deformation spheroidizes the lamellar or fibrous eutectic carbides and aligns the carbides in bands. Further increases in reduction bring the bands closer together. The net effect of the hot work is to approach a uniform dispersion of alloy carbides in an austenitic matrix. However, in order to completely eliminate banding of the dispersed carbides, hot reductions in excess of 97% have been shown to be necessary (Ref 8).

The type, amount, and dispersion of alloy carbides continue to be altered by thermal processing after solidification and hot work. Cooling from

hot-work temperatures, annealing, and austenitizing for hardening all affect the primary carbide distributions in high-speed steels as microstructures attempt to approach equilibrium under changing thermal conditions. Early studies by x-ray diffraction and chemical analyses of extracted carbides established the variety of alloy carbides that form in high-speed steels (Ref 9-15) and established, for the purposes of alloy design, the importance of assessing carbide composition by atomic percent rather than weight percent. For example, Fig. 14-6 shows the weight and atomic percentages of the principal elements found in the carbides electrolytically separated from T1, M10, and M2 high-speed steels (Ref 9). The carbides from each steel have about the same total of tungsten, molybdenum, and chromium atoms, while the vanadium and carbon atom contents in the M10 and M2 steels are significantly higher than those in the T1 steel, consistent with the compositions of the steels and the higher fraction of MC carbides in the M10 and M2. However, on a weight basis, tungsten appears to dominate the carbide compositions.

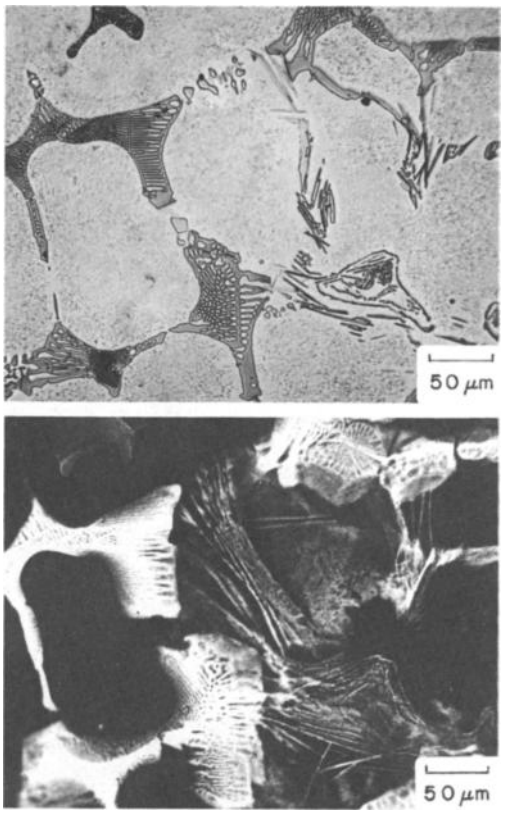

Fig. 14-4 Feathery, herringbone, and MC eutectics in M2 high-speed steel. (a) Light micrograph, $KMnO_4$ etch. (b) Microradiograph of same area. Source: Ref 7

Depending on steel composition, the following alloy carbides have been identified in high-speed steels (Ref 9–15): according to convention, M represents the sum of the metal atoms—tungsten, molybdenum, chromium, vanadium, and iron—in the carbides:

- *M_6C*, a tungsten- or molybdenum-rich carbide corresponding to the complex fcc carbide of the composition range Fe_3W_3C to Fe_4W_2C in tungsten steels, or Fe_3Mo_3C to Fe_4Mo_2C in molybdenum steels, and capable of dissolving some chromium, vanadium, and cobalt
- *$M_{23}C_6$*, a chromium-rich carbide corresponding to the fcc carbide $Cr_{23}C_6$ and capable of dissolving iron, tungsten, molybdenum, and vanadium
- *MC*, a vanadium-rich carbide corresponding to the fcc carbide of composition range VC to V_4C_3 and capable of dissolving limited amounts of tungsten, molydenum, chromium, and iron
- *M_2C*, a tungsten- or molybdenum-rich carbide corresponding to the hcp carbide W_2C in tungsten steels or M_2C in molybdenum steels. This carbide has been observed only as a transition phase formed during tempering of high-speed steels.

Recommended temperature ranges for forging and annealing of the various high-speed steels are listed in Tables 14-2 (a) and (b). Because of the high hardenability of the high-speed steels, air cooling will produce hardened microstructures. Therefore, normalizing is not recommended, and it is essential to anneal hot-worked tools prior to machining and austenitizing for hardening. The objective of annealing is to produce a low-hardness microstructure that consists of dispersed spheroidized carbides in a matrix of ferrite. The annealing process may be performed at temperatures where some austenite forms, in which case slow furnace cooling is required to ensure that the austenite transforms to ferrite, or it may be performed subcritically at temperatures where ferrite and various carbides are stable (Ref 1,16). In high-speed tool steels, the spheroidized carbide arrays will contain the primary carbides, M_6C and MC, formed on solidification and spheroidized by hot work, as described above. However, the annealed structures will also contain secondary carbides, notably $M_{23}C6$, which are stable and form only during lower-temperature processing and annealing.

Figure 14-7 shows how selective etching has been used to reveal the various types of carbides present in the annealed microstructure of an M2 steel (Ref 10). Each successive etch with different reagents developed another type of carbide, until the final nital etch revealed the complete array of spheroidized carbides in the matrix of ferrite. The composite array of spheroidized carbides consists of subsets of M_6C, MC, and $M_{23}C_6$ carbides, with the coarser particle arrays consisting of M_6C and

MC carbides and the finer particle array consisting of $M_{23}C_6$, consistent with the stages of processing at which the various carbides formed. Kayser and Cohen (Ref 9) have measured the total volume fraction of carbides and the volume fractions of M_6C, $M_{23}C_6$, and MC carbides in a number of high-speed steels in the annealed condition and after hardening. A summary of those data is presented in Fig. 4-24. That summary shows that austenitizing for hardening significantly reduces the total volume percentages of alloy carbides from those present in the annealed steels and that, in particular, the $M_{23}C_6$ carbides, present in significant fractions in the annealed steels, are totally dissolved during high-temperature austenitizing for hardening.

Austenitizing for Hardening of High-Speed Steels

Austenitizing for hardening is a critical step in the heat treatment of high-speed steels. As shown in Fig. 14-1, austenitizing is accomplished very high in the austenite-carbide phase field, just below or at temperatures where melting initiates. Austenitizing times are very short, on the order of 2 to 5 min. In view of the very high temperatures, two preheating steps prior to heating to the final austenitizing temperature are recommended to minimize thermal shock.

Just as in the other tool steels discussed to this point, the function of austenitizing of high-speed steels is to adjust carbide volume fractions and matrix chemistries to develop optimum responses to subsequent hardening and tempering. Where the high-speed steels differ from other steels is in the remarkable stability of the alloy carbides that have been incorporated into annealed microstructures by alloying and primary processing. As discussed above, $M_{23}C_6$ carbides dissolve at relatively low austenitizing temperatures and are completely dissolved at 1095 °C (2000 °F). However, the primary M_6C and MC carbides are stable to much higher temperatures and, in fact, are never completely dissolved despite the high austenitizing temperatures used for hardening.

Figure 14-8 shows the changes in volume percentages of the M_6C and MC alloy carbides as a function of austenitizing temperature for a number of high-speed steels (Ref 9). The M_6C carbides tend to dissolve somewhat more rapidly than the MC carbides. All of the high-speed steels contain some of each type of alloy carbide, but the amounts of the various carbides typically retained in a given hardened steel are dependent on steel composition. Table 14-3 lists the amounts of M_6C and MC carbides retained in some hardened T- and M-type high-speed steels; similar data have been shown in Fig. 4-24. The higher-melting-point, high-tungsten types of high-speed steels are normally heated to temperatures near 1290 °C (2350 °F), while the lower-melting-point, high-molybdenum types of high-speed steels are not heated above 1220 to 1230 °C (2225 to 2250 °F).

In addition to establishing the volume fraction of primary carbides in hardened high-speed steel microstructures, austenitizing controls the chemical composition of the matrix, which will transform to

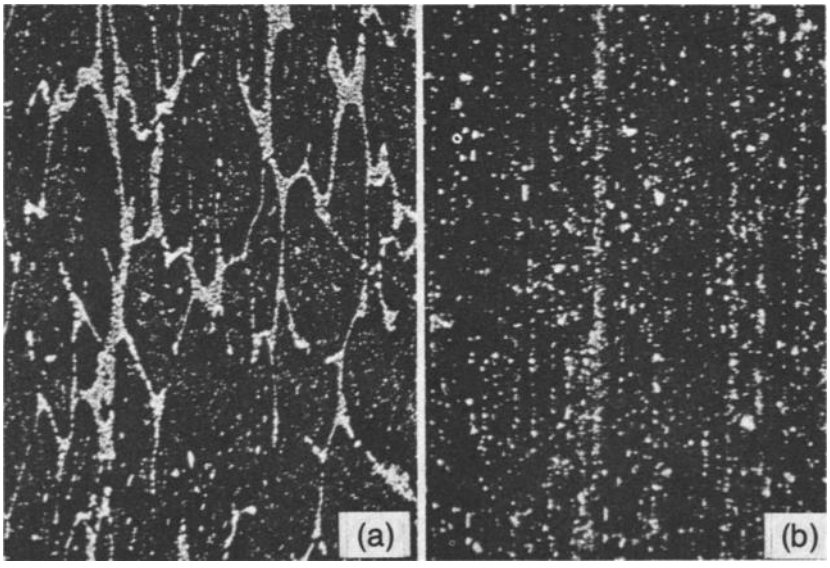

Fig. 14-5 Microstructure of high-speed steel showing alteration in carbide aggregates caused by forging. (a) Longitudinal microstructure after moderate reduction. (b) Longitudinal microstructure after modre severe reduction

martensite and in turn be subjected to tempering. Table 14-4 lists the carbide and matrix compositions of some high-speed steels in the annealed and hardened conditions. The data show the necessity of austenitizing as a means to increase the matrix carbon content, from a negligible amount in ferrite of the annealed structures, to an amount that will be adequate for supersaturating martensite and sufficient for carbide formation during secondary hardening. This level of carbon is shown to be uniformly between 0.4 and 0.5% for all of the steels, with the remainder of the carbon incorporated to varying amounts, depending on the alloy and carbon content of the steel, in the residual primary carbides. Table 14-4 also shows that the alloy element content of the matrix is increased by austenitizing, and thus is available to combine with carbon and form the alloy carbides necessary for secondary hardening.

Figure 14-9 shows examples of microstructures of T1 steel austenitized at various temperatures.

Table 14-3 Percentage of excess carbide existing as M_6C and MC in various high-speed steels

Type	Austenitizing temperature °C	Austenitizing temperature °F	Content, % M_6C	Content, % MC
T1	1290	2350	97	3
T4	1290	2350	96	4
T2	1290	2350	92	8
M1	1205	2200	87	13
M2	1220	2225	85	15
M10	1205	2200	61	39
M4	1220	2225	44	56
M15	1250	2280	34	66

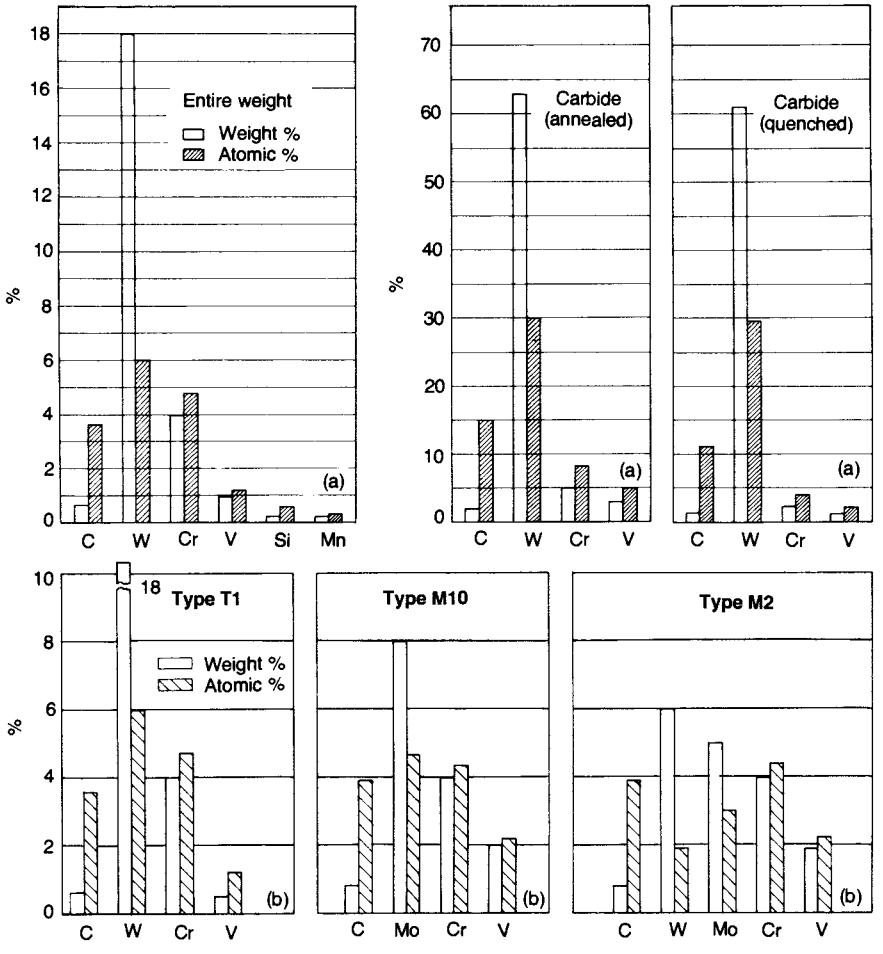

Fig. 14-6 (a) Relationship between atomic and weight percentages of the elements in T1 high-speed steel containing 18% W, 4% Cr, 1% V, 0.70% C, 0.25% Si, and 0.25% Mn. Left: relationship for entire steel; center: relationship for carbides in annealed steel; right: relationship for carbides in hardened steel. (b) Comparison of alloy content in weight and atomic percent for T1, M10, and M2 high-speed steels. Source: Ref 9

Figure 14-9(a) shows the microstructure, dominated by a high volume fraction of undissolved carbides, produced by underheating at 870 °C (1600 °F). A microstructure properly heated at 1260 °C (2300 °F) is shown in Fig. 14-9(b). Residual alloy carbides are dispersed within a matrix of martensite. The martensite crystals are not resolved, but prior-austenite grain boundaries have been brought out by the etch. Figures 14-9(c) and (d) show, respectively, microstructures that have been overheated at 1290 and 1320 °C (2350 and 2410 °F). At 1290 °C (2350 °F), compared to austenitizing at 1260 °C (2300 °F), the alloy carbides have coarsened and more have gone into solution. As a result, the austenite has been so enriched in carbon and alloying elements that the M_s temperature has been drastically reduced. On cooling to room temperature, therefore, only a few large, dark-etching plates of martensite have formed and most of the microstructure consists of retained austenite. The specimen overheated to 1320 °C (2410 °F) has undergone significant melting, to the point where eutectic colonies have again formed

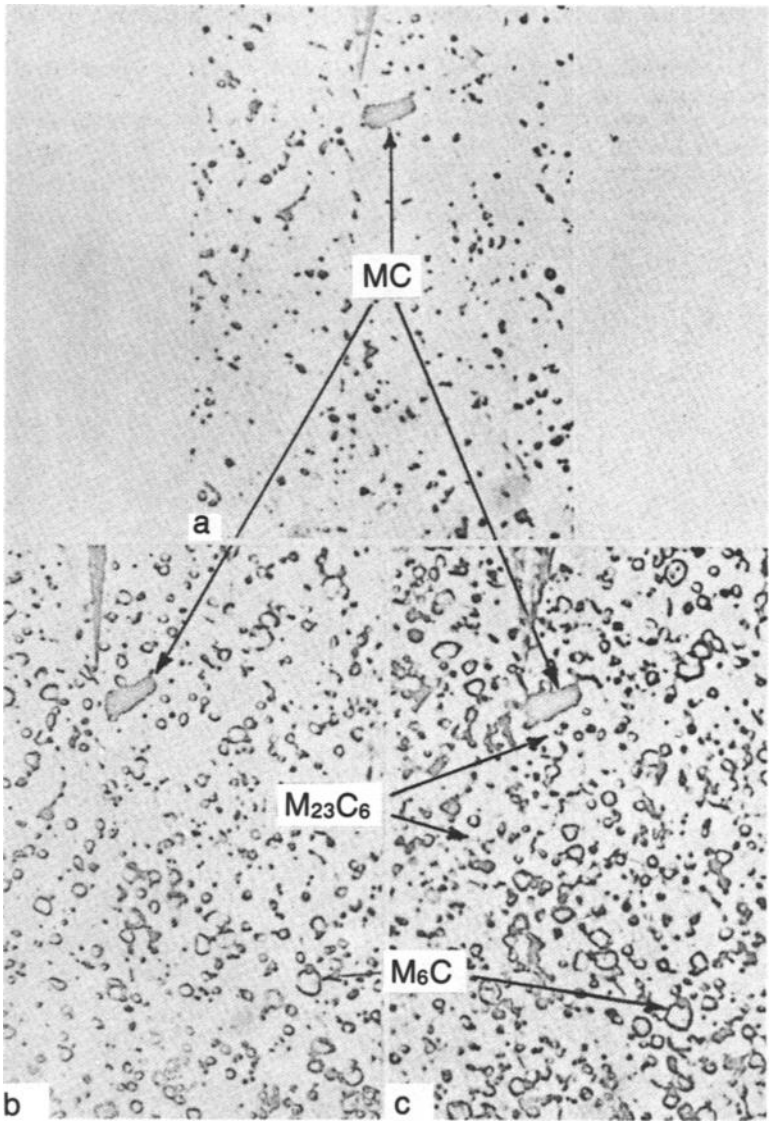

Fig. 14-7 Microstructure of annealed M2 high-speed steel. 2000×. (a) Etched electrolytically in 1% chromic acid, 3 V. 1.7% MC. (b) As (a) and etched in 4% NaOH saturated with $KMnO_4$. 1.7% MC plus 13.0% M_6C. (c) As (b) and etched in 1% nital. 1.7% MC plus 13.0% M_6C plus 8.5% $M_{23}C_6$. Source: Ref 10

from the liquid regions on cooling and all uniformity produced by thermomechanical treatment after casting has been lost.

Grain Size Control during Austenitizing

Austenitizing for hardening also serves to establish the austenitic grain size of hardened high-speed steels. Tools that are properly hardened generally have fine austenitic grain size because of the grain-boundary pinning effects of the retained alloy carbides. Of the two parameters of a particle distribution that control grain size (Eq 5-2) in high-speed steels, the high volume fraction (f) of retained carbides is more influential in restraining grain growth than carbide particle size (r), which is relatively coarse as a result of the high-temperature austenitizing of high-speed steels.

Figure 14-10 shows the austenitic grain size of a T6 steel austenitized at various temperatures. The grain sizes produced by austenitizing between 1260 and 1300 °C (2300 and 2375 °F) are remarkably fine, although grain size continuously increases with increasing temperature and carbide solution in that temperature range and higher. Uniform grain sizes are dependent on uniform distributions of carbides. If hot work and annealing have not produced a uniform microstructure, then mixed grain sizes may develop on hardening. Fine grain sizes will be maintained where carbide particles are present, and

Table 14-4 Carbide and matrix compositions of common high-speed steels in the annealed and hardened conditions

	Carbide composition, %							Matrix composition, %						
Type	C	Fe	W	Mo	Cr	V	Co	C	Fe	W	Mo	Cr	V	Co
T1	2.5	25.4	60.7	1.3	7.1	3.2	...	0	95.3	1.5	0.1	3.0	0.2	...
	2.1	19.4	73.2	1.4	2.5	1.4	...	0.5	85.3	8.6	0.2	4.4	1.0	...
T2	2.6	23.4	59.9	2.6	6.3	3.3	2.0	0	89.0	1.1	0.1	3.4	0.3	6.2
	2.6	20.2	70.0	2.5	1.6	1.4	1.6	0.4	79.5	8.3	0.5	4.7	1.1	5.6
T4	2.9	22.8	58.5	1.3	8.3	6.3	...	0	95.4	1.8	0.1	2.6	0.3	...
	2.8	18.9	70.2	1.3	3.3	3.6	...	0.5	85.3	8.0	0.2	4.4	1.7	...
T15	6.4	21.5	22.3	20.3	9.3	20.2	...	0	95.3	1.0	0.4	3.3	0	...
	8.7	11.2	27.5	20.4	3.0	29.1	...	0.5	86.1	3.5	3.2	4.7	1.9	...
M1	6.3	15.7	47.2	1.2	7.2	21.2	1.2	0.2	91.4	1.5	0.1	4.2	0.1	2.9
	9.1	8.7	47.2	1.4	2.9	29.8	1.0	0.4	81.2	7.3	0.2	5.1	1.4	4.3
M2	5.5	28.2	...	44.5	11.3	10.5	...	0	95.5	...	1.0	2.9	0.4	...
	8.0	7.3	...	60.5	5.9	18.3	...	0.5	88.8	...	5.4	4.2	1.1	...
M4	4.0	27.9	29.4	22.5	7.7	8.5	...	0	95.5	0.3	0.7	3.3	0.2	...
	3.7	23.6	39.7	22.3	2.0	8.8	...	0.5	89.0	2.0	3.0	4.6	1.0	...
M10	3.9	34.9	7.6	39.9	8.7	5.0	...	0	96.9	0.2	0.3	2.5	0.2	...
	3.5	34.5	9.8	45.0	3.0	4.3	...	0.6	89.1	0.9	4.7	3.9	0.9	...

Source: Ref 9

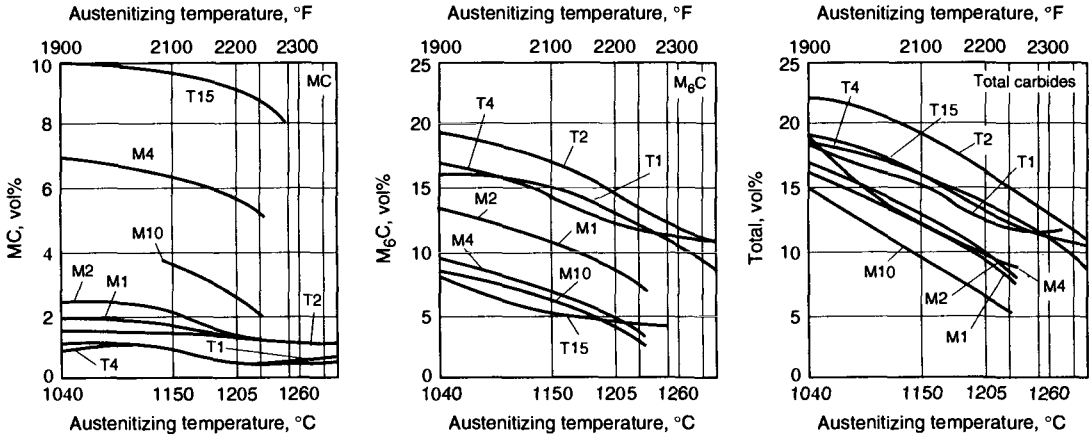

Fig. 14-8 Volume percentage of M_6C, MC, and total carbides as a function of temperature in eight commercial high-speed steels after oil quenching from temperature. Source: Ref 9

coarse grains will grow in regions where particles are absent. Figure 14-11 shows an example of a mixed grain size associated with marked segregation of carbide particles in a high-speed steel.

If a high-speed steel needs to be rehardened after a first hardening and tempering heat treatment, severe discontinuous grain coarsening may develop during the second austenitizing treatment. The coarse grain boundaries are quite brittle and the resulting intergranular fracture results in a characteristic faceted fracture, which because of its appearance is termed "fishscale" fracture. The lower toughness of high-speed steels that have coarsened discontinuously generally makes them unfit for cutting tool service. A tracing of discontinuous coarsening in T1 steel has been shown in Fig. 5-14, where a single, very large grain is shown to have consumed many fine surrounding grains (Ref 17), and an example of fishscale fracture is shown later in Fig. 17-10.

Figure 14-12 shows the abrupt grain coarsening that occurs in T1 and M2 high-speed steels as a function of second austenitizing temperature. Up to a critical temperature, the grain size is quite fine, consistent with the pinning effects of a fine carbide particle distribution. This particle distribution in rehardened specimens is especially fine because of the very fine carbide distributions formed by hardening and tempering in the first heat treatment. However, the fine particles with their high surface areas dissolve readily during the second austenitizing treatment. Rapid coarsening thus is a result of a sudden elimination of a critical amount of grain-boundary pinning force when a sufficient number of the fine particles dissolve at some point in the austenitizing process (Ref 17, 18). Figure 14-13 shows that the coarsening temperature developed during the second hardening treatment is a function of the first austenitizing temperature. In order to prevent discontinuous grain coarsening, tools that need to be rehardened should be reannealed before the second hardening treatment. The reannealing will create coarser carbide dispersions, which more gradually coarsen and dissolve during austenitizing, and thereby cause a more gradual increase in grain size.

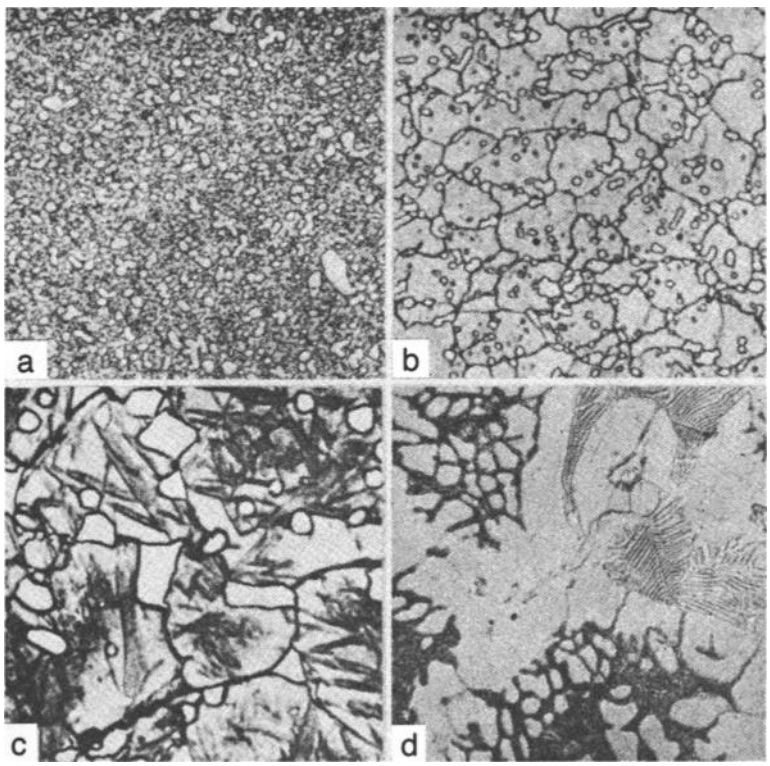

Fig. 14-9 Microstructure of quenched T1 high-speed steel. (a) Quenched in oil from 870 °C (1600 °F); underheated. Nital etch, 500×. (b) Quenched in oil from 1260 °C (2300 °F); typical hardened microstructure showing prior-austenite grain size and carbides. Nital etch, 500×. (c) Quenched from 1290 °C (2350 °F). Sulfuric acid etch, 2500×. (d) Quenched from 1320 °C (2410 °F); overheated. Nital etch, 500×

Cooling Transformations and Hardening

The highly alloyed high-speed tool steels have excellent hardenability and are deep hardening. Figure 14-14 shows an IT diagram for T1 high-speed steel (Ref 19). This diagram is typical of those for all high-speed steels. The diffusion-controlled transformations of austenite to pearlitic and bainitic mixtures of ferrite and carbides are quite sluggish, and a considerable temperature range separates the C-curves for the high- and low-temperature decomposition products. Although the bainite transformation is initiated rapidly, its progress is slow and the transformation of austenite eventually ceases. For example, Fig. 14-15 shows the amount of bainite formed as a function of time at 315 °C (600 °F) in a T1 steel; transformation stops after about 40% of the microstructure consists of bainite. The austenite that does not transform to bainite during an isothermal hold is remarkably stable and does not transform to martensite on cooling to room or even subzero temperatures.

A much more rapid transformation is the formation of proeutectoid carbides at the higher temperatures, as indicated by the dashed line in Fig. 14-14. The proeutectoid carbides form preferentially on austenite grain boundaries and never achieve a large volume fraction of the transformed microstructures in high-speed steels. Although not resolvable in the light microscope, the grain-boundary carbides are believed to contribute to the prominent appearance of prior-austenite grain boundaries in etched hardened microstructures, as shown in Fig. 14-9 (b), and have been identified by electron diffraction of extracted particles from M2 steel as vanadium carbides (Ref 20). The thin networks of grain-boundary carbides do not affect hardness, but could lower toughness under some conditions of stress, espe-

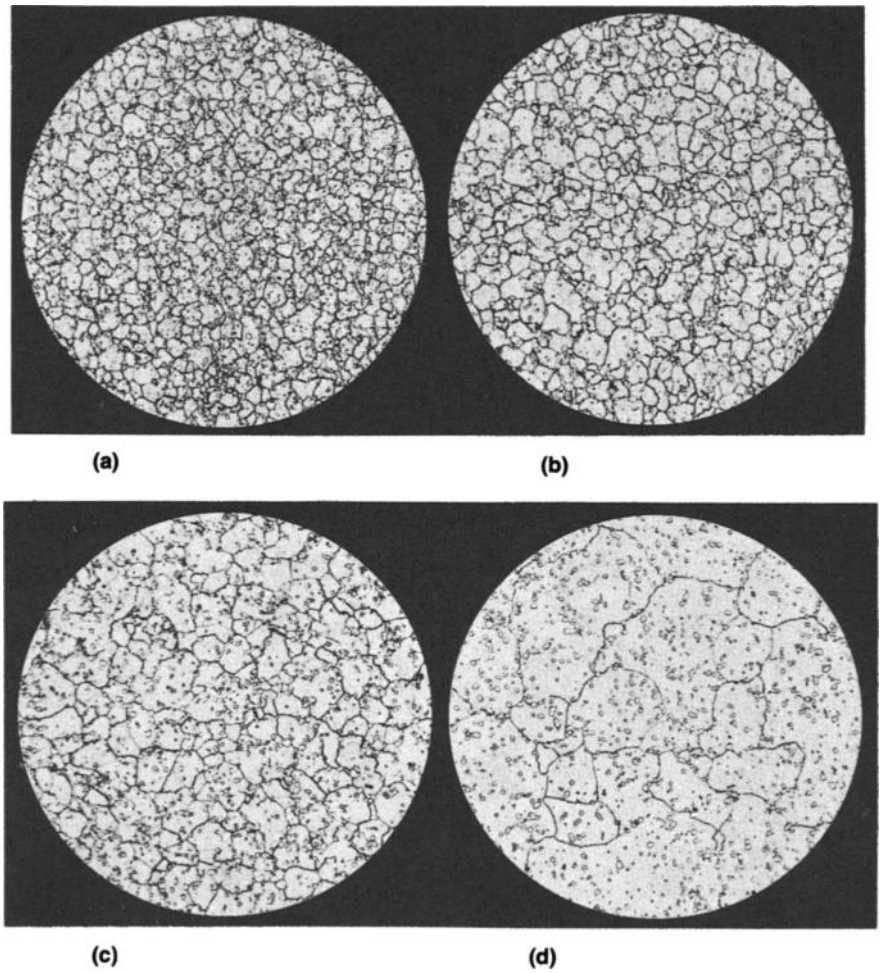

Fig. 14-10 Effect of austenitizing temperature on grain size of T6 high-speed steel. Light micrographs, 300×. (a) 1260 °C (2300 °F); grain size, 18. (b) 1290 °C (2350 °F); grain size, 14. (c) 1300 °C (2375 °F); grain size, 10; (d) 1315 °C (2400 °F); grain size, 6

cially in microstructures of coarse prior austenitic grain size.

Although the high-speed steels have sufficient hardenability to harden on air cooling, they are frequently hardened by quenching into salt or martempering at temperatures in the range of 540 to 650 °C (1000 to 1200 °F). The wide bay that separates the high- and low-temperature transformations to ferrite-carbide aggregates ensures that no loss in hardening will occur as a direct result of austenite transformation during salt bath quenching. The salt bath quenches will accelerate cooling somewhat, and thus minimize the formation of grain-boundary carbides. A major benefit of an isothermal hold in

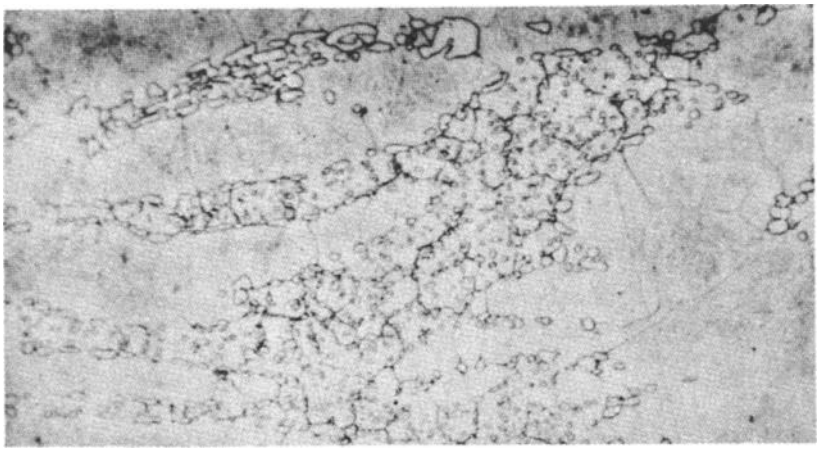

Fig. 14-11 Mixed grain size in high-speed steel, heated to 1295 °C (2360 °F), caused by marked segregation of carbide particles

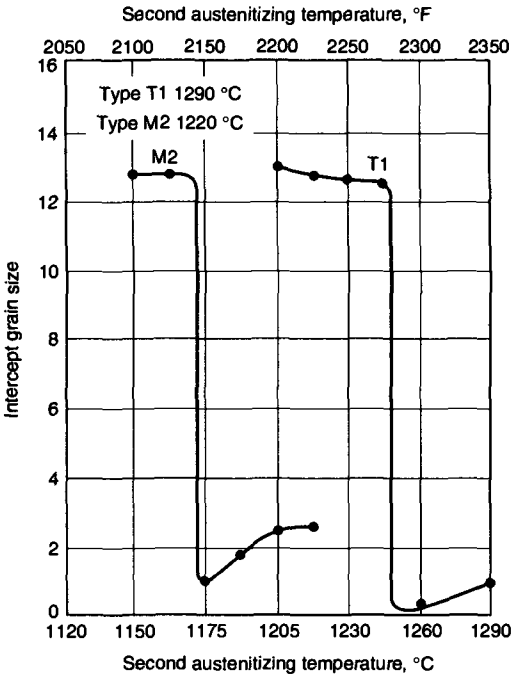

Fig. 14-12 Austenitic grain size versus second austenitizing temperature for T1 and M2 high-speed steels. Type T1 was prequenched from 1290 °C (2350 °F) and type M2 from 1220 °C (2225 °F). Source: Ref 17

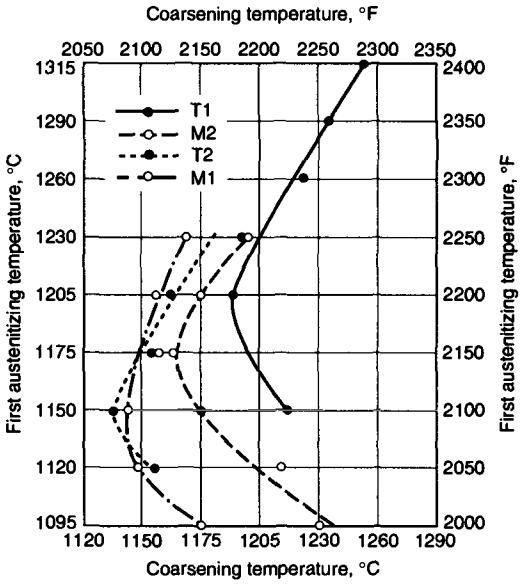

Fig. 14-13 Relationship of first and second (coarsening) temperatures for several high-speed steels. Source: Ref 17

the metastable austenite condition is associated with the equalization of temperature throughout a tool. When a tool is cooled through the martensite transformation range after the isothermal hold, the absence of temperature gradients will minimize distortion and the potential of cracking that might occur if the volume changes associated with martensite formation developed nonuniformly through the cross section of the tool.

The objective of hardening is to form martensitic microstructures that incorporate sufficient carbon and alloying elements to provide for secondary hardening during tempering. The as-quenched microstructures of hardened high-speed steels consist of mixtures of martensite and retained austenite, which are in turn dependent on austenitizing and the manner in which tools are cooled after austenitizing. Figure 14-16 shows the effect of austenitizing temperature and time on the hardness of T1 steel. At any given austenitizing temperature, as-quenched hardness reaches a constant value within a few minutes at temperature. Also, maximum hardness increases with increasing austenitizing temperature. These data show the importance of high-temperature austenitizing in accelerating the dissolution of the stable alloy carbides in high-speed steels and the attendant benefits on austenite formation and martensite strength.

With higher austenitizing temperatures, increased carbon in the austenite would be expected to result in more retained austenite on cooling to room temperature, as well as martensite of higher hardness. The increased retained austenite is related to reduced M_s temperatures, as austenite is increasingly enriched in carbon and alloying elements with increasing austenitizing temperatures. Figure 14-17 shows the effect of austenitizing temperature on M_s temperature in a tungsten high-speed steel, as well as the amount of austenite retained at room temperature and after cooling to −120 °C (−185 °F)(Ref 21). Figure 14-18 shows the effect of austenitizing temperature and time on M_s temperatures of a tungsten high-speed steel and indicates that some adjustments in the composition of austenite that lower M_s temperature occur with increasing austenitizing time (Ref 22). The matrix compositions of many properly hardened high-speed tool steels as shown in Table 14-4, are quite similar, and consequently many have M_s temperatures typically about 200 °C (400 °F).

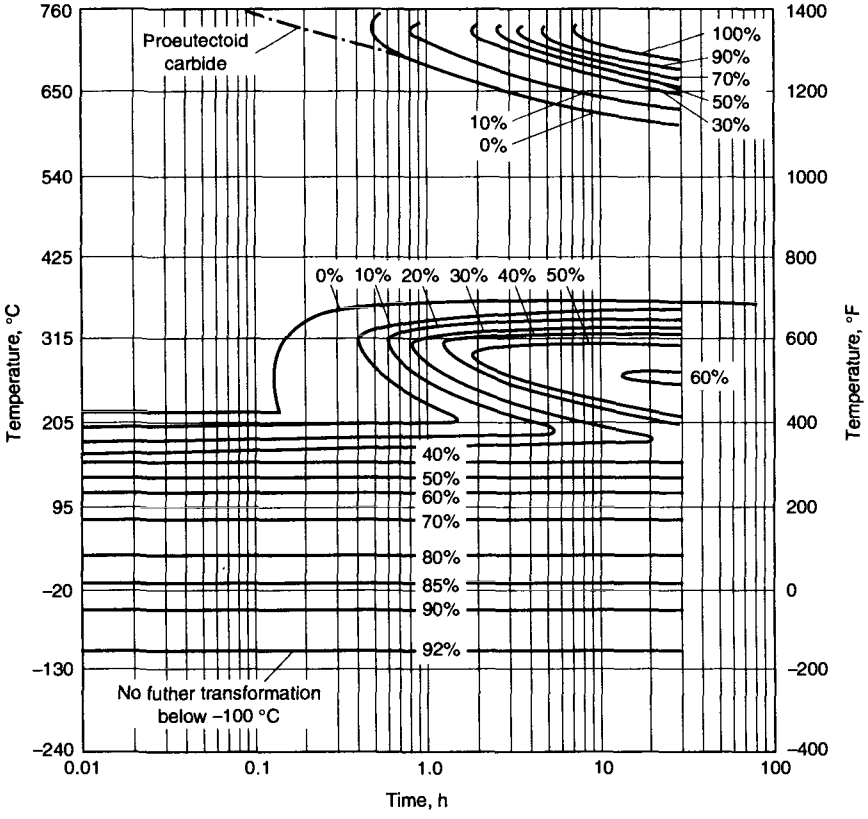

Fig. 14-14 IT diagram for T1 high-speed steel. Austenitizing temperature, 1290 °C (2350 °F). Source: Ref 19

Generally, if austenitizing temperatures are held below the melting points of high-speed steels, the amounts of austenite retained at room temperature do not significantly lower the hardness of as-quenched structures. Figures 14-19 and 14-20 (Ref 23) confirm that as-quenched hardness values of high-speed steels generally approach constant maxima after austenitizing at temperatures approaching melting, but that slight decreases in hardness may occur depending on alloy composition and the highest austenitizing temperature attained. Although the amounts of retained austenite may vary widely, it is estimated that at least 15% retained austenite exists in all high-speed steels, and that 20 to 25% retained austenite represents a good average value for commercial practice.

Another cause of variations in retained austenite content may be a result of interrupted quenching. If

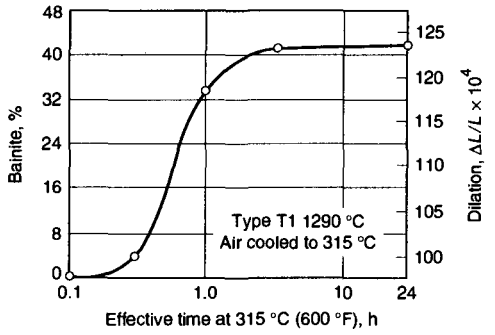

Fig. 14-15 Bainite formation in T1 high-speed steel as a function of time at 315 °C (600 °F). Note that the reaction does not proceed to completion. Source: Ref 19

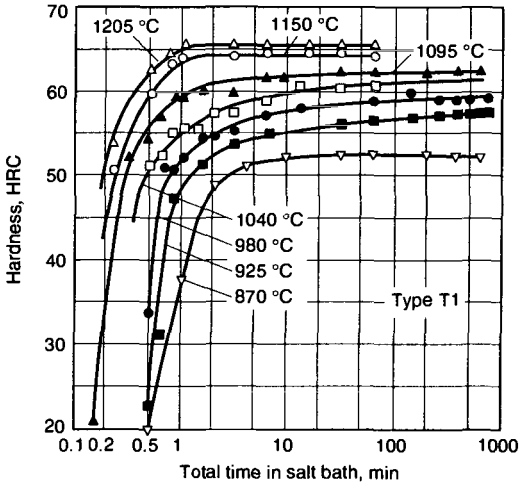

Fig. 14-16 Effect of austenitizing time and temperature on the hardness of T1 high-speed steel. Specimens austenitized in salt bath and brine quenched.

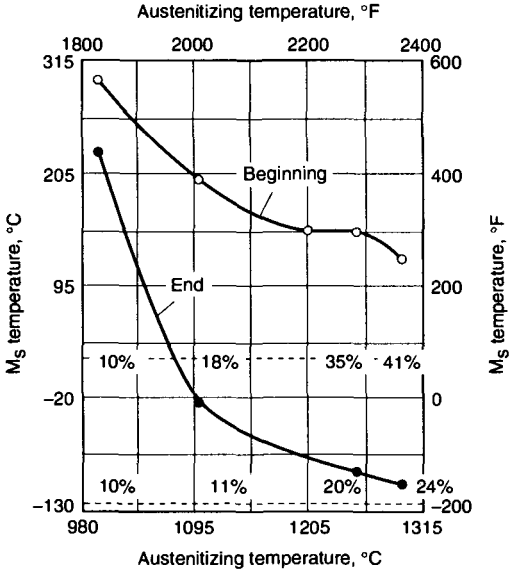

Fig. 14-17 Effect of austenitizing temperature on beginning and end of martensite transformation in high-speed steel containing 0.74%C, 18,2% W, 4.0% Cr, and 0.58% V. Percentages listed on dashed horizontal lines at room temperature and −120 °C (−185 °F) refer to the amount of retained austenite at these temperatures after quenching from 1000, 1100, 1250, and 1300 °C (1835, 2015, 2280, and 2375 °F). Source: Ref 21

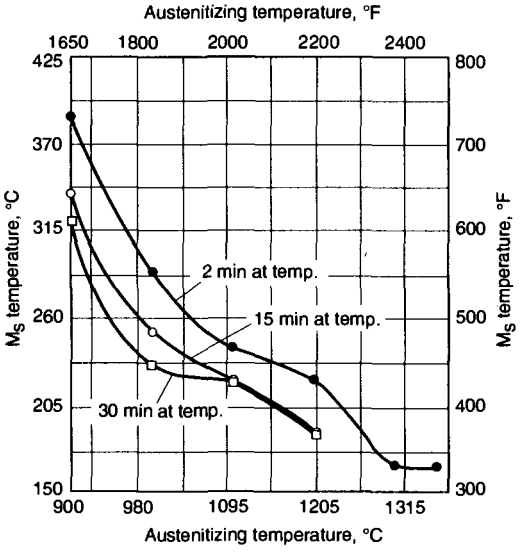

Fig. 14-18 M_s temperature as a function of austenitizing time and temperature for a high-speed steel containing 0.75% C, 17.4% W, 4.2% Cr, and 0.62% V. Source: Ref 22

high-speed steels are continuously cooled, the transformation of austenite to martensite is continuous and a function only of decreasing temperature below M_s, as characterized by Eq 5-1. For example, Fig. 14-21 shows the continuous transformation, as measured by length changes that accompany martensite formation, of a T1 steel continuously cooled between an M_s temperature of 215 °C (420 °F) and a effective M_f temperature of about −100 °C (−150 °F) (Ref 24). However, if cooling is interrupted and then resumed, the austenite is stabilized, as discussed in Chapter 5, and transformation to martensite does not begin immediately when cooling is resumed (Ref 25). Figure 14-22 shows the effect of room-temperature aging or stabilization on the transformation of austenite on subsequent cooling below room temperature in a T1 steel (Ref 24). Increased aging substantially lowers the temperature at which transformation resumes, but eventually the transformation finishes at about the same temperature.

Interrupted cooling above the martensite transformation range may also affect martensite transformation kinetics and the amount of retained austenite. These effects may be due to conditioning or composition changes in austenite that promote bainite formation on cooling rather than martensite formation. Whenever bainite forms, whether by cooling from a high hot quenching temperature or by isothermal transformation, the M_s temperature is lowered and more austenite is retained on cooling to room temperature. Figure 14-23 shows the effect of holding time at several temperatures on M_s temperatures of an M2 steel (Ref 19). Major effects on M_s temperatures are created by isothermal holding at high temperatures, where conditioning occurs and

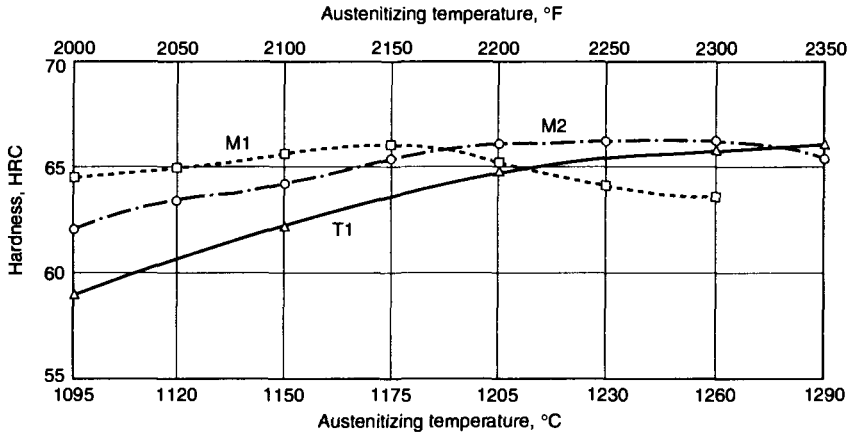

Fig. 14-19 Effect of austenitizing temperature on the quenched hardness of several high-speed steels

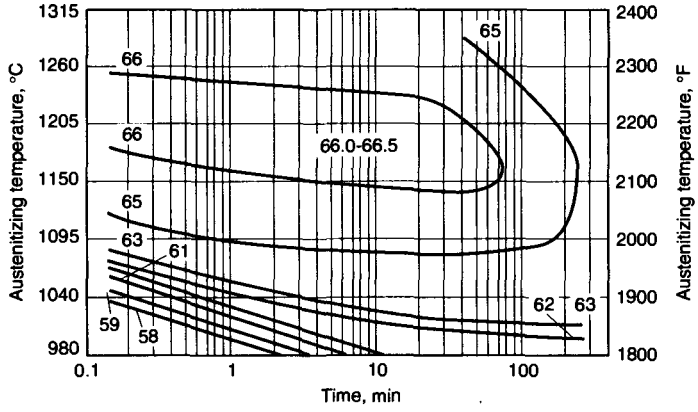

Fig. 14-20 Oil-quenched hardness (HRC) of type T1 high-speed steel as a function of austenitizing time and temperature. Source: Ref 23

conditioning occurs and bainite forms on cooling, or at low temperatures, where isothermal transformation to bainite occurs; relatively little change in M_s temperatures is caused by holding at temperatures in the bay region of the IT diagram.

Tempering and Hardness of High-Speed Steels

Tempering is the final critical heat treatment step applied to high-speed steels. The microstructure at the start of tempering consists of primary carbides, martensite, and retained austenite, the exact amounts of which depend on many alloying and processing factors, as described to this point, but typically are on the order of 10%, 70%, and 20%, respectively. The coarse primary alloy carbide particles are unchanged by the relatively low temperatures used for tempering. The martensite and retained austenite in a given steel, although they have different crystal structures, have identical compositions. It is assumed that the quenching permits no composition change in the austenite, and since martensite formation is a diffusionless process, the composition of the martensite is identical to that of its parent austenite. However, the stable compositions established during high-temperature austenitizing, at room temperature and at the temperatures used for tempering, are highly unstable, in that the martensite and austenite are supersaturated with carbon and alloying element atoms. As a result, during tempering, when diffusion of alloying elements is possible, a number of structural changes

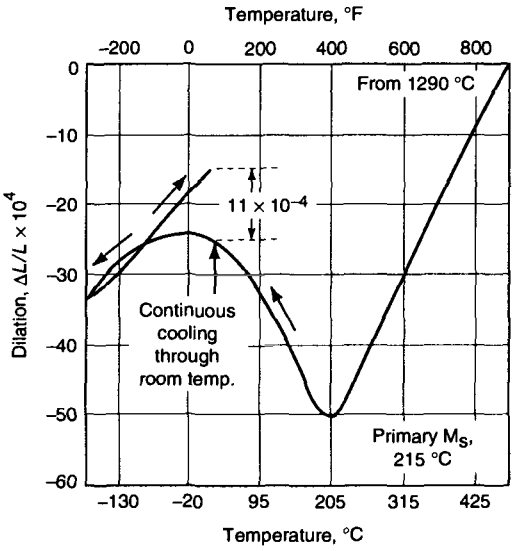

Fig. 14-21 Dilatation curve for the continuous cooling of T1 high-speed steel, showing expansion caused by austenite-to-martensite transformation, which continues through room temperature. Source: Ref 24

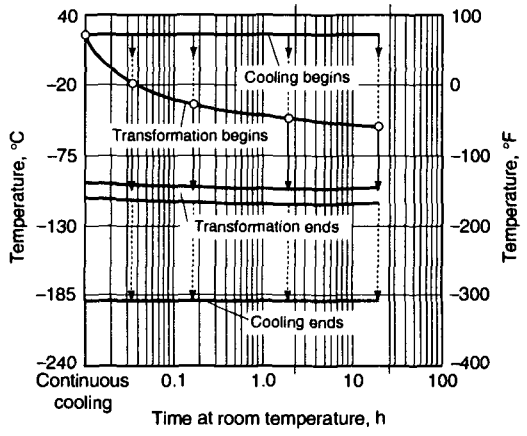

Fig. 14-22 Effect of room-temperature aging on the transformation range of the retained austenite in hardened T1 high-speed steel during subsequent cooling to -190 °C (-310 °F) Source: Ref 24

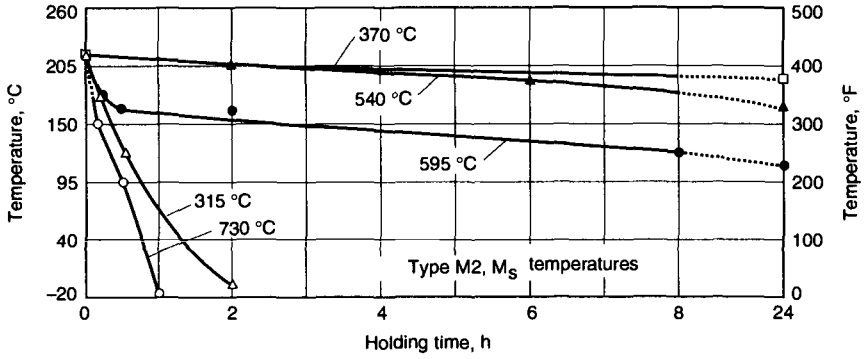

Fig. 14-23 Effect of holding time at various temperatures after cooling from 1225 °C (2235 °F) on the M_s temperature on cooling from the holding temperature to room temperature. Cooling rate from holding temperature, 3 to 6 °C/min (5 to 10 °F/min). Source: Ref 19

are initiated—in particular, the precipitation of alloy carbides.

Figure 14-24 shows typical tempering curves for M1 and T15 high-speed steels. The curves differ from those of tool steels with lower alloy content with respect to the intensity of secondary hardening, which equals or exceeds the hardness of the as-quenched martensite. The early stages of tempering of hardened high-speed steels are similar to those of other tool steels and involve the precipitation of iron carbides (i.e., ε/η transition carbides and Fe_3C in the martensitic matrix at tempering temperatures too low for alloy element diffusion. During these stages, the hardness of the as-quenched martensite decreases.

The secondary hardening is caused by the precipitation of very fine, stable alloy carbides. Depending on steel composition, the carbides that have been identified in this stage of tempering are M_2C and MC carbides based on the isomorphous hexagonal Mo_2C and W_2C carbides and cubic VC carbide (Ref 1, 11, 12, 26–28). For constant tempering times on the order of 1 or 2 h, the hardening due to the alloy carbide precipitation starts at around 315 °C (600 °F) and reaches a peak between 510 and 565 °C (950 and 1050 °F). At higher tempering temperatures, the fine distributions of M_2C and MC particles are replaced by precipitation of $M_{23}C_6$ and M_6C carbides. These carbides coarsen rapidly, and hardness decreases sharply with increasing tempering temperature.

All high-speed steels have similar curves of hardness versus tempering temperature. Figure 14-25 illustrates variations in hardness levels and peak hardness temperatures due to differences in high-speed steel alloying. The peak hardness associated with secondary hardening is dependent on having sufficient carbon atoms available to stoichiometrically combine with the alloying elements to produce the highest volume fraction of closely spaced alloy carbide particles possible (Ref 27). The fact that the alloy carbides must nucleate from a supersaturated martensitic matrix at temperatures where the mobility of the carbide-forming element atoms is limited ensures that the particles will be fine and closely spaced. The T15 steel, which is highly alloyed with molybdenum and cobalt, shows the most intense secondary hardening peak, at a hardness in excess of 70 HRC. The cobalt does not take part in carbide formation but nevertheless consistently enhances hardness when added as an alloying element.

Figure 14-26 shows the effect of austenitizing temperature on the tempering response of a T1 steel. Higher austenitizing temperatures, at which more carbon and alloying elements go into solution, increase the supersaturation of as-quenched martensite and make possible a greater intensity of carbide precipitation, increasing peak secondary hardness and hardness at all other tempering temperatures relative to specimens austenitized at lower temperatures. Thus, austenitizing temperatures at the high end of recommended ranges are preferred for cutting applications that require maximum hardness, provided austenite grain size is not severely coarsened. As discussed earlier relative to hardening, retained austenite will also increase with increasing austenitizing temperature, but the amount of austenite retained has little effect on the maximum tempered hardness that can be obtained. It has been observed that high-speed steels that have been air cooled have the same as-quenched hardness as when they are oil quenched but have lower resis-

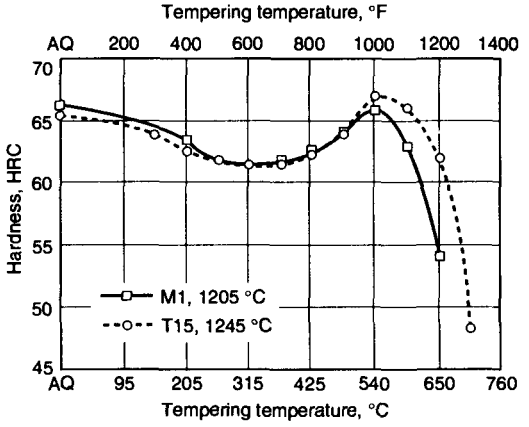

Fig. 14-24 Hardness versus tempering temperature for M1 and T15 high-speed steels. AQ, as quenched

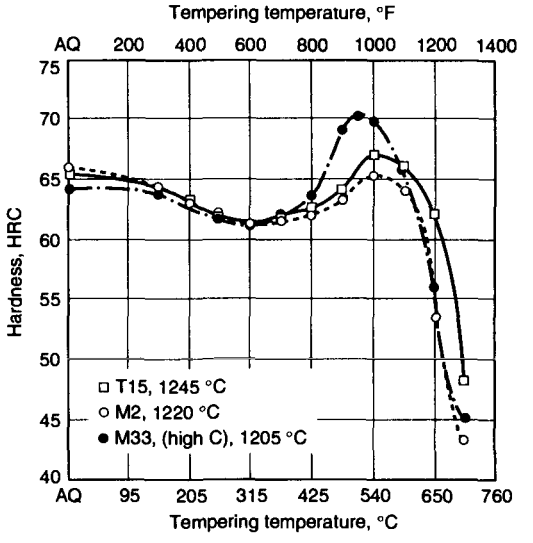

Fig. 14-25 Effect of tempering temperature on the hardness of three high-speed steels, illustrating the range in tempering characteristics within the group

tance to tempering. For any constant tempering temperature and time, the hardness of air-cooled specimens tends to be one or two HRC points lower than that of oil-quenched specimens.

The microstructural changes that produce the hardness changes during tempering are diffusion controlled and therefore dependent on both tempering time and temperature. The curves of hardness versus tempering temperature shown to this point have been obtained by holding tempering time constant and varying temperature. The combined effect of temperature and time can be characterized by the use of Holloman-Jaffe time-temperature parameters (Ref 29), as shown in Fig. 14-27 for an M2 steel austenitized at 1190 °C (2175 °F) and 1220 °C (2225 °F). From the time-temperature parameters, combinations of tempering time and temperature to produce specific hardness values can be calculated. Figures 14-28 and 14-29 show the tempering time-temperature combinations that produce isohardness lines as calculated from the data shown in Fig. 14-27 for the M2 steel austenitized at two temperatures. Note that two sets of conditions produce constant hardness values on either side of the hardness peaks of 65/66 and 64/65 HRC for specimens austenitized at 1220 and 1190 °C (2225 and 2175 °F), respectively. For a given hardness, combinations of time and temperature on the high side of those that produce maximum hardness (i.e., conditions on the overaging side of the hardness peaks) should be chosen to provide for adequate levels of toughness. Despite the apparently wide choice of time and temperature combinations that produce a given hardness, tempering times on the order of 1 to 3 h are selected for convenience and to avoid the possibility of oversoftening in actual furnace conditions.

A major difference between the tempering behavior of high-speed steels and other tool steels of lower alloy content is the very high stability of the retained austenite in hardened high-speed steels. As a result, the retained austenite does not transform during tempering to any significant degree. However, tempering conditions the retained austenite so that it transforms to martensite during cooling after tempering. The martensite formed during cooling after the first tempering cycle is untempered, thus lowering the toughness of a high-speed steel. This condition necessitates the double and triple tempering cycles applied to high-speed steels.

Figures 14-30 and 14-31 show examples of diagrams that plot combinations of tempering times and temperatures required to produce maximum secondary hardness and complete transformation, as defined by the complete transformation of all

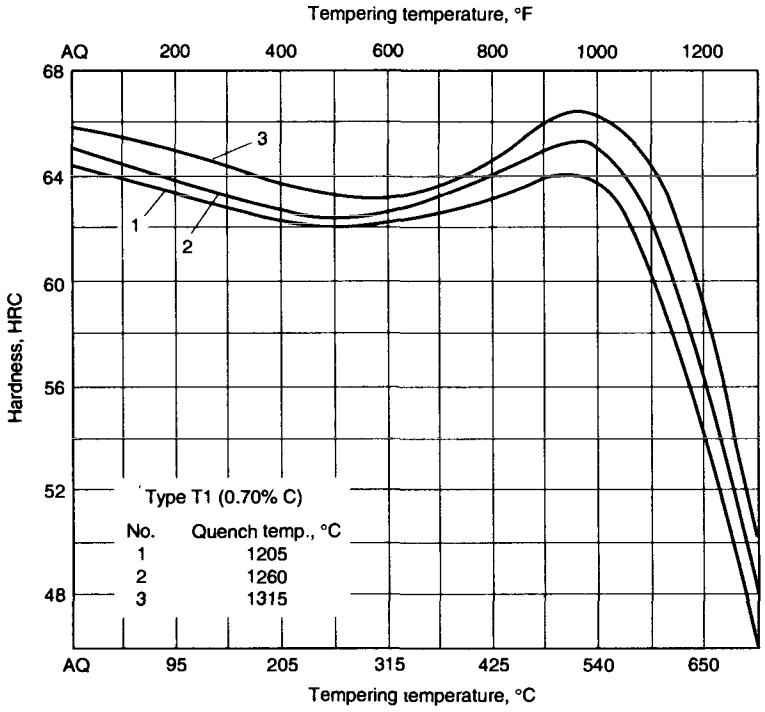

Fig. 14-26 Effect of tempering temperature on the hardness of a 0.70% C T1 high-speed steel after quenching from three temperatures. For this steel, 1290 °C (2350 °F) is the usual austenitizing temperature. Tempering time, 2.5 h

retained austenite on a first cooling after tempering, for T1 and M2 high-speed steels (Ref 30). These diagrams show that the tempering-induced changes which render retained austenite susceptible to transformation on cooling require tempering beyond that which produces maximum secondary hardness. Although the diagrams define the conditions that would necessitate only a second temper, in actual practice three and even four tempering cycles may be applied. Similar diagrams that show tempering conditions for maximum hardness and complete transformation for T2, T4, T6, M4, and M10 high-speed steels have been published (Ref 31).

Kulmburg et al (Ref 22, 33) have evaluated by dilatometric analysis the transformation of retained austenite as a result of tempering of high-speed steels. Figure 14-32 shows length changes as a function of temperature for M2 high-speed steel tem-

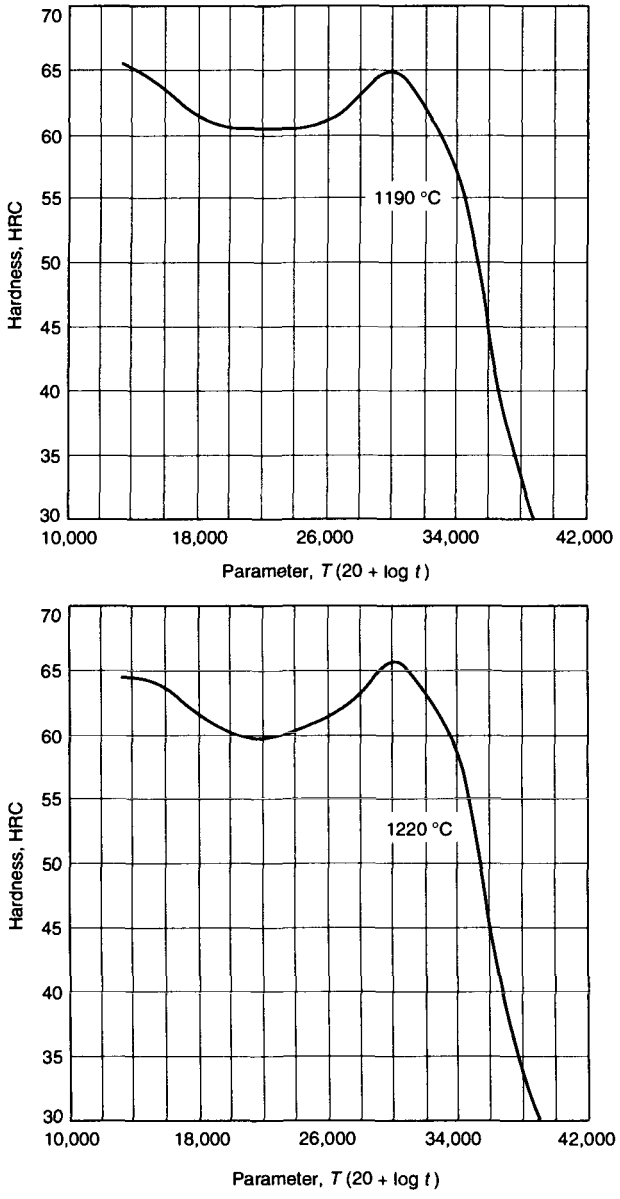

Fig. 14-27 Master tempering curves for M2 high-speed steel hardened from two different austenitizing temperatures

pered four times after holding 10 min at either 540 or 570 °C (1000 or 1060 °F). After tempering at 540 °C (1000 °F), there is essentially no detectable change in dimensions related to martensite formation on cooling. After tempering at 570 °C (1060 °F), however, significant amounts of martensitic transformation occur on cooling, as shown by deviation from the linear curve associated with thermal contraction and marked by the indicated M_s temperatures.

Figure 14-33 shows the interrelationships among hardness, retained austenite, and M_s and M_f temperatures of retained austenite as a function of tempering for hardened M2 steel. The hardness and retained austenite scatter bands are a combination of data from Kulmburg et al. (Ref 33) and data from Haberling and Martens (Ref 34). The increased ability of the retained austenite to transform to martensite during cooling with increasing tempering, as marked by the increase in M_s and M_f temperatures,

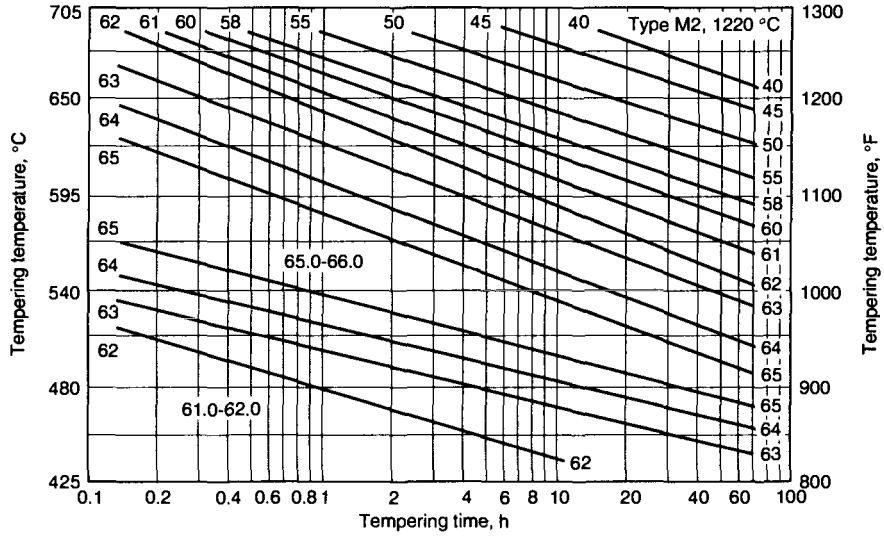

Fig. 14-28 Isohardness lines for tempering M2 high-speed steels oil quenched from 1220 °C (2225 °F)

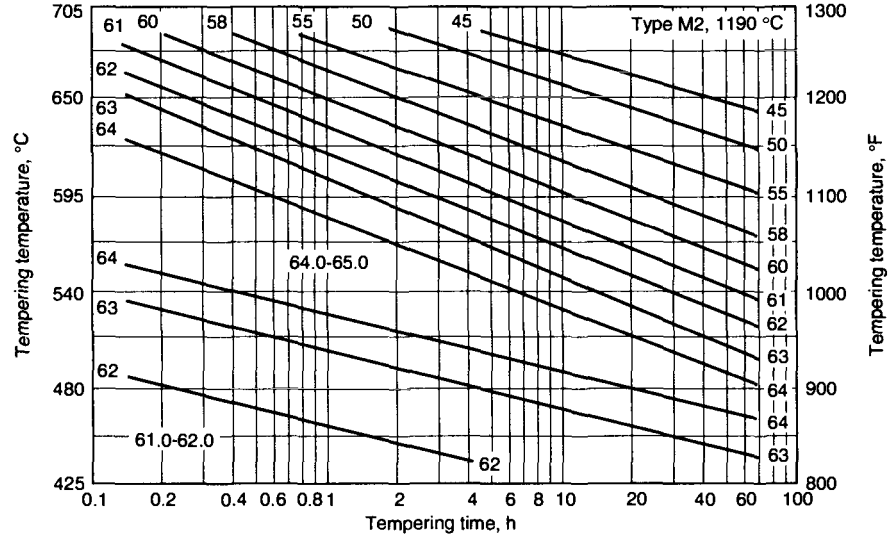

Fig. 14-29 Isohardness lines for tempering M2 high-speed steel quenched from 1190 °C (2175 °F)

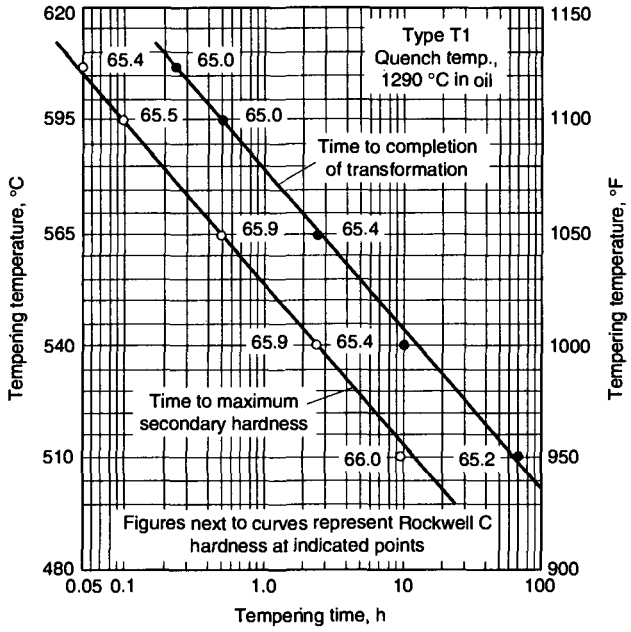

Fig. 14-30 Relationship between the tempering time and the tempering temperature required to produce maximum secondary hardness and to complete the transformation of retained austenite on cooling from the tempering temperature for T1 high-speed steel oil quenched to room temperature from 1290 °C (2350 °F). Source: Ref 30

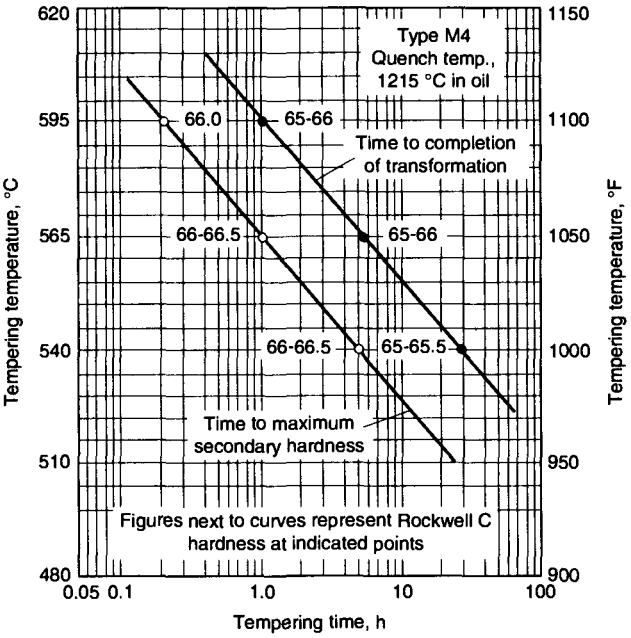

Fig. 14-31 Same as Fig 14-30, but for M4 high-speed steel oil quenched from 1215 °C (2220 °F)

is attributed to the precipitation of alloy carbides in the retained austenite during tempering. The alloy carbides remove carbon and alloying elements from solution in the austenite. This composition change raises M_s temperatures, with the result that austenite, retained after austenitizing and quenching for hardening, becomes unstable after tempering with respect to athermal martensite formation.

As discussed above, maximum secondary hardness is a function of austenitizing time and temperature, which establish the supersaturation of as-quenched martensite, as well as tempering time and temperature, which establish the intensity of secondary hardening. Kulmburg et al. (Ref 33), with the data of Bungardt and Oppenheim (Ref 35), have plotted hardness contours for hardened and tempered M2 steel as a function of time-temperature hardening and time-temperature tempering parameters, as shown in Fig. 14-34. This plot identifies the combination of hardening and tempering parameters capable of producing maximum hardness of 66 HRC in M2 high-speed steels.

Other Property Changes in Tempered High-Speed Steels

The preceding section discussed the effect of tempering on hardened high-speed steels primarily by describing the changes produced in room-temperature hardness. High-speed steels are expected to operate at high temperatures; therefore, hot hardness is also a valuable measure of performance. Figures 14-35 to 14-37 show various curves of hardness as a function of test temperature. For high-speed steels, hot hardness decreases gradually up to temperatures of 595 °C (1100 °F) and then drops more abruptly. Figure 14-35 shows a typical dependence of hot hardness on test temperature for a T1 steel (Ref 36).

Hot hardness bands for high-speed steels compared to those of other relatively highly alloyed steels—namely, cold-work die steels and chromium and tungsten hot-work steels—are shown in Fig. 14-36. The superiority of high-speed steels, especially the highly alloyed superhigh-speed steels with respect to hot hardness is clearly shown. These comparisons reflect differences in alloy design

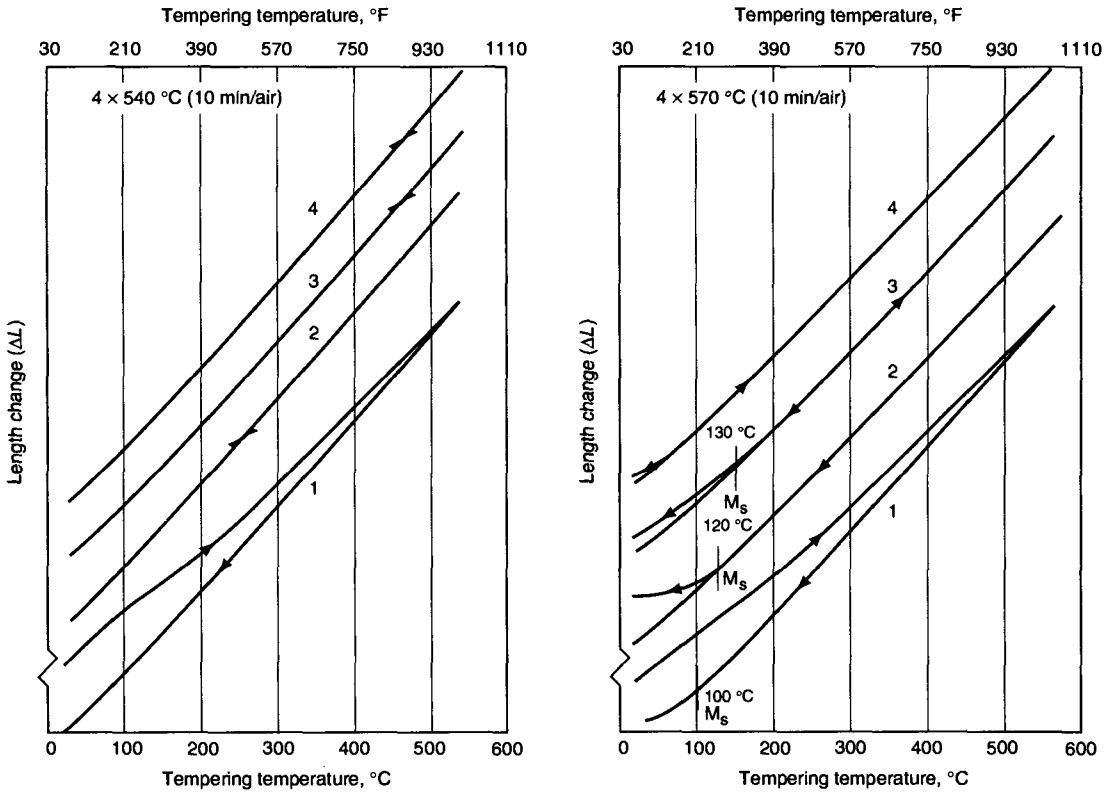

Fig. 14-32 Length changes as a function of temperature for M2 high-speed steel subjected to four cycles of tempering. Source: Ref 33

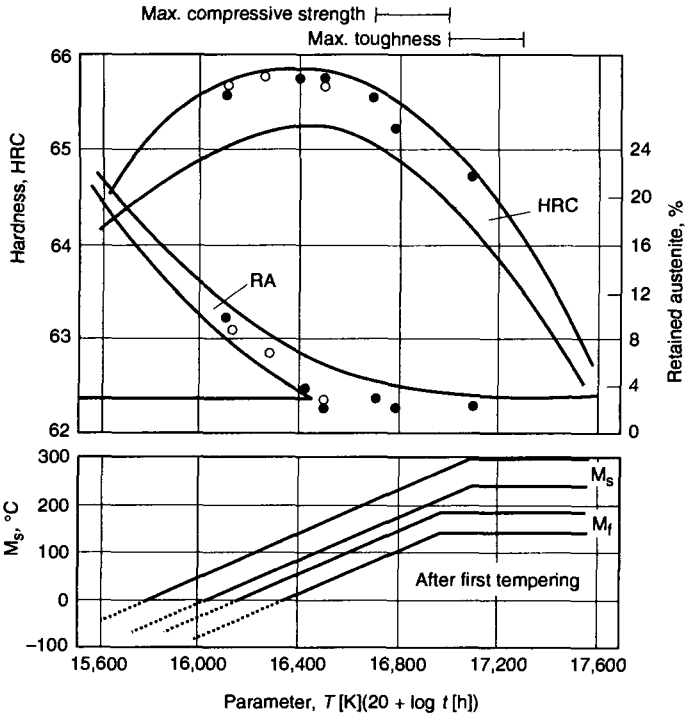

Fig. 14-33 Relationships among tempering parameter, hardness, retained austenite, and M_s and M_f temperatures of retained austenite in M2 high-speed steel. Source: Ref 33

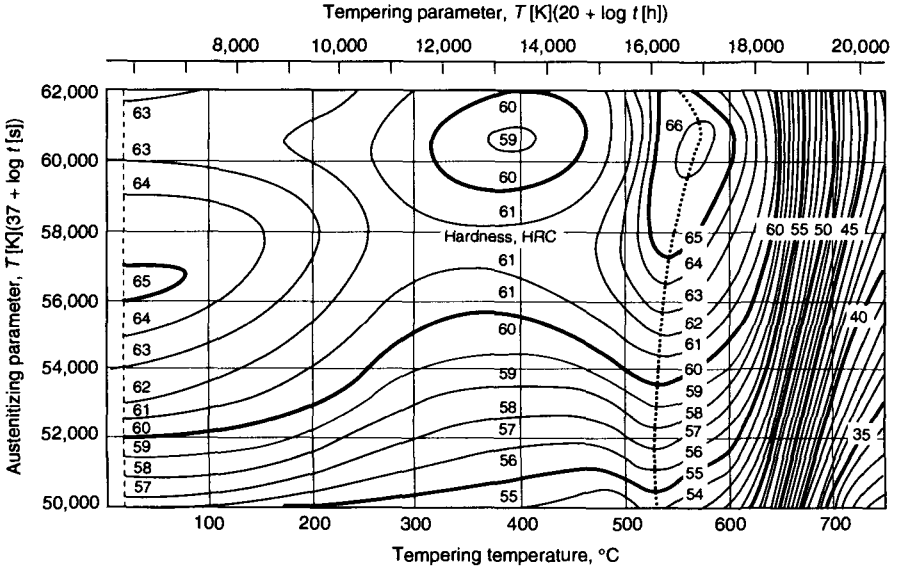

Fig. 14-34 Combinations of austenitizing and tempering conditions that produce various hardness levels in M2 high-speed steel. Source: Ref 33

strategies for quite different applications. The hot-work steels have a gradual softening behavior similar to that of the high-speed steels but have much lower overall hardness because of lower carbon content. The lower hardness is associated with microstructures with the higher toughness and fracture resistance required by hot-work steels. In contrast, wear resistance and hot hardness, made possible by the high carbon and alloy content of the high-speed steels, are primary requirements for cutting tools. Although all high-speed steels are rated very high with respect to hot hardness (Tables 14-2a and b), there are differences between the various types, as shown in Fig. 14-37.

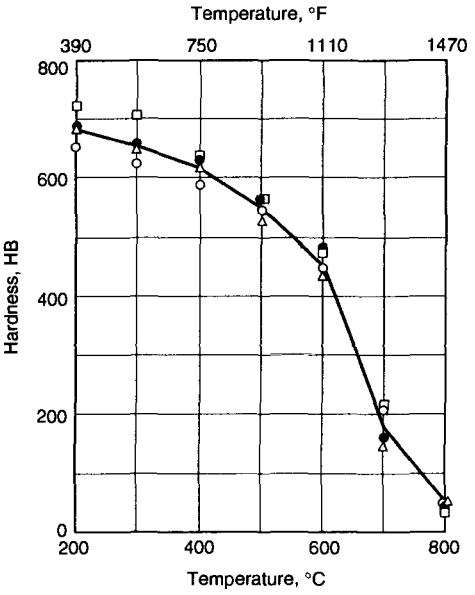

Fig. 14-35 Hot hardness of T1 high-speed steel as a function of testing temperature. Source: Ref 36

Without question, tools fabricated from high-speed steels require excellent wear resistance and hot hardness. However, high elastic limits and yield strengths are also required, especially for fine-edge tools, which must resist deformation. Good toughness and fracture resistance are also required for situations, such as overloads or loads in the presence of notches and sharp corners, where applied stresses exceed elastic limits. Tools often spall at edges when they first come into contact with workpieces. Under these conditions, the limited room-temperature fracture toughness of high-speed steels is more critical than toughness at higher operating temperatures.

Figure 14-38 shows strength and ductility, as measured by bend testing, as a function of austenitizing temperature for a T1 steel double tempered for 2.5 h at 555 °C (1030 °F) (Ref 37). Hardness increased from 57 to 64.5 HRC as the temperature was raised. Yield and total bend strength increase to a maximum with increasing austenitizing temperature and then fall sharply on overheating. The greater the difference between the yield and bend strengths, the greater the ability to accommodate

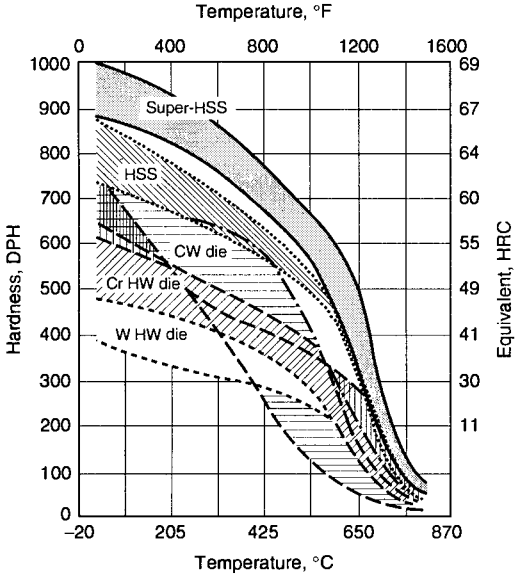

Fig. 14-36 Hot hardness versus testing temperature for high-speed steels (HSS), cold-work (CW) die steels, and hot-work (HW) die steels

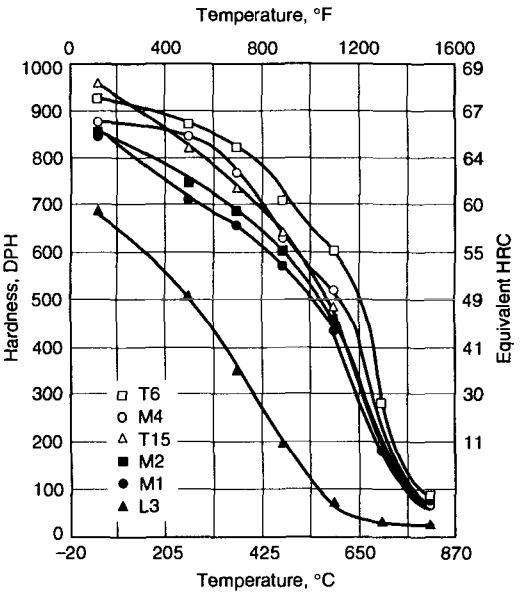

Fig. 14-37 Hot hardness versus testing temperature for several high-speed steels and a low-alloy steel, L3

plastic deformation without fracture. When the yield strength equals the bend strength, fracture occurs as soon as the yield strength is exceeded. The measures of ductility are inverse to the strength measurements up to overheating.

The effect of tempering temperature on the hardness and bend properties of T1- and M2-type tool steels is shown in Fig. 14-39 (Ref 37). The T1 steel was austenitized at 1290 °C (2350 °F) and the M2 steel at 1220 °C (2225 °F); the hardened specimens were tempered for 1 h at the temperatures shown. At lower tempering temperatures, as residual stresses are relieved and transition carbides precipitate in the martensite, deflection and strength increase to maxima. Strength and ductility then decrease, as cementite precipitates. With secondary hardening, yield strength increases sharply and plastic deflection drops to a minimum. After tempering at 565 °C (1050 °F), yield and bend strengths are at or close to their maximum values for the 1 h tempering. Longer tempering times would shift the minimum in plastic deflection to lower tempering temperatures. Double tempering below the temperatures used in the first temper causes little change in bend properties, but if performed at temperatures that reduce hardness, significant improvements in properties occur.

The yield strength determined in bend testing correlates well with hardness. Figure 14-40 plots yield strength as a function of hardness for M2 and T1 high-speed steels and shock-resisting and oil-hardening tool steels (Ref 38). There is an excellent correlation of yield strength with hardness up to the point for each steel where tempering has been insufficient to stabilize the substructure and residual stresses, as marked by the dashed lines for such undertempered conditions. The high-speed steels show superior ranges of usable yield strength and hardness compared to the other steels.

Torsion tests provide useful evaluation of high-speed steels used for taps and drills. The static torsion test evaluates strength and ductility in terms of torsional elastic limit, the torque to fracture, and the elastic and plastic twist to fracture. The torsional impact test measures, from the area under the torque-twist curve, the energy expended in twisting a specimen to fracture. Figure 14-41 shows torsional properties as a function of tempering temperature for T1 steel austenitized at three different temperatures (Ref 39). All the specimens show a sharply reduced ability to sustain plastic deformation after tempering at conditions that produce peak hardness and strength. Figure 14-42 shows that torsional impact falls as peak secondary hardening develops in a T1 high-speed steel and continues to fall even when specimens are tempered beyond peak hardness (Ref 40). This decrease in toughness may be associated with the coarse alloy carbide particles that develop when hardness starts to drop.

The low toughness of hardened high-speed steels requires impact testing with unnotched specimens. Figure 14-43 shows unnotched Izod impact toughness as a function of tempering temperature for T1 and M2 high-speed steels austenitized at 1290 and

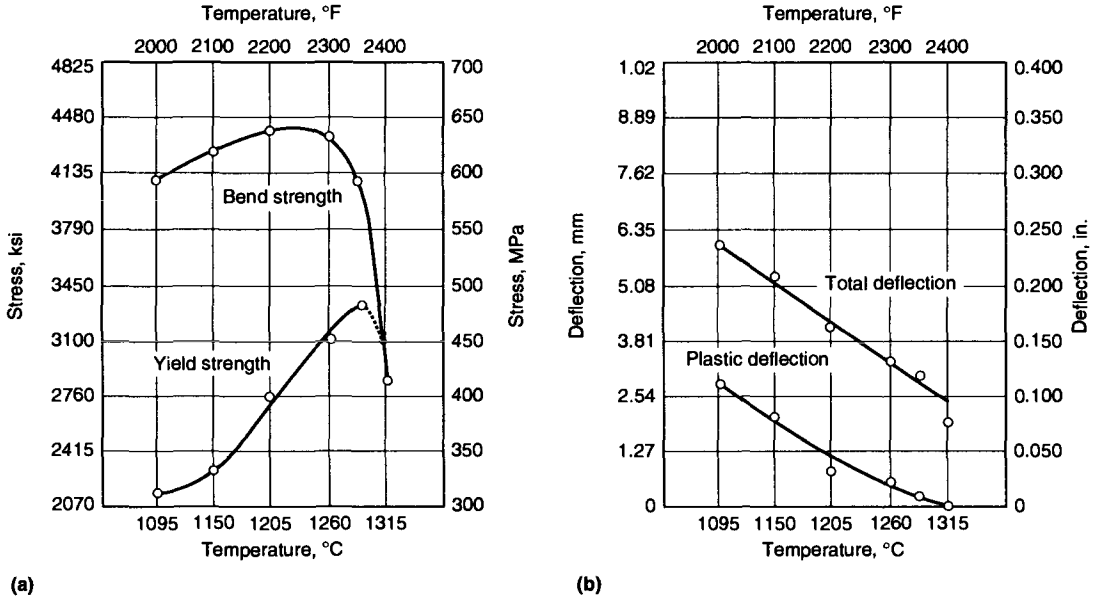

Fig. 14-38 Effect of austenitizing temperature on the yield strength and bend strength (a) and the plastic deflection and the total deflection (b) of T1 high-speed steel. Specimens were double tempered for 2.5 h periods at 555 °C (1030 °F). Source: ref 37

1220 °C (2350 and 2225 °F), respectively (Ref 41). A well-defined drop in impact toughness coincides with peak secondary hardness. The decrease in impact toughness is more severe in the M2 steel, which had a higher retained austenite content (25 to 32%) compared to that of the T1 steel (15 to 22%). Thus, the impact toughness decrease may be caused by a combination of cementite formation, from the transformation of at least some of the retained austenite, and maximum matrix strength, as developed by alloy carbide precipitation. This has been related to similar toughness minima that develop in H11/H13- type hot-work steels (Ref 42) (see Chapter 13).

Figure 14-44 shows unnotched Izod impact toughness as a function of hardness for double-tempered T1 and M2 steels hardened from various temperatures. Increasing austenitizing temperatures severely lower impact toughness in specimens tempered to high hardness. This information must be factored into the selection of heat treatment conditions for cutting tools. The cutting ability and hot hardness of high-speed steels are enhanced by high austenitizing temperatures, which take more carbon and alloying elements into solution. On the other hand, Fig. 14-44 demonstrates that toughness is degraded by high-temperature austenitizing. Thus, the need for good fracture resistance versus hot hardness in a given cutting application must be carefully considered to select the best heat-treating conditions. Figure 14-45 compares unnotched impact strength as a function of hardness for a number of high-speed steels and shows that considerable variations in toughness exist based on alloy content.

The measurement of fracture toughness, or K_{Ic}, provides another method to evaluate toughness of high-speed steels. Fracture toughness is the stress intensity at which a sharp crack, usually introduced by fatigue testing, becomes unstable under maximum constraint or plane strain conditions and is considered to be a material property that can be used to evaluate the stresses at which flaws of various sizes will become unstable and lead to fracture (Ref 43). Thus, unlike Izod or Charpy impact testing, a crack does not first have to be generated by a sequence of deformation and fracture initiation mechanisms.

Kim, et al. (Ref 44) have measured the fracture toughness of an M2 high-speed steel and a matrix steel whose composition simulates the matrix of M2 high-speed steel hardened according to commercial practice, and which does not contain

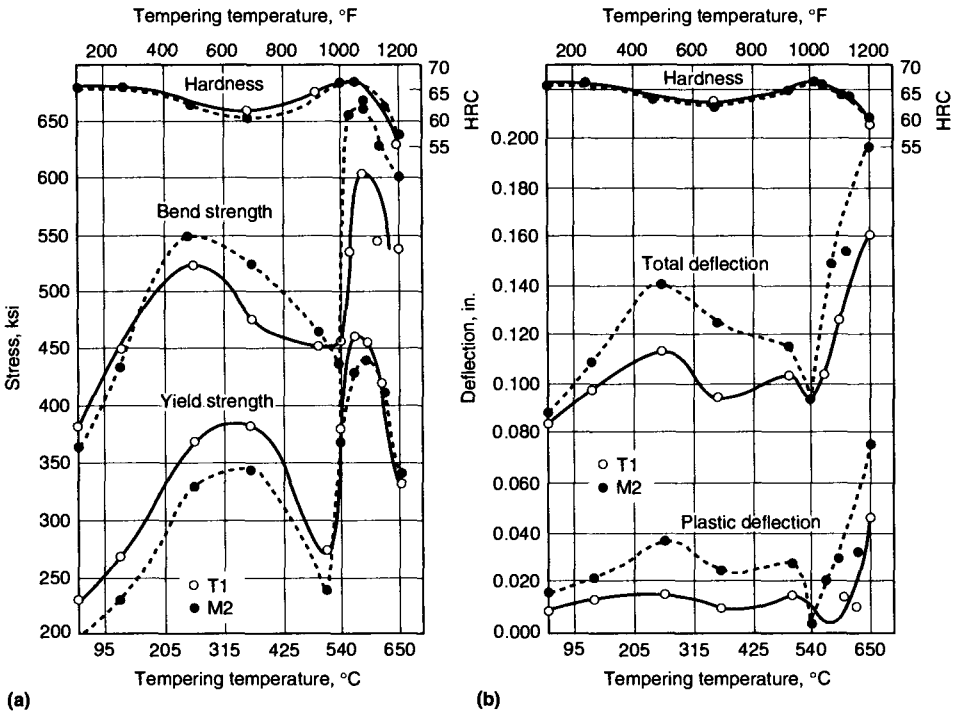

Fig. 14-39 (a) Effect of tempering temperature on the yield strength, bend strength, and hardness of T1 and M2 high-speed steels. Tempering time was 1 h. The T1 steel was austenitized at 1290 °C (2350 °F) and M2 steel was austenitized at 1220 °C (2225 °F). (b) Effect of tempering temperature on the total deflection, plastic deflection, and hardness of T1 and M2 high-speed steels heat treated at the same conditions as (a). Source: Ref 37

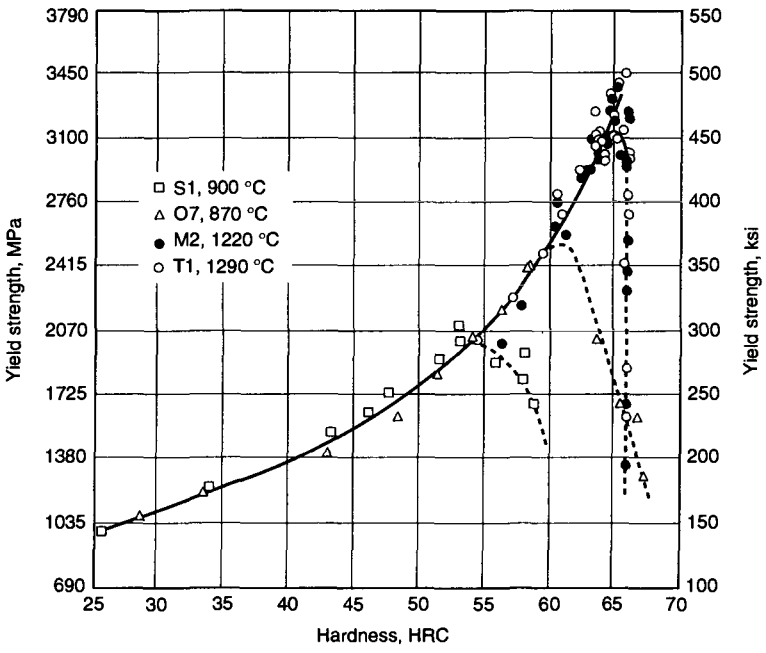

Fig. 14-40 Yield strength and hardness combinations in two medium-alloy tool steels (S1 and O7) and two high-speed tool steels (M2 and T1). Dashed lines indicate where each steel is untempered for its composition. Source: Ref 38

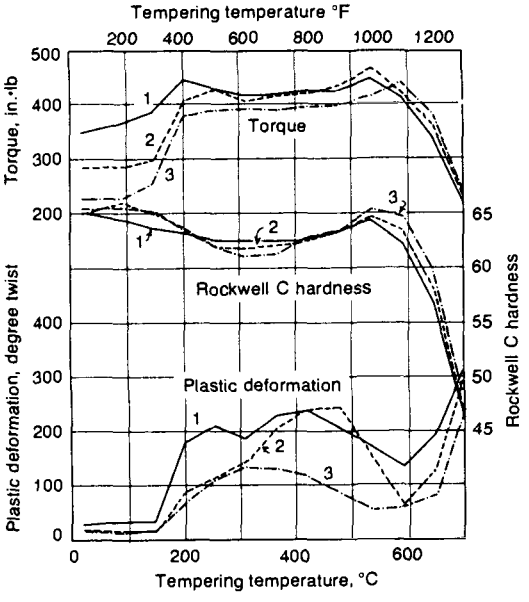

Fig. 14-41 Torsional properties and hardness as a function of tempering temperature for quenched-and-tempered T1 high-speed steel. Curve 1, quenched from 1260 °C (2300 °F); curve 2, quenched from 1290 °C (2350 °F); curve 3, quenched from 1315 °C (2400 °F). Source: Ref 39

the primary carbides of a typical hardened high-speed steel. Figures. 14-46 and 14-47 show the fracture toughness values measured for the M2 and matrix steels as a function of austenitizing temperature in the as-quenched and quench and double-tempered conditions, respectively. The fracture toughness for the as-quenched M2 steel specimens falls sharply with increasing austenitizing temperature, consistent with the results of Izod impact testing. Tempering raises fracture toughness, especially in high-hardness specimens, and decreases the rate at which fracture toughness decreases with increasing austenitizing temperature. The matrix steel in the as-quenched condition had lower fracture toughness after high-temperature austenitizing, even though it has lower hardness, than the M2 steel. The low toughness of the matrix steel was related to intergranular fracture along grain boundaries with thin grain-boundary carbide films. After tempering, the matrix steel showed higher fracture toughness than the M2 steel, apparently because the grain-boundary carbides coarsened and lost continuity. Coarse grain sizes and high contents of retained austenite increased fracture toughness.

Another consequence of hardening and tempering high-speed tool steels is dimensional change. Expansion occurs as a result of hardening, the extent of which depends on the carbon content and tetragonality of the martensite and the

of retained austenite, which if present in sufficient amounts will limit expansion. Figure 14-48 shows the dimensional changes that develop on tempering M2 tool steels after quenching from various austenitizing temperatures. There is a slight contraction on tempering up to tempering temperatures of between 480 and 540 °C (900 and 1000 °F). After tempering above that temperature range, there is a sharp expansion attributed to the transformation of retained austenite to martensite on cooling from the tempering temperature.

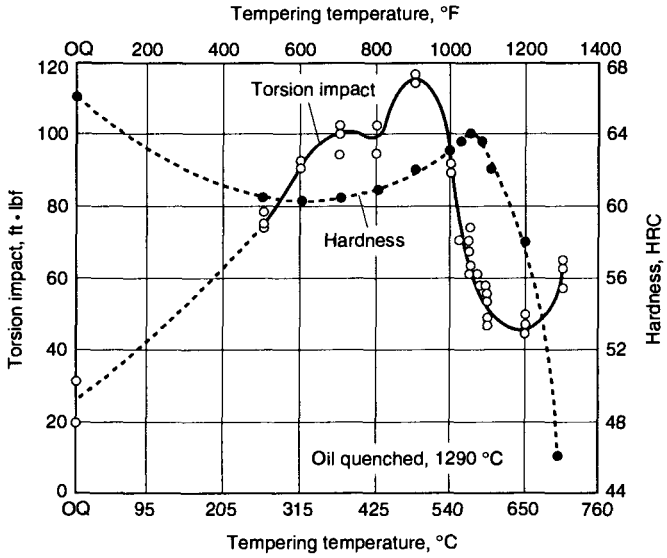

Fig. 14-42 Torsion impact properties and hardness of quenched-and-tempered T1 high-speed steel containing 0.70% C, 18% W, 4% Cr, and 1% V. OQ, oil quenched. Source: Ref 40

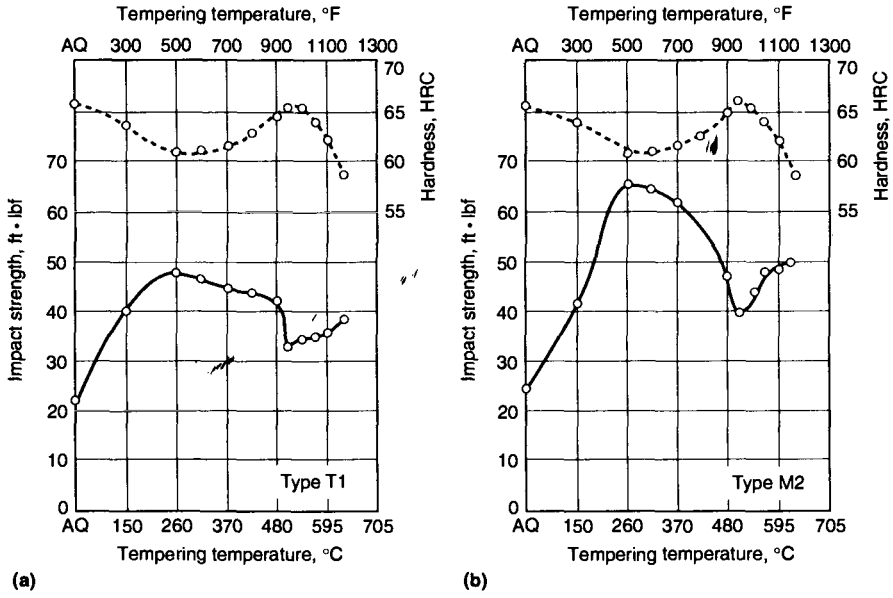

Fig. 14-43 Hardness and unnotched Izod impact strength as a function of tempering temperature for (a) T1 high-speed steel austenitized at 1290 °C (2350 °F) and (b) M2 high-speed steel austenitized at 1220 °C (2225 °F). Source: Ref 41

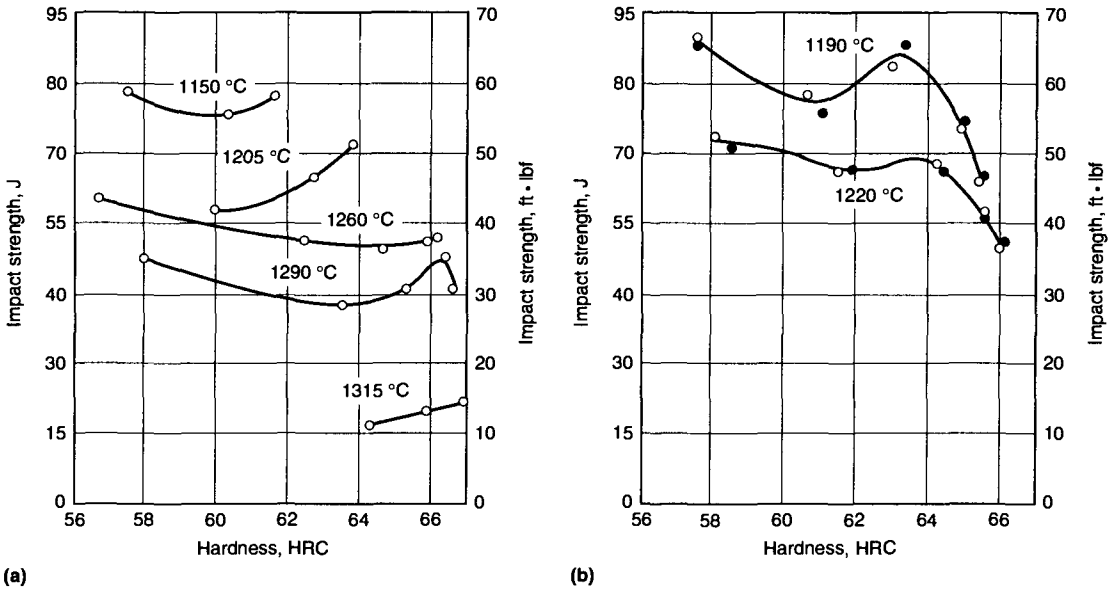

Fig. 14-44 Impact strength as measured by unnotched Izod testing versus hardness for (a) T1 high-speed steel hardened from various temperatures and (b) M2 high-speed steel hardened from 1190 and 1220 °C (2175 and 2225 °F). Source: Ref 41

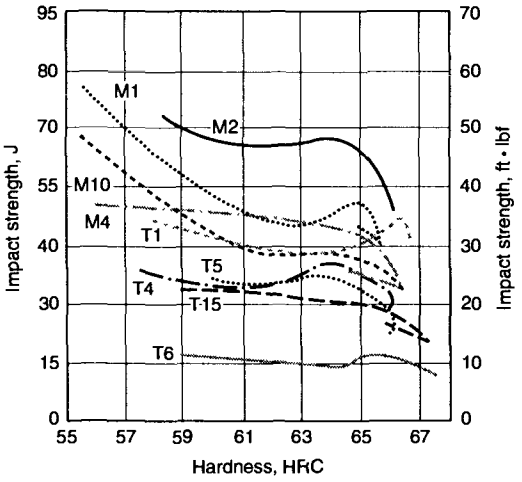

Fig. 14-45 Unnotched Izod impact strength versus hardness for several high-speed steels. The steels and their austenitizing temperatures are as follows: T1, 1315 °C (2400 °F); M2, 1220 °C (2225 °F); M10, 1220 °C (2225 °F); M1, 1220 °C (2225 °F); M4, 1220 °C (2225 °F); T15, 1250 °C (2285 °F); T4 1290 °C (2350 °F); T5, 1290 °C (2350 °F); T6, 1290 ° C (2350 °F). Source: Ref 41

Summary: Alloying Elements in High-Speed Steels

The effects of the complex alloying of high-speed tool steels have been repeatedly described to this point. In particular, the principles of alloying with regard to the microstructures and properties of high-speed steels produced by solidification, hot deformation, and heat treatment have been described by reference to various grades of high-speed steels. These grades have been developed by systematic studies, which followed the effects of carbon and the other alloying elements added to high-speed steels in order to optimize properties and performance (Ref 1, 30).

The essential design approach for high-speed steels consists of incorporating distributions of hard alloy carbides in a matrix of tempered martensite. As shown earlier in Fig. 4-22 and 4-23, the alloy carbides incorporated into the microstructures of high-speed steels have very high strengths and stabilities compared to the iron carbides and martensite of carbon steels, and thus contribute significantly to high-speed steel performance. The alloying elements come from the transition metal periods of the periodic table (Ref 45), as has been shown in Table 4-3 and repeated here as Table 14-5 for purposes of discussion of the effects of individual elements on alloying. Almost all of the transition metals in groups IV, V, and VI have been incorporated in one or another of the high-speed tool steels, primarily because of their strong carbide-forming capabilities. The elements of groups VII and VIII are weak carbide formers or do not form carbides.

There must be sufficient carbon to effectively convert the alloying elements to alloy carbides. At first glance, the amounts of carbon and other alloying elements, given in weight or mass percent in

their contents in the many types of high-speed steels. However, when considered on an atomic basis, all of the high-speed steels have very similar atomic ratios of the sum of all of the carbide-forming elements to the atomic percentage of carbon. Figure 14-49 shows the composition ranges for many of the commonly used tool steels plotted on a ternary composition diagram where one of the axes is the sum of all the carbide-forming elements in atomic percent. When viewed in this framework, the range of high-speed tool steel compositions that have evolved to usable grades is quite narrow. Within an overall alloy composition, each alloying element, depending on its concentration in the alloy and on the ratio of carbon to metal atoms in the crystal structure of its carbides, requires different stoichiometric amounts of carbon in order to be fully utilized in carbide formation (Ref 1, 26, 27). As discussed in earlier sections of the chapter, many time-temperature-dependent phenomena during primary processing, hardening, and tempering must also be controlled to develop the best carbide distributions in a given steel.

Table 14-1 shows that the carbon content of high-speed steels ranges from a low of 0.65% to a high of 1.60%. Although the carbon content of a given steel is fixed within narrow limits, variations within these limits may cause variations in mechanical properties and cutting performance. Also, some of the high-speed steels are available in several ranges of carbon content.

Carbon in any high-speed steel, depending on austenitizing temperature, will be in large part consumed by alloy carbide formation and, if present in too low a concentration, will result in low matrix carbon content after hardening. Also, appreciable quantities of ferrite may become stable at austenitizing temperatures in lower-carbon steels. Figure 14-50 shows as-quenched hardness as a function of austenitizing temperature in T1 steel with various levels of carbon and illustrates the combined effect of low matrix carbon and ferrite formation on lowering the hardness of steels with lower carbon contents. Lower quenched hardness is followed by a lower tempered hardness, as shown in the master tempering curves for the T1 carbon series of alloys in Fig. 14-51 and 14-52 for austenitizing temperatures of 1205 and 1290 °C (2200 and 2350 °F), respectively (Ref 23). The highest-carbon steel is most sensitive to austenite formation at the highest austenitizing temperature, and therefore has a lower quenched hardness than that of steels of intermediate carbon content. However, the higher available carbon content in this steel makes possible higher peak secondary hardness, as shown in Fig. 14-43.

The role that the carbide-forming elements chromium, molybdenum, tungsten, and vanadium play in carbide formation and stability in the processing and performance of high-speed tool steels has been described throughout this chapter. Cobalt, however, is a weak carbide-forming element and in tool steels is not considered to be a carbide-forming element. Instead, cobalt influences performance by being present in solid solution in the austenite and tempered martensite. Cobalt contributes significantly to the hot hardness of high-speed steels, as shown in Fig. 14-53, and is a major alloying element in the high speed steels that attain superhigh hardness of 70 HRC after tempering. The latter effects of cobalt may be due to indirect effects on alloy carbide precipitation. One explanation may be that cobalt raises the melting point of high-speed steels, thus making possible the use of higher hardening temperatures, which enable greater solution of the carbide-forming elements and carbon for subsequent carbide precipitation during secondary hardening on tempering. Another explanation, proposed by Speich (Ref 46) relative to secondary hardening in ultrahigh-strength structural steels, is based on the observation that cobalt retards the recovery of the dislocation substructure of as-quenched martensite.

Table 14-5 Transition metal carbides

Carbide formation is fairly common among the transition elements, except for the second and third rows of group VIII (a).

III	IV	V	VI	VII	VIII		
$Sc_{2-3}C$ ScC_2 Sc_2C_3	TiC	V_2C VC	$Cr_{23}C_6$ Cr_7C_3 Cr_3C_2	$Mn_{23}C_6$ Mn_3C Mn_5C_2 Mn_7C_3	Fe_3C	Co_3C Co_2C	Ni_3C
Y_2C Y_2C_3 YC_2	ZrC	Nb_2C NbC	Mo_2C Mo_3C_2 MoC_{1-x}	TcC	Ru	Rh	Pd
LaC_2	HfC	Ta_2C TaC	W_2C W_3C_2 WC	ReC	OsC	Ir	Pt

(a) ☒ indicates no carbide formation for this element. Source: Ref 31

dislocation substructure of as-quenched martensite. As a result, many more sites are available for the nucleation of alloy carbides in tempered martensite, resulting in a finer alloy carbide dispersion and more intense strengthening during secondary hardening.

High-Speed Tool Steel Applications

The following sections are taken from Ref 47 and are based on information provided in Ref 48.

Single-Point Cutting Tools

The simplest cutting tools are single-point cutting tools, which are often referred to as tool bits, lathe tools, cutoff tools, or inserts. They have only one cutting surface or edge in contact with the work material at the given time. Such tools are used for turning, threading, boring, planing, or shaping, and most are mounted in a toolholder that is made of some type of tough alloy steel. The performance of such tools is dependent on the tool material as well as factors such as the material being cut, the speeds and feeds, the cutting fluid, and fixturing. Following is a discussion of material characteristics and recommendations for the most popular lathe tools.

M1, M2, and T1 are suitable for all-purpose tool bits. They offer excellent strength and toughness, are suitable for both roughing and finishing, and can be used for machining wrought steel, cast steel, cast iron, brass, bronze, copper, aluminum, and so on. These are good economical grades for general shop purposes.

M3 class 2 and M4 high-speed tool steels have high carbon and vanadium contents. Their wear resistance is several times that of standard high-speed steels. These bits are hard and tough, withstanding intermittent cuts even under heavy feeds. They are useful for general applications and are especially recommended for cast steels, cast iron, plastics, brass, and heat-treated steels. On tool bit applications where failure occurs from rapid wearing of the

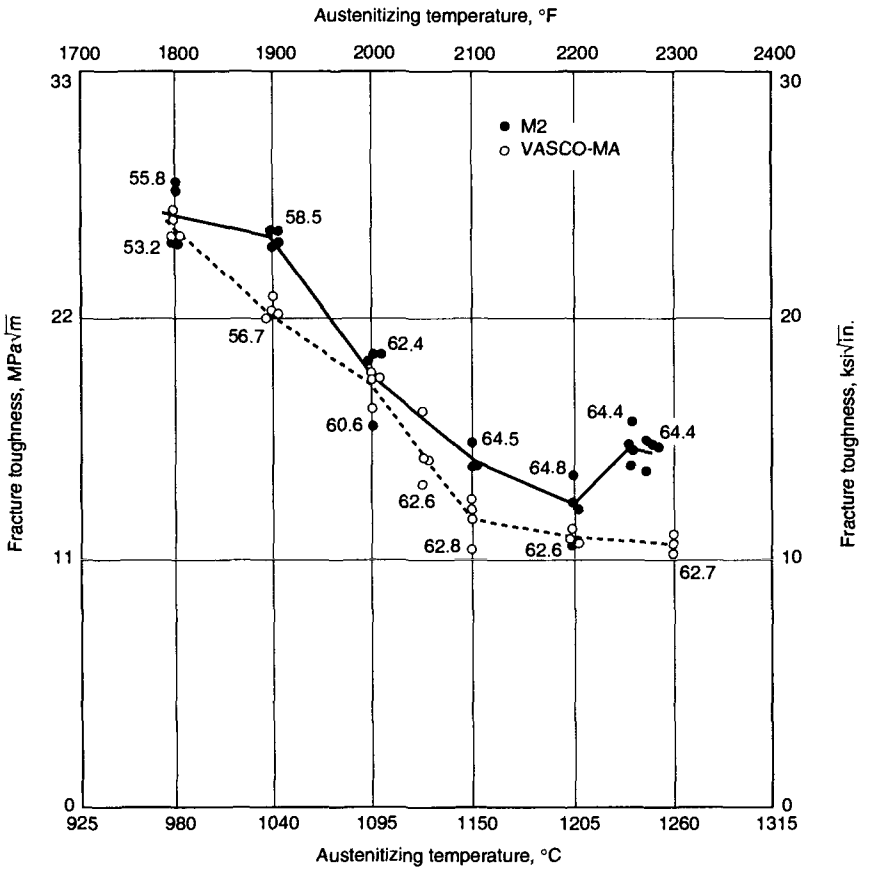

Fig. 14-46 Effect of austenitizing temperature on fracture toughness of as-hardened M2 and a matrix tool steel. Numbers adjacent to data points refer to hardness in HRC. Source: Ref 44

T4, T5, and T8 combine wear resistance, resulting from the higher carbon and vanadium contents, with a higher hot hardness, resulting from the cobalt content. These steels offer good resistance to abrasion and high hot hardness, so they can be applied to the cutting of hard, scaly, or gritty materials. They are well adapted for making hogging cuts, cutting hard materials, and cutting materials that throw a discontinous chip, such as cast iron and nonferrous materials. The high degree of hot hardness permits T4, T5, and T8 to cut at greater speeds and feeds than most high-speed tool steels. They are much more widely used for single-point cutting tools such as lathe, shaper, and planer tools, than for multipoint tools.

Superhard tool bits made from M40 series offer the highest hardness available for high-speed tool steels. The M40 steels are economical cobalt-bearing alloys that can be treated to reach a hardness as high as 69 HRC. Tool bits made from them are easy to grind and offer top efficiency on difficult-to-machine aerospace materials (e.g., titanium- and nickel-base alloys) and heat-treated high-strength steels requiring hot hardness.

Often an engineer specifies a grade that is not necessary for a given application. For example, selecting M42 for a general application that could be satisfied with M2 does not always prove to be beneficial. The logic is that the tool can be run faster and therefore generate a higher production rate. What happens many times is that the M42 chips because of its lower toughness, level, whereas the M2 does not. T15 tool bits are made from a steel capable of being treated to a high hardness, with outstanding hot hardness and wear resistance. The exceptional wear resistance of T15 has made it the most popular high-speed tool steel for lathe tools. It has higher hardness than most other steels and its wear resistance surpasses that of all other conventional high-speed tool steels as well as certain cast cutting tool materials. It has ample toughness for most types of cutting tool applications and will withstand

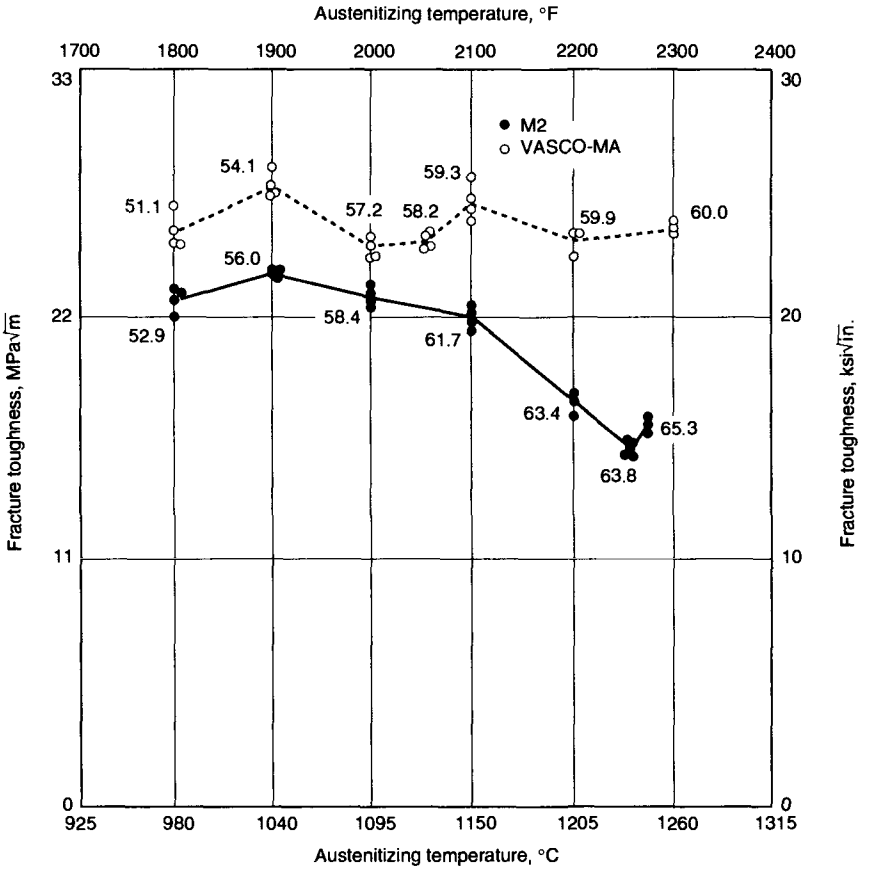

Fig. 14-47 Effect of austenitizing temperature on fracture toughness of hardened and tempered M2 and a matrix tool steel. The steels were double tempered at 565 °C (1050 °F) for 1.5 h per temper. Numbers adjacent to the data points refer to hardness in HRC. Source: Ref 44

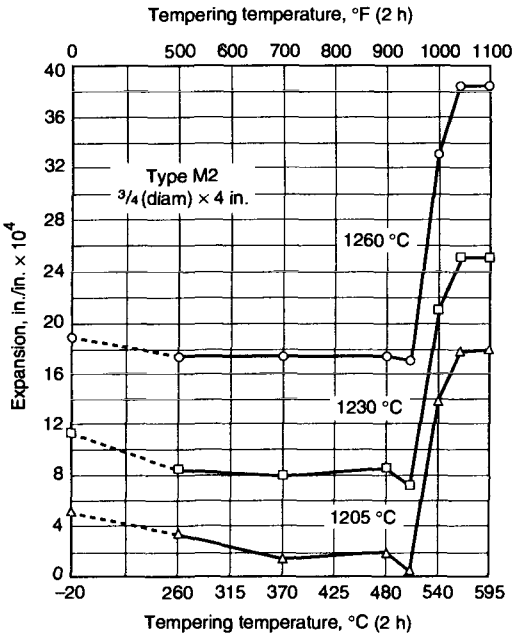

Fig. 14-48 Dimensional changes as a function of tempering temperature in an M2 high-speed tool steel quenched from three different austenitizing temperatures.

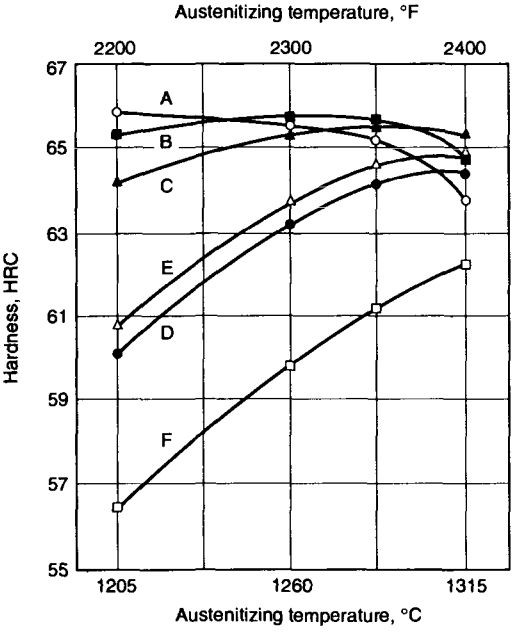

Fig. 14-50 Effect of austenitizing temperature on the quenched hardness of 18-4-1, type T1 high-speed steel, at different carbon levels: steel A, 0.78% C; steel B, 0.72% C; steel C, 0.67% C; steel D, 0.57% C, steel E, 0.58% C; steel F, 0.52 %C. Source: Ref 23

intermittent cuts. T15 bits are especially adapted for machining materials of high tensile strength, such as heat-treated steels, and for resisting abrasions encountered with hard cast iron, cast steel, brass, aluminium, and plastics. Tool bits of T15 can cut

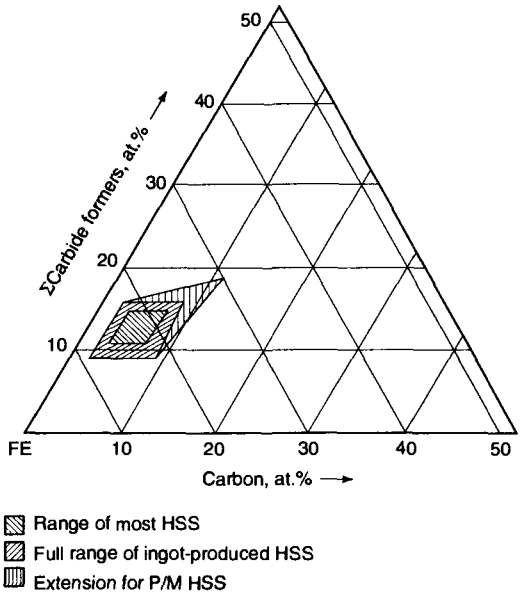

Fig. 14-49 Location of high-speed steel compositions on a ternary plot of Fe-C-carbide-forming elements. Source: Ref 1

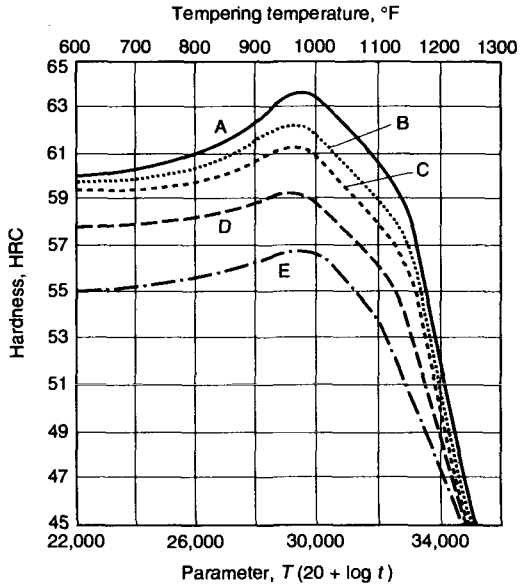

Fig. 14-51 Master tempering curves for T1 high-speed steel at five different carbon levels (see steels A to E in Fig 14-50). Hardened from 1205 °C (2200 °F), tempering times of 5 h. Source: Ref 23

ordinary materials at speeds 15 to 100% higher than average.

Multipoint Cutting Tools

Applications of high-speed tool steels for other cutting-tool applications (e.g., drills, end mills, reamers, taps, threading dies, milling cutters, circular saws, broaches and hobs) are based on the same parameters of hot hardness, wear resistence, toughness, and economics of manufacture. Some of the cutting tools that require extensive grinding have been produced of P/M high-speed tool steels.

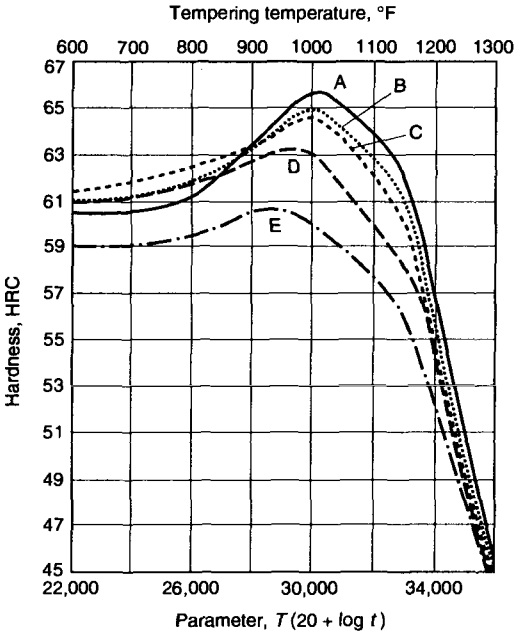

Fig. 14-52 Master tempering curves for T1 high-speed steel at different carbon levels (see Fig. 14-50), similar to Fig. 14-51, but hardened from1290 °C (2350 °F). Source: Ref 23

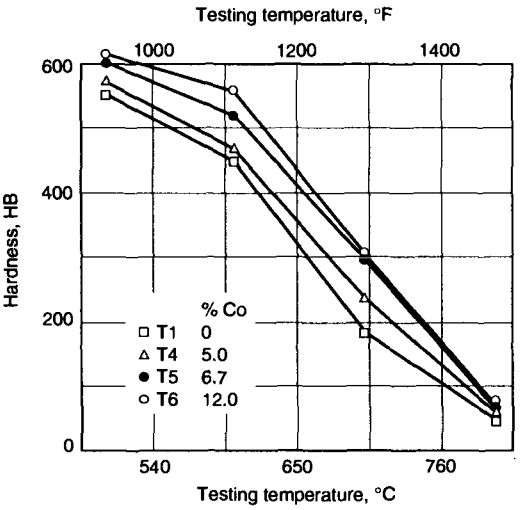

Fig. 14-53 Hot hardness of high-speed steels with various additions of cobalt as a function of testing temperature. Source: Ref 36

General-purpose drills, other than those made from low-alloy steels for low production on wood or soft materials, are made from high-speed tool steels, typically M1, M2, M7, and M10. For lower-cost hardware-quality drills, intermediate high-speed tool steels M50 and M52 are sometimes used, although they cannot be expected to perform as well as standard high-speed tool steels in production work. M33, M42, or T15 are used for the high hot hardness required in the drilling of the more difficult-to-machine alloys, such a nickel-base or titanium products.

High-speed tool drills are not currently being coated as extensively as gear cutting tools because many drills are not used for production applications. Also, the cost of the coating (predominantly with titanium nitride) is prohibitive because it represents a higher percentage of the total tool cost.

Drills coated with titanium nitride reduce cutting forces (thrust and torque) and improve the surface finishes so much that they eliminate the need for prior core drilling and/or subsequent reaming. Coated drills are especially suitable for cutting highly abrasive materials, hard nonferrous alloys, and difficult-to-machine materials, such as heat-resistant alloys. These tools are not recommended for drilling titanium alloys because of possible chemical bonding of the coating to the workpiece material. When drilling gummy materials (e.g., 1018 and 1020 steels) with coated tools, it may be necessary to provide for chip-breaking capabilities in the tool design (Ref 49).

End mills are produced in a variety of sizes and designs, usually with two, four, or six cutting edges on the periphery. This shank-type milling cutter is

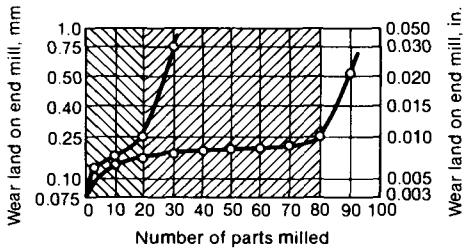

Fig. 14-54 Wear lands developed with uncoated end mills and end mills coated with titanium nitride. Tool life increased fourfold with coated tools. The cross-hatched area at left (extending from 0 to 30 parts) indicates the number of pieces produced by an uncoated end mill after 0.25 mm (0.010 in.) wear land on the tool. The cross-hatched area at right represents the number of pieces produced by a coated end mill after 0.25 mm (0.010 in.) wear land on the tool. Source: Ref 49

typically made from the general purpose high-speed tool steels M1, M2, M7, and M10. For workpieces made from hardened materials (over 300 HB), a grade such as T15, M33, or M42 is more effective. Increased cutting speeds can be used with these cobalt-containing high-speed tool steels because of their improved hot-hardness.

One manufacturer realized a fourfold increase in the tool life of end mill wear lands when it switched to a tool coated with titanium nitride (Fig 14-54). End mills coated with titanium nitride also outperform uncoated solid carbide tools. In an operation for machining valves made from type 304 stainless steel, a switch from solid carbide end mills increased tool life from 30 parts to 150 parts (Ref 1). Furthermore, the cost of the coated, end mills was only one-sixth that of the carbide tools. Both types of 19 mm (¾ in.) fluted end mills were used to machine a 1.6 mm (1/16 in.) deep slot at a speed of 300 rev/min and a feed of 50 mm/min (2 in./min.)

Reamers are designed to remove only small amounts of metal and therefore require very little flute depth for the removal of chips. For this reason, reamers are designed as rigid tools, requiring less toughness from the high-speed tool steel than a deeply fluted drill. The general-purpose grades M1, M2, M7, M10, and T1 are typically used at maximum hardness levels. For applications requiring greater wear resistance, grades such as M3, M4, and T15 are apropriate.

Milling cutters. The size, style, configuration, complexity, and capacity of milling cutters are almost limitless. Milling cutters are available with staggered-tooth or straight-tooth configurations, form relieved or formed, in sizes from 50 to 300 mm (2 to 12 in.). They are used to machine slots, grooves, racks, sprockets, gears, splines, and so on, and they cut a wide variety of materials, including plastics, aluminum, steel, cast iron, superalloys, titanium, and graphite structures. The general-purpose high-speed tool steel used for more than 70% of milling cutter applications is M2, usually the free-machining type. It has a good balance of wear resistance, hot hardness, toughness, and strength and work well on carbon, alloy, and stainless steels, aluminum, cast iron, and some plastics (generally any material that is under 30 HRC in hardness). When higher-hardness materials or more wear-resistent materials need to be milled, M3 or M4 are selected. The higher carbon and vanadium contents in those materials improve wear resistance and allow for the machining of materials greater than 35 HRC in hardness. For workpiece hardness levels above that and as high as 50 HRC, either M42, with its high hardness and high hot hardness, or T15, with its high wear resistance and high hardness, is desirable. The P/M grades in M4 and T15 are increasing in popularity for milling cutters because they offer ease of grinding and regrinding.

Hobs are milling cutters that cut a repeated form about a center, such as a gear teeth, by meshing and rotating about the workpiece, forming a helical pattern. This type of metal cutting creates less force at the cutting edge (less chip load on the teeth) than ordinary milling cutters. Accordingly, less toughness and edge strength are required of hob materials; wear is more commonly a mode of failure. Most hobs are made from a high-carbon version of M2, although normal carbon levels are also used. M2 with a sulfur addition or P/M product for improved machinability and surface finish is often used for hobs.

Saws are quite similar to milling cutters in style and application, but they are usually thinner and tend to be smaller in diameter. Sizes range from 0.075 mm (0.003 in.) thick by 13 mm (½ in.) outside diameter to more than 6.4 mm (¼ in.) thick by 200 mm (8 in.) outside diameter. Used for cutting, slitting, and slotting, saws are available with straight-tooth, staggered-tooth, and side-tooth configuration and are made from alloys similar to those used for milling cutters. Again, M2 high-speed tool steel is the general-purpose saw material, but because of the typical thinness of these products, toughness is optimized with lower hardness. Relatively few saws are made from M3 or M4 high-speed tool steels, because T15 and M42 are generally the two alternative materials to M2. M42 is often used to machine stainless steels, aluminum, and brass because it increases saw production life and can be run at considerably higher speeds. T15 is used for very specialized applications. Saws made of high-speed tool steel are used to cut, slit, and slot everything from steel, aluminum, brass, pipe, and titanium to gold jewelry, fish, frozen foods, plastic, rubber and paper.

Broaches. M2 high-speed tool steel is the most frequently used material for broaches. This includes the large or circular broaches that are made in large quantities as well as the smaller keyway and shape broaches. Sometimes the higher-carbon material is used, but free-machining M2 is generally used because it results in a better surface finish. Powder metallurgy products are very popular for broaches in M2, M3 class 2, and M4 when they are used to improve wear resistance. M4 is probably the second most widely used material for this application. M42 and T15 are often used for difficult-to-machine materials such as nickel-base alloys and other aerospace-type alloys.

Using a 3.2 by 13 by 305 mm (⅛ by ½ by 12 in.) flat broach, a manufacturer of high-nickel (48%) alloy magnets made of M2 increased tool life from 200 to 3400 pieces by adding a titanium nitride coating. A smoother surface finish was also obtained. Replacing the flat broach with an uncaoted round broach, 11.99 mm (0.472 in.) in diameter by 660 mm (26 in.) long, increased magnet production to about 7000 pieces, an coating the round broach

660 mm (26 in.) long, increased magnet production to about 7000 pieces, an coating the round broach with titanium nitride increased production to about 19,000 pieces (Ref 49). Overall, the changes increased production by a factor of 95.

Factors in Selecting High-Speed Tool Steels

No single composition of high-speed tool steel can meet all cutting tool requirements. The general-purpose steels such as M1, M2, M7, and T1 have the highest toughness and good cutting ability, but they possess the lowest hot hardness and wear resistance of all the high-speed tool steels. The addition of vanadium offers greater wear resistance and hot hardness, and steels with intermediate vanadium contents are suited for fine and roughing cuts on both hard and soft materials. The 5% V steel (T15) is especially suited for cutting hard metals and alloys or high-strength steels, and it is particularly suitable for machining aluminum, stainless steels, austenitic alloys, and refractory metals. Wrought high-vanadium high-speed tool steels are more difficult to grind than their P/M product counterparts. The addition of cobalt in various amounts allows still-higher hot hardness, the degree of hot hardness being proportional to the cobalt content. Although cobalt-bearing steels are more brittle than noncobalt types, they give better performance on hard, scaly materials that are machined with deep cuts at high speeds.

REFERENCES

1. G. Hoyle, *High Speed Steels*, Butterworths, London, 1988
2. T. Murakami and A. Hatta, *Sci. Rep. Tōhoku Univ., Honda Anniversary Volume*, 1936, p 882
3. K. Kuo, *J. Iron Steel Inst.*, Vol 181, 1955, p 128
4. K. Kuo, *J. Iron Steel Inst.*, Vol 181, 1955, p 218
5. H.J. Goldschmidt, *J. Iron Steel Inst.*, Vol 186, 1957, p 68
6. E. Horn and H. Brandis, *DEW-Tech. Ber.*, Vol 11, 1971, p 147–154
7. R.K. Barkalow, R.W. Kraft, and J.I. Goldstein, Solidification of M2 High Speed Steel, *Metall. Trans. A*, Vol 3, 1972, p 919–926
8. F.A. Kirk, H.C. Child, E.M. Lowe, and T.J. Wilkins, High-Speed Steel Technology—Manufacturers Viewpoint, *J. Iron Steel Inst.*, Vol 209 (No. 8), 1971, p 606–619
9. F. Kayser and M. Cohen, Carbides in High Speed Steel—Their Nature and Quantity, *Met. Prog.*, Vol 61 (No. 6), 1952, p 79
10. D.J. Blickwede, M. Cohen, and G.A. Roberts, The Effect of Vanadium and Carbon on the Constitution of High Speed Steel, *Trans. ASM*, Vol 42, 1950, p 1161
11. K. Kuo, Carbides in Chromium, Molybdenum, and Tungsten Steels, *J. Iron Steel Inst.*, Vol 173, 1953, p 363–375
12. K. Kuo, Carbide Precipitation, Secondary Hardening, and Red Hardness of High Speed Steel, *J. Iron Steel Inst.*, Vol 174, 1953, p 223–228
13. A.P. Gulyaev, Study of the Phase Composition of High Speed Steels, *Stal*, Vol 6, 1946, p 181
14. H.J. Goldschmidt, The Structure of Carbides in Alloy Steels, *J. Iron Steel Inst.*, Vol 160, 1948, p 345; Vol 170, 1952, p 189
15. T. Malkiewicz, Z. Bojarski, and J. Foryst, Carbides in Annealed and Quenched High Speed Steels, *J. Iron Steel Inst.*, Vol 193, 1959, p 25
16. A. Omsen, *The Annealing of High Speed Steel, J. Iron Steel Inst*, Vol 207 (No. 5), 1969, p 610–620
17. A.H. Grobe, G.A. Roberts, and D.S. Chambers, Discontinuous Grain Growth in High Speed Steel, *Trans. ASM*, Vol 46, 1954, p 759–788
18. E. Kula and M. Cohen, Grain Growth in High Speed Steel, *Trans. ASM*, Vol 46, 1954, p 727–752
19. P. Gordon, M. Cohen, and R.S. Rose, The Kinetics of Austenite Decomposition in High Speed Steel, *Trans. ASM*, Vol 31, 1943, p 161
20. P. Payson, *The Metallurgy of Tool Steels*, John Wiley & Sons, 1962, p 206–208
21. A. Gulyaev, The Martensite Transformation in High Speed Steel, *Kachestvennaya Stal*, Vol 5 (No. 1), 1937, p 41
22. I. Bornatski, Aging of Supercooled Austenite in High Speed Steel, *Metallurg*, Vol 14 (No. 3), 1939, p 56
23. A.H. Grobe and G.A. Roberts, Effect of Carbon Content on 18-4-1 High Speed Steel, *Trans. ASM*, Vol 45, 1953, p 475
24. M.P. Gordon and M. Cohen, Transformation of Retained Austenite in High Speed Steel at Subatmospheric Temperatures, *Trans. ASM*, Vol 30, 1952, p 569
25. M. Cohen, Retained Austenite, *Trans. ASM*, Vol 41, 1949, p 35
26. H.W. Rayson, Tool Steels, *Constitution and Properties of Steels*, F.B. Pickering, Ed., Vol 7, *Materials Science and Technology*, VCH Publishers, 1992, p 583–640
27. F.B. Pickering, *Physical Metallurgy and Design of Steels*, Elsevier Applied Science, London, 1978
28. R.W.K. Honeycombe, *Steels: Microstructure and Properties*, Edward Arnold, London, 1981
29. J.H. Hollomon and L.D. Jaffe, Time-Temperature Relations in Tempering High Carbon Steels, *Trans. TMS-AIME*, Vol 162, 1945, p 223–249
30. M. Cohen and P.K. Koh, Tempering High Speed Steels, *Trans. ASM*, Vol 27, 1939, p 1015
31. G.A. Roberts and R.A. Cary, *Tool Steels*, 4 ed., American Sociey for Metals, 1980
32. A. Kulmburg, E. Kaiser, and S. Wilmes, Rationalisierungsmöglichkeiten beim Anlassen von Schnellarbeitsstahlen, *Härt.-Tech. Mitt.*, Vol 42, 1987, p 133–138
33. A. Kulmburg, E. Kaiser, F. Korntheuer, and S. Wilmes, Einfluss der Haltedauer auf die Vorgänge beim

34. E. Haberling and H. Martens, Härteannahme und Restaustenitumwandlung beim Anlassen von gehärteten Schnellarbeitsstählen im Salzbad und im Luftumwalzofen, *TEW-Tech. Ber.*, Vol 1, 1975, p 131–135
35. K. Bungardt and R. Oppenheim, Beziehung zwischen Temperatur und Zeit bei der Härtung eines Molybdan-Vanadin-Wolfram-Schnellarbeitsstahles, *Stahl Eisen*, Vol 76, 1956, p 689–700
36. O.E. Harder and H.A. Grove, Hot Hardness of High-Speed Steels and Related Alloys, *Trans. TMS-AIME*, Vol 105, 1933, p 88–124
37. A.H. Grobe and G.A. Roberts, The Bend Test for Hardened High Speed Steel, *Trans. ASM*, Vol 40, 1948, p 435
38. J.C. Hamaker, Jr., V.C. Strang, and G.A. Roberts, Bend: Tensile Relationships for Tool Steels at High Strength Levels, *Trans. ASM*, Vol 49, 1957, p 550
39. J.V. Emmons, Physical Properties of High Speed Steel, *Trans. ASST*, Vol 19, 1931, p 289
40. G.V. Luerssen and O.V. Greene, The Torsion Impact Test, *Trans. ASTM*, Vol 33, 1933, p 315
41. A.H. Grobe and G.A. Roberts, Unnotched Impact Strength of High Speed Steels, *Trans. ASM*, Vol 42, 1950, p 686
42. J.R.T. Branco and G. Krauss, Toughness of H11/H13 Hot Work Die Steels, *New Materials, Processes, Experiences for Tooling*, H. Berns, M. Hofmann, L.-A. Norstrom, K. Rasche, and A.-M. Schindler, Ed., MAT SEARCH, Andelfingen, Switzerland, 1992, p 121–134
43. J.F. Knott, *Fundamentals of Fracture Mechanics*, John Wiley & Sons, 1973
44. C. Kim, A.R. Johnson, and W.F. Hosford, Jr., Fracture Toughness of AISI M2 High-Speed Steel and Corresponding Matrix Tool Steel, *Processing and Properties of High Speed Tool Steels*, M.G.H. Wells and L.W. Lherbier, Ed., TMS-AIME, 1980, p 32–74.
45. L.E. Toth, *Transition Metal Carbides and Nitrides*, Academic Press, 1971
46. G.R. Speich, Secondary Hardening Ultrahigh-Strength Steels, *Innovations in Ultrahigh-Strength Steel Technology*, G.B. Olson, M. Azrin, and E.S. Wright, Ed., U.S. Army Materials Technology Laboratory, 1990, p 89–111
47. Wrought High-Speed Tool Steels, *ASM Speciality Handbook: Tool Materials*, J.R. Davis, Ed., ASM International, 1995
48. A.M. Bayer and B.A. Becherer, High-Speed Tool Steels, *Machining*, Vol 16, *ASM Handbook* (formerly 9th ed., *Metals HAndbook*), ASM International, 1989, p 51–59
49. C. Wick, HSS Cutting Tools Gain a Productivity Edge, *Manuf. Eng.*, May 1987, p 38

Tool Steels: 5th Edition
George Roberts, George Krauss, Richard Kennedy, p 291-304
DOI:10.1361/toos1998p291

Copyright © 1998 ASM International®
All rights reserved.
www.asminternational.org

CHAPTER 15
Mold Steels

The steels used for plastic molding and some die-casting applications, designated as group P steels in the AISI classification system, have fabrication and performance requirements that differentiate them from other types of tool steels. The following list, based on literature published up to 1957, describes some of the essential characteristics required in mold steels (Ref 1):

- *Ease of hubbing or hubbability.* This requirement is met by low annealed hardness.
- *Machinability.* When hubbing is not possible or economical, or when hubbing must be followed by machining, the machinability of mold steel becomes of paramount importance.
- *Polishability* is especially important in dies for molding transparent plastics, where a smooth surface on the final product is mandatory. Freedom from inclusions, chemical and structural uniformity, and high surface hardness are essential for good polishability.
- *Wear resistance.* The flow of material into a die or mold can cause an appreciable amount of wear. A hard, wear-resistant surface is required.
- *High surface hardness.* In addition to promoting polishability and wear resistance, high surface hardness is necessary for resistance to indentation.
- *High core strength* is necessary to prevent "sinking" of the cavity when acted upon by high pressures.
- *Toughness.* Dies and molds may be subjected to shock from several sources, including mechanical operation of opening and closing dies, injection of plastics or alloys at high velocity, and thermal shock of rapid heating and cooling. A tough, ductile material is advantageous for shock resistance.
- *Minimum dimensional change on hardening.* Die materials that require a minimum amount of finishing to size after heat treatment are generally preferable.
- *Resistance to corrosion.* Some plastics are highly corrosive. Rusting may become a problem, especially under high-humidity conditions.
- *Resistance to hardness loss on tempering.* Slightly elevated temperatures are involved in the molding of some products. A die that loses its hardness soon shows signs of wear.

All of these requirements are still valid, especially with the current and anticipated very high production of plastics by injection molding of thermoplastics and by compression molding of thermoset plastics, the need for high quality, the need to maintain costs in mold manufacture, and the need for increased life of steels in mold applications. The need for high polishability, as achieved by low inclusion content and uniformity, has driven the application of improved steelmaking and forging practices for mold steels, including vacuum degassing, special deoxidation treatments, and electroslag or vacuum arc remelting. In addition to the standard grades of mold steels, as described below, martensitic stainless steels are used for applications that require corrosion resistance higher than achievable with low-alloy carbon grades.

Hubbing, sometimes also called hobbing, is a technique for forming mold cavities by forcing hardened steel master hubs, which replicate the cavities to be formed, into softer die blanks. Hubbing is often the least time-consuming and most cost-effective way to fabricate die cavities, especially in multicavity molds with identical impressions (Ref 2). Hubbing is restricted to relatively simple shapes because it is not possible to hub cavities with undercuts, and most cavities thus are machined. Master hubs require high compressive strengths and high polishability and are manufactured from shock-resisting steels (S1 and S4), oil-hardening steels (O1 and O2), or cold-work steels (including A2, A6, D2, and D4). Water-hardening tool steels will generally not harden deeply enough to provide the high compressive strengths required for hubbing.

Table 15-1 lists the compositions of the low- and medium-carbon mold steels, and Table 15-2 lists

performance factors and processing information for these steels. There are three major groups of P-type steels: carbon steel grades used for hubbed cavities, carbon steel grades used for machined cavities, and stainless steel grades. The steels of the first group have very low carbon contents, less than 0.12%, and must be carburized to develop high surface hardness and wear resistance for molding applications. Wear resistance is a function of alloy content as well as carbon content, and the wear resistance of the carburized surface of the P4 steel with its high chromium content approaches that of the air-hardening cold-work die steel A2. The low carbon content of the hardened cores of carburized P steels provides microstructures with high toughness and shock resistance. The second group of mold steels, which includes the P20 and P21 steels with higher carbon contents must have cavities machined and may be carburized to increase surface hardness and wear resistance.

Martensitic stainless steels constitute the third type of steels used for molds. These steels are used in applications requiring high corrosion resistance, either because some plastics (such as polyvinyl chloride, which may generate HCl) are highly corrosive or because the general operating conditions cause the formation of rust on cavity surfaces or mold cooling channels. Cooling during injection molding of plastics is critical, and although the thermal conductivity of stainless steel is lower than that of carbon steel, stainless steel molds perform better than carbon steels, which have greatly reduced thermal conductivity because of rusting (Ref 3). The martensitic mold steels are typically modifications of AISI 4*xx* martensitic stainless steels and contain 13% Cr or more and various levels of carbon (Ref 1, 3, 4). Nominal compositions of three martensitic stainless steels used for molds are also listed in Table 15-1.

Hubbing Grades

The ability to effectively create cavities by cold working of mold steels is related to annealed hardness, which in turn depends on carbon and alloy content. Figure 15-1 shows that the depth of hubbed cavities increases rapidly when the annealed hardness of mold steels drops below 150 HB (Ref 5, 6). Although the correlation of hubbability with annealed hardness is good, some investigators have suggested that the rate of work hardening is a better indicator of formability during hubbing (Ref 7–9). The P1 steel, the most readily hubbed according to Fig. 15-1, was essentially a plain carbon steel and thus had very low hardenability after carburizing. The low hardenability necessitated water quenching, which increased distortion on hardening. The P1 steel is no longer widely used and has been replaced by the P-type steels with higher, but still moderate, alloy content for improved hardenability. Higher hardenability makes possible martensite formation during oil quenching, and the resulting more uniform cooling, as compared to that achievable in water quenching, results in better dimensional control during mold hardening.

Alloy design of the low-carbon mold steels is based on a need to balance hubbing characteristics for cavity formation and hardenability after carburizing. The P3 steel contains nickel, chromium, and manganese but has relatively low workability. The P2 grade has lower nickel content, a higher chromium content, and a molybdenum addition to compensate for lower hardenability due to the reduced nickel content. Nickel acts as a ferrite strengthener and tends to promote high annealed hardness. Therefore, its reduced content in the P2 grade promotes hubbability. Figures 15-2 and 15-3 show, respectively, IT diagrams for the core and carburized case of a P2 steel. The carburized P2

Table 15-1 Composition limits for low-carbon mold steels and nominal compositions of stainless mold steels

Type	UNS No.	Composition(a), %								
		C	Mn	Si	Cr	Ni	Mo	W	V	Al
Low-carbon mold steels										
P2	T51602	0.10 max	0.10–0.40	0.10–0.40	0.75–1.25	0.10–1.50	0.15–0.40	...	...	...
P3	T51603	0.10 max	0.20–0.60	0.40 max	0.40–0.75	1.00–1.50	...	...	...	...
P4	T51604	0.12 max	0.20–0.60	0.10–0.40	4.00–5.25	...	0.40–1.00	...	...	...
P5	T51605	0.10 max	0.20–0.60	0.40 max	2.00–2.50	0.35 max	...	...	...	...
P6	T51606	0.05–0.15	0.35–0.70	0.10–0.40	1.25–1.75	3.25–3.75	...	...	...	...
P20	T51620	0.28–0.40	0.60–1.00	0.20–0.80	1.40–2.00	...	0.30–0.55	...	...	...
P21	T51621	0.18–0.22	0.20–0.40	0.20–0.40	0.50 max	3.90–4.25	...	...	0.15–0.25	1.05–1.25
Stainless mold steels										
13Cr–0.12C	...	0.12	0.40	0.25	13.00	...	...	...	...	...
13Cr–0.35C	...	0.35	0.40	0.25	13.25	...	...	...	...	...
17Cr–0.65C	...	0.65	0.30	0.30	17.00	...	...	...	...	...

(a) 0.25% max Cu, 0.03% max P, and 0.03% max S

Table 15-2 Performance factors and processing information for mold steels

Factor	For hubbed and/or carburized cavities					For machined cavities				
	P2	P3	P4	P5	P6	P20	P21	13Cr–0.12C	13Cr–0.35C	17Cr–0.65C
Major factors										
Wear resistance	1(a)	1(a)	1(a)	1(a)	1(a)	1(a)	1	2	3	5
Toughness	9	9	9	9	9	8	8	8	6	5
Hot hardness	2(a)	2(a)	4(a)	2(a)	3(a)	2(a)	4	5	6	6
Minor factors										
Usual working hardness, HRC	58–64(a)	58–64(a)	58–64(a)	50–64(a)	58–61(a)	30–50	36–39	40–42	50–53	51–57
Depth of hardening	S	S	M	S	M	M	D	M	M	M
Finest grain size at full hardness, Shepherd standard	...	...	...	...	...	7½	...	...	7	7½
Surface hardness as-quenched, HRC	62–65(a)	62–64(a)	62–65(a)	62–65(a)	60–62(a)	52–54	22–26	40–43	50–53	55–58
Core hardness (25 mm, or 1 in., diam round), HRC	15–21	15–21	33–35	20–25	35–37	45–50	22–26	40–43	50–53	55–58
Manufacturing factors										
Availability	2	1	2	2	2	3	2	1	1	1
Cost	1	1	2	1	1	1	2	2	2	2
Machinability	7	7	5	7	6	8	5	4	4	4
Quenching medium	O	O	A,O	O, W	O	O	O	O, A	O	O,A
Hardening temperature, °C (°F)	830–845(a) (1525–1550)	800–830(a) (1475–1525)	885–925(a) (1625–1700)	845–870(a) (1550–1600)	790–815(a) (1450–1500)	815–870 (1500–1600)	870–900 (1600–1650)	955–1010 (1750–1850)	980–1040 (1800–1900)	1010–1065 (1850–1950)
Dimensional change on hardening	M	M	M	M	M	M	M	M	M	M
Safety on hardening	M	M	M	M	M	M	H	H	M	M
Susceptibility to decarburization	M	M	M	M	M	M	L	M	M	M
Approximately hardness as-rolled or forged, HB	200	200	350	230	280	310	...	400	500	550
Annealed hardness, HB	103–123	109–137	116–135	103–123	180–207	150–180	248–269	150–180	160–202	187–228
Annealing temperature, °C (°F)	730–815 (1350–1500)	730–815 (1350–1500)	870–900 (1600–1650)	845–870 (1550–1600)	675–695 (1250–1280)	760–790 (1400–1450)	870–900 (1600–1650)	790–845 (1450–1550)	845–900 (1550–1650)	845–900 (1550–1650)
Tempering range, °C (°F)	150–260 (300–500)	150–260 (300–500)	150–260 (300–500)	150–260 (300–500)	150–230 (300–450)	150–260 (300–500)	580–540 (900–1000)	260–425 (500–800)	150–425 (300–800)	150–425 (300–800)
Forging temperature, °C (°F)	1010–1120 (1850–2050)	1010–1120 (1850–2050)	1010–1120 (1850–2050)	1010–1120 (1850–2050)	1065–1175 (1950–2150)	1010–1120 (1850–2050)	...	1120–1175 (2050–2150)	1095–1205 (2000–2200)	1095–1150 (2000–2100)

Note: Ratings are explained in Chapter 2. (a) After carburizing

steel is usually hardened by oil quenching, and surface hardness may be as high as 65 HRC.

The P5 grade contains chromium as the major alloying element and has high hubbability and core strength, as related to good hardenability, equivalent to that of the P3 grade. It can be hardened by quenching in oil or water and may attain surface hardness of 65 HRC after carburizing and hardening. Type P6 mold steel contains nominally 3.5% Ni and cannot be readily annealed to hardness below 180 HB. As shown in Fig. 15-1, P6 steel has low hubbability and thus is frequently used for machine-cut cavities. However, hardenability is good, and P6 steel molds develop core strength superior to all other carburizing grades of mold steel except P4. Figure 15-4 shows end-quench hardenability for P6 steel at various carbon levels (Ref 10). Hardness goes through a maximum with increasing carbon content. The reduced hardness at carbon levels above 0.60% is due to increasing amounts of retained austenite as carbon content increases. Figure 15-5 shows typical core properties of P6 steel as a function of tempering temperature, and Fig. 15-6 shows the effect of carbon content on as-quenched core properties after a simulated carburizing treatment (Ref 11).

Type P4 mold steel is the deepest-hardening grade of low-carbon mold steel, by virtue of its high chromium and molybdenum contents, and can be hardened by oil quenching or air cooling. The oil quench results in a minimum of scale, and the air cool results in a minimum of distortion. With carbon and chromium on the low side of the range, an annealed hardness of 95 HB is possible for P4 steel (Ref 12). Typical compositions of P4 can be annealed to hardness as low as 125 HB. As a result, P4 hubbability is comparable to or exceeds that of P3 mold steel. Although P4 steel is readily machined in the annealed condition, machinability can be improved by first air cooling from 870 to 885 °C (1600 to 1625 °F).

After case hardening, type P4 mold steels are the most wear resistant and least susceptible to softening on tempering of all the low-carbon mold steels. Figure 15-7 shows the effect of tempering on case hardness of carburized P4 steel in comparison to the hardness of a plain carbon tool steel. The effect of tempering on the case and core hardness of P4 steels is shown in Fig. 15-8. Maintaining somewhat lower surface carbon content, as was the case for carburizing in cast iron chips, results in a case which has been found to be effective for die cavities in molds

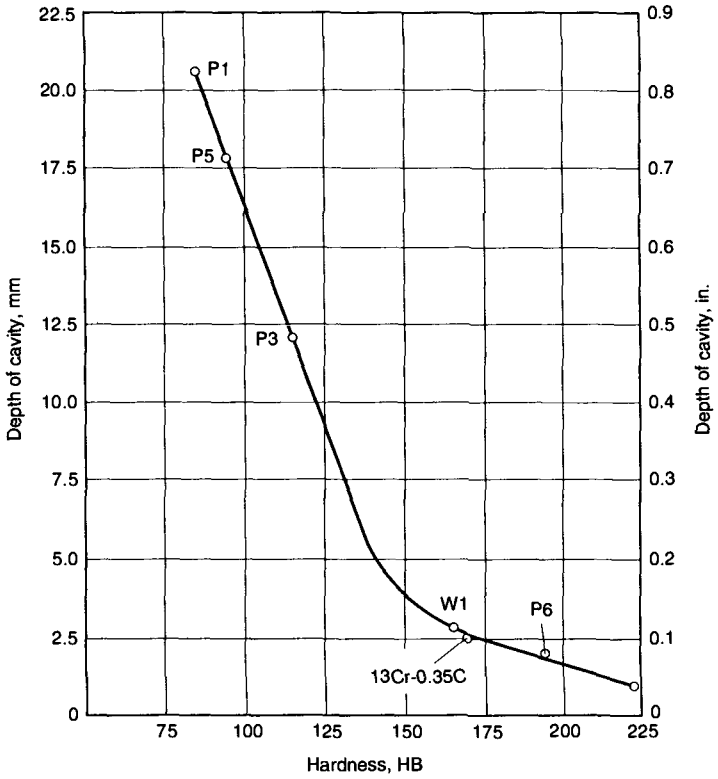

Fig. 15-1 Depth of hubbed cavity as a function of annealed hardness. Note the rapid increase in depth of hubbed cavity at hardnesses below 150 HB. Data from Ref 5 and 6

used in die casting of low-melting alloys. Table 15-3 presents the core mechanical properties of P4 steel air cooled from 955 °C (1750 °F) and tempered at 425 °C (800 °F) (Ref 13, 14).

Machined Cavity Grades

Type P20 mold steel is a medium-hardenability grade that is normally oil quenched. Figures 15-9 and 15-10 show, respectively, Jominy end-quench curves and an IT diagram for P20 steel. For die casting of low-melting alloys, P20 is often machined in the heat-treated condition at about 300 HB and placed in service without subsequent hardening and tempering. For plastic molding applications, P20 is frequently carburized. As-quenched surface hardness of carburized molds may be as high as 65 HRC, but the resistance to softening of the carburized surface during tempering is relatively low, comparable to that of plain carbon steel. Figure 15-11 shows the effect of tempering temperature on the surface hardness of P20 steel pack carburized for 2 h at two temperatures. Lull (Ref 15) has studied the effect of heat treatment, particularly carburizing temperature, on the polishability of P20 steel and found that carburizing temperatures in

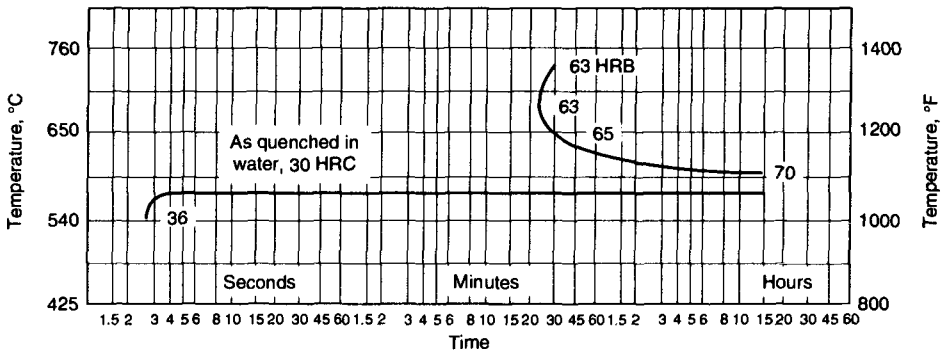

Fig. 15-2 IT diagram for P2 steel. This diagram characterizes transformation in the unhardened core of molds made from P2 steel. Courtesy of Crucible Steel Co.

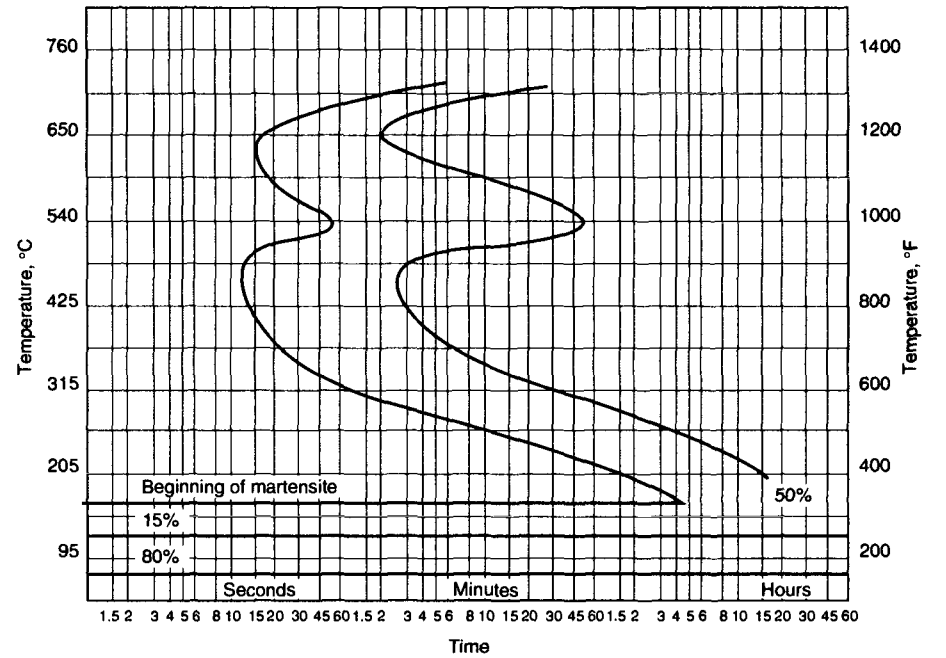

Fig. 15-3 IT diagram for carburized case of P2 steel. Courtesy of Crucible Steel Co.

excess of 870 °C(1600 °F) are detrimental to good polishability. The effect of carburizing temperature on surface hardness and case depth of P20 steel is shown in Table 15-4, and mechanical properties of a P20 steel after a typical heat treatment are given in Table 15-5.

Type P21 mold steel is alloyed with nickel and aluminum and is hardened by the precipitation of a nickel-aluminum intermetallic compound. Blanks are solution treated by slow cooling to 705 to 730 °C (1300 to 1350 °F) and holding at temperature for times between 60 and 180 min, depending on section size. Preheating should not be performed. Cooling from the solution temperature can be done in air or in oil to accelerate cooling. After solution treatment, hardness is in the range of 24 to 28 HRC, and mold cavities can be readily machined. After machining, final hardening to aged hardness between 30 and 40 HRC is accomplished by heating between 510 and 550 °C (950 and 1020 °F) for 20 h for small sections and up to 24 h for large sections. The P21 mold steel cannot be carburized but can be nitrided. Nitriding for 20 to 24 h at 510 to 525 °C (950 to 975 °F) produces case depths between 0.152 and 0.203 mm (0.006 and 0.008 in.) with a surface hardness equivalent to 70 HRC. Table 15-6 lists mechanical properties of P21 steel in the solution-treated and aged conditions, and Table 15-7 shows the effect of aging temperature on specimens aged between 20 and 24 h.

Table 15-3 Core mechanical properties of P4 mold steel air cooled from 955 °C (1750 °F) and tempered at 425 °C (800 °F)

Property	Value
Tensile strength, MPa (ksi)	1289 (187)
Yield strength, MPa (ksi)	1034 (150)
Elongation in 50 mm (2 in.), %	15
Reduction of area, %	53
CVN impact, J (ft·lbf)	43 (32)
Hardness, HB	390

Corrosion-Resistant Mold Steels

Although not included in the AISI classification of tool steels, the hardenable martensitic stainless steels have long been used for mold applications that require high corrosion resistance. Table 15-1 presents the nominal compositions of three corrosion-resistant mold steels described in the 4th Edition of *Tool Steels* (Ref 1). These steels fall into the category of steels designated as mold steels for machined cavities. More recent references describing the need for corrosion-resistant mold steels were introduced earlier in this chapter (Ref 2–4). Hardenability and performance of the corrosion-resistant mold steels are a function of carbon and chromium content. The steel with 13Cr and 0.12C is an oil-hardening grade of medium hardenability, and effectively equivalent to an AISI 420 martensitic stainless steel. An IT diagram for this type of steel is shown in Fig. 15-12. The diffusion-controlled transformations are quite sluggish, and small sections can be hardened

Table 15-4 Effect of carburizing temperature on case depth and surface hardness for P20 mold steel(a)

Carburizing temperature		Surface hardness,	Case depth	
°C	°F	HRC	mm	in.
845	1550	65.6	0.36	0.014
870	1600	64.2	0.43	0.017
900	1650	62.5	0.41	0.016
925	1700	59.2	0.51	0.020
955	1750	58.6	0.56	0.022
980	1800	58.6	0.71	0.028

(a) Specimens were 25 mm (1 in.) cubes, held 2 h at temperature in carburizing compound and quenched in oil. Courtesy of Teledyne VASCO

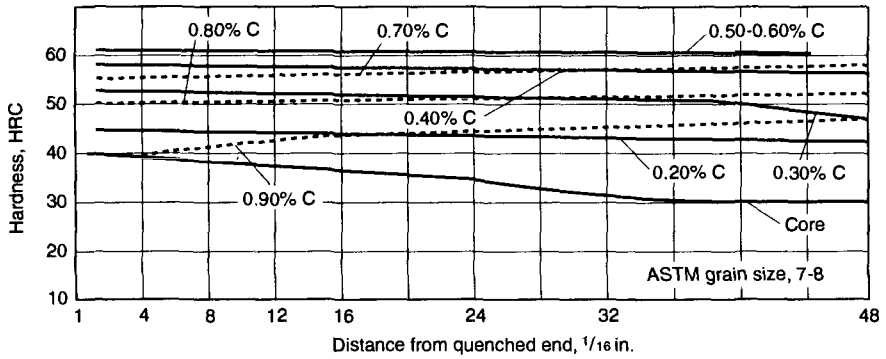

Fig. 15-4 Hardness of type P6 mold steel along end-quench hardenability bar at various case-depth levels corresponding to various carbon contents. Hardness at high carbon contents decreases with increasing carbon content because of increasing amounts of retained austenite. Source: Ref 10

by air cooling. Figure 15-13 shows mechanical properties as a function of tempering temperature for a 13Cr-0.12C mold steel. Tensile strength as high as 1400 MPa (200 ksi) can be attained, and a toughness minimum develops after tempering between 425 and 540 °C (800 and 1000 °F).

The corrosion-resistant mold steel with 13% Cr and 0.35% C has slightly less corrosion resistance than that of the 0.12% C steel but better wear resistance. The IT diagram of the 13Cr-0.35C steel (Fig. 15-14) indicates lower hardenability for this steel compared to that of the 13Cr-0.12C steel (Fig. 15-12). The higher carbon content, however, makes possible higher tensile strengths and hardness than can be attained in the lower carbon steels (Fig. 15-15).

The corrosion-resistant 17Cr-0.65C mold steel is similar in composition to an AISI 440A martensitic stainless steel and is the most wear resistant of the martensitic types of stainless mold steels. Figure 15-16 shows an IT diagram for a 17Cr-0.65C mold steel, and hardness as a function of tempering tem-

Table 15-5 Mechanical properties of P20 mold steel after oil quenching from 845 °C (1550 °F) and tempering 2 h at 205 °C (400 °F)

Property	Value
Tensile strength, MPa (ksi)	1310 (190)
Yield strength, MPa (ksi)	1172 (170)
Elongation in 50 mm (2 in.), %	13
Reduction of area, %	51
Hardness, HRC	36–38

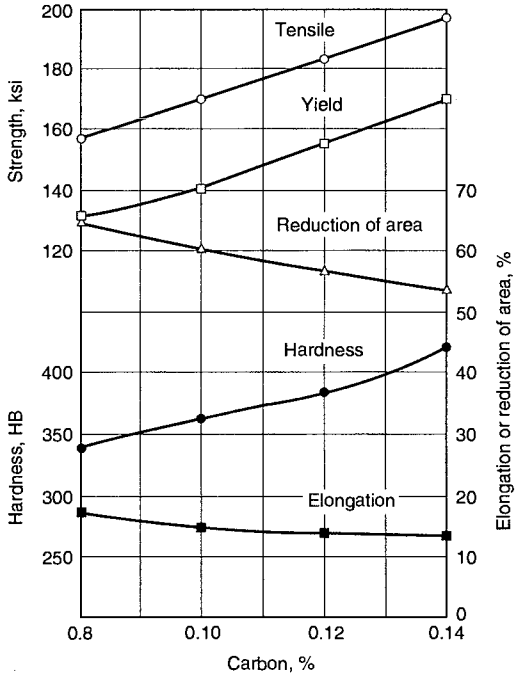

Fig. 15-6 Core mechanical properties of P6 mold steel as a function of carbon content. Specimens were oil quenched from 900 to 925 °C (1650 to 1700 °F). Source: Ref 11

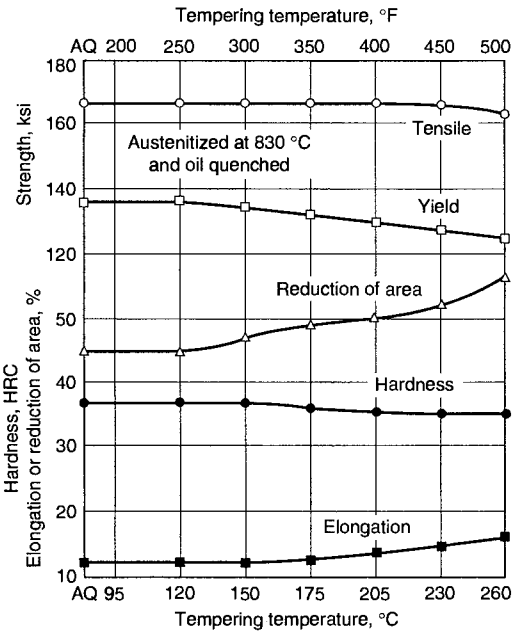

Fig. 15-5 Core mechanical properties of carburized P6 mold steel as a function of tempering temperature. AQ, as quenched. Source: Ref 11

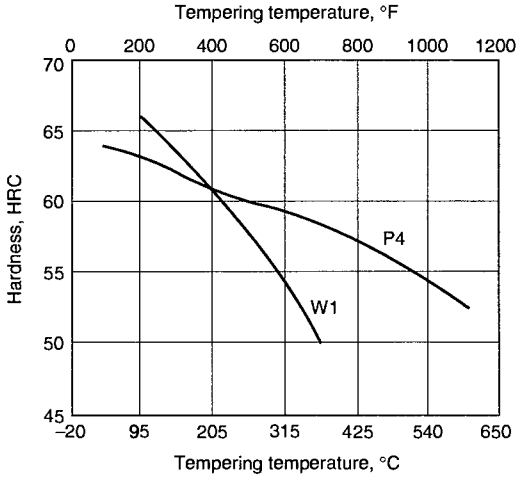

Fig. 15-7 Comparison of the effect of tempering temperature on carburized surface hardness of P4 steel and W1 carbon tool steel. The P4 steel was carburized at 925 °C (1700 °F) for 8 h and oil quenched. Courtesy of Uddeholm Co.

Table 15-6 Mechanical properties of P21 mold steel

Condition	Tensile strength MPa	Tensile strength ksi	Yield strength (0.2% offset) MPa	Yield strength (0.2% offset) ksi	Elongation in 50 mm (2 in.), %	Reduction of area, %	Hardness HRC	Hardness HB
Solution treated	862	125	586	85	24	59	26 max	262 max
Aged	1234	179	1138	165	16	40	36–39	341–375

Table 15-7 Effect of aging temperature on hardness of P21 mold steel

Aging temperature °C	Aging temperature °F	Hardness, HRC
510	950	38–41
525	975	36–39
540	1000	34–38
550	1025	29–34
565	1050	27–32

(a) Aging time, 20 to 24 h

perature is shown in Fig. 15-17. For a high-carbon, high-chromium mold steel specimen quenched from 1040 °C (1900 °F) and tempered at 150 °C (300 °F), the ultimate tensile strength is 1827 MPa (265 ksi), but ductility is low, with an elongation of 3.7% in a gage length of 50 mm (2 in.) and a reduction of area of 11.5%.

Forging, Annealing, and Stress Relieving

Table 15-2 lists forging temperatures for the various mold steels. No special precautions are necessary. It is desirable to slow cool oil- and air-hardening grades after forging, either in a furnace or an insulating medium such as lime or ashes. The annealing temperatures given in Table 15-2 are for full annealing; after cooling slowly from these temperatures, optimum machinability or hubbability should result. For a machine-cut mold, it is often advantageous to stress relieve prior to final finishing in order to minimize dimensional changes on hardening. Similarly, hubbed molds may require several intermediate stress-relief treatments before the cavity has been sunk to the desired depth. Recommended stress-relief temperatures increase with alloy content. P3 and P6 steels should be stress relieved at temperatures between 675 and 695 °C (1250 and 1280 °F); P2, P5, and P20 steels between 705 and 730 °C (1300 and 1350 °F); and P4 and the stainless mold steels between 745 and 775 °C (1375 and 1425 °F).

Carburizing, Hardening, and Tempering

The molds made from low-carbon steels in which cavities are formed by hubbing are invariably carburized before hardening and tempering, and molds made from P20 steel, with its higher carbon content, are frequently carburized when used for plastic molding. It is extremely important that the surfaces of parts to be carburized be as clean as possible, because foreign matter on surfaces may lead to nonuniform carburizing, which in turn leads to polishing difficulties. Carburizing is a well-established heat-treating technology and can be accomplished by gas carburizing, pack carburizing in solid carbon-containing compounds, liquid carburizing in salt baths, vacuum carburizing, and plasma or ion carburizing (Ref 16). Carburizing temperatures range from 870 to 925 °C (1600 to 1700 °F), with carburizing times ranging between 2 and 24 h depending on the desired case depth.

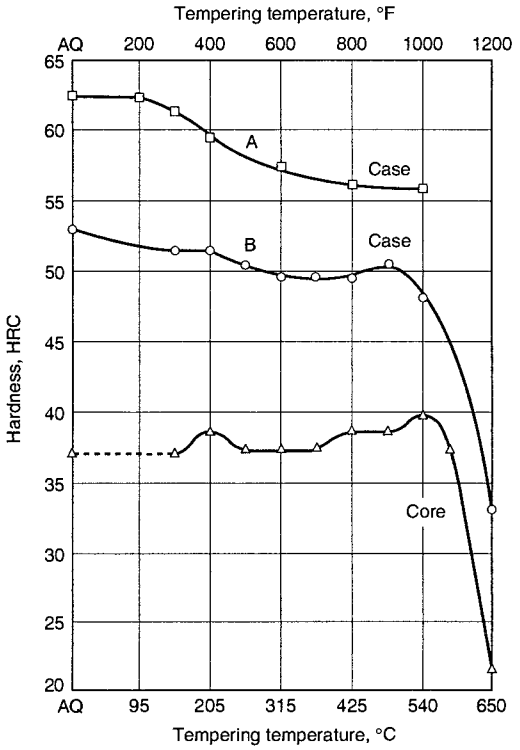

Fig. 15-8 Case and core hardness of P4 steel as a function of tempering temperature. Curves A and B are from specimens pack carburized in charcoal and cast iron chips, respectively. Courtesy of Carpenter Steel Co.

Austenitizing temperatures for hardening mold steels and the usual tempering temperature ranges are shown in Table 15-2. All the low-carbon hubbing grades and P20 are typically cooled in air or in the pack after carburizing and are therefore reheated for hardening. Reheating for hardening at temperatures below A_{cm} produces a dispersion of small carbide particles and a fine austenite grain size. This structure then transforms on quenching to a fine martensitic microstructure of high hardness and low susceptibility to intergranular cracking (Ref 17). The carbide particles retained on austenitizing are incorporated into the martensitic structure, and the retained austenite content of reheated and hardened case microstructures is low. Mold steels with higher hardenability, such as P4, can be hardened by air cooling directly after carburizing, but the retained austenite content may be high and the hardened microstructure will be susceptible to intergranular cracking (Ref 17, 18). The retained austenite content can be reduced by refrigeration at subzero temperatures, but reheating, as noted above, may more effectively lower retained austenite and increase hardness.

Austenitizing, quenching, and solution treating of type P21 mold steel are usually done by the tool steel manufacturer. Therefore, the only heat treat-

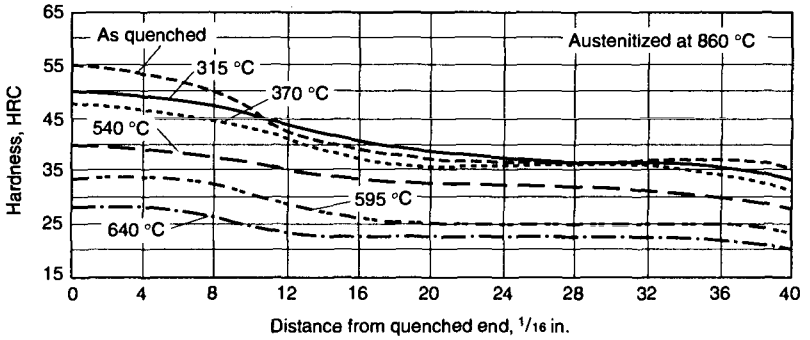

Fig. 15-9 Jominy end-quench hardenability curves for type P20 mold steel after quenching and tempering at indicated temperatures for 2 h. Courtesy of Teledyne VASCO

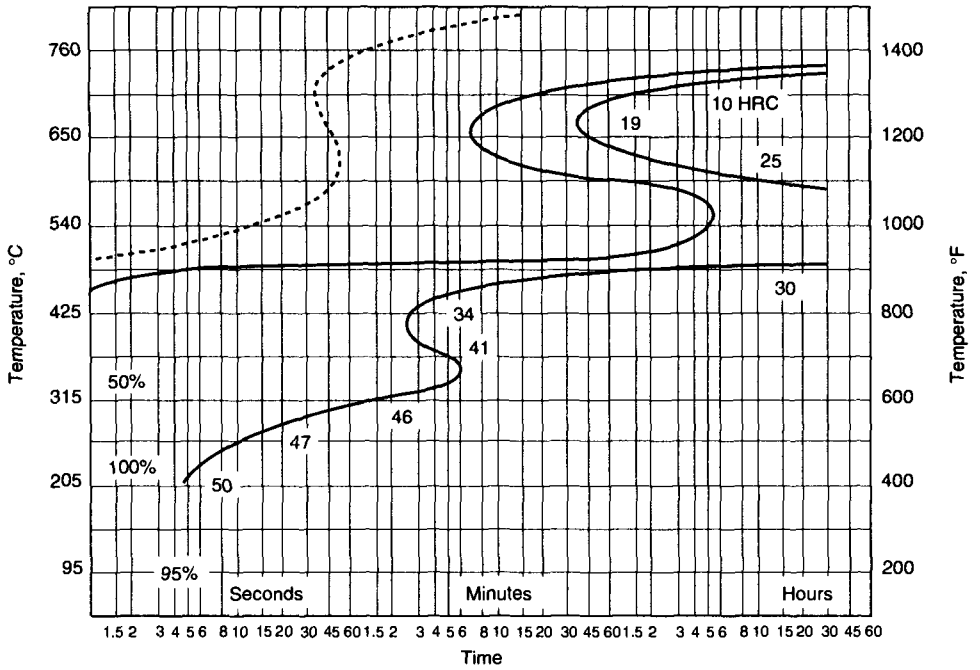

Fig. 15-10 IT diagram for type P20 mold steel. Austenitizing temperature was 845 °C (1550 °F). Courtesy of Crucible Steel Co.

ment required after machining is relatively low-temperature aging between 510 and 540 °C (950 to 1000 °F) for 20 to 24 h. No surface protection is necessary during the aging treatment. Type P21 can be simultaneously nitrided and aged in one operation. Once P21 steel is nitrided, it is very difficult to resoften or remove the nitrided case.

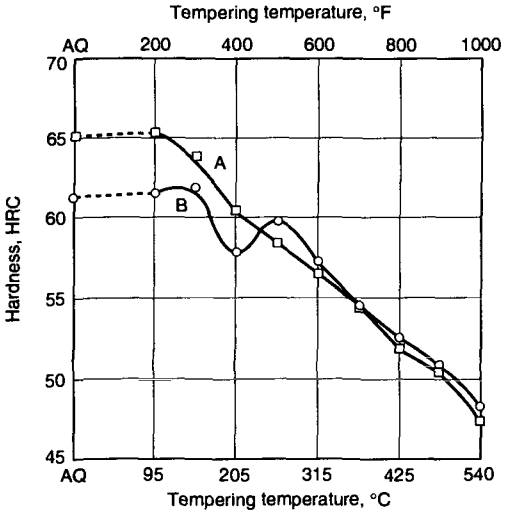

Fig. 15-11 Effect of tempering temperature on the surface hardness of carburized P20 steel. Curve A is for specimens carburized at 845 °C (1550 °F) and curve B is for specimens carburized at 900 °C (1650 °F). Courtesy of O.I. Lemmer, Teledyne VASCO

Tempering of mold steels requires no special precautions. For plastics molding, a surface hardness near 60 HRC is advantageous for polishability and wear resistance, while molds for die casting of low-melting alloys are operated satisfactorily at a hardness of about 50 HRC or lower. To ensure structural stability and hardness retention during operation, a tempering temperature close to maximum operating temperature of the mold is desirable, though not always mandatory. Tempering of the martensitic stainless grades in the temperature range of 425 to 595 °C (800 to 1100 °F) should be avoided because of attendant embrittlement and loss of corrosion resistance after tempering in this range.

Selection and Applications of Mold Steels

Major applications for mold steels are for molds with cavities for plastics molding and die casting of

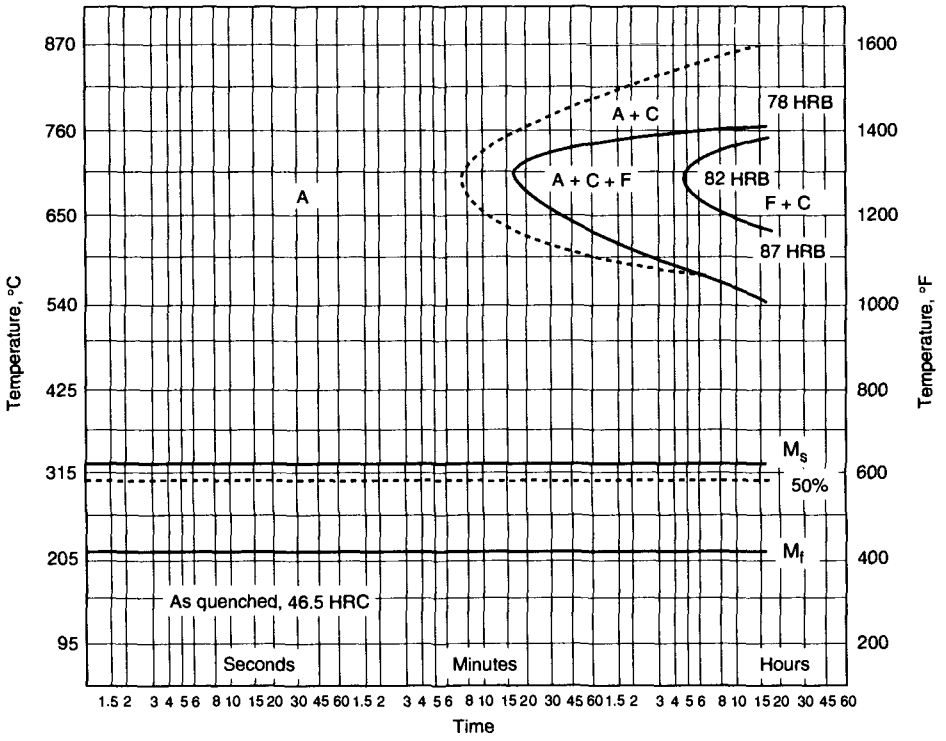

Fig. 15-12 IT diagram for a 13Cr-0.12C mold steel austenitized at 980 °C (1800 °F). Courtesy of Crucible Steel Co.

low-melting alloys such as tin, zinc, and lead alloys. Certain mold steels are used for backing plates, cavity plates, and spacer blocks. Type P20 is a convenient reference material for comparing mold steels. Tables 15-1 and 15-2 show that P20 is low in alloy content and yet has adequate hardenability for all except the largest cavities. P20 steel is hardened by oil quenching from a relatively low temperature, and dimensional changes on hardening are not as great as with water-hardening steel grades. It cannot be hubbed easily but is the most easily machined mold steel. P20 has sufficient wear resistance for intermediate-length production runs and can be carburized if greater wear resistance or surface hardness is required. It is suitable for either molding plastic or die casting of low-melting alloys. Higher alloy modifications of P20, with higher hardenability and wear resistance, have been used in the past (Ref 1), but these grades are no longer listed in the AISI classification system.

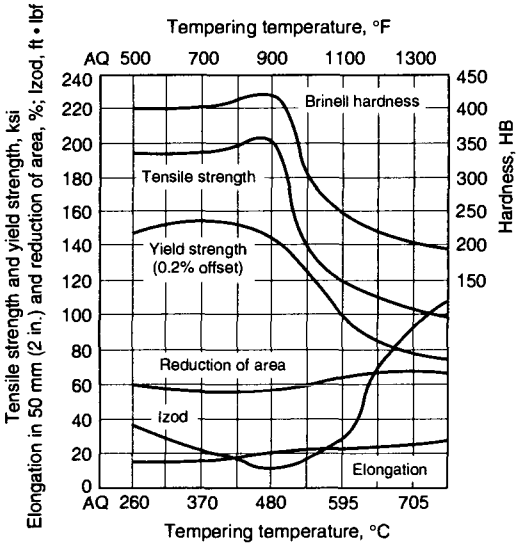

Fig. 15-13 Mechanical properties of a hardened 13Cr-0.12C mold steel as a function of tempering temperature. Specimens were quenched in oil from 980 °C (1800 °F) and tempered for 3 h at the various tempering temperatures. Courtesy of Crucible Steel Co.

Type P21 mold steel can develop a maximum hardness of 40 HRC and has wear resistance and toughness comparable to that of P20 steel heat treated to the same hardness. Although P21 steel is less easily machined than P20, it requires no surface protection during its unique low-temperature aging treatment.

If toughness greater than that of type P20 is desirable with a minimum sacrifice in strength, as in large dies subject to severe shock, then mold steels P4 and P6 should be considered. Type P6 steel has better machinability than P4.

Although chromium plating can be used to prevent corrosion of mold surfaces, it is often more

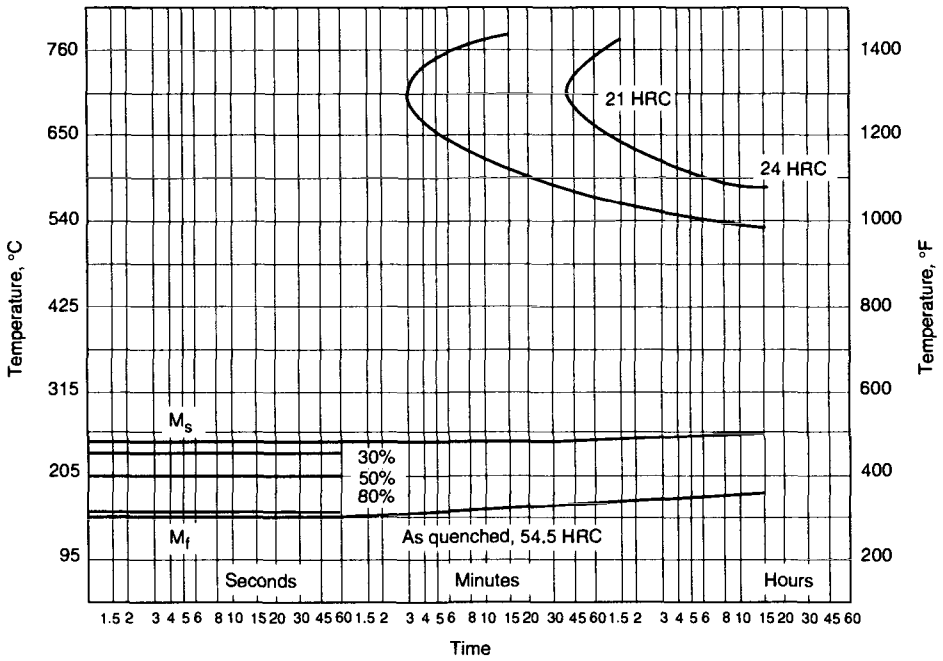

Fig. 15-14 IT diagram for a 13Cr-0.35C mold steel. Courtesy of Crucible Steel Co.

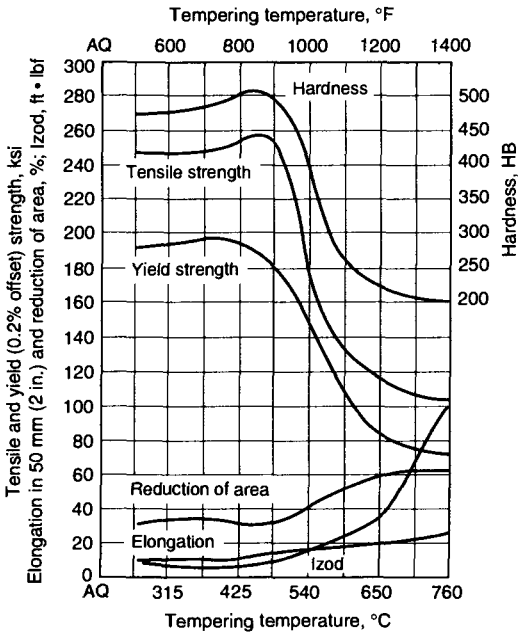

Fig. 15-15 Mechanical properties of hardened 13Cr-0.35C mold steel as a function of temperature. Specimens were oil quenched from 1010 °C (1850 °F) and tempered for 5 h at the various tempering temperatures. Courtesy of Crucible Steel Co.

desirable to make the entire mold from corrosion-resisting steel. This eliminates the possibility of spalling of the plating and the rounding off of sharp corners that occurs on plating. The martensitic stainless steels are all suitable for molding of highly corrosive plastics, such as the urea and vinyl types, and will resist the rusting associated with high-humidity atmospheric conditions. The 13Cr-0.12C grade is at least equivalent to P20 in wear resistance and toughness, but cannot be treated to a hardness much above 43 HRC. The martensitic stainless steels must be quenched and tempered to develop corrosion resistance, but embrittlement and loss of corrosion resistance occurs on tempering between 425 and 595 °C (800 and 1100 °F) and limits the hardness levels that can be produced by tempering. The 17Cr-0.65C grade is the most wear resistant of the corrosion-resisting types, equaled only by P4 in the carburized condition, but has the lowest toughness of any of the mold steels. The martensitic stainless steel grades, in addition to being widely used in plastics molding, are used for the demanding manufacture of molds for many glass products, including glass screens for television sets and computers (Ref 19). Glass manufacture requires high wear resistance, resistance to scaling, high-temperature strength, and high polishability.

To aid in the selection of mold steels, Table 15-8 ranks the various mold steels with respect to prop-

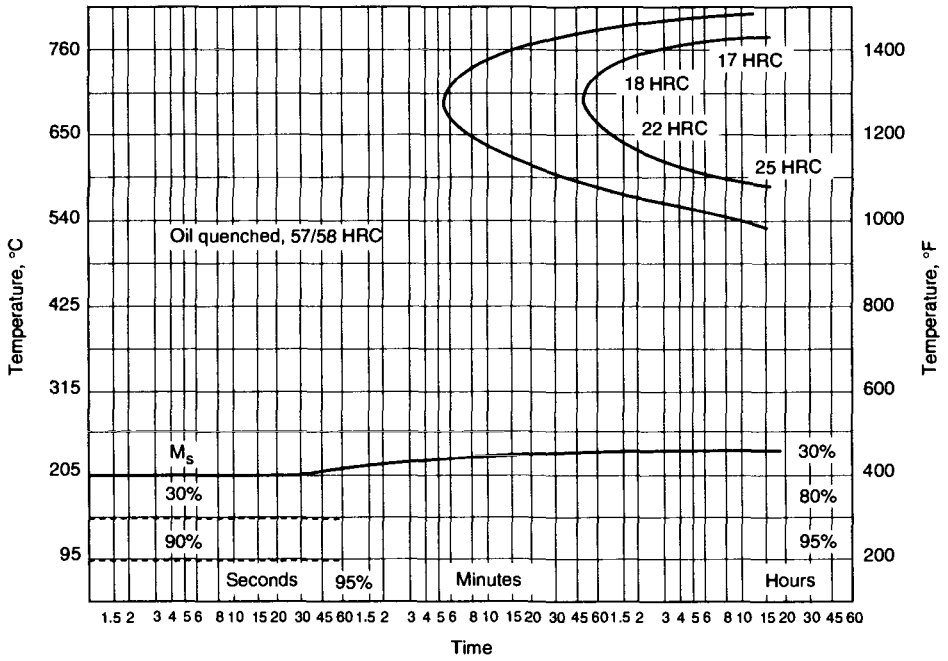

Fig. 15-16 IT diagram for a 17Cr-0.65C mold steel. Specimens were austenitized at 1040 °C (1900 °F). Courtesy of Crucible Steel Co.

erties related to mold manufacture and performance. This table includes and supplements the data of Table 15-2 by incorporating factors such as hubbability and corrosion resistance. Steels with equivalent properties are grouped, and the groups are arranged in order of decreasing property value. For example, P4 in the carburized condition and the 17Cr- 0.65C stainless have equivalent wear resistance and the highest wear resistance of all the alloys.

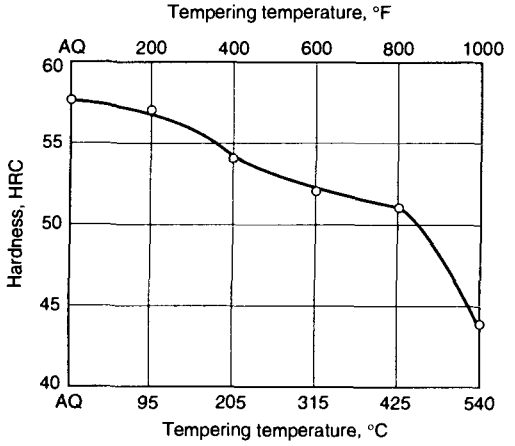

Fig. 15-17 Hardness as a function of tempering temperature for a 17Cr-0.65C mold steel oil quenched from 1040 °C (1900 °F). Courtesy of Crucible Steel Co.

An example of the use of Table 15-8 follows. Assume that a mold made of uncarburized P20 steel, a steel in which cavities must be machined, has suffered considerable wear in the compression molding of a highly abrasive plastic, and as a consequence, out-of-tolerance parts are produced long before the required number of parts has been manufactured. As replacement steel, P21 with equivalent wear resistance can be eliminated from consideration. Types P3 and P2 in the carburized condition have higher wear resistance, but lower core strength, and in an application with high compression would not be suitable. Carburized P20 and P6 steels would be good solutions to the wear problem. However, on the basis of machinability, the P6 steel ranks lower than the P20, and this consideration might be the deciding factor.

REFERENCES

1. G.A. Roberts and R.A. Cary, *Tool Steels,* 4th ed., American Society for Metals, 1980, p 449
2. D.W. Lundy, Manufacture of Stainless Steel Plastic Molds, *Tool Materials for Molds and Dies,* G. Krauss and H. Nordberg, Ed., Colorado School of Mines Press, 1987, p 244–248
3. O. Sandberg and W. Roberts, Relation between Properties of Tool Steels and Mold/Die Performance, *Tool Materials for Molds and Dies,* G. Krauss and H. Nordberg, Ed., Colorado School of Mines Press, 1987, p 263–286
4. H. Jan, J. Sammer, M. Gstettner, K. Leban, and I. Jung, Bohler M340—A New Development in

Table 15-8 Properties and ranking of mold steels

Wear resistance	Toughness	Hot hardness	Machinability	Hubbability	Core strength	Corrosion resistance
5 P4(a), 17Cr-0.65C	9 P2, P3, P4, P5, P6	6 13Cr-0.35C, 17Cr-0.65C	8 P20	7 P2, P5	6 13Cr-0.35C, 17Cr-0.65C	High: 13Cr-0.12C, 13Cr-0.35C, 17Cr-0.65C
4 P5(a), P6(a)		5 P4(a), 13Cr-0.12C	7 P2, P3, P5	6 P3	5 P20	
3 P2(a), P3(a), P20(a), 13Cr-0.35C	8 P20, P21, 13Cr-0.12C	4 P6(a), P21	6 P6	5 P4	4 P21, 13Cr-0.12C	Low: All others
	6 13Cr-0.35C	3 P5(a)	5 P4, P21	4 P20, 13Cr-0.12C	3 P4, P6	
2 13Cr-0.12C	5 17Cr-0.65C	2 P2(a), P3(a), P20	4 13Cr-0.12C, 13Cr-0.35C, 17Cr-0.65C	3 13Cr-0.35C	2 P2, P3, P5	
1 P20, P21				2 P6, 17Cr-0.65C		
				1 P21		

Note: This table is so arranged as to aid in material selection. Under each tabular heading, steels having equivalent ratings as to a particular property are grouped and the groups are arranged in decreasing order of that property; for example, types P4 and 17Cr-0.65C are equivalent in wear resistance and have the highest wear resistance.(a) After carburizing

the Field of Corrosion Resistant Plastic Mold Steels, *Progress in Tool Steels,* H. Berns, H.-F. Hinz, and I.-M. Hucklenbroich, Ed., Schurmann and Klagges KG, Bochum, Germany, 1996, p 297–306

5. I. Thomas and E. Spitzig, When and How to Hob, *Mod. Plast.,* Vol 32, 1955, p 117
6. G.E. Brumbach, A High Strength Die Steel That Can Be Cold Hobbed, *Machinery,* Nov 1951, p 154
7. F. Halward, Flow Test of Hubbing Steel, *Met. Prog.,* Vol 59 (No. 3), 1959, p 356
8. A.L. Pranses, Better Steel Devised for Hubbing, *Am. Mach.,* July 1948, p 84
9. R.W. Brown, Two Steels Make Our Plastic Molds, *Am. Mach.,* January 1951, p 112
10. F.X. Kayser, R.F. Thomson, and A.L. Boegehold, An End-Quench Test for Determining the Hardenability of Carburized Steels, *Trans. ASM,* Vol 45, 1953, p 1056
11. *Alloy Digest,* Engineering Alloy Digest, Inc.
12. Data sheets, Uddeholm Co.
13. Properties of Steels Commonly Used for Plastic Molds, *Mat. Methods,* March 1950, p 81
14. High Strength, High Temperature Die Steel for Cold Hobbing, *Tool. Prod.,* Feb 1952, p 192
15. E.E. Lull, The Effect of Heat Treatment on the Polishability of Mold Steels, *J. Soc. Plast. Eng.,* Vol 12 (No. 4), 1956
16. *Heat Treating,* Vol 4, *ASM Handbook,* ASM International, 1991, p 312–375
17. G. Krauss, *Steels: Heat Treatment and Processing Principles,* ASM International, 1990, p 291–305
18. C.A. Apple and G. Krauss, Microcracking and Fatigue in a Carburized Steel, *Metall. Trans.,* Vol 4, 1973, p 1195–1200
19. R. Breitler and J. Mayerhofer, Superclean Tool Steel for TV-Panel Production, *Progress in Tool Steels,* H. Berns, H.-F. Hinz, and I.-M. Hucklenbroich, Ed., Schurmann and Klagges Publishers, Bochum, Germany, 1996, p 287–296

Tool Steels: 5th Edition
George Roberts, George Krauss, Richard Kennedy, p 305-323
DOI:10.1361/toos1998p305

Copyright © 1998 ASM International®
All rights reserved.
www.asminternational.org

CHAPTER 16
Surface Modification of Tool Steel

Tool steels are subjected to severe wear, high stresses, elevated temperatures, and corrosive environments. By virtue of alloy content, thermomechanical processing, and heat treatment, tool steels are designed to withstand such destructive forces not only at the tool/workpiece interface, but also to a considerable depth below that interface. Subsurface strength is imparted by through-hardening and is the reason for the great concern with hardenability or depth of hardening during the final hardening heat treatments of the various tool steels. Despite the high uniform hardness and strength profiles of hardened tool steels, tool surface and near-surface regions are subjected to the most destructive forces, and, almost from the beginning of the widespread application of tool steels, ways to improve surface properties have been evaluated. For example, some of the first technical papers regarding the nitriding of high-speed tool steels were published in the 1930s, and pack carburizing has long been used to maintain surface carbon contents of high-carbon tool steels during heat treatment (Ref 1).

Today many additional surface modification technologies are available to improve the performance of tool steels. Figure 16-1 shows a variety of currently available surface modification techniques and compares the depth to which structure and properties are modified by the various processes (Ref 2). Four classes of processes are identified: implantation, plating and coating, thermochemical, and thermal. Implantation changes surface chemistry, similar to the other thermochemical techniques, but because of unique processing and the associated very shallow hardened surface layers, implantation is often considered a separate class of surface treatment. Plating, especially the chemical vapor deposition (CVD) and physical vapor deposition (PVD) processes of great importance to tool steels, deposits thin layers or coatings of hard materials, such as nitrides or carbides, on substrates. Other than the coating, little change in surface chemistry is produced. Thermochemical treatments, such as nitriding and carburizing, cause significant changes in surface chemistry by the diffusion of atoms such as nitrogen or carbon into a steel substrate. Thermal treatments cause no change in surface chemistry, but do cause localized surface heating and thereby make possible surface hardening by austenite formation on heating and subsequent transformation to martensite on cooling.

The surface modification treatments shown in Fig. 16-1 are applied by many processes. Some of the treatments, such as the carburizing and nitriding thermochemical treatments and induction and flame thermal treatments, are well established and continue to benefit from advances in equipment and instrumentation. However, many of the techniques shown are of much more recent application to tool and other steels. The newer surface modification technologies applied to steels incorporate high-energy beams, plasmas, magnetic and electrical fields, and vacuum systems (Ref 3–6), and many of these techniques were first developed and applied for thin-film and circuit manufacture in electronic applications (Ref 7).

The large number of surface modification techniques now available and the range of surface properties that can be produced for engineering components have led to the interdisciplinary activity of surface engineering, defined (Ref 2) as:

> Surface engineering involves the application of traditional and innovative surface technologies to engineering components and materials in order to produce a composite material with properties unattainable in either the base or surface material. Frequently, the various surface technologies are applied to existing designs of engineering components but, ideally surface engineering involves the design of the component with a knowledge of the surface treatment to be employed.

With respect to selection of surface treatment, coating thickness, as noted in Fig. 16-1, is a critical design parameter. Some coatings—for example,

those produced by PVD and CVD processes—are quite thin but provide excellent surface wear resistance and lower friction at tool/workpiece interfaces. However, applications subjected to high bending or contact stresses require deeper case depths, as provided, for example, by thermochemical or thermal surface modification techniques. The alloy and processing design of tool steels provides high through-hardened strength and hardness; therefore, tool steels do not benefit from the traditional thermochemical and thermal techniques to the same extent as surface-hardened low-carbon and medium-carbon steels which have lower through-hardened strengths. Thus, with the exception of the low-carbon P-type mold steels, as described in Chapter 15, tool steels are rarely carburized. However, the concept of composite design, where a ceramic layer is deposited on a steel substrate, has greatly expanded the performance of tool steels. Figure 16-2 shows hardness ranges achievable by various heat treatments and surface coating techniques and materials (Ref 8). Nitriding and various oxide, boride, carbide, and nitride coatings provide substantially higher surface hardnesses compared to those of hardened steel substrates and provide a major driving force for surface modification of tool steels.

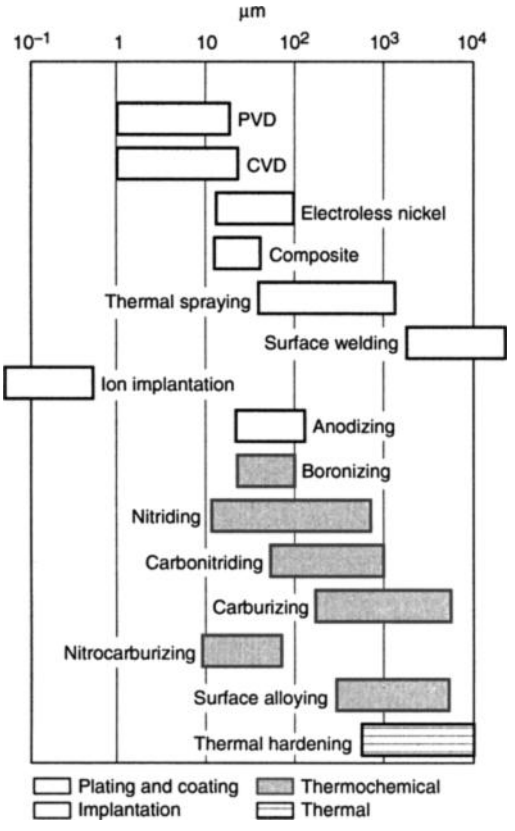

Fig. 16-1 Classification of surface modification processes and comparison of typical depths of surfaces modified by the various processes. Source: Ref 2

Oxide Coatings

Oxide coatings improve the performance of hot-work and high-speed tool steels. In the hot-work steels, an adherent black oxide scale forms during the course of heat treatment. This scale is very resistant to abrasion and helps to hold die lubricants. If the scale is removed by grinding or polishing after heat treatment, a die may be reheated in air to a temperature below the final tempering temperature to re-form the protective oxide scale.

Techniques such as exposure to steam at temperatures of about 565 °C (1050 °F), or heating in liquid sodium hydroxide/sodium nitrate salts for 5 to 20 min at 140 °C (285 °F), are used to produce hard oxide coatings on high-speed steel cutting tools (Ref 6). Black, oxidized layers less than 5 μm (0.2 mil) thick are produced on the surfaces of the tools by these treatments. These oxide layers are remarkably adherent under service conditions and result in significant increases in cutting tool performance and life, as shown in Tables 16-1 and 16-2.

Nitriding

Nitriding is a thermochemical surface treatment that introduces nitrogen into the surfaces of steels in the ferritic or tempered martensitic condition. Thus, in contrast to carburizing, which introduces carbon into austenite at high temperatures and therefore necessitates quenching to martensite with its atten-

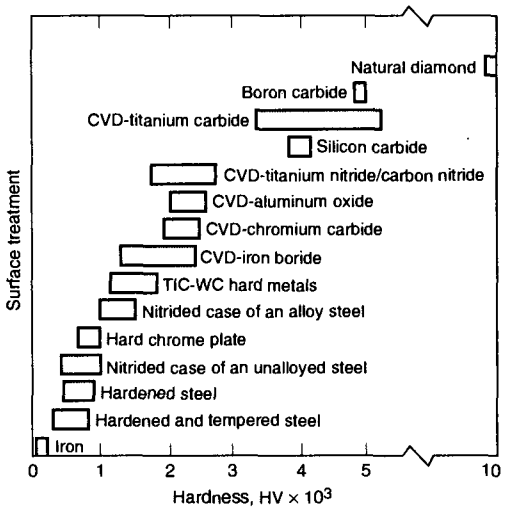

Fig. 16-2 Ranges of surface hardness produced by various surface modification treatments. Source: Ref 8

dant volume changes, nitriding is accomplished with very little distortion and dimensional change. Nitriding is commonly applied to medium-carbon steels containing strong nitride-forming elements such as chromium, aluminum, vanadium, tungsten, and molybdenum, which are also major components of tool steels. Therefore, tool steels—including H11, H12, and H13 hot-work steels; A2, A6, D2, D3, and S7 air-hardening steels; M2 and M4 high-speed steels; and P20 plastic mold steel—benefit from nitriding. The various tool steels are commonly nitrided by conventional gas nitriding (Ref 9, 10) and, more recently, by plasma or ion nitriding (Ref 11), as described later in this section.

Salt bath treatments are also used for the nitriding of tool steels, and often the composition of the molten salts used introduces carbon as well as nitrogen into the surface of workpieces (Ref 12, 13). These treatments thus are referred to as nitrocarburizing surface treatments (Fig. 16-1). The liquid nitriding treatments find especially wide use in the surface modification of low-carbon steel automotive components but are also applied to various types of tool steels, including high-speed steels (Ref 13, 14).

As nitrogen diffuses into a tool steel, it combines with alloying elements to form very fine nitride precipitate particles or zones consisting of atom layers of substitutional alloying elements and interstitial nitrogen atoms (Ref 15). The distributions of very fine, closely spaced nitride particles dispersed in tempered martensite produce very high hardness (>1000 HV, Fig. 16-2) compared to conventionally hardened and tempered steels. The alloy nitrides are also quite stable and resist coarsening to temperatures, generated by friction or operation, on the order of those typically used for nitriding, about 500 °C (930 °F). Therefore, nitriding produces excellent wear, galling, and seizing resistance during metal-to-metal contact. Figure 16-3 shows examples of the hardness gradients produced by gas nitriding H11, H12, and D2 tool steels for various times at 525 to 540 °C (975 to 1000 °F) (Ref 9). Increasing tool steel chromium content lowers the depth of hardening for a given nitriding time

Nitriding is most commonly performed by exposure to ammonia gas atmospheres at temperatures between 495 and 565 °C (925 and 1050 °F). The ammonia dissociates on the surface of the steel according to this reaction:

$$NH_3 = N + 3H \qquad \text{(Eq 16-1)}$$

and the resulting nitrogen atoms are adsorbed at the surface of the steel and diffuse into the tool interior. Because of the relatively low nitriding temperatures and the fact that the nitrogen combines with the alloying elements as it diffuses into the steel, nitriding times are quite long, ranging from 10 to 130 h depending on the steel and the application. Nitrided

Table 16-1 Machining tool life improvements due to steam oxidation

Tool	Application	Tool life	
		Before steam treating	After steam treating
M2 broachers	Cutting AISI 1010 latch	20 h per grind	70 h per grind
M2 drills	Drilling Bakelite plastic insulating blocks	10 holes	25 holes
	Phenolic terminal plates	1700 holes per grind	8500 holes per grind
	Drilling AISI 4030 steel 25 mm (1 in.) thick	17 holes	81 holes
M7 end mill tools	Cutting 8740 steel forgings	30 pieces	200 pieces
A6 hobs	Cutting teeth on AISI 3140 forged gear	...	62.2% increased life
M2 milling cutters	Two slots in 1020 steel	150 cuts per grind	306 cuts per grind
	Slotting 1020 steel bars	2000 per grind	7000 per grind
M2 saw blades	Cutting 75 mm (3 in.) rods, austenitic steel	100% endurance at 0.52 m/s (102 sfm)	120% endurance at 0.57 m/s (112 sfm)
M2 taps	Cutting SAE 52100 steel	1800 pieces	3000 pieces

Table 16-2 Effect of steam oxidation on tool life in forming various carbon steel nuts and bolts

M2 tool	Application (steel type)	Tool life	
		Before steam treating(a)	After steam treating(b)
4th station punch	Castle nut (1030)	21,000 nuts	42,000 nuts
4th station punch	Slotted insert nut (1030)	22,000 nuts	38,000 nuts
4th station punch	Castle nut (1030)	29,000 nuts	80,000 nuts
3rd station punch	Castle nut (1110)	20,000 nuts	35,000 nuts
4th station punch	Castle nut (1110)	15,000 nuts	35,000 nuts
Trim die	Bolt head (1335)	7,000 bolts	16,000 bolts

(a) Hardened and triple tempered. (b) Hardened, triple tempered, and steam treated

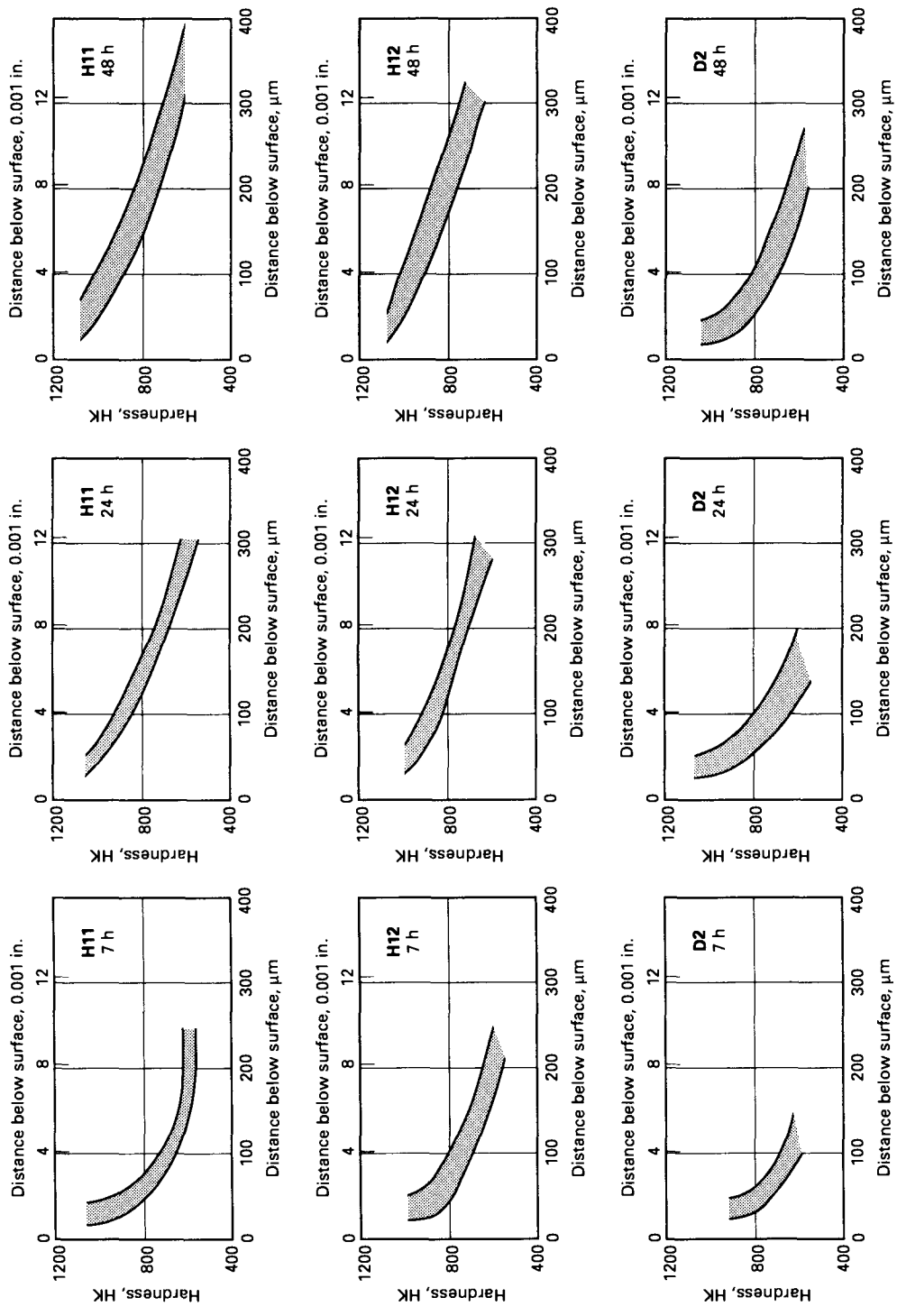

Fig 16-3 Hardness profiles for H11, H12, and D2 tool steels after nitriding at 525 °C (975 °F) for the times shown. Source: Ref 9

case depths are relatively shallow, usually less than 0.5 mm (0.02 in.), and typically on the order of 0.1 mm (0.004 in.). Prior to nitriding, hardened steels should be tempered above nitriding temperatures in order to produce a core structure that will not soften during long nitriding treatments. This requirement matches well with the relatively high secondary-hardening temperatures used for tempering many tool steels.

Plasma or ion nitriding is the most recent modification of nitriding applied to steels and has received considerable attention in the technical literature (Ref 16-19). Plasma nitriding is accomplished in vacuumtight, cold-wall chambers in which the workpiece is made cathodic (negative), and the chamber walls are anodic and grounded. Figure 16-4 shows a schematic diagram of an ion-nitriding system (Ref 5). First hydrogen, for heating and cleaning the workpiece surfaces, and then a mixture of hydrogen and nitrogen, for the nitriding stage, are added to the chamber. An applied direct-current (dc) potential across the workpiece and the chamber wall creates a plasma. The plasma consists of ions, electrons, and charged and neutral atoms and molecules and, in the voltage-current combinations used for ion nitriding, creates a uniform purple glow around the cathodic workpiece. The nitrogen atoms diffuse into the workpiece, which generally is heated to nitriding temperatures by the impact of the plasma-driven nitrogen ions and atoms, without the need for external heating. Newer system designs, however, may use external heat to reduce cycle times.

A major advantage of plasma nitriding is the enhanced mass transfer of high-energy nitrogen molecules and ions to steel surfaces under the action of an electric field. The penetration of the nitrogen atoms into the steel is, of course, still controlled by diffusion and nitride formation. Other advantages of ion nitriding in comparison to conventional gas nitriding include safety, lower temperatures of operation (as low as 375 °C, or 700 °F), reduced distortion, reduced gas consumption, reduced energy consumption in cold-wall furnaces, clean environmental operation (Ref 17), and good control of the brittle iron nitrides that sometimes form on the surface of nitrided parts (Ref 20).

Although improved wear and corrosion resistance are major benefits of the high surface hardness and surface compressive stresses produced by nitriding, toughness of tool surfaces is reduced (Ref 11). As a result, spalling or chipping of tools and dies may occur on nitrided edges in some applications. In such cases, reducing nitrided surface hardness and reducing case depth are recommended to improve performance (Ref 11).

Ion Implantation

Ion implantation is a surface modification process by which surface chemistry and properties are modified by ions forced into workpiece surfaces by very-high-energy beams (Ref 3, 21-23). Figure 16-1 indicates that ion implantation represents a unique

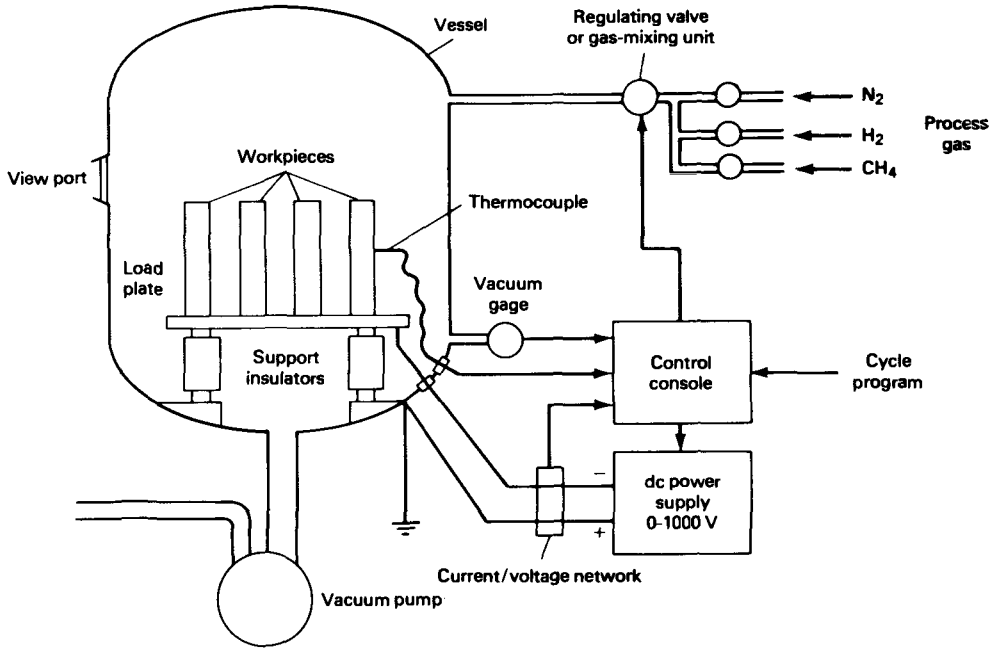

Fig. 16-4 Schematic of a typical ion-nitriding vessel. Source: Ref 19

class of treatments and that the depth of the affected surface zone is quite shallow. The ion beams are produced in a source or gun that ionizes gas molecules by electrons emitted from a source at an energy of about 100 to 200 eV (Ref 22). The ion beam is then focused and extracted from the source by an exit electrode. Figure 16-5 shows a schematic diagram of a typical ion source. Ion implantation is a line-of-sight process; that is, only areas directly exposed to the beam are implanted. For coverage of areas larger than the ion beam, the specimen must be translated or the ion beam rastered over the specimen surface.

The ion implantation process imparts high strength, high hardness, and residual compressive stresses into substrate surfaces by the lattice damage induced by the ion impact. Point defects, such as vacant lattice sites and ions and atoms forced into nonequilibrium interstitial sites, as shown schematically in Fig. 16-6, account for much of the structural change. The implantation is usually carried out close to room temperature; therefore, the case depth is largely determined by ion trajectories during impact rather than atomic diffusion. However, heat is generated by the ion bombardment, and some short-range diffusion and fine-scale precipitation may take place (Ref 22).

Any kind of ion can be implanted, but nitrogen is commonly implanted in steels to improve near-surface corrosion resistance and tribological properties. As noted above, the case depths produced by ion implantation are very shallow, on the order of 0.2 μm (0.008 mil) compared to nitrided case depths of typically 100 μm (4 mils). The low temperatures of ion implantation result in almost no distortion. Hoyle (Ref 13) reports that ion implantation of nitrogen into M2 steel thread-cutting dies for cast iron and gear cutting tools results in increased life, but that very little improvement in the life of high-speed steel drills results from ion implantation. Minimal improvements in life may be a result of the very thin case depths of ion-implanted surfaces and the softening of these layers by heat generated in applications such as cutting tools. Ion-implanted forming tools not subjected to significant heating may benefit significantly from enhanced surface properties induced by ion implantation. Several tool steel applications where ion implantation has improved wear resistance have been listed by Hirvonen (Ref 24), and improvements in wear resistance of hardened M2, D2, and 420 steels by nitrogen implantation have been described (Ref 25). Various tool steel parts and the benefits of ion implantation to the associated cutting and forming performance of those parts are described in Ref 10.

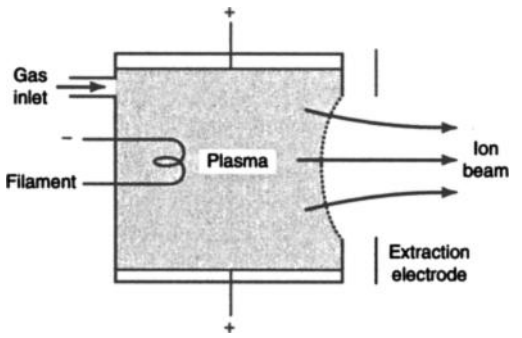

Fig. 16-5 Schematic of a typical ion source. Shown are an electron-emitting filament, anode, provision for gas input, and the ion extraction system. Source: Ref 22

Ion beam bombardment may be superimposed on other surface modification techniques. For example, a thin coating applied by a PVD technique, as described below, may be subjected to ion bombardment. In addition to the creation of point defects in the collision zone, the impact of the ion beam may cause displacement of some of the coating atoms into the substrate. This process is illustrated on a schematic atomic scale in Fig. 16-7, where simultaneous coating deposition by evaporation and ion bombardment are shown (Ref 22). The mixing of the coating and substrate atoms lends the term "ion beam mixing" to this process and results in excellent bonding and adhesion of the coating. When the ion beams are applied concurrently with the coating deposition technique, the combined processing is referred to as ion-assisted coating (IAC) or ion-beam-assisted deposition (IBAD) (Ref 22, 23). Middleton et al. (Ref 26) have recently evaluated the rolling contact fatigue behavior of M50 IBAD coated with titanium nitride and found increases in life and excellent adherence of the IBAD coatings.

Chemical and Physical Vapor Deposition Processing

Two quite different processing approaches are used to deposit the thin coatings or layers of ceramic compounds that provide dramatic improvements in wear resistance and life to hardened tool steel substrates. Physical vapor deposition physically generates and deposits atoms or molecules on substrates in high-vacuum environments. The atom flux that impinges on a substrate may be generated by a number of techniques, as described below. Chemical vapor deposition exposes substrates to gaseous reactants that chemically react to produce the desired surface coating products. Many of the terms used relative to PVD and CVD processing, as well as to other surface modification techniques, have been defined and illustrated in a recent publication (Ref 27).

The PVD processes are accomplished in high vacuums and the coating atoms travel relatively

large distances without collisions (Ref 28). As a result, the PVD processes are line-of-sight processes. The CVD processes are accomplished at atmospheric pressures and therefore have better throwing power, or the ability to uniformly coat complex shapes, than do the PVD processes. Physical vapor deposition processes for titanium nitride coatings are typically applied at substrate temperatures of about 500 °C (930 °F), whereas substrate temperatures in CVD processes are higher, typically about 1000 °C (1830 °F). Thus, tool steels coated by PVD processes need not be heat treated subsequent to deposition, whereas tool steels coated by CVD processes must be hardened after coating. Despite reheating, the hardening treatments applied to CVD TiN-coated D2 steel have been found to maintain homogeneous, defect-free coatings and residual surface compressive stresses of about –1000 MPa (–145 ksi) (Ref 29).

Coating atoms in PVD processes may be generated by evaporation, sputtering, or ion plating in vacuum environments. When gases such as nitrogen, methane, or oxygen are introduced into the vacuum chambers, the metal atoms react with the gas atoms to form nitrides, carbides, or oxides, and the PVD processes are referred to as reactive processes. Evaporation is accomplished by heating source materials in high vacuums (10^{-6} kPa, or 7.5 $\times$ 10^{-6} torr, or better) to cause the thermal evaporation of atoms or molecules that travel through the vacuum and deposit on a substrate surface (Ref 30). Deposition processes based solely on evaporation are being replaced by more efficient sputtering or ion-plating processes using glow discharge plasmas.

Sputtering is a PVD coating process in which atoms are ejected mechanically from a target by the impact of ions or energetic neutral atoms. Figure 16-8 shows schematically the mechanism of sputtering in a simple diode system (Ref 31). The chamber is initially evacuated, then backfilled with argon

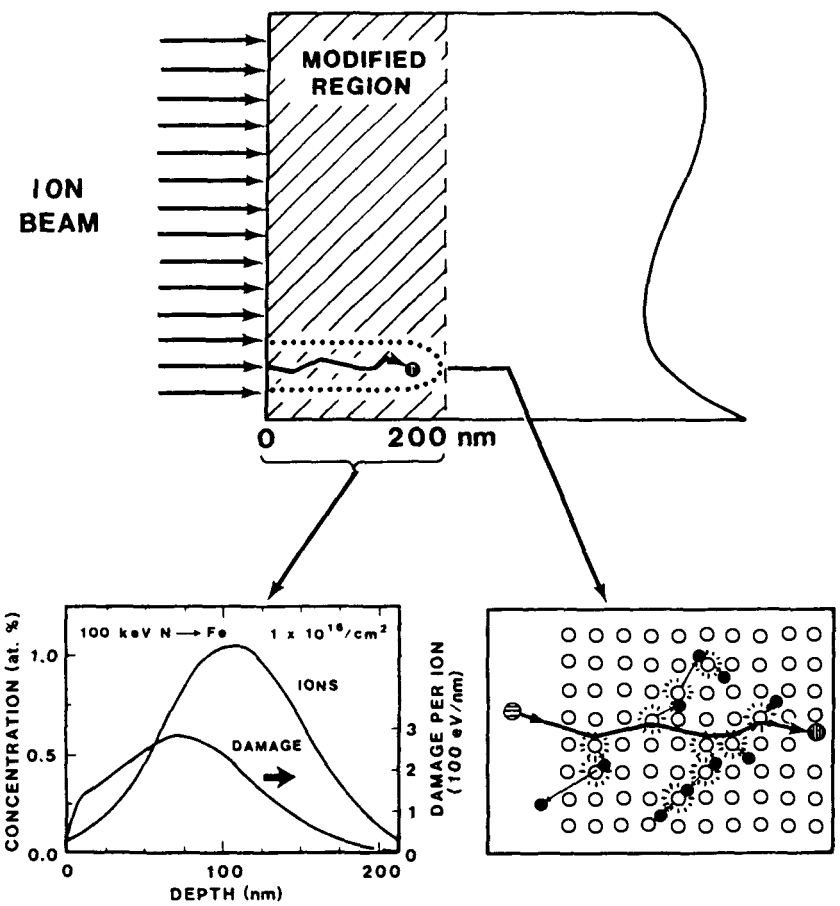

Fig. 16-6 Schematic of nitrogen atom implantation in iron (top), N and damage profiles (lower left), and defect generation (lower right). Source: Ref 3

gas, and the target is made cathodic or negative by the application of a dc potential between −500 and −5000 V. A low-pressure glow discharge plasma is produced around the target cathode, creating positively charged argon ions that are accelerated to the target. The momentum transfer due to the impact of the argon ions is sufficient to eject target atoms that travel to the substrate and other parts of the chamber. The mechanical transfer of atoms by sputtering is more readily controlled than transfer of atoms by thermal evaporation, and the sputtered atoms have higher energies (Ref 30).

Simple diode sputtering systems have relatively low rates of deposition. Thus, improved sputtering systems, with magnetic fields applied at the targets, have been developed. The resulting process is referred to as magnetron sputtering, shown schematically in Fig. 16-9 (Ref 31). The magnetic fields trap secondary electrons generated by the target and greatly increase ionization in the cathode plasma. Thus, more argon ions strike the target, and sputtering and deposition rates are significantly increased relative to diode sputtering. A more recent modification of magnetron sputtering is unbalanced magnetron sputtering (Ref 32). In this process (in contrast to conventional magnetron sputtering, where the magnetic field is closely restricted to the target), magnets are arranged to create a plasma that extends between the target and the substrate, with attendant benefits of ion bombardment at the substrate. As a result, unbalanced magnetron sputtering is capable of producing fully dense coatings on large, complex surfaces (Ref 32).

Ion plating, also referred to as plasma-assisted PVD or evaporative-source PVD, is a plasma-assisted deposition process in which the coating atoms are generated by thermal evaporation from an appropriate source (Ref 30, 33, 34). The sources may be electrically heated wire, arc, electron beam, or hollow cathode designs. The source is made the anode, and the substrate becomes the cathode by the application of a dc or radio-frequency (rf) voltage ranging between −500 and −5000 V. In the resulting substrate cathode glow discharge, atoms and ions are accelerated at high energies to the substrate coating. The bombardment of the substrate by the high-energy particles produces dense coatings with excellent adhesion, and the cathode glow discharge enhances substrate coverage. The diode ion plating systems have been further improved by designs which enhance ionization with ion currents that can be controlled independently of the bias voltage between the evaporative source and the substrate (Ref 31, 34). These modified PVD system designs are referred to as triode ion plating systems.

Chemical vapor deposition produces surface coatings by chemical reactions at the surfaces of heated substrates, as shown schematically in Fig. 16-10. Gaseous reactants are introduced into a reactor, which may be of cold-wall or hot-wall design, then chemically react at the surface of a heated substrate, deposit a solid coating, and create gaseous reaction products that are exhausted from the reactor (Ref 35). General equations for CVD carbide and nitride ceramic coatings deposited on tool steels are of the form (Ref 27):

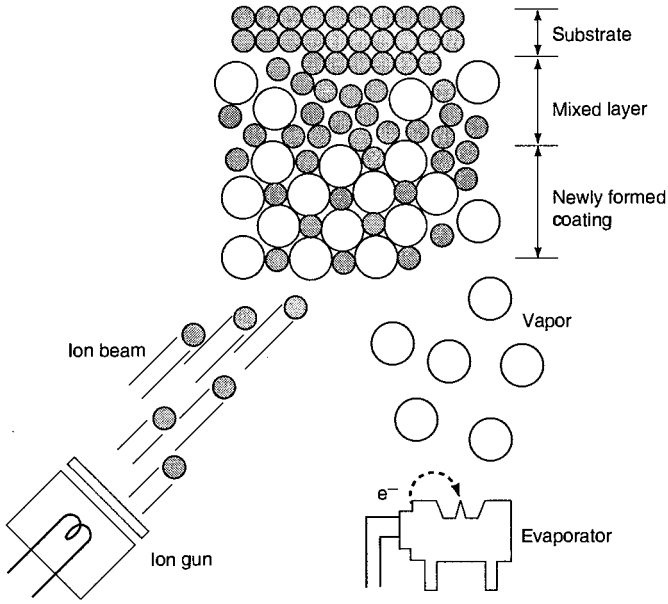

Fig. 16-7 Schematic of ion-beam-assisted deposition and mixing of ions and atoms in and below evaporation coating. Source: Ref 22

$$MCl_x + H_2 + 0.5N_2 = MN + xHCl \quad \text{(Eq 16-2)}$$

$$MCl_x + CH_4 = MC + xHCl \quad \text{(Eq 16-3)}$$

Specific reactions for TiN and TiC coatings include (Ref 35, 36):

$$TiCl_4 + CH_4 = TiC + 4HCl \quad \text{(Eq 16-4)}$$

$$TiCl_4 + \tfrac{1}{2}N_2 + 2H_2 = TiN + 4HCl \quad \text{(Eq 16-5)}$$

$$TiCl_4 + NH_3 + \tfrac{1}{2}H_2 = TiN + 4HCl \quad \text{(Eq 16-6)}$$

Often, for improved adhesion, TiN coatings on tool steels are combined with very thin undercoatings of titanium carbide or titanium carbonitride. The deposition temperatures for the CVD TiC and TiN coating reactions are relatively high, around 1000 °C (1830 °F). However, CVD deposition temperatures can be lowered if the CVD reactions are carried out in an environment of glow discharge plasmas maintained at the substrate/vapor interface (Ref 37). These processes are referred to as plasma-assisted chemical vapor deposition (PACVD) processes, and such techniques can lower substrate deposition temperatures to the range between 500 and 600 °C (930 and 1110 °F). The CVD and PACVD processes have also been used to deposit diamond and diamondlike coatings on substrates from gaseous mixtures of hydrogen and hydrocarbons, and these coatings show promise for improved performance in cutting tool applications (Ref 36, 37).

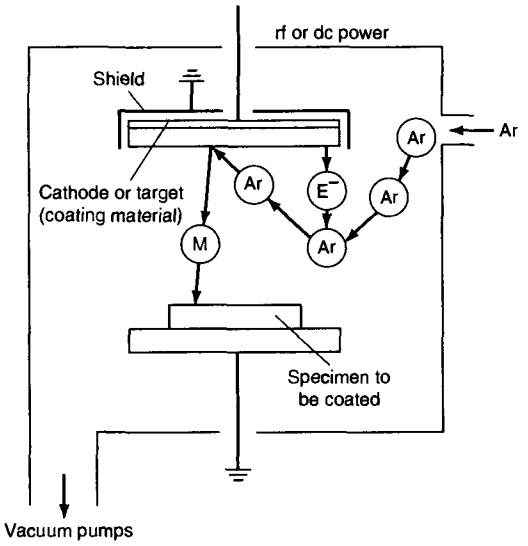

Fig. 16-8 Schematic of sputtering mechanisms. Source: Ref 31

CVD and PVD Coating Structure and Performance

The thin coatings produced on tool steels by CVD and PVD deposition processes tend to have very fine microstructures because of rapid cooling during deposition, but coating morphology, structure, and adhesion are quite sensitive to deposition parameters such as the energy of the incident atoms, substrate temperature, and sputtering gas pressures (Ref 30). The coatings are generated by nucleation and growth processes that first involve the adsorption of incident atoms, referred to as adatoms, on a substrate surface. The adatoms then diffuse on the substrate surface to preferred bonding sites such as ledges or vacancies or to growing clusters of atoms that become the nuclei of the crystals, which will grow to create the coating.

Three different coating growth mechanisms, as reviewed by Rigsbee (Ref 30), have been identified:

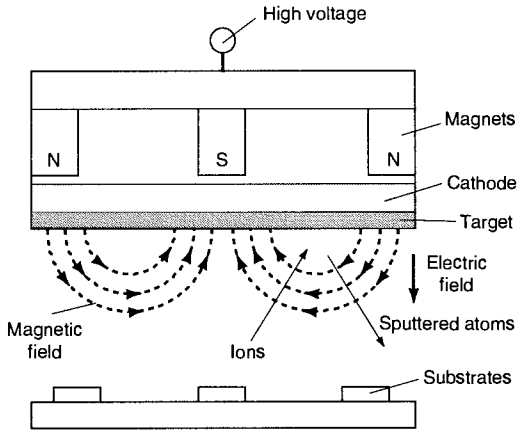

Fig. 16-9 Schematic of magnetron sputtering. Source: Ref 31

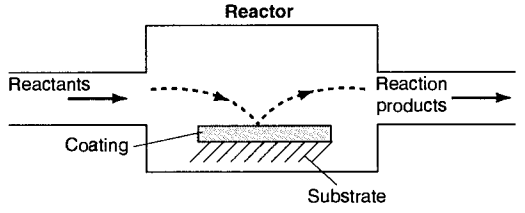

Fig. 16-10 Schematic of CVD deposition processes in a cold-wall reactor. Source: Ref 35

(1) three-dimensional island or Volmer-Weber growth, (2) two-dimensional layer-by-layer or Frank-van der Merwe growth, and (3) initial layer-by-layer growth followed by island growth. The latter mixed-mode growth is referred to as Stranski-Krastanov growth. The first mode consists of the formation of clusters, the growth of individual islandlike clusters to critical size, and the eventual impingement of the islands to produce a continuous film. Layer growth is typical of systems where adatoms have high surface mobility and bind more strongly to substrate atoms than with each other to form clusters. The mixed-mode growth may be due to initial epitaxial layer growth, which is terminated at some point by the buildup of residual stresses that produce defect sites for island nucleation and growth.

Figures 16-11 and 16-12 show schematic diagrams of coating microstructures and morphologies that may develop as a function of substrate temperature and argon pressure during sputtering. Figure 16-11 was developed for evaporated coatings by Movchan and Demchishin (Ref 38) for evaporated coatings, and Fig. 16-12 was developed for sputtered coatings by Thornton (Ref 39, 40). The Thornton diagram subdivides the zone 1 structures formed at low substrate temperatures into two zones, zone 1′ and zone T, to account for variations induced by sputtering.

Zone 1 coating morphologies are porous and consist of conical arrays of crystallites that taper from narrow nucleating clusters to broader, dome-shaped crystals with increasing film thickness. The rounded surfaces of these tapered crystals produce relatively rough coating surfaces. The tapered morphology is a result of low adatom surface diffusivity at low substrate temperatures (Ref 30, 41). Few nuclei develop as a result of the low surface diffusivity. Those nuclei, which do grow effectively, shield or shadow intervening areas from incident atoms; consequently, a high degree of porosity is incorporated between the growing tapered crystallites. In addition, there is accumulating evidence that the tapered zone microstructures contain a very high density of atomic scale microvoids and that sputtering produces a more imperfect fine structure than does thermal evaporation (Ref 41). As shown in Fig. 16-12, higher argon pressures shift the boundaries of zone 1 to higher substrate temperatures. This shift is due to increased vapor scattering of incident sputtered atoms, a process that effectively reduces adatom energy and therefore adatom surface mobility.

Zone T microstructures are transition microstructures formed at higher substrate temperatures. The coatings are denser and the coating surfaces are smoother than zone 1′ microstructures because of increased adatom surface diffusion at higher substrate temperatures. These transition microstructures are still very fine and are characterized by columnar crystal growth. Increased substrate surface diffusion and bulk diffusion in coatings are reflected in the coatings that form in zone 2, where coarser columnar crystals nucleate and grow, and in zone 3, where coarse columnar and even equiaxed crystals may grow. Crystal perfection increases with deposition at increasing substrate temperatures. Figures 16-13 and 16-14 show examples of tapered crystal morphology and columnar crystal morphology, respectively, in PVD coatings deposited by reactive triode ion plating (Ref 42-44).

Many high-speed tool steels for cutting and machining and tool steels for hot and cold working are coated with CVD and PVD coatings such as TiN. Examples of the improvements in tool life attainable by TiN coating of cutting tools are shown in Table 16-3 (Ref 10). Matthews (Ref 33) has reviewed many of the commercial PVD processes used to apply TiN coatings and also has documented the dramatic improvements in performance that are possible with application of the coatings. Coatings produced by the various processes range in thickness from less than 1 μm (0.04 mil) to 6 μm (0.24 mil) and give the tools a uniform gold color. Deposition temperatures are 500 °C (930 °F) or lower.

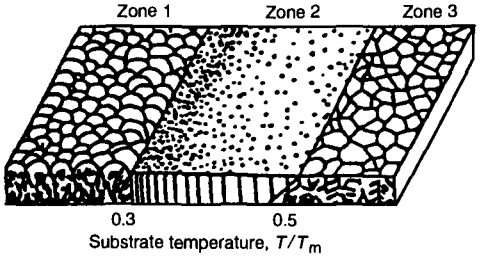

Fig. 16-11 Schematic of structural zones in PVD coatings as a function of substrate temperature as proposed by Movchan and Demchishin. Source: Ref 38

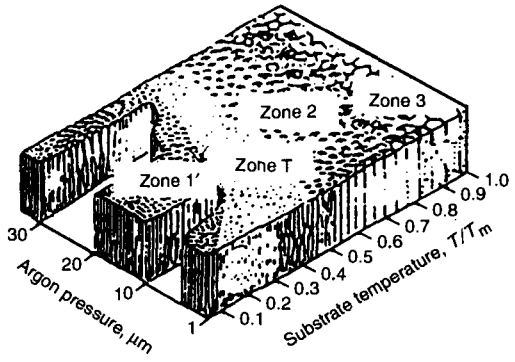

Fig. 16-12 Schematic of structural zones in PVD coatings as a function of substrate temperature and argon pressure in sputtering as proposed by Thornton. Source: Ref 39, 40

The hardness of the coatings for TiN are typically around 2500 HV but are a function of coating composition (Ref 42). Coatings applied at low substrate temperatures, which produce dense microstructures, develop high compressive residual stresses, and under certain conditions, stresses high enough to cause plastic deformation and cracking of the coating may develop (Ref 40, 41).

Table 16-4 presents the results of residual stresses and hardness measurements of PVD TiN and Ti(C,N) coatings applied to two high-speed steels by ion plating (Ref 45). The ASP 30 steel is the equivalent of an M4 high-speed steel, and the ASP 60 steel contains 2.28% C and higher amounts of molybdenum, vanadium, and cobalt than the ASP 30 steel. The residual stresses in all the coatings are compressive, and the hardness and residual stresses in the Ti(C,N) coatings are substantially higher than those in the TiN coatings. The higher hardness of the Ti(C,N) coatings has been found to correlate with enhanced life, compared to TiN-coated steels, in forming operations (Ref 46). In another study, the changes in hardness and compressive residual stresses as a function of temperature were measured in TiN coatings deposited on an austenitic stainless steel substrate (Ref 47). Both the hardness and re-

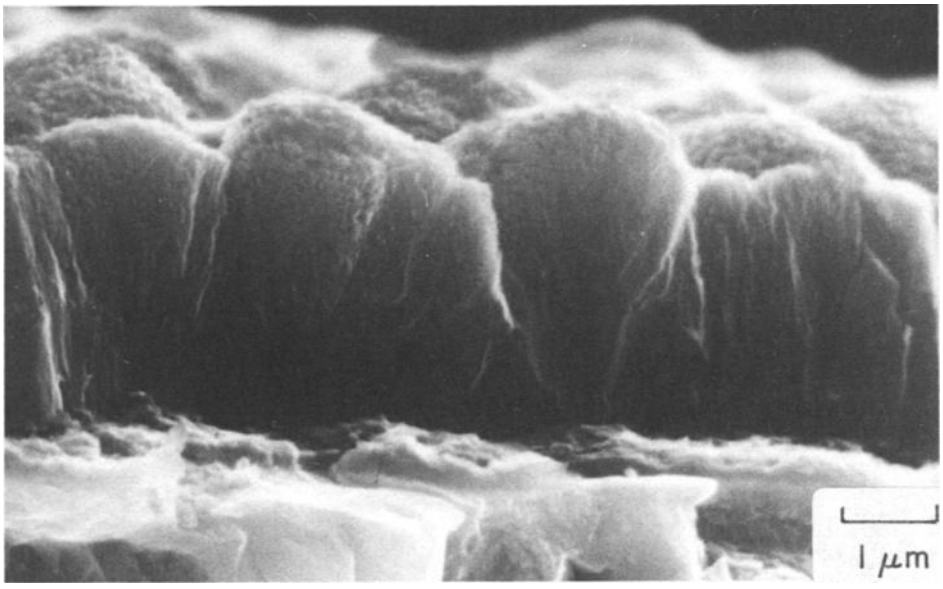

Fig. 16-13 $(Ti_{33}Al_{17})N$ deposited by triode ion plating at low substrate current density. Courtesy of A.S. Korhonen, Helsinki University of Technology

Table 16-3 Increased tool life attained with PVD coated cutting tools

Cutting tool				Workpieces machined before resharpening	
Type	High-speed tool steel	Coating	Workpiece material	Uncoated	Coated
End mill	M7	TiN	1022 steel, 35 HRC	325	1,200
End mill	M7	TiN	6061-T6 Al alloy	166	1,500
End mill	M3	TiN	7075T Al alloy	9	53
Gear hob	M2	TiN	8620 steel	40	80
Broach insert	M3	TiN	Type 303 stainless steel	100,000	300,000
Broach	M2	TiN	48% Ni alloy	200	3,400
Broach	M2	TiN	Type 410 stainless steel	10,000–12,000	31,000
Pipe tap	M2	TiN	Gray iron	3,000	9,000
Tap	M2	TiN	1050 steel, 30–33 HRC	60–70	750–800
Form tool	T15	TiC	1045 steel	5,000	23,000
Form tool	T15	TiN	Type 303 stainless steel	1,840	5,890
Cutoff tool	M2	TiC-TiN	Low-carbon steel	150	1,000
Drill	M7	TiN	Low-carbon steel	1,000	4,000
Drill	M7	TiN	Titanium alloy 662 layered with D6AC tool steel, 48–50 HRC	9	86

sidual stresses decreased with increasing temperature, and on cooling to room temperature did not return to the starting values, a result discussed in terms of microstructural changes induced by heating.

Characterization of the properties of very thin CVD and PVD coatings requires the application of special experimental techniques. Nix (Ref 48) has reviewed some of the recently developed techniques to evaluate the residual stresses, deformation, and fracture of electronic thin films. Techniques such as laser scanning to measure residual stresses, and micron and microbeam deflection techniques to measure elastic and plastic properties, are described. Similarly, Saunders (Ref 49) has reviewed measurement methods used to characterize the properties of thin coatings deposited on tool steels and other materials. The measurement of composition, fracture strains, adhesion, and mechanical properties by means of mechanical property microprobes or nanoindenters are described.

Coating adhesion correlates with performance and, for hard coatings, adhesion is frequently measured by scratch tests. Bull and Rickerby (Ref 50) describe the application of scratch testing to TiN coatings on steel substrates and identify five types of coating failure: gross spallation, buckling, chipping, conformal cracking, and tensile cracking. Deformation and fracture mechanisms of TiN coatings on M2 tool steel by hardness indentation and scratch testing have been described by Ma and Bloyce (Ref 51).

Salt Bath Coating

Hard alloy carbide, nitride, and carbonitride coatings can be applied to steels by means of salt bath processing. One such technique, the TD process (Toyota diffusion coating process), uses molten borax with additions of carbide-forming elements,

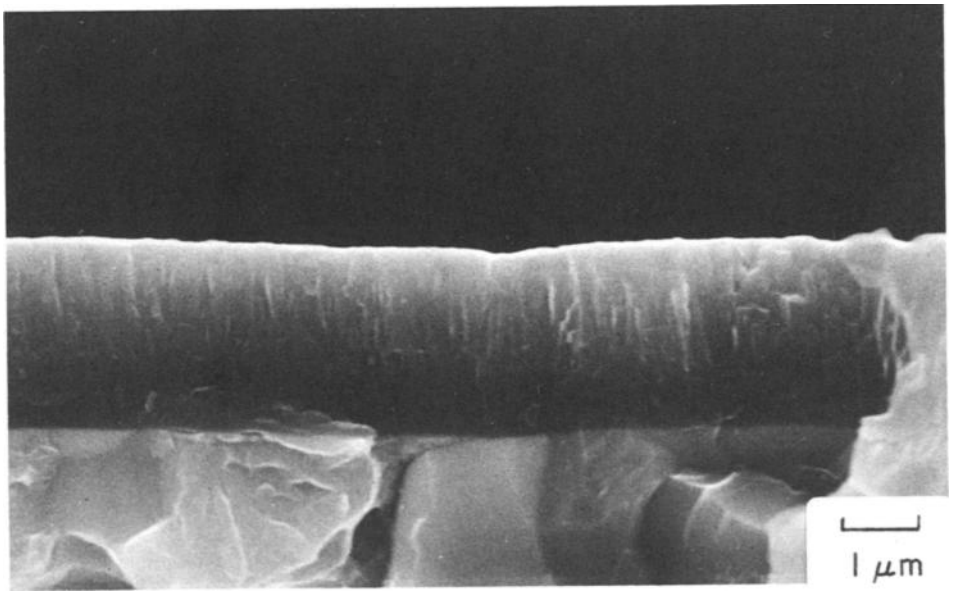

Fig. 16-14 (Ti_1Al) coating deposited by triode ion plating at high substrate current density. Courtesy of A.S. Korhonen, Helsinki University of Technology

Table 16-4 Characterization of PVD TiN and Ti(C,N) coatings on tool steels
See text for details.

Substrate	Coating	Residual stress, GN/M^2	Coating thickness, μm	Coating hardness, HV	Substrate hardness, HV	Composite hardness, HV (50 gf)
ASP 30	TiN	−3.2 ± 1.2	3.9 ± 0.3	2300 ± 300	920 ± 20	1950 ± 300
ASP 60	TiN	−2.4 ± 1.0	4.2 ± 0.2	2500 ± 200	940 ± 30	2250 ± 100
ASP 30	Ti(C, N)	−20.0 ± 8.2	3.8 ± 0.3	3000 ± 200	920 ± 20	2700 ± 100
ASP 60	Ti(C, N)	−17.0 ± 7.6	4.3 ± 0.4	3300 ± 400	940 ± 30	3000 ± 100

Source: Ref 45

such as vanadium, niobium, titanium, or chromium (Ref 52–54). The carbide-forming elements combine with carbon from the substrate steel to produce alloy carbide layers or coatings similar to those produced by PVD and CVD techniques. However, the growth of the layers depends on carbon diffusion, and the process requires relatively high temperatures, ranging between 800 and 1250 °C (1470 and 2280 °F), to maintain adequate rates of coating growth. Carbide coating thicknesses of 4 to 7 μm (0.16 to 0.28 mil) are produced in times ranging from 10 min to 8 h, depending on bath temperature, bath composition, and type of steel. The coated steels may be cooled and reheated for hardening, or the bath temperature may be selected to correspond to the steel austenitizing temperature, permitting the steel to be quenched directly after coating.

In order to lower salt bath deposition temperatures, techniques to produce alloy carbonitride layers have been developed (Ref 54). Such coatings are produced on hardened and nitrided steels in vanadium- or chromium-containing chloride baths at temperatures between 550 and 600 °C (1020 and 1110 °F). The nitrided surface contributes nitrogen to the coating, and carbide growth is negligible at the relatively low processing temperatures.

Coating hardnesses greater than 3000 HV have been reported for VC and NbC layers produced by salt bath processing. Thus, applications similar to those for which PVD and CVD coatings are used also are suitable for hard salt-bath coatings. In particular, the TD coatings have significantly increased the life of mold and die steels for sheet metal stamping, aluminum die casting, cold forging, and extrusion.

Laser and Electron Beam Surface Modification

Laser and electron beams provide very-high-energy, directed sources of heat and are used for many types of surface modification. As shown in Fig. 16-15, depending on power input, high-energy laser beams can be used for a variety of applications, including cutting, welding, surface melting and alloying, and localized surface hardening (Ref 3, 55–58). Welding and cutting technologies are highly developed and have followed the continuous development of high-energy density power sources (Ref 55, 56). Of the laser and electron beam surface modification techniques, localized surface hardening is the most widely developed and applied.

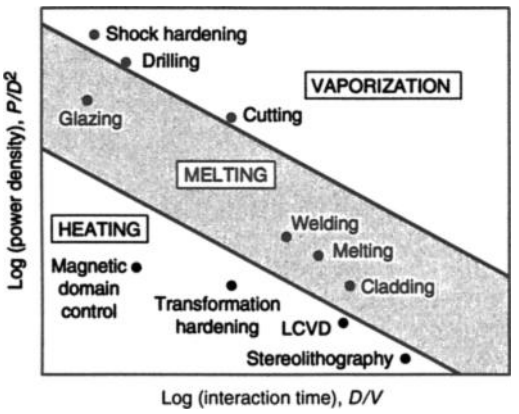

Fig. 16-15 Processing conditions for various types of laser treatments. Source: Ref 57

Heating by laser and electron beams is accomplished by photon interactions of the incident radiation with the electronic structures of the substrate material. The incident energy is very rapidly converted into heat just below the surface, on the order of a few tens of nanometers for laser light, and a few microns for electron beams, depending on the accelerating voltage, which varies between 10 and 100 keV (Ref 59, 60). Figure 16-16 shows schematically the effects of laser and electron beam irradiation on surface heating, melting, and solidification (Ref 59). Electron beam treatments must be conducted in vacuum, but laser light is not subject to this constraint and thus offers considerable flexibility in manufacturing operations. Also, unlike induction and flame heating, lasers can be located at some distance from workpieces, and the laser light can be reflected by mirrors to focusing lenses that control the width of the heated spot or track (Ref 60, 61).

The term *laser* stands for "light amplification by stimulated emission of radiation," and three different types of lasers have been developed: Nd:YAG (neodymium dissolved in yttrium aluminum garnet), CO_2, and excimer. Bass (Ref 60) presents an excellent review of the operation and characteristics of the various types of lasers. The Nd:YAG lasers operate at wavelengths of 1.06 μm, and are widely used for welding and drilling operations. The CO_2 lasers have the highest commercially available power and operate in the infrared range, frequently at a wavelength of 10.6 μm, while the more recently developed excimer lasers operate in the near-ultraviolet range, with wavelengths between 0.193 and 0.351 μm. Laser light may be reflected, depending on the irradiated material and laser beam wavelength. Therefore, for effective laser heating, wavelengths that are absorbed by the workpiece must be selected, or the irradiated workpiece must be coated with a light-absorbing material.

Laser and electron beam surface heat treatments are used to selectively harden localized areas of steel and cast iron components. The heat generated by irradiation is controlled to prevent melting; therefore, local regions can be austenitized. Rapid cooling of the austenitized regions by conduction of heat into the bulk of the workpiece then causes the austenite to transform to very fine martensitic microstructures. In laser surface heating applications, the hardening process is sometimes referred to as

laser transformation hardening, as indicated in Fig. 16-15, in order to differentiate it from laser surface melting phenomena.

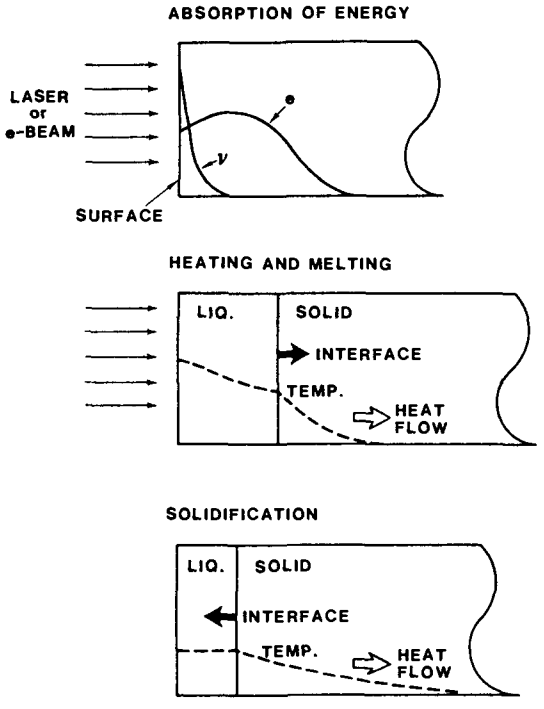

Fig. 16-16 Schematic of the effects of laser and electron beam heating, melting, and solidification. Source: Ref 63

Laser surface heat treatment produces thin surface zones that are very rapidly heated and cooled. Thus, distortion is minimized, because of the low heat input per unit bulk volume, and alloys of low hardenability can be hardened. Molian (Ref 61) has reviewed a number of applications of laser transformation hardening. The energy-absorbing coatings for each application are listed; for steels, typical case depths range from 250 to 750 μm (10 to 30 mils). Most of the applications are to increase wear resistance of machine components manufactured from medium-carbon steels or cast irons, but a few tool steel applications are listed. Similarly, for electron beam surface heating, Zenker et al. (Ref 62) have reviewed processing considerations, microstructures, properties, and applications.

In contrast to transformation hardening, the melting of surfaces by laser and electron beams, as also shown schematically in Fig. 16-16, makes possible surface alloying and unique solidification microstructures. Heating may be extremely rapid, on the order of nanoseconds, and cooling, accomplished by thermal conduction into the unheated mass of the substrate, is similarly very rapid. Exact rates of heating and cooling depend on many factors, such as power input, time of irradiation, laser pulsing, and surface and bulk characteristics of the heated substrate (Ref 63, 64). The very high heating and cooling rates attainable, 10^8 to 10^{10} °C/s, produce extremely rapid solidification and thus make possible very fine nonequilibrium microstructures. In the extreme, new metastable crystalline phases, glassy or

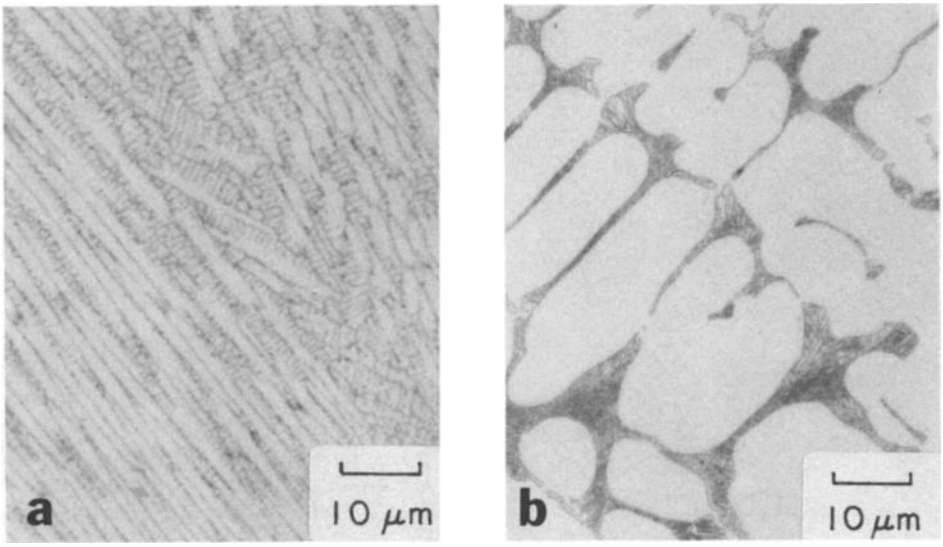

Fig. 16-17 (a) Laser-melted dendritic structure of M42 tool steel. (b) Chill-cast dendrite structure of M42 tool steel. Light micrographs. Courtesy of T. Bell, University of Birmingham

amorphous structures, or highly supersaturated phases may be developed in rapidly cooled surface layers.

Laser and electron beam surface alloying can be accomplished by injecting powders into melted surface layers or by chemical modification by another technique prior to irradiation (Ref 65). When the object of laser treatment is to produce an amorphous or glassy layer, that process is referred to as laser glazing. Glass formation in materials such as silicon, Pd-Cu-Si and Fe-Ni-P-B alloys is readily accomplished but is much more difficult in metals. For example, a study of laser glazing of iron and tool steels, which had been pack boronized to promote amorphization, did not produce evidence of amorphous structures (Ref 66). Nevertheless, the laser surface alloying of the tool steels produced surface layers of high hardness, 2100 HV, containing very fine boride particles. Cracking and porosity were encountered under some conditions of the laser glazing study.

The dramatic changes in surface microstructure produced by laser surface melting of M42 tool steel are shown in Fig. 16-17 and 16-18 (Ref 67). Figure 16-17 shows considerable refinement of the dendritic microstructure of laser-melted M42 compared to that of chill-cast M42, as well as the absence of primary carbides in the laser-melted zone. Dissolution of the alloy carbides is a function of traverse speed, and at high speeds, carbides are not completely dissolved. In the laser-melted surfaces produced by slow traverse speeds, much higher peak hardness compared to conventionally heat-treated steels was observed after triple tempering, apparently because of the greater solution in the molten zone of alloying elements that were subsequently available for precipitation during tempering. Substantial life increases of laser melted M2 and M35 tool bits, compared to those that were conventionally hardened, have been reported (Ref 68).

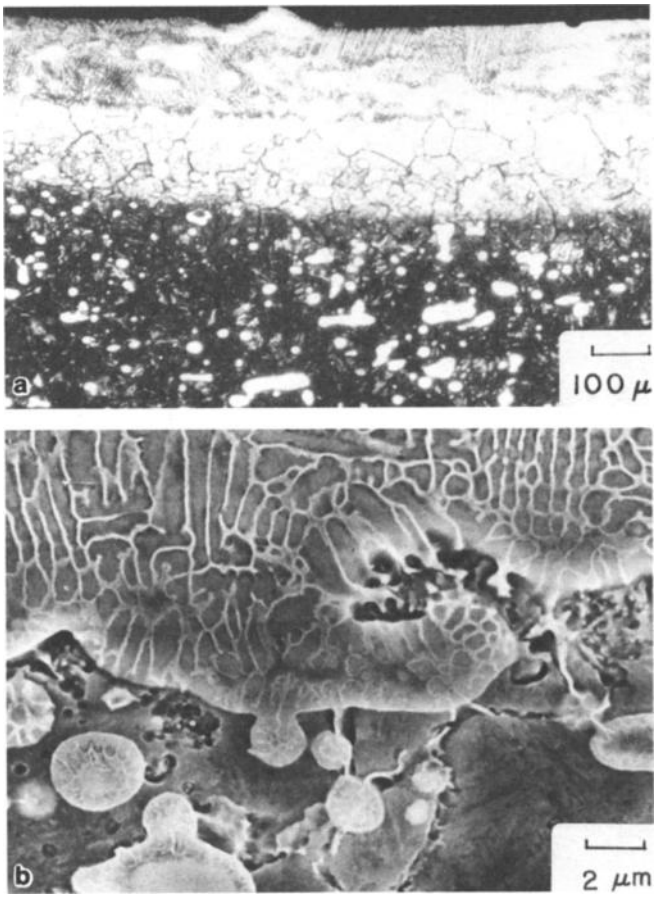

Fig. 16-18 (a) Laser-melted surface layer on M42 tool steel. (b) Higher-magnification view of (a), showing particle melting of carbides at melt interface. Light micrographs. Courtesy of T. Bell, University of Birmingham

Boride Coatings

Boriding or boronizing is a thermochemical process that produces wear-resistant boride coatings on tool steels, carbon and alloy steels, and other materials (Ref 10, 69-71). The boron may be supplied by gaseous, liquid, and solid media, and plasma, PVD, and CVD techniques of applying boron and boron compounds have been evaluated (Ref 69). The use of solid boronizing agents, containing largely boron carbide, as applied by packing tools in powders or applying pastes, has proved the most technologically viable method of boronizing (Ref 71). Steels are boronized at temperatures between 850 and 950 °C (1560 and 1740 °F), and a layer of iron boride, Fe_2B forms on the surface. The iron boride FeB may also form but is considered undesirable because of its tendency to flake from coatings. When present, the FeB can be removed by diffusion annealing. Some elements, such as chromium, molybdenum, nickel, manganese, vanadium, and cobalt, are incorporated into the boride layer, and others, such as carbon, silicon, aluminum, and copper, are insoluble in the boride layer and diffuse into the steel substrate as the boride layer forms. Thus, most of the alloying elements in steel retard the growth of the boride layer to some degree and tend to reduce the attainable thickness of the boride layers.

Table 16-5 Examples of boronized tool steels and applications

DIN designation	Equivalents		Applications
	AISI/SAE	U.K.	
ST 37	...	...	Pins for pinned disk mills, bushes, bolts, nozzles, pipe bends, conveyor tubes, baffle plates, runners, base plates, blades, thread guides
St 50-1	...	...	Casting inserts, nozzles, handles
C15(Ck15)	1015	080A15/080M15	Gear drives, pump shafts
C45	1045	060A47/080M46	Pins, guide rings, grinding disks, bolts
45S20	1146	...	Shaft protection sleeves, mandrels
Ck45	1045	080M46/060A47	Swirl elements, nozzles, rollers, bolts
C45W	...	...	Gate plates
C60W	...	...	Clamping chucks, guide bars
X210Cr12	D3	BD3	Bushes, press tools, plates, mandrels, punches, dies
115CrV3	L2	...	Drawing dies, ejectors, guides, insert pins
40CrMnMo7	...	...	Gate plates, bending dies
X38CrMoV5 1	H11	BH11	Plungers, injection cylinders, sprues
X40CrMoV5 1	H13	BH13	Orifices, ingot molds, upper and lower dies and matrices for hot forming, disks
X32CrMoV3 3	H10	BH10	Injection molding dies, fillers, upper and lower dies and matrices for hot forming
X155CrVMo12 1	D2	BD2	Threaded rollers, shaping and pressing rollers, pressing dies and matrices
105WCr6	...	...	Engraving rollers
X210CrW12	...	...	Straightening rollers
60WCrV7	S1	BS1	Press and drawing matrices, mandrels, liners, dies, necking rings
X165CrMoV12	...	...	Drawing dies, rollers for cold mills
56NiCrMoV7	L6	...	Extrusion dies, bolts, casting inserts, forging dies
X45NiCrMo4	...	...	Embossing die, pressure pad and die
90MnCrV8	02	B02	Molds, bending dies, press tools, engraving rollers, bushes, drawing dies, guide bars, disks, piercing punches
100Cr6	52100	535A99	Balls, rollers, guide bars, guides
Ni 36	...	...	Parts for nonferrous metal casting equipment
X50CrMnNiV22 9	...	...	Parts for unmagnetizable tools (heat treatable)
X10Cr13	410	410S21/410C21	Valve components, fittings
X46Cr13	420	420S45	Valve components, plunger rods, fittings, guides
X35CrMo17	...	...	Shafts, spindles, valves
X12CrNi18 8	302	...	Screw cases and bushes
X5CrNiMo17 12 2	316	316S13-31	Perforated screens, slotted-hole screens, parts for the textile and rubber industry
G-X10CrNiMo18 9	...	...	Valve plugs, parts for the textile and chemical industry
X6CrNiTi18 10	321	321S18-59	Rings, conveyor jets, screw cases, parts for the chemical industry
X6CrNiMoTi17 12 2	316Ti	320S18/320S31	Rings, conveyor jets, screw cases, parts for the chemical industry
30CrNiMo8	...	...	Rollers, heat-treatable machine components
17CrNiMo6	4317	...	Bevel gears, screw and wheel gears, shafts, chain components
16MnCr5	5115	527M17/590M17	Helical gear wheels, guide bars, guiding columns
20MnCr5	5120	...	Helical gear wheels, guide bars, guiding columns
42CrMo4	4140	708A42/708M40	Press tools, extruder screws, rollers, extruder barrels and cylinders, plungers, rings, guides
50CrMo4	4150	708A47	Nonreturn valves, dies
30CrMoV9	...	...	Extruder dies, disks, cylinders, bushings, nozzle base plates
50CrV4	6150	735A51/735H51	Thrust plates, clamping devices, valve springs, spring contact strip

Source: Ref 71

The iron boride layers have high hardness, between 18 and 20 GPa (1800 and 2000 kgf/mm^2), and therefore provide good resistance to wear, especially that caused by abrasive particles. The boride coatings are typically 50 to 150 μm (2 to 6 mils) thick and thus do not provide good resistance to rolling contact fatigue when compared to carburized and nitrided steels with deeper case depths. Table 16-5 lists some applications for boronized tool steels. High-speed tool steels are not suitable for boronizing, since at their high hardening temperatures, above 1150 °C (2100 °F), eutectic decomposition of Fe_2B occurs (Ref 71).

REFERENCES

1. G.A. Roberts and R.A. Cary, *Tool Steels*, 4th ed., American Society for Metals, 1980
2. T. Bell, Surface Engineering: Past, Present, and Future, *Surf. Eng.*, Vol 6 (No. 1), 1990, p 31–40
3. L.E. Rehn, S.T. Picraux, and H. Wiedersich, Ed., *Surface Alloying by Ion, Electron, and Laser Beams*, American Society for Metals, 1987
4. D.S. Rickerby and A. Matthews, Ed., *Advanced Surface Coatings: A Handbook of Surface Engineering*, Chapman and Hall, 1991
5. P.H. Morton, Ed., *Surface Engineering and Heat Treatment: Past, Present and Future*, Institute of Metals, London, 1991
6. *Surface Engineering*, Vol 5, *ASM Handbook*, ASM International, 1994
7. L.I. Maissel and R. Glang, Ed., *Handbook of Thin Film Technology*, McGraw-Hill, 1970
8. W.H. Roberts, Surface Engineering and Tribology in General Engineering, *Surface Engineering and Heat Treatment: Past, Present and Future*, P.H. Morton, Ed., Institute of Metals, London, 1991, p 12–42
9. C.H. Knerr, T.C. Rose, and J.H. Fikowski, Gas Nitriding, *Heat Treating*, Vol 14, *ASM Handbook*, ASM International, 1991, p 387–409
10. J.R. Davis, Surface Engineering of Specialty Steels, *Surface Engineering*, Vol 5, *ASM Handbook*, ASM International, 1994, p 762–775
11. E. Haberling and K. Rasche, Plasma Nitriding of Tool Steels, *New Materials, Processes, Experiences for Tooling*, H. Berns, M. Hofmann, L.-A. Norstrom, K. Rasche, and A.-M. Schindler, Ed., MAT SEARCH, Andelfingen, Switzerland, 1992, p 369–392
12. Liquid Nitriding, *Heat Treating*, Vol 4, *ASM Handbook*, ASM International, 1991, p 410–419
13. G. Hoyle, *High Speed Steels*, Butterworths, London, 1988, p 166–193
14. G. Wahl, Salt Bath Nitrocarburizing of Tools at 480–630 C, *Progress in Tool Steels*, H. Berns, H.-F. Hinz, and I.-M. Hucklenbroich, Ed., Schurmann and Klagges, Bochum, Germany, 1996, p 341–350
15. K. H. Jack, Nitriding, *Heat Treatment '73*, The Metals Society, London, 1973, p 39–50
16. T. Spalvins, Ed., *Ion Nitriding*, ASM International, 1987
17. *Plasma Heat Treatment Science and Technology*, PYC Editions, Paris, 1987
18. T. Spalvins and W.L. Kovacs, Ed., *Ion Nitriding and Ion Carburizing*, ASM International, 1990
19. J.M. O'Brien, Plasma (Ion) Nitriding, *Heat Treating*, Vol 4, *ASM Handbook*, ASM International, 1991, p 420–424
20. G. Krauss, *Steels: Heat Treatment and Processing Principles*, ASM International, 1990, p 281–350
21. R.F. Hochman, Ed., *Ion Plating and Implantation*, American Society for Materials, 1986
22. G. Dearnaley, Ion Implantation and Ion-Assisted Coating, *Advanced Surface Coatings: A Handbook of Surface Engineering*, D.S. Rickerby and A. Matthews, Ed., Chapman and Hall, 1991, p 41–65
23. G. Dearnaley, Materials Science Aspects of Ion Beam Technology, *Surf. Eng.*, Vol 7 (No. 2), 1991, p 127–136
24. J.K. Hirvonen, The Industrial Applications of Ion Beam Processes, *Surface Alloying by Ion, Electron, and Laser Beams*, L.E. Rehn, S.T. Picraux, and H. Wiedersich, Ed., American Society for Metals, 1987, p 373–388
25. J.I. Onate, F. Alonso, J.K. Dennis, and S. Hamilton, Microindentation and Tribological Study of Nitrogen Implanted Martensitic Steels, *Surf. Eng.*, Vol 8 (No. 3), 1992, p 199–205
26. R.M. Middleton, P.J. Huang, M.G.H. Wells, and R.A. Kant, Effect of Coatings on Rolling Contact Fatigue Behavior of M50 Bearing Steel, *Surf. Eng.*, Vol 7 (No. 4), 1991, p 319–326
27. E. Tyrkiel and P. Dearnley, Ed., *A Guide to Surface Engineering Terminology*, Book No. 575, Institute of Materials, London, 1995
28. D.S. Rickerby and A. Matthews, *Advance Surface Coatings: A Handbook of Surface Engineering*, D.S. Rickerby and A. Matthews, Ed., Chapman and Hall, 1991, p 1–13
29. O. Kessler, F. Hoffmann, and P. Mayr, Distortion of CVD-Coating and Gas Quenched Tool Steels, *Proc. 2nd Int. Conf. Quenching and Control of Distortion*, G.E. Totten, M.A.H. Howes, S.J. Sjostrom, and K. Funatani, Ed., ASM International, 1996, p 171–178
30. J.M. Rigsbee, Physical Vapor Deposition, *Surface Modification Engineering*, R.P. Kossowsky, Ed., CRC Press, 1989, p 231–255
31. T. Spalvins, Plasma Assisted Surface Coating/Modification Processes: An Emerging Technology, *Heat Treatment '73*, The Metals Society, London, 1973, p 1–8
32. P.J. Kelly, R.D. Arnell, and W. Ahmed, Some Recent Applications of Materials Deposited by Unbalanced Magnetron Sputtering, *Surf. Eng.*, Vol 9 (No. 4), 1993, p 287–291
33. A. Matthews, Titanium Nitride PVD Coating Technology, *Surf. Eng.*, Vol 1 (No. 2), 1985, p 93–104
34. K.S. Fancey and A. Matthews, Plasma-Assisted Physical Vapor Deposition, *Advanced Surface Coat-*

ings: A Handbook of Surface Engineering, D.S. Rickerby and A. Matthews, Ed., Chapman and Hall, 1991, p 127–159
35. J.-O. Carlsson, Thermally Activated Chemical Vapor Deposition, *Advanced Surface Coatings: A Handbook of Surface Engineering,* D.S. Rickerby and A. Matthews, Ed., Chapman and Hall, 1991, p 162–193
36. H.O. Pierson, Chemical Vapor Deposition of Nonsemiconductor Materials, *Surf. Eng.*, Vol 5, *ASM Handbook,* ASM International, 1994, p 510–516
37. D.S. Rickerby, Plasma-Assisted Chemical Vapor Deposition, *Advanced Surface Coatings: A Handbook of Surface Engineering,* D.S. Rickerby and A. Matthews, Ed., Chapman and Hall, 1991, p 194–216
38. B.A. Movchan and A.V. Demchishin, Study of the Structure and Properties of Thick Vacuum Condensates of Nickel, Titanium, Tungsten, Aluminum Oxide and Zirconium Oxide, *Fiz. Met. Metalloved.*, Vol 28, 1969, p 653
39. J.A. Thornton, High Rate Thick Film Growth, *Ann. Rev. Mater. Sci.*, 1977, p 239–260
40. J.A. Thornton, The Microstructure of Sputter-Deposited Coatings, *J. Vac. Sci. Technol.*, Vol A4, 1986, p 3059–3065
41. D.W. Hoffman and R.C. McCune, Microstructural Control of Plasma-Sputtered Refractory Coatings, *Plasma-Based Processing,* J.J. Cuomo, S.M. Rossnagel, and W.D. Westwood, Ed., Noyes Publications, 1989
42. A.S. Korhonen, J.M. Molarius, S. Osenius, and M.S. Sulonen, Ion Plating of Tools and Dies, *Tool Materials for Molds and Dies,* G. Krauss and H. Nordberg, Ed., Colorado School of Mines Press, 1987, p 217–230
43. J.M. Molarius, A.S. Korhonen, E. Harju, and R. Lappalainen, Comparison of Cutting Performance of Ion-Plated NbN, ZrN, TiN, and (Ti,Al)N Coatings, *Surf. Coat. Technol.*, Vol 33, 1987, p 117–131
44. I. Penttinen, J.M. Molarius, A.S. Korhonen, and R. Lappalainen, Structure and Composition of ZrN and (Ti, Al)N Coatings, *J. Vac. Sci. Technol.*, Vol A6, 1988, p 2158–2161
45. P. Hedenqvist, M. Olsson, and S. Hogmark, Characterization of Ti(C,N) and TiN Coatings on Powder Metallurgy High Speed Steels, *Surf. Eng.*, Vol 8 (No. 1), 1992, p 39–47
46. H. Schulz, New PVD-Coatings for Forming Tools, *New Materials, Processes, Experiences for Tooling,* H. Berns, M. Hofmann, L.-A. Norstrom, K. Rasche, and A.-M. Schindler, Ed., MAT SEARCH, Andelfingen, Switzerland, 1992, p 567–575
47. S.J. Bull, D.S. Rickerby, J.C. Knight, and T.F. Page, High Temperature Mechanical Properties of Physical Vapour Deposited Titanium Nitride, *Surf. Eng.*, Vol 8 (No. 3), 1992, p 193–198
48. W.D. Nix, Mechanical Properties of Thin Films, *Metall. Trans. A,* Vol 20A, 1989, p 2217–2245
49. S.R.J. Saunders, Measurement Methods in Surface Engineering, *Surf. Eng.*, Vol 9 (No. 4), 1993, p 293–299
50. S.J. Bull and D.S. Rickerby, Failure Modes in Scratch Adhesion Testing: Some Observations, *Surface Modification Technologies III,* T.S. Sudarshan and D.G. Bhat, Ed., TMS, 1990, p 153–169
51. K.J. Ma and A. Bloyce, Observations of Deformation and Failure Mechanisms in TiN Coatings after Hardness Indentation and Scratch Testing, *Surf. Eng.*, Vol 11 (No. 1), 1995, p 71–74
52. T. Arai, Carbide Coating Process by Use of Molten Borax Bath in Japan, *J. Heat Treat.*, Vol 1 (No. 2), 1979, p 15–22
53. T. Arai, H. Fujita, Y. Sugimoto, and Y. Ohta, Diffusion Carbide Coatings Formed in Molten Borax Systems, *J. Mater. Eng.*, Vol 9, 1987, p 183–189
54. T. Arai, H. Fujita, Y. Suimoto, and Y. Ohta, Vanadium Carbonitride Coating by Immersing into Low Temperature Salt Bath, *Heat Treatment and Surface Engineering,* G. Krauss, Ed., ASM International, 1988, p 49–53
55. Y. Arata, *Plasma, Electron and Laser Beam Technology,* American Society for Metals, 1986
56. E.A. Metzbower and D. Hauser, Ed., *Power Beam Processing: Electron, Laser, Plasma-Arc,* ASM International, 1988
57. F.C.J. Fellowes and W.M. Steen, Laser Surface Treatment, *Advanced Surface Coatings: A Handbook of Surface Engineering,* D.S. Rickerby and A. Matthews, Ed., Chapman and Hall, 1991, p 244–277
58. R. Zenker, Electron Beam Surface Modification State of the Art, *Proc. 1st ASM Heat Treatment and Surface Engineering Conf. in Europe,* Part 2, E.J. Mittemeijer, Ed., Trans Tech Publications, Switzerland, 1992, p 459–476
59. L.E. Rehn, S.T. Picraux, and H. Wiedersich, Overview of Surface Alloying by Ion, Electron and Laser Beams, *Surface Alloying by Ion, Electron, and Laser Beams,* L.E. Rehn, S.T. Picraux, and H. Wiedersich, Ed., American Society for Metals, 1987, p 1–17
60. M. Bass, Lasers and Electron Beams, *Surface Alloying by Ion, Electron, and Laser Beams,* L.E. Rehn, S.T. Picraux, and H. Wiedersich, Ed., American Society for Metals, 1987, p 357–372
61. P.A. Molian, Engineering Applications and Analysis of Hardening Data for Laser Heat Treated Ferrous Alloys, *Surf. Eng.*, Vol 2, 1986, p 19–28
62. R. Zenker and M. Mueller, Electron Beam Hardening, Part I: Principles, Process Technology and Properties, *Heat Treat. Met.*, Vol 15 (No. 4), 1988, p 79–88; R. Zenker, W. John, D. Rathjen, G. Fritsche, and B. Kamfe, Electron Beam Hardening, Part 2: Influence on Microstructure and Properties, *Heat Treat. Met.*, Vol 16 (No. 2), 1989, p 43–51
63. D.M. Follstaedt and S.T. Picraux, Microstructures of Surface-Melted Alloys, *Surface Alloying by Ion, Electron, and Laser Beams,* L.E. Rehn, S.T. Picraux, and H. Wiedersich, Ed., American Society for Metals, 1987, p 175–221
64. C.W. White and M.J. Aziz, Energy Deposition, Heat Flow, and Rapid Solidification during Pulsed-Laser and Electron Beam Irradiation of Materials, *Surface*

Alloying by Ion, Electron, and Laser Beams, L.E. Rehn, S.T. Picraux, and H. Wiedersich, Ed., American Society for Metals, 1987, p 19–50

65. J.H. Perpezko and W.J. Boettinger, Kinetics of Resolidification, *Surface Alloying by Ion, Electron, and Laser Beams,* L.E. Rehn, S.T. Picraux, and H. Wiedersich, Ed., American Society for Metals, 1987, p 51–90
66. P.A. Molian and H.S. Rajasekhara, Laser Glazing of Boronized Iron and Tool Steels, *Surf. Eng.,* Vol 2, 1986, p 269–276
67. T. Bell, I.M. Hancock, and A. Bloyce, Laser Surface Treatment of Tool Steels, *Tool Materials for Molds and Dies,* G. Krauss and H. Nordberg, Ed., Colorado School of Mines Press, 1987, p 197–216
68. M. Hsu and P.A. Molian, *Wear,* Vol 127, 1988, p 253
69. P.A. Dearnley and T. Bell, Engineering the Surface with Boron Based Materials, *Surf. Eng.,* Vol 1, 1985, p 203–217
70. A.V. Reddy, Boronising Behaviour of Ni-Si-Cr Steel, *Surf. Eng.,* Vol 8, 1992, p 136–140
71. H.-J. Hunger and G. Trute, Boronizing to Produce Wear-Resistant Surface Layers, *Heat Treat. of Met.,* Vol 21 (No. 2), 1994, p 31–39

Tool Steels: 5th Edition
George Roberts, George Krauss, Richard Kennedy, p 325-343
DOI:10.1361/toos1998p325

Copyright © 1998 ASM International®
All rights reserved.
www.asminternational.org

CHAPTER 17
Troubleshooting: Manufacturing and Performance Problems

Tool steels are remarkable materials which must perform the most difficult tasks of any structural materials. The alloying and processing of each type of tool steel is designed to perform well under specific sets of operating conditions. However, each type of steel, even when manufactured to the highest quality, has its operational limits, and factors such as wear under recommended operating conditions are inevitable. Also, problems that arise during manufacture or application may severely limit tool life or even cause catastrophic failure. The following considerations have been identified as essential factors contributing to successful tool, die, and mold making (Ref 1):

- High-quality steel
- Good mechanical design
- Proper selection and application of steel
- Correct heat treatment
- Proper finishing by grinding and EDM

Problems related to all these factors have long been documented in the tool steel literature (Ref 1–5) and, when the causes were understood, provided the basis for applying corrections that result in dependable or improved tool steel performance.

The previous chapters have described the alloying, processing, microstructures, and properties of the various groups of tools steels, the operating advantages and limitations of the various groups, and the reasons for the selection of various grades within each group, depending on performance requirements. These chapters should be referred to for specific selection, processing, and performance characteristics of the various tool steels. This chapter presents an overview of some of the major causes of tool and die failures as related to manufacturing and performance problems associated with the factors on the above list.

In order to troubleshoot causes of premature failure, the contributions of two major causes of failure must be assessed: (1) the source of stress and (2) microstructural condition. In some cases the microstructure has been manufactured to state-of-the-art quality, and failure is caused by excessive stresses caused by poor mechanical design, improper use, or overloads in service. In other cases, tools and dies may be properly designed and used, but flaws, stresses, or detrimental microstructures responsible for poor performance have been introduced during manufacture. In view of the importance of fracture to premature failures, the next section describes general aspects of tool steel fracture and its relation to tool steel microstructure. Subsequent sections present examples of failure associated with various processing and heat treatment problems. In addition to fracture problems, distortion is discussed.

Fracture and Toughness of Tool Steels: General Considerations

Tool steels must have very high strength, hardness, and wear resistance. These properties are inconsistent with high toughness or fracture resistance, and tool steels are very susceptible to fracture if stresses during manufacture or service exceed those which the microstructure can sustain. Fracture may be strain controlled, where generalized plastic deformation precedes fracture, or stress controlled, where fracture is caused largely by stress without any appreciable plastic flow.

Ductile fracture is a strain-controlled fracture that occurs by the deformation-induced nucleation and growth of microvoids around hard particles (Ref 6). Although ductile fracture is not a brittle mechanism, the ductile fracture resistance of tool steels tends to be low because of the high rates of strain hardening in tempered martensitic matrices and high densities

of hard alloy carbide particles built into tool steel microstructures. Operating loads within recommended limits, below the high ultimate tensile or shear strengths of properly processed tool steels, do not initiate ductile fracture. However, such factors as overloads, stress concentrations, surface flaws, or nonuniform distributions of coarse carbides may significantly lower the resistance of a tool steel to ductile fracture. Ductile fractures of tool steels tend to be macroscopically flat and have a smooth, gray, silky appearance consistent with the fine microstructure of properly processed tool steels.

Brittle fracture is stress-controlled fracture that occurs with little or no plastic deformation (Ref 7). Frequently, the stresses that cause brittle fracture are well below those expected from ultimate tensile strengths or reasonable operating conditions. Brittle fracture may be initiated by cleavage cracks in hard particles, which in turn lead to unstable cleavage crack propagation in matrix structures of low toughness. Cleavage cracking develops in steels stressed at low temperatures and high strain rates or under other conditions where dislocation mobility is severely restricted (Ref 8).

In tool and other high-carbon steels, a major mechanism of brittle fracture is intergranular cracking along embrittled austenite grain boundaries. This form of brittle fracture is caused by excessive austenitizing and is exacerbated by hydrogen if present. To the unaided eye, intergranular fractures have a faceted appearance, and light reflects from the coarse austenite grain boundaries typically associated with the conditions that produce intergranular fracture. This characteristic fracture appearance led the early heat treaters to conclude that the steel had "crystallized." All components of a hardened steel microstructure are, of course, crystalline, but are usually much too fine to be resolved with the naked eye. In the case of intergranular fracture, the faceted appearance confirms that significant coarsening of austenite crystals or grains has occurred.

The intergranular fracture is promoted by coarse austenite grain size, phosphorus segregation to austenite grain boundaries, and cementite particle precipitation on grain boundaries (Ref 9) and is driven by tensile stresses or bending stresses generated by heat treatment or in service. Tools and dies properly heat treated to produce fine austenite grain sizes and carbide dispersions, and applications where the loading is primarily in compression and shear, are not sensitive to brittle, intergranular fracture and will fail by transgranular ductile, but characteristic low-toughness, mechanisms of microvoid formation and coalescence.

Figure 17-1 compares the toughness of a number of tool steels heat treated to typical service levels of hardness (Ref 10). Three measures of toughness are shown: fracture toughness, K_{Ic}, or the stress intensity to cause crack propagation at the tip of a sharp crack; energy absorbed on CVN impact testing; and energy absorbed on unnotched Izod impact testing. Specimen and testing details are given in Ref 11. The toughness of the steels varies widely because of various levels of heat-treated matrix strength and different densities of carbide dispersions.

Differences in toughness of the steels as ranked by the different testing techniques are affected by the nature of the tests. Charpy V-notch testing gives

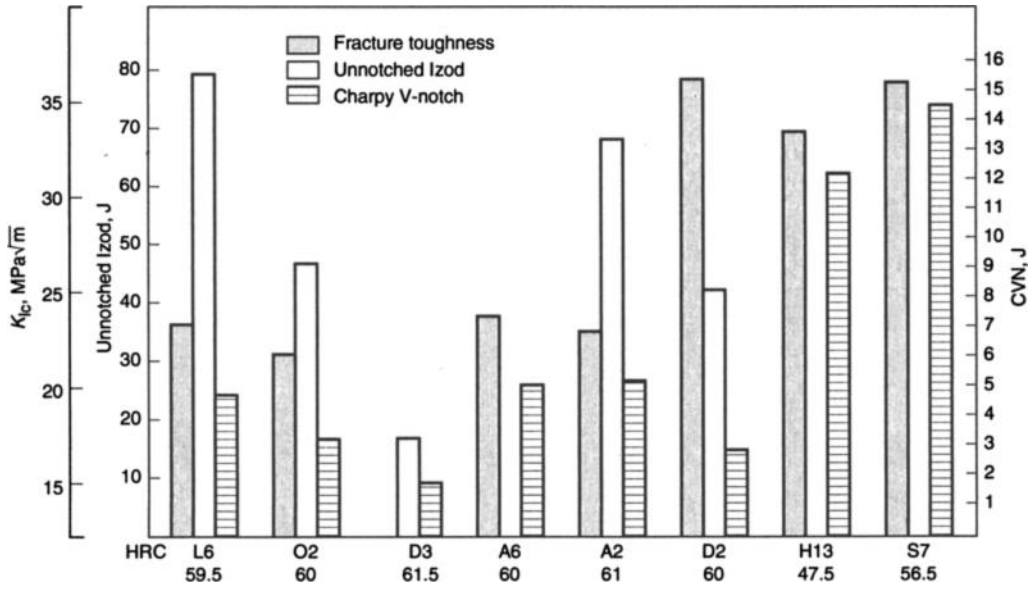

Fig. 17-1 Comparison of fracture toughness, longitudinal unnotched Izod, and longitudinal CVN impact toughness for various tool steel specimens taken from 89 mm square stock and tested at working hardness. Source: Ref 10

very low values of energy absorbed for tool steel fracture, even for those with higher toughness, because of the severe stress concentration at the notch root and the application of load at very high-strain rates. A large plastic process zone develops ahead of the notch, and the associated stresses are distributed over large volumes of the microstructure. Thus, carbides, inclusions, and other fracture-sensitive features are subjected to stresses that initiate and propagate the fracture. In comparison to notched bar testing, the energy absorbed in the fracture of the various tool steels as measured by the unnotched Izod tests is much higher, reflecting the deformation required to cause fracture in the absence of any stress concentration.

In contrast to impact toughness testing, fracture toughness testing is performed at slower strain rates, and the plastic zone ahead of the sharp crack is small, especially in tool steels with very high yield strengths (Ref 12, 13). As a result of the small process zone, fracture stresses may not build up at all fracture-sensitive microstructural features, and the measurement of fracture toughness of tool steels reflects more the fracture resistance of typical local regions of the microstructure and less the effect of more widely spaced inclusions or carbides.

In summary, the toughness or fracture resistance of tool steels by any measure is generally low. By design, hardness, strength, and wear resistance of tool steels are maximized, and sacrifices in toughness are accepted. Nevertheless, certain differences in toughness can be caused by alloying and heat treatment. Lower carbon content, which lowers strain-hardening rates of the tempered matrix martensite, and lower alloy content, which reduces the volume fraction of hard alloy carbide particles that initiate fracture, are used to increase toughness at the expense of wear resistance. Earlier chapters have described specific alloying and heat treatment approaches used to balance strength and toughness in the various groups of tool steels.

Steel Quality and Primary Processing

As discussed, fracture resistance of tool steels is greatly influenced by coarse second-phase particles dispersed throughout a matrix of tempered martensite. Two types of particles influence fracture: inclusions and carbides. Excessive sizes or densities of either type of particle, or inhomogeneous distributions of particles, could contribute to premature tool and die failures.

Inclusions are nonmetallic phases such as alumina, sulfides, and silicates, in many combinations and morphologies, which are introduced during various phases of steelmaking (Ref 14, 15). Some inclusions are hard, such as oxides, and resist deformation during hot work, while others, notably manganese sulfides, are plastic and deform during hot work. The resulting elongated and flattened inclusions may introduce considerable anisotropy in the properties and fracture of hot-worked steels. Alloy carbide particles are present by design in most tool steels but should be distributed as uniformly as possible to optimize fracture resistance.

With the recognition of the detrimental role that coarse, second-phase particles play in the fracture resistance of tool steels have come significant improvements in steelmaking since the publication of earlier work on tool steel technology (Ref 1–5). The oxide and sulfide inclusion contents of tool steels are now at very low levels because of melting improvements, including improved deoxidation, the use of shrouding to prevent reoxidation of liquid streams, enhanced desulfurization, electroslag refining, and vacuum arc refining, as described in Chapter 3.

Alloy carbide arrays, especially the as-cast cells of primary eutectic carbides, must be dispersed and uniformly distributed by high-temperature soaking and controlled hot-work schedules in cast and wrought tools steels. A major advantage of tool steels manufactured by powder metallurgy processing is the ability of this technique to produce uniform dispersions of small randomly distributed carbides without the need for homogenization of solidification structures and segregation by hot work (Ref 16).

Hot work by rolling or forging of highly alloyed tool steels must be done with caution, since the deformation is accomplished in the two-phase, carbide-austenite phase field. Under the action of certain stress and strain states, voids may be initiated at carbides and coalesce along carbide bands to form cracks (Ref 17). Hot ductility in the cast condition is a function of the size of the eutectic cells or the secondary dendrite arm spacing as controlled by solidification. The finer the cell spacing, the better the hot ductility, because microcracks created by the coalescence of voids are shorter and require more strain to cause fracture (Ref 17). Figure 17-2 shows an example of a central burst in a forged bar of high-speed steel caused by improper forging (Ref 1). Ultrasonic inspection techniques today would readily reveal such defects at the steel mill prior to shipment.

Another difficulty sometimes encountered during primary processing of tool steels is the formation of flakes or hairline cracks within the interior of heavy sections and forgings (Ref 18). The flaking is due to excessive hydrogen trapped during solidification. At high temperatures, in liquid steel and in δ-iron, the solubility of hydrogen is high, about 7 ppm, but with decreasing temperature the solubility of hydrogen drops to less than 1 ppm at room temperature. In section sizes greater than 75 mm (3 in.) in diameter, the hydrogen, not trapped at permanent sites such as sulfide inclusions, cannot diffuse from the steel during cooling after finish rolling or forging.

This hydrogen then concentrates, often at prior-austenite grain boundaries, and severely lowers the cohesive strength of the microstructure to the point where cooling stresses are sufficient to cause cracking. The diffusion of hydrogen to critical sites is time dependent and may take up to 2 weeks to cause cracking.

Today, the susceptibility of tool steels to flaking is significantly lowered by the use of vacuum degassing to reduce hydrogen to very low levels in liquid steel. Without the use of degassing, heavy sections of steel may be held at temperatures between 500 and 650 °C (930 and 1200 °F) to allow the hydrogen to diffuse from the steel to a level consistent with its reduced solubility in that temperature range.

Mechanical Design

Many tool and die failures have occurred during heat treatment or in service as a result of poor mechanical design (Ref 1, 2). Sharp changes in section thickness, sharp corners, and inadequate section size after machining of holes are common design causes of tool and die failure. Often, discontinuous changes in section thickness and square corners create stress concentrations that are sufficient to generate stresses high enough to cause quench cracking on cooling during hardening heat treatments. The stress concentrations associated with sharp corners—for example, sharp keyways in rotating shafts—may also induce fatigue failures during operation. The latter problem is readily corrected by introducing half-round keyways, and other causes of stress concentration are often corrected by introducing generous fillets to sharp corners. In chisels and other pneumatic tools, tapered shanks are even better than fillets to accommodate changes in section (Ref 1).

Examples of failures due to poor design are shown in Fig. 17-3 to 17-7. Figure 17-3 shows the fracture surface of a high-carbon, high-chromium

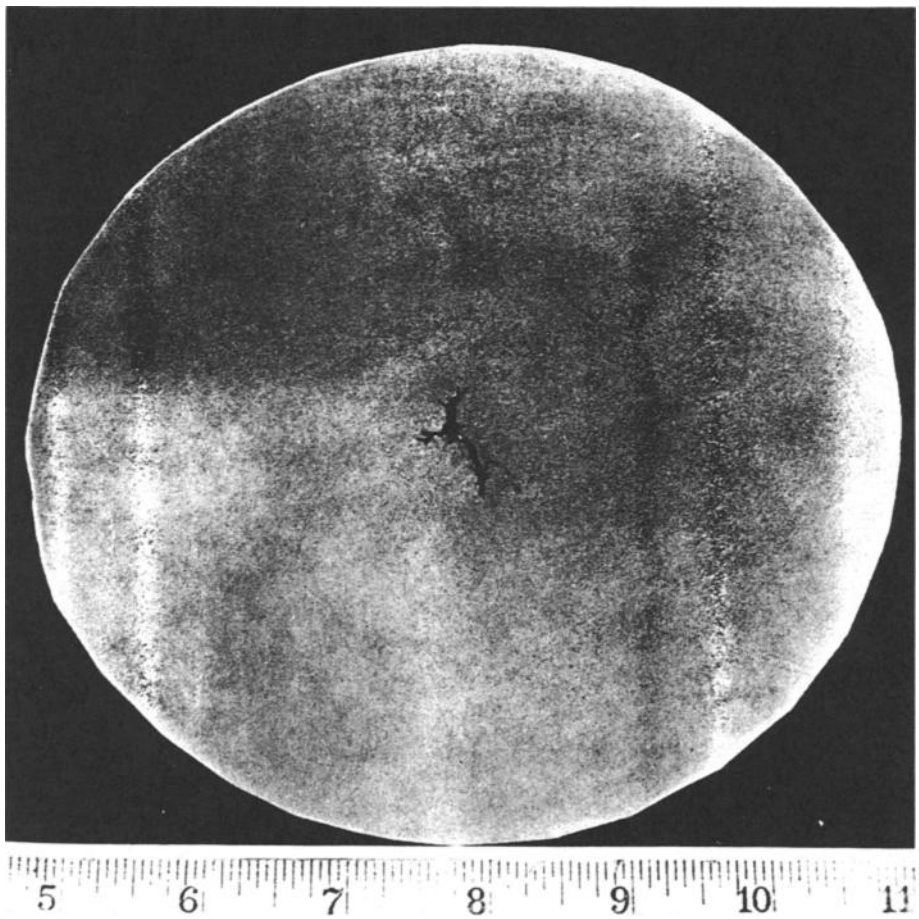

Fig. 17-2 Central burst in a 125 mm (5 in.) diam forged bar of high-speed steel. Source: Ref 1

die that failed in service because of inadequate steel left between the threaded holes and the inner surface of the die. This example emphasizes the need to retain adequate section thicknesses to lower the stresses created by operating loads in tool and die applications. Figure 17-4 shows a high-speed steel punch that cracked during heat treatment. The cracking was caused by the high stresses induced by cooling due to the sharp change in section thickness between the two parts of the punch. Deep identification stamp marks are another common cause of stress concentration leading to fracture in low-toughness tool steels; Fig. 17-5 shows an example of a die that failed as a result of such overenthusiastic stamping. Figure 17-6 shows premature failure of a 5% Cr hot-work die steel due to cracks initiated by stress concentrations at very sharp corners of the die.

Figure 17-7 presents an example of a failure that may arise during assembly of die components. Shown is a die holder, made from 5% Cr hot-work steel, that split when a cold-heading die insert was forced into it. The oversize die insert clearly generated stresses sufficient to cause overload fracture of the low-toughness tool steel. This example, and the others presented, show that fracture and cracking in hardened tool steels develop with almost no macroscopically visible plastic deformation.

Heat Treatment Problems

The Tool Steel Trouble-Shooter (Ref 1), published in 1952, states, "Faulty heat treatment causes most tool failures." Whether or not this statement is still true today with current instrumentation and heat-treating equipment, every step of the heat treatment process, including stress relief, preheating, austenitizing, quenching, and tempering, must be carried out with care according to recommended practices for each grade of steel.

Excessive distortion, especially in nonsymmetric tools, may develop in several stages of the hardening process. One stage is during heating after tools have been shaped by rough machining or other shaping process such as cold hubbing. Residual stresses are introduced by these processes, and when a part is heated, the flow strength of the steel may decrease to the level where the residual stresses can cause localized plastic flow or distortion. Thus, stress-relief treatments are highly recommended for precision tools. Any dimensional changes produced by the stress relief should be adjusted by finish machining prior to hardening. Such finish machining on an annealed part will be more cost effective than making corrections on the part when hardened.

Heating to the austenitizing temperature for hardening is another stage in the hardening process where distortion, and even cracking, especially for tools and dies with complex shapes or major changes in section thickness, may take place. Single and double preheating steps, depending on how high an austenitizing temperature is recommended, are necessary to provide uniform heating throughout a part and to minimize distortion on austenitizing. Tool steels that must be austenitized at high temperatures also benefit from preheating, in that the time at the high austenitizing temperature can be minimized and the potential for scaling and decarburization reduced accordingly.

Overheating during austenitizing for hardening is a major source of problems during tool steel heat treatment. Overheating, to temperatures above the recommended austenitizing temperatures for a given tool steel, results in increased dissolution of alloy carbides, increased carbon content of the austenite, and austenite grain coarsening. Curves of austenite grain size as a function of austenitizing temperature for various tool steels have been shown in earlier chapters. When an overheated microstructure is quenched, it is highly susceptible to quench cracking by intergranular fracture along

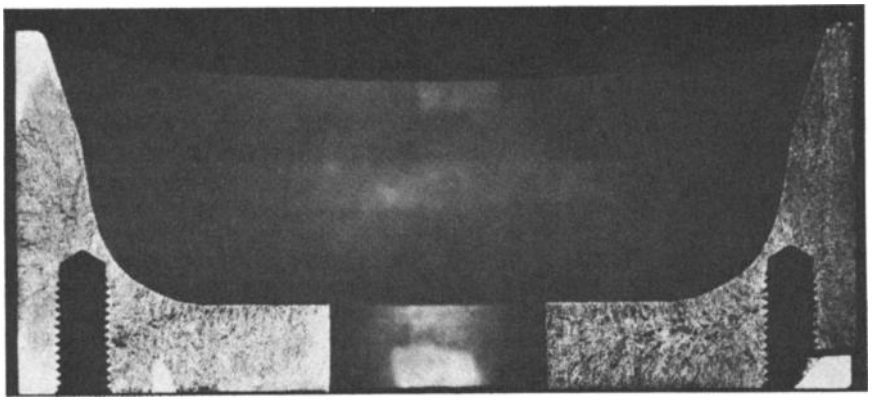

Fig. 17-3 Fracture surface of a high-carbon, high-chromium die that failed in service. Poor design left extremely thin walls in a highly stressed portion of the die.

coarsened and embrittled austenite grain boundaries, as described earlier in this chapter. Figure 17-8 shows an extreme example of overheating. The microstructures are from opposite ends of an M2 steel broach, 40 mm (1.5 in.) in diameter, that cracked during heat treatment. At one end was a correct

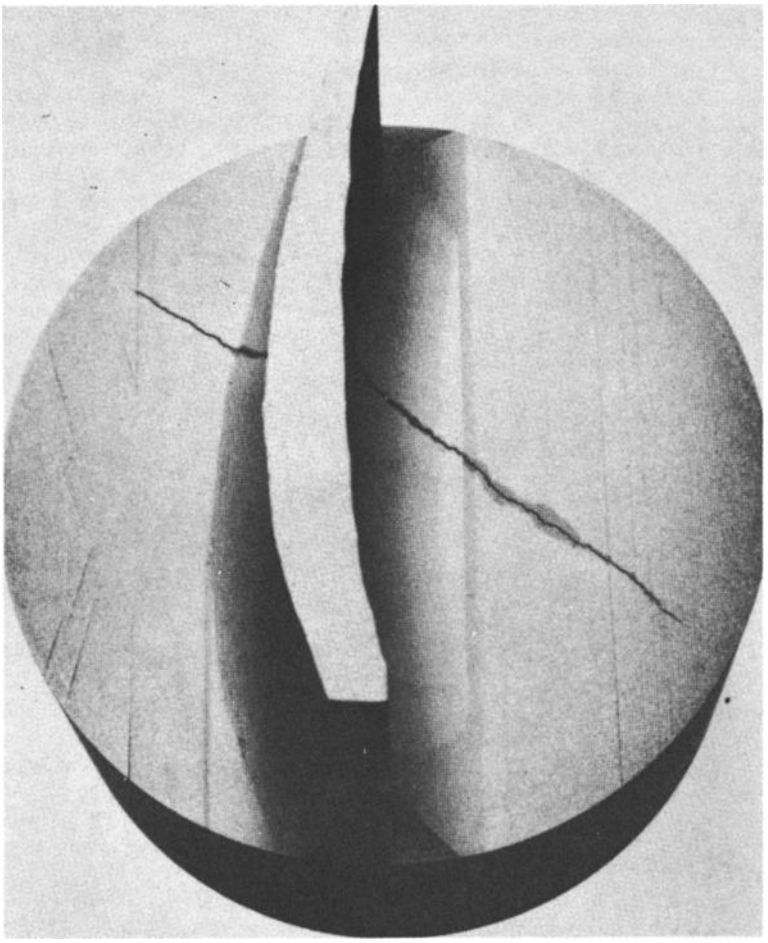

Fig. 17-4 High-speed steel punch that cracked on heat treatment because of the large difference in section size

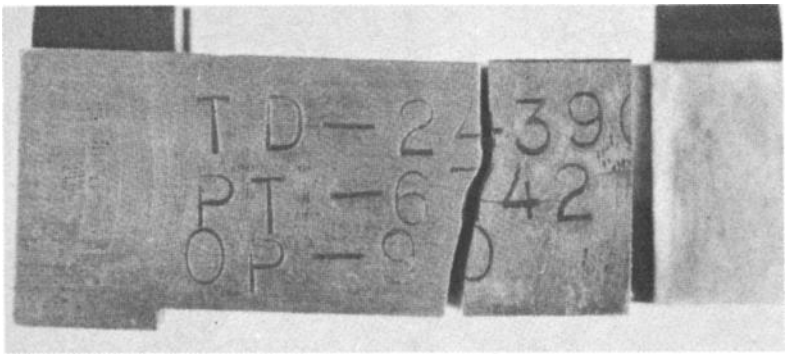

Fig. 17-5 Failure of die by cracking caused by the stress-concentration effect of deep stamp marks

microstructure of uniformly dispersed carbides in a matrix of martensite, but at the other end was a network of coarse carbides on coarsened austenite grain boundaries typical of an overheated microstructure. This premature failure resulted from overheating caused by temperature variations in the austenitizing furnace.

When a tool steel is overheated, not only is the susceptibility to quench cracking and intergranular fracture in service increased, but the retained austenite content in quenched specimens also is greatly increased. As a result, as-quenched hardness will be lower than anticipated. Figure 14-9(c) has shown the microstructure of overheated T1 tool steel. Excessive retained austenite is present, most of the carbides have dissolved, and the coarse martensite plates reflect very coarse austenite grain size. This type of microstructure typically accompanies austenite grain boundaries embrittled by phosphorus segregation and carbide formation.

The very high austenitizing temperatures and high-alloy content of high-speed steels make them especially sensitive to overheating. Overheating of high-speed steels may in fact cause melting of portions of the microstructure and a return to an undesirable solidification structure in those areas. Figure 17-9(a) and (b) show microstructures of properly austenitized and hardened high-speed steel and overheated and hardened high-speed steel from milling cutters that failed in service, respectively. The overheated microstructure shows that a eutectic carbide cell structure has been reestablished by the overheating. The latter microstructure not only reduces service life, but also greatly increases susceptibility to quench cracking.

A special type of grain coarsening and embrittlement occurs when high-speed steels have been reaustenitized after a first hardening heat treatment. Rehardening is sometimes necessary to salvage a tool for one reason or another. Figure 17-10 shows an example of such grain coarsening and the associated "fishscale" fracture appearance in a rehardened high-speed steel. The causes of this unique discontinuous grain growth have been discussed in earlier chapters. Conditions for the grain growth associated with fishscale fracture can be eliminated by annealing the hardened steel prior to reheating for hardening a second time.

Many tool steel heat treatment problems have been traced to inadequate surface protection during austenitizing. The maintenance of surface carbon content is critical to achieve the correct micro-

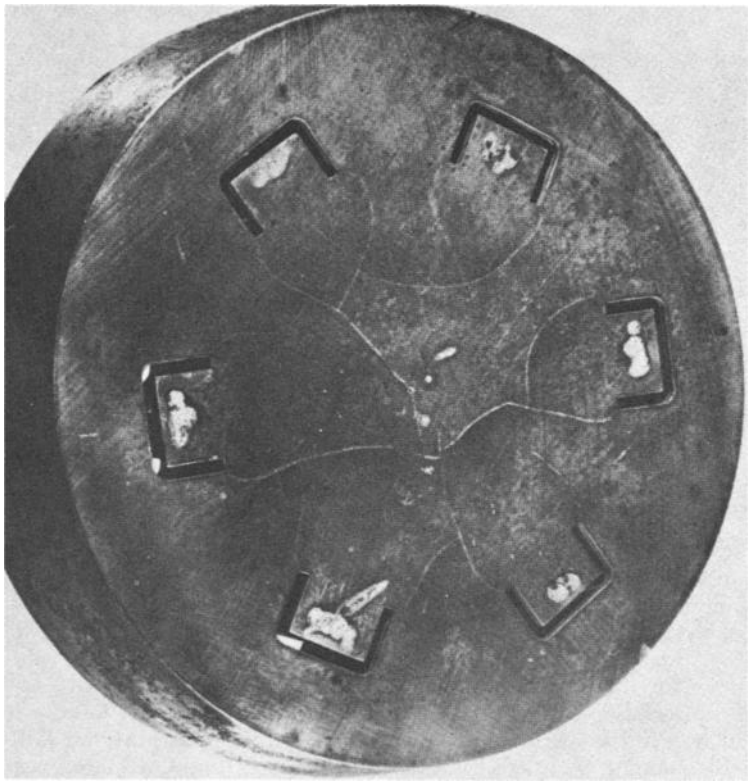

Fig. 17-6 Premature failure of a 5% Cr hot-work die steel caused by the severe stress-concentration effect of very sharp corners

structure and performance of tools and dies. These problems should be avoided by proper instrumentation and atmosphere control or the use of vacuum furnaces. If a furnace atmosphere is not neutral, a tool surface may be decarburized, leading to softer microstructures and rapid wear, or it may be carburized, leading to brittle behavior.

Figure 17-11 shows microstructures from M1 tool steel twist drills that exhibited various surface microstructures and performance. The twist drill with the normal microstructure (Fig. 17-11a) showed satisfactory performance, but the other two drills, one carburized (Fig. 17-11b) and the other decarburized (Fig. 17-11c), showed unacceptable performance. The surface of the carburized drill chipped in a brittle manner, and the surface of the decarburized drill wore rapidly in service. Figure 17-12 shows another example of a decarburized surface microstructure, in this case from a T1 form-cutting tool. The surface is almost completely decarburized, resulting in the formation of ferrite rather than martensite in the decarburized layer.

Another example of an inadvertently carburized tool steel surface is shown in Fig. 17-13. Here the surface of an M2 steel tap consists of a layer of austenite because the high carbon content has substantially lowered the M_s temperature. Carburization can be so severe that the high carbon lowers the surface melting point to where melting or fusion of the surface occurs. Figure 17-14 shows the surface microstructure of a T2 broach that was decarburized and then carburized. The decarburized layer is marked by the white band of ferrite grains, and the carburized zone is marked by the dark band and a dendritic surface layer, indicating that melting has occurred. When carburization is severe enough to cause surface melting, the tool surface assumes a macroscopically rippled appearance, as illustrated in Fig. 17-15.

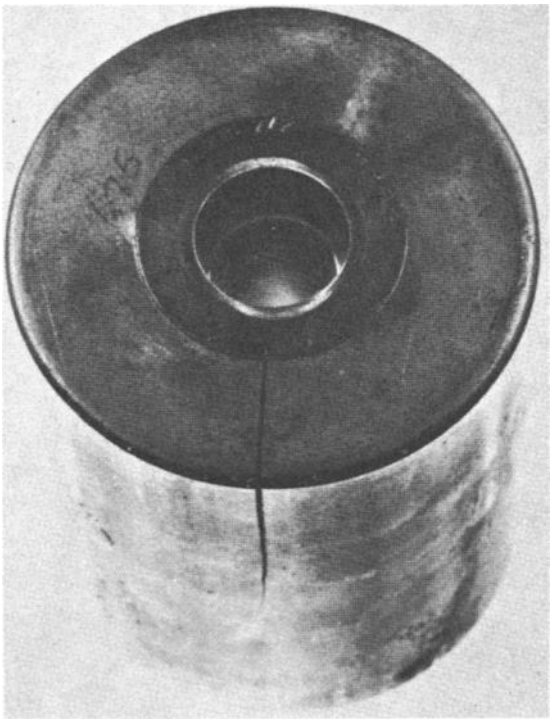

Fig. 17-7 Failure of holder for a cold-heading die insert caused by overstressing associated with forcing the insert into the poorly designed holder

Tool steel troubles may also originate during quenching from the austenitizing temperature. Although the microstructural conditions for quench cracking are established primarily during austenitizing, as discussed above, the stress that causes the cracking originates during the quench. Temperature gradients between the surface and interior or different sections of a tool mean that some parts transform to martensite before others. Those parts which transform last, undergo the volume expansion last, and this expansion applies tensile stresses to regions transformed previously. If the stresses are high enough, and if the microstructure is sufficiently weakened, as at austenite grain boundaries embrittled during high-temperature austenitization, quench cracking will occur.

Quenching stresses decrease as cooling rates decrease and temperature drops more uniformly throughout a tool cross section. This principle is one of the major reasons steels are alloyed for high hardenability. High hardenability not only increases depth of hardening, but also makes possible the use of less aggressive quenches to achieve hardening. In the extreme, highly alloyed steels can be hardened by air cooling with great benefits for both the prevention of quench cracking and the minimization of distortion.

Martempering—the quenching of tools into molten salt until temperature equalizes just above the M_s temperature, followed by air cooling—is another approach used to eliminate quench cracking and reduce distortion. Martempering requires steels of high hardenability to avoid transformation of austenite to soft microstructures such as ferrite, pearlite, and bainite in the salt bath. Thus, many highly alloyed tool steels are well suited to martempering. Interrupted oil quenching is also sometimes used to reduce temperature gradients during cooling (Ref 5). The workpiece is quenched until color disappears from the surface, is removed from the oil, and, when color reappears, is again placed in the oil. This procedure may be repeated a number of times until the color becomes a dark red, at which time the work may be cooled in air.

Water-hardening tool steels have very low hardenability and therefore must be severely water quenched for hardening. A problem that may readily develop in water-hardening steels is the formation of soft spots due to incomplete martensite for-

mation. These soft spots may result in cracking, especially in large tools and tools with irregular shapes or section changes (Ref 1). Frequently the soft spots (i.e., regions where austenite has transformed to nonmartensitic microstructures) are a result of the vapor blanket that forms around red-hot steel parts when they are first immersed in water. The hardenability of the W-type steels is so low that even a short delay in cooling is sufficient for diffusion-controlled transformation of austenite. Agitation of the quenchant or the workpiece, or the use of a brine quench, will produce more rapid, uniform cooling and prevent the formation of soft spots.

Examples of soft spots formed on water-hardening steel are shown in Fig. 17-16 and 17-17. The darker areas are properly hardened, and the soft spots have the same light appearance as the unhardened interiors of the parts. On the part shown

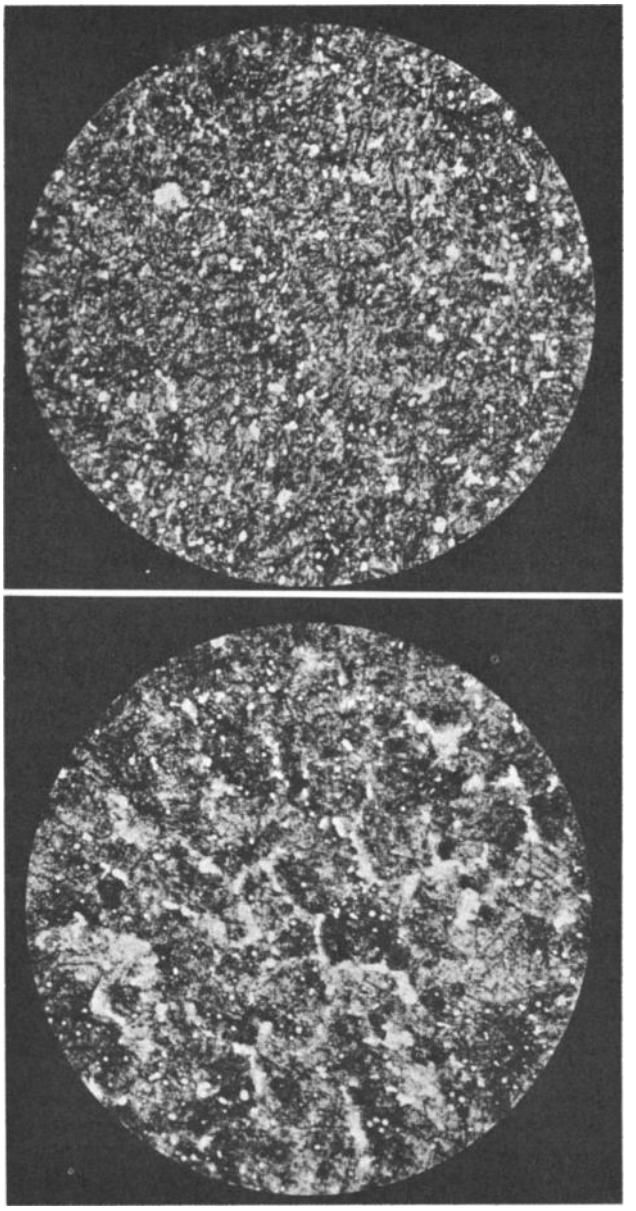

Fig. 17-8 Structures illustrating overheating in an M2 broach. Top: Proper microstructure found at one end of broach. Bottom: Overheated structure found at the other end of broach. Very uneven furnace heating was responsible for the quite different microstructures. Light micrographs. 400×

in Fig. 17-16, the dark, properly quenched areas had a hardness of 63 HRC and the soft spots a hardness of 45 HRC.

Good quenching practice requires that tools be removed from the quenchant before they reach room temperature and that they be transferred im-

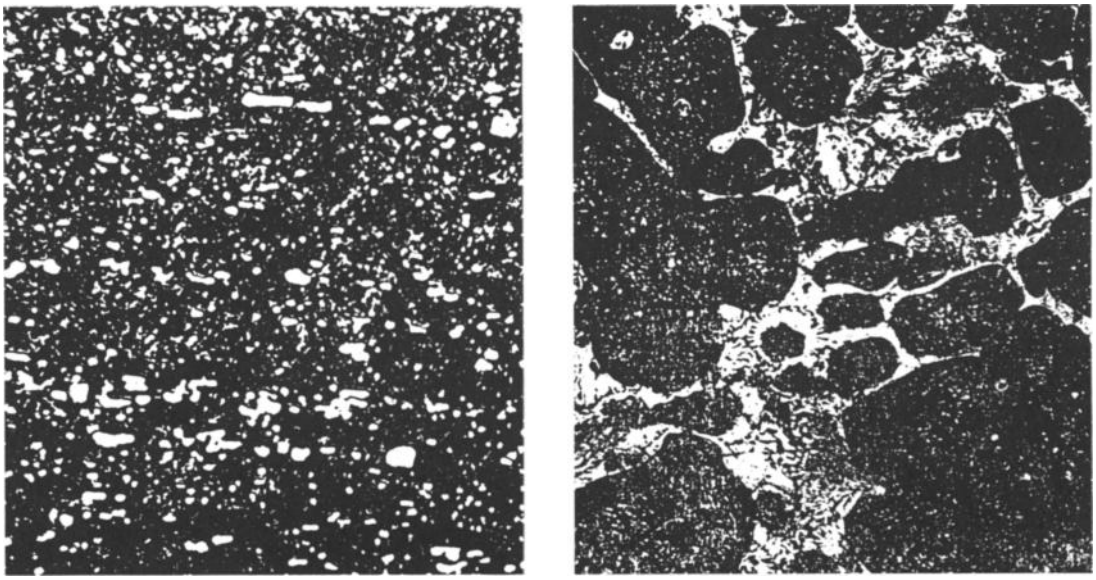

(a) (b)

Fig. 17-9 Comparison of hardened microstructures from properly austenitized (a) and overheated (b) high-speed steel. Light micrographs, 700×. Source: Ref 1

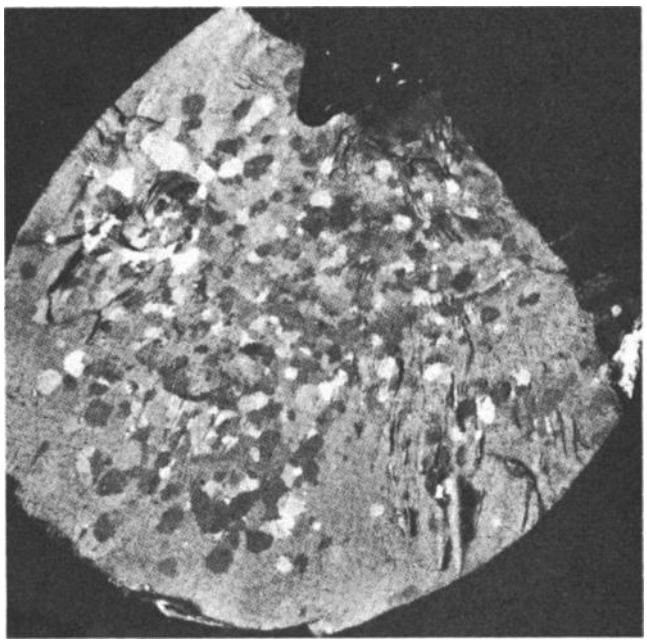

Fig. 17-10 Appearance of fishscale fracture associated with coarse austenite grains in a rehardened high-speed steel

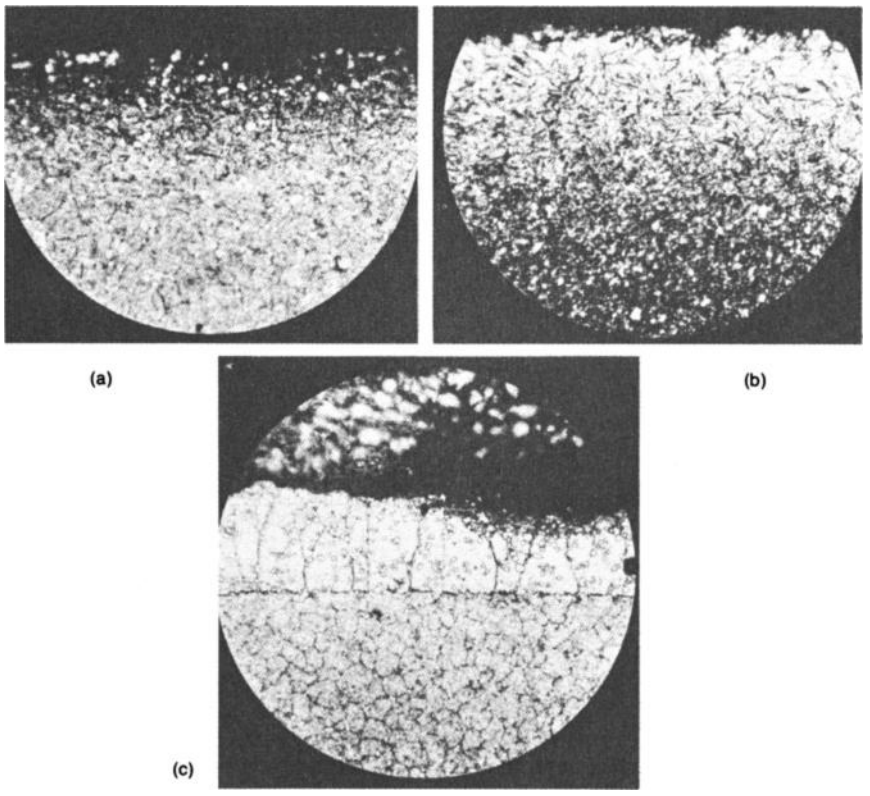

Fig. 17-11 Microstructures of hardened M1 twist drills. (a) Normal microstructure with good performance. (b) Carburized surface microstructure that failed by chipping. (c) Decarburized surface microstructure that failed by rapid wear. Light micrographs, 300×

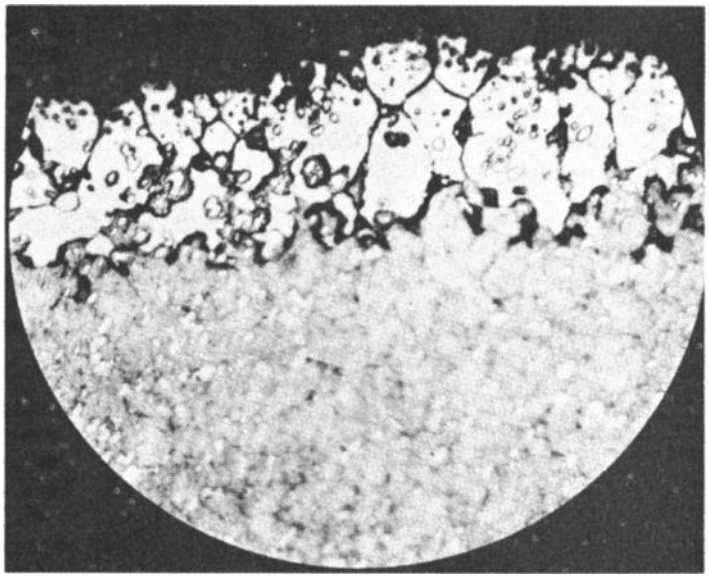

Fig. 17-12 Decarburized layer, composed of ferrite grains, in a hardened T1 steel form-cutting tool. Light micrograph, 500×

mediately to the tempering furnace. Steels quenched in liquid baths should be removed at 65 to 95 °C (150 to 200 °F), and more highly alloyed air-hardening steels with low M_s temperatures should be cooled to a somewhat lower temperature and held long enough at that temperature to achieve more martensite formation. Quenching to room temperature will increase stresses and the risk of

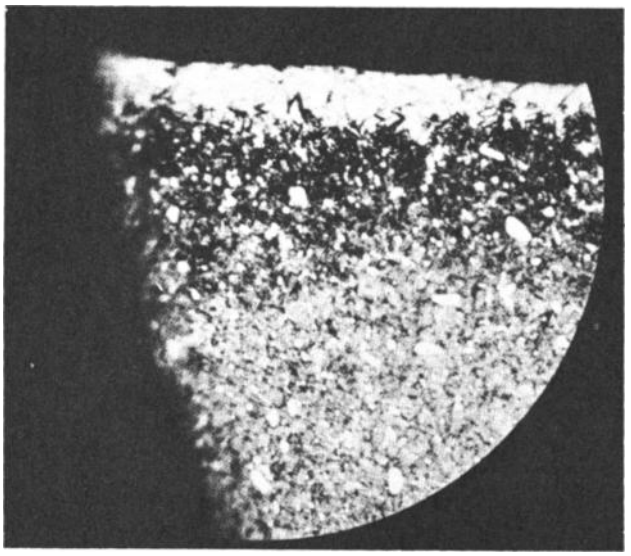

Fig. 17-13 Microstructure of an M2 tap that failed because of a surface layer of retained austenite due to carburization during austenitizing. Light micrograph. 500×

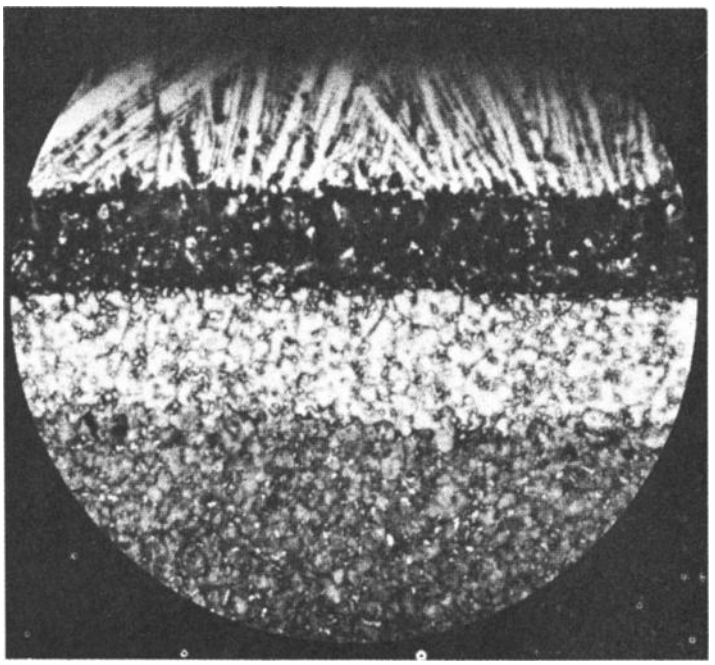

Fig. 17-14 Surface microstructure of a T2 steel broach that was first decarburized to produce the white ferrite layer and then carburized to produce the black band and a dendritic surface layer indicating melting. Light micrograph. 150×

cracking, and holding as-quenched parts too long at room temperature before tempering may result in time-dependent cracking if parts have not already cracked in the quench. A major function of tempering, in addition to making the microstructural adjustments necessary for good performance, is to relieve stresses introduced by quenching. Double and triple tempering of tool steels, as discussed in earlier chapters, is a necessary to improve toughness by spheroidizing coarse carbide arrays and tempering martensite that form after the first tempering treatments.

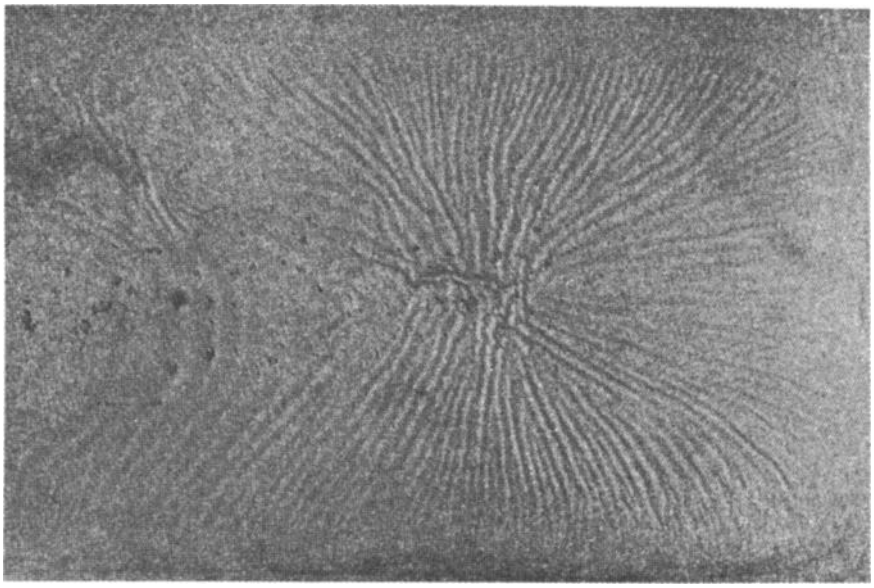

Fig. 17-15 Rippled appearance of a fused or molten tool surface due to carburization. Unmagnified photograph

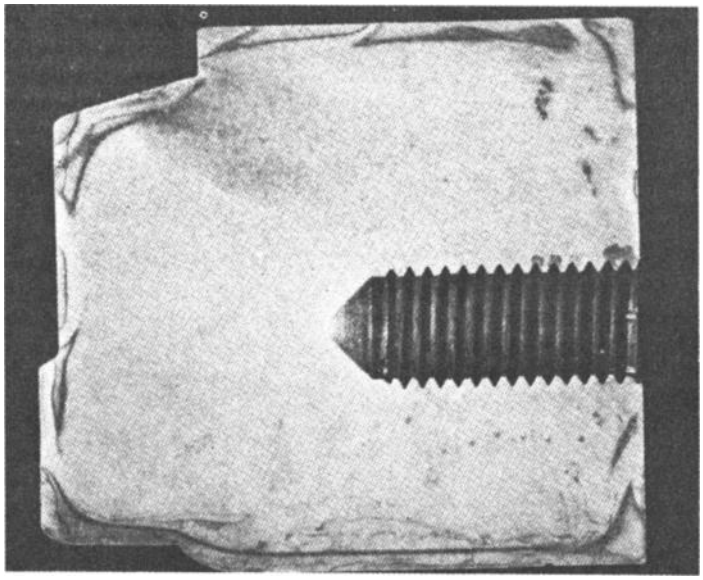

Fig. 17-16 Cross section showing soft spots (white areas adjacent to dark areas) on surfaces of a water-hardening steel. Unmagnified photograph

Grinding and Finishing of Hardened Tools

Grinding is frequently performed on hardened tools to produce final tool dimensions and to correct for dimensional changes caused by heat treatment. Even properly designed and heat-treated tools may create trouble, in the form of cracking or poor service, if improper grinding is applied after the hardening heat treatment. The grinding may generate enough localized heat by action of the abrasive to actually heat the surface of the steel above its hardening temperature and thereby cause a rehardening of the surface. In extreme conditions the surface stresses caused by grinding may cause cracks or checks in the tool surface, which, if undetected, will ultimately cause premature failure of the tool in service. Short of reaustenitizing a surface layer, grinding may cause overtempering and surface softening.

Figures 17-18 to 17-20 show examples of grinding damage in various tool steel applications. In many cases, deep acid etching or magnetic particle testing is required to reveal small, tightly closed grinding cracks. Grinding speed, effective coolants, cleanliness of the grinding wheel, and proper grit size must all be considered to ensure that excessive heat is not generated during grinding (Ref 1), and stress-relief treatments may be used to reduce residual stresses introduced by grinding. Proper heat treatment to ensure the absence of embrittled microstructures produced by overheating or insufficient tempering is also a necessary condition for good grinding.

Electrodischarge machining is also used to finish and shape hardened tools. This technique is capable of producing slots or complex shapes that could not be produced by conventional machining techniques. The EDM process works by melting away the tool material, leaving a white surface layer that consists of as-cast material and a heat-affected zone that transforms to as-quenched martensite. This surface layer is brittle and contains high residual stresses and may cause cracking in service. References presented in Chapter 13 showed that EDM surfaces have lowered resistance to heat checking by hot-work die steels. Therefore, removal of the white layer, by light polishing or grinding, and stress-relief treatments are recommended for hardened tools finished by EDM.

Distortion and Dimensional Change

Changes in size and shape during heat treatment may be an additional source of trouble in the manufacture of a tool or die, in that such changes necessitate expensive finishing operations to bring a part into required tolerances. Already this chapter has mentioned the distortion that may occur during heating and quenching, and the benefits that slow or interrupted rates of heating and cooling may confer on the control of distortion and cracking during heat treatment. This section, following Lement (Ref 19),

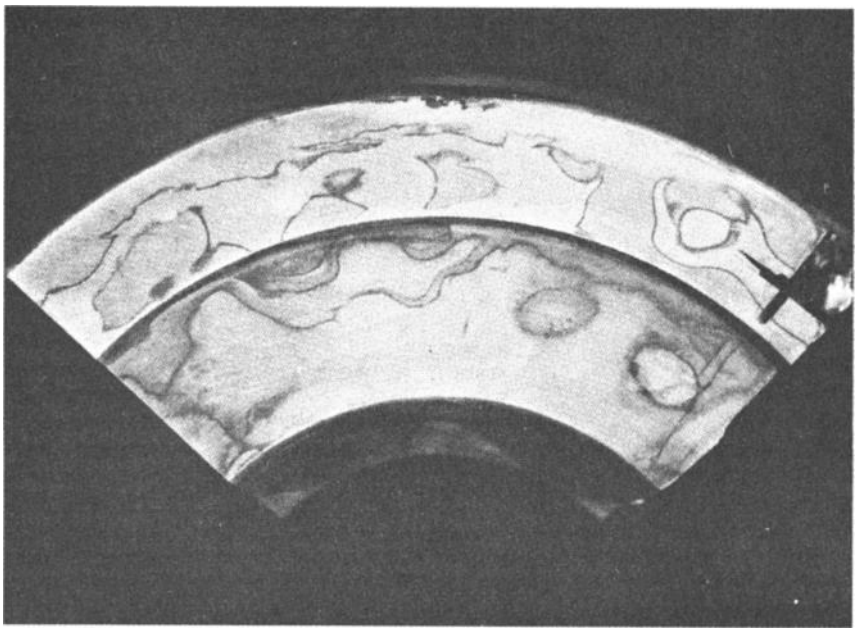

Fig. 17-17 Mottled appearance associated with soft spots on a water-hardening steel die

examines more systematically the causes of distortion and dimensional change in tool steels.

Two principal types of distortion or dimensional changes occur during heat treatment of tool steels: size and shape. Size distortion is related to changes in volume—either expansion, where dimensions increase or grow, or contraction, where dimensions decrease or shrink. Shape distortion is associated with changes in the geometry of a part, caused by bending or twisting. Figure 17-21 shows schematically examples of size and shape distortion due to hardening heat treatments of an L-shape tool steel

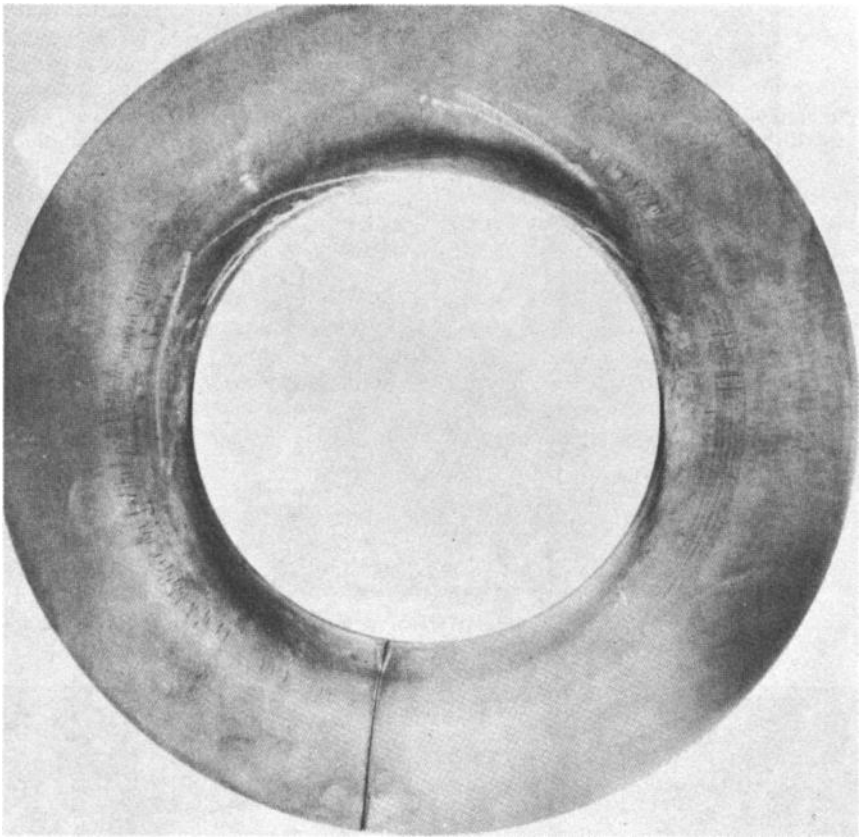

Fig. 17-18 Failure of a high-carbon, high-chromium drawing die due to grinding cracks. Grinding cracks around the inner diameter were revealed by deep etching

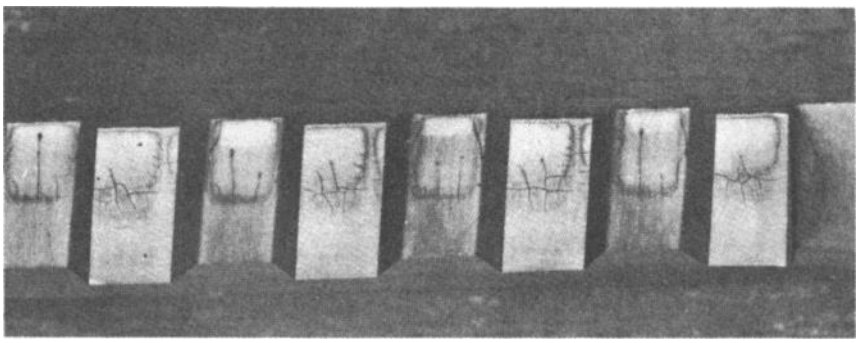

Fig. 17-19 Grinding damage on a T1 steel tap that failed in service

part, and Table 17-1 lists the many causes of size and shape distortion that may occur during tool steel heat treatment.

Size distortion is caused by thermal expansion and contraction during heating and cooling and by the changes in crystal structure that accompany phase transformations during heat treatment. If changes in size are related primarily to room-temperature differences before and after heating, the expansion and contraction due to temperature changes may be neglected and the dimensional changes related directly to changes in microstructure and the phases that compose the microstructures. On hardening, when an annealed microstructure consisting of ferrite and spheroidized carbides is converted to martensite, a volume expansion will occur. The magnitude of this expansion will depend on the carbon content of the martensite, which, as shown in Chapter 4, establishes the tetragonality of the martensite unit cell and the amount of retained austenite that coexists with the martensite. The formation of the martensite is accomplished by way of conversion of the annealed ferrite-carbide microstructure to austenite and the subsequent transformation of the austenite to martensite. Because of the low specific volume of austenite compared to martensite, there is a volume expansion of about 4.1% when austenite containing 1.0% C transforms to martensite.

Table 17-2 lists the specific volumes of the various phases that form in carbon tool steels, and Table 17-3 presents the volume and dimensional changes associated with various changes in microstructures during the hardening of carbon tool steels. All the changes are dependent on carbon content, and as carbon content decreases, the changes in dimension also decrease. The size changes associated with the various reactions assume complete replacement of one microstructure by another. This assumption is rarely valid in tool steel heat treatment. For example, there are generally carbides left undissolved during austenitizing and therefore incomplete transformation of a spheroidized microstructure to austenite, and, after quenching, not all of the austenite transforms to martensite, leaving some fraction of retained austenite in the hardened microstructure. These changes can significantly reduce the size changes associated with hardening, and Lement points out that for a 1% C steel, if 7.5 vol% undissolved cementite and 20 vol% retained austenite are present in a hardened steel, there should be no volume change on hardening (Ref 19).

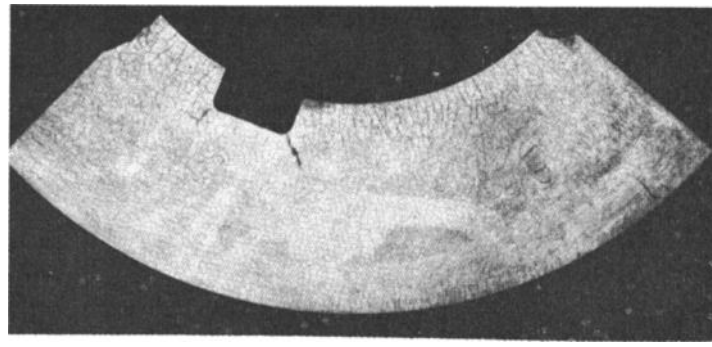

Fig. 17-20 Grinding damage on a high-carbon, high-chromium tool steel slitter knife that spalled in service

Table 17-1 Causes of size and shape distortion during heat treatment of tool steels

Operation	Sequence	Size distortion	Shape distortion
Hardening	Heating to and holding at austenitizing temperature	Formation of austenite Solution of carbides	Relief of residual stress Thermal stresses Sagging
	Quenching	Formation of martensite Formation of nonmartensite products	Thermal stresses Transformation stresses Introduction of residual stresses
Cold treatment	Subcooling to and holding at subzero temperature and returning to room temperature	Formation of martensite	Thermal stresses Transformation stresses Introduction of residual stresses
Tempering	Heating to and holding at tempering temperature	Decomposition of martensite Transformation of retained austenite	Stress relief Thermal stresses
	Cooling from tempering temperature	Transformation of retained austenite	Thermal stresses Introduction of residual stresses

Source: Ref 19

Tempering causes contraction as carbides precipitate from martensite supersaturated with carbon and expansion when retained austenite transforms to mixtures of ferrite and carbides or to bainite or martensite after cooling from tempering temperatures. The chapters on the various tool steels have presented examples of the dimensional changes that occur during tempering of specific tool steels, and Fig. 17-22 and 17-23 show, respectively, changes in dimensions of hardened D2 and H13 tool steels as a function of tempering temperature. Differences in the dimensional changes at various orientations to the rolling direction may be due to preferred crystallographic orientation or the elongation of residual solidification structures and segregation during hot rolling.

Shape distortion is caused by nonuniform thermal and transformation stresses due to nonuniform temperature distribution throughout a part. Localized regions, which expand or contract due to heating or cooling or a phase transformation due to more rapid heating or cooling than adjacent regions, exert stresses on those adjacent regions which may be high enough, especially at higher temperatures, to generate plastic deformation and changes in shape. If the stresses cannot be relieved by plastic flow, considerable residual stresses will be incorporated into a quenched part. Nonuniform quenching, higher quenching rates, larger section sizes, and large variations in section all contribute to large variations in temperature during heating or cooling and increase the possibility of significant shape distortion or high residual stresses. As described earlier, good mechanical design, preheating, interrupted cooling, the selection of high-hardenability steels that can harden during slower rates of cooling, and rapid tempering of hardened parts are all factors which will minimize distortion, cracking, and residual stresses.

Although good heat treatment practice, based on an understanding of the physical changes and phase transformations by which hardening is accomplished, can minimize or compensate for dimensional changes, there is a great need to be able to precisely predict dimensional changes caused by hardening, especially in parts of complex shapes. As a result, characterizing the quenching process and mathematical modeling of the heat treatment process in order to predict distortion and residual stresses are of much interest (Ref 20-23). Modeling requires knowledge of quenchants, the quenching process, heat-transfer coefficients at the quenchant/workpiece interface, and thermal conductivity and specific heat as a function of chemical composition, phase distribution, and temperature within the workpiece, in order to establish the temperature gradients that develop in the workpiece as a function of time during quenching. The temperature

Table 17-2 Specific volume of phases present in carbon tool steels

Phase or phase mixture	Range of carbon, %	Calculated specific volume at 20 °C (68 °F), cm^3/g
Austenite	0–2	0.1212 + 0.0033 (% C)
Martensite	0–2	0.1271 + 0.0025 (% C)
Ferrite	0–0.02	0.1271
Cementite	6.7 ± 0.2	0.130 ± 0.001
Epsilon-carbide	8.5 ± 0.7	0.140 ± 0.002
Graphite	100	0.451
Ferrite plus cementite	0–2	0.1271 ± 0.0005 (% C)
Low-carbide martensite plus ε-carbide	0–2	0.1277 ± 0.0015 (% C –0.25)
Ferrite plus ε-carbide	0–2	0.1271 ± 0.0015 (% C)

Source: Ref 19

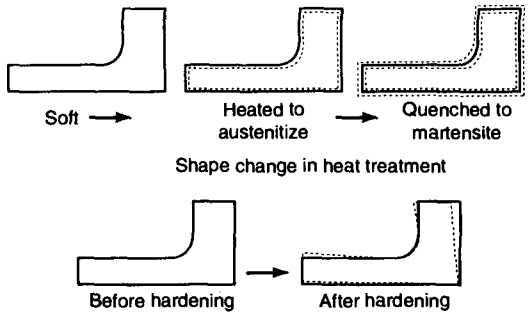

Fig. 17-21 Schematic examples of size and shape changes caused by heat treatment. Courtesy of Latrobe Steel Co.

Table 17-3 Size changes on hardening carbon tool steels

Reaction	Volume change, %	Dimensional change, mm/mm or in./in.
Spheroidite→austenite	–4.64 + 2.21 (% C)	–0.0155 + 0.0074 (% C)
Austenite→martensite	4.64 – 0.53 (% C)	0.0155 – 0.0018 (% C)
Spheroidite→martensite	1.68 (% C)	0.0056 (% C)
Austenite→lower bainite(a)	4.64 – 1.43 (% C)	0.0155 – 0.0048 (% C)
Spheroidite→lower bainite(a)	0.78 (% C)	0.0026 (% C)
Austenite→aggregate of ferrite and cementite(b)	4.64 – 2.21 (% C)	0.0155 – 0.0074 (% C)
Spheroidite→aggregate of ferrite and cementite(b)	0	0

(a) Lower bainite is assumed to be a mixture of ferrite and ε-carbide. (b) Upper bainite and pearlite are assumed to be mixtures of ferrite and cementite. Source: Ref 19

gradients must then be related to phase transformation kinetics and the accompanying stress and strains associated with the phase transformations as a function of temperature and position. A discussion of the modeling efforts to date is outside the scope of this book, and the reader is referred to the recent literature for state-of-the-art reviews of the characterization of quenching processes and the mathematical modeling of heat treatment distortion (Ref 20–23).

REFERENCES

1. *The Tool Steel Trouble-Shooter,* Bethlehem Steel Co., 1952
2. G. Roberts and R. Cary, *Tool Steels,* 4th ed., American Society for Metals, 1980
3. P. Payson, *The Metallurgy of Tool Steels,* John Wiley & Sons, 1962
4. F.R. Palmer and G.V. Luerrssen, *Tool Steel Simplified,* 3rd ed., Carpenter Steel Co., 1960
5. *Tool Steel for the Non-Metallurgist,* Crucible Specialty Metals, 1985
6. W.M. Garrison, Jr., and N.R. Moody, Ductile Fracture, *J. Phys. Chem. Solids,* Vol 48 (No. 11), 1987, p 1036–1074
7. J.F. Knott, *Fundamentals of Fracture Mechanics,* Butterworths, London, 1973
8. G. Krauss and C.J. McMahon, Jr., Low-Toughness and Embrittlement in Steels, *Martensite,* G.B. Olson and W.S. Olson, Ed., ASM International, 1992, p 295–321
9. G. Krauss, Heat Treated Martensitic Steels: Microstructural Systems for Advanced Manufacture, *Iron Steel Inst. Jpn. Int.,* Vol 35 (No. 4), 1995, p 349–359
10. R.M. Hemphill and D.E. Wert, Impact and Fracture Toughness Testing of Common Grades of Tool Steels, *Tool Materials for Molds and Dies,* G. Krauss and H. Nordberg, Ed., Colorado School of Mines Press, 1987, p 66–89
11. *Mechanical Testing,* Vol 8, *Metals Handbook,* 9th ed., American Society for Metals, 1985
12. F.B. Pickering, The Properties of Tool Steels for Mould and Die Applications, *Tool Materials for Molds and Dies,* G. Krauss and H. Nordberg, Ed., Colorado School of Mines Press, 1987, p 3–32
13. H. Berns, Strength and Toughness of Hot Working Tool Steels, *Tool Materials for Molds and Dies,* G. Krauss and H. Nordberg, Ed., Colorado School of Mines Press, 1987, p 45–65
14. R. Kiessling and N. Lange, *Non-metallic Inclusions in Steel,* 2nd ed., The Metals Society, London, 1978
15. W.C. Leslie, Inclusions and Mechanical Properties, *ISS Trans.,* Vol 2, 1983, p 1–24
16. K.E. Pinnow and W. Stasko, P/M Tool Steels, *Properties and Selection: Irons, Steels, and High-Performance Alloys,* Vol 1, *Metals Handbook,* 10th ed., ASM International, 1990, p 780–792
17. W. Roberts, Dynamic Changes that Occur during Hot Working and Their Significance Regarding Microstructural Development and Hot Workability, *Deformation Processing and Structure,* ASM International, 1984, p 109–184
18. G.F. Vander Voort, Embrittlement of Steels, *Properties and Selection: Irons, Steels, and High-Performance Alloys,* Vol 1, *Metals Handbook,* 10th ed., ASM International, 1990, p 689–736
19. B.S. Lement, *Distortion in Tool Steels,* American Society for Metals, 1959

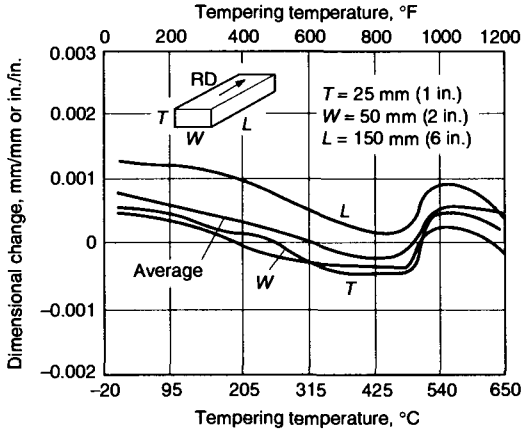

Fig. 17-22 Dimensional changes in air-hardened D2 tool steel as a function of tempering temperature and orientation. Courtesy of Latrobe Steel Co.

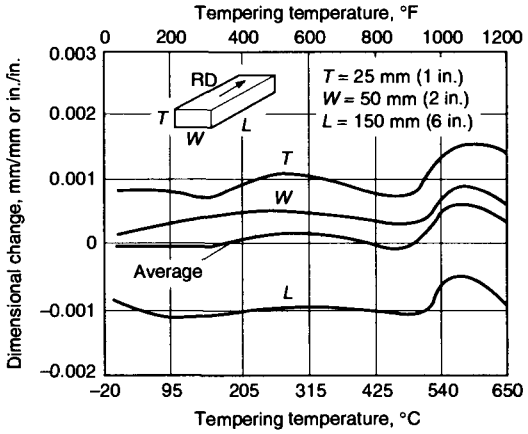

Fig. 17-23 Dimensional changes in air-hardened H13 tool steel as a function of tempering temperature and orientation. Courtesy of Latrobe Steel Co.

20. B. Liscic, H.M. Tensi, and W. Luty, Ed., *Theory and Technology of Quenching,* Springer-Verlag, Berlin, 1992
21. *Quenching and Carburizing,* Institute of Materials, London, 1993
22. G.E. Totten, Ed., *Quenching and Distortion Control,* ASM International, 1992
23. G.E. Totten, M.A.H. Howes, S.J. Sjostrom, and K. Funatani, Ed., *2nd International Conference on Quenching and the Control of Distortion,* ASM International, 1996